GEOMAGNETIC INDUCTION STUDIES IN SOUTHERN SCOTLAND

ALAN GEORGE JONES

GEOMAGNETIC INDUCTION STUDIES

IN SOUTHERN SCOTLAND

by

Alan George Jones

Thesis presented for the degree of

Doctor of Philosophy of the

University of Edinburgh in the Faculty of Science

1977

DECLARATION

I hereby declare that the work presented in this thesis is my own unless otherwise stated in the text, and that the thesis has been composed by myself.

Alan George Jones

ABSTRACT

The Southern Uplands of Scotland is at present a region of great interest to both geologists and geophysicists. The complex tectonic history associated with the closing of the proto-Atlantic ocean has yet to be determined. Previous geophysical studies have shown that the Southern Uplands is atypical of normal continent. Geomagnetic investigations have indicated a zone of anomalously high electrical conductivity underlying the Southern Uplands region at a depth of 12-30 km.

In order to determine further the exact structure and spatial variation of this conductivity zone, two geomagnetic studies have been carried out in the region. A Geomagnetic Deep Sounding Array of 19 Gough-Reitzel variometers recorded the naturally varying Earth's magnetic field during December 1973 and January 1974. This was followed by Magneto-Telluric observations on lines perpendicular and parallel to the strike of the supposed anomaly.

In this thesis, reviews of various regional MT studies, the geophysical significance of conductivity measurements and the known geology and geophysics of the Southern Uplands region are given. The aims, and relevant theory, of induction studies are also presented. The observational procedures for both the GDS and MT techniques, and the type and form of the MT activity, are described. Techniques for analysing the MT data are developed in some detail. Methods are proposed, and examples given, for (a) estimating the gross structural strike direction, (b) averaging response function estimates, (c) estimating the confidence intervals of the response functions, (d) estimating new forms of coherence functions, which exhibit many desirable properties, and (e) a frequency-time analysis for estimating the response functions for sub-intervals of the data set.

The full MT and GDS estimates from analysis of the single station data - rotated major and rotated minor impedance estimates, azimuthal angles, skew factors and real and imaginary induction vectors - are presented and qualitatively discussed.

A one-dimensional interpretation of two-dimensional MT data is examined and shown to be valid for 'rotated major' impedance estimates from locations sufficiently distant from gross lateral inhomogeneity. Various methods for determining an 'optimum model' that best satisfies, in some manner, the observed MT responses are reviewed. A Monte-Carlo inversion procedure is developed and applied to the 'rotated major' data from six of the thirteen locations. It was considered, for various reasons, unjustifiable to interpret all the data.

The GDS and MT results agree on the complexity of the conductivity variations in the Midland Valley, the Southern Uplands and Northern England. The simple 'Eskdalemuir anomaly' proposed by Edwards et al. (1971) cannot explain the observations. A conductive layer is required beneath the Midland Valley at a depth of no greater than 11 km. The conductive zone underlying the Southern Uplands is at a depth greater than 24 km. For the Northern England response, the top layer of highly conducting sediments 'screen' the possible effects of a 'lower crustal/ upper mantle' conductive layer. The geological and geophysical implications of the acceptable MT models are discussed.

In this work, the quantitative information, offered by the MT technique, is shown to be necessary for a full interpretation of the conductivity distribution. Also, estimation of the phase response, as well as the amplitude response, of the impedance tensor elements is shown to resolve the surface structure of the acceptable models.

Various suggestions are made about further investigation of the region.

ACKNOWLEDGEMENTS

I gratefully acknowledge the help and direction given me by my supervisor, Dr. Rosemary Hutton. Dr. Hutton has not only encouraged me throughout my research but also has ensured that I was not too side-tracked by peripheral issues. I am indebted to her for the years of preparation and organisation she spent on the project before I came to Edinburgh. I should like to express my gratitude to the Geophysics Department of Edinburgh University for providing the wherewithal for my research. I wish to thank all members of the Department for furnishing a refreshing and stimulating atmosphere in which to work. In particular, I would like to mention Drs. Jane Sik (co-supervisor), Dennis Rooney, Dave Summers and Bruce Hobbs, all of whom gave me much food for thought. Dennis Rooney is to be especially thanked for his guidance during the initial stages of data processing, and Bruce Hobbs for theoretical assistance. The fieldwork and technical assistance given me by Mr. Alex Jackson and Mr. Hugh Muir did not go unnoticed. It was much appreciated. The fieldwork for the GDS Array study was more amusing because of the companionship of Mr. Surrinder Chita, whose help is thankfully acknowledged. Also, I am grateful to my two colleagues, Mr. Dave McKirdy and Ms. Sheila Kirkwood, for their patience and assistance during the last six months. Sheila Kirkwood is also thanked for proof-reading the typescript of this thesis.

I am pleased to extend warm thanks to Dr. Ian Gough for his invitation to process the GDS Array data initially at the Department of Physics of the University of Alberta, Edmonton, Canada. During my two-month visit to that Department, Dr. Remi Alabi gave up much of his time both to train me in the data reduction procedure and to entertain me during the weekends - for which I am very grateful.

I wish to thank most sincerely all the people on whose land the instruments were located, many of whom gave up garages, outbuildings and even houses to provide shelter for the MT filtering and recording equipment. Their overwhelming generosity and hospitality made the fieldwork for the MT project very enjoyable.

I should like to thank all the staff of the Edinburgh Regional Computing Centre who have helped me at the data processing stage of my research. I express appreciation especially to Ms. Beth Egan for digitising some of the MT data sections.

My financial support for this research was by a Natural Environment Research Council studentship, for the initial two years, and a University of Edinburgh studentship for the final 18 months. The Royal Society of London provided the funds for the purchase and construction of the MT equipment. I express gratitude to all three bodies.

Finally, I wish to thank Ms. Fiona Train for aiding me in inumerable ways, and Ms. Kathy Dodds who gave up many hours to type this thesis - an achievement for which I am indebted to her.

CONTENTS

LIST OF FIGURES

LIST OF TABLES

CHAPTER 1

INTRODUCTION

1.1 General comments

Many geophysical methods exist for studying the structure of the Earth on global, regional and local scales. All invoke measurement of one or more physical parameter(s), either time variant or invariant, and then attempt to invert the observed data to derive a model structure which is both unique and representative of the true Earth. Of those techniques which are applied for regional studies, geomagnetic induction methods offer the most powerful approach for deducing temperature profiles within the Earth. Of all lithological parameters that are temperature dependent, conductivity is the most sensitive to thermal variation. However, the primary aim of the majority of induction studies is to derive a (unique) conductivity model that satisfies the observed data. When this aim is achieved, inferences, and possibly deductions, about past and present crustal and mantle processes can be made.

Much interest is focussed at present on the theory of plate tectonics and its orogenic implications. In order to verify upper mantle convection theories that would lead to plate motion, it is necessary to know not only the present positions of plate boundaries but also the past ones. The locations of present spreading ridges, subduction zones, island arcs, etc. have largely been determined by seismic methods. However, to delineate past tectonic zones, it is necessary to recognise relic geological features which are clearly related to plate edge tectonic processes. This has been accomplished with some degree of success using geomagnetic induction methods by identifying various forms of geomagnetic variation anomalies (Law and Riddihough, 1971).

Geomagnetic induction studies utilise the natural magnetic field variations as the energy source. These variations diffuse into the Earth and induce electric currents by the elementary Faraday-Henry law. The induced electric currents will in turn induce secondary magnetic fields according to the Biot-Savart law. An observer on the surface of the Earth measures either (i) three components of the varying magnetic field (Geomagnetic Deep Sounding technique) or (ii) the variations of two horizontal components of both magnetic and electric fields (Magneto-Telluric technique). The Geomagnetic Deep Sounding (GDS) method is usually employed to delineate anomalous structures by mapping current concentrations. The conductance (conductance (s) = conductivity (σ) x thickness (d)) - or 'integrated conductivity - of the anomalous region can be estimated but the actual conductivity cannot unless the spatial gradients of the horizontal magnetic field components are also known (Kuckes, 1973a, b). For a one-dimensional Earth, the Magneto-Telluric (MT) method is more powerful in that direct estimates of the conductivity distribution with depth can be attained. In the proximity of two-dimensional conductivity structures, it is still possible to invert the MT data either by a quasi-one-dimensional (Wright, 1970) or a full two-dimensional (Wiedelt, 1975a) interpretation. However, three-dimensional structures pose problems which have yet to be solved. 'Parkinson vectors' (Parkinson, 1959, 1962, 1964) can locate such anomalies but quantitative interpretation is extremely difficult (Hewson-Browne and Kendall, 1976).

Penetration into the Earth by magnetic variations occurs naturally because of the skin-depth phenomenon of electro-magnetic fields. In this respect, induction methods are superior to galvanic resistivity techniques because highly resistive strata will be penetrated and currents will be induced in the underlying geological successions.

A further advantage of the MT technique when compared to galvanic methods is that estimate is made not only of apparent resistivity but also of the phase lead of the induced electric field to the inducing magnetic field. Accordingly, the model interpretation is constrained by two sets of approximately independent information (Parker, 1970; Summers, 1976). The extra set of constraints will lead to a more well-defined conductivity model.

1.2 Natural Source Field Characteristics

The natural variations of the geomagnetic field are utilised as the source for induction studies. They cannot be controlled and thus it is desirable that some knowledge is gained of the properties of the various magnetic disturbances prior to undertaking fieldwork. For example, if the recording equipment is not continuously monitored, a general sensitivity level will have to be chosen which will enable maximum possible recording of the desired variations. To choose such a level, probable amplitudes of the variations have to be ascertained.

A generalised geomagnetic spectrum in the interval 1 cycle per year to 1 cycle per second (Serson, 1973) is shown in figure 1.1. The telluric response that would be observed over a uniform earth of resistivity 20 Ωm is also illustrated in the figure. The geomagnetic spectrum has the form of a logarithmic increase in amplitude with decreasing frequency from 1 Hz to 3×10^{-3} Hz (a period of one hour), then a subsequent decrease in amplitude to a continuous level of about 3 nT for frequencies less than 10^{-4} Hz. Superimposed on this general shape are spectral lines, mainly due to various interactions between the Earth's magnetic field and plasma emitted by the Sun.

At frequencies greater than 1 Hz, the amplitude of the natural magnetic field again rises due to lightning discharges (sferics). At

Figure 1.1a Amplitudes of natural variations in the horizontal geomagnetic field useful in induction research

Figure 1.1b Corresponding amplitudes in the earth-electric field, computed for a model earth of uniform resistivity 20 ohm.m

reproduced from Serson (1973)

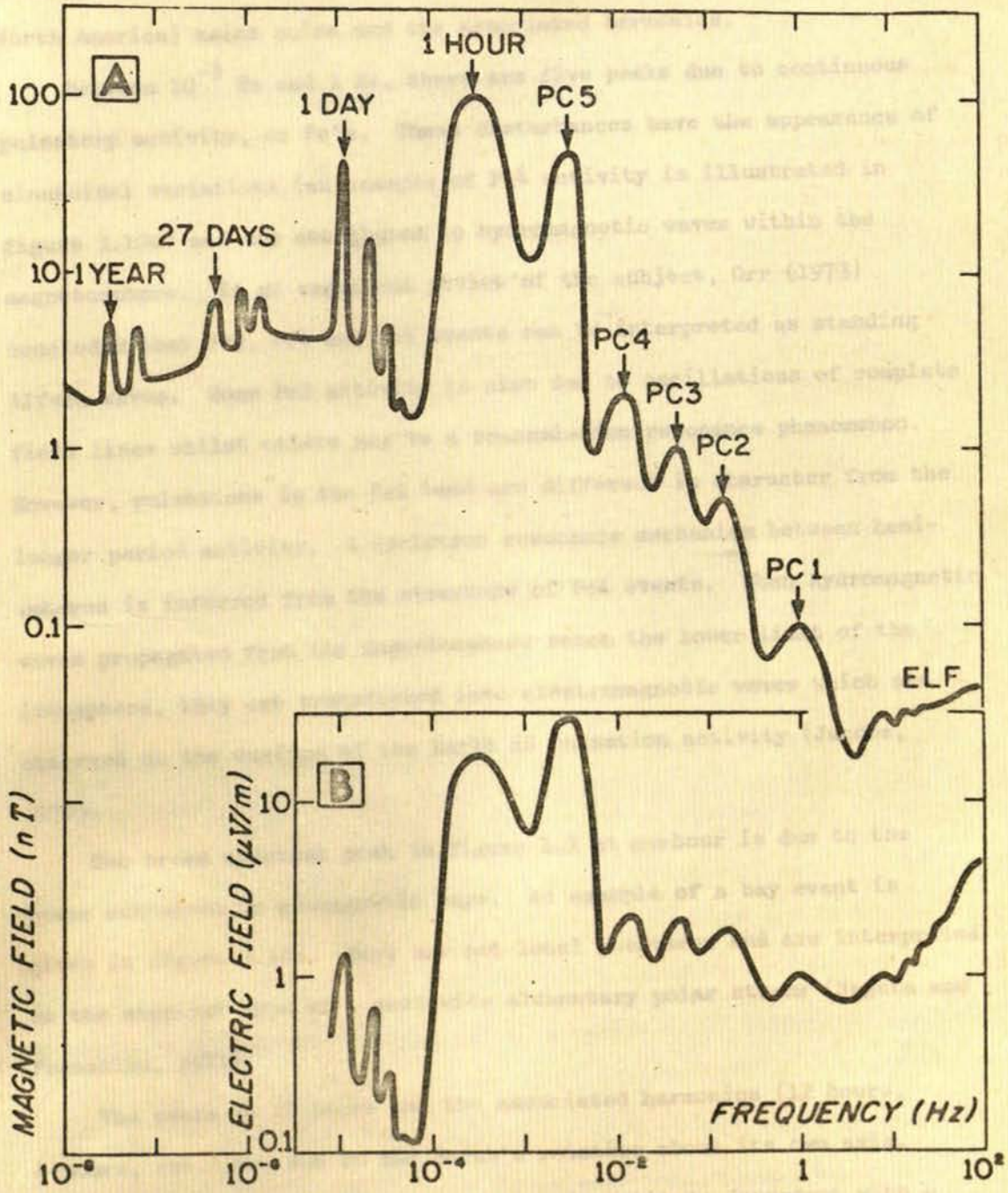
A
100
10
1
0.1
1 YEAR
27 DAYS
1 DAY
1 HOUR
PC 5
PC4
PC3
PC2
PC1
ELF
MAGNETIC FIELD (nT)
B
10
1
0.1
ELECTRIC FIELD (μV/m)
FREQUENCY (Hz)
10⁻⁶
10⁻⁶
10⁻⁴
10⁻²
1
10²

large distances from thunderstorms, sferics provide a nearly uniform source which is essential for applying the Cagniard MT relationship (Wait, 1954). Difficulties arise when undertaking Audio Magneto-Telluric (AMT, 1 Hz - 10 KHz) surveys in cultural areas due to 50 Hz (60 Hz in North America) mains noise and its associated harmonics.

Between 10^{-3} Hz and 1 Hz, there are five peaks due to continuous pulsatory activity, or Pc's. These disturbances have the appearance of sinusoidal variations (an example of Pc4 activity is illustrated in figure 3.10b) and are attributed to hydromagnetic waves within the magnetosphere. In an excellent review of the subject, Orr (1973) concluded that Pc3, Pc4 and Pc5 events can be interpreted as standing Alfvén waves. Some Pc2 activity is also due to oscillations of complete field lines whilst others may be a transmission resonance phenomenon. However, pulsations in the Pc1 band are different in character from the longer period activity. A cyclotron resonance mechanism between hemispheres is inferred from the structure of Pc1 events. When hydromagnetic waves propagated from the magnetosphere reach the lower limit of the ionosphere, they are transformed into electromagnetic waves which are observed on the surface of the Earth as pulsation activity (Jacobs, 1970).

The broad spectral peak in figure 1.1 at one hour is due to the power contained in geomagnetic bays. An example of a bay event is given in figure 3.10c. Bays are not local phenomena and are interpreted as the simplest type of worldwide elementary polar storms (Nagata and Fukushima, 1971).

The peaks at 24 hours and the associated harmonics (12 hours, 8 hours, etc.) are due to the Earth's rotation about its own axis. The amplitude of this diurnal variation is latitude dependent with a magnitude of the order of 10 nT in mid-latitudes (Matsushita, 1967).

Because this is so low, the daily variation is best observed during geomagnetically quiet periods. The generating current mechanism is thought to be predominantly an ionospheric dynamo action (Mishin et al., 1975).

The broad spectral peak at 27 days and those of the harmonics (13.5 days, 9 days, etc.) are associated with the sidereal solar rotation period. The main peak is not sharp because the outer surfaces of the Sun rotate with a latitudinal dependency. The rotation period of equatorial regions of the Sun is 26.4 days, whilst at 35° latitude it is 28.7 days (Chapman and Bartels, 1940). Regions of the Sun where there is a local low magnetic field will emit plasma at higher than normal levels. The plasma, on interacting with the Earth's magnetosphere, gives rise to 'geomagnetic storms' which last typically two or three days. Storms due to one region of the Sun will obviously recur at about 27 day intervals, and this has been observed (Chapman and Bartels, 1940).

The semi-annual peak is not the first harmonic of the annual line, as was first thought. Currie (1966) and Banks (1969) conclude that it is a ring current phenomenon, while the annual line is considered to be an ionospheric dynamo effect.

1.3 Regional Magneto-Telluric Studies

Although work for this project dealt with both GDS and MT techniques, the interpretations and model studies were based mainly on the MT results. Accordingly, it is more appropriate if a review of MT investigations is given rather than a general review of induction studies.

Figure 1.2 illustrates those regions of the world where reasonably thorough multi-station MT investigations have been, or are being, carried out. Some of the substantial papers published from these

TABLE 1.1

Location of multi-station MT investigations

- also GDS array investigations if undertaken in the same region

Code: 1 = MT only; 2 = GDS array only; 3 = MT and GDS

Location No.	Reference
1	Everett and Hyndman (1967 - 3).
2	Tammemagi and Lilley (1973 - 1), Gough et al. (1974 - 2), Lilley and Tammemagi (1972 - 3).
3	Febrer et al. (1976 - 1).
4	Rooney (1976 - 3), Banks and Ottey (1974 - 2).
5	Berktold et al. (1974 - 3), Haak (1976 - 1).
6	Winter (1976 - 1).
7	Swift (1967 - 1), Madden and Swift (1969 - 1), Schmucker 1970 - 2), Porath and Gough (1971 - 2).
8	Word et al. (1970 - 1), Mitchell and Landisman (1971 - 1), Vozoff (1973 - 1).
9	Caner et al. (1967 - 2), Morrison et al. (1968 - 1), Schmucker (1970 - 2).
10	Porath et al. (1970 - 2), Rankin and Reddy (1973 - 1), Learly and Phinney (1974 - 1), Alabi et al (1975 - 2).
11	Dowling (1970 - 1), Bentley (1974 - 1).
12	Kasameyer (1974 - 1), Edwards and Greenhouse (1975 - 2).
13	Caner et al. (1967 - 2), Caner et al. (1969 - 1), Cochrane and Hyndman (1970 - 2), Camfield et al. (1971 - 2), Nienaber et al. (1973 - 1), Dragert (1974 - 1).
14	Srivastava et al. (1963 - 1), Vozoff and Ellis (1966 - 1), Reddy and Rankin (1971, 1972 - 1), Porath et al. (1971 - 2), Peeples and Rankin (1973 - 1).

(Contd)

Figure 1.2 Locations of multi-station Magneto-Telluric investigations

-each number refers to a paper, or papers, indexed in table 1.1

If a GDS array study has also been undertaken in the same region as an M-T study, the published work(s) from the GDS investigation is also listed in table 1.1

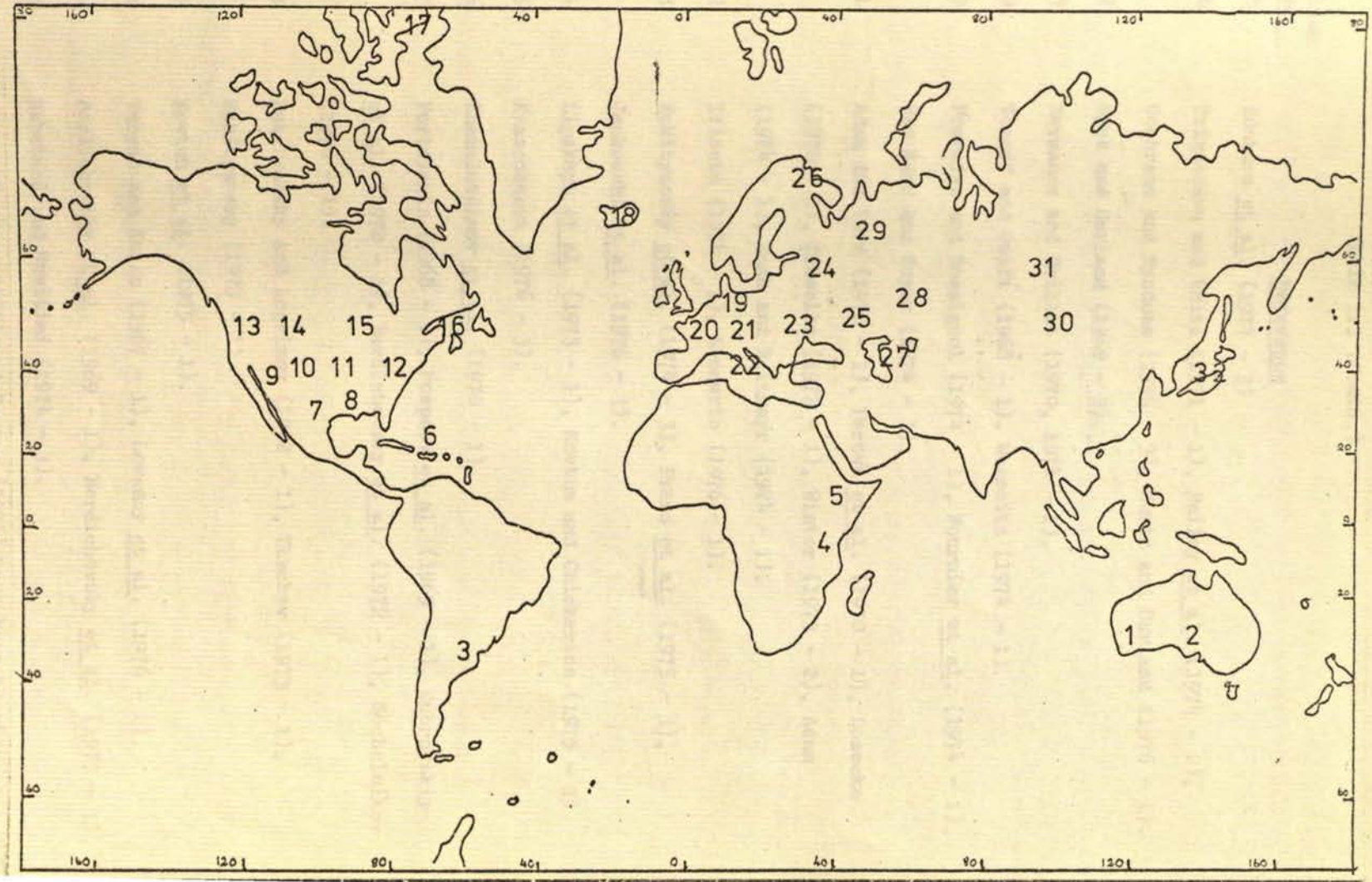
160
120
80
40
0
40
80
120
160
60
40
20
0
20
40
60
1
2
3
4
5
6
7
8
9
10
11
12
13
14
15
16
17
18
19
20
21
22
23
24
25
26
27
28
29
30
31

Table 1.1 (Contd.)

Location No.	Reference
15	Honkura et al. (1977 - 3)
16	Srivastava and White (1971 - 1), Bailey et al. (1974 - 2), Cochrane and Hyndman (1974 - 3), Kurtz and Garland (1976 - 1).
17	Dyck and Garland (1969 - 3).
18	Hermance and Grillot (1970, 1974 - 1).
19	Vozoff and Swift (1968 - 1), Wagenitz (1974 - 1).
20	Fournier and Rossignol (1974 - 1), Fournier et al. (1974 - 1), Van Ngoc and Boyer (1974 - 1).
21	Adam and Vero (1970 - 1), Pecova et al. (1970 - 1), Losecke (1970 - 1), Scheelke (1972 - 1), Winter (1973 - 2), Adam (1974 - 1), Haak and Reitmayr (1974 - 1).
22	Iliceta (1974 - 1), Kemmerle (1976 - 1).
23	Rukityansky et al. (1974 - 3), Praus et al. (1975 - 3), Jankowski et al. (1976 - 3).
24	Lipskaya et al. (1973 - 1), Kovtun and Chicherina (1975 - 1).
25	Krasnobaeva (1976 - 3).
26	Zhemaletdinov et al. (1970 - 1).
27	Portnyagin (1968 - 1), Pospeev et al. (1969 - 1), Dubrovskiy et al. (1970 - 1), Berdichevsky et al. (1972 - 1), Sochelnikov (1976 - 1).
28	Rokityansky and Logvinov (1972 - 1), Tkachev (1973 - 1), Rokityansky (1975 - 1).
29	Kovtun et al. (1975 - 1).
30	Vanyan and Karin (1967 - 1), Levadny et al. (1976 - 2).
31	Berdichevsky et al. (1969 - 1), Berdichevsky et al. (1975 - 1).
32	Nabetani and Noritimi (1974 - 3).

Note: The reviews of Hutton (1976) and Kovtun (1976) have been heavily relied on for information concerning studies undertaken in eastern Europe and Siberia.

studies are listed in table 1.1. Keller (1971) showed the location of earlier deep electrical (MT, galvanic resistivity and controlled-source electromagnetic) experiments and Lilley (1975) presented an equivalent map indicating regions studied by two-dimensional magnetometer arrays. To be added to Lilley's map are the following array studies; (i) Scandinavia (Küppers, 1976), (ii) north West Germany (Küppers, 1976), (iii) the central part of Russian platform (Rokityansky et al., 1976), (iv) the area north of Quebec City, Canada (Camfield, 1976), (v) the Baikal region of southern Siberia (Levadny et al., 1976), (vi) the Caucasian Mountains (Dadunashvily et al., 1976) and (vii) Argentina and Chile (Aldrich et al., 1973).

Global coverage by MT and GDS studies is obviously of severely limited extent. It is difficult to make gross generalisations about crustal and mantle conductivity structures until tectonically important areas such as South Asia, Antarctica, west Siberia, Alaska, northern South America and the Middle East have been studied. However, several points can be made about certain regions.

In a review on induction studies over stable shield and platform areas, Kowtun (1976) concluded that a 'normal' distribution of conductivity with depth under Precambrian shields has yet to be established. For these regions, a conducting zone at lower crustal/upper mantle depths, of conductance as high as 1000 S, is often reported. In the crust, this zone is considered to be due to either (i) sulphidisation and/or graphitisation of rocks (Gough, 1973), (ii) a hydrated zone (Hyndman and Hyndman, 1968) or (iii) a partial melt zone at low temperatures due to high water content (Berdichevsky et al., 1972). When the conducting layer appears to be in the upper mantle, it is usually interpreted as a partial melt zone, as in (iii) above (Chan et al., 1973; Berdichevsky et al., 1972).

Conducting zones either in the crust or upper mantle or both are almost always reported when induction studies have been carried out over rifts and other active regions (Hutton, 1976a). A partial melt zone is the most likely explanation due to the high heat flows usually observed in these areas.

Almost all published MT curves exhibit a decreasing asymptote for periods greater than about 10^4 s (Kovtun, 1976). This is due to a conductive layer of about 1 $S.m^{-1}$ at a depth of the order of 400-700 km (Banks, 1969; Parker, 1971). It is probable, but not certain, that the conductivity increase occurs at the same depth as the compressional and shear wave seismic velocities increase. This is considered to be at about 400 km and is concluded to be either (i) a phase transition of olivine to the more closely-packed beta or spinel structures (Ringwood and Major, 1970) or (ii) a phase transition with an associated increase in fayalite (Fe_2SiO_4) content (Kaila and Krishna, 1976). If the seismic boundary is due to a phase transformation alone, then the conductivity discontinuity should be at least as sharp as the corresponding seismic discontinuity (Tolland and Strens, 1972; Tolland, private communication). However, the interpreted complex structure transformations of olivine to beta at 400 km (Burdick and Anderson, 1975), beta to spinel at 500 km (Burdick and Anderson, 1975), followed by spinel to post-spinel (Anderson, 1967) over the range 590 to 710 km (Massé, 1974), perhaps with a chemical change occuring at the latter (Burdick and Anderson, 1975), could cause a gradual conductivity increase with depth. A gradual change was determined by the Cantwell-McDonald mantle conductivity model (McDonald, 1957; Cantwell, 1960) rather than a sharp transition as was suggested by uniform core (Chapman, 1919; Rikitake, 1966) or Lahiri-Price type (Lahiri and Price, 1939) models. A gradual transition in conductivity from 10 $S.m^{-1}$ at

250 km depth to 1 $S.m^{-1}$ at 800 km was suggested when Parker (1971) applied Backus-Gilbert inversion theory to data published by Banks (1969). An overall conductivity distribution presented by Rikitake (1973) - figure 1.3 - based mainly on a model presented by Banks (1972), which indicates a fairly steep conductivity increase, is concluded to be the most reliable throughout the Earth at present.

Although knowledge of the phase between the electric and magnetic fields constrains the number of acceptable models considerably, very few investigators attempt to extract such information. Even when estimated, it is rarely utilised. To determine phase accurately demands a high degree of relative time control between the magneto-telluric components. This does not present any problems when recording with coincident pen-position analogue recorders or multi-track tape recorders, but can cause difficulties when employing non-coincident pen-position analogue recorders (e.g. Watenabe) or sequential sampling cassette recorders. However, even if using either of the latter types of recording system, it is desirable to try to retain phase information. The importance of phase data for resolving surface structure was suggested by Parker (1971) and was shown by Summers (1976).

Of all the literature cited in table 1.1, only Everett and Hyndman (1967b), Swift (1967), Vozoff and Swift (1969), Mitchell and Landisman (1971), Kurtz and Garland (1976), Rooney (1976) and Beblo (1976) presented phase estimates. Everett and Hyndman employed their phase information in a qualitative sense only and Mitchell and Landisman utilised theirs to examine possible source effects. Only Rooney and Beblo constrained acceptable models by both their amplitude and phase estimates. More sophistication is required of both the instrumentation and the data analysis procedures to try to evaluate reliable phase information.

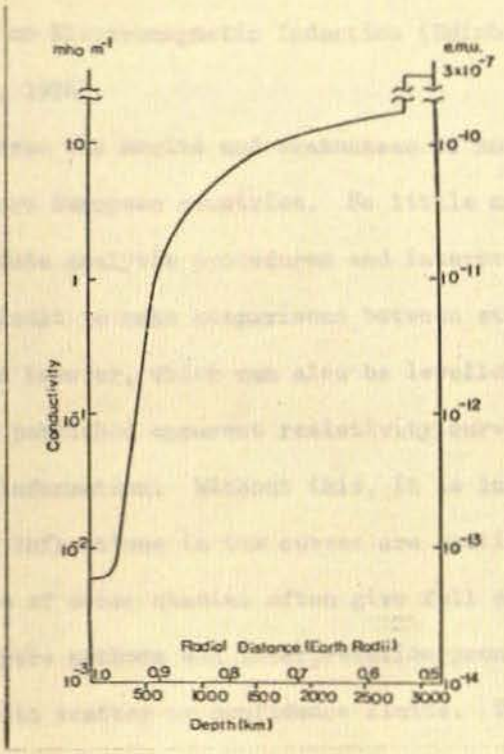

Figure 1.3 Global conductivity v. depth profile proposed by Rikitake (1973)

-reproduced from Rikitake (1973)

Excellent reviews and collations of the vast number of regional MT studies undertaken can be found in Fournier (1966), Barsczus (1970), Untiedt (1970), Fournier et al. (1971), Keller (1971), Porstendorfer (1975), Adam (1975), Hutton (1976b) and the various review papers presented at the Workshops on Electromagnetic Induction (Edinburgh, 1972; Ottawa, 1974; Sopron, 1976).

It is difficult to assess the merits and weaknesses of most MT studies undertaken in Eastern European countries. So little account is given of instrumentation, data analysis procedures and interpretative techniques that it is difficult to make comparisons between studies. One of the major criticisms however, which can also be levelled at some other workers, is that the published apparent resistivity curves often lack any scatter or error information. Without this, it is impossible to determine whether minor inflections in the curves are statistically meaningful or not. Reports of other studies often give full details of instrumentation, data analysis methods and interpretation procedures and also plot the curves with scatter or confidence limits. This practice should be standardised in some manner and adopted for the publication of all MT results.

With these points in mind, several MT studies have been selected for review on the merits of methods, site locations and ensuing interpretations.

The tectonic history of the Southern Uplands of Scotland is believed to be closely related to that of the Gulf of St. Lawrence area of Canada (Phillips et al., 1976). This relationship is discussed in greater detail in section 1.5. The region has been extensively studied by two independent groups, Cochrane and Hyndman at Nova Scotia and Garland and his colleagues at Toronto. Each group employed both MT and GDS methods. Figure 1.4 illustrates the region and the locations

of the observation sites of both groups. In an earlier investigation, Srivastava and White (1971) made MT measurements at three locations - Sable Island, Halifax and Fredericton - but did not present apparent resistivity results or interpretations. They did however state that there was a strong attenuation of the vertical magnetic field at Sable Island which was not in agreement with the usual ocean edge effect. To account for this, lateral conductivity variations beneath both the continent and ocean were postulated.

When analysing their GDS data, Hyndman and Cochrane (1971) also obtained small transfer function estimates for their Sable Island (SI) station. This feature and the frequency response observed at Dartmouth (DM) were the major constraints when two-dimensional modelling was attempted. A bounded high conductivity zone ($\sigma \sim 0.3$ S.m^{-1}) at lower crustal depths was necessary to account for the SI response. A second high conductivity zone ($\sigma \sim 1$ S.m^{-1}) at about 120 km, terminating under the western side of Nova Scotia, was required to explain the DM observations. They concluded that the shallow zone was hydrated lower crust (Hyndman and Hyndman, 1968) under Nova Scotia and as far east as Sable Island. In a later analysis, Cochrane and Hyndman (1974) incorporated data from 7 MT stations in Atlantic Canada, 13 additional magnetic stations in eastern North America and also some GDS data of Pitcher (1972). The model that best accounted for both these magnetic field observations and the prior ones differed only in minor detail from the one earlier proposed (Hyndman and Cochrane, 1971). A section across this optimum model along line AA' of figure 1.4 is illustrated in 1.5a. This Scotia Shelf conductive zone was concluded to be part of a larger region of high conductivity at lower crustal depths underlying much of the Appalacian system and the North American Atlantic Coastal Plain. This zone was considered best modelled in the lower crust rather than

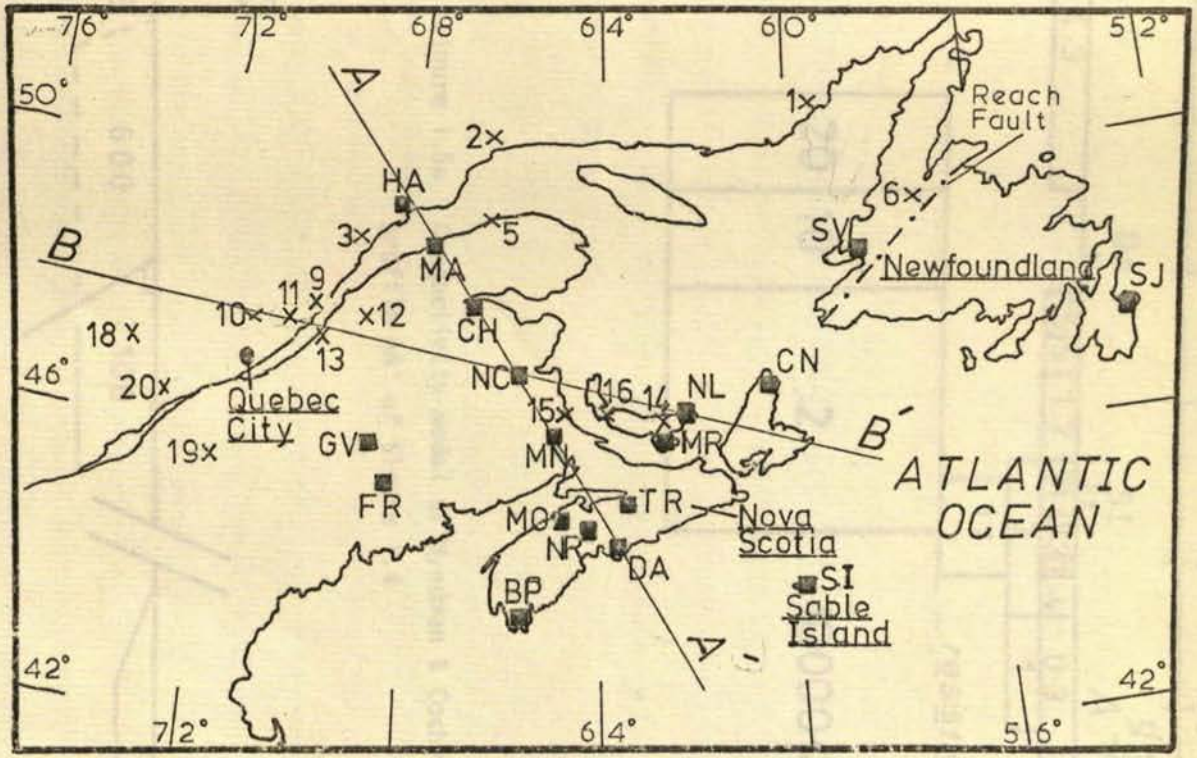

Figure 1.4 Map of Atlantic Canada showing the locations of GDS and MT observations

XY - Stations of Cochrane & Hyndman (1974), profile AA' illustrated in figure 1.5a

x12 - Stations of Kurtz & Garland (1976), profile BB' illustrated in figure 1.5b

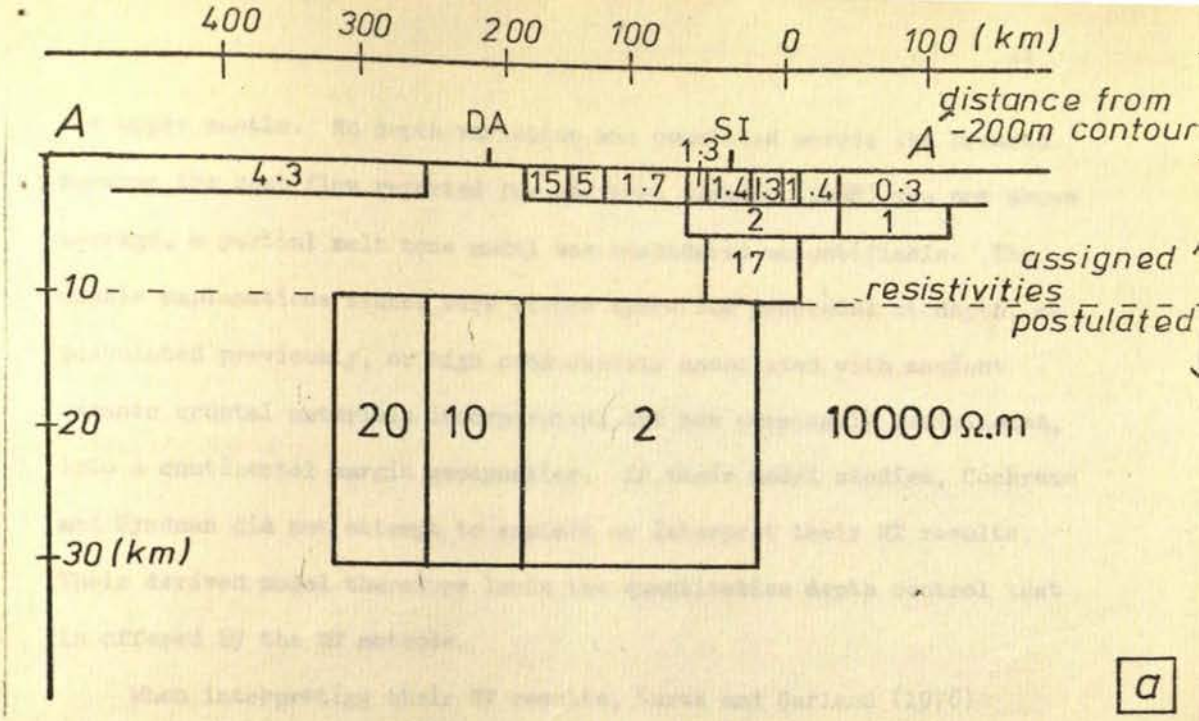

Figure 1.5a Conductivity model of Hyndman & Cochrane (1974) profile AA' of figure 1.4

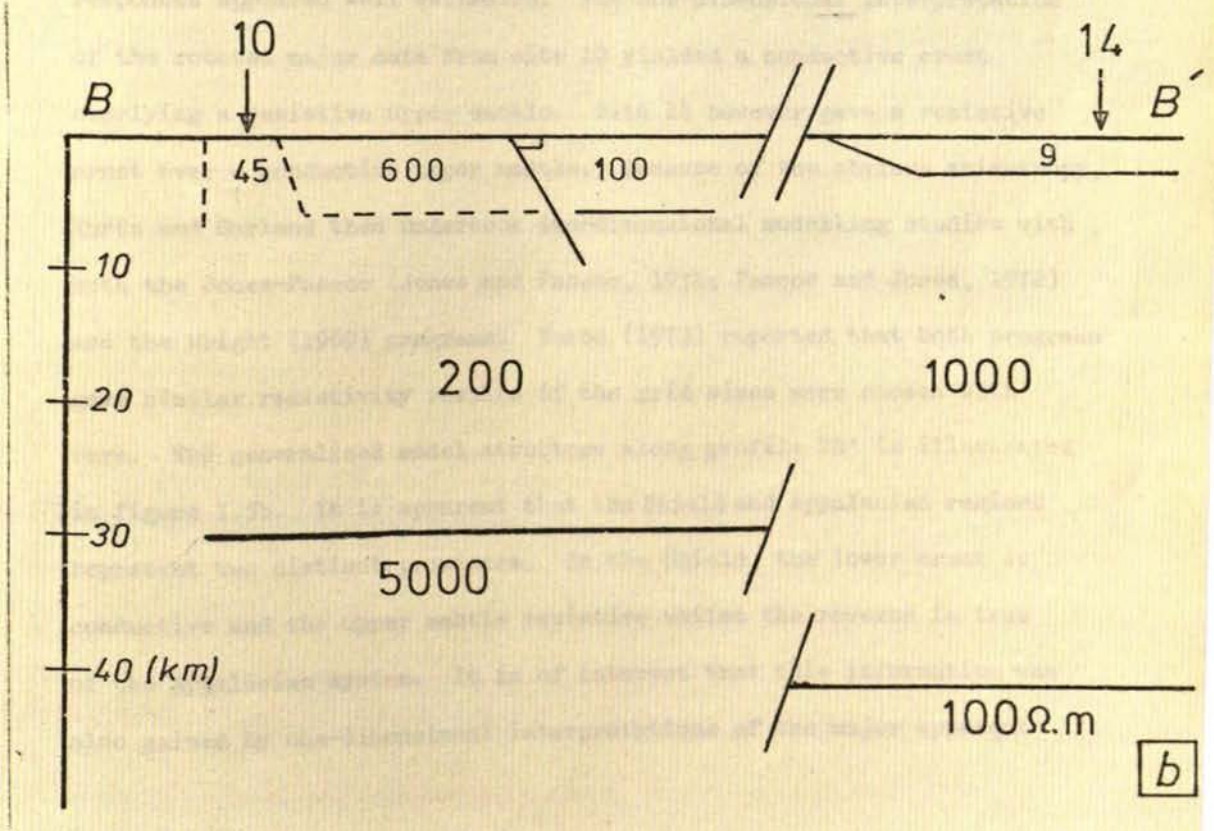

Figure 1.5b Conductivity model of Kurtz & Garland (1976) profile BB' of figure 1.4

the upper mantle. No depth variation was concluded across its breadth. Because the heat flow reported for the area (Jessop, 1968) was not above average, a partial melt zone model was considered unjustifiable. The viable explanations stated were either hydration processes at depth, as postulated previously, or high conductivity associated with ancient oceanic crustal materials incorporated, but not chemically assimilated, into a continental margin geosyncline. In their model studies, Cochrane and Hyndman did not attempt to explain or interpret their MT results. Their derived model therefore lacks the quantitative depth control that is offered by the MT methods.

When interpreting their MT results, Kurtz and Garland (1976) initially fitted one-dimensional models although all stations except those on Prince Edward Island exhibited strong anisotropy. These models were derived from the amplitude responses only even though the phase responses appeared well estimated. The one-dimensional interpretation of the rotated major data from site 10 yielded a conductive crust overlying a resistive upper mantle. Site 14 however gave a resistive crust over a conductive upper mantle. Because of the obvious anisotropy, Kurtz and Garland then undertook two-dimensional modelling studies with both the Jones-Pascoe (Jones and Pascoe, 1971; Pascoe and Jones, 1972) and the Wright (1969) programs. Kurtz (1973) reported that both programs gave similar resistivity results if the grid sizes were chosen with care. The generalised model structure along profile BB' is illustrated in figure 1.5b. It is apparent that the Shield and Appalacian regions represent two distinct provinces. In the Shield, the lower crust is conductive and the upper mantle resistive whilst the reverse is true of the Appalacian system. It is of interest that this information was also gained by one-dimensional interpretations of the major apparent

resistivity curves from sites 10 and 14. This will be discussed further in chapter 6.

When comparing the two models given in figure 1.5, it is obvious that both groups concur about the existence of a conductive zone under Nova Scotia. The disparity between the models is in the depth to this zone. Cochrane and Hyndman suggest 10 km, i.e. lower crustal conductor, whilst Kurtz and Garland believe it is about 40 km, i.e. upper mantle conductor. Under the Shield however, the models totally disagree. Cochrane and Hyndman postulate a normal Cantwell-McDonald conductivity distribution (Madden and Swift, 1969) but Kurtz and Garland propose a fairly conductive zone in the crust. These differences may be because of the higher frequency information obtained by Kurtz and Garland coupled with the quantitative depth control of the MT method.

A conductive zone at lower crustal depths under stable continental crust has been reported by Dowling (1970) who made wide-band (.05 s - 10^4 s) MT measurements at 16 locations in Wisconsin. Automatic one-dimensional inversion of both rotated major and rotated minor apparent resistivity curves by steepest-descent methods was undertaken. The data analysis procedures applied by Dowling are commendable - application of acceptance criteria and utilising a 'quality factor' as a weighting function - but certain points about the interpretations could be queried. As scatter or error bars were not given, it is impossible to assess the statistical meaning of the results or the interpretations. The two resistivity curves - major and minor - for any one of sites 1 - 4 appear identical in form to each other and each is separated from its counterpart by a nearly frequency independent factor of approximately x10. Accordingly, interpretation of either curve will yield interfaces at the same depths as the other but layer resistivities which are x10 different. However, that these 4 sites, separated from each other by

over 70 km, all display this effect is surprising. They would all need to be close to a graben-type lateral inhomogeneity (Wright, 1970) which was suggested by Porath (1971). Dowling selected the interpretation of either the major or the minor curve from each site as representative of the Earth's conductivity structure. The criterion for selection was that interpretation which maintained the structural congruity between adjacent sites. The dangers of interpreting the rotated minor curve in some situations have been stressed by Rankin (personal communication). The comparison between the 'preferred' models and the seismic sections of the area published by Steinhart and Meyer (1961) showed close agreement. No alternative models that also satisfy the data are given. However, although in the author's opinion some quantitative aspects of the interpretations can be doubted, the qualitative result that a conductive zone underlies a stable region at lower crustal/upper mantle depths cannot. This is in contrast to the remarks by Porath (1971) who considered the low resistivities in the period range 40 s - 100 s were due to lateral inhomogeneity effects.

Although MT variations have only been measured at a few locations in Iceland, the full consideration given by Hermance to many other geophysical parameters warrants a review of this investigation. In 1964, Garland and Ward (1965) operated three magnetic variometers on an EW traverse in the north-eastern part of Iceland. Subsequent analysis of the data led to the conclusion that there was a broad zone of enhanced conductivity at a depth of approximately 30 km. In 1967, Hermance and Garland (1968) followed this up by recording MT variations at 4 locations, also in the north-eastern region. Data were analysed using narrow band pass filters then computing time-dependent Cagniard resistivities by power ratio estimation. The results from three stations were presented and all exhibited high scatter even though only

visually correlatable signals were taken. Preliminary interpretations of the data from each site were in agreement about the existence of a conductive zone ($\sigma \sim 0.03$ S.m^{-1}) within 25 km of the surface. The apparent spatial extent of this zone led to the conclusion that it represented a manifestation of the regional state of the crust under Iceland and was not just due to volcanism. The spectral observation bandwidth was increased by improved instrumentation and MT variations in the period band 1 s - 10^4 s were recorded at 3 further locations during 1969 (Hermance and Grillot, 1970). The data from one location were analysed by power spectral methods and Cagniard resistivities estimated. These resistivities appeared isotropic, therefore relaxing the need to estimate tensor impedances. One-dimensional interpretation of the data necessitated a conductive zone of .05 S.m^{-1} and 20 km thick within 1.5 km of the surface. From laboratory studies of the variation of the conductivity of rocks with temperature, Hermance and Grillot (1970) considered that the base of the conductive zone must be at a temperature of 1100 - 1400 K. These conclusions support the suggestion of Heirtzler et al. (1966) that the Curie isotherm (770 K) upwarps along the Rekjanes spreading ridge. The base of the conductive zone also coincides with a P-wave seismic velocity increase from 6.6 km.s^{-1} to 7.5 km.s^{-1} at 15 - 20 km depth. That the conductive zone is within 1.5 km of the surface is presumed to be due to hot brackish water in the sedimentary layers. The depth of the transition from predominantly electrolytic conduction to predominantly solid conduction was estimated to be at about 3 km. This depth coincides with a seismic velocity interface between the 4 - 5 km.s^{-1} overburden and a 6.6 km.s^{-1} crustal layer. However, in a later analysis, Hermance (1973b) considered fully the possible conduction mechanisms which could give rise to the observed conductive zone and concluded that the transition occurred at a greater

depth than previously thought, about 8 - 10 km. The original data from Lake Thingvullavatn (THI) was reprocessed in terms of a full tensor impedance relationship and it was discovered, not surprisingly, that the diagonal elements (Z_{XX} and Z_{YY}) were small (Hermance and Grillot, 1974). Accordingly, it was assumed that the MT fields were insensitive to lateral inhomogeneity and that they described the vertical conductivity distribution. The apparent resistivity data were inverted by a Monte-Carlo technique (Greenfield and Turnbull, 1970) and a conductive layer of resistivity 1 - 33 Ωm, thickness 7 - 17 km, with its top interface at 3 km was well defined. When the inversion scheme was constrained so as to include an interface at 10 km depth, which coincided with the seismic crust-mantle boundary, the depth to the conductive zone was reduced to 2 km and its resistivity to 10 - 20 Ωm, becoming more conductive (1 - 15 Ωm) in the range 6 - 10 km. The temperature of the crust-mantle interface at 10 km depth appropriate for these conductivity values is of the order of 1300 K. This is consistent with the high thermal gradients (60 - 120 $K.km^{-1}$) observed in boreholes on Iceland. At 10 km depth however, there must be a sharp decrease in the thermal gradient to about 1 $K.km^{-1}$ to accommodate the MT results. Although local lateral inhomogeneities are obviously not present around THI, it would be interesting to know whether the data from Audkuluheidi (AUD) and Tungnaa (TUN), also recorded during 1969, are in agreement with those from THI. If they are not, do they exhibit effects due to regional variations of depths, thicknesses and resistivities of the layers?

The plains of Alberta have been extensively studied by both MT and GDS techniques for over a decade. Magneto-telluric investigations were undertaken during the early 1960's by various groups (Niblett and Sayn-Wittgenstein, 1960; Srivastava et al., 1963; Srivastava and Jacobs,

1964) and all proposed a zone of high conductivity around 80 km depth to explain their observed responses. Caner et al. (1969), from an analysis of both their own data and those of Vozoff and Ellis (1966), also concluded that a conductive zone underlies the Rockies and south-western Alberta at upper mantle depths. However, interpretations of MT observations made at over 20 locations in Alberta by Rankin and colleagues (Reddy and Rankin, 1971, 1972; Peeples and Rankin, 1973) led to the conclusion that there was no evidence in their data for a high conducting upper mantle zone. Their results were explainable solely by the Western Canadian Sedimentary Basin. The longest period at which tensor elements were estimated by Rankin et al. was 300 s. However, Caner et al.'s (1969) apparent resistivity data show clearly that the inflection in the curves, due to current penetrating the deep high conductivity zone, occurs at around 400 s. Thus, it is possible that two conductive zones exist, one at the surface due to the sedimentary basin and mapped by Rankin, the other in the upper mantle discovered by the longer period investigations. Phase information would clearly show a deep conductive zone even at periods as short as 100 s. A GDS study of the region (Camfield et al., 1971) shows a remarkable consistency in the magnetic fields over Alberta. The main feature of the variations was a westward decrease in normal Z, interpreted as due to the rise of a conducting zone in the lower crust or upper mantle to shallower depths to the west of the Rockies. This conclusion is in full agreement with that of Caner et al. (1969).

The conductivity distribution beneath the oceans is being investigated by both island-based and ocean-bottom MT observations. A rise in the conductive mantle off the Californian coast is strongly suggested from analysis of variations recorded by Cox et al. (1970). This feature is supported by Larsen (1976), who found that the upper 400 km

is generally less conducting at Tucson than at Bermuda and Hawaii, and by Winter (1976), who analysed data from the MODE (Mid-Oceanic Dynamic Experiment) project. Kharin et al. (1976) re-analysed the results of Cox et al. (1970) by contraining the amplitude data to be consistent with the observed phase response. The analytical method for undertaking such a procedure has been detailed by Weidelt (1972), who determined a 'reconstructed' phase response from the MT data published by Wiese (1963). Kharin et al. concluded that there is a conductive layer in the 70 - 150 km depth interval which was interpreted as the oceanic asthenosphere.

1.4 Geophysical significance of conductivity measurements

When deducing a temperature profile and/or bulk composition model within the Earth from an estimated conductivity distribution, it must always be borne in mind that little is known of the effects on conductivity, and other lithological parameters, of many fundamental variables. Inferences and deductions about the Earth's structure from any surface observations must be approached with caution. This has been stressed by many workers and perhaps in its strongest form by Professor F. Birch (1952) who states:

"Unwary readers should take warning that ordinary language undergoes modification to a high-pressure form when applied to the interior of the Earth: a few examples of equivalents follow:

High Pressure form	Ordinary meaning
certain	dubious
undoubtedly	perhaps
positive proof	vague suggestion
unanswerable argument	trivial objection
pure iron	uncertain mixture of all the elements."

The questionable exercise of inferring conditions prevailing within the Earth from high pressure, high temperature conductivity experiments in the laboratory on rocks with low pressure, low temperature histories has been queried by experimentalists, notably Schlossen (1976) and Duba (1976). Schlossen considers that the major differences between true conditions in the Earth and those attainable in the laboratory are, (i) that either powder or polycrystal samples are used and (ii) that different ambient atmospheres are present. Duba is of the opinion that the time factor is of paramount importance and it cannot be reconstructed in the laboratory.

Some of those parameters known to affect conductivity are: composition, pressure, temperature, oxygen fugacity, phase, transition-metal ion content, orientation, twinning, order-disorder, water content, partial-melt and porosity (Keller and Frischneckt, 1966; Keller, 1966; Green, 1973; Shankland, 1975; Duba, 1976). It is obvious that nothing is known of those parameters that do affect conductivity but which are not known to do so. The relative importance of each of the parameters cited above is depth dependent. For example, water content is of major importance for upper crustal layers whilst temperature is for mantle depths. At the depths of interest for this study, i.e. lower crust and upper mantle, the variables of main importance in the interpretation of laboratory conductivity measurements are: water content, temperature, oxygen fugacity, percentage of partial melt and mineral content. Pressure is not significant (Duba et al., 1974) except when it produces crack closure in near surface rocks (Brace et al., 1975) and at depths where phase transitions may be involved (Duba, 1976).

A full review of the probable chemical composition of the crust is given by Ronov and Yaroshevsky (1969), who conclude that the most widespread minerals in the crust are: feldspars (over 50%), quartz (10 -

20%), pyroxenes and amphiboles (10 - 20%) and micas (3 - 5%). However, for saturated rocks, electrolytic conduction by the interstitial fluids will dominate other conduction mechanisms. The bulk rock conductivity will be given by Archies law (1942) which states:

$$\sigma_r = \sigma_f \eta^m \qquad (1.1)$$

where σ_r - rock conductivity

σ_f - pore fluid conductivity

η - porosity

and m - exponent, commonly $1 \rightarrow 2$ (Keller, 1966).

The effects of decreasing porosity have been investigated by resistor array modelling studies (Greenberg and Brace, 1969; Shankland and Waff, 1974). These experiments indicate $m = 2$ for pressures greater than 3-4 kbar, i.e. after crack closure.

As was discussed in the previous section, there is a depth at which electrolytic conduction becomes less dominant than semi-conduction with ions, ion vacancies, electrons and electron vacancies as the charge carriers. For most regions of the Earth, this transition from one dominant mechanism to another can be considered to occur in the upper mantle. It was originally believed to take place at the Mohorovicic discontinuity which divides the crust from the mantle. This discontinuity is not always located however, especially in regions of tectonic instability. It was first discovered in 1910 by Mohorovicic from observations of compressional wave travel times from earthquakes but, although much effort has been expended, there is still disagreement about its nature. Two explanations have been suggested, a compositional change from basic gabbro to ultrabasic peridotite or a phase boundary between either gabbro and eclogite or serpentine and peridotite

(McKenzie, 1970). The transition zone between the crust and upper mantle is considered to be of the order of 0.5 km wide (Nakamura and Howell, 1964) which is too small for a gabbro-eclogite phase change (Ringwood and Green, 1970). A full discussion of the other two possibilities was given by McKenzie (1970) who concludes that either is tenable. Both, however, give a peridotitic composition for the upper mantle whose properties can be investigated by approximating it to an olivine layer (Birch, 1970) of composition $Mg_{1.8}Fe_{0.2}SiO_4$ (Fujisawa, 1968).

Virtually all minerals display an increase in conductivity with increasing temperature, governed by terms of the form

$$\sigma_i = \sigma_{oi}\, e^{-E_i/kT} \qquad (1.2)$$

(Kittel, 1953) where E_i is the activation energy

σ_i is the conductivity of the i'th mechanism at temperature T

σ_{oi} is the conductivity of the i'th mechanism at temperature 0 K

and k is Boltzmann's constant.

The exponential temperature dependence ensures a single conduction mechanism dominates in a given temperature range (Shankland, 1975). However, no one single conduction mechanism has been defined for silicate materials likely to exist in the mantle.

Early laboratory experiments by various workers on olivine, of a composition near 10 mole % fayalite (Fe_2SiO_4), showed very poor agreement between them (Duba and Lilley, 1972). The values ranged over three orders of magnitude at most temperatures. This gave rise to widely varying geothermal profiles when conductivity-depth distributions were inverted. Duba and Nicholls (1973) showed the significant effect oxygen fugacity has on the conductivity of olivine. Because of this,

the majority of experiments are now carried out with controlled oxygen pressure. The present state of the art has been reviewed by Duba (1976). He derived an olivine electrogeotherm by combining (i) the temperature dependence of olivine, estimated from a Red Sea sample (Duba et al., 1974) and an Arizonan sample (Duba and Nicholls, 1973), and (ii) mantle conductivity distributions given in the literature. The electrogeotherm is consistent with estimated temperatures below 150 km but at shallower depths, the temperatures are considerably higher than can be explained by semi-conduction in olivine. This result is taken by Duba to suggest that the conductivity in the outer 150 km of the Earth is controlled either by more conducting phases, perhaps interstitial water, partial melting or grain boundary impurities, or by some other mineral species. Figure 1.6 illustrates the temperature-depth profile for olivine calculated by Duba, together with pyroxene geotherms (MacGregor and Basu, 1974; Mercier and Carter, 1975) and postulated continental and oceanic geotherms of Ringwood (1966).

It is apparent that a strict discontinuity between predominantly electrolytic conduction and predominantly semi-conduction does not occur. Until more is known of the possible conduction mechanisms that will dominate in the upper mantle, petrological and geophysical interpretations of the derived conductivity in the upper 100 km of the mantle are not possible. Many effects can be postulated, notably partial-melting and hydration processes, but none can be assumed exclusively.

1.5 Geology and Geophysics of the Southern Uplands Region

1.5.1 Geology

A simplified geological map of the survey area is illustrated in figure 1.7. The main feature is the Southern Uplands fault, which divides the Southern Uplands from the Midland Valley. Little is known

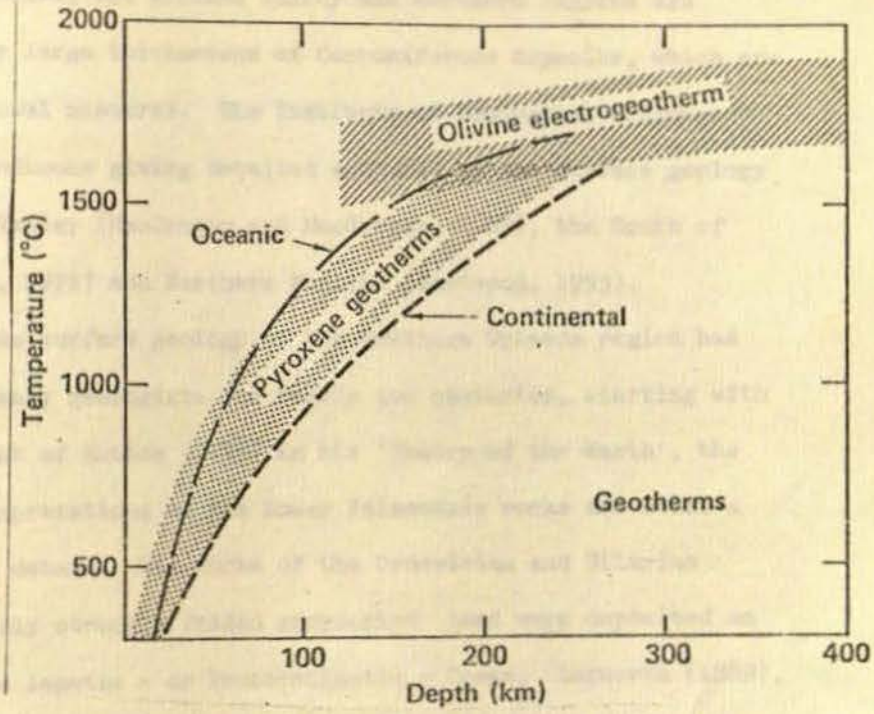

Figure 1.6 Temperature v. depth profile calculated by Duba (1976) -'olivine geotherm'

reproduced from Duba (1976)

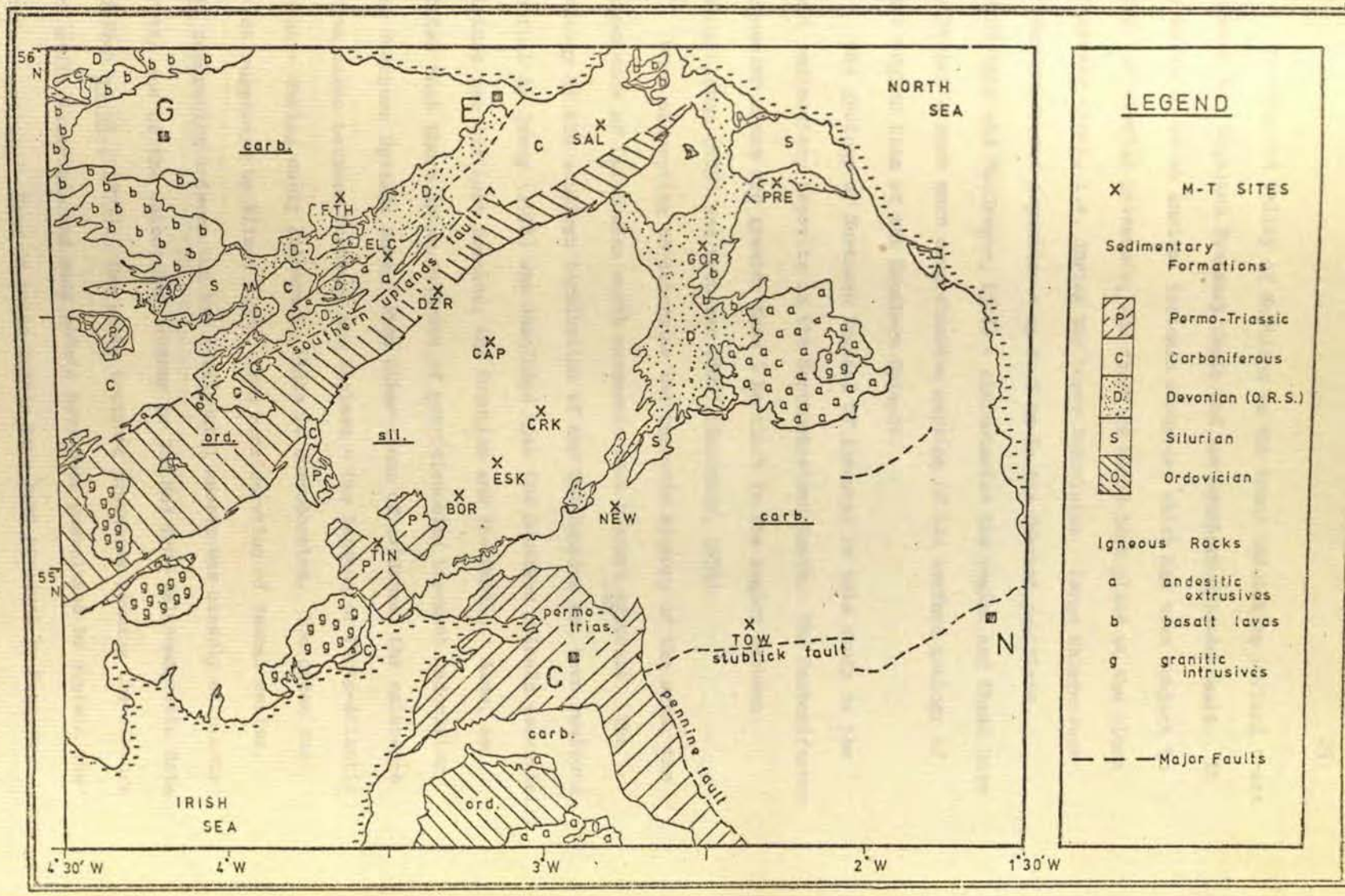

Figure 1.7 Sketch map of the geology of the investigation region

Note: M-T sites indicated by crosses

The Midland Valley of Scotland is the broad undulating lowland tract between the Highland Boundary fault and the Southern Uplands fault. It is known to be an ancient tectonic structure which has been subject to powerful crustal movements, the first of which took place at the close of Arenig times, i.e. during the Lower Ordovician. Large thicknesses of Carboniferous deposits - up to 2 km in the Central coalfield (MacGregor and MacGregor, 1948) - characterise the region and these have motivated a much more comprehensive mapping of the surface geology of this region than of the Southern Uplands.

The geology of Northern England of interest in this study is the vast sedimentary deposits in the Northumberland basin. The Carboniferous sequences alone are greater than 3 km thick in the region between Newcastleton (NEW) and Towhouse (TOW) (Eastwood, 1953).

When attempting to determine the tectonic history of the area, the importance of Caledonian earth movements soon becomes apparent. The geology of the southern termination of the Caledonides has been reviewed in full by Dewey (1974) who concluded that the Southern Uplands essentially divides two distinct domains, the Grampian and the Celtic. Also, he states that there is no evidence of pre-Caledonian basement underlying the Southern Uplands zone. From other lines of evidence, the existence of an ocean between Scotland and England - the Iapetus or Proto-Atlantic Ocean - during early Palaeozoic times is corroborated. The ocean was first suggested by Wilson (1966) from consideration of faunal realms. The separation between the two continental masses was clearly eliminated by the end of the Caledonian orogeny (c.360 Ma) from palaeomagnetic data (Briden et al., 1973). The plate tectonic processes causing the closure are still uncertain and many models have been postulated to explain the surface geology. Some of these models have been reviewed by Moseley (1975). Models that accepted Powell's (1971) hypothesis of continental

crust under the Southern Uplands and interpreted the Midland Valley as the oceanic remnant (Gunn, 1973; Jeans, 1973) were quickly rejected on palaeontological grounds (Williams, 1972). Closure by two subduction zones, one Benioff zone in the north-west along the Southern Uplands fault (approximately) and the other in the Solway-Northumberland basin, was first postulated by Dewey (1969) and has received support from Church and Gayer (1973), Williams (1972) and Phillips et al. (1976). Other authors concur on the existence during the Ordovician of a northward dipping Benioff zone between the Midland Valley and the Southern Uplands (Garson and Plant, 1973). Some of them suggest that obduction occurred at this boundary (Church and Gayer, 1973; Mitchell and McKerrow, 1975; Floyd, 1976). Fitton and Hughes (1970) suggest the closure of the Iapetus was by the southward dipping Benioff zone. The most recent and comprehensive work on the subject (Phillips et al., 1976) proposed that the Iapetus ocean was a minimum of 600 - 800 km wide during Arenig (c.500 Ma). This is comparable with the width of 1000 $\pm$ 800 km estimated by Briden et al. (1973). Phillips et al. also propounded that the two Benioff zones were not parallel but at an angle of 14° - 18° to each other. This caused the collision point of the two zones to migrate from NE to SW at a rate of about 17 $mm.yr^{-1}$, a value deduced from volcanism ending at progressively later dates towards the south-west. A post-collisional dextral slip of 980 km along this Iapetus suture was suggested. This was postulated to explain the convincing evidence of Mitchell and McKerrow (1975) that north-westerly subduction continued until lower Old Red Sandstone times (c.415 Ma) whilst volcanism in the Lake District ceased in the lower Caradoc (c.473 Ma). The Iapetus suture in Britain was concluded to be along the Northumberland trough-Solway Firth line due to the existence of an elongated basin in the region during the lower Carboniferous (Leeder, 1974). The model of

Phillips et al. for the suture zone during Llandeilo (c.480 Ma) is illustrated in figure 1.8.

Due to the parallel tectonic history of eastern Canada (Phillips et al., 1976) it is appropriate to note here that from faunal evidence, the Iapetus suture has recently been located in Newfoundland as the Reach fault and its southern continuation, the Cape Ray fault (McKerrow and Cocks, 1977). This gives a strong basis for assuming that the Gibbs Fracture Zone (Grant, 1972) represents the manifestation of the Iapetus suture on the Newfoundland and Irish continental margins (Scrutton, 1974).

1.5.2 Geophysics

When comparing the British Isles with some other high technology countries, e.g. North America, Germany or Russia, it becomes apparent that little geophysical exploration of the mainland has been accomplished. This is possibly due to the complete and comprehensive geological mapping of Britain which, in part, circumvents the need for exploration of economic regions by applied geophysical techniques.

Considering the South of Scotland in particular, a complete Bouguer anomaly gravity map has yet to be published. An aeromagnetic map of Great Britain has been published by the Institute of Geological Sciences and the region of interest for this work is shown on sheet 1 (1972). Certain areas in southern Scotland and northern England have been surveyed in detail by either gravity or ground based magnetics or both. These areas include the Ballantrae complex (gravity and magnetics - Powell, 1977a), the Fleet granites (gravity - Parslow, 1968; gravity and magnetics - Powell, 1977b), the western Midland Valley (gravity - McLean and Qureshi, 1966) and the north eastern Southern Uplands (gravity - Hipkin and Lagios, personal communication). A Bouguer

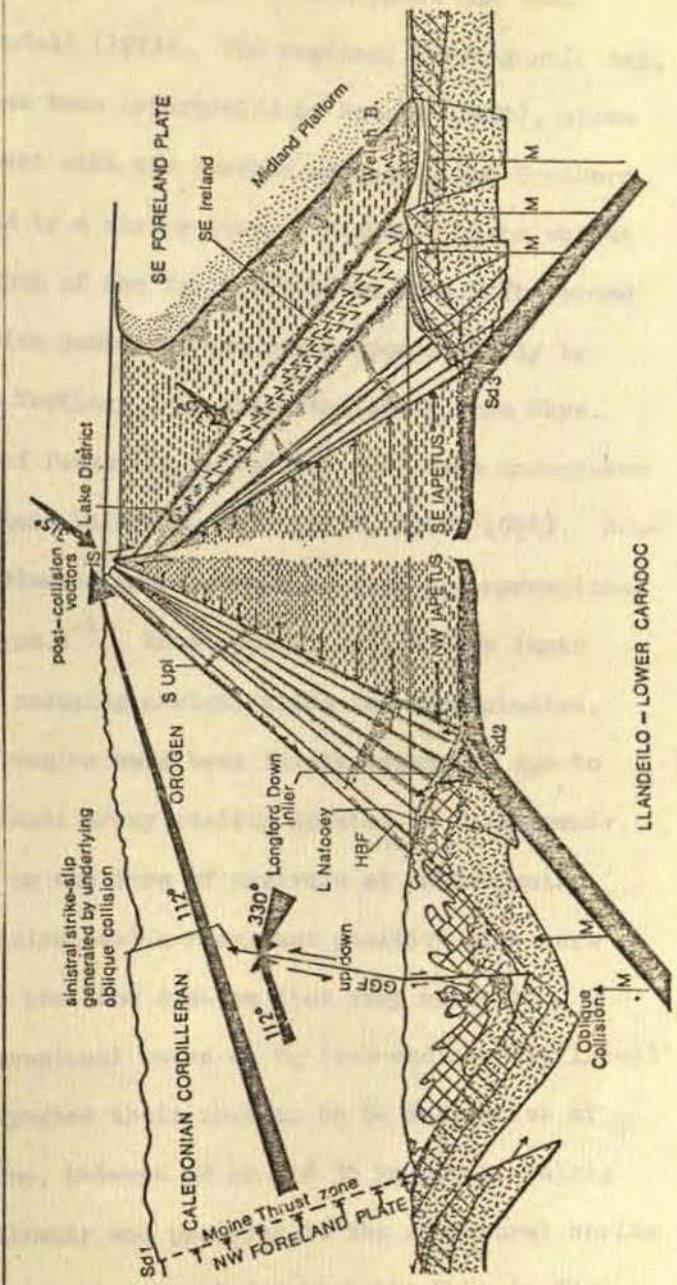

Figure 1.8 Palaeographical and structural reconstruction of the Iapetus suture zone during the Llandeilo-lower Caradoc

-reproduced from Phillips et al (1976)

anomaly map of the coastal and inland region around Fleet has been presented by Parslow and Randall (1973). The regional aeromagnetic map, the western part of which has been interpreted by Powell (1970), shows features reasonably consistent with the surface geology. The Southern Uplands fault is represented by a narrow line of magnetic highs whilst the Ordovician sediments south of the fault are broad lows. The broad line of highs for the Silurian sediments are cut perpendicularly by magnetic lows caused by the Tertiary dyke swarm radiating from Skye.

Local seismic studies of formation velocities have been undertaken at various sites in the Midland Valley by Hall (1970, 1971, 1974). Near surface Lower Palaeozoic sediments are reported to have a compressional wave velocity of 3.65 - 4.3 km.s^{-1}. Knowledge of sedimentary layer velocities is important for reducing arrival times for deep studies. Deep seismic studies of the region have been fairly extensive due to the U.K.A.E.A. permanent seismic array station located at Eskdalemuir. In one of the first reports on the form of arrivals at Eskdalemuir, Agger and Carpenter (1964) calculated a resultant positive time term for the array. This implies that the station lies very close to materials transmitting compressional waves at Pg (sub-sedimentary layer) velocities. They also interpreted their results to be indicative of lateral variations in the Moho, between 22 km and 35 km depth. Along a line passing through Eskdalemuir and parallel to the structural strike of the Southern Uplands geology, they concluded that the Moho is flat at a depth of 28 km. In a later investigation, Collette et al. (1970) concluded that this depth is underestimated and state a Moho depth of 33 - 35 km. They concur with an interpretation by Jacob (1969), who analysed crustal phase velocities recorded by the array, of a velocity increase at 10 - 12 km from approximately 6.0 km.s^{-1} to 6.5 km.s^{-1}. However, to ensure their model was consistent with their data, Collette

et al. had to propose a layer of velocity about 7.0 km.s^{-1} at the base of the crust.

A major seismic study has recently been carried out by a joint Anglo-German group. This Lithospheric Seismic Profile in Britain (LISPB) was operated as four reversed lines and the preliminary results were reported by Bamford et al. (1976). The initial $T^2 - X^2$ fits to P_MP arrivals infer a clear Moho discontinuity at 32 - 36 km beneath the Southern Uplands. A more detailed analysis however (Bamford, 1977; Nunn et al., 1977) revealed that the Moho discontinuity changes in nature from a sharp transition under the northern part of the Midland Valley to a gradational change (over 5 km) under the Southern Uplands. Also, there is a possible horizontal discontinuity in the pre-Caledonian basement between the Southern Uplands fault and the Stublick fault and a lower crustal layer appears to shallow beneath the Southern Uplands. The interpreted seismic section is illustrated in figure 1.9.

Various electromagnetic studies have been operated in the Southern Uplands prior to this work. Their locations are illustrated in figure 1.10. The first reported was an MT investigation at Eskdalemuir and the Irish Sea by Jain (1964) and Jain and Wilson (1967). The time-varying fields were recorded in the period band 8 - 6000 s. The Irish Sea telluric observations were by telephone cables connecting various points. They had previously been employed by Bowden and Hughes (1961) for estimating the rate of flow of water in the Sea. The magnetic observations were of the horizontal field variations perpendicular to the cables and were made at the end of each cable. At Eskdalemuir, both components (NS and EW) of both fields were measured. Because of the single component resistivity measurement for the Irish Sea observations, meaningful interpretations are valid only if the sub-surface is exactly one-dimensional. Any departure from this ideal

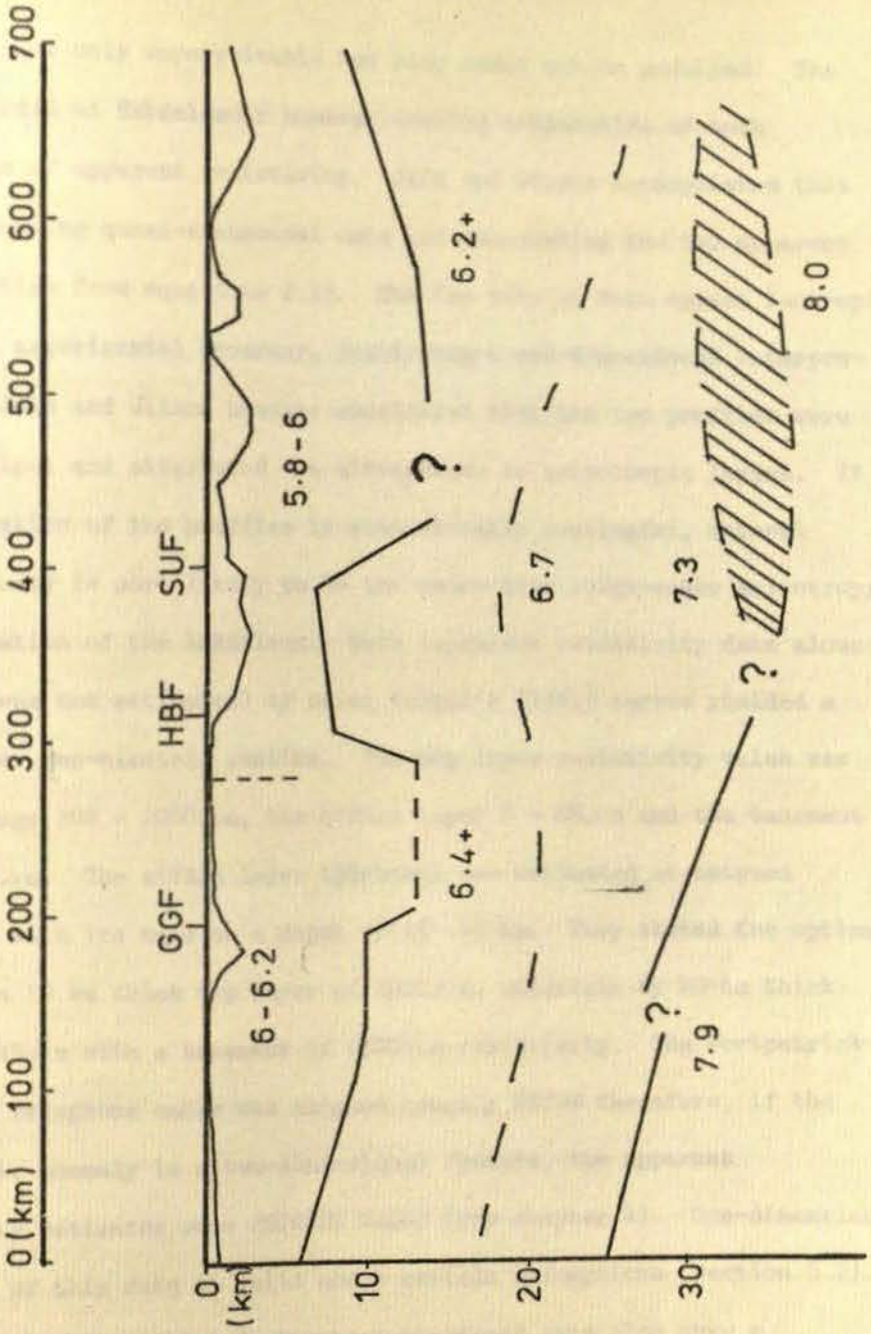

Figure 1.9 Seismic cross-section through Scotland and Northern England

-reproduced from Bamford & Prodehl (1977)

state was not only unperceivable but also could not be modelled. The data recorded at Eskdalemuir however enabled computation of both components of apparent resistivity. Jain and Wilson accomplished this by hand-scaling quasi-sinusoidal data and calculating the two apparent resistivities from equations 2.13. The two sets of data appear isotropic to within experimental accuracy, justifying a one-dimensional interpretation. Jain and Wilson however considered that the two profiles were not identical and attributed the differences to anisotropic layers. If the separation of the profiles is statistically meaningful, lateral inhomogeneity is more likely to be the cause than large-scale anisotropy. Interpretation of the Eskdalemuir data (apparent resistivity data alone as phase was not estimated) by using Yungul's (1961) curves yielded a three layer geo-electric section. The top layer resistivity value was in the range 300 - 2000Ωm, the middle layer 8 - 88Ωm and the basement over 1000Ωm. The middle layer thickness was estimated at between 3 - 40 km with its base at a depth of 18 - 44 km. They stated the optimum model as a 10 km thick top layer of 3000Ωm, underlain by 20 km thick layer of 45Ωm with a basement of 2500Ωm resistivity. The Portpatrick-Stranraer telephone cable was aligned roughly NE/SW therefore, if the Eskdalemuir anomaly is a two-dimensional feature, the apparent resistivity estimates were ROTATED MAJOR (see chapter 4). One-dimensional inversion of this data is valid under certain assumptions (section 6.2). The interpretation of the Portpatrick-Stranraer data also gave a conductive zone of 40Ωm between 18 - 38 km depth.

Osemeikhian and Everett (1968) operated 3 three-component proton magnetometers at 10 locations in Northern Ireland and Southern Scotland. The field components were sampled at minute intervals and, after band averaging, 12 minutes was the shortest period at which estimates were made. They noted high frequency attentuation at Eskdalemuir (ESK) and

Glenlee (GL) - see figure 1.10 - but not at the other stations. This was interpreted as due to a lens of high conductivity materials, within the top 100 km, restricted to the south-western Southern Uplands of Scotland. That the Z attentuation was not apparent at Aldergrove (AL) in Northern Ireland is surprising due to the tectonic position of the station. The anomalous zone was not considered to continue to the north-eastern Southern Uplands from seismic evidence alone, as magnetic variations were not recorded in the area.

Edwards et al. (1971) undertook a large scale geomagnetic study of the British Isles and Eire with 5 to 8 instruments operated. They recorded geomagnetic variations at 49 locations. Those stations in the Southern Uplands region are illustrated in figure 1.10. The data were averaged into 14 period bands, with centre period from 12 mins to 480 mins. Plots of power levels, relative phase and induction vectors all reveal an anomalous region in the Southern Uplands which was interpreted as a lower crustal or upper mantle conductor. The in-phase induction vectors also identified the Atlantic Ocean and the shallow seas as conductors. Edwards et al. proposed that current in the North Sea 'leaked' to the Irish Sea through the anomalous Southern Uplands conductor. There was no indication that it extended as far as the Isle of Man or into Northern Ireland. Three possible explanations were suggested to account for the 'Eskdalemuir anomaly'. They were (i) an compositional change at an unknown depth causing an increased fayalite content in the olivine, (ii) high water content of deformed marine sediments, or (iii) graphitic schists existing at depth. In a revised interpretation utilising the 'Hypothetical Event Technique' (Bailey et al., 1974), Bailey and Edwards (1976) showed that the Eskdalemuir anomaly could be an expression of Caledonian orogeny. The NS polarised hypothetical event showed a NE-SW lineation in the quadrature vertical component.

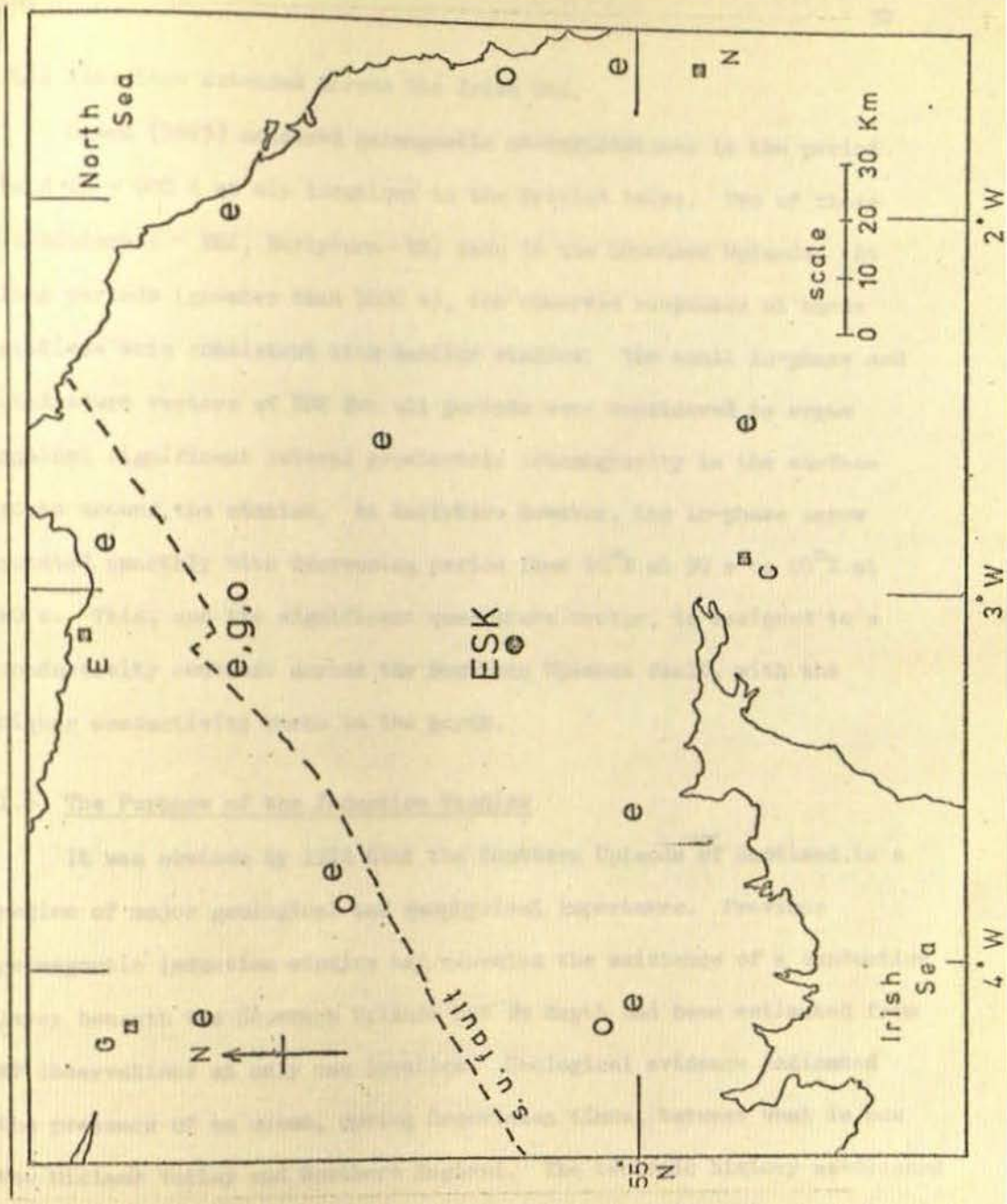

Figure 1.10 Locations of previous geomagnetic studies in the Southern Uplands

e Edwards et al (1971) - GDS
g Green (1973) - GDS
o Osemeikhan & Everett (1968) - GDS

At Eskdalemuir observatory (ESK) , e,g,o, & M-T by Jain and Wilson (1967)

This lineation extended across the Irish Sea.

Green (1975) measured geomagnetic micropulsations in the period band 10 - 600 s at six locations in the British Isles. Two of these (Eskdalemuir - ESK, Earlyburn - EB) were in the Southern Uplands. At long periods (greater than 1000 s), the observed responses at these stations were consistent with earlier studies. The small in-phase and quadrature vectors at ESK for all periods were considered to argue against significant lateral geoelectric inhomogeneity in the surface rocks around the station. At Earlyburn however, the in-phase arrow rotated smoothly with decreasing period from 90°E at 90 s to 20°E at 20 s. This, and the significant quadrature vector, is assigned to a conductivity contrast across the Southern Uplands fault, with the higher conductivity rocks to the north.

1.6 The Purpose of the Induction Studies

It was obvious by 1972 that the Southern Uplands of Scotland is a region of major geological and geophysical importance. Previous geomagnetic induction studies had revealed the existence of a conductive layer beneath the Southern Uplands but its depth had been estimated from MT observations at only one location. Geological evidence indicated the presence of an ocean, during Ordovician times, between what is now the Midland Valley and Northern England. The tectonic history associated with the closing of this ocean was, and still is, subject to ver ification.

The GDS studies were long period (greater than 700 s) geomagnetic investigations. Such observations could not give information about crustal conductivity distributions due to the large skin depth at such periods. The generalised skin depth (equation 2.27) at 700 s for the optimum model of Jain and Wilson (1967) is over 170 km. Thus, higher frequency information was required. Synoptic array studies at long

periods are known to indicate crustal conductivity structure because the derivable real-time phase estimates are sensitive to crustal layers.

In order to investigate the anomaly further, it was decided to operate a twenty station synoptic array study with Gough-Reitzel magnetometers - kindly lent by Dr. I. Gough - then make single station wide band MT observations at desirable locations.

CHAPTER 2

THEORY

This chapter will begin with a brief history of research into geomagnetic induction phenomena, concentrating mainly on the development of the magneto-telluric technique. Relationships, which can be developed from the basic Maxwell's equations, useful for both geomagnetic depth sounding and magneto-tellurics, will be stated. General geomagnetic induction in structures of increasing complexity will be considered and parameters that aid identification of the form of the real earth below the recording site will be formulated.

Full theoretical treatment will be given only where considered expedient.

2.1 Brief Historical Review

The first systematic study of magnetic and telluric field relations appears to have been performed by Airy (1868). However, it was not until Schuster (1889) separated the observed Sq geomagnetic field variations into parts of internal and external origin that a method for gaining qualitative information about the electrical conductivity structure of the earth became viable.

Prior to 1940, research concentrated on the spherical harmonic analyses of Sq (quiet day), L (lunar) and Dst (storm time) variations to derive the conductivity and depth of a uniform sphere model that was most consistent with the observed data (Chapman, 1919; Chapman and Price, 1930; Hasegawa, 1936). The simple uniform core model for the earth was soon rejected in favour of non-uniform models (Lahiri and Price, 1939) and data from secular variations were utilised (McDonald, 1957) to estimate the conductivity of the lower mantle.

Differing magnetic fields, particularly in the vertical component (H_z), were observed at two very closely spaced stations by Schmidt (1909) but were not attributed to local induction effects until much later (Meyer, 1951). The dependence of the magnetic and telluric field relationships on the conductivity of the earth was measured (Tereda, 1917; Hirayama, 1934; Hatakeyama, 1938) and Schelkunoff (1938) introduced the concept of impedance in electromagnetic studies. Tikhonov (1950) realised the potential of utilising the natural electromagnetic fields of the earth. However, it was Cagniard (1953) who published the first paper to show a method of deriving the conductivity distribution with depth, below the recording site, from the amplitude and phase of the orthogonal horizontal magnetic and telluric field vectors. Recursion algorithms to derive the apparent resistivity and phase response at a certain frequency on the surface of a plane layered model were given by Wait (1954) and Lipskaya and Troitskaya (1955). Interpretation was by curve-matching the observed response to a theoretical response.

Wait (1954) cast aspersions on the validity of Cagniard's assumption of plane wave sources, since finite ionospheric sources do not give rise to normally incident plane waves. Also, magneto-telluric results inferring conductivity distributions well into the mantle (Migaux, Astier and Reval, 1960) did not agree with spherical harmonic analyses of the geomagnetic field (Lahiri and Price, 1939). This led Price (1962) to develop a general theory for the magneto-telluric method with finite dimensions of the source fields. Srivastava (1965) extended the recursion algorithm of Lipskaya and Troitskaya to include the effect of finite source dimensions and gave a curve-matching technique for estimating not only the conductivity layering parameters but also

the wavelength of the source (if both horizontal components of the magnetic field are measured).

However, computer modelling studies undertaken by Madden and Nelson (1964) and Srivastava (1965) indicated that for realistic earth conductivity profiles, the plane wave source field assumption is valid for periods up to 10^3 seconds. Swift (1967) analysed magnetograms from two stations 1300 km apart (Dallas and Tucson) at mid-geomagnetic latitude and concluded that, for the period band 10^3 s to 10^5 s, the wavelength of the source field must be in excess of 10^4 km. This corresponds to a wavenumber ($k_T = 2\pi/\lambda$) of the order of 10^{-5} m^{-1} and therefore, from Srivastava's studies (1965), Cagniard's assumption is valid at mid-geomagnetic latitudes for periods up to 10^5 s.

It soon became apparent that the scalar nature of Cagniard's impedance relationship, given by

$$\begin{bmatrix} E_X \\ E_Y \end{bmatrix} = \begin{bmatrix} 0 & Z_{XY} \\ Z_{YX} & 0 \end{bmatrix} \begin{bmatrix} H_X \\ H_Y \end{bmatrix}, \qquad (2.1)$$

did not give interpretable, meaningful or consistent results in areas of lateral conductivity variations. Neves (1957) was the first to recognise the tensor nature of the relationship between the magnetic and telluric fields, and employed a tensor admittance formalism, namely

$$\begin{bmatrix} H_X \\ H_Y \end{bmatrix} = \begin{bmatrix} Y_{XX} & Y_{XY} \\ Y_{YX} & Y_{YY} \end{bmatrix} \begin{bmatrix} E_X \\ E_Y \end{bmatrix}.$$

Bostick and Smith (1962) showed that the admittance tensor could be rotated so as to minimise the diagonal elements ($Y'_{XX}(\theta)$, $Y'_{YY}(\theta)$). The tensor is thus reduced, as far as possible, to the Cagniard representation.

Other workers however, followed the lead of Berdichevskii (1960, 1963) and Tikhonov and Berdichevskii (1966) and expressed the relationships in the form of an impedance tensor,

$$\begin{bmatrix} E_X \\ E_Y \end{bmatrix} = \begin{bmatrix} Z_{XX} & Z_{XY} \\ Z_{YX} & Z_{YY} \end{bmatrix} \begin{bmatrix} H_X \\ H_Y \end{bmatrix}. \qquad (2.2)$$

Many methods have since become available for computing the tensor impedance elements by employing statistical and spectral techniques (Swift, 1967; Morrison et al., 1968; Sims and Bostick, 1969; Reddy and Rankin, 1973). Various criteria have been used to decide on the angle that best represents the gross structural strike of the anomaly, if a quasi-two-dimensional structure could be assumed. This is discussed more fully in section 2.4.3.

As the instrumentation for data acquisition became more reliable, greater quantities of data became available for analysis from each recording site. However, apparent resistivity results derived from a large number of data sets exhibited a high degree of scatter. Thus workers became more critical of their data. This implies some data qualification techniques need to be employed which, because of the large quantity of data involved, must be computerisable. Intuitive data screening methods became too impractical.

The first type of data qualification technique utilised was to employ acceptance criteria. The most favoured in magneto-telluric studies is that the coherence between one telluric component and one, or both, of the magnetic components (i.e. γ^2_{ND} or γ^2_{NHD}) should be above a certain level. Examples of acceptable coherences are given in table 2.1. The large variability between authors indicates the difficulty of rigorous comparison. A fuller discussion of a more satisfactory coherence function to employ is given in section 4.4.4. Another

TABLE 2.1

Minimum coherence criterion, employed in recent MT studies, for acceptance of data

	γ^2_{ND}	γ^2_{NHD}
Swift (1967)		0.8
Caner *et al.* (1969)	0.56	
Word *et al.* (1970)		0.64
Reddy & Rankin (1971)		0.9
Vozoff (1972)		0.9
Kurtz (1973)		0.8
Nienaber *et al.* (1973)	0.56	
Cochrane & Hyndman (1974)		0.765
Reddy *et al.* (1976)		0.9
Rooney (1976)		0.8

acceptance criterion commonly used is that the power of all four traces should exceed a certain 'noise' power level. This noise could be due to instrumentation noise, digitising procedure, digital recording errors, etc.

Once data acceptance criteria had been applied, workers began to use weighting functions to emphasise the well estimated data points when averaging. Intuitive weighting was employed by Ward et al. (1970), who plotted resistivities with an associated coherence greater than 0.8 with a different symbol from those with coherence less than 0.8. Caner et al. (1969) gave resistivities with a coherence greater than 0.9 a weighting of three (unity weighting for those with coherence less than 0.8) when averaging. Dowling (1970) utilised an 'empirically derived quality factor', dependent on polarisation characteristics, coherences and rotational properties, as a weighting function.

Indicators of the gross dimensionality of the subsurface can aid interpretation of the data. The first signature formulated exploits the skew properties of the impedance tensor (Swift, 1967) and is rotationally invariant. Other dimensionality indicators utilise the vertical magnetic field component (H_Z) related to the horizontal components by

$$H_Z = AH_X + BH_Y \qquad (2.3)$$

(Everett and Hyndman, 1967a) and are the 'tipper' (Vozoff, 1972) and its associated 'skew', 'phase' and 'coherency' (Jupp and Vozoff, 1976).

The role of the H_Z component in induction studies was shown by Parkinson (1959, 1962, 1964) who introduced the concept of the 'best correlating direction' of the horizontal magnetic field (H_X, H_Y) with the vertical. The frequency domain form (2.3) gave rise to the single station induction arrows defined as

$$|R| = \{A_r^2 + B_r^2\}^{\frac{1}{2}} \text{ (a)} \qquad \theta_R = \arg(R) = \tan^{-1}\left(\frac{-B_r}{A_r}\right) \text{(b)}$$

$$|I| = \{A_i^2 + B_i^2\}^{\frac{1}{2}} \text{ (c)} \qquad \theta_I = \arg(I) = \tan^{-1}\left(\frac{-B_i}{A_i}\right) \text{(d)} \qquad (2.4)$$

The direction of the real induction arrow is reversed so as to point toward areas of current flow, following Parkinson (1964). There is much dissention between GDS workers about the meaning of the imaginary arrow. Its direction is reversed for consistency with 2.4b and with other workers (Gough, McElhinny and Lilley, 1974; Banks and Ottey, 1974; Green, 1975).

Comprehensive accounts of methods of estimating and presenting the transfer functions (A, B) are given by Schmucker (1970), Banks (1973) and Lilley (1974).

2.2 Relationships from Maxwell's Equations

Maxwell's basic equations in a source-free medium state

$$\text{div } \underline{B} = 0, \qquad (2.5a)$$

$$\text{div } \underline{D} = \rho, \qquad (2.5b)$$

$$\text{curl } \underline{H} = \underline{J} + \frac{\delta \underline{D}}{\delta t}, \qquad (2.5c)$$

$$\text{curl } \underline{E} = -\frac{\delta \underline{B}}{\delta t}. \qquad (2.5d)$$

From equations 2.5, the vector Helmholtz equations (dependence on exp ($i\omega t$) assumed)

$$\nabla^2 \underline{F} - k_\omega^2 \underline{F} = 0, \qquad (2.6)$$

where $\underline{F}$ is either $\underline{E}$ or $\underline{H}$ and the propagation constant,

$$k_\omega^2 = \omega\mu\,(i\sigma - \omega\varepsilon),$$

can be derived by utilising the relationships,

$$\underline{D} = \varepsilon \underline{E}, \tag{2.7a}$$

$$\underline{B} = \mu \underline{H}, \tag{2.7b}$$

$$\underline{J} = \sigma \underline{E}, \tag{2.7c}$$

where ε, μ and σ are the uniform permittivity, permeability and conductivity respectively of the medium. This development has been well covered in the literature (Grant and West, 1965; Ward et al., 1973).

The wave equation formalism of 2.6 can be reduced to the diffusion equation by neglecting the displacement current term ($\omega^2 \mu\varepsilon$) of the propagation constant and considering conduction currents only. Then the propagation (more correctly 'diffusion') constant will be

$$k_d^2 = i\omega\mu\sigma. \tag{2.8}$$

Consideration of minimum conductivity and maximum permittivity values possible within the earth's crust and mantle give a ratio of the amplitude of conduction currents to that of displacement currents of

$$\sigma : \omega\varepsilon \equiv 1 : 7 \times 10^{-5}\omega$$

(for $\sigma_{min} = 10^{-5}$ S.m^{-1}, $\varepsilon_{max} \simeq 7 \times 10^{-10}$ F.m^{-1} for saturated porous rocks with a dielectric capacitivity of 80, Grant and West, 1965). For a radian frequency of 0.628 rad s^{-1} (corresponding to a period of 10 s, the shortest period variations recorded in this study) the ratio is one to 5×10^{-5}.

The vector diffusion equation given by

$$\nabla^2 \underline{F} = \sigma\mu \dot{\underline{F}} \tag{2.9}$$

does not represent the propagation of steady waves but the diffusion of vector field $\underline{F}$ into the medium, the amplitude of the vector decaying

exponentially with penetration. The depth at which the field $\underline{F}$ has an amplitude of 1/e of that at the surface of the medium, called the 'skin depth', is considered in the following sections.

General solutions to 2.9 are given by linear combinations of the elementary solution

$$Ae^{i(k_x x + k_y y + k_z z)} + Be^{-i(k_x x + k_y y + k_z z)} \qquad (2.10)$$

where $$|k_x^2 + k_y^2 + k_z^2| = |k_d^2| = \omega\mu\sigma.$$

Three inter-related inductive response functions can be defined for the medium (Schmucker, 1973). These functions are dependent on frequency and tangential source wavenumber k_T, where $k_T^2 = k_x^2 + k_y^2$. They are the impedance $Z(\omega, k_T)$, the inductive scale length $C(\omega, k_T)$, and the ratio of the internal to external parts of the magnetic surface field $S(\omega, k_T)$. The primary objective for magneto-telluric investigations is to estimate $Z(\omega)$ whilst GDS studies attempt to evaluate $S(\omega)$.

The relationship between the spatial gradient of the horizontal magnetic field, and the ratio of the orthogonal components of the horizontal electric and magnetic fields, has been shown by Schmucker (1970) and Kuckes (1973a and b) to be

$$\frac{H_z}{\frac{\delta}{\delta x} H_x + \frac{\delta}{\delta y} H_y} = \frac{i}{\omega\mu} \frac{E_{x,y}}{H_{y,x}} = -C(\omega). \qquad (2.12)$$

The impedance of the earth has been estimated from the spatial character of the magnetic field by very few workers, notably Kuckes (1973a) and Lilley and Sloane (1976). Much scope exists in GDS studies for utilising 2.12.

2.3 General Geomagnetic Induction Over One-Dimensional Structures

2.3.1 Homogeneous Half-Space

The most rigorous theory of electromagnetic induction in an homogeneous earth having a plane boundary was advanced by Price (1950), and was reviewed by Rikitake (1966). Price showed that two types of solutions to the diffusion equation (2.9), constrained by the usual boundary conditions at the air/medium interface (i.e. the tangential components of $\underline{E}$ and $\underline{H}$, and the normal component of $\underline{B}$, are continuous), are possible. Only one set of solutions need be considered for electric field induction by a magnetic source field (solutions of the first type). Conversely, solutions of the second type correspond to the free modes of decay of a varying current distribution which is unaffected by any external electric field and demands a zero magnetic field outside the medium. One important conclusion to be drawn from first-type solutions is that the induced currents flow everywhere parallel to the surface of the conductor. It can also be shown from Snell's law of refraction,

$$k_o \sin \theta_o = k_1 \sin \theta_1$$

where k_o - wavenumber of the field in the air

θ_o - angle of incidence

k_1 - wavenumber of the field in the medium

θ_1 - angle of refraction into the medium

that $\theta_1 \sim 0^o$ (Kurtz, 1973). Therefore, regardless of the angle of incidence, the low frequency electromagnetic waves will propagate vertically downward.

Cagniard's definitive paper (1953) on the basic theory of the magneto-telluric method established that the resistivity of a medium is related to orthogonal electric and magnetic horizontal field

components observed at the surface by

$$\rho_{XY} = \frac{1}{\omega\mu} \left| \frac{E_X}{H_Y} \right|^2 , \qquad (2.13a)$$

$$\rho_{YX} = \frac{1}{\omega\mu} \left| \frac{E_Y}{H_X} \right|^2 , \qquad (2.13b)$$

$$\text{and } \rho_{XY} = \rho_{YX}.$$

The phase of the magnetic field is retarded by an angle of $\pi/4$ with respect to that of the electric field. The skin depth is given by

$$\delta = \frac{1}{\mathrm{Re}(k_d)} = \left(\frac{2}{\omega\mu\sigma} \right)^{\frac{1}{2}}. \qquad (2.14)$$

Equations 2.13a, 2.13b and 2.14 can be expressed in terms of the experimentalists 'field' units as

$$\rho_{XY} = 0.2T \left| \frac{E_X}{H_Y} \right|^2 \qquad (2.15)$$

$$\text{and } \delta = 0.503 \, (\rho T)^{\frac{1}{2}} \qquad (2.16)$$

where $\underline{E}$ is measured in mV/km,

$\underline{H}$ is measured in gamma, γ,

T is the period in seconds,

ρ is the resistivity in ohm.m,

and δ is the skin depth in km.

In Cagniard's development, it was implicitly assumed that

$$|k_d|^2 \approx |k_z|^2 \gg |k_x^2 + k_y^2| \qquad (2.17)$$

which is equivalent to

$$\delta^2 << \frac{1}{k_T} .$$

This requires the source field to be reasonably spatially uniform (i.e. k_x, $k_y \rightarrow 0$). A more general theory was developed by Price (1962) in which he considered a source of non-infinite horizontal extent with a wavelength of $\lambda = 2\pi/k_T$. Both Wait (1954), and later Price (1962), gave the necessary correction to 2.13a and b. Defining the resistivity to be related to the complex impedance by

$$\rho_{XY,\ YX} = \frac{1}{\omega\mu} \left| Z_{XY,\ YX}(\omega,\ k_T) \right|^2 \qquad (2.18)$$

then Z, as given by Price (1962), is

$$Z\ (\omega,\ k_T) = \left(\frac{E_X}{H_Y}\right)\left(1 - \frac{k_T^2}{2i\omega\mu\sigma}\right)^{-1} . \qquad (2.19)$$

Thus, the resistivity of the half space is underestimated by a factor of

$$\left| 1 - \frac{k_T^2}{2i\omega\mu\sigma} \right|^{-2} , \qquad (2.20)$$

which is a function of frequency.

For reasons specified in the earlier section however, this factor need not be corrected for if the period is less than 10^5 s.

2.3.2 N-Layered Isotropic Half-Space

Cagniard (1953) showed that an 'apparent' resistivity, analagous to the apparent resistivity of the DC sounding method, could be calculated from an extension of 2.13 to

$$\rho_a(T) = \frac{1}{\omega\mu}\left|\frac{E_X}{H_Y}(T)\right|^2 = \frac{1}{\omega\mu}\left|\frac{E_Y}{H_X}(T)\right|^2 \qquad (2.21)$$

and also the 'apparent' phase to

$$\psi_a(T) = \arg\left(\frac{E_X}{H_Y}(T)\right) = \arg\left(\frac{E_Y}{H_X}(T)\right) - \pi \qquad (2.22)$$

Cagniard suggested curve-matching the measured apparent resistivity and phase responses to that of a layered earth model. He presented the master curves for two-layer models and master curves for models of more complexity have been published in the literature (Yungul, 1961; Srivastava, 1967). The forward problem of calculating the response function measured at the surface of an N-layered isotropic half space is discussed in detail by Ward et al. (1973), who restated the recursion algorithm of Wait (1962), and by Keller and Frischknecht (1966), who expounded that of Lipskaya and Troitskaya (1955). The latter states

$$Z_o(\omega) = \frac{+i\mu\omega}{k_1}\coth\left[k_1h_1 + \coth^{-1}\left(\frac{k_1}{k_2}\coth\left[k_2h_2 + \coth^{-1}\left(\cdots\right.\right.\right.$$

$$\left.\left.\left.\cdots\coth^{-1}\left(\frac{k_{n-2}}{k_{n-1}}\coth\left[k_{n-1}h_{n-1} + \coth^{-1}\left(\frac{k_{n-1}}{k_n}\right)\right]\right)\cdots\right)\right]\right)\right] \qquad (2.23)$$

where $Z_o(\omega)$ is the impedance

k_i is the propagation constant for the ith layer given by

$$k_i = \left(\frac{\omega\mu_i\sigma_i}{2}\right)^{\frac{1}{2}} + i\left(\frac{\omega\mu_i\sigma_i}{2}\right)^{\frac{1}{2}} \qquad (2.24)$$

h_i is the thickness of the ith layer.

A program was written to calculate the apparent resistivity and phase response for an N-layered geometry employing the algorithm of 2.23. Some typical results are given in figure 2.1.

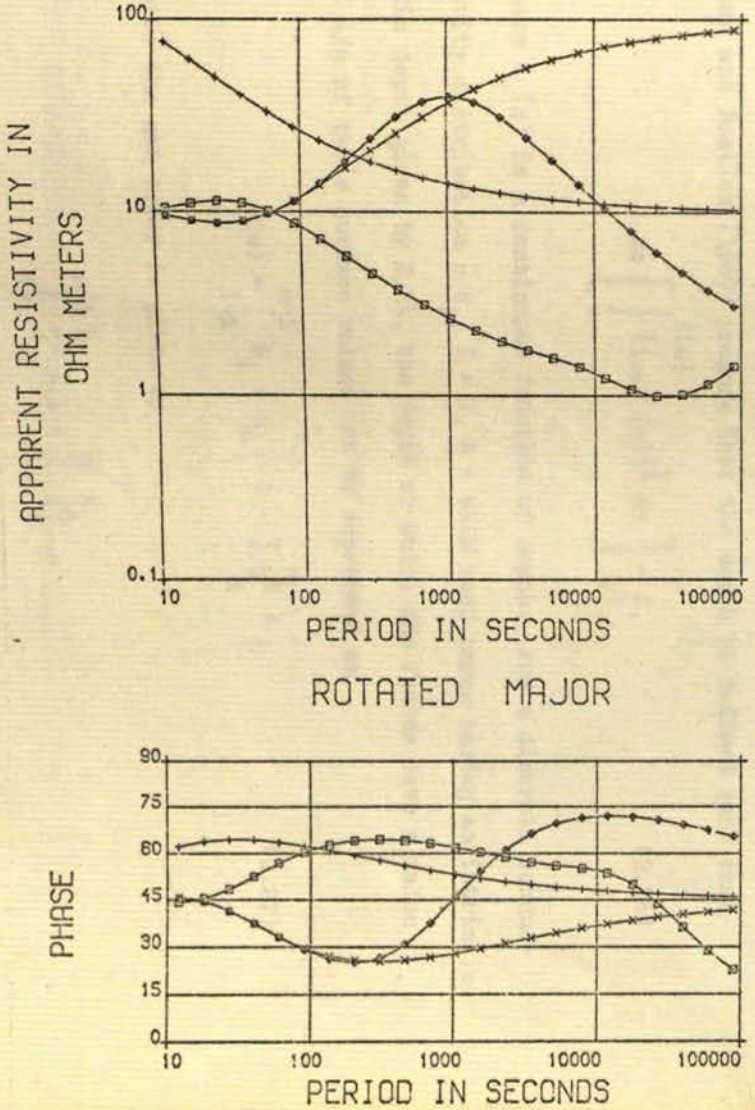

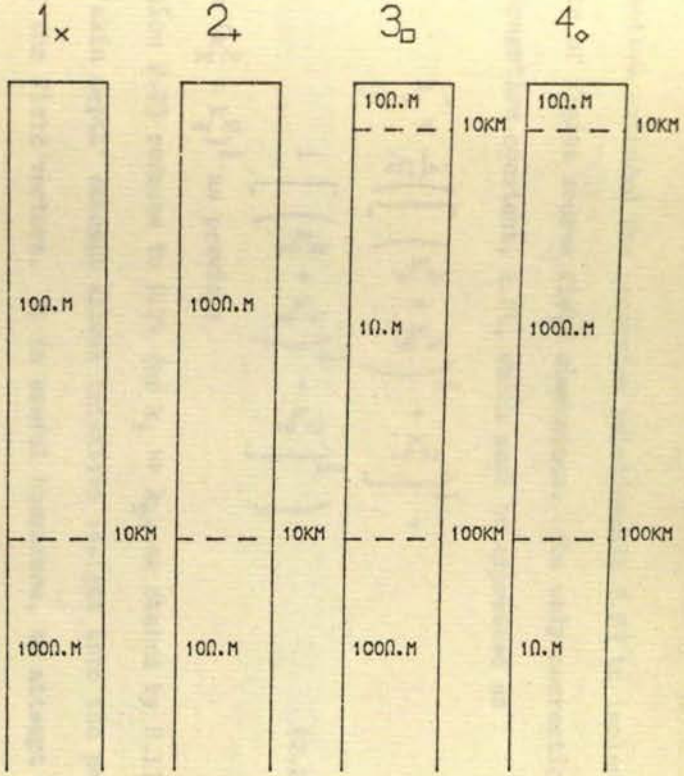

Figure 2.1 Typical M-T responses for theoretical models

Srivastava extended the recursion relationship 2.23 to include the effects of finite source field dimensions. The only correction is to the propagation constant, 2.24, which must be expressed as

$$k_i' = \frac{1}{\sqrt{2}}\left(\left[\left(k_i^4 + k_T^4\right)^{\frac{1}{2}} + k_T^2\right]^{\frac{1}{2}} + i\left[\left(k_i^4 + k_T^4\right)^{\frac{1}{2}} - k_T^2\right]^{\frac{1}{2}}\right) \qquad (2.25)$$

where $k_T = (k_X^2 + k_Y^2)^{\frac{1}{2}}$ as previous.

Equation 2.25 reduces to 2.24 for $k_i >> k_T$, as stated by 2.17.

The 'skin depth' concept allows intuitive insight into the penetration of the field vectors. It is useful therefore, to attempt to generalise the relationship given by 2.14 for an N-layered geometry. Sims and Bostick (1969) propose that the depth be defined such that

$$\mathrm{Re}\left[\int_0^{\delta(\omega)} (i\omega\mu\sigma\,(z))^{\frac{1}{2}}\,dz\right] = 1, \qquad (2.26)$$

where $\sigma\,(z)$ is a continuous function of depth. For a discrete conductivity distribution - σ_i, i = 1, N - with each layer having an intrinsic skin depth given by 2.14, the depth at which the fields have a value of 1/e of their surface values can be expressed as

$$\delta(\omega) = \sum_{i=1}^{m-1} h_i + \delta_m\left(1 - \sum \frac{h_i}{\delta_i}\right), \qquad (2.27)$$

where the mth layer is given by

$$\sum_{i=1}^{m-1} \frac{h_i}{\delta_i} < 1 < \sum_{i=1}^{m} \frac{h_i}{\delta_i}\ .$$

Figure 2.2 illustrates use of 2.27 by computing the generalised skin depths at different periods for the conductivity distributions of figure 2.1.

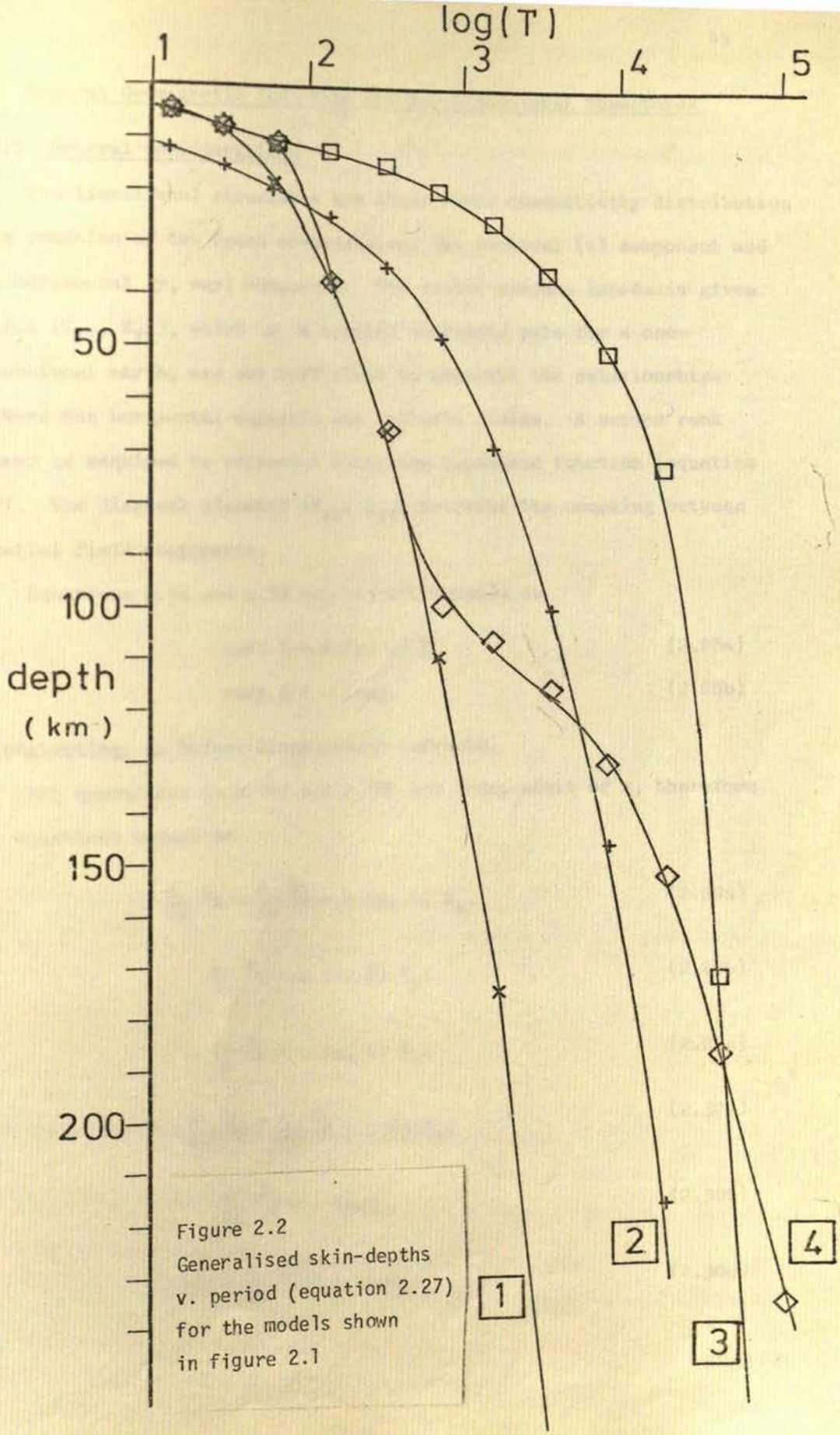

Figure 2.2
Generalised skin-depths
v. period (equation 2.27)
for the models shown
in figure 2.1

2.4 General Geomagnetic Induction for Two-Dimensional Structures

2.4.1 General Considerations

Two-dimensional structures are those whose conductivity distribution is a function of two space co-ordinates, the vertical (z) component and one horizontal (y, say) component. The scalar surface impedance given by 2.1 (Z_{XY}, Z_{YX}), which is a complex conjugate pair for a one-dimensional earth, are not sufficient to describe the relationships between the horizontal magnetic and telluric fields. A second rank tensor is required to represent fully the impedance function (equation 2.2). The diagonal elements (Z_{XX}, Z_{YY}) describe the coupling between parallel field components.

Equations 2.5c and 2.5d can be reformulated as

$$\text{curl } \underline{H} = \sigma\ (y,\ z)\ \underline{E}, \tag{2.28a}$$

$$\text{curl } \underline{E} = -\ i\omega\mu\underline{H}, \tag{2.28b}$$

by neglecting, as before displacement currents.

All quantities in 2.28a and 2.28b are independent of x, therefore the equations reduce to

$$\frac{\delta}{\delta y} H_z - \frac{\delta}{\delta z} H_y = \sigma\ (y,\ z)\ E_x, \tag{2.29a}$$

$$\frac{\delta}{\delta z} H_x = \sigma\ (y,\ z)\ E_y, \tag{2.29b}$$

$$-\frac{\delta}{\delta y} H_x = \sigma\ (y,\ z)\ E_z. \tag{2.29c}$$

$$\frac{\delta}{\delta y} E_z - \frac{\delta}{\delta z} E_y = -\ i\omega\mu H_x, \tag{2.30a}$$

$$\frac{\delta}{\delta z} E_x = -\ i\omega\mu H_y, \tag{2.30b}$$

$$-\frac{\delta}{\delta y} E_x = -\ i\omega\mu H_z. \tag{2.30c}$$

These six equations can be decoupled into two distinct modes. In one mode, the electric vector is polarised along the independent axis (E_x) and the mode is described by 2.29a, 2.30b and 2.30c, which involve field vectors, E_x, H_y, H_z only. The other mode, which employs field components H_x, E_y, E_z, is totally independent of the first. This mode is characterised by having its magnetic vector polarised along the independent axis and the field relationships are given by 2.29b, 2.29c and 2.30a.

The magnetic vectors, H_y and H_z, can be eliminated from equations 2.29a, 2.30b and 2.30c to give an elliptic equation in E_x

$$\frac{\delta^2}{\delta y^2} E_x + \frac{\delta^2}{\delta z^2} E_x = k_d^2 E_x. \qquad (2.31a)$$

The equation describes the E-polarisation (Jones and Price, 1970) or TE (transverse electric, Sims and Bostick, 1969) mode. Analagously, an elliptic equation in H_x, namely,

$$\frac{\delta^2}{\delta y^2} H_x + \frac{\delta^2}{\delta z^2} H_x = k_d^2 H_x, \qquad (2.31b)$$

can be derived by eliminating the electric vectors from 2.29b, 2.29c and 2.30a. This corresponds to the H-polarisation or TM (transverse magnetic) mode.

2.4.2 Typical Two-Dimensional Models

(a) Fault

One of the two-dimensional models studied most extensively is the vertical fault structure (figure 2.3). D'Erceville and Kunetz (1962) examined analytically the problem for H-polarisation and concluded that continuity of the normal component of the current sheet across the boundary ($j_{y1} = j_{y2}$ at $y = 0$) demands a discontinuity in the electric

component ($\sigma_1 E_{y1} = \sigma_2 E_{y2}$ from 2.7c). The orthogonal magnetic vector (H_x) however is continuous across the boundary. Therefore, the ρ_{YX} apparent resistivity, as defined by 2.13b, will itself be discontinuous. Weaver (1963) considered both H- and E-polarisation, and his results for H-polarisation concur with those of d'Erceville and Kunetz. For E-polarisation, it was necessary for Weaver to assume that the horizontal magnetic field was constant along the surface (i.e. $(H_Y)_{Z=0}$ = constant for $-\infty < y < +\infty$). He was then able to solve for the ρ_{XY} resistivity. Although this assumption was shown to be incorrect by Jones and Price (1970), the general conclusion that ρ_{XY} was a monotonically continuous and smooth function across the boundary was upheld. Figure 2.3 illustrates the difference between ρ_{XY} and ρ_{YX} curves to be observed for different resistivity contrasts.

In terms of physical processes, Price (1973) explains that the electric field is discontinuous for the H-polarisation case because an alternating surface charge is continually being placed on the boundary by impinging currents. The effects of this surface change on the E-field are illustrated in Jones and Price (1970).

Whether the discontinuous ρ_{YX} resistivity, as displayed by figure 2.3, will be observed in practice has been seriously questioned by Rankin and co-workers (Rankin, Reddy and Schneider, 1976; Rankin, Reddy and Kao, 1976). By modelling the fault as a quasi-continuous distribution, rather than a stepwise discontinuous function, they were able to show that the ρ_{YX} resistivity differed by a maximum of only 15% from the ρ_{XY} resistivity and that it was continuous (figure 2.4). A geological fault would be expected to possess a finite transition zone length due to fault metamorphism, therefore Rankin and colleagues' representation appears to be more reasonable. Reddy and Rankin (1973) also show that the discontinuous effect in ρ_{YX} is reduced if the contact

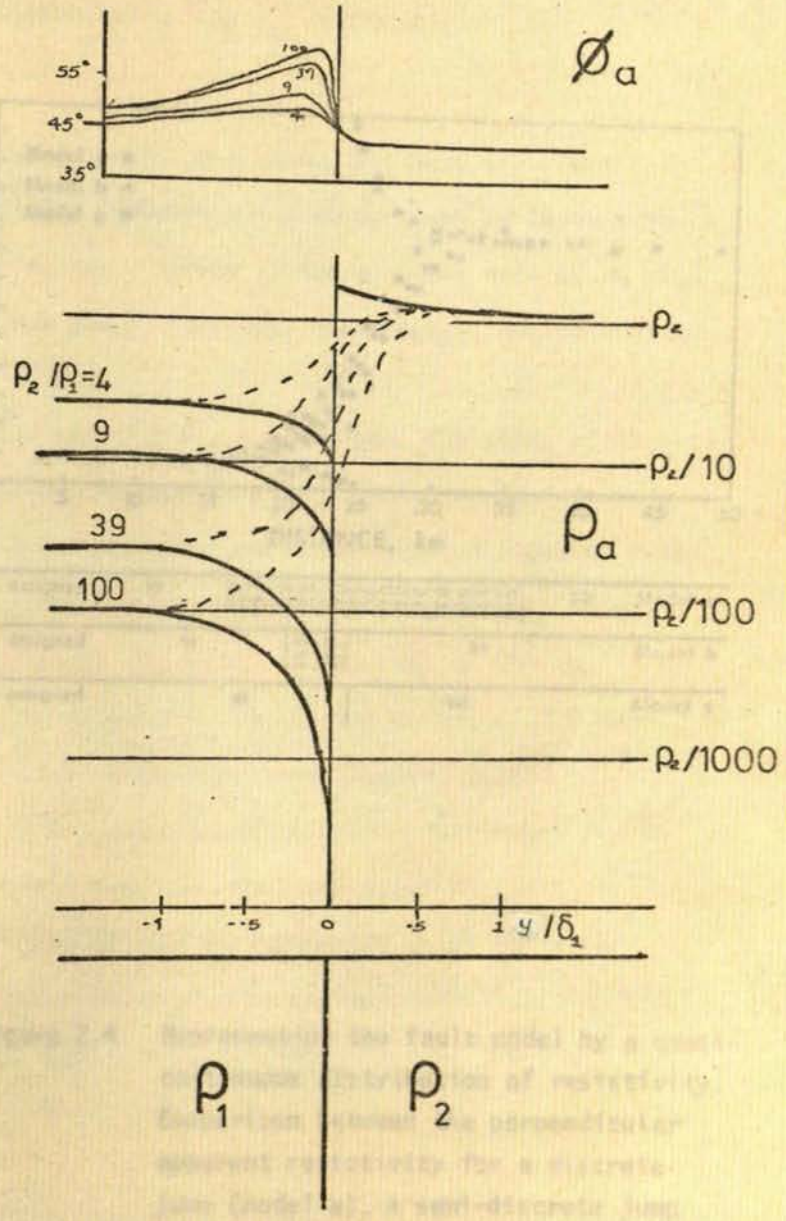

Figure 2.3 Parallel (- - -) and Perpendicular (———) apparent resistivities to be observed on traversing a fault. The phase of the perpendicular impedance is also shown

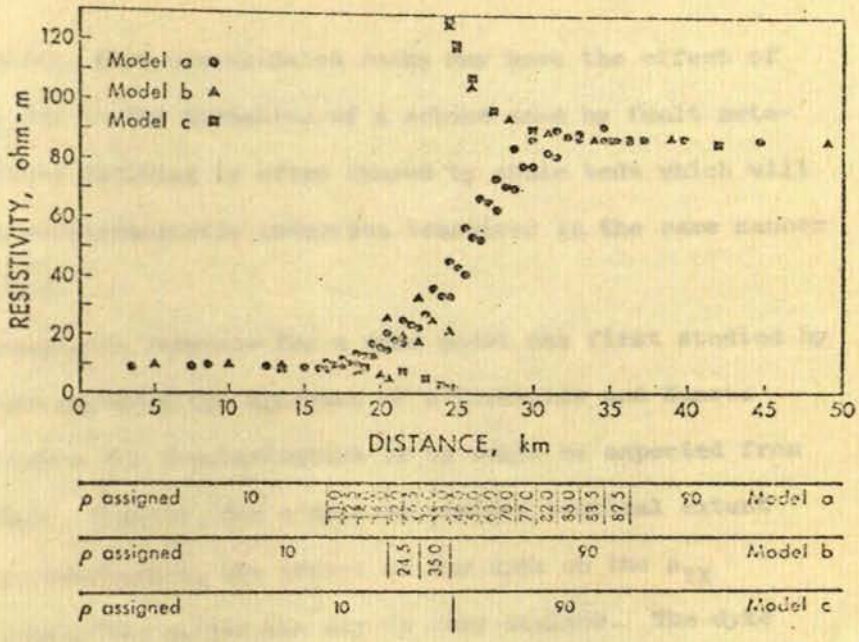

Figure 2.4 Representing the fault model by a quasi-continuous distribution of resistivity. Comparison between the perpendicular apparent resistivity for a discrete jump (model a), a semi-discrete jump (model b) and a continuous variation (mcdel c) im resistivity across the fault.

is sloping rather than vertical. Furthermore, the existence of an overburden also smooths and attenuates all of the boundary effects (Vozoff, 1972), most noticeably in the ρ_{YX} resistivity.

(b) Dyke

Faults in older, more consolidated rocks may have the effect of conductive dykes due to the formation of a schist zone by fault metamorphism. Imbricate faulting is often caused by shale beds which will also perturb the electromagnetic induction behaviour in the same manner as conductive dykes.

The electromagnetic response for a dyke model was first studied by Rankin (1962), who extended the approach of d'Erceville and Kunetz (1962). The response for H-polarisation is as would be expected from a dual-fault model. However, for a dyke of limited vertical extent with a conductive overburden, the effect of the dyke on the ρ_{YX} resistivity is negligible unless the dip is very shallow. The dyke would then be modelled as a conductive layer (Vozoff, 1972).

Swift (1971) has investigated numerically the dyke model for E-polarisation. He concluded that the anomalous magnetic field, defined as the total magnetic field (H_y and H_z components only) minus the ambient field, is primarily vertical and does not exhibit pronounced attenuation with depth. The induced electric field is concentrated just above the centre of the body.

(c) General Body

Electromagnetic induction in bodies of simple geometry can be studied analytically. As mentioned, analytic solutions have been published for fault (d'Erceville and Kunetz, 1962; Weaver, 1963) and dyke (Rankin, 1962) models. Schmucker (1971) has examined the problem of induction in a non-uniform surface above a layered substratum and

Weidelt (1971) has investigated induction effects in two adjacent half-sheets with different uniform conductivities.

For structures of more generality than those cited above, analytic solutions have not yet been presented. Accordingly, to investigate electromagnetic induction in inhomogeneous bodies of arbitrary shape, numerical techniques have to be utilised. Of the numerical methods available, the three that have become most prominent for induction studies are; the transmission surface formulation applied by Madden and co-workers (Dulaney and Madden, 1962), the finite element method (Coggon, 1971) and the finite difference method applied first by Neves (1957). A brief review of these three techniques is given by Jones (1973) and a full description by Ward et al. (1973).

Of the three, the most utilised is the finite difference approach. This is because Jones and co-authors published not only the theory (Jones and Price, 1970), but also FORTRAN programs (Jones and Pascoe, 1971; Pascoe and Jones, 1972) of their method for solving the electromagnetic induction problem in a general two-dimensional structure embedded in a layered earth for both H- and E-polarisations. A program package for two-dimensional modelling employing the finite element method is available (Kisak and Silvester, 1975) and is reported to be more efficient and to require less computing time than finite-difference methods (Kisak, 1976). Nevertheless, the widespread use of the Jones-Pascoe (J-P) programs warrants full consideration of the techniques employed.

The basic theory of the J-P programs was presented by Jones and Price (1970). The regions for solution, and their corresponding equations and relevant boundary conditions, for the simple two quarter-space model are illustrated in figure 2.5. Equations 2.31a and 2.31b are of the form

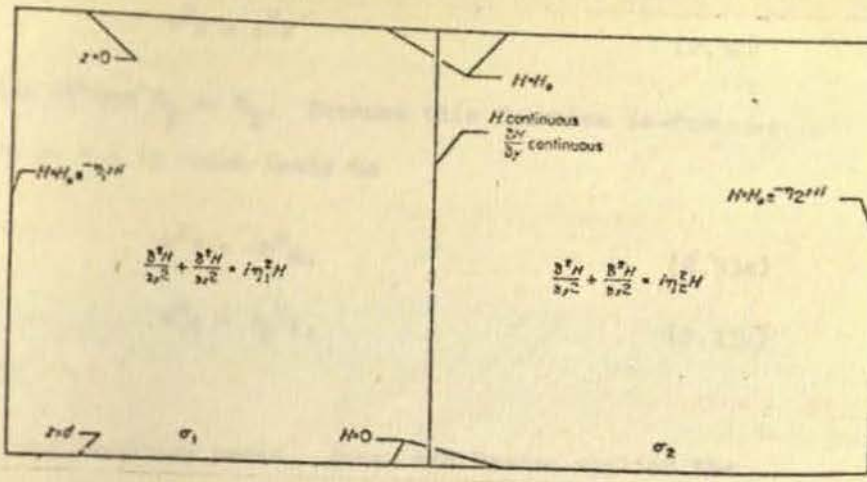

(a)

(b)

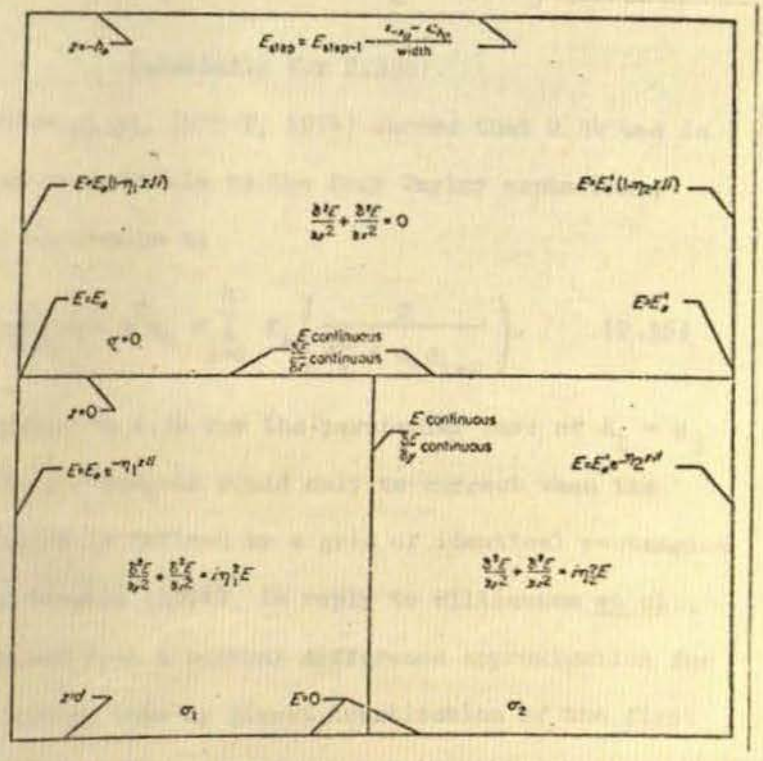

Figure 2.5 Equations and boundary conditions for the two quarter-space model

(a) H-polarisation

(b) E-polarisation

$$\nabla^2 F = k^2 F \tag{2.32}$$

where F represents either E_x or H_x. Because this function is complex, it can be written as f + ig which leads to

$$\nabla^2 f = -\eta^2 g, \tag{2.33a}$$

$$\nabla^2 g = \eta^2 f, \tag{2.33b}$$

(where $\eta^2 = \omega\mu\sigma$)

on equating real and imaginary parts. Jones and Pascoe applied the finite difference technique to the conductive structure depicted by figure 2.6. By neglecting terms of $O(d^3)$ and greater in the Taylor expansion of partial derivatives about the zeroth point, they obtained for the finite difference representation of 2.33a

$$f_o \sum_{i=1}^{4} \left(\frac{1}{d_i^2} \right) - \eta^2 g_o = \sum_{i=1}^{4} f_i \left(\frac{1}{d_i^2} + \frac{1}{(d_i + d_{i+2})} \left[\frac{1}{d_{i+2}} - \frac{1}{d_i} \right] \right) \tag{2.34}$$

where $5 \equiv 1$, $6 \equiv 2$ (similarly for 2.33b).

However, Williamson et al. (W-H-T, 1974) showed that 2.34 was in error and, by applying Cramer's Rule to the four Taylor expansions, they gave the correct expression as

$$f_o \left(\frac{2}{d_1 d_2} + \frac{2}{d_2 d_4} \right) - \eta^2 g_o = \sum_{i=1}^{4} f_i \left(\frac{2}{d_i^2 + d_i d_{i+2}} \right). \tag{2.35}$$

Equation 2.35 reduces to 2.34 for the particular case of $d_1 = d_3$ and $d_2 = d_4$. Thus, the J-P program would only be correct when the conductivity configuration is defined by a grid of identical rectangles or squares. Jones and Thomson (1974), in reply to Williamson et al., state that 2.34 is derived from a central difference approximation for the first derivative, rather than by direct substitution of the first derivative by Cramer's Rule. They concede that 2.35 will introduce a

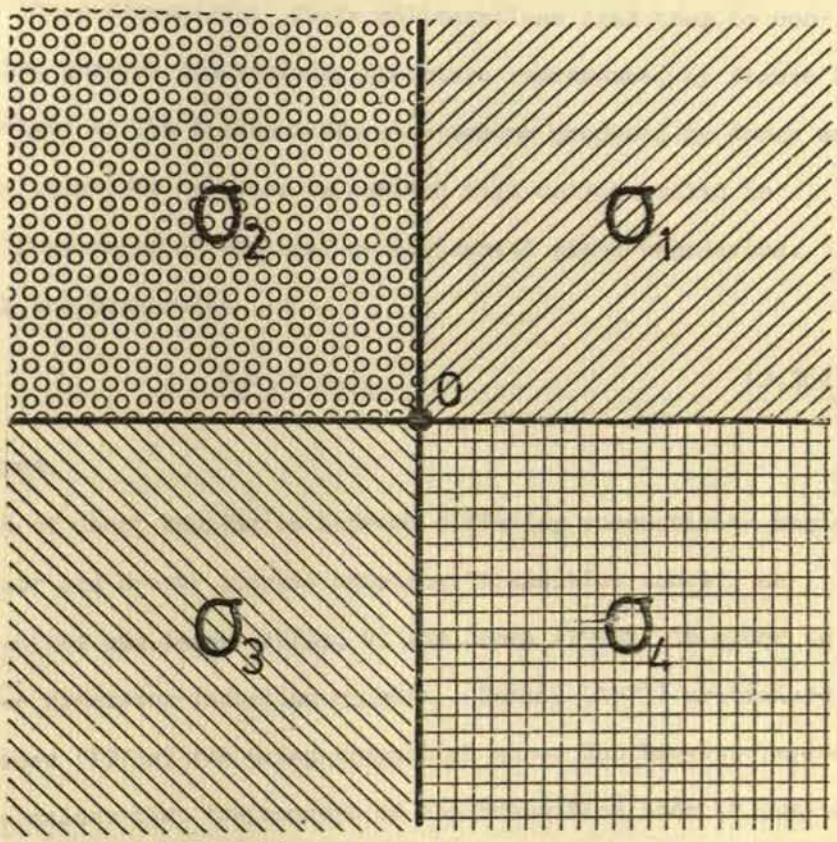

Figure 2.6 Generalised node point (0) for a finite difference scheme

greater degree of accuracy but caution strongly that the grid configuration must still be chosen with care.

Brewitt-Taylor and Weaver (BT-W, 1976) have re-examined the two-dimensional theory as a prelude to extending the finite difference approach to three dimensions. Their deliberations lead them to conclude that the general conductivity structure represented by figure 2.6 cannot be solved by the finite difference scheme proposed by Jones and Pascoe. The equations that can be derived will only be valid in homogeneous regions or at vertical or horizontal plane boundaries. This implies the constraint

$$\sigma_1\sigma_3 = \sigma_2\sigma_4. \qquad (2.36)$$

must be obeyed.

Instead of sharp boundaries between differing conductivity regions, Brewitt-Taylor and Weaver suggest adopting 'transition zones', as employed by Lines and Jones (1973a, b) and Jones (1973b) in order to solve a three dimension induction problem. Rankin (1973) criticised Lines and Jones (1973a) for using transition zones but Brewitt-Taylor and Weaver consider that the concept of the transition zone is just as implicit in the two-dimensional case as in the three-dimensional one. Although equation 2.31a will still be valid for transition zones rather than sharp boundaries for E-polarisation, the H-polarisation equation (2.31b) will have to be supplemented by terms involving the partial derivative of resistivity $\rho(= 1/\sigma)$ with respect to both y and z directions. The full equation becomes

$$\rho\left(\frac{\delta^2}{\delta y^2} H_x + \frac{\delta^2}{\delta z^2} H_x\right) + \frac{\delta\rho}{\delta y}\frac{\delta}{\delta y} H_x + \frac{\delta\rho}{\delta z}\frac{\delta}{\delta z} H_x = i\omega\mu_o H_x \qquad (2.37)$$

(ρ is defined differently here than in Brewitt-Taylor and Weaver (1976) to be notationally consistent throughout the thesis).

Brewitt-Taylor and Weaver present the finite difference equations for E- and H-polarisations for a transition zone concept and a comparison between their results and those of Jones and Pascoe (with and without the W-H-T correction) is given in figure 2.7. Although the E-polarisation results differ at most by ten per cent (which is still a propagated error of twenty per cent in the apparent resistivity value), the H-polarisation figures are inconsistent in form. The BT-W method gives a narrower dip over the conducting block. Their derived H-polarisation finite difference representation for the case of sharp boundaries (i.e. $\delta\rho/\delta y = \delta\rho/\delta z = 0$)

$$4(\rho_o + i(\omega\mu h)^2)H_o = \rho_{41}H_1 + \rho_{12}H_2 + \rho_{23}H_3 + \rho_{34}H_4, \qquad (2.38)$$

where $\rho_{ij} = \frac{1}{2}(\rho_i + \rho_j)$ and $\rho_o = \frac{1}{4}(\rho_1 + \rho_2 + \rho_3 + \rho_4)$, differs from that of Jones and Pascoe's except for the special case of $\sigma_1 = \sigma_2 = \sigma_3 = \sigma_4$. As 2.38 will still be subject to constraint 2.36, a transition zone concept is still required. Brewitt-Taylor and Weaver confirmed their results of figure 2.7 by analysing the problem using more formal procedures and conclude that although the J-P E-polarisation equations need only be modified, the J-P H-polarisation equations are incorrect and can lead to substantial errors (up to 50 per cent in the apparent resistivity value).

The J-P program solves the W-H-T equations by Gauss-Sidel iteration (Smith, 1965) which can be an extremely costly technique if a small relaxation error is desired. Losecke and Muller (1975) suggest various methods of decreasing the required computing time and still obtaining the same accuracy. The most efficient of those suggested is to employ successive over-relaxation (Smith, 1965) when iterating. The author attempted to improve the rate of convergence of the (W-H-T corrected) J-P program by applying the successive over-relaxation method and also

Figure 2.7 Comparison between Brewitt-Taylor & Weaver (1976) and Jones & Pascoe (1971) solutions for E-polarisation (left-hand diagrams) and H-polarisation fields over a block of conductivity ten times the half-space conductivity

———— solutions of B-T & W

- - - - - - solutions of J & P with WHT correction applied

..... solutions of J & P without WHT correction

-reproduced from Brewitt-Taylor and Weaver

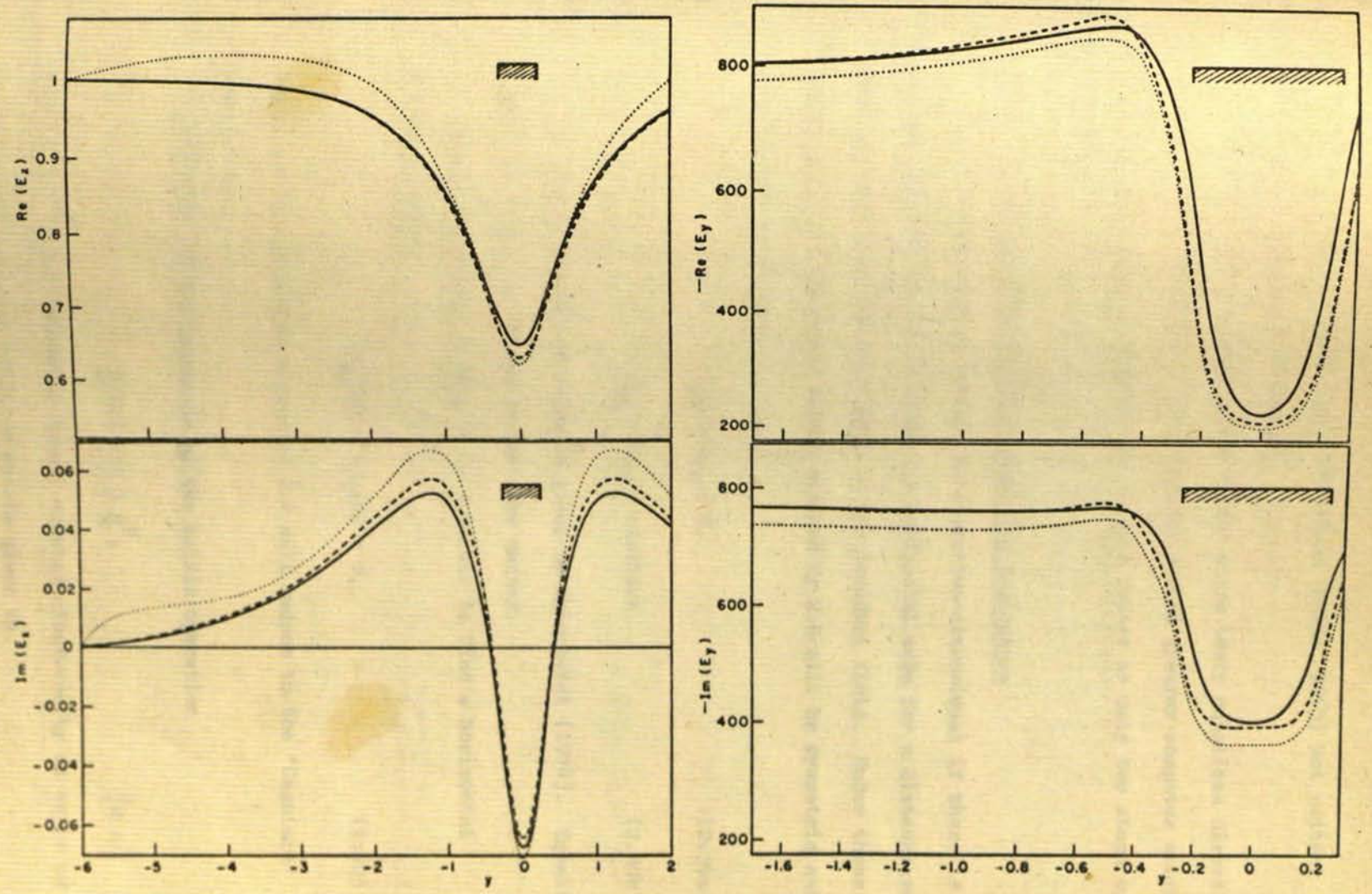
Re (E_z)
1
0.9
0.8
0.7
0.6
Im (E_z)
0.06
0.04
0.02
0
-0.02
-0.04
-0.06
-6
-5
-4
-3
-2
-1
0
1
2
y
-Re (E_y)
800
600
400
200
-Im (E_y)
600
600
400
200
-1.6
-1.4
-1.2
-1.0
-0.8
-0.6
-0.4
-0.2
0
0.2
y

the alternating-direction implicit method (Smith, 1965) but neither method gave converging iterates.

However, Brewitt-Taylor and Weaver solve their equations directly by Gaussian elimination. This requires a much greater computer storage capacity than the J-P program but is much faster as only two steps are required.

2.4.3 Dimensionality and Directionality Indicators

A structure can be defined as quasi-two-dimensional if there is no conductivity variation along one horizontal axis for a distance very much greater than the skin depth of the incident field. Under these conditions, the impedance tensor defined by 2.2 will be symmetric and the elements will obey

$$Z_{XX} + Z_{YY} = 0, \tag{2.39a}$$

$$Z_{XY} - Z_{YX} = \text{constant}. \tag{2.39b}$$

A rigorous proof of 2.39a is given by Abramovici (1974). Equation 2.39b can easily be proven in the same manner.

Under constraint 2.39a, it is possible to find a horizontal direction where

$$Z'_{XX}(\theta) = Z'_{YY}(\theta) = 0, \tag{2.40}$$

and hence the impedance tensor of 2.2 will reduce to the 'Cagniard' form of 2.1.

Rotation of the tensor is by the matrix operation

$$\underline{\underline{Z}}'(\theta) = \underline{\underline{R}}\,\underline{\underline{Z}}\,\underline{\underline{R}}^{T}, \tag{2.41}$$

where $\underline{\underline{Z}}'(\theta)$ is the impedance tensor rotated clockwise by an angle of θ and $\underline{\underline{R}}$ is the Cartesian rotation matrix given by

$$\underline{\underline{R}} = \begin{bmatrix} \cos\theta & \sin\theta \\ -\sin\theta & \cos\theta \end{bmatrix}. \qquad (2.42)$$

By calculating the rotated tensor given by 2.41, it is easily shown that constraints 2.39a and 2.39b are rotationally invariant. Therefore, the 'skew' of the impedance tensor, given by

$$\text{Skew} = \frac{|Z_{XX} + Z_{YY}|}{|Z_{XY} - Z_{YX}|}, \qquad (2.43)$$

(Swift, 1967) is also rotationally invariant, and, for one-dimensional or true two-dimensional cases, will equal zero. For a three-dimensional earth, the skew will be non-zero (except when the measurements are made on a plane of symmetry, Word et al., 1970) and its value will indicate the 'degree of three-dimensionality'.

Various methods have been presented for estimating the gross structural strike of the earth beneath the recording site. All of them converge to the correct result when the data is actually two-dimensional. Table 2.2 lists the 'strike' angle estimation method employed in some recent MT investigations. As an analytic technique for deriving the angle that maximises $|Z_{XY}|$ has not been presented, computer rotation of the impedance tensor is required. Swift (1967) demonstrated that the angle at which

$$|Z'_{XY}(\theta_o)|^2 + |Z'_{YX}(\theta_o)|^2 = \text{maximum}, \qquad (2.44)$$

also satisfies

$$|Z'_{XX}(\theta_o)|^2 + |Z'_{YY}(\theta_o)|^2 = \text{minimum}, \qquad (2.45)$$

and is given by

$$\tan(4\theta_o) = \frac{(Z_{XX} - Z_{YY})(Z_{XY} + Z_{YX})^* + (Z_{XX} + Z_{YY})^* (Z_{XY} - Z_{YX})}{|Z_{XX} - Z_{YY}|^2 - |Z_{XY} + Z_{YX}|^2}. \qquad (2.46)$$

TABLE 2.2

Methods of determining the gross-structural strike of the anomaly in recent MT studies

	Criterion	Method
Bostick & Smith (1962)	maximise $\|Y_{xy}(0)\|$	computer rotation
Everett & Hyndman (1967)	maximise $\|Z_{xy}(0)\|$	computer rotation
Swift (1967)	maximise $\|Z_{xy}(0)\|^2 + \|Z_{yx}(0)\|^2$	analytic
Sims & Bostick (1969)	as Swift (1967)	
Reddy & Rankin (1971)	maximise $\|Z_{xy}(0)\|^2 + \|Z_{yx}(0)\|^2$	computer rotation
Vozoff (1972)	as Swift (1967)	
Kurtz (1973)	as Swift (1967)	
Peeples & Rankin (1973)	as Reddy & Rankin (1971)	
Cochrane & Hyndman (1974)	as Swift (1967)	
Hermance & Grillot (1974)	as Everett & Hyndman (1967)	
Reddy & Rankin (1974)	minimise $\gamma^2_{NH.D}$	computer rotation
Reddy et al. (1976)	as Everett & Hyndman (1967)	
Rooney (1976)	as Everett & Hyndman (1967)	

Swift and others (table 2.2) consider that the angle calculated from 2.46 best represents the gross structural strike of the anomalous region.

The rotated $Z'_{XY}(\theta)$ tensor element, from 2.41, is

$$2Z'_{XY}(\theta) = (Z_{XY} - Z_{YX}) + (Z_{XY} + Z_{YX}) \cos 2\theta - (Z_{XX} - Z_{YY}) \sin 2\theta. \quad (2.47)$$

Let $A = Z_{XY} - Z_{YX}$, $B = Z_{XY} + Z_{YX}$ and $C = -(Z_{XX} - Z_{YY})$, then 2.47 can be written as

$$2Z'_{XY}(\theta) = A + B \cos 2\theta + C \sin 2\theta. \quad (2.48)$$

The square of the modulus of 2.48 is

$$4|Z'_{XY}(\theta)|^2 = |A|^2 + 2\mathrm{Re}(AB^*) \cos 2\theta + 2\mathrm{Re}(AC^*) \sin 2\theta +$$
$$|B|^2 \cos^2 2\theta + |C|^2 \sin^2 2\theta + 2\mathrm{Re}(BC^*) \sin 2\theta \cos 2\theta. \quad (2.49)$$

The direction at which 2.49 is a maximum (or a minimum) is given by the angle which satisfies

$$\frac{d}{d\theta} |Z'_{XY}(\theta_o)|^2 = 0. \quad (2.50)$$

The first derivative of 2.49 with respect to θ is (adopting the notation $R_{AB} = \mathrm{Re}(AB^*)$)

$$4 \frac{d}{d\theta} |Z'_{XY}(\theta)|^2 = -4R_{AB} \sin 2\theta + 4R_{AC} \cos 2\theta -$$
$$4|B|^2 \sin 2\theta \cos 2\theta + 4|C|^2 \sin 2\theta \cos 2\theta +$$
$$4R_{BC} (2 \cos^2 2\theta - 1). \quad (2.51)$$

If condition 2.50 is to be satisfied then

$$\left[R_{AB} + (|B|^2 - |C|^2) \cos 2\theta_o\right] . \sin 2\theta_o$$
$$= 2R_{BC} \cos^2 2\theta_o + R_{AC} \cos 2\theta_o - R_{BC}. \quad (2.52)$$

Squaring both sides of 2.52 and substituting $(1 - \cos^2 2\theta_o)$ for $(\sin^2 2\theta_o)$ gives a quartic equation in $\cos 2\theta_o$, namely

$$\left(4R_{BC}^2 + (|B|^2 - |C|^2)^2\right)\cos^4 2\theta_o + \left(2(2R_{BC}R_{AC} + R_{AB}(|B|^2 - |C|^2))\right)\cos^3 2\theta_o$$

$$+ \left(R_{AC}^2 - 4R_{BC}^2 + R_{AB}^2 - (|B|^2 - |C|^2)^2\right)\cos^2 2\theta_o$$

$$+ \left(-2(R_{AB}(|B|^2 - |C|^2) + R_{AC}R_{BC})\right)\cos 2\theta_o + \left(R_{BC}^2 - R_{AB}^2\right) = 0. \quad (2.53)$$

There will be four solutions for $2\theta_o$ in the range $(0, 2\pi)$. A method for finding analytically the solutions to quartic equations is given by Mostow et al. (1963, page 160). Alternatively, Newton-Raphson iterative techniques can be employed. To determine which of the four roots represent the maximising, rather than the minimising, directions for $|Z'_{XY}(\theta)|^2$, a test as to whether the second derivative of 2.49 is greater or less than zero can be performed.

The maximising angle would then be given by

$$\text{either} \quad \theta_r = \frac{1}{2} \text{ arc cos } (r_{max}),$$

$$\text{or} \quad \theta_r = \pi - \frac{1}{2} \text{ arc cos } (r_{max}) \quad (2.55)$$

(where r_{max} represents a maximising root) because the root is a function of 2θ and not θ.

Various tests were conducted on real data to discover if the maximising angle calculated from 2.53 was in agreement with that found by evaluating 2.48 in 2^o increments from 0^o to 180^o. Both the analytic and the numerical method of solution gave the same four roots to 2.53 but, in a few cases, some or all of the roots were either complex or had an absolute value greater than one. For the majority of data however, the two methods of evaluating the maximising, and minimising,

angles were in agreement. An example of a comparison at two periods (236 s and 28.5 s) for a data set from Saltoun (SALC) is illustrated in figure 2.8.

The author however, for reasons specified in section 4.5.3, chose not to rotate the impedance tensor to the angle that maximised $|Z_{XY}|^2$ but rather to that angle which maximised the partial coherence function γ^2_{NDH}. This function measures the coherence between the North telluric and the East magnetic vectors with the influence of the North magnetic vector removed in a least squares sense (Bendat and Piersol, 1971). An analytic expression which calculated the angle that maximised $\gamma^2_{NDH}(\theta)$ could not be determined. Computer rotation of the coherence function was necessary therefore.

Another dimensionality indicator is the eccentricity of the rotation ellipse for the complex impedance tensor (Word et al., 1970). This is defined by

$$\beta(\theta) = \frac{|Z'_{XX}(\theta) - Z'_{YY}(\theta)|}{|Z'_{XY}(\theta) + Z'_{YX}(\theta)|} . \qquad (2.56)$$

This function however, is not rotationally invarient but will reduce to zero for two-dimensional structures when θ equals the strike direction. The function therefore may be useful as a directionality rather than a dimensionality indicator.

Because it is possible for the skew, as defined by 2.43, to be zero if the measurements are made on a plane of symmetry of a three-dimensional structure, Word et al. (1970) state that the conditions

$$\begin{aligned} \text{SKEW} &= 0 \\ \beta(\theta_o) &= 0 \end{aligned} \qquad (2.57)$$

are necessary and sufficient conditions for assuming true two-

Figure 2.8 Comparison of analytic solution, with the computer rotation, for the maximum $Z_{xy}(0)$ angle

EVENT SALC

ROTATED IMPEDANCES PLOT

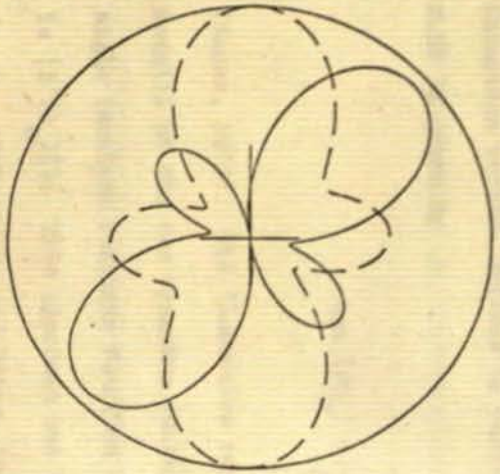

PERIOD = 235.8 SECS

$$\underline{\underline{Z}} = \begin{bmatrix} (10.46 + 9.306i) & (-2.771 - 1.422i) \\ (1.790 + 3.424i) & (-7.994 + 1.002i) \end{bmatrix}$$

Angles from solving 2.53

$\theta_{min} = 9.2^\circ$ or $\underline{170.8}^\circ$

$\theta_{max} = \underline{45.4}^\circ$ or 134.6°

EVENT SALC

ROTATED IMPEDANCES PLOT

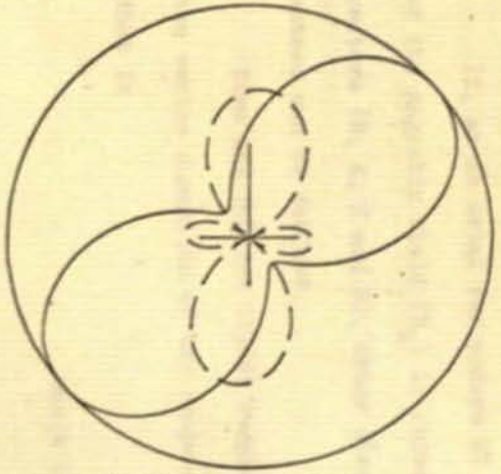

PERIOD = 28.5 SECS

$$\underline{\underline{Z}} = \begin{bmatrix} (1.256 + 2.624i) & (-0.3124 - 2.178i) \\ (0.6603 + 2.802i) & (-0.4060 - 1.130i) \end{bmatrix}$$

$\theta_{min} = 12.4^\circ$ or $\underline{167.6}^\circ$

$\theta_{max} = \underline{45.4}^\circ$ or 134.6°

dimensionality. However, because $\beta(\theta)$ is not rotationally invariant, and because of the limited availability of the publication of Word et al. (1970), the function has not been employed by many investigators.

If, as is usual for modern MT investigations, the vertical component of the magnetic field (H_Z) is recorded as well as the four horizontal vectors (N, E, H and D), other directionality and dimensionality indicators can be defined.

Sims and Bostick (1969) suggest that the direction which maximises the vector summation of the response functions (A, B) given by 2.3, that is

$$\text{Max}|A'(\theta)|^2, \tag{2.58}$$

where $$A'(\theta) = A \cos \theta + B \sin \theta, \tag{2.59}$$

is a good estimate of the strike direction.

This was first suggested for GDS studies by Everett and Hyndman (1967a) as a method for displaying the transfer functions (they, however, preferred to display their transfer functions as the two induction vectors defined by equation 2.4). The angle which satisfies 2.58 is given by

$$\tan (2\theta_o) = \frac{AB^* - A^*B}{|A|^2 - |B|^2} \tag{2.60}$$

(Banks, 1973). The 'inductive response' functions are defined as the modulii of the two transfer functions rotated into the maximising angle (maximum response function is $|A'(\theta_o)|$, minimum response function is $|B'(\theta_o)|$). This approach has been widely accepted for GDS studies (Banks, 1973; Banks and Ottey, 1974; Green, 1975; Beamish, 1976; Robinson, 1976; Rooney, 1976) but not for MT investigations. Banks and Ottey (1974) point out that the function $|A'(\theta)|^2$ is not elliptic

in form as stated by Everett and Hyndman (1967a). The two combining oscillations are both in the vertical direction, not in two orthogonal directions as required for an ellipse. But the rotation of $|A'(\theta)|^2$ can be described by formulae that are of the same form as ellipse formulae. Other methods of presenting the geomagnetic induction tensor are given by Lilley (1974).

Vozoff (1972) suggests that another estimate of strike direction is given by

$$\theta_o = \frac{R(\pi - \theta_R) + I(\pi - \theta_I)}{R^2 + I^2} \qquad (2.61)$$

and Jupp and Vozoff (1976) show that, if there is uncorrelated noise on the magnetic vectors, the arithmetic average of the angles given by 2.60 and 2.61 is an unbiased estimate of the strike direction.

Vozoff (1972), later amended by Jupp and Vozoff (1976), defined four functions which he considers indicative of two-dimensionality. They are (a) the 'tipper' (so called because the transfer functions (A, B) operate on the horizontal magnetic field and 'tip' part of it into the vertical direction) defined by

$$T = \{R^2 + I^2\}^{\frac{1}{2}}, \qquad (2.62)$$

(b) the 'tipper skew'

$$TS = \frac{2(A_r B_i - A_i B_r)}{T^2}, \qquad (2.63)$$

(c) the 'tipper phase'

$$S_T = \frac{|A|\,\phi_A + |B|\,\phi_B}{T^2}, \qquad (2.64)$$

and (d) the 'tipper coherency' or multiple coherency γ_{ZHD} (Bendat and Piersol, 1971).

CHAPTER 3

DATA ACQUISITION

This chapter will detail the methods employed to record the GDS and MT data. A description will be given of the site locations, the instrumentation utilised and the data recorded for both studies.

The GDS array will be discussed in section 3.1 and a fuller discussion of the MT project will be given in sections 3.2, 3.3 and 3.4.

3.1 The GDS Array

As outlined in the introduction, the geomagnetic deep sounding experiment was conducted with nineteen Gough-Reitzel magnetometers placed at the positions illustrated in figure 3.1. The Eskdalemuir observatory provided a twentieth location at which simultaneous measurement of the magnetic field variations were made. For each site, the three letter station title, full station name (usually the nearest town), geographic and geomagnetic co-ordinates and geomagnetic declination are given in table 3.1.

The construction of the magnetometer is described fully in Gough and Reitzel (1967) and is reviewed by Serson (1973). The design is classical in principle; three magnets suspended in three orthogonal orientations (magnetic north, H; magnetic east, D; magnetic vertical, Z) by taut torsion wires rotate through small angles in response to variations of the geomagnetic field. The rotations are magnified by optical levers and are recorded on film strip as displacements of images. The three variometers, and the associated electronic circuits and camera, are mounted on an aluminium frame which is placed within an aluminium tube set vertically in a hole in the ground. Diurnal

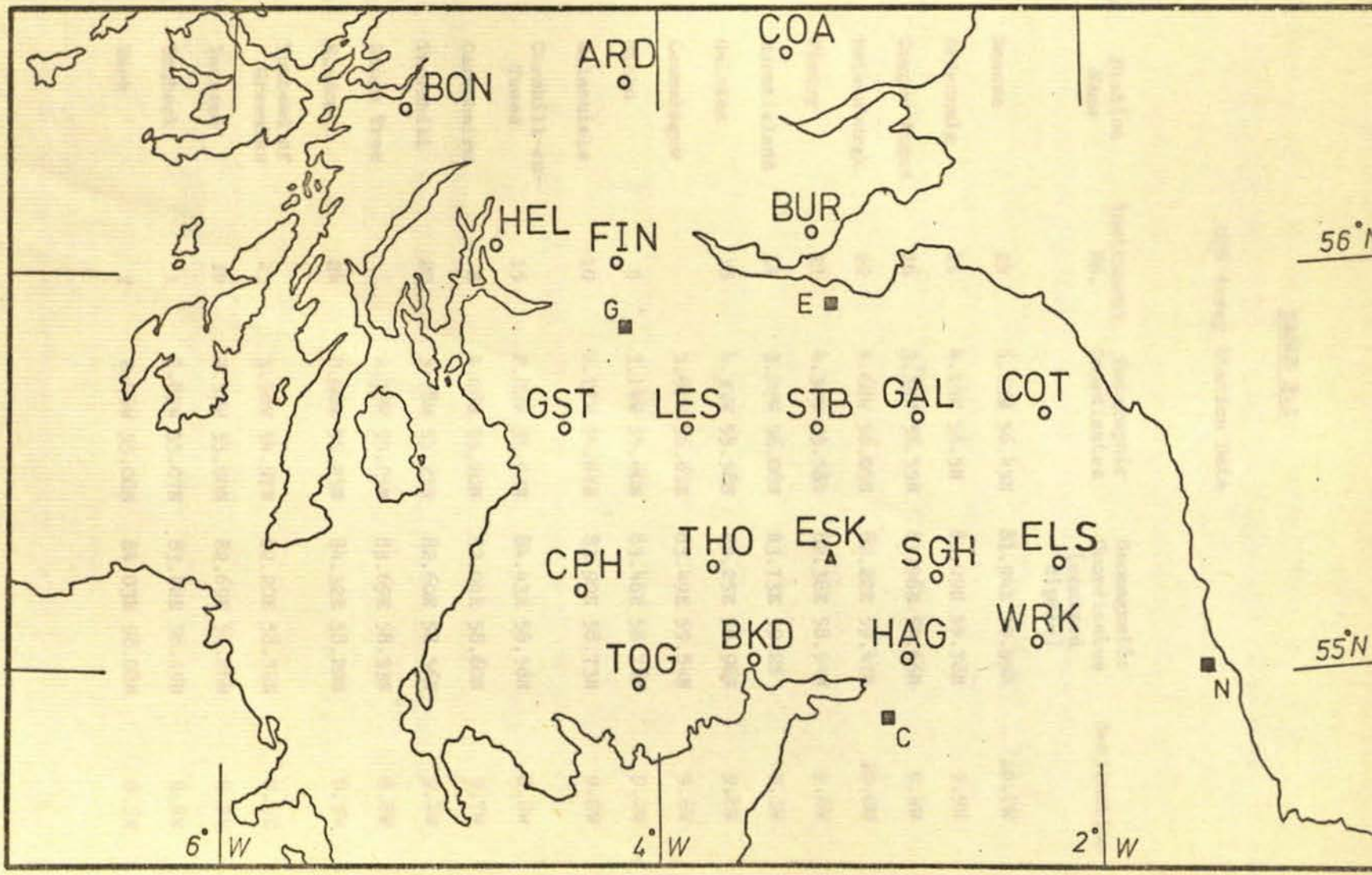

Figure 3.1 Locations of the GDS Array stations

TABLE 3.1

GDS Array Station Data

Station Title	Station Name	Instrument No.	Geographic Coordinates	Geomagnetic Coordinates (centred dipole)	Declination
BON	Bonawe	19	5.23W 56.45N	81.94E 59.95N	10.7W
ARD	Ardeonaig	11	4.15W 56.5N	83.09E 59.78N	9.9W
COA	Couper Angus	16	3.33W 56.55N	83.96E 59.66N	9.4W
HEL	Helensburgh	22	4.68W 56.05N	82.22E 59.47N	10.0W
FIN	Fintry	21	4.30W 55.58N	82.38E 58.94N	9.6W
BUR	Burntisland	14	3.22W 56.08N	83.73E 59.2N	9.3W
GST	Galston	18	4.33W 55.58N	82.25E 58.96N	9.8W
LES	Lesmahagow		3.85W 56.63N	83.49E 59.84N	9.6W
STB	Stobo	5	3.14W 55.60N	83.48E 58.74N	9.2W
GAL	Galashiels	10	2.77W 55.67N	83.90E 58.73N	9.0W
COT	Cornhill-on-Tweed	15	2.22W 55.63N	84.43E 58.58N	8.8W
CPH	Carsphairn	8	4.28W 55.20N	82.04E 58.60N	9.7W
THO	Thornhill	20	3.78W 55.27N	82.60E 58.56N	9.4W
SGH	Saugh Tree		2.70W 55.25N	83.69E 58.33N	8.8W
ELS	Elsdon	24	2.08W 55.25N	84.32E 58.20N	8.5W
TOG	Towhead of Greenlaw	25	3.98W 54.97N	82.20E 58.32N	9.5W
BKD	Bankend	12	3.52W 55.00N	82.69E 58.26N	9.3W
HAG	Hagbeck	1	2.85W 55.07N	83.42E 58.19N	8.8W
WRK	Wark	7	2.25W 55.08N	84.03E 58.08N	8.5W

temperature variation at the depth of the topmost magnet (D) is of the order of 0.1 K, and first order temperature compensation is provided by auxiliary magnets. The auxiliary magnets are also used to vary the required sensitivity of each component. The sensitivity used will depend on the expected level of geomagnetic activity.

Three major modifications have been made to the magnetometer by Dr. I. Gough since the basic design was published by Gough and Reitzel.

The vertical spacing between adjacent components was reduced from .5 m to .25 m, which gave an overall shortening of .5 m. This made the instruments less unwieldy in the field and also required shallower holes than previously. However, the interaction between components was enhanced to a significant level (4 per cent of H recorded on Z) and accordingly, corrections have to be applied when the data are processed.

The accutron timer (Bulova, model TE-11-16) was replaced by a crystal clock.

The time interval between successive recordings of the geomagnetic field components was increased from ten to twenty seconds. This reduced the Nyquist frequency from 0.05 Hz to 0.025 Hz which could introduce aliasing effects from Pc3 micropulsations (the Pc3 frequency band is 0.0285 Hz to 0.05 Hz). However, the amplitude of Pc3 activity in mid-latitudes is typically 1 γ (Orr, 1973) which is effectively negligible when compared to variations which are likely to be analysed, e.g. Pc5 activity, bay and storm disturbances, typically of order 100 γ.

In use, the magnetometers were found in general to be robust and fairly trouble-free. A data coverage of approximately 75 per cent was realised. The main causes for loss of records were (a) faulty camera drive, (b) misting of the mirrors and (c) images going off scale.

There were no records at all from ELS, very little from WRK and no Z data from BON and COA.

Four major improvements about the design of the magnetometer can be suggested. It would have been greatly beneficial if the magnetometers had been air tight. They had previously been operated in fairly arid climates (North America, South Africa and Australia) and accordingly problems resulting from high humidity and high rainfall had not been encountered. During the Scottish project, two magnetometers became completely waterlogged and data were lost from six others due to misting of the mirrors. Attempts were made to reduce these effects to a minimum by liberal use of silicon grease around seals and by inserting packets of silica gel inside the magnetometer.

The orienting and levelling of the magnetometers were extremely critical. An error of 1^{o} in either of these would cause the record of one variation field component to include about 2 per cent of another component. An inexact orientation would produce an error in each horizontal component due to the other of approximately the same magnitude. However, an equivalent inexact levelling would produce a much amplified error in the vertical component from the horizontal components than vice versa due to the higher sensitivity of the vertical variometer. For the Gough-Reitzel magnetometers employed for the Scottish work, the tube was levelled and oriented rather than the aluminium variometer frame itself. Should the magnetometer subsequently settle, the aluminium frame has to be removed completely and the tube re-oriented and/or re-levelled. A design to be preferred is one in which the chassis can be precisely levelled and oriented independently of the outer casing.

The necessity for the power supplies to be external to the instrument gave problems in localities of high water table. These difficulties could be circumvented by utilising internal power sources.

The fourth suggestion concerns the required calibration of the components at the beginning and the end of each film strip. Because the film drive could not be accelerated, certain periods of time were spent waiting for the film to advance sufficiently so that critical sections of film were not fogged by opening the instrument. An exterior control which increased the film drive rate would reduce the required waiting time. Alternatively, a time controlled calibration would have produced the desired affect.

Instruments built by the University of Münster, based on the Gough-Reitzel design, incorporate these recommendations and are able to operate satisfactorily in the extreme North Scandinavian climate (Küppers, 1976).

3.2 The MT Project

The results from the GDS array were intended to aid choice of suitable locations at which to measure magneto-telluric field variations. However, due to lack of time, the array data were not fully analysed prior to the commencement of the MT fieldwork. Therefore, approximate positions were chosen at which recordings of the MT fields would best delineate the anomaly described by previous geophysical work (section 1.2).

During the late summer of 1974, records were taken of the time varying fluctuations of the magnetic and telluric fields at four locations (FTH, DZR, CRK, NEW) in a line perpendicular to the strike of the anomaly (figure 3.2). In the following spring, the variations were recorded at eight other sites, three more on the NE to SW line (ELC, CAP and NEW) and four on a line parallel to the strike of the modelled anomaly (TIN, BOR, GOR and PRE). It was hoped that data from the eighth site, SAL, would given an indication of any coast effect that might perturb the geomagnetic fields at PRE, GOR and TIN.

Figure 3.2 Locations of stations at which M-T variations were recorded

During the summer of 1975, a visitor to the department, Mr. T. Odera, recorded MT variations at the Eskdalemuir observatory with the Geophysics Department's equipment. This was part of a training programme of the technique organised for Mr. Odera by Dr. Hutton, and Mr. Odera was advised whilst on fieldwork by the author. The data recorded by Mr. Odera has been subsequently analysed and interpreted as part of the research programme.

The fieldwork procedure adopted at each location often varied in minor detail but essentially consisted of four operations - site preparation, instrument installation, recording of variations and instrument retrieval. The necessary requirements at a location at which MT observations were to be made were much more constricting than those at which geomagnetic observations only were made, with Gough-Reitzel type magnetometers. Correct observation of the telluric field requires a large, relatively flat field far from artificial electric disturbances and preferably free of livestock - both to prevent the lines being bit through and to prevent injury to the livestock. As the magnetometers had to be buried for temperature stabilisation, it was preferable if the top 1.5 m of overburden could be dug with ease. Because of the power requirements of the recorders, mains supply had to be used for observing the long period variations. This imposed severe restrictions on site suitability. Finally, the filters and recorders had to be protected from the elements. This required some form of out-building which could be made secure against unwanted entry.

Once a suitable location had been found and permission granted, the first course of action was to install the electrodes. This gave the electrodes as much time as possible to stabilise before commencing recording. The four (or three) magnetometer holes were then dug, one

for each Jolivet variometer and one for the three-component fluxgate head (if long period measurements were to be made). The magnetometers were oriented approximately and then covered over. In this way the sensors were able to acclimatise to the temperature environment and re-settle after the agitation caused by repositioning before recording began. The filtering and recording equipment were then set-up and tested for possible malfunction caused by re-location.

This completed the first two operations of the fieldwork procedure and took typically one to two days, depending on the nature of the top 1.5 m of overburden.

As will be described in the next section, the MT equipment consisted of two independent systems. One system made observations of the short period (either 10 s to 300 s or 10 s to 1200 s) variations, the other recorded the more slowly varying phenomena (200 s to dc). These were termed the fast variation (FVSa and FVSb) and slow variation (SVS) systems respectively. The SVS required a much longer observation time than did the FVS to obtain a worthwhile amount of reasonable data. Thus it was possible to 'pair' stations and record both short and long period fluctuations at the main station, then move only the FVS to a nearby location whilst still recording with the SVS at the main station. Sites ELC and CAP, TIN and BOR and GOR and PRE were paired in this manner.

Table 3.2 lists the three letter location name, full name, geographic and geomagnetic co-ordinates, declination and observations made for each of the thirteen locations at which MT variations were recorded for this project.

Before embarking on the fieldwork programme however, it was important to discover the diurnal temperature variation at depth within the overburden. Diurnal thermal variations would considerably

TABLE 3.2

Magneto-telluric station data

Station Title	Station Name	Geographic Coordinates	Geomagnetic Coordinates (centred dipole)	Declination	Recording Period (not always continuous)
BOR	Borland	3.324W 55.224N	83.036E 58.426N	9.2W	FVS 24/4/75-01/5/75
CAP	Cappercleuch	3.217W 55.364N	83.330E 58.660N	9.1W	FVS 02/4/75-10/4/75
CRK	Craik	3.025W 55.364N	83.435E 58.497N	9.0W	FVS 06/8/74-11/8/74 SVS 06/8/74-24/8/74
DZR	Drumelzier	3.390W 55.595N	83.221E 58.786N	9.2W	FVS 18/9/74-28/9/74 SVS 15/9/74-03/10/74
ELC	Elsrickle	3.533W 55.664N	83.123E 58.879N	9.4W	FVS 24/3/75-30/3/75 SVS 24/3/75-11/4/75
ESK	Eskdalemuir	3.200W 55.314W	83.223E 58.485N	9.1W	FVS 05/8/75-11/8/75
FTH	Forth	3.681W 55.782N	83.054E 59.019N	9.5W	FVS 29/8/74-03/9/74 SVS 26/8/74-12/9/74
GOR	Gordon	2.533W 55.686N	84.154E 58.698N	8.8W	FVS 16/5/75-23/5/75 SVS 16/5/75-09/6/75
NEW	Newcastleton	2.796W 55.196N	83.554E 58.293N	8.8W	FVS 04/5/75-09/5/75 SVS 04/5/75-12/5/75
PRE	Preston	2.255W 55.836N	84.703E 58.782N	9.2W	FVS 04/6/75-09/6/75
SAL	Saltoun	2.853W 56.910N	84.703E 59.903N	9.0W	FVS 26/5/75-03/6/75
TIN	Tinwald	3.561W 55.110N	82.718E 58.367N	9.3W	FVS 16/04/75-23/4/75 SVS 16/4/75-02/5/75
TOW	Towhouse	2.369W 54.968N	83.836E 57.994N	9.3W	FVS 16/10/74-24/10/7 SVS 06/10/74-24/10/7

affect the electrode potential associated with each electrode. This could lead to an incorrect estimate of the amplitude of the telluric field at periods close to diurnal. Also, the Jolivet variometers were considered to be temperature variant and thermal fluctuations would affect their recordings.

Daily temperature data for 1963 were obtained from the Eskdalemuir observatory. The year 1963 was chosen because it was the year that exhibited the widest recorded temperature variations in recent times. Table 3.3 gives the mean monthly values of the daily maximum, minimum and four foot earth temperatures, together with their associated sample standard deviations. The values are plotted in figure 3.3. The amplitude of the annual variation at the surface is about 17 K and at four feet is 8.2 K.

The amplitude of the thermal variation at depth in a medium, $T_Z(w)$, with respect to that at the surface of the medium, $T_0(w)$, is given by

$$T_Z(w) = T_0(w) \exp\left[-Z\sqrt{\frac{w}{2k}}\right], \qquad (3.1)$$

where w is the frequency of the incident variation

Z is the depth into the medium

and k is the thermal diffusivity of the medium.

Substituting the values T_0 = 17 K, T_Z = 8.2 K, Z = 1.22 m and $w = 2 \times 10^{-7}$ gives a value of thermal diffusivity of 2.8×10^{-7} m^2 s^{-1}. The possible range of diffusivities for soils is given by Monteith (1973), who states a maximum of 8.5×10^{-7} m^2 s^{-1} for damp sandy soil and a minimum of 1×10^{-7} for dry peat. Assuming the extreme value of 8.5×10^{-7}, and a daily variation of 17.5 K (the largest recorded in 1963) gives the variation of T_Z with Z plotted in figure 3.4 for a diurnal frequency. A more realistic maximum variation at a depth Z

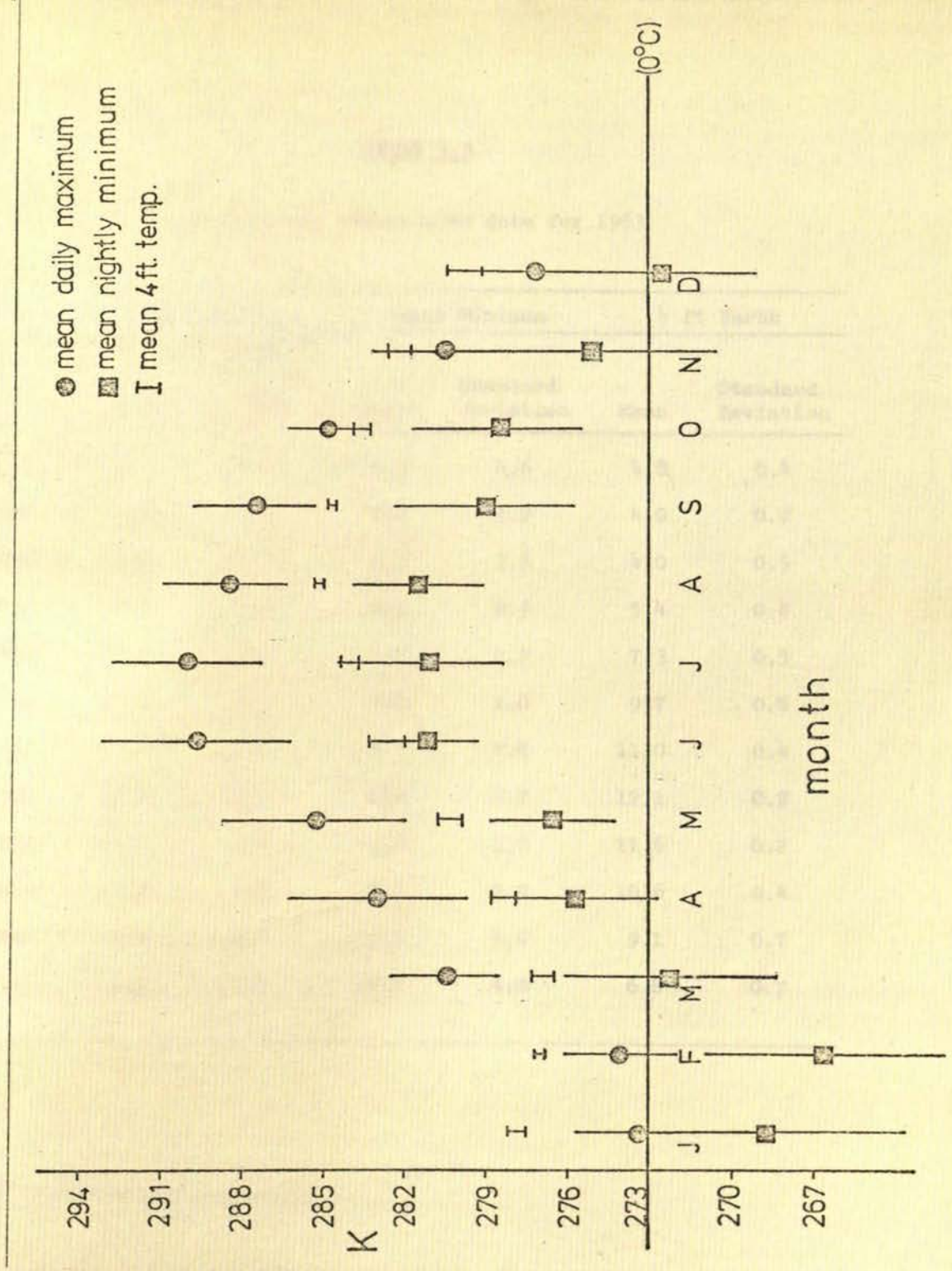

Figure 3.3 Eskdalemuir temperature data for 1963 -monthly means with sample standard deviations

TABLE 3.3

Eskdalemuir temperature data for 1963

	Day Maximum		Night Minimum		4 ft Earth	
	Mean	Standard deviation σ_{n-1}	Mean	Standard deviation	Mean	Standard deviation
Jan	0.6	2.2	-4.3	4.6	4.8	0.4
Feb	1.2	2.2	-6.3	3.9	4.0	0.2
Mar	7.4	1.9	0.8	3.8	4.0	0.5
Apr	9.9	3.2	2.7	2.9	5.4	0.4
May	12.2	3.3	3.6	2.2	7.3	0.5
Jun	16.9	3.6	8.2	1.8	9.7	0.8
Jul	17.2	2.9	8.1	2.8	11.0	0.4
Aug	15.6	2.2	8.4	2.7	12.1	0.2
Sep	14.5	2.2	5.9	3.2	11.6	0.2
Oct	11.7	1.3	5.5	2.9	10.6	0.4
Nov	7.5	2.7	2.2	4.6	9.1	0.7
Dec	4.1	2.4	-0.4	4.0	6.8	0.7

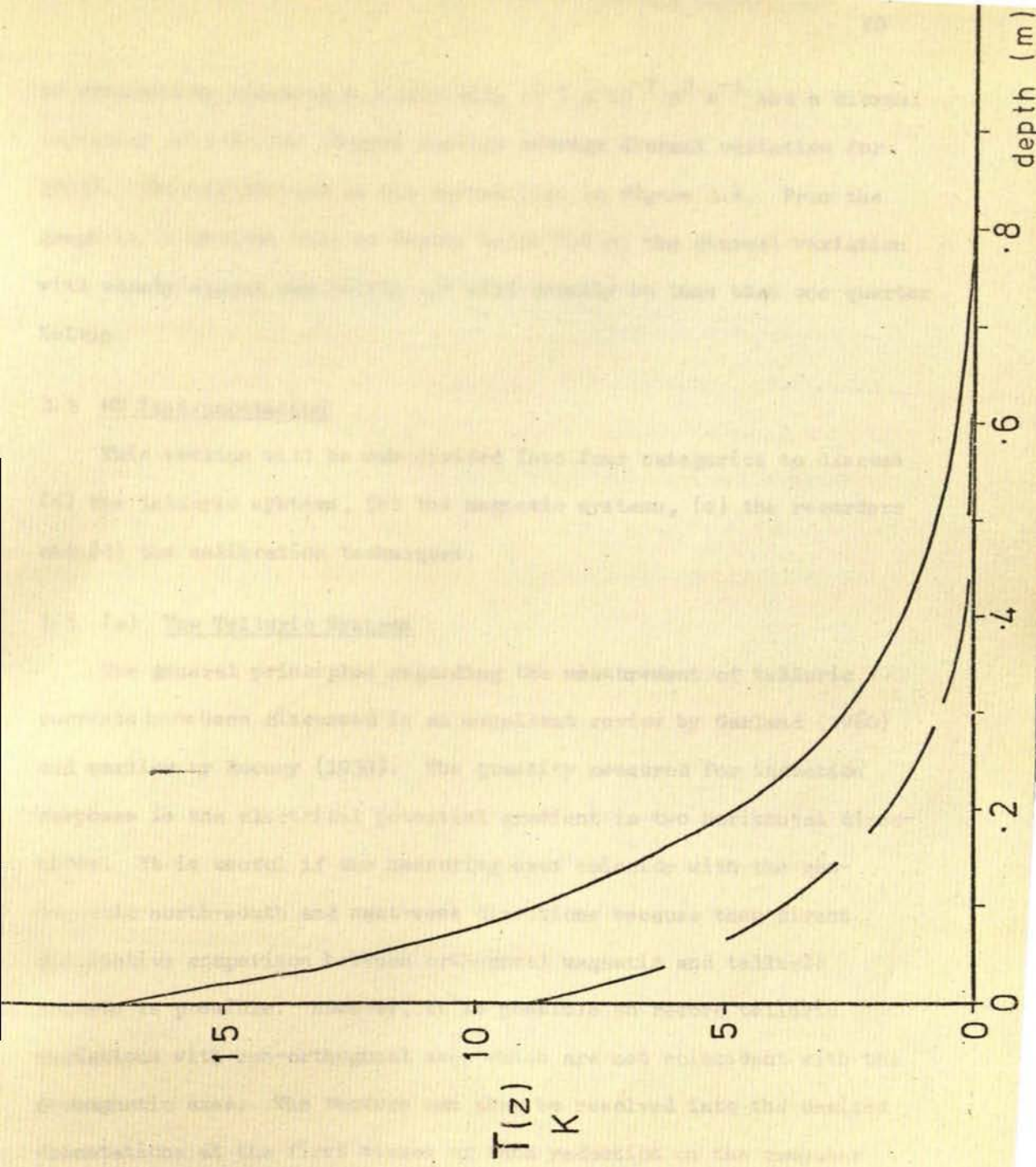

Figure 3.4 Diffusion of diurnal thermal variation with depth

——— T_o=17 K, κ=8.5x10^{-7} m^{2}s^{-1}

— — — T_o= 9 K, κ=5.0x10^{-7} m^{2}s^{-1}

is obtained by assuming a diffusivity of 5×10^{-7} m^2 s^{-1} and a diurnal variation of 9 K (the largest monthly average diurnal variation for 1963). This is plotted as the dashed line in figure 3.4. From the graph it is obvious that at depths below 0.4 m, the diurnal variation will rarely exceed one Kelvin and will usually be less than one quarter Kelvin.

3.3 MT Instrumentation

This section will be sub-divided into four categories to discuss (a) the telluric systems, (b) the magnetic systems, (c) the recorders and (d) the calibration techniques.

3.3 (a) The Telluric Systems

The general principles regarding the measurement of telluric currents have been discussed in an excellent review by Garland (1960) and earlier by Rooney (1939). The quantity measured for induction purposes is the electrical potential gradient in two horizontal directions. It is useful if the measuring axes coincide with the geomagnetic north-south and east-west directions because then direct qualitative comparison between orthogonal magnetic and telluric records is possible. However, it is possible to record telluric variations with non-orthogonal axes which are not coincident with the geomagnetic axes. The vectors can then be resolved into the desired orientations at the first stages of data reduction on the computer (Rooney, 1939).

All that is required to measure the potential gradient is a recording of the potential difference between electrodes placed in the earth. Most of the problems encountered when measuring telluric currents can be traced to the electrodes and accordingly, the design and form of the electrodes must be chosen with care. Non-polarising

electrodes commonly employed for DC resistivity surveying have the advantages of low contact resistance and low contact potential. However, these factors must be balanced against a diurnal contact potential variation (due to the necessity of having the electrodes close to the surface) and solution infiltration of the soil. Buried metal electrodes are considered to be more effective for recording low frequency variations of the telluric field (Garland, 1960). Of the commonly available metals, lead appears most suitable because of the low value of electromotive force between it and a solution of its salt (typically -0.1 V, Garland, 1960). Also, lead will not deteriorate appreciably with use. Accordingly, the electrodes employed for the MT project were constructed of lead.

It was decided to use cylindrical electrodes rather than the more conventional flat plate design. This was to reduce the installation and retrieval time of the electrode array. Each electrode was constructed from a lead sheet of thickness 2.5 mm and sides 0.45 m by 0.45 m, which formed a cylinder of radius 0.13 m. The external surface area of the electrodes was therefore 0.2 m^2. Approximately 0.3 m of each flex of a three-core cable was bared and soldered to the electrode, ensuring that the copper was not exposed. Finally, a nylon bar was fixed internally, approximately 0.05 m from the top of the cylinder, to facilitate removal of the electrode from the ground. The cable was knotted to the bar to ensure that any stresses on the electrode lines would not result in loss of connection to the electrode.

The electrode holes were bored out with a hand auger to a depth of approximately 1 m. The top of the electrode was therefore at a depth greater than 0.5 m and accordingly, the diurnal variation in electrode temperature was less than 0.25 K. The thermal variation in

contact potential was thus kept below 0.1 per cent. When covering an electrode, the inner part of the cylinder was filled first to ensure that the cylinder would not collapse on compacting the top soil and that ground contact would be as firm as possible. Inter-electrode contact resistances were very dependent on overburden material but were typically of the order of a few hundreds of ohms.

The electrode configuration utilised was the 'L' shape with each arm usually 100 m long. Electrode separations as small as 15 m (Simon and Rossignol, 1974) and as large as 262 km (Berlin observatory) have been reported in the literature. However, a balance must be made between short lengths that will be greatly influenced by near-surface inhomogeneities and long lengths that will average the field variation. Also, it is obviously desirable to keep the electrode separations as small as possible because of the logistics involved. The cable employed for the electrode lines was three-core 15 amp rubber-covered mains flex. Each flex was 50 m long thus necessitating joining cable lengths together. Great care was taken that the joints were insulated from the ground, both by liberal use of silicon grease and insulating tape and by slightly raising the joint above ground surface. If there was live-stock in the field, the cables were checked thoroughly at least twice a day to ensure there were no cuts, etc. which could act as alternative earthing points.

The telluric amplifiers and filter stages were based on a design by Trigg (1972) and are reported fully in Rooney (1976). Problems were encountered with the high-pass (-3dB point at 10^{-4} Hz) filter stages of the system. The capacitor of each stage intermittently discharged, which caused the telluric records to go off scale for a period of three hours, i.e. the recharging time of the capacitor. This was considered to be due to high humidity in the atmosphere

causing shorting across the high value resistances (113 MΩ and 226 MΩ) in the filter stage. The discharges could not be eliminated therefore the high pass filter stage was bypassed and the dc potential between electrodes was backed-off for the SVS. This potential was typically of the order of a few tens of millivolts and was backed-off across a 1 MΩ resistor. Thus, the current taken from the dry batteries used as power sources for the back-off unit was less than a microamp.

Supplementary filters, of the same design as those outlined by Trigg (1972), were employed to give three band widths, 10 s - 300 s (FVSa), 10 s - 1200 s (FVSb) and 200 s to dc (SVS). If the two systems (FVS and SVS) were at different locations, the SVS telluric variations were common-mode rejected and then amplified by Keithley null-detector microvoltmeters (model 155). A block diagram of the telluric systems is given in figure 3.6.

The only problem encountered when measuring the telluric field variations, apart from the high-pass filter discharge, was with very long period variations of the potential between electrodes. This was only important for the SVS because either of the two FVS high pass supplementary stages (300 s for a and 1200 s for b) filtered out the dc components. At most sites, the electrodes settled after three or four days and the longest period variation discernable was diurnal. However, at GOR both the telluric components showed a linear variation in potential levels and accordingly the back-off system had to be constantly re-adjusted.

3.3 (b) The Magnetic Systems

Because of the vastly different scales between magnetic field variations at Pc3 and Pc4 micropulsation periods (typically of order one nanotesla) compared to those at one hour (typically one hundred

nanotesla), it is extremely difficult to construct a sensor that covers the whole frequency range 10^{-4} Hz to 10^{-1} Hz. The magnetometer would need to have high sensitivity and extremely low drift characteristics and would therefore be costly. To facilitate recording the magnetic field variations as accurately as possible over a wide band width therefore, two types of magnetometer were employed for this study.

For the FVS band (10 s to either 300 s or 1200 s), the variometers used were basically suspended magnet type. Each of the three components was measured by a single-component Jolivet magnetometer . The instrument, designed by Jolivet (1966) and modified by Albouy et al. (1971) is superior in design to conventional suspended magnet systems because it does not measure the field strength by deflection. A feedback current flowing through Helmholtz coils induces a magnetic field which re-orientates the magnet back to the (arbitrary) zero position. The required field to perform the operation is evaluated by an optical system consisting of a light source, various mirrors and a differentiating photocell. Thus, the field variation is measured by monitoring the variation of the feedback current. The output voltage of the sensor is 0.5 mV per nanotesla with a flat frequency response for periods greater than 5 s. The magnet and its suspension were protected from shocks by being immersed in a transparent liquid of the same density as the magnet.

The method for orienting each variometer into the required H, D and Z co-ordinates is described in full by Rooney (1976).

The variometers were buried in three separate thermally insulated containers, the tops of which were greater than 0.5 m below the surface, and were separated from each other by a distance greater than 2 m. The outputs from each variometer were amplified by Keithley micro-voltmeters and then band-pass filtered by identical circuits to those

used for the FVS telluric components. A block diagram of the Jolivet magnetometer system is given in figure 3.6.

The magnet and suspension of the Jolivet variometer had a natural resonant frequency of 0.5 Hz. On some occasions, for no apparent reason, one or more Jolivets began to resonate. The low pass filter response at 0.5 Hz was -17 dB, but this was not sufficient to filter the high amplitude oscillation output. One remedy, which worked on occasion, was to turn the power to the variometer off for a period of a couple of hours. At one site however, GOR, use of the Jolivet magnetometers had to be discontinued.

For the SVS band (0.005 Hz to 0 Hz), a three-component magnetometer based on the fluxgate principle was employed. The magnetometer was manufactured by EDA Electronics of Ottawa and was based on a design by Trigg et al. (1971). The output voltage of the unit was about 30 mV per nanotesla with a quoted resolution of one nanotesla (the resolution was in fact found to be better than that quoted). A temperature dependence of less than one nanotesla per Kelvin was specified by the manufacturers. With the head under more than 0.5 m of topsoil, the diurnal variation due to thermal diffusion was of the order of one tenth of a nanotesla. The output level from the fluxgate unit was sufficiently high not to warrant amplification and accordingly, the variations had only to be low pass filtered - 3 dB point at about 200 s - before recording. The block diagram of the Fluxgate magnetometer system is illustrated in figure 3.6.

The internal hour timer was removed from the unit because of the filter decay effect produced. Otherwise, the magnetometer performed very satisfactorily.

The problem of resonant oscillations of the Jolivet magnetometers became too serious to continue using them. Accordingly, the Fluxgate

magnetometer had to be used for the FVS at three locations - GOR, SAL and PRE. A comparison between Jolivet and Fluxgate H-components was made at GOR. Part of the run is illustrated in figure 3.5a and the ordinary and normalised transformed ordinary coherences between the traces are given in 3.5b. Although the Fluxgate record contained more noise, the coherences show that the traces contain correlatable signal for periods greater than about 20 s. After a visual inspection of the comparison test, it was decided to attempt to record MT variations at the remaining three locations with the Fluxgate magnetometer rather than abandon the FVS programme. This decision proved worthwhile for SAL and PRE but not for GOR.

3.3 (c) The Recorders

The recorders employed for the MT work were Watenabe five-channel servo-type potentiometric recorders, model HC611-L. The five field variations were inscribed by liquid ink pens with five different colours of ink onto paper chart 0.282 m wide. A sixth pen inscribed a timing pulse at minute intervals for the FVS and also an event pulse at hour intervals on both systems. The chart drive was governed by the supply frequency and, because mains power was used, was extremely regular. The chart speed selected was 15 mm per minute for FVSa (10 s - 300 s band), 7.5 mm per minute for FVSb (10 s - 1200 s), or 30 mm per hour for the SVS. The five pens were designed so that each could travel the full chart width and the thickness of an ink trace was typically 0.5 mm. This gave a dynamic range for the recorder of 55 dB which compares favourably with most other analogue recorders. Because the pens were not coincident, it was necessary to record the parallax between them. An accurate determination of parallax was critical if reliable estimates of phase were desired. An error of

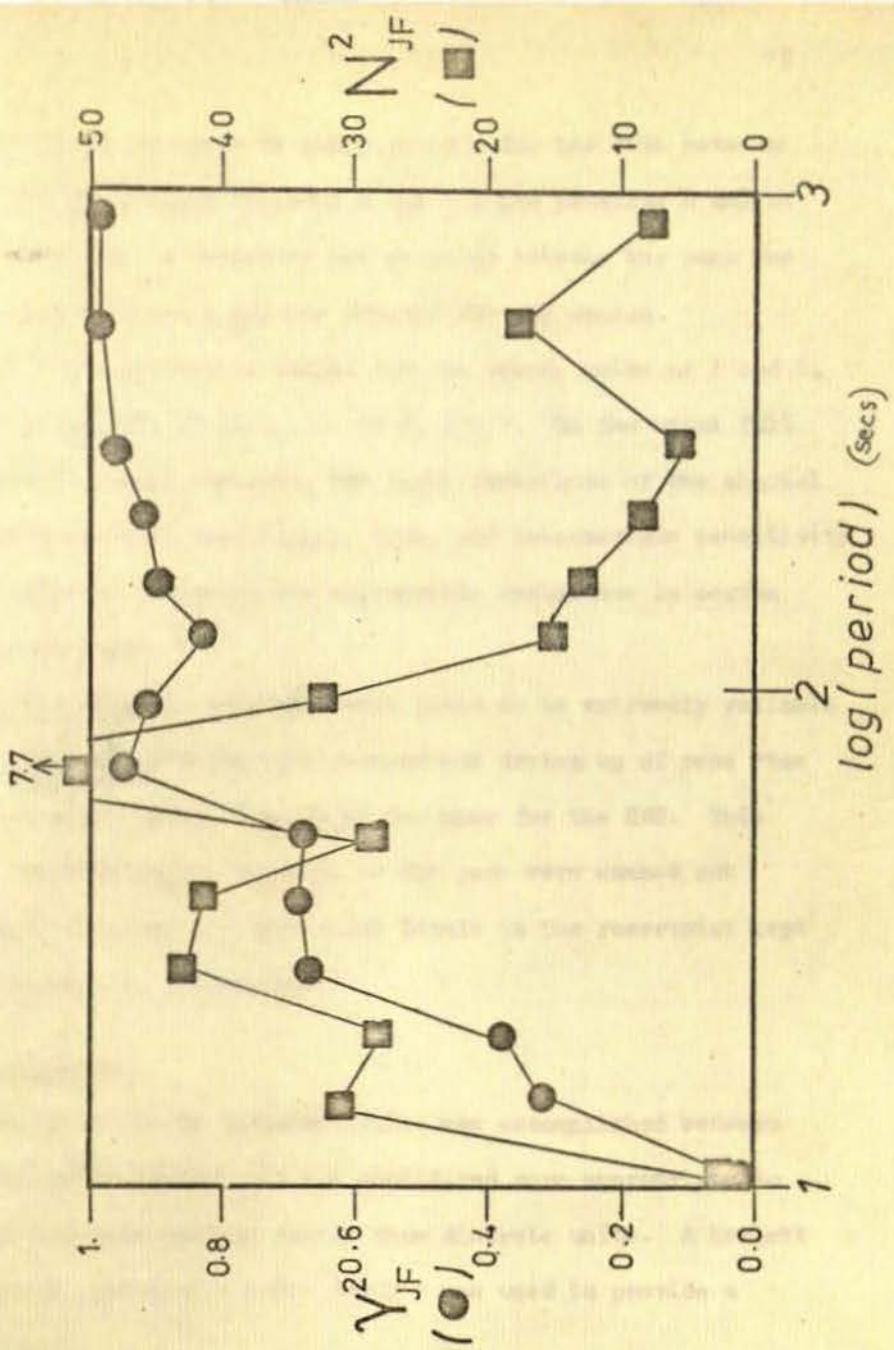

Figure 3.5b Ordinary coherences(circles) and Normalised transformed ordinary coherences(squares) between the Jolivet and the Fluxgate records of figure 3.5a

2 mm would introduce an error in phase at 10 s for the FVSb between the N trace and the D trace (typical N pen - D pen parallax 8 mm) of over 360°. Therefore, a record of the parallax between the pens was taken daily, and whenever a pen was removed for any reason.

The full scale deflection ranges were in decade units of 1 and 5, i.e. 1 mV, 5 mV, 10 mV, 50 mV ..... 50 V, 100 V. On the usual full scale deflection ranges employed, the input resistance of the channel was one megaohm per unit volt range. Thus, any intermediate sensitivity could be selected by inserting the appropriate resistance in series with the channel input.

In use, the Watenabe recorders were found to be extremely reliable and robust. The only problem that occured was drying up of pens when on the slowest chart speed, i.e. 30 mm per hour for the SVS. This proved most frustrating but usually, if the pens were washed out thoroughly and often and the liquid ink levels in the reservoirs kept high, could be kept to a minimum.

3.3 (d) Calibration

Calibration of the MT instrumentation was accomplished between the two stages of fieldwork. It was considered more appropriate to calibrate the complete systems rather than discrete units. A Hewlett Packard function generator - model 3310B - was used to provide a sinusoidal signal.

For the telluric system, the calibration technique was as illustrated in figure 3.6a. For each component, the function generator output, the 10 s - 300 s band pass system (FVSa) output, the 10 s - 1200 s band pass system (FVSb) output and the two 200 s - DC systems (SVS) outputs were monitored on the Watenabe recorder. The sinusoidal signal was varied from 8 s to 2000 s and at least twenty complete

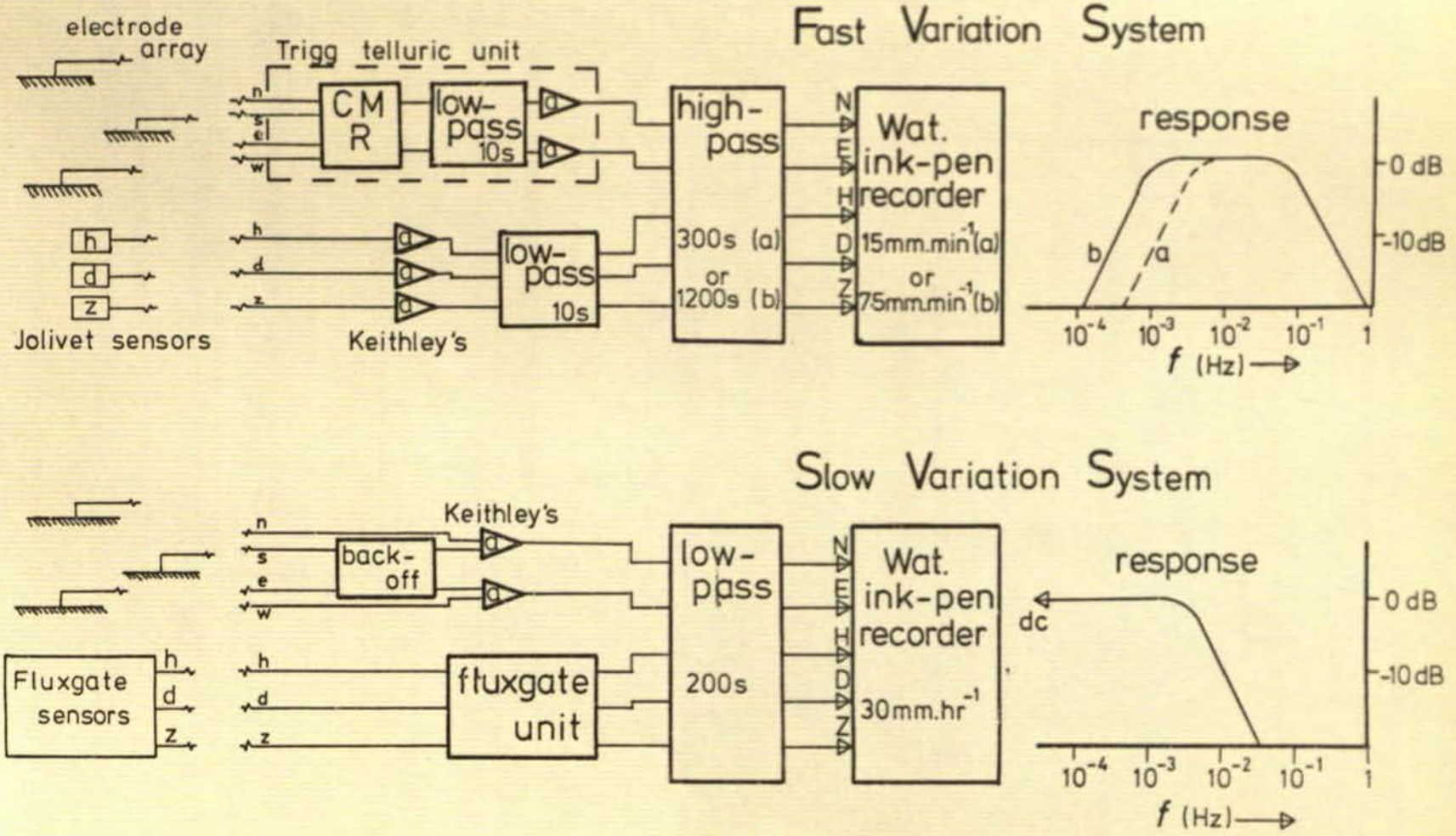
Fast Variation System
electrode array
Trigg telluric unit
n
s
e
w
CM R
low-pass 10s
high-pass
300s (a)
or
1200s (b)
N
E
H
D
Z
Wat. ink-pen recorder
15mm.min⁻¹(a)
or
75mm.min⁻¹(b)
h
d
z
Jolivet sensors
Keithley's
low-pass 10s
response
0 dB
-10dB
b
a
10⁻⁴ 10⁻³ 10⁻² 10⁻¹ 1
f (Hz)
Slow Variation System
Keithley's
back-off
low-pass
200s
Wat. ink-pen recorder
30mm.hr⁻¹
Fluxgate sensors
fluxgate unit
response
dc
0 dB
-10dB
10⁻⁴ 10⁻³ 10⁻² 10⁻¹ 1
f (Hz)

Figure 3.6 Block diagram of the Magneto-Telluric systems

FVSa - 10s-300s Period Band
FVSb - 10s-1200s " "
SVS - 200s-d.c. " "

Figure 3.6a Block diagram of method of calibrating the telluric systems

Figure 3.6b Block diagram of method of calibrating the magnetic systems

(i) -FVS, Jolivet magnetometers
(ii)-SVS, Fluxgate magnetometers

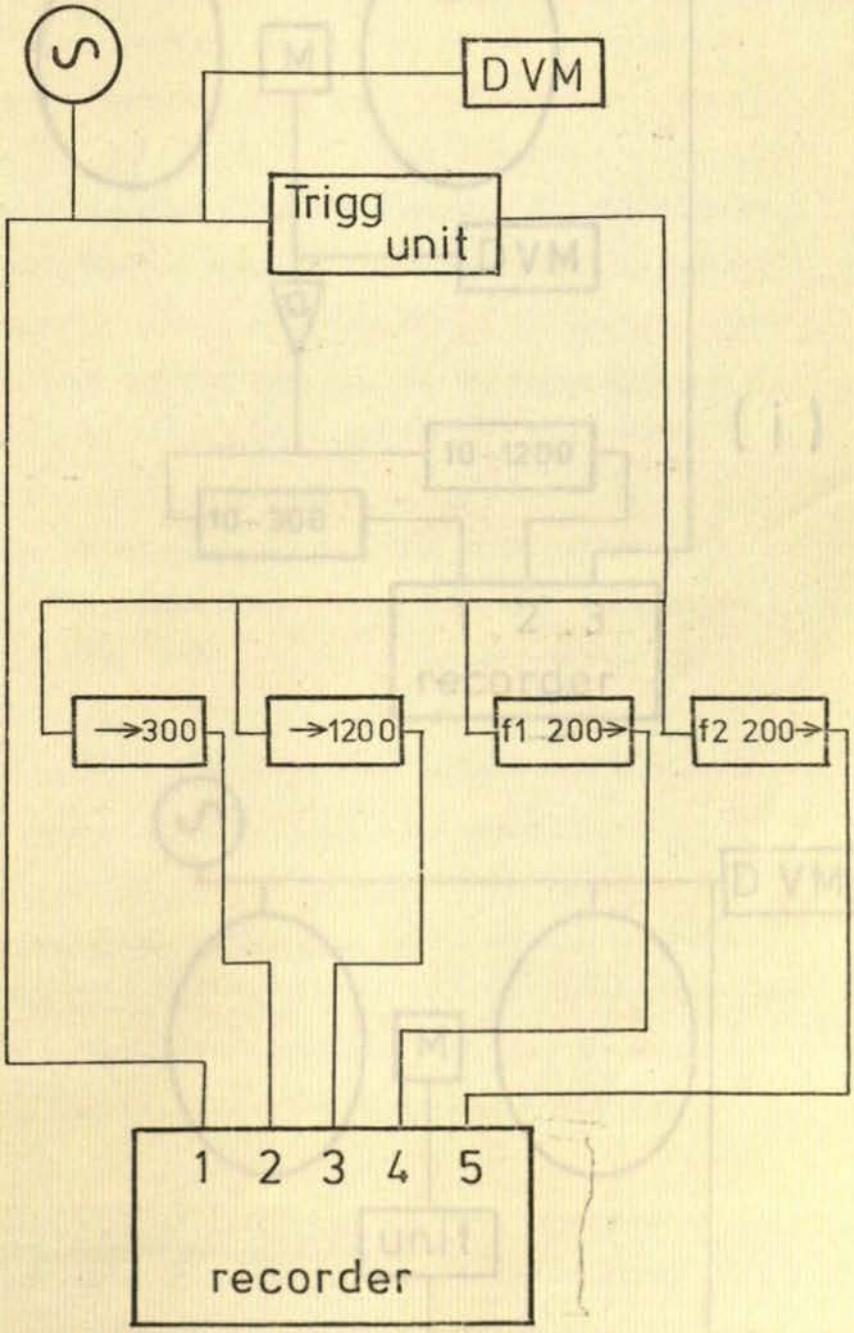
DVM
Trigg unit
→300
→1200
f1 200→
f2 200→
1 2 3 4 5
recorder

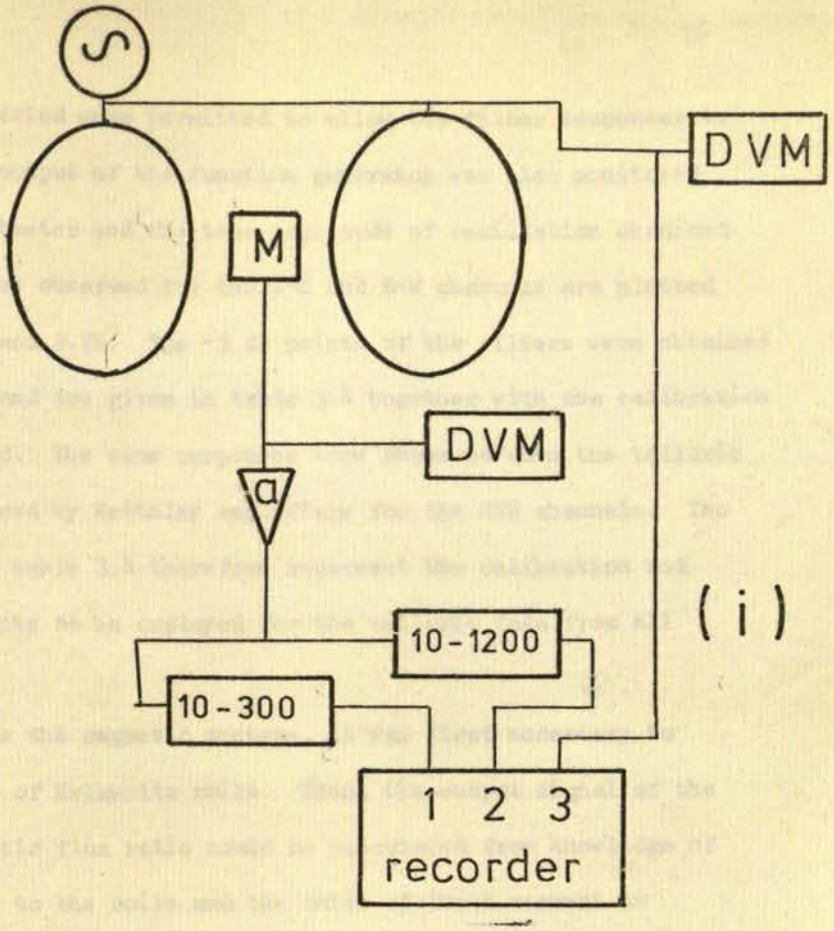
S
DVM
M
DVM
a
10-1200
10-300
1 2 3
recorder

(i)

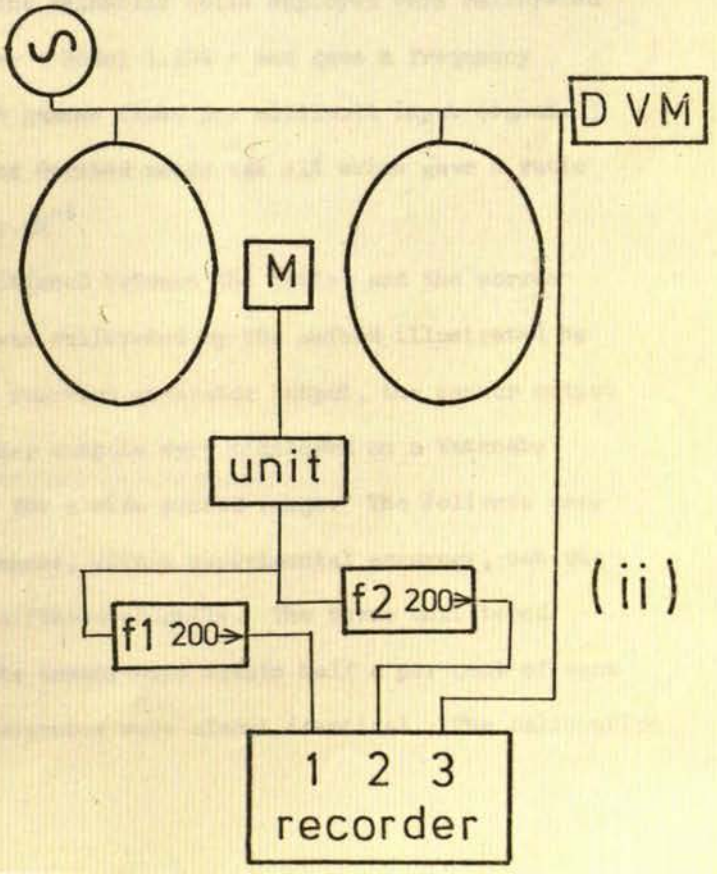
S
DVM
M
unit
f2 200
f1 200
1 2 3
recorder

(ii)

cycles at each period were permitted to allow the filter responses to stabilise. The output of the function generator was also monitored on a digital voltmeter and the true amplitude of oscillation obtained.

The responses observed for the N-S and E-W channels are plotted in figures 3.7a and 3.7b. The -3 dB points of the filters were obtained from the graphs and are given in table 3.4 together with the calibration factors estimated. The same responses were observed when the telluric units were replaced by Keithley amplifiers for the SVS channels. The values listed in table 3.4 therefore represent the calibration and filter coefficients to be employed for the telluric data from all sites.

To calibrate the magnetic systems, it was first necessary to calibrate a pair of Helmholtz coils. Then, the output signal of the systems to magnetic flux ratio could be calculated from knowledge of the input signal to the coils and the ratio of input current to magnetic flux induced. The Helmholtz coils employed were calibrated by a Forster Oersted meter - Model 1.104 - and gave a frequency independent ratio of 5.04 gammas field per millivolt input signal. The quoted accuracy of the Oersted meter was ±1% which gave a ratio accuracy of $5.04 \pm 0.05\ \gamma.mV^{-1}$.

Each sensor was positioned between the coils, and the corresponding magnetic system was calibrated by the method illustrated by block diagram 3.6b. The function generator output, the sensor output and the two relevant filter outputs were monitored on a Watenabe recorder for each sensor for a wide period range. The Jolivets were found to give equal responses, within experimental accuracy, but the response of the filters differed slightly. The three unfiltered components of the Fluxgate sensor were within half a per cent of each other and their filter responses were almost identical. The calibration

Figure 3.7 Responses of the telluric channels

0dB = 1 (mV/km)/FSD in (mV/km)

Figures 3.8 & 3.9 Responses of the magnetic channels

a - Jolivet magnetometers

0dB = 0.19 nT/FSD in mV for H & D

= 0.18 nT/FSD in mV for Z

b - Fluxgate magnetometers

0dB = 0.032 nT/FSD in mV for H,D & I

N-channel

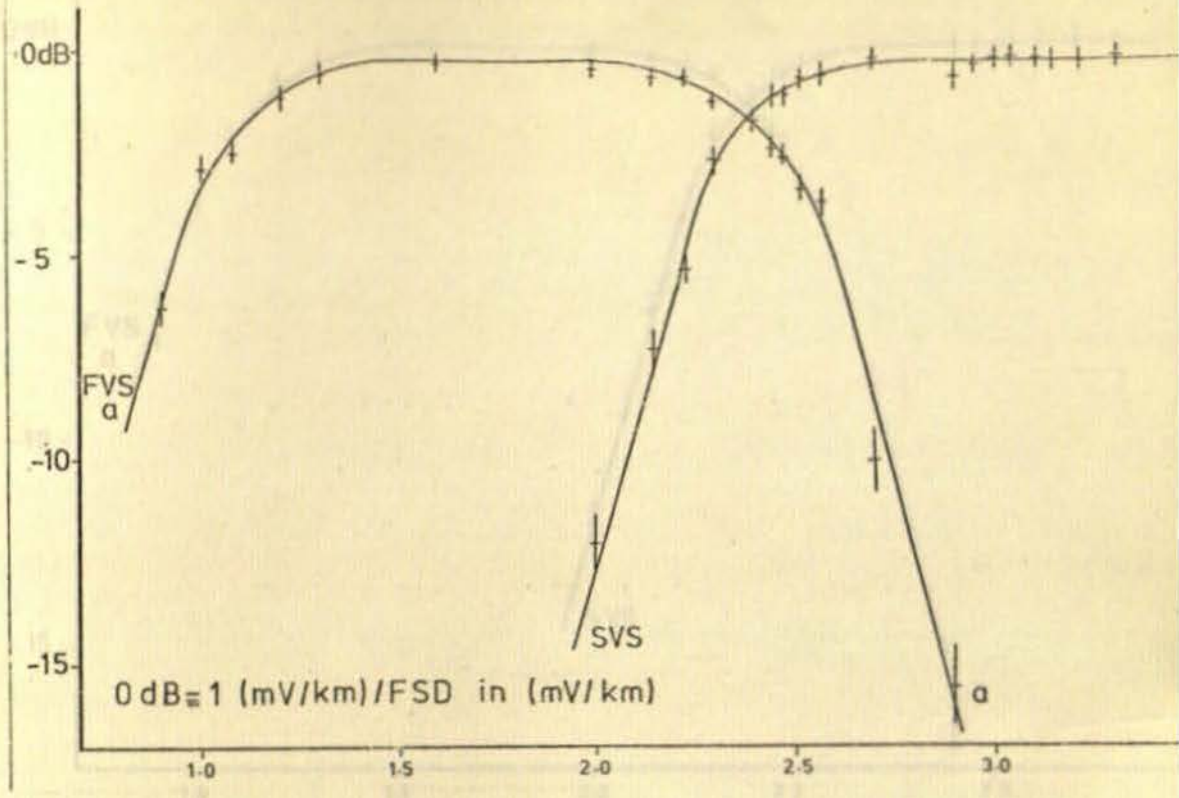
0dB
-5
-10
-15
FVS
a
SVS
a
0 dB = 1 (mV/km)/FSD in (mV/km)
1.0
1.5
2.0
2.5
3.0

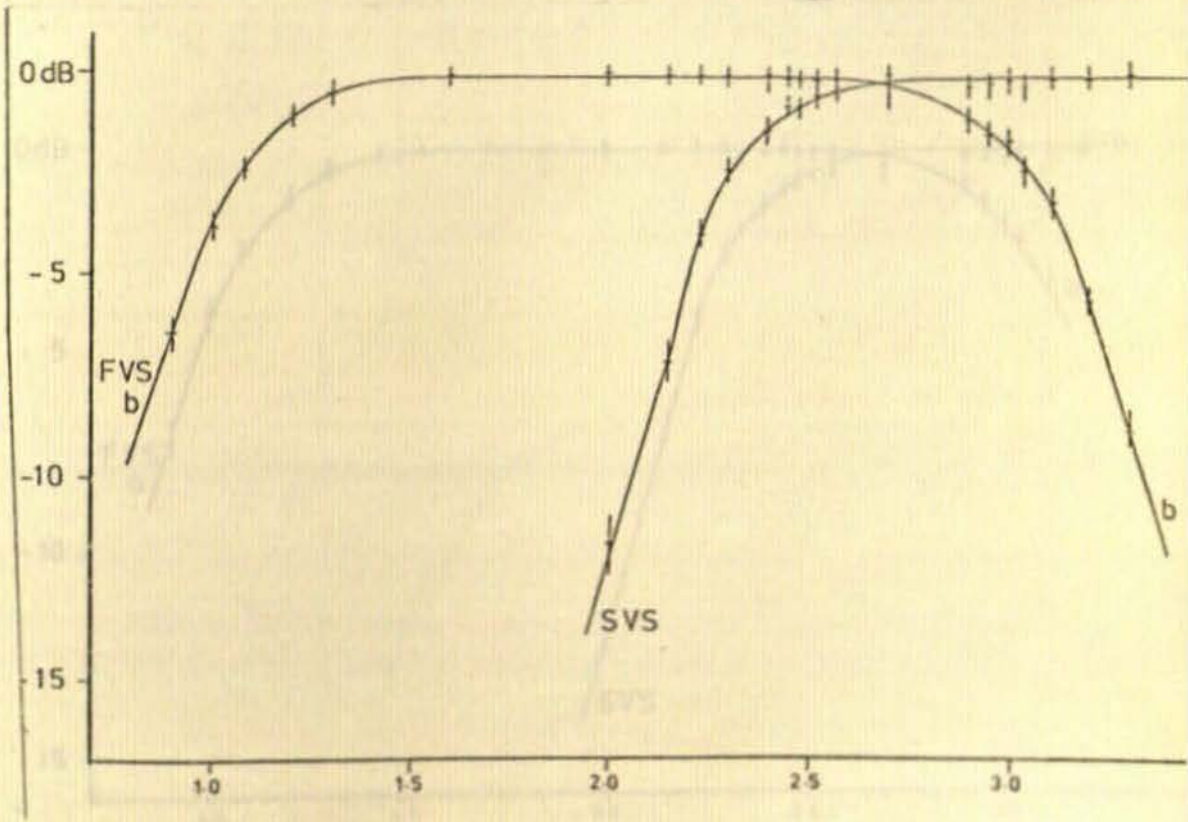
0dB
-5
-10
-15
FVS
b
SVS
b
1.0
1.5
2.0
2.5
3.0

E-channel

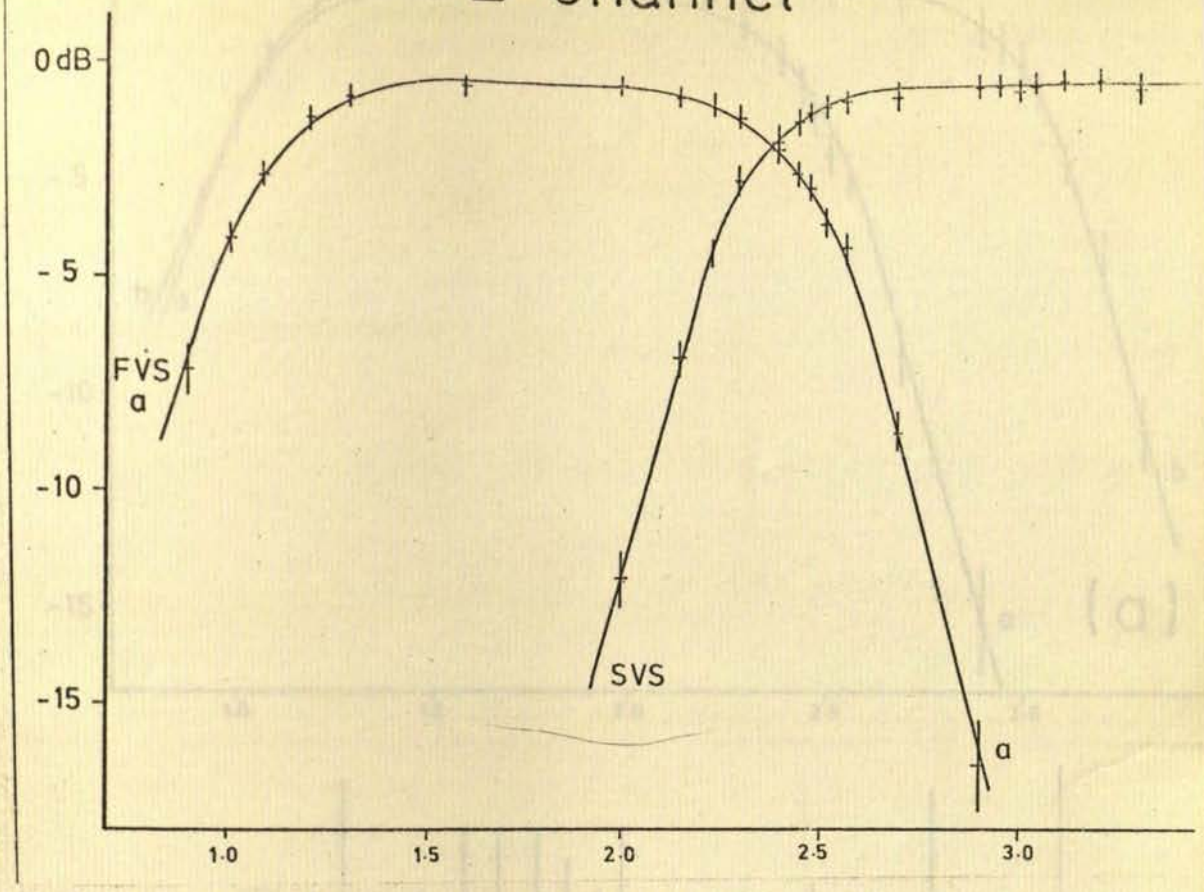
0 dB
- 5
-10
-15
FVS
a
SVS
a
1·0
1·5
2·0
2·5
3·0

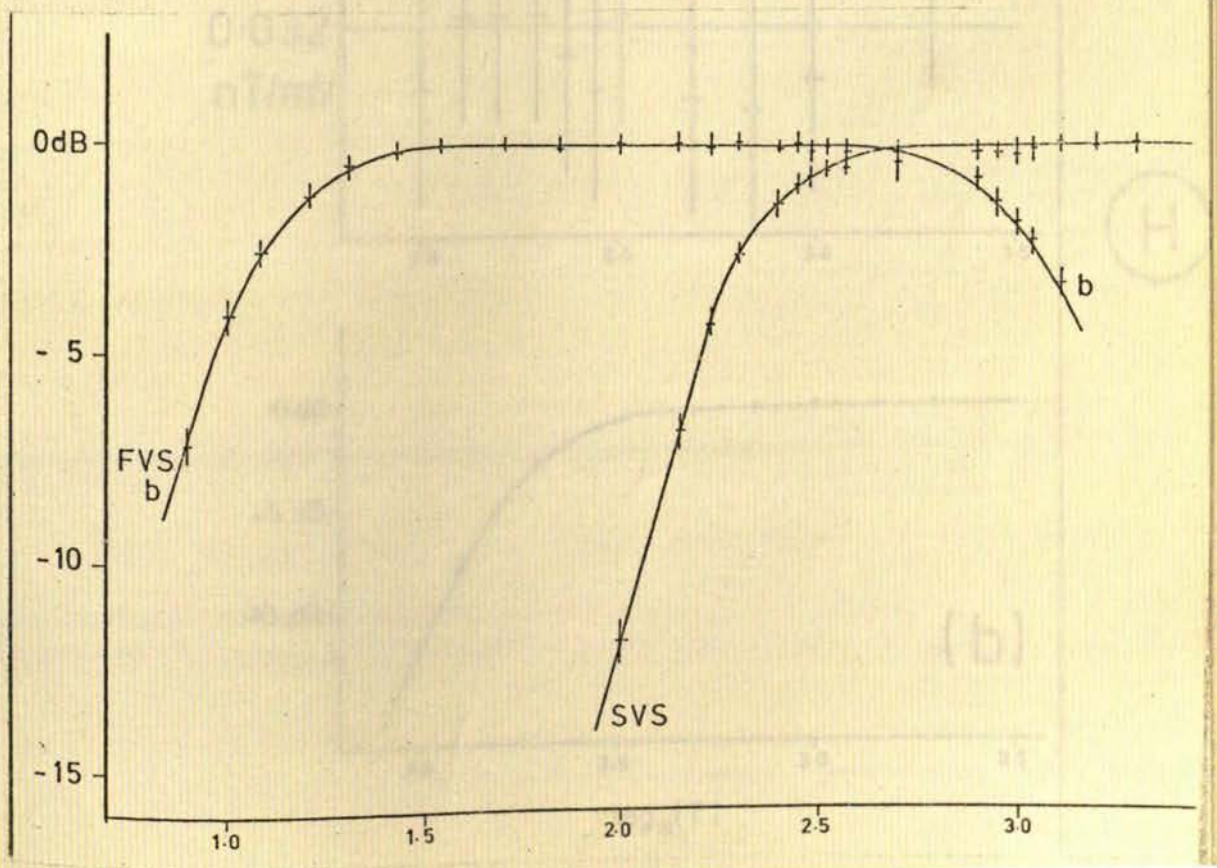
0dB
- 5
-10
-15
FVS
b
SVS
b
1·0
1·5
2·0
2·5
3·0

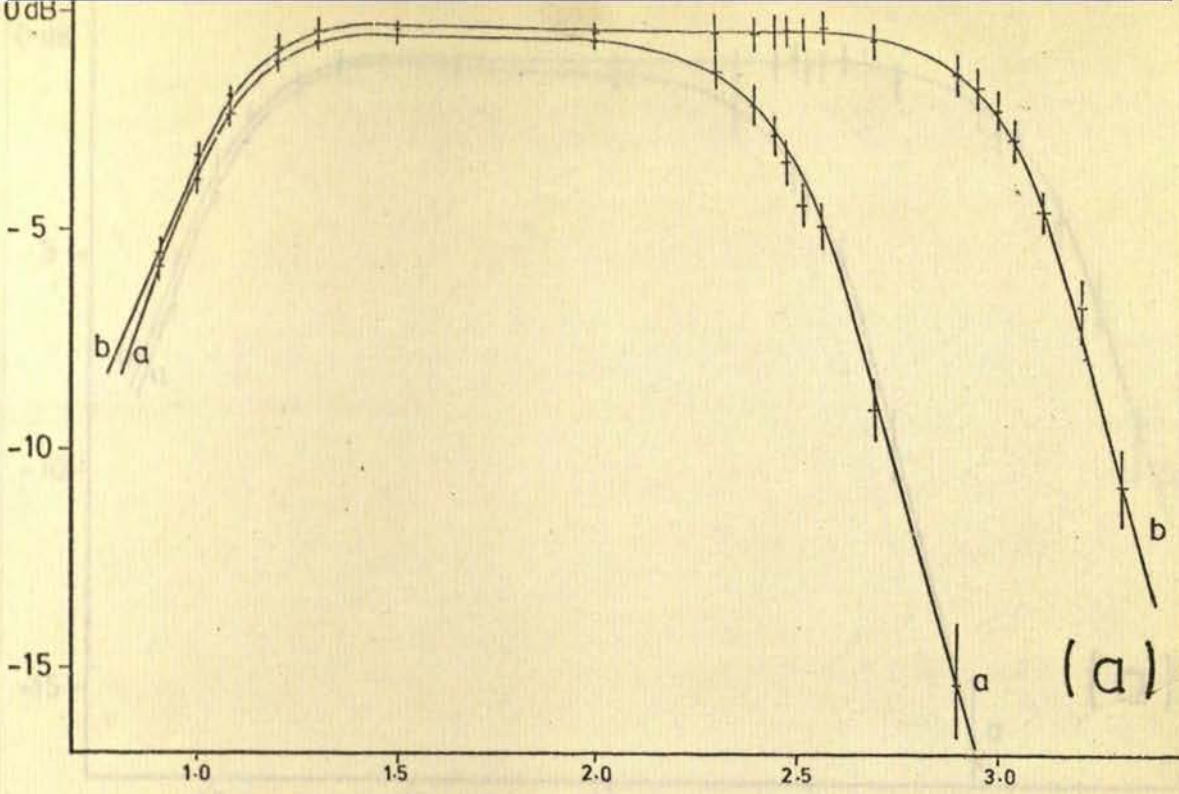
0 dB
-5
-10
-15
b
a
a
b
(a)
1·0
1·5
2·0
2·5
3·0

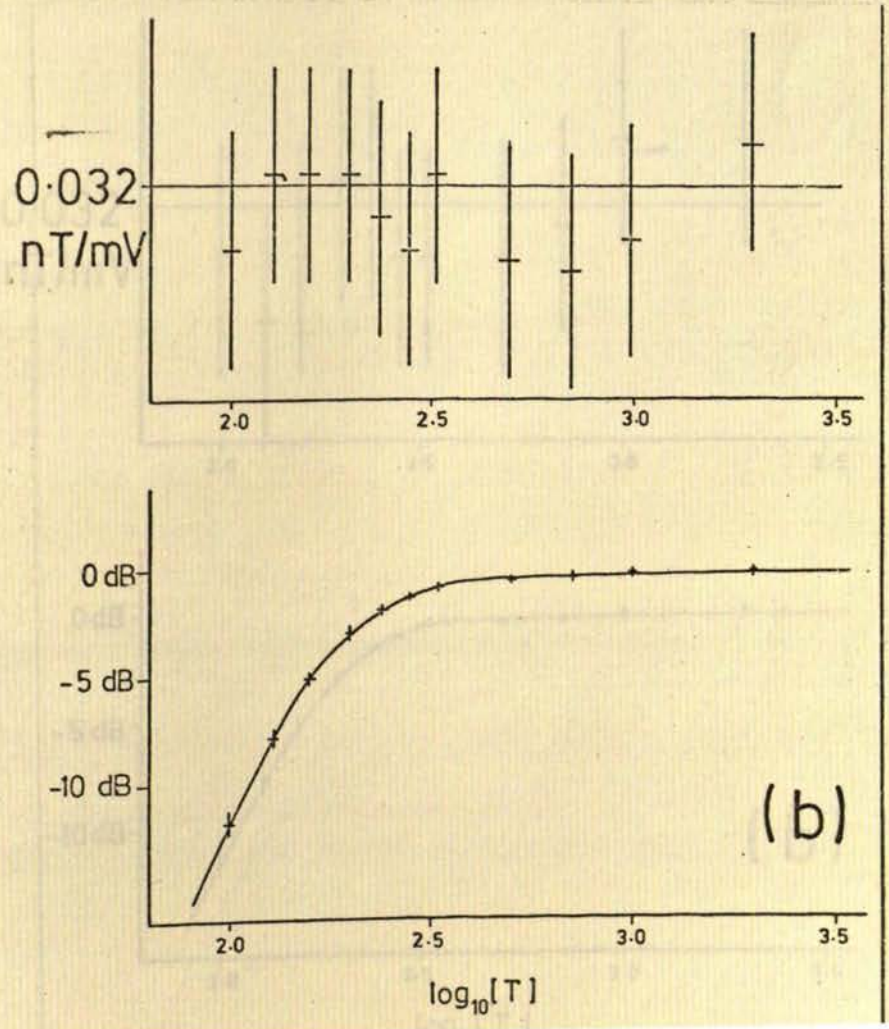
0·032
nT/mV
2·0
2·5
3·0
3·5
0 dB
-5 dB
-10 dB
(b)
2·0
2·5
3·0
3·5
log10[T]

H

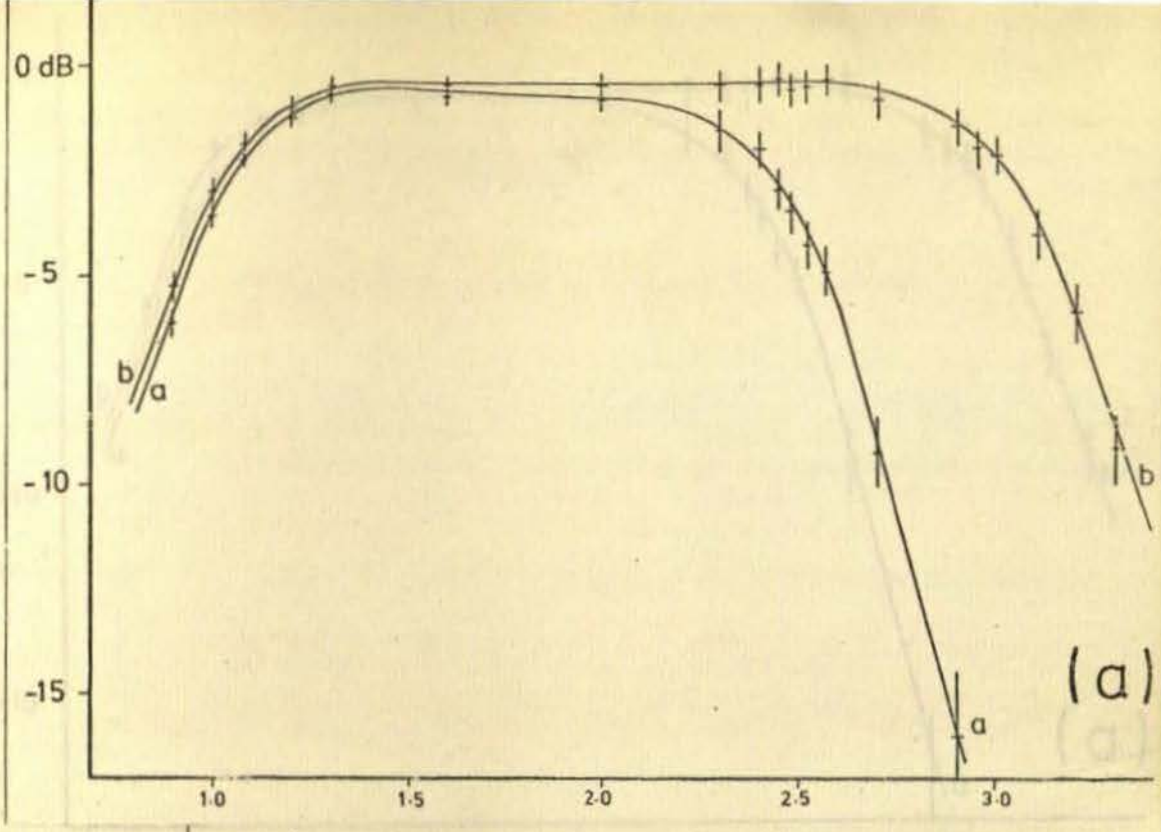
0 dB
-5
-10
-15
b
a
a
b
(a)
1·0
1·5
2·0
2·5
3·0

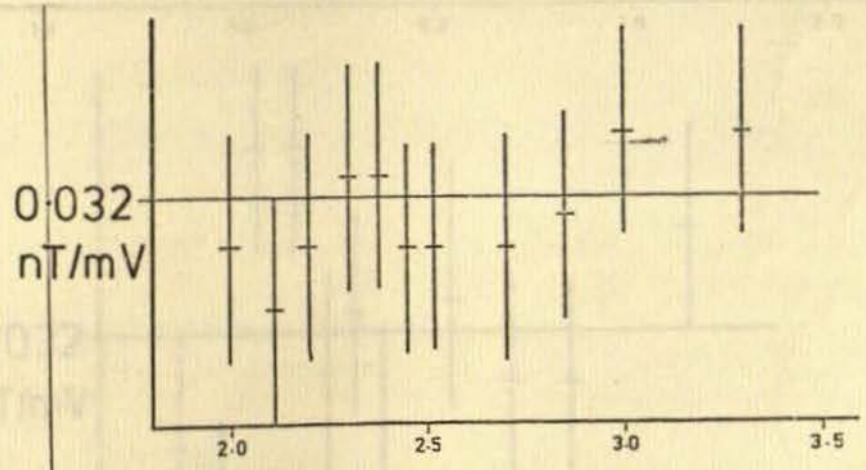
0·032
nT/mV
D
2·0
2·5
3·0
3·5

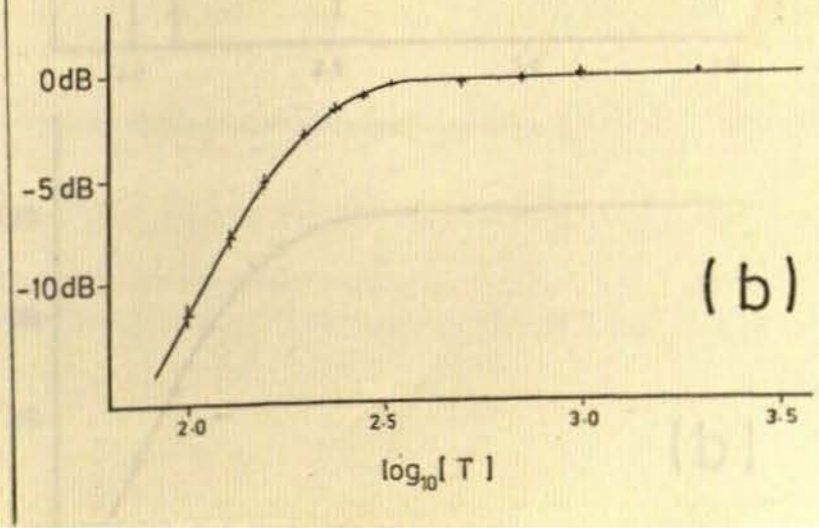
0dB
-5 dB
-10dB
(b)
2·0
2·5
3·0
3·5
log10[T]

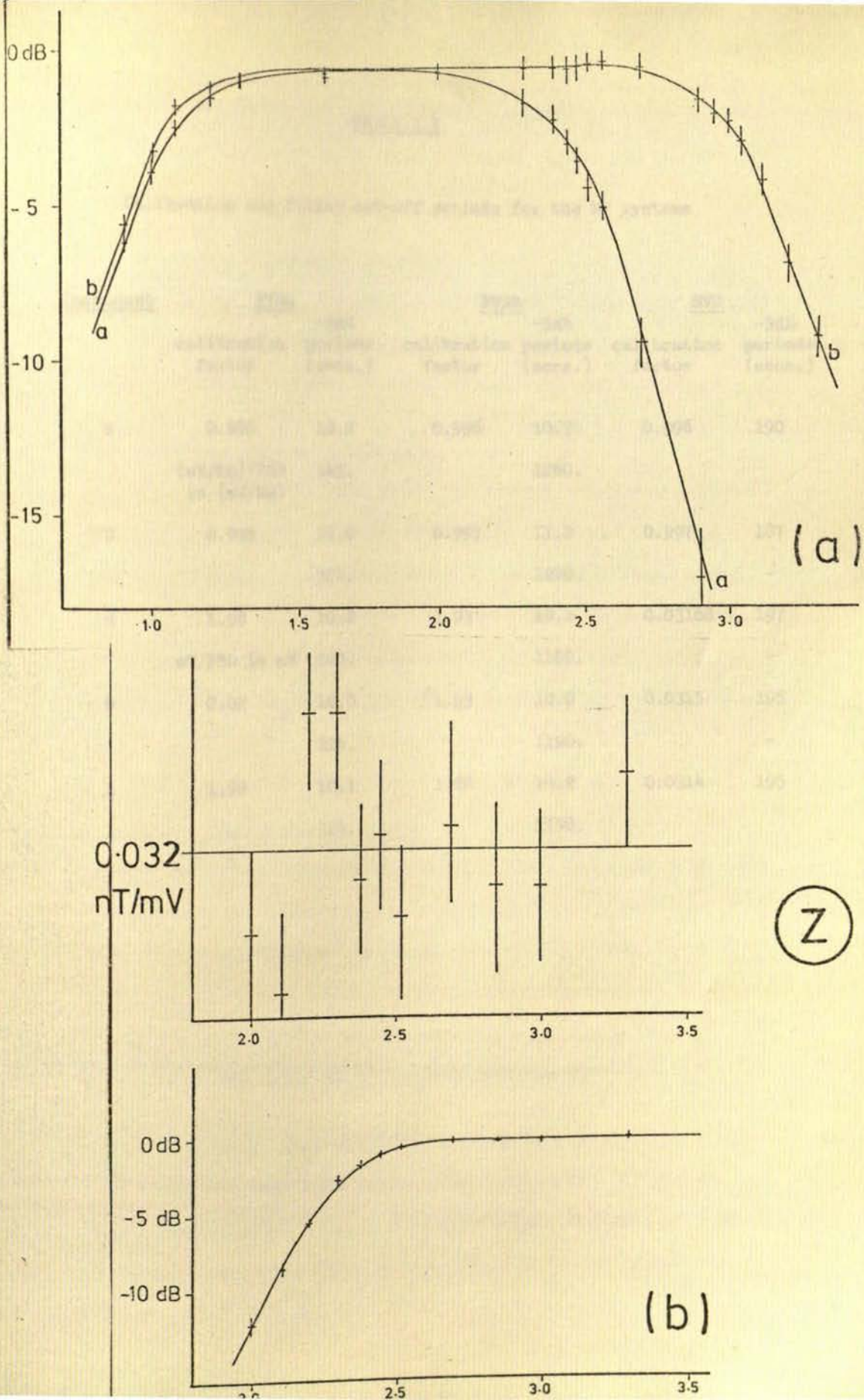
0 dB
-5
-10
-15
b
a
a
b
(a)
1·0
1·5
2·0
2·5
3·0
0·032
nT/mV
Z
2·0
2·5
3·0
3·5
0 dB
-5 dB
-10 dB
(b)
2·5
3·0
3·5

TABLE 3.4

Calibration and filter cut-off periods for the MT systems

Component	FVSa		FVSb		SVS	
	calibration factor	-3dB periods (secs.)	calibration factor	-3dB periods (secs.)	calibration factor	-3dB periods (secs.)
N	0.996	10.2	0.996	10.7	0.996	190
	(mV/km)/FSD in (mV/km)	343.		1260.		
E	0.995	11.0	0.997	11.2	0.997	187
		324.		1220.		-
H	1.98	10.2	1.93	10.2	0.03188	197
	nT/FSD in mV	320.		1180.		-
D	2.02	10.0	1.93	10.0	0.0315	195
		324.		1190.		-
Z	1.92	10.1	1.86	10.2	0.0314	195
		324.		1190.		

and filter coefficients for both magnetic systems are given in table 3.4 and the Jolivet responses are plotted in figure 3.8, the Fluxgate in 3.9.

3.4 Discussion of MT Data Collected

In this section, a description of (a) the factors that governed the quality and quantity of data recorded, (b) the type and form of data recorded and (c) site problems encountered, will be given.

3.4 (a) Data Quality and Quantity

The quality of the magnetotelluric records taken at a location was dependent on many factors. The two most important were the magnitude of geomagnetic activity and the level of cultural noise. A high level of activity recorded at a site where there was little noise gave a high signal to noise ratio, and vice versa. This was reflected in the amount of data finally accepted for the particular site.

The quantity of data recorded was almost entirely instrument dependent. Some of the factors governing quantity were directly controlled by the investigator. These include full scale deflection settings and the choice of site. Factors indirectly controllable by the investigator include ink pen maintenance, electrode potential drift, electrode line surveillance and instrument response vigilance. Almost the only uncontrollable factor was power supply failure. Fortunately, the mains power supply failed rarely.

3.4 (b) Type and Form of Activity Recorded

There were many types of activity recorded and it would be impossible to classify all of them distinctly. However, a 5-fold categorisation of the activity that was most frequently observed can

be made. These are (i) Pi2 activity around local midnight, (ii) local midday micropulsation activity, (iii) bay type events, (iv) long period oscillatory phenomena and (v) general activity.

There were over twenty records of Pi2 activity which usually took the form of three or more separate 'bursts' of oscillation. An example of the phenomenon is illustrated in figure 3.10a. With few exceptions, the events occurred between 2100 and 0300 hours with the majority between 2300 and 0100 hours. A 26 to 29 day recurrence tendency for Pi2 pulsations reported by Saito and Matsushita (1968) was not observed but pulsations seemed to exhibit a 14 day recurrence. This could be a manifestation of the first harmonic of the sidereal solar rotation period. The dominant period of the Pi2 pulsations was found to decrease with increasing Kp index, as observed by Channon and Orr (1970). However, an approximate relationship between the two for 1974/75 is given by $T = 100 - 10\ Kp$ rather than the form $T = 92 - 11.4\ Kp$ for 1966 stated by Channon and Orr. This is probably due to a sunspot number dependence of the relationship. The dominant period of the few Pi2 pulsations recorded between 0300 and 2100 hours did not exhibit any dependence on Kp index.

The midday micropulsation activity consisted of Pc3 or low period Pc4 pulsations, as shown in figure 3.10b. The majority of the ten events occurred between 1030 and 1330 hours and did not demonstrate any obvious relationship between period and Kp index. The horizontal field was usually elliptically polarised and was not preferentially orientated.

The bay type events were of traditional form, a single half-sinusoidal excursion then a return to normal, sometimes with an over-compensation effect. An example of one of the events analysed is illustrated in figure 3.10c. The main period and local time of the

Figure 3.10 Examples of activity recorded

a - Pi2 activity arround local midnight
b - Pc3 activity at local midday
c - Bay-type activity
d - Pc5 pulsation
e - general activity
f - " "
g - " "
h - " "

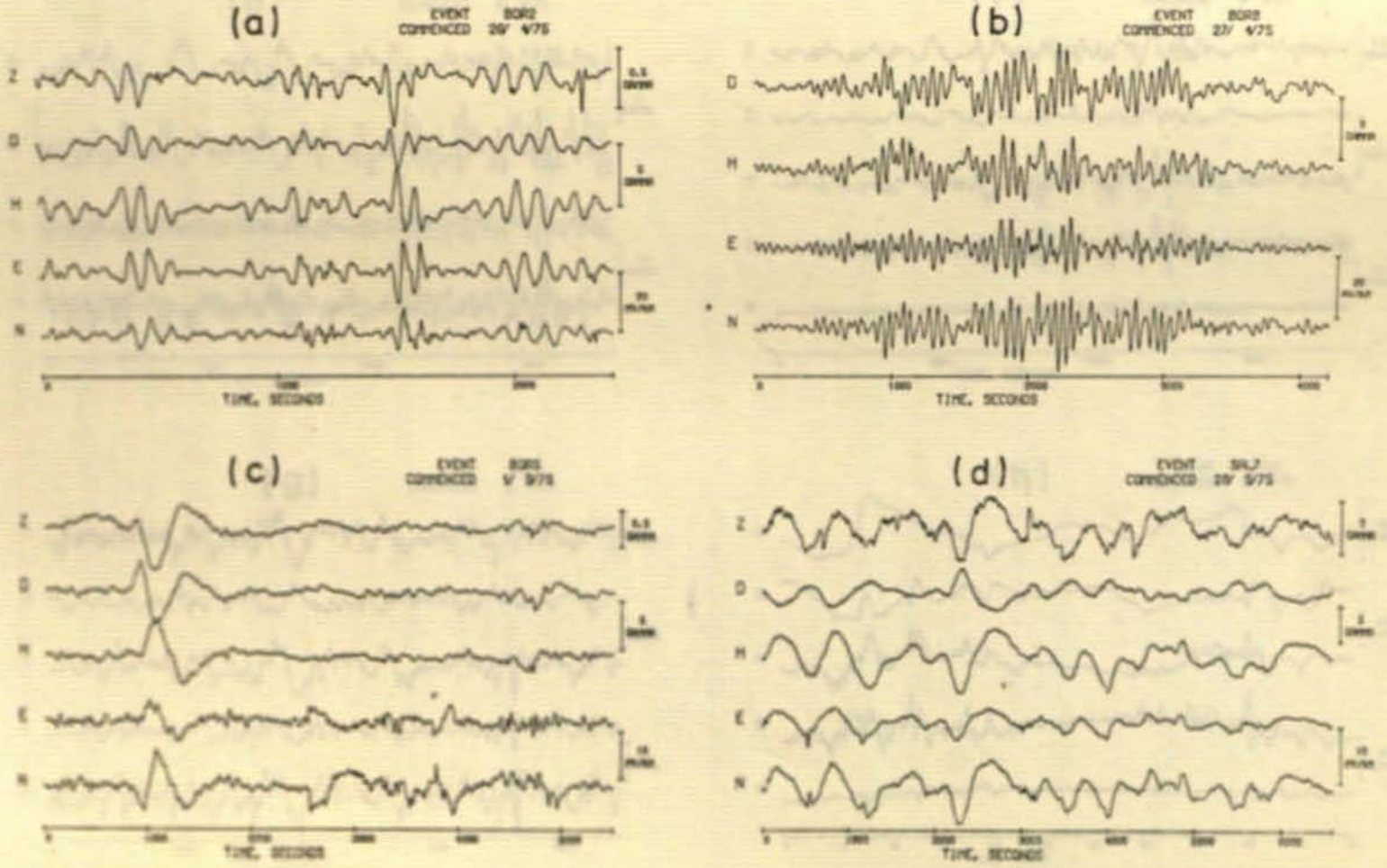
(a)
EVENT BORE
COMMENCED 26/ 4/75
Z
D
H
E
N
TIME, SECONDS
(b)
EVENT BORE
COMMENCED 27/ 4/75
D
H
E
N
TIME, SECONDS
(c)
EVENT BORE
COMMENCED 4/ 5/75
Z
D
H
E
N
TIME, SECONDS
(d)
EVENT SALT
COMMENCED 28/ 5/75
Z
D
H
E
N
TIME, SECONDS

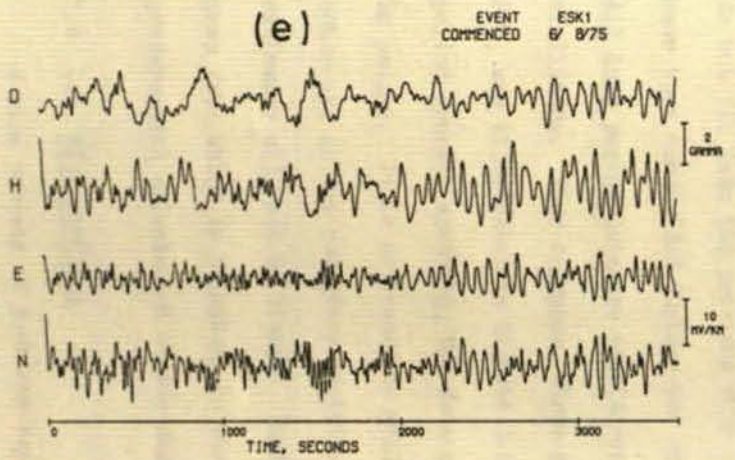
(e)
EVENT ESK1
COMMENCED 6/ 8/75
D
H
E
N
2
10
0
1000
2000
3000
TIME, SECONDS

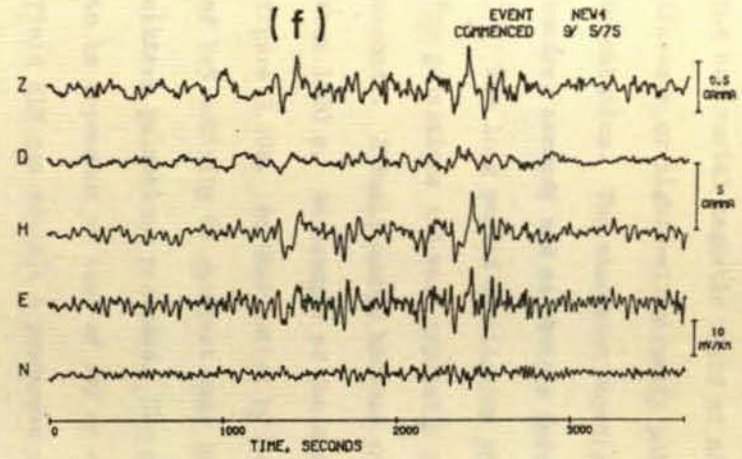
(f)
EVENT NEW1
COMMENCED 9/ 5/75
Z
D
H
E
N
0.5
5
10
0
1000
2000
3000
TIME, SECONDS

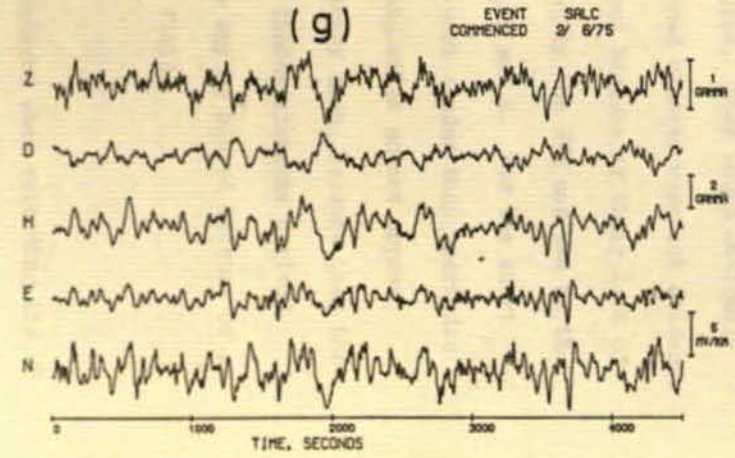
(g)
EVENT SALC
COMMENCED 2/ 6/75
Z
D
H
E
N
1
2
5
0
1000
2000
3000
4000
TIME, SECONDS

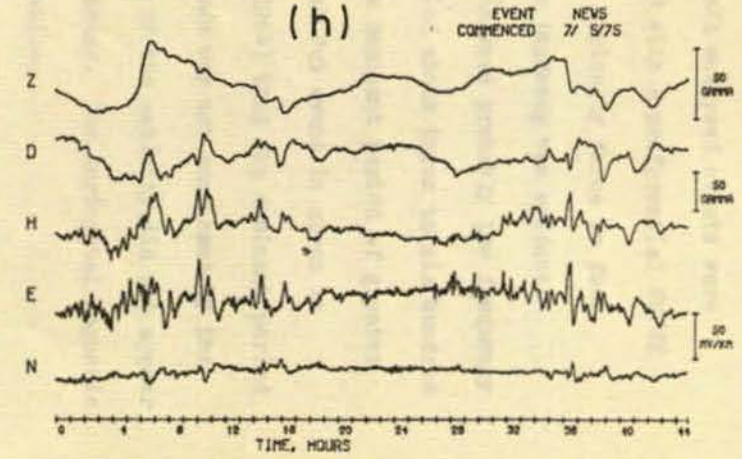
(h)
EVENT NEW5
COMMENCED 7/ 5/75
Z
D
H
E
N
50
50
50
0
4
8
12
16
20
24
28
32
36
40
44
TIME, HOURS

eleven events analysed did not appear Kp index dependent. However, the horizontal magnetic field of almost all analysed events were linearly or highly-elliptically polarised with a preferential NW/SE orientation. The excursion duration was typically three to four hundred seconds and no obvious recurrence tendency was evident.

The long period oscillatory phenomena were probably low frequency Pc5 pulsations and were typically of period about three to six hundred seconds. A small number however showed a dominant period of greater than 1000 s. An example of the more usual Pc5 event is given in figure 3.10d. An observation by Saito (1964) that the dominant period of Pc5 activity is shortest near local dawn was not confirmed by the sixteen pulsations recorded. The period of the activity did not appear to be dependent on time of day or on Kp index. The horizontal magnetic field did not exhibit a preferred orientation.

The classification of general activity covers those data which do not fit into the previous four categories. They could obviously have been subdivided further but other broad classes were not evident. All long period data are considered general because of their lack of similitude. Four examples, three recorded by the FVS and one by the SVS, are illustrated in figures 3.10e, f, g and h. For the short period general activity, the data appear more random than aperiodic in nature. It is necessary to analyse data which do not appear coherent, as the pulsatory activity obviously does, because then the estimates will not be biased. Impedance tensor elements derived from data which is pulsatory in character may be biased because of a preferential orientation of the magnetic field.

3.4 (c) Site Problems

A wide variety of problems was encountered when recording the MT data at the various locations. Most involved the instrumentation,

as already discussed in section 3.3, but some were due to the sites themselves.

During the initial stages of fieldwork, it was realised that if the mains earth was employed as the systems' earth, then step-like transients were recorded simultaneously on all five channels. These transients were not due to geomagnetic activity but were a result of mains loading and unloading by domestic users. Accordingly, the systems were earthed by the common electrode of the telluric array. This alleviated problems of this nature.

Mains 'noise' was a common difficulty which was totally uncontrollable. The noise appeared on all traces and took the form of large amplitude rapid oscillations which completely overwhelmed the natural signals. It appeared without apparent cause, lasted for an indeterminate time then ceased, also without reason. This effect had to be suffered but fortunately was fairly infrequent.

During the first recording at CAP, one of the telluric records (N) was found to be very noisy. It was realised that the non-common electrode for the N-S telluric line was buried close to a mains transformer. When the electrode was repositioned, the record became much 'cleaner'.

After the first recording at GOR, the N-S and E-W traces were found to be identical for any polarisation of magnetic field. This was considered too coincidental to be a real phenomenon and it was discovered that a North Sea gas pipe ran directly through the electrode array at an orientation of N 45° E. Thus, the natural telluric field had become perturbed by the pipe. The electrodes were re-located and observations of the natural telluric field ensued.

Recording at FTH was proceeding well until about 1700 hours on 29 August 1974 when both tellurics suddenly went off-scale. Because

of the high-pass filter time constants for the FVSb, it was about an hour before the traces returned to zero off-set. This effect was traced to a blast at a nearby open cast mine which had altered the dc potential between the pairs of electrodes. Fortunately, this did not occur often.

Mechanical vibrations caused movement of the Jolivet variometers which was recorded as spurious high frequency noise. This noise completely overwhelmed the natural variations and accordingly, it was desirable to place the magnetometers as far from roads and tracks as possible. Because of the strict requirements for an MT field site however, it was occasionally necessary to place the Jolivets close to known sources of intermittent vibration.

CHAPTER 4

DATA ANALYSIS

4.1 General Considerations

With the advent of high-speed, large storage capacity modern computers, data analysis has become, in the main, computer oriented The first objective of any computer processing of analogue records is calibration of the data to permit study of it in the time domain. This usually involves computer re-plotting of the data in a manner which enables direct qualitative comparison between observations made either at different locations at the same time or at the same location at different times. The second objective is the derivation, from the time domain recordings, of frequency domain parameters which might aid the delineation of causal anomalous conductivity structures.

With data from an array of variometers, the first objective provides a relatively quick method of gaining a qualitative impression of what may, or may not, be a local induction anomaly. However, it is usually necessary to employ frequency domain analysis if a more rigorous interpretation is sought. The research worker nevertheless should not bypass time domain procedures. The very worthwhile papers by Gough and his colleagues reporting their preliminary analyses of array data from visual inspection only illustrate its usefulness.

Single station data, by its very nature, is more easily interpreted in the frequency domain. Accordingly, it is not usual when conducting an investigation with only one set of instruments to try to gain much qualitative information from the time domain characteristics of the observations.

A time domain analysis of data allows estimation of parameters that are time dependent, e.g. of the source, etc. Frequency domain

analysis however permits derivation of time independent parameters, for example the conductivity distribution.

Two types of spectral analysis are discussed in this chapter. Techniques applicable to Fourier transient phenomena have been used for the analysis of the array data, and those expedient for Fourier intransient data have been employed for the analysis of the single station magneto-telluric records.

4.2 Processing of Fourier transient events from the GDS array

The initial processing of the GDS data from Array B was carried out by the author during a two month visit to the University of Alberta, Edmonton, Canada in 1974, using methods described in this section. As has been mentioned, shortage of time has not permitted the author to analyse the data from the array fully.

4.2.1 Data selection

All the data from the 19 variometers were scanned quickly to determine those sites which had complete records for the whole of the observational period. Data from one of these sites was re-inspected and a note made of the characteristics (i.e. estimated polarisation, estimated spectral content, duration, type and form of activity and local time) of magnetically active intervals. Nine of these 'events' were chosen as being the most suitable for study. The film records for each site were then examined for the data quality during each of the nine chosen events. Two of the nine were then selected for processing on the bases of their coverage - table 4.1 - and their characteristics. Figure 4.1a shows an example of the Pc5 micropulsation event, of period about 400 s, duration approximately 90 minutes, and commence time just prior to 1200 (UT) on 9th December 1973. The second event is illustrated in figure 4.1b. It is a bay type phenomenon

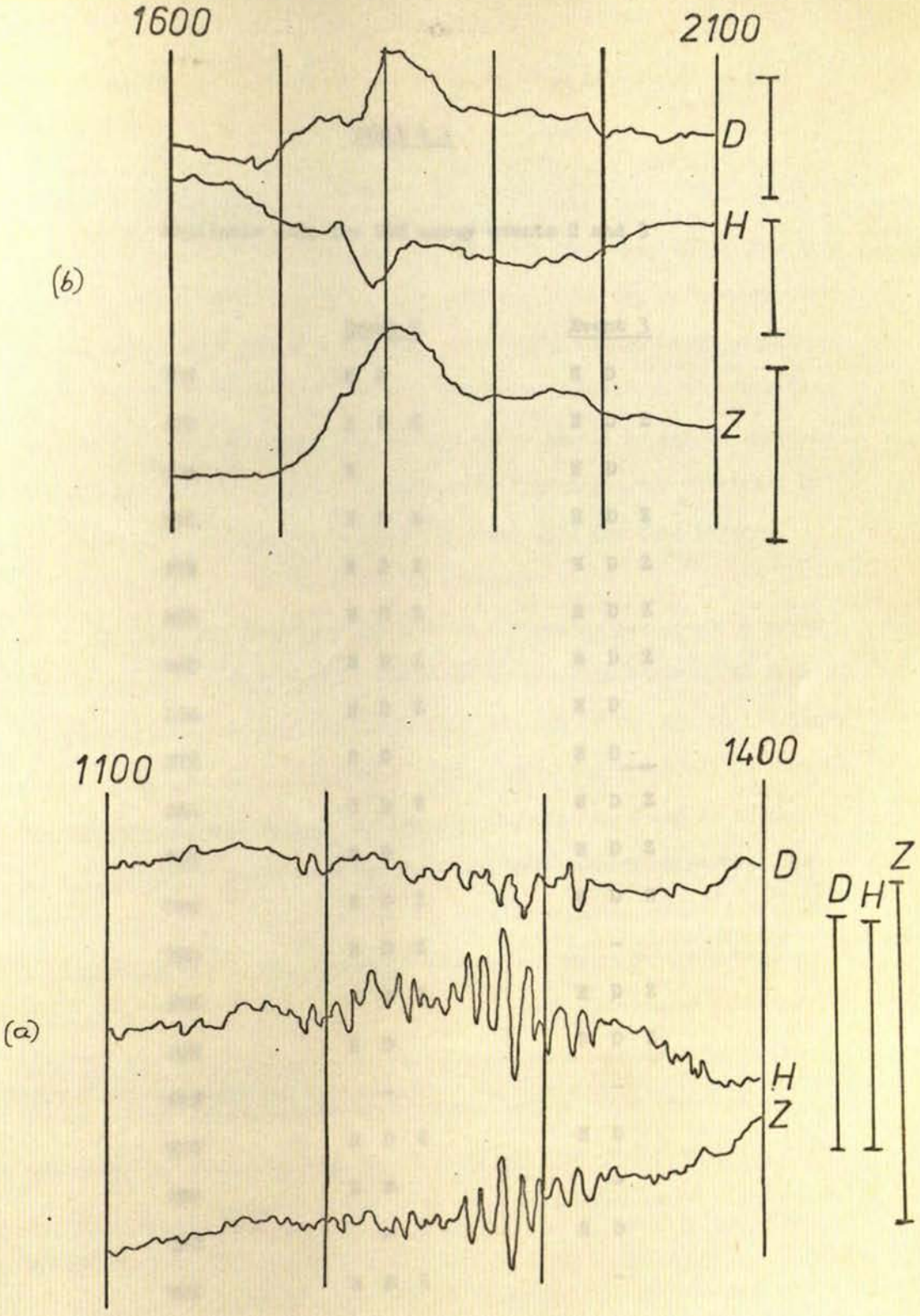

Figure 4.1 Example of Events 2 & 3 - data recorded at station BUR
top - event 3 bottom - event 2
[illegible] indicate amplitude of 100 nT

TABLE 4.1

Available data for GDS array events 2 and 3

	Event 2	Event 3
BON	H D	H D
ARD	H D Z	H D Z
COA	H	H D
HEL	H D Z	H D Z
FIN	H D Z	H D Z
BUR	H D Z	H D Z
GST	H D Z	H D Z
LES	H D Z	H D
STB	H D	H D
GAL	H D Z	H D Z
COT	H D	H D Z
CPH	H D Z	H D Z
THO	H D Z	-
ESK	H D Z	H D Z
SGH	H D	H D Z
ELS	-	-
TOG	H D Z	H D
BKD	H D	-
HAG	-	H D
WRK	H D Z	-

with a preceding sudden impulse which occurred at 16.45 (UT) on 19th December 1973.

4.2.2 Data Reduction

As reported in section 3.1, recording was on photographic film with a time interval of 20 s between data points. If it can be assumed that the film transport was at a constant rate (which should be reasonably valid for the short sections of data being analysed), and that the film burn is contrasting enough, the data presents itself in a form suitable for automatic digitisation. The automatic film-digitiser developed by the University of Edmonton (Alabi, 1974) was used for this purpose.

The operations involved were as follows:

(i) The roll of film was placed in a scanning device which moved the film across a differential photocell at a constant rate. At preset intervals (corresponding to a film-time interval of one minute), a light source above the film illuminated. This caused the photocell to register the position of the five spots (two baselines and H, D and Z) on the film, plus any other transparent sections such as scratch marks. The film scanner then transmitted the (x, y) co-ordinates of all points with intensity greater than a threshold intensity. These co-ordinates were written onto magnetic tape by the PDP15 computer interfaced with the film scanner. The computer also displayed the points on a Tektronix screen, where they appeared in sequential order. When the display screen was full, a hard copy was made of the data on the screen. This was used by the operator at the next stage of processing to distinguish between traces.

(ii) Using Edmonton's IBM 360/165 computer, the information on the digitiser tapes was processed by an interactive graphics program written by Dr. A. O. Alabi. On prompts from the program, the user, employing a

light pen follower, traced the two baselines and the three magnetic records in turn on the interactive graphics display screen. Recognition of each trace was made by reference to the hard copy from the automatic digitising process. If there were not exactly sixty digitised points in any one hour, an interpolation program made the necessary adjustments. Other prompts from the program requested such pertinent information as calibration factors, geomagnetic co-ordinates of the station and timing of the hour marks, etc. The calling program then output the (60x no. of hours) calibrated points for each trace.

As absolute magnetic observations had not been made at the field sites, absolute baseline control was not possible. To give all the data an equivalent baseline therefore, it was necessary to digitise data in advance of the start of the event and take relative differences. For both events examined, digitisation started at least 40 minutes prior to the magnetically active period.

Three main problems arose when the automatic digitising procedure was applied to Scottish records:-

(i) For reasons discussed in chapter 3, the traces were frequently very faint. Lower threshold illumination levels were tried but this resulted in an unacceptable level of background noise.

(ii) When the variations were sufficiently rapid, the differential photocell recorded two, or even three, x-y co-ordinates for one trace when only one should have been recorded. This multiplicity could not be resolved at the interactive program stage.

(iii) If the traces were too close together and crossed many times, the resulting digitisation became too Gordian for processing by the interactive graphics procedure.

If any one of these problems arose, the automatic digitising process was abandoned for the pertinent trace or traces, and manual

digitising was performed. The procedure involved using a film viewer, the screen of which was covered by a grid. The film was adjusted in the reader so that the base lines were horizontal. Then every third point, corresponding to a time interval of one minute, had its y co-ordinate noted for each of the traces being digitised in this fashion. These co-ordinates were then punched on cards.

For the micropulsation event (fig. 4.1a), an attempt was made to process the data automatically but difficulties arose due to problems (ii) and (iii) above. Accordingly, all the data were digitised manually.

For the bay event (fig. 4.2b), the only problem was with a few faint traces; these were digitised manually.

One major problem that presented itself during data reduction procedures was the exact timing of the individual magnetograms. As has been mentioned in section 3.1.6, the film drive sometimes completely or intermittently jammed. In the latter case, exact timing of the event could not be obtained by the usual method of counting hour marks from the beginning or the end. To overcome these difficulties, exact times of (a) the very first inflection for the micropulsation event and (b) the sudden impulse for the second event were obtained from Eskdalemuir observatory records. It was assumed that these two precursors were simultaneous over the whole array. By using this method, a timing inaccuracy of one spot, i.e. ±10 s, was the maximum possible. This corresponds to an error of $\pm 8^{o}$ in phase for the micropulsation period and less than half a degree for the main periodicities of the bay event.

4.2.3 Time Domain Analysis

Analysis in the time domain, as has been referred to in the introductory remarks to this chapter, provides a qualitative indication

of the variation of the geomagnetic field over the whole array. Whether the variation is due to external source effects or internal induction effects cannot in general be resolved. However, in mid-latitudes, it is reasonable to assume that the source will remain relatively uniform over large horizontal distances (compared to the size of the array).

The usual procedure is to stack the magnetograms in lines of equivalent geomagnetic latitude and to inspect the plots for inherent differences. This can be performed on two scales.

On a regional scale, examination of the direction in which the horizontal field increases or decreases can give an indication of the type and position of the inducing source. An excellent example of this approach has been given by Alabi et al. (1975) from visual examination of substorm activity on 28 August 1972. They concluded that the H_Y component of the magnetic field was a field-aligned Birkeland current whereas much of the structure of the H_X component variation was probably due to the ionospheric east-west morning current.

Consideration of more localised variations in the horizontal field, together with the variations in the vertical field, can indicate the position of anomalous internal current concentrations. Indicative of current concentration in a conducting body are the following important signatures;

(a) there is a large phase shift in Hz, or even reversals on either side of the current, and

(b) the horizontal field normal to the strike of the body is enhanced on one side, and depressed on the other side, of current concentrations.

By observing these signatures in their array data from central U.S.A., Alabi et al. (1975) were able to plot the axis of a conducting body (approximated by a line current) through their eight lines of magnetometer recording sites.

4.2.4 Frequency Domain Analysis

Many methods are currently available for transforming a data set from the time domain to the frequency domain. A brief summary of these will be given in the following discussion of spectral estimation.

The procedure used for the analysis of the array events was the Fast Fourier Transform algorithm of Cooley and Tukey (1965). Pre-transformation operations were; removal of the mean and linear trend, application of a cosine bell window to the initial and final ten per cent of the data, and extension to 4096 points by the addition of zeros. Extension from no. of hours x 60 (either 180 or 300 points for the first and second events respectively) to 4096 and not to the next power of two (256 and 512 respectively) as is usual, may appear erroneous, but it must be remembered that the data being analysed is 'transient' data. As such it can be defined as non-periodic deterministic data for which a discrete spectral representation is not possible but a continuous spectral representation is. One method for gaining a more continuous spectral coverage, thus a more correct representation, is by the addition of zeros. This addition is by its very nature justifiable as assumption is made from the outset that

$$\begin{matrix} x(t) \\ y(t) \\ z(t) \end{matrix} = 0 \text{ for } 0 > t \text{ and } t > T$$

Assurance that the procedures appropriate for the estimation of spectra of stationary random data (i.e. the FFT algorithm) can be applied directly to the estimation of spectra of transient data is given by Bendat and Piersol (1971) and Hermance (1973).

When the spectral content of the event had been computed for all stations, the amplitude spectra of the two horizontal components were examined to choose a period (or periods) at which the field exhibited

a local maximum. In the following section on spectral estimation for intransient data, the need to band average the Fourier co-efficients will be stressed. However, for non-periodic deterministic transient data, the estimate does not have an associated random variance, hence band averaging is not necessary.

Maps of Fourier spectral amplitudes have been prepared at a number of frequencies of interest and using an algorithm given by Fowler et al. (1967), the polarisation parameters were estimated and plotted. These results will be discussed further in Chapter 5.

Further sophisticated techniques, such as transfer function analysis and an attempt to separate the internal and external fields, were not attempted.

4.3 Processing of Fourier intransient record sections for single station MT and GDS data

As inferred in 4.1 and 4.2, the data recorded by the MT equipment at the 13 locations is inherently different in character from that recorded by the array study. The data are not Fourier transient phenomena but rather Fourier intransient phenomena which can be analysed statistically to gain information about the frequency content. An example of a typical record section is illustrated in figure 4.2. Assuming that the data are generated by random processes, or at the very least obey the Central Limit Theorem (Jenkins and Watts, 1968), the first objective of computer processing stated in 4.1 is less relevant. By analysing a sufficient number of variations to satisfy the central limit theorem, the dependence of the frequency domain parameters on the time of observation ideally can be reduced to zero. Thus, qualitative comparison of simultaneous MT data is not essential. The aim of Fourier intransient data processing is therefore the estimation of frequency dependent characteristics - the second objective of 4.1.

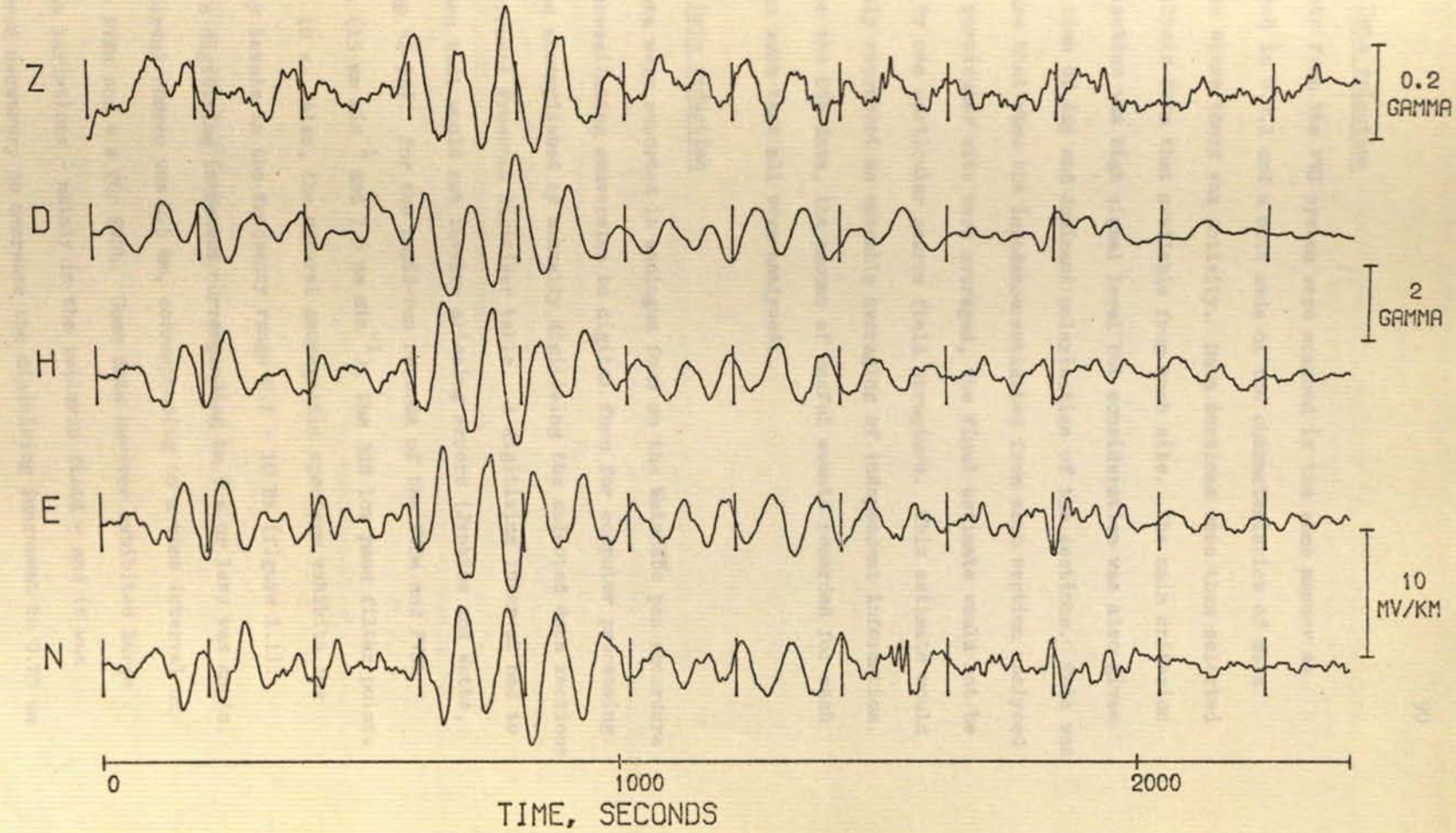

Figure 4.2 Data section BOR1

4.3.1 Data selection

Data from the FVS system were scanned in the same manner as described in 4.2.1 and a note made of the characteristics of data sections where there was activity. Data sections were then selected for analysis from that available from each site. The main criterion for selection was high signal level but consideration was also given to the time of day and dominant polarisation of the sections. This was to ensure that when the impedances estimated from each section analysed from a particular site were averaged, the final estimate would not be biased by one particular source field structure. This estimate would hopefully represent an ensemble averaging of independent information.

For the SVS data, the amount of useful events recorded for each site was such that all were analysed.

4.3.2 Data reduction

Data were recorded in analogue form on the Watenabe pen recorders thus necessitating conversion to digital form for computer processing. This was accomplished by manually digitising the selected data sections on a Ferranti Freescan Digitiser table. A digitising interval had to be chosen that would not involve aliasing errors (Jenkins and Watts, 1968, pp 52-53). For the rapid-run records of the FVSa and FVSb systems (15 mm min^{-1} and 7.5 mm min^{-1}), the 3dB low pass filter points were at 10 s. Also, the natural geomagnetic spectrum exhibits low activity levels in the frequency range 0.1 - 10 Hz (figure 1.1). Hence, a digitising increment corresponding to 5 s or less was ample. The interval chosen was 0.5 mm, corresponding to a time interval of 2 s for FVSa and 4 s for FVSb. Some data however exhibited large gradient variations - mainly in the telluric field - and it was considered necessary to decrease the digitising increment to 0.25 mm (1 s and 2 s) to reduce errors in spectral estimation.

For the slow run data of the SVS (30 mm hr^{-1}), the low pass 3dB cut off was at 200 s. The filter response at 60 s - corresponding to 0.5 mm digitising increment - was about -15dB. This was considered sufficient to remove signals with period less than 60 s. Therefore, aliasing problems would not occur.

Prior to digitising any trace from a data section, a trace header was keyed onto the magnetic tape. The header was mainly for trace recognition but it also contained other pertinent information: recorder full scale deflection setting, sign, time of event, chart speed and trace parallax.

Chart tilt relative to the digitiser x-axis was recorded by digitising a point at either end of the base line on the chart. The digitised points were then reduced to zero tilt at the first stage of computer processing. The necessity for this correction was shown by Stuart et al. (1971) who demonstrated that a tilt as small as 7^{o} introduced spectral distortion in the form of second and third harmonics of the main peak. These harmonics were not present in the data.

A total of 137 data sections were digitised, 93 by the author and the remainder by the Edinburgh Regional Computing Centre. For each digitised section, a check was made of the digitising procedure by plotting out the digitised data and comparing it by overlay with the original. Discrepancies of greater than 2 mm resulted in re-digitising of the erroneous data trace.

4.3.3 Data conditioning

Certain pre-processing operations have to be undertaken before spectral estimation procedures can be applied to the data. This is because the frequency domain windows often include side lobes which can introduce gross harmonic distortion about spectral peaks.

Fourier transformation from the time series - x(t) - to its complex frequency domain series - X(f) - is made by

$$X(f) = \int_{-\infty}^{\infty} x(t)e^{-i\omega t}\, dt. \qquad (4.1)$$

However, data sets are of finite length, therefore an estimate of X(f) given by

$$\hat{X}(f, T) = \int_{0}^{T} x(t)e^{-i\omega t}\, dt \qquad (4.2)$$

must be made. Equation 4.2 is equivalent to

$$\hat{X}(f, T) = \int_{-\infty}^{\infty} x(t)U_T(t)e^{-i\omega t}\, dt \qquad (4.3)$$

where

$$U_T(t) = \begin{cases} 0 & t < 0 \\ 1 & 0 < t < T \\ 0 & t > T. \end{cases} \qquad (4.4)$$

Function $U_T(t)$, given by 4.4, is usually called a "box-car" function (Kanasewich, 1973, p 91) and represents the restriction of knowledge of x(t) to the range (0, T). Equation 4.3 can be re-written as a frequency domain convolution between X(f) and the Fourier transformation of $U_T(t)$, i.e. $U_T(f)$, as

$$\hat{X}(f, T) = U_T(f) * X(f). \qquad (4.5)$$

The shapes of $U_T(t)$ and $U_T(f)$ are illustrated in figure 4.3a and b. The large side lobes of $U_T(f)$ - 24% first negative lobe, 13% first positive lobe - will cause spectral distortion by permitting 'leakage' of power through the lobes. The shape of $U_T(f)$ is given by the Fourier transformation of $U_T(t)$ - given by equation 4.4 - and is

$$U_T(f) = T\left(\frac{\sin \pi fT}{\pi fT}\right) = T \operatorname{sinc} \pi fT. \qquad (4.6)$$

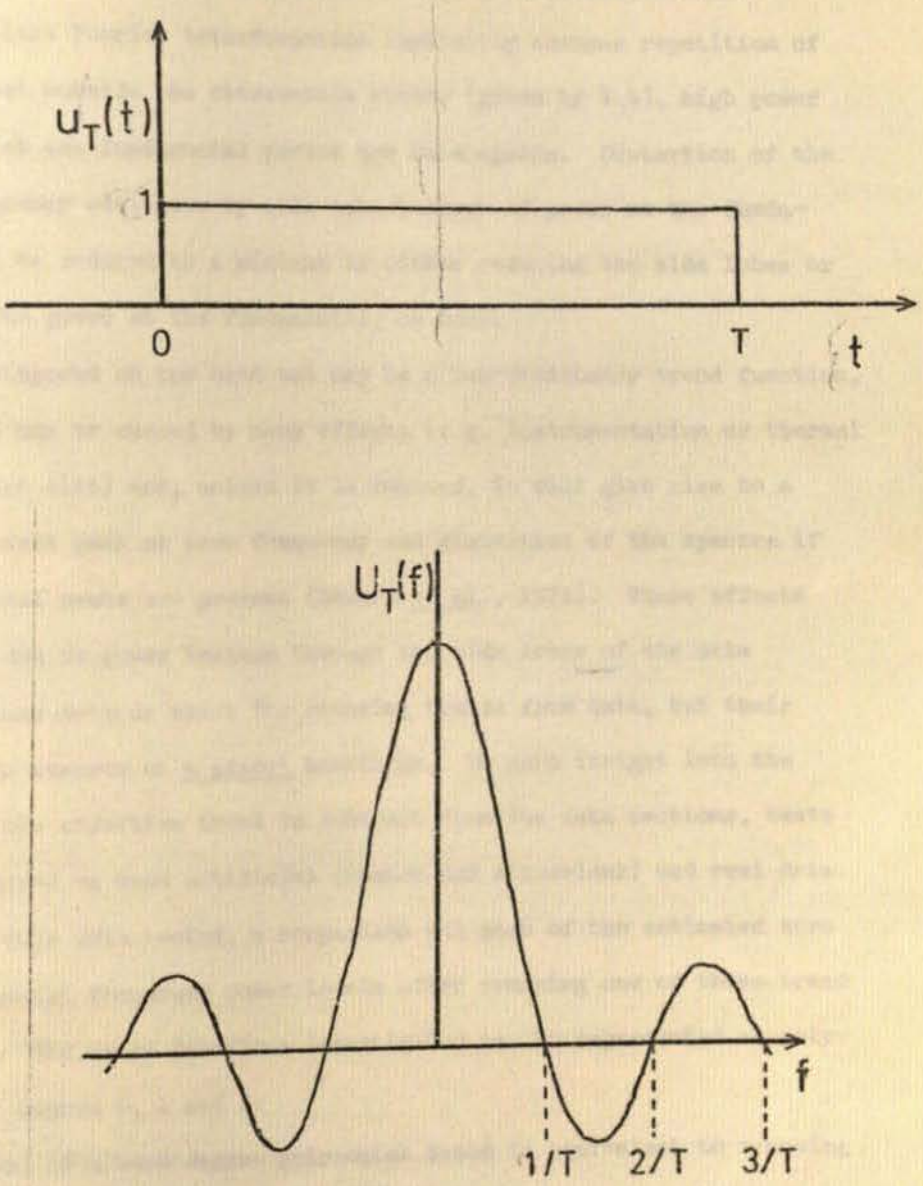

Figure 4.3 The 'box-car' window -$u_T(t)$- and its Fourier Transform -$U_T(f)$

For the data sections digitised, variations with period the length of the data set, i.e. the fundamental, were not apparent. Hence, power estimates at the zero and fundamental frequencies should be zero. However, since Fourier transformation implicitly assumes repetition of the data set outside the observation window (given by 4.4), high power estimates at the fundamental period are inescapable. Distortion of the other frequency estimates by side lobe leakage of power at the fundamental can be reduced to a minimum by either reducing the side lobes or reducing the power at the fundamental, or both.

Superimposed on the data set may be a non-stationary trend function. This trend may be caused by many effects (e.g. instrumentation or thermal drift, chart tilt) and, unless it is removed, it will give rise to a sharp spectral peak at zero frequency and distortion of the spectra if real spectral peaks are present (Stuart et al., 1971). These effects are again due to power leakage through the side lobes of the data window. Many methods exist for removing trends from data, but their application assumes an a priori knowledge. To gain insight into the most suitable objective trend to subtract from the data sections, tests were conducted on both artificial (random and sinusoidal) and real data. For those dats sets tested, a comparison was made of the estimated zero and fundamental frequency power levels after removing one of three trend functions. The trend functions investigated can be represented as polynomials of degree 0, 1 and 2.

Removal of a zero degree polynomial trend is equivalent to removing the sample mean of the data set. This is given by

$$x = s + c = s + \frac{1}{N} \sum_{i=1}^{N} x_i, \qquad (4.7)$$

where [x] is the original data set

[s] is the reduced data set

and c is the sample mean.

The form of c given by 4.7 has been shown to be an unbiased estimate of the true mean (Bendat and Piersol, 1971, p 101).

Removal of a polynomial of the first order represents reduction of the form

$$x = bs + c \tag{4.8}$$

where b is the linear trend of x .

The term b can be estimated using either an average slope technique or a least squares procedure (Bendat and Piersol, 1971, pp 288-290). In the tests, the average slope algorithm was employed.

A second degree polynomial trend can be removed by deriving s from x by

$$x = as^2 + bs + c$$

where a is the quadratic, or half-sinusoidal, trend of the data. This trend was removed by first estimating the Lagrangian second-order interpolation polynomial to x from

$$L_2(i) = \frac{(i - N|2)(i - N)}{N^2|2} x_o + \frac{i(i - N)}{(N^2|4 - N)} x_1 + \frac{i(i - N|2)}{(N^2 - N|2)} x_2 \tag{4.9}$$

(Jeffrey, 1971, pp 336-337)

where i is the point number

x_o, x_1 and x_2 are the values at the beginning, middle and end of the data set respectively

and N is the data set point length.

The polynomial, $L_2(n)$ was then removed from each data point to give s from

$$s_i = x_i - L_2(i) \tag{4.10}$$

The values x_o, x_1 and x_2 were estimated by averaging over the first 10%,

middle 20% and end 10% respectively, viz:

$$x_o = \frac{1}{10}\sum_{i=1}^{N/10} x_i,\quad x_1 = \frac{1}{20}\sum_{i=\frac{N}{2}-\frac{N}{10}}^{\frac{N}{2}+\frac{N}{10}} x_i,\quad x_2 = \frac{1}{10}\sum_{i=N-\frac{N}{10}}^{N} x_i. \qquad (4.11)$$

The tests indicated that removal of a quadratic trend by employing equations 4.9, 4.10 and 4.11 gave the smallest power levels at the zeroth and fundamental frequencies. This is illustrated in figure 4.4.

As well as reducing the spectral power at the lowest frequencies to a minimum, it is desirable to modify $U_T(f)$, given by 4.6, to reduce the side lobe amplitudes. Application of a cosine taper to the first and last 10% of the data, first suggested by Bingham, Godfrey and Tukey (1967), has been widely accepted. The cosine taper is given by

$$C_T(t) = \begin{cases} 0 & t < 0 \\ \frac{1}{2}\left(1 + \cos\left(10t/T - 1\right)\pi\right) & 0 < t < \frac{T}{10} \\ 1 & T/10 < t < T - T/10 \\ \frac{1}{2}\left(1 + \cos\left(10(T - t)/T - 1\right)\pi\right) & T - T/10 < t < T \\ 0 & t > T. \end{cases} \qquad (4.12)$$

The Fourier transformation of $C_T(t)$ to $C_T(f)$ is given by Kanasewich (1973, p 93) and is illustrated in figure 4.5b. The reduction in the side lobe amplitudes is obvious by comparing 4.3b with 4.5b. The estimate of the function X(f) (equation 4.1) after utilising cosine bells is given by

$$\hat{X}_C(f, T) = C_T(f) * X(f). \qquad (4.13)$$

However, a correction term of (1/0.875) must be employed to scale $\hat{X}_C(f, T)$ because of the smaller area of $C_T(t)$ to $U_T(t)$ (Bendat and Piersol, 1971, p 323). The spectral estimate of x(t) in the range (0, T) is thus given by

$$\hat{X}(f, T) = 1.143\, C_T(f) * X(f). \qquad (4.14)$$

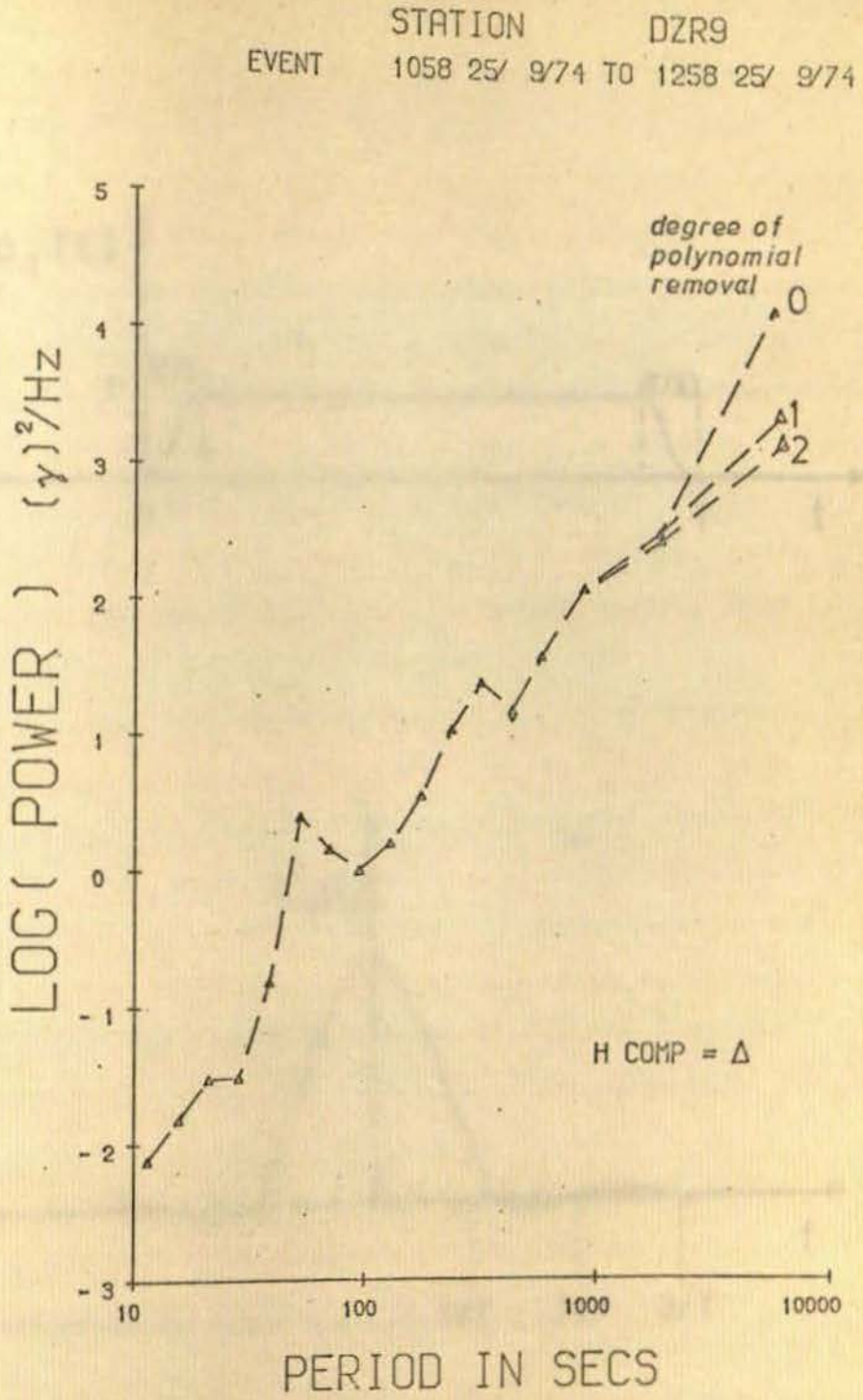

Figure 4.4 Example of different trend removal -a polynomial trend of degree 0,1 & 2 has been removed from the H-component of data section DZR9

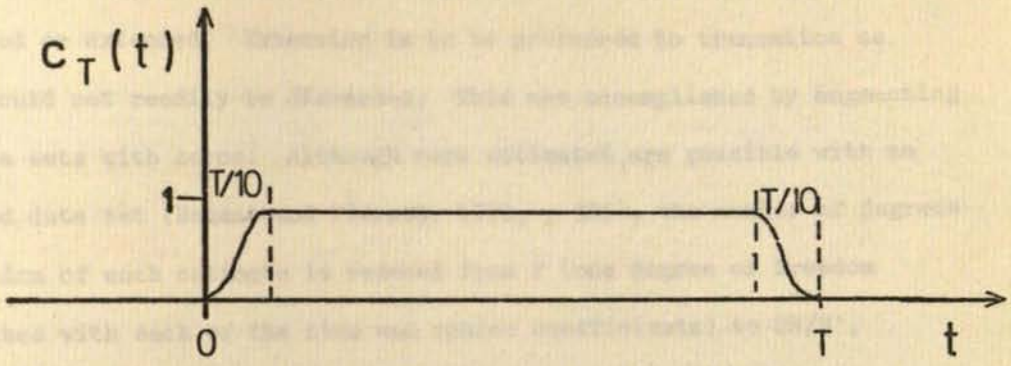

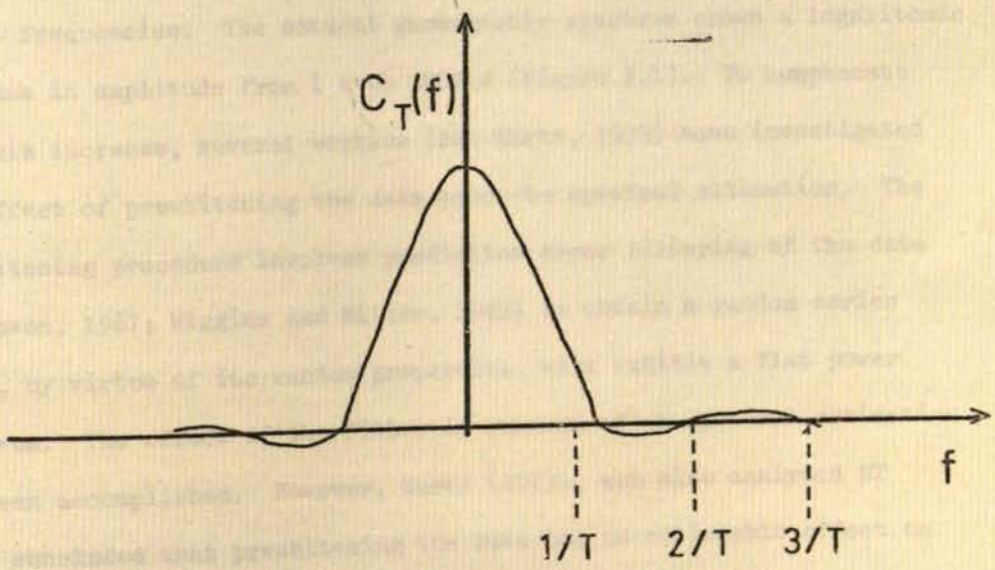

Figure 4.5 The cosine taper window -$c_T(t)$- and its Fourier transform -$C_T(f)$

When computing $\hat{X}(f, T)$ from $x(t)$ by the Fast Fourier Transform algorithm of Cooley and Tukey (1965), the data set point length has to be a power of 2. Accordingly, the data sections had to be either truncated or extended. Extension is to be preferred to truncation as data should not readily be discarded. This was accomplished by augmenting the data sets with zeros. Although more estimates are possible with an extended data set (Bendat and Piersol, 1971, p 325), the number of degrees of freedom of each estimate is reduced from 2 (one degree of freedom associated with each of the sine and cosine coefficients) to $2N/N'$, where N is the original point length and N' is the extended point length. Augmentation of the data set by zeros also has the desirable feature of smoothing the spectral window (Kanasewich, 1973, p 100).

Spectral estimation of random data assumes a flat power spectrum. Real data analysed in geophysics rarely, if ever, exhibits equal power at all frequencies. The natural geomagnetic spectrum shows a logarithmic increase in amplitude from 1 s to 3000 s (figure 1.1). To compensate for this increase, several workers (see Kurtz, 1973) have investigated the effect of prewhitening the data prior to spectral estimation. The prewhitening procedure involves prediction error filtering of the data (Robinson, 1967; Wiggins and Miller, 1972) to obtain a random series which, by virtue of its random properties, will exhibit a flat power spectrum. The effect of the filter is removed after spectral estimation has been accomplished. However, Kurtz (1973), who also analysed MT data, concluded that prewhitening the data had no noticeable effect on estimated spectra, calculated apparent resistivities or polarisation parameters. The procedure was therefore considered not to be an essential pre-processing operation for data recorded for this project also.

4.3.4 Spectral estimation and band averaging

Many procedures exist for estimating the spectral content of a time series. Methods useful for geomagnetic data have been reviewed by Sims and Bostick (1969) and Hermance (1973a). There are three basic procedures, (i) autocorrelation techniques (Blackman and Tukey, 1967), (ii) Fourier transformation methods (Bingham et al., 1967) and (iii) filter methods (Behannon and Ness, 1966; Berdichevsky et al., 1973).

Two other methods which have recently become available are non-linear data-adaptive spectral estimators which give greatly increased resolution. They are the Maximum Entropy Method of Burg (1967, 1968, 1970, 1972, 1973), suggested independently in the form of an auto-regressive spectral estimator by Parzen (1969), and the Maximum Likelihood Method of Capon (1969), both reviewed by Lacoss (1971). However, as shown by various workers (Chan and Stegen, 1974; Courtillot and LeMouel, 1975; Fougere et al., 1975; Ulrych, 1975), the spectral amplitudes have an associated high variance. In geomagnetic induction studies, a low variance for an estimate is far more desirable than a high degree of resolution. Hence, these methods were not employed in this study.

For computational efficiency, Fast Fourier Transformation is preferable to autocorrelation. Various workers (Gentleman and Sande, 1966; Bingham et al., 1967; Rader, 1970) suggest that the most efficient way of estimating the autocorrelation function of a time series is to transform the series by FFT into the frequency domain, perform a convolution and then inverse Fourier transform the convolved parameter, again by FFT. The equivalence of the time domain auto-correlation function and the power spectrum is given by the Wiener-Khintchine theorem (Kanasewich, 1973, pp 75-77).

In a comparison between spectral estimators (i) and (ii), the Cagniard apparent resistivity estimates derived by both methods were in close agreement. A program in the Biomedical Computer Program Package, BMD02T (Dixon, 1971), was used to calculate the autocorrelation characteristics. For the Fourier transformation, subroutine RHARM, based on the algorithm of Cooley and Tukey (1965), was employed. Because of the similarity of the Cagniard estimates and of the much smaller computing cost of method (ii), RHARM, a routine in the IBM Scientific Subroutine Package, was used for all spectral estimations.

After the pre-processing operations described in 4.3.3 and transformation by RHARM, each of the five frequency series (N(f), E(f), H(f), D(f) and Z(f)) was multiplied by the complex conjugate of each of the five series. This gave a 5 x 5 cross-spectral matrix at each frequency. Ten of the cross-spectral series represent the complex conjugate of ten others since

$$(N * D) = (N D^*)^*.$$

Each estimate from a random time series is mutually independent of any other estimate and is chi-square distributed with two (or 2N/N' if augmentation has been used) degrees of freedom (Jenkins and Watts, 1968, pp 230 - 233). Even if the data are not Normally Distributed, as is required of random data, the Fourier cosine and sine estimates will be very nearly Normal, by the Central Limit Theorem, and the distribution of the cross-spectra will be chi-squared (Jenkins and Watts, 1968, p 233). However, the normalised standard error of an estimate, which defines the random portion of the estimated error, is

$$E_r = (2/n)^{0.5} \qquad (4.15)$$

(Bendat and Piersol, 1973, p 191), where n is the number of degrees of freedom. Hence, for n = 2 or less, the standard deviation of the

estimate is as great as the estimate itself. Also, the variance of each estimate is independent of the sample size (Jenkins and Watts, 1968, p 233; Bendat and Piersol, 1973, p 191). Therefore, auto- and cross-spectral estimates of the form

$$\hat{S}_x(f) = \frac{2}{T}|\hat{X}(f, T)|^2 \qquad (4.16)$$

are inconsistent.

There are three basic techniques for reducing the variance of an estimate by increasing the number of degrees of freedom associated with that estimate. The method most commonly employed involves averaging neighbouring frequencies (Daniell, 1946). For the Bartlett spectral estimate (Bartlett, 1948), the data set is segmented into non-overlapping sub-sections and the spectral estimates from each sub-section are averaged. The third approach consists of averaging the spectral estimates from an ensemble of independent events and hence can be considered an extension of Bartlett's suggestion. Each of these procedures then results in a 'smoothed' spectral estimate with a smaller variance than the 'raw' estimates.

For the main analysis program - PROGRAM ONE - the first technique described of frequency smoothing over adjoining estimates was applied. The smoothing window applied was the rectangular box-car shape in the frequency domain. This form is recommended by Kanasewich (1973, p 102) rather than the usual autocorrelation windows (e.g. Hanning, Hamming or Parzen). During the initial processing, a Daniell window which was independent of frequency was used, i.e. the same number of raw estimates were averaged together regardless of the centre frequency. However, this resulted in many closely-spaced smoothed estimates for periods close to the Nyquist period and a few widely-spaced smoothed estimates at the longer periods. A more reasonable window to employ for geomagnetic

studies is one that gives approximately equi-spaced smoothed estimates on a log T scale. The window commonly used to obtain this result is a Constant Q (Swift, 1967; Vozoff, 1972; Reddy et al., 1976) or a logarithmic Daniell (Fournier and Rossignol, 1974) window. A comparison between a normal Daniell window, averaging 8 raw estimates to obtain each smoothed estimate, and a Constant Q window, with a Q of 0.3, for the estimated power spectra of 5 random series, is illustrated in figure 4.6 (note: the Constant Q spectra have been offset upwards). For a random series with zero mean, the power spectral density should be flat with magnitude equal to the variance of the series (Jenkins and Watts, 1968, pp 224-226). The reduction in statistical scatter obtained by applying the Constant Q filter can be seen in figure 4.6. Accordingly, a Constant Q window was employed throughout for smoothing the raw spectral estimates.

For all data analysed, the first terms of the Fourier series were discarded as they represent the average power levels of the series, i.e. the dc components. Also, it was found necessary to discard the first harmonics as they were extremely sensitive to the form of detrending function used - see section 4.3.3. This problem has been reported by Hermance (1973a).

4.3.5 Correction for instrument response

Two different corrections have to be applied to the data due to the response of the instrumentation. The effects of the parallax between the traces (3.3c) and of the filter responses (3.3a) have to be removed at the computer processing stage.

As described in section 3.3c, the parallax between the five pens was recorded at least daily. If a data section was selected from a chart, the nearest parallax check was located and the parallax of each

Figure 4.6 Comparison of employing a Daniell window, or a Constant Q window, for averaging

Note: the power levels derived using the Constant Q window have been increased to avoid overlap

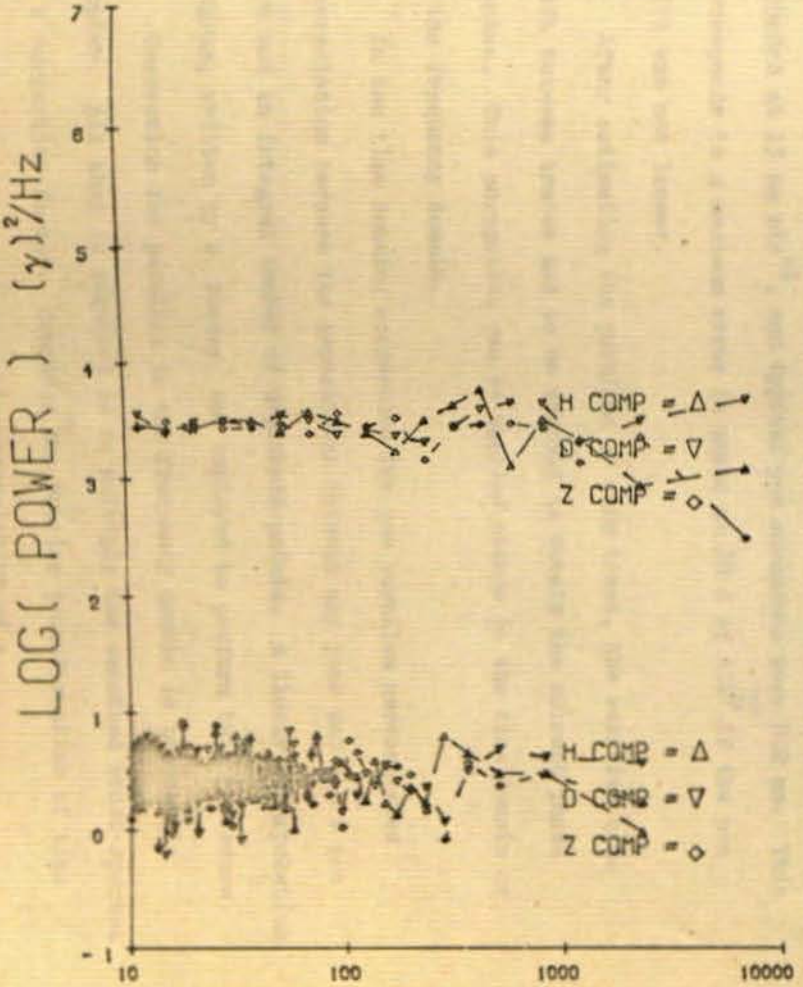
LOG(POWER) (γ)²/Hz
7
6
5
4
3
2
1
0
-1
10
100
1000
10000
H COMP = Δ
D COMP = ∇
Z COMP = ◇
H COMP = Δ
D COMP = ∇
Z COMP = ◇
PERIOD IN SECS

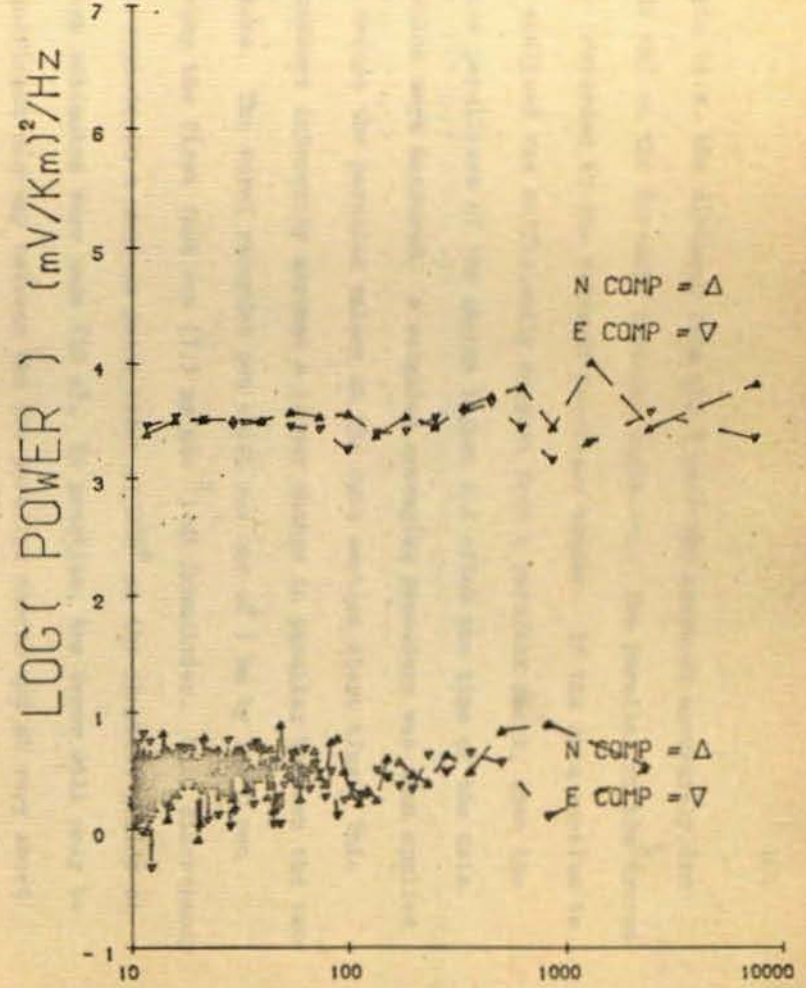
LOG(POWER) (mV/Km)²/Hz
7
6
5
4
3
2
1
0
-1
10
100
1000
10000
N COMP = Δ
E COMP = ∇
N COMP = Δ
E COMP = ∇
PERIOD IN SECS

trace (i.e. the distance from the Z pen) was measured accurately (to 0.01 mm) on the Ferranti Freescan Digitiser. The parallax of the traces was recorded in the relevant pre-trace header. If the data section to be analysed was sufficiently distant from a parallax check, then the trace parallaxes of the checks before and after the time of the data section were measured. A weighted averaging procedure was then applied to deduce the parallax values at the data section start time. This procedure inherently assumes a linear change in parallax between the two checks. The worst recorded pen shift was one of 1 mm by the D pen during the first fast run (7.5 mm min^{-1}) at Drumelzier. This discrepancy corresponds to a maximum phase error of 288° at the shortest period at which estimates were made (10 s). In practise, the error will only be significant mid-way between the two parallax checks and at very short periods. Most high frequency data were obtained from FVSa, which was recorded at 15 mm min^{-1}, and typical pen movements were 0.2 mm. This corresponds to a maximum error in phase at 10 s of $\pm 14^{\circ}$ if the pen shift was not linear.

After estimating the parallax of each trace, the relative time shift between traces had to be removed to obtain the correct phase spectra. This correction can be applied either in the time domain or in the frequency domain.

In the time domain, correction for pen parallax necessitated interpolation because the separations between any pens and the Z pen were not an integral number of digitised points. A linear interpolation program, written by D. Rooney, was employed to perform this procedure.

Correction for parallax in the frequency domain is inherently simpler. All that is required is to multiply the smoothed cross-spectra by a correction factor. Consider the Fourier transformation of time series $x(t)$ with a parallax time translation of a,

$$X(f) = \int_{-\infty}^{\infty} x(t + a)e^{-i\omega t}\, dt.$$

Substitute, $t' = t + a$, then

$$X(f) = e^{i\omega a} \int_{-\infty}^{\infty} x(t')e^{-i\omega t'}\, dt'$$

$$= e^{i\omega a}\, X'(f).$$

Similarly for $y(t)$ with a parallax time translation of b,

$$Y(f) = e^{i\omega b}\, Y'(f).$$

The cross-spectrum between the true Fourier spectras $X(f)$ and $Y(f)$ is given by

$$\begin{aligned} Sxy(f) &= X^*(f)\ \ Y(f), \\ &= X'^*(f)\ \ Y'(f)e^{i\omega(b-a)}, \\ &= S'_{xy}(f)e^{i\omega(b-a)} \end{aligned} \qquad (4.17)$$

Hence, the cross-spectral estimates, $\hat{S}'_{xy}(f)$, have to be multiplied by $\exp(i\omega(b - a))$.

A comparison was made between these two methods of parallax correction. As shown clearly in figure 4.7, it was found that the frequency domain methods provided more reliable phase estimates at short periods. The frequency domain method also gave a considerable saving of computer time.

As reported in section 3.3a, the analogue filters employed at the recording stage were designed by Trigg (1972). They were Butterworth second-order low and high pass filters. The response of these filters had to be removed at the processing stage. For the FVS systems, both low-pass (-3dB points at 0.1 Hz) and high-pass (-3dB points at 0.003 Hz

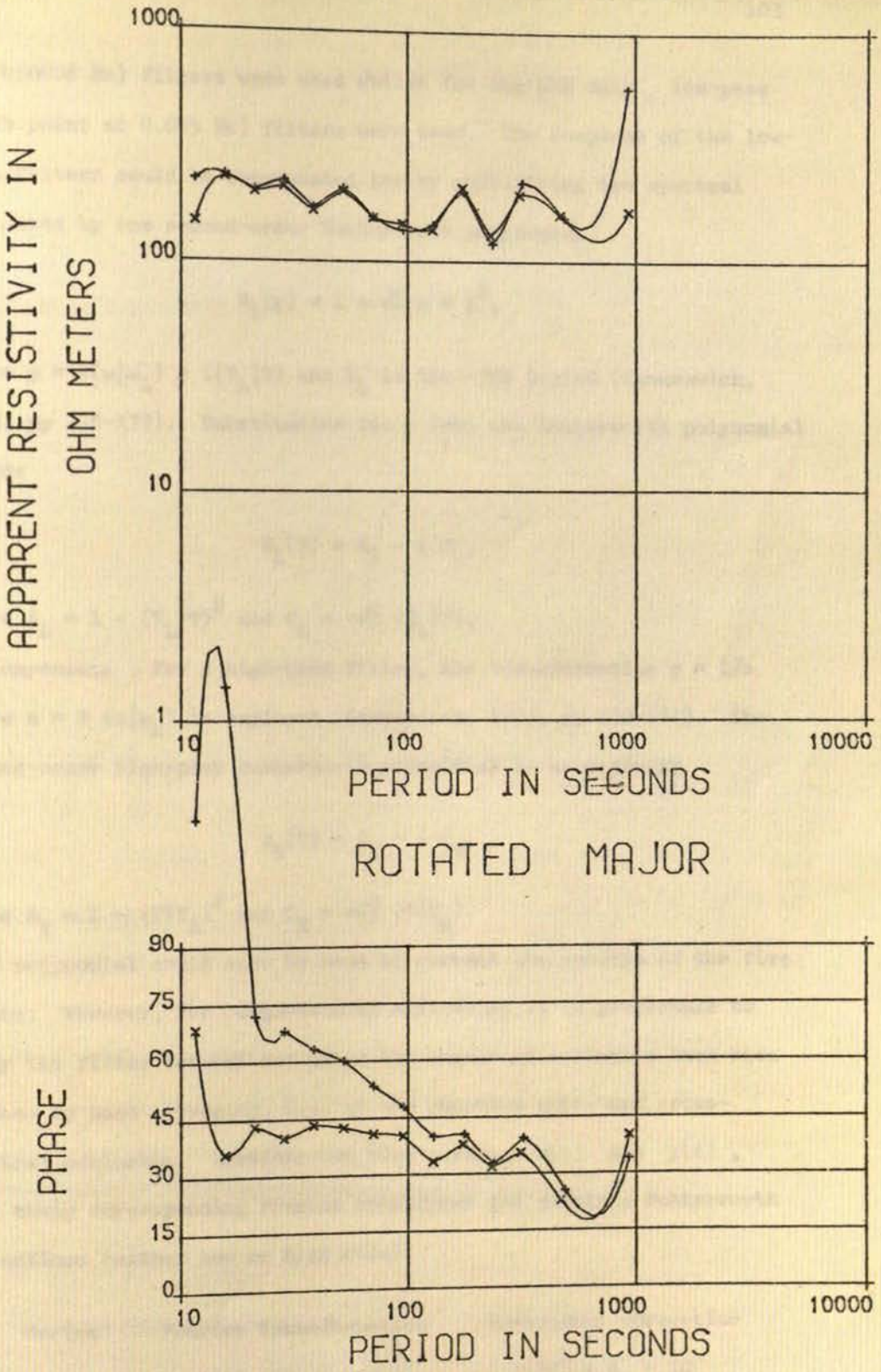

Figure 4.7 Comparison of correcting for parallax in the time domain (+) and the frequency domain (x)

and 0.0008 Hz) filters were used whilst for the SVS only low-pass (-3dB point at 0.005 Hz) filters were used. The response of the low-pass filters could be compensated for by multiplying the spectral estimates by the second-order Butterworth polynomial

$$B_L(p) = 1 + \sqrt{2}\, p + p^2,$$

where $p = i(\omega|\omega_L) = i(T_L|T)$ and T_L is the -3dB period (Kanasewich, 1973, pp 175-179). Substitution for p into the Butterworth polynomial yields

$$B_L(T) = A_L - i\, C_L,$$

where $A_L = 1 - (T_L|T)^2$ and $C_L = -\sqrt{2}\ (T_L|T)$.

To compensate for a high-pass filter, the transformation $p = 1/s$ where $s = i\ (\omega|\omega_H)$ is employed (Kanasewich, 1973, pp 179-181). The second-order high-pass Butterworth polynomial is accordingly

$$B_H(T) = A_H - i\, C_H,$$

where $A_H = 1 - (T|T_H)^2$ and $C_H = +\sqrt{2}\ (T|T_H)$.

This polynomial could also be used to correct the spectra of the five traces. However, for computational efficiency it is preferable to apply the filter corrections after the number of estimates have been reduced by band averaging, i.e. to the smoothed auto- and cross-spectral estimates. Consider two time series, x(t) and y(t), with their corresponding Fourier transforms and required Butterworth corrections (either low or high pass)

Series	Fourier transformation	Instrument correction
x(t)	$X(f) = a_x - iC_x$	$B_x(f) = A_x - iC_x$
y(t)	$Y(f) = a_y - iC_y$	$B_y(f) = A_y - iC_y$.

The cross-spectral estimate of the two series is

$$S_{xy}(f) = X^*(f)\, Y(f) = (a_x + ic_x)(a_y - ic_y),$$

$$= a_s - ic_s,$$

where $a_s = a_x a_y + c_x c_y$ and $c_s = a_x c_y - a_y c_x$.

The corrected cross-spectral estimate is given by

$${}_cS_{xy} = {}_cX^*(f)\ {}_cY(f),$$

$$= (X(f)\ B_x(f))^*\ Y(f)\ B_y(f),$$

$$= {}_ca_s - i_c c_s,$$

where
$${}_ca_s = (A_x A_y + C_x C_y)\, a_s - (A_x C_y - A_y C_x)\, c_s, \qquad (4.18a)$$

$${}_cc_s = (A_x C_y - A_y C_x)\, a_s + (A_x A_y + C_x C_y)\, c_s, \qquad (4.18b)$$

and a_s and c_s are as previously defined.

The corrections to the cross-spectral estimates for the filter responses were applied by inserting the relevant -3db cut off periods into the equations for A_L and C_L (for low pass filters) or A_H and C_H (for high pass filters) and employing 4.18a and b.

A block diagram of the main analysis program - PROGRAM ONE - showing the procedural steps described by 4.3.3 and 4.3.4 to estimate the auto- and cross-spectral matrix, $S_{xy}(f)$, is illustrated in figure 4.8.

4.3.6 Digital filtering

The powerful numerical technique of digital band-pass filtering the raw data to gain a qualitative impression of the behaviour of the spectral components with time has not until recently found much support in geomagnetic induction studies. Primarily this is because the

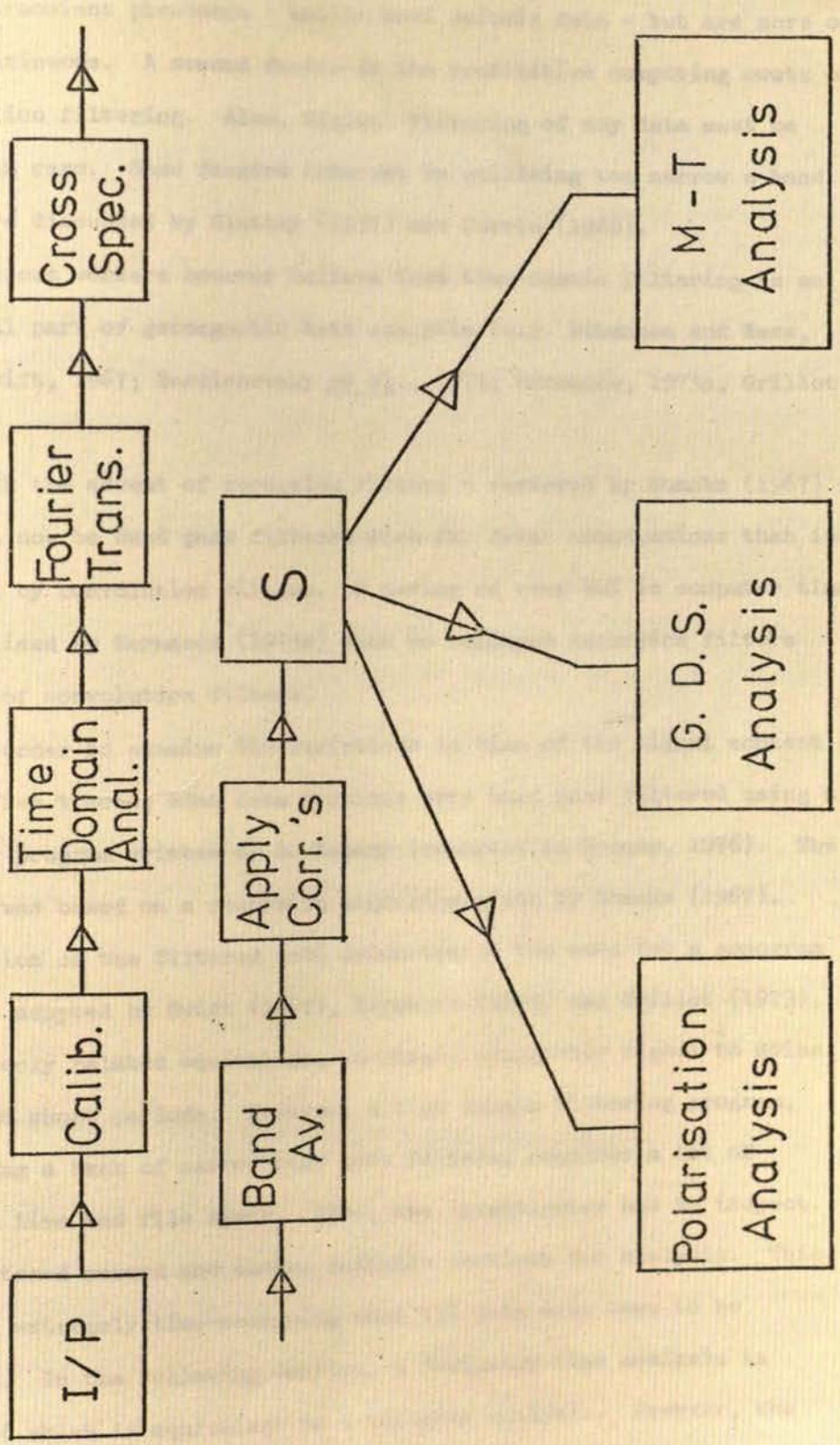

Figure 4.8 Block diagram of PROGRAM ONE analysis

geomagnetic and telluric variations at low periods (1 s - 10^3 s) are not always transient phenomena - unlike most seismic data - but are more or less continuous. A second factor is the prohibitive computing costs of convolution filtering. Also, digital filtering of any data must be done with care. Some dangers inherent in utilising too narrow a band pass were discussed by Slutsky (1937) and Currie (1966).

Various workers however believe that time-domain filtering is an essential part of geomagnetic data analysis (e.g. Behannon and Ness, 1966; Swift, 1967; Berdichevsky et al., 1973; Hermance, 1973a; Grillot, 1975).

With the advent of recursion filters - reviewed by Shanks (1967) - data can now be band pass filtered with far fewer computations than is required by convolution filters. A saving of over 90% in computer time was realised by Hermance (1973a) when he employed recursion filters instead of convolution filters.

In order to examine the variations in time of the signal content of the five traces, some data sections were band pass filtered using a computer program written by D. Rooney (reported in Rooney, 1976). The program was based on a recursion algorithm given by Shanks (1967). Examination of the filtered data demonstrated the need for a sonogram analysis adopted by Swift (1967), Hermance (1973) and Grillot (1973), or a closely related equivalent, to obtain acceptable signal to noise ratios at short periods. However, a time domain filtering program, containing a bank of narrow band pass filters, requires a lot of computer time and file space. Also, the investigator has to inspect each filtered record and choose suitable sections for analysis. This would be extremely time-consuming when 137 data sets have to be analysed. In the following section, a frequency-time analysis is presented which is equivalent to a sonogram analysis. However, the

proposed frequency-time analysis requires less computer resource, both time and file space, and also less effort on the part of the investigator.

4.3.7 Frequency-time analysis

As described in 4.3.6, digital band pass filtering of the raw data indicated that, at short periods, the signal to noise ratios of the geomagnetic and telluric fields varied substantially with time. This effect warranted an analysis which could isolate times of high signal to noise ratio from those of low signal to noise ratio. One of the acceptance criteria employed was that the power levels of all relevant traces (i.e. N, E, H and D for MT estimates; H, D and Z for GDS estimates) at the period of interest must be above a digitiser error power. Whilst this criterion might reject estimates made at short periods from the whole data section, estimates made at times of high signal content would be accepted. Although a sonogram analysis (Swift, 1967) would indicate those times of high signal content, it employs a lot of resources.

A frequency-time analysis has been developed for studying the time varying characteristics of the geomagnetic data. The characteristics of interest are signal to noise ratios, horizontal field polarisations and coherence functions. The method is related to the Bartlett spectral estimation procedure (1948) in that the original data section is segmented into short lengths, either with or without overlap. For each sub-section, a trend is removed, a data window is applied, and the sub-sample size is augmented (by zeros) to a power of two. Each modified sub-data set is then Fourier transformed and the raw estimates are frequency band averaged by a constant Q window. Analysis of the nonstationary properties of a data set by this approach was suggested

by Welch (1967). Two choices of data window are stated by Welch to be of reasonable form. One has the shape $1 - t^2$: $-1 < t < 1$, and gives a spectral window close in shape to that of the hanning, or cosine arch, window (Kanasewich, 1973, pp 101-103). The other window has the shape $1 - |t|$: $-1 < t < 1$, and is the Bartlett (1950) data window (Kanasewich, 1973, pp 104-105). Tests were conducted on artificial and real data to evaluate which of the two data windows was most suitable to employ. The tests showed little, if any, difference between them. The former $(1 - t^2)$ was arbitrarily chosen for subsequent data windowing.

Welch's paper was written to illustrate how Bartlett's spectral estimation method (1948) could be improved by using one of the data windows and, if the original series is short, overlapping the sub-data sets. The smoothed spectral estimates were obtained by averaging arithmetically the raw estimate from each modified periodogram. The author however, was concerned with the nonstationary aspects of the data. Hence, a Constant Q Daniell window was used to smooth the raw estimates of each sub-data set.

To illustrate the procedure: consider two data sets, $x(t)$ and $y(t)$, which are segmented to give K sub-data sets, $x_1(t)$, $x_2(t)$, ..., $x_K(t)$ and $y_1(t)$, $y_2(t)$, ..., $y_K(t)$, of length L. The raw spectral estimates are obtained by taking a discrete Fourier transform of the sub-data sets modified by a data window, viz.

$$X_k(n) = \frac{1}{L} \sum_{j=0}^{L-1} x_k(j)\, w(j) \exp(-2ijkn/L) \qquad (4.19)$$

where $w(j)$ is the selected data window. For the $1 - t^2$ window, as was applied, $w(j)$ is given by

$$w(j) = 1 - \left[j - \frac{L-1}{2} \Big/ \frac{L+1}{2} \right]^2. \qquad (4.20)$$

Estimates for $Y_k(n)$ are obtained in a similar fashion to 4.19. The smoothed cross-spectral estimates in the k'th sub-set are obtained by frequency averaging raw cross-spectral estimates from that sub-set, i.e.

$$\hat{S}_{xy,k}(\bar{n}) = \langle X_k^*(n).\ Y_k(n) \rangle. \qquad (4.21)$$

A flow chart of this procedure - PROGRAM TWO - is illustrated in figure 4.9.

From the smoothed auto- and cross-spectral estimates of the sub-data sets, it is possible to evaluate desired parameters. The non-stationary properties of these parameters can then be displayed in various manners. The methods chosen were (i) the frequency-time variations of various coherence functions and Z/H and Z/D ratios were written out on the line-printer, and (ii) the frequency-time variations of power levels, polarisation characteristics and normalised transformed partial coherence functions were contoured and plotted out by a Calcomp software graphics plotter. The sub-data sets which display the required characteristics, either high signal to noise ratio, high coherence or, a certain horizontal magnetic field polarisation, etc., are then chosen for subsequent analysis.

To illustrate use of PROGRAM TWO, consider the data section DZR9 - of sample size 3526 points - shown in 4.10. Using PROGRAM ONE, these data were analysed and apparent resistivity and phase estimates obtained. However, estimates at periods less than 50 s were not accepted because the smoothed auto-spectral density of one, or more, of the traces was less than the estimated digitising error power. A sonogram analysis with band-pass recursion filters of selectivity 0.2 centred on various periods - figure 4.11 - indicated that there was more power at short periods, which was apparently coherent on all traces, during the second half-hour of the data section.

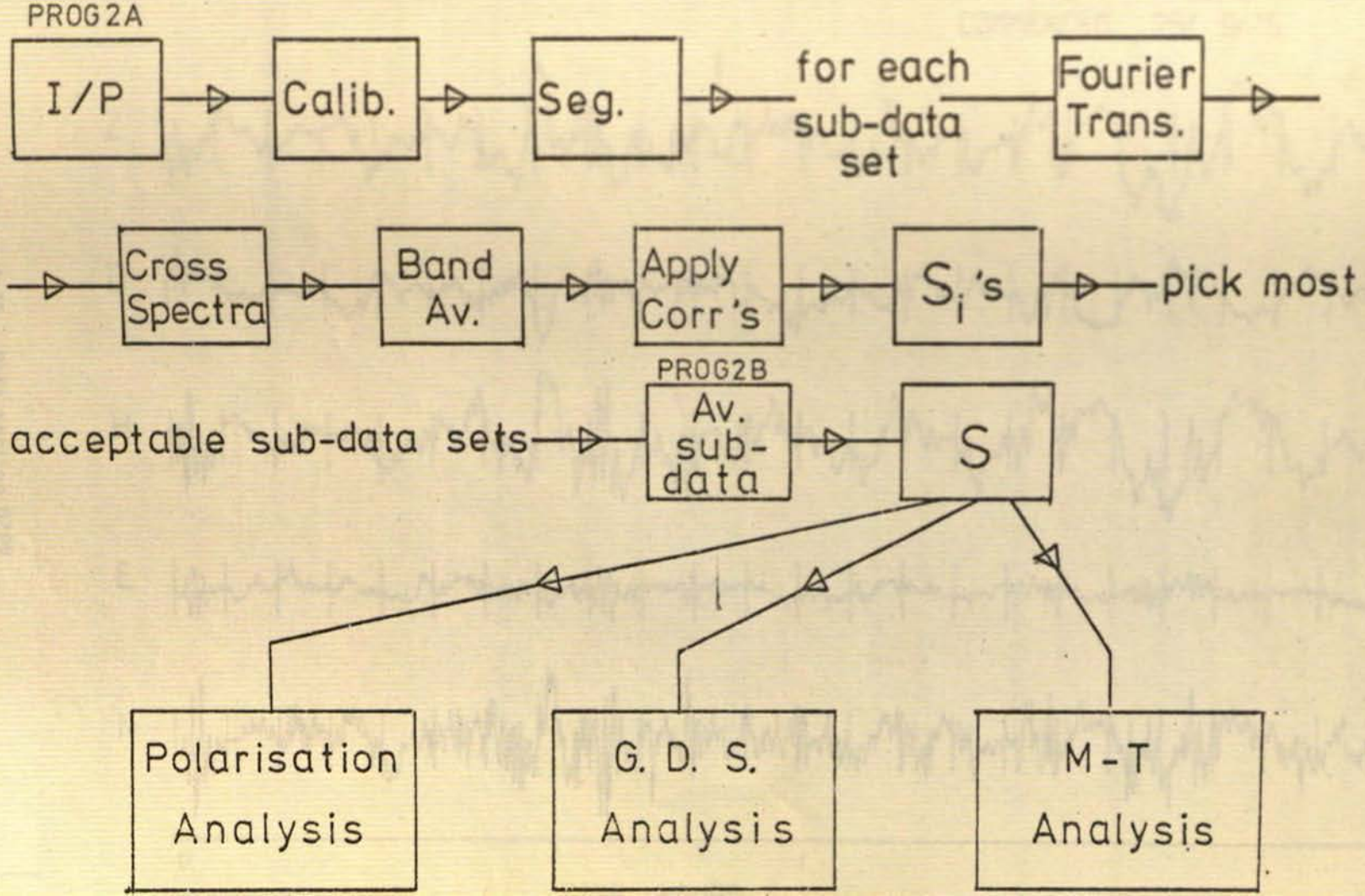

Figure 4.9 Block diagram of PROGRAM TWO analysis

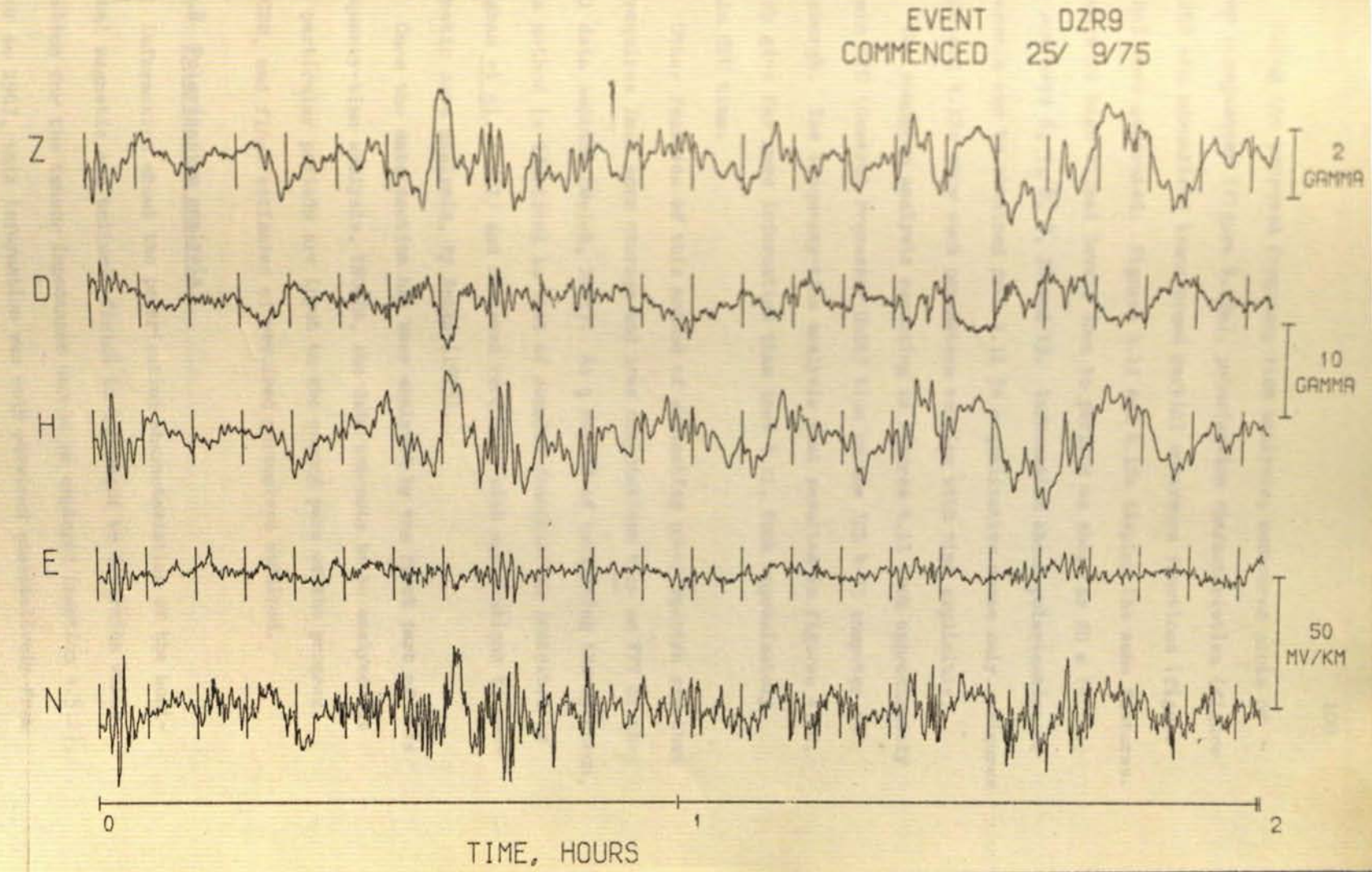

Figure 4.10 Data section DZR9

Using the proposed frequency-time analysis, contoured plots of power acceptances (figure 4.12a), polarisation characteristics (figure 4.12b) and normalised transformed partial coherence functions (figure 4.12c) were generated. Figures 4.11 and 4.12a display the same features. There were high signal levels down to periods as short as 20 s (4.11c) for sub-sets 6, 7, 8, 9, 18 and 19. Information about polarisation or coherence can be obtained from 4.11 in a qualitative sense only. Figures 4.12b and 4.12c show such parameters varying with time explicitly.

The sonogram analysis resulting in figures 4.11 took approximately 30 min CPU (Central Processor Unit) time on the ICL 4-75 computer at Edinburgh. The frequency-time analysis that resulted in figures 4.12, which give far more information than does 4.11, took approximately 5 min CPU time.

Other features of this method of estimating power spectra are that it requires less core storage and less computations than an FFT of the full data section (Welch, 1967). As a method of estimating the spectrum, this method is identical to that of complex demodulation described by Bingham et al. (1967) and reviewed recently, with applications to geomagnetic data analysis, by Banks (1975).

Once the data section has been analysed by the first part of this frequency-time analysis, PROG2A, the data sub-sets to be analysed at the particular periods are input to the second part of the program, PROG2B, and final estimates of required parameters obtained.

4.3.8 Polarisation analysis

Information about the polarisation characteristics of the horizontal magnetic and telluric fields is important to determine which equation for the tensor impedances should be employed (section 4.5.2). Prior to 1967, this information was only obtained qualitatively from

Figure 4.11 Sonogram analysis of data section DZR9

a original series'
b narrow band-pass filtered series', with a centre period of 11s.
c as above for 13.5s.
d as above for 16.5s.
e as above for 20s.
f as above for 25s.
g as above for 30s.
h as above for 36s.
i as above for 45s.

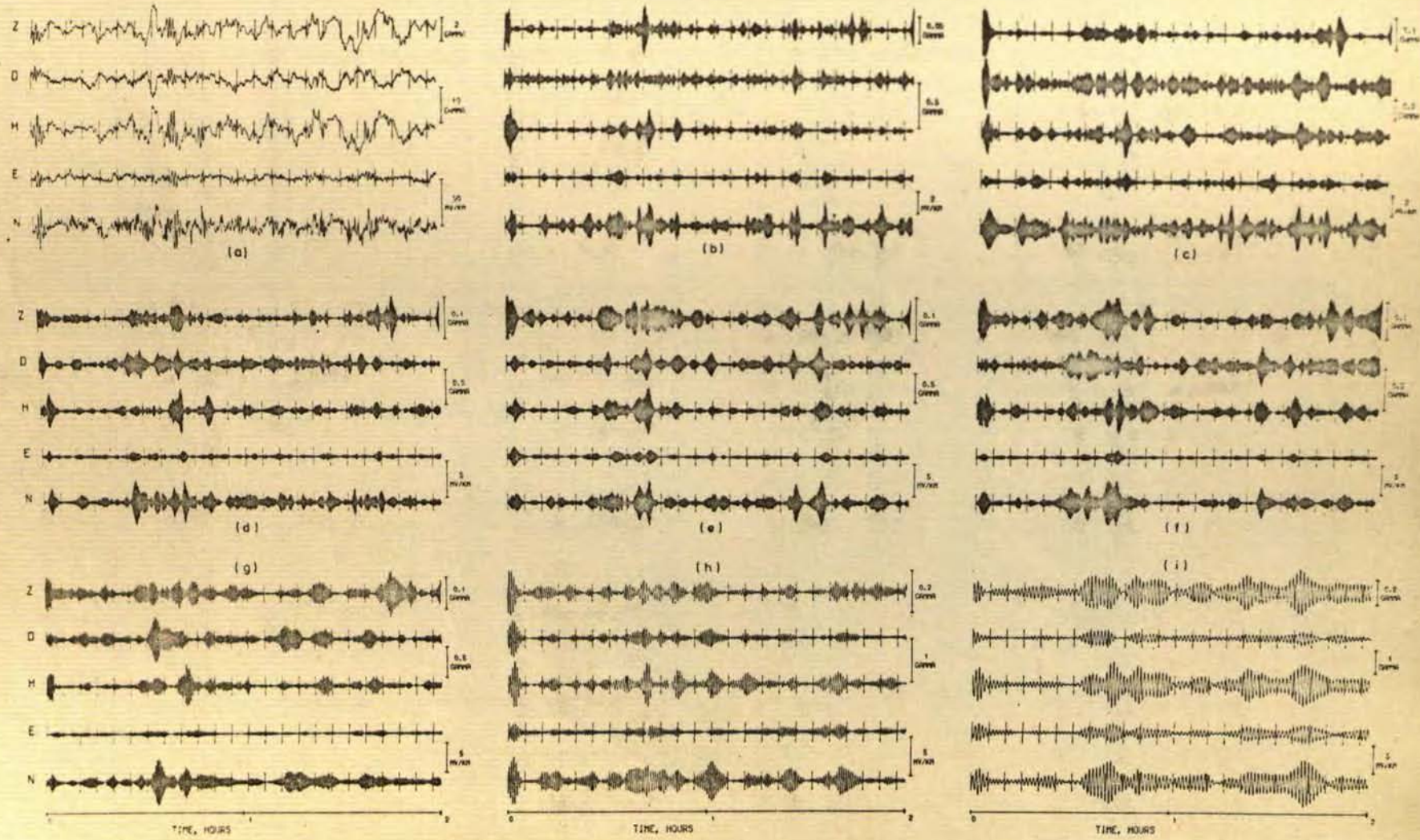
Z
D
H
E
N
(a)
(b)
(c)
(d)
(e)
(f)
(g)
(h)
(i)
TIME, HOURS
TIME, HOURS
TIME, HOURS

Figure 4.12 Contour plots of frequency/time analysis of data section DZR9

(a) Power acceptance regions

(b) Polarisation parameters

(c) Normalised Transformed Partial Coherences

(D)

EVENT DZR9

POWER ACCEPTANCES FOR M-T ANALYSIS

LOG(H) = -1.62 LOG(D) = -1.62 LOG(N) = -0.20 LOG(E) = -0.20

PERIODS

1	524.0	2	149.7	3	65.5	4	40.3
5	29.9	6	24.4	7	20.2	8	16.4
9	13.4	10	11.0				

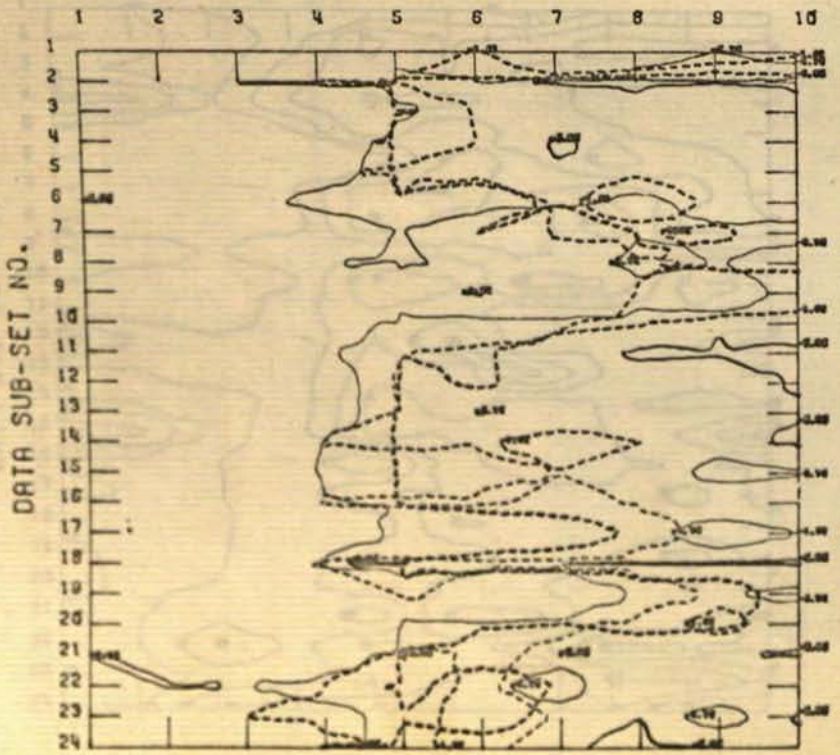

EVENT DZR9

POWER ACCEPTANCES FOR G.D.S. ANALYSIS

LOG(H) = -1.62 LOG(D) = -1.62 LOG(Z) = -2.23

PERIODS

1	524.0	2	149.7	3	65.5	4	40.3
5	29.9	6	24.4	7	20.2	8	16.4
9	13.4	10	11.0				

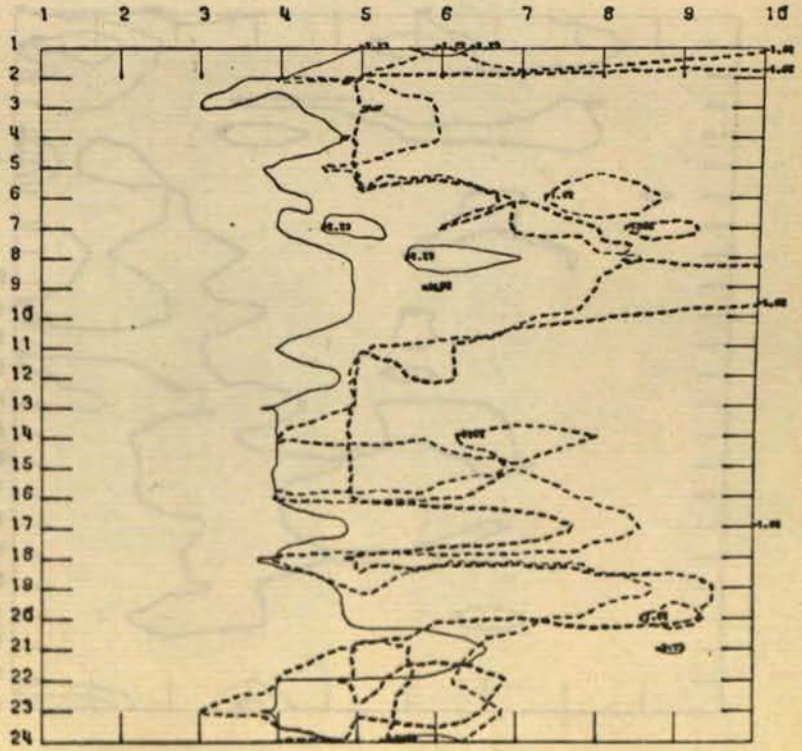

EVENT DZR9

MAGNETIC FIELD POLARISATION CHARACTERISTICS

MINIMUM VALUE = -43.244 MAXIMUM VALUE = 89.977

PERIODS

1	524.6	2	149.7	3	65.5	4	40.3
5	29.9	6	24.4	7	20.2	8	16.4
9	13.4	10	11.6				

PERIOD NO.

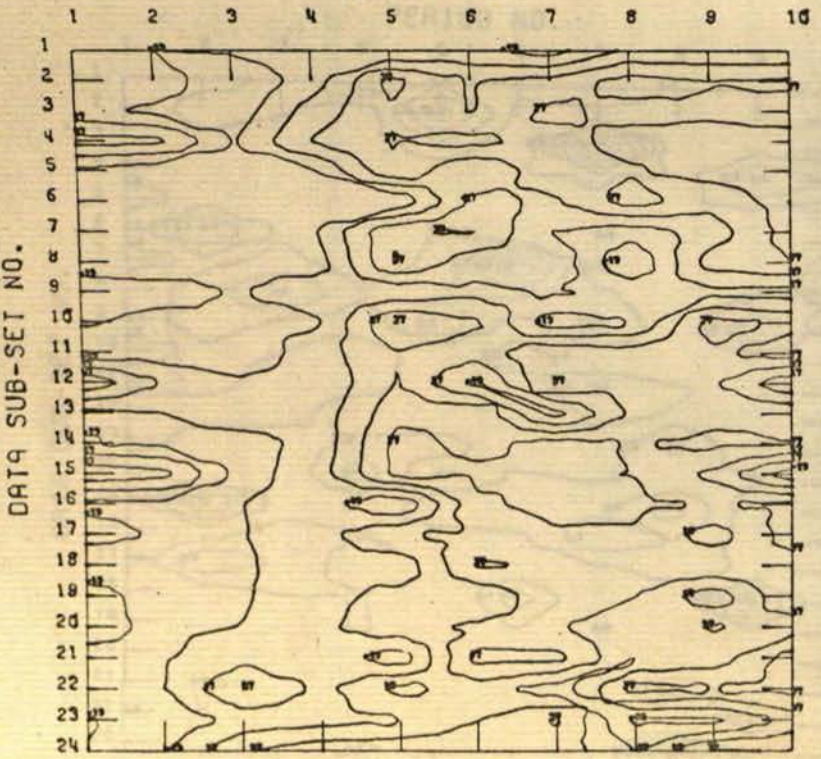

(a)

EVENT DZR9

TELLURIC FIELD POLARISATION CHARACTERISTICS

MINIMUM VALUE = -42.966 MAXIMUM VALUE = 88.372

PERIODS

1	524.6	2	149.7	3	65.5	4	40.3
5	29.9	6	24.4	7	20.2	8	16.4
9	13.4	10	11.6				

PERIOD NO.

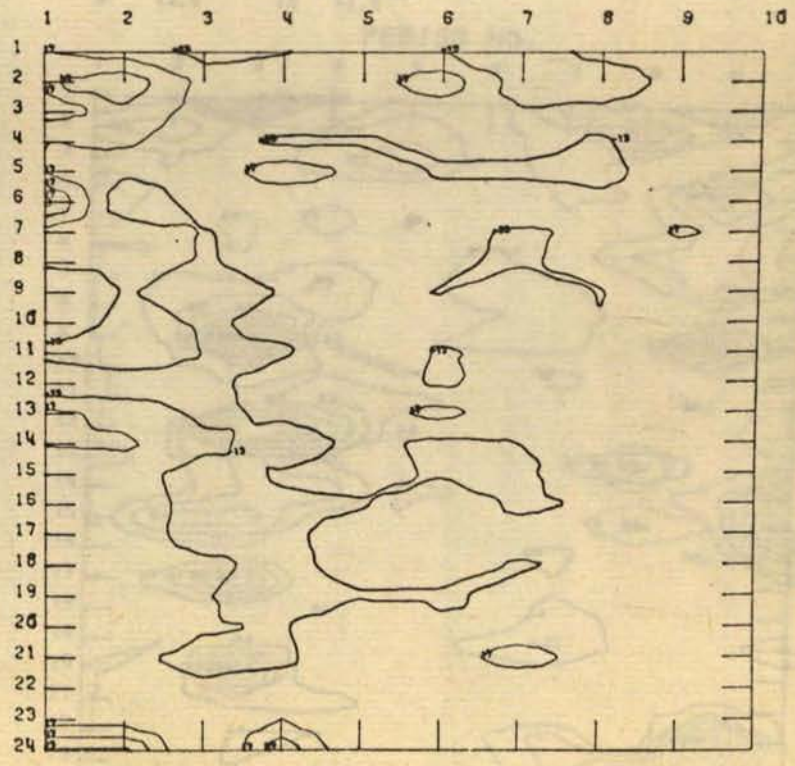

EVENT DZR9

NORMALISED TRANSFORMED PARTIAL COHERENCE ND.H

MINIMUM VALUE = 0.034 MAXIMUM VALUE = 13.167

PERIODS

1	524.0	2	149.7	3	65.5	4	40.3
5	29.9	6	24.4	7	20.2	8	16.4
9	13.4	10	11.0				

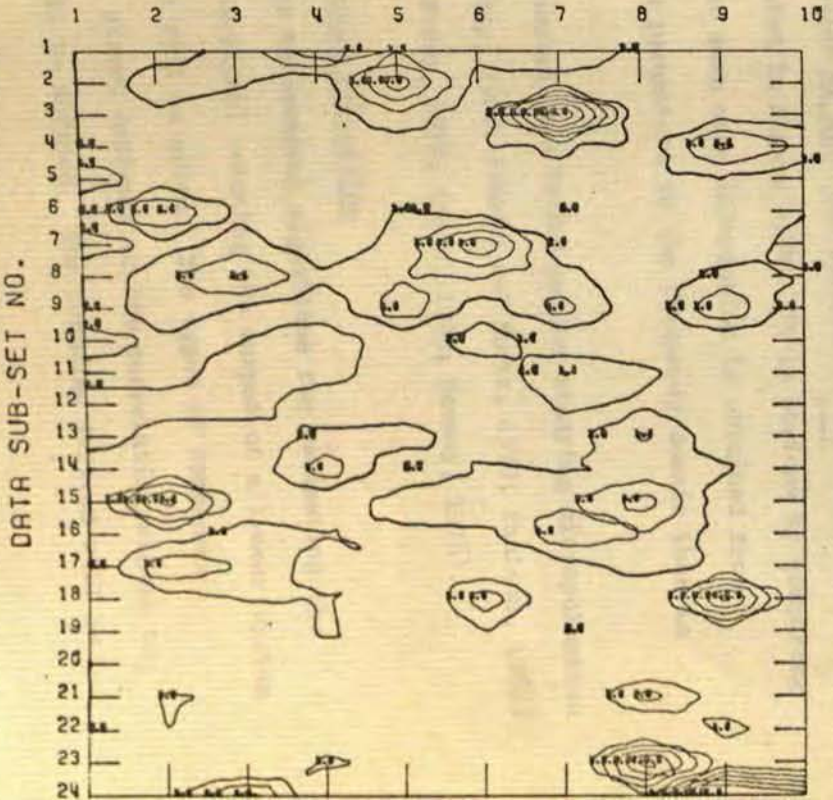

EVENT DZR9

NORMALISED TRANSFORMED PARTIAL COHERENCE EH.D

MINIMUM VALUE = 0.259 MAXIMUM VALUE = 18.026

PERIODS

1	524.0	2	149.7	3	65.5	4	40.3
5	29.9	6	24.4	7	20.2	8	16.4
9	13.4	10	11.0				

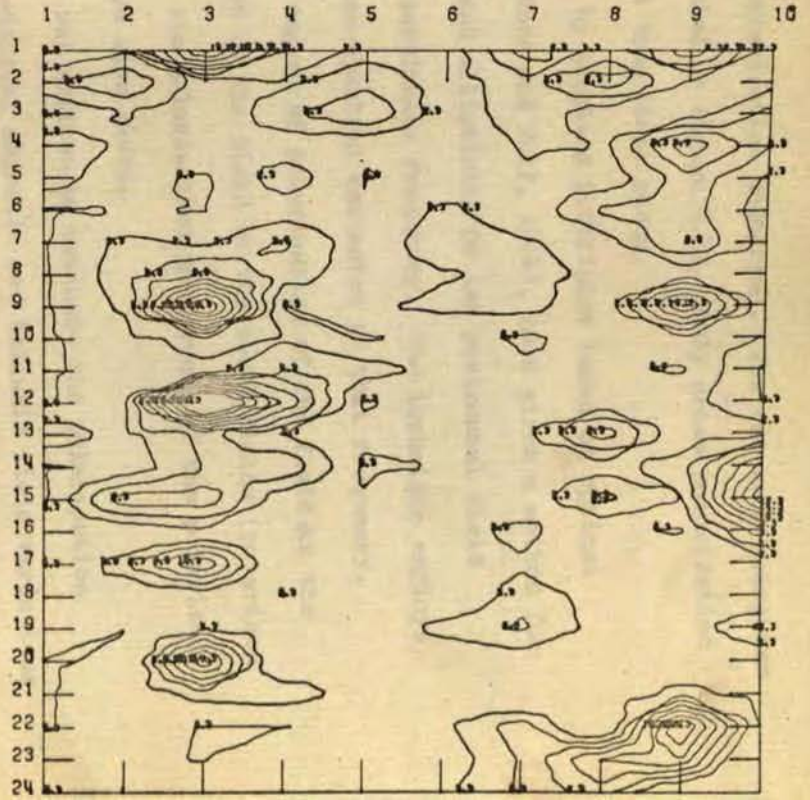

(c)

inspection of time domain polarisation hodograms. The two such hodograms for event DZR9 are illustrated in figure 4.13. Only gross polarisation information can be obtained from these plots.

Fowler et al. (1967), by adapting principles based on optical phenomena (O'Neill, 1963; Born and Wolf, 1964), have given a method for calculating the direction and ellipticity of the horizontal field polarisation ellipse at a particular frequency. The technique employs the smoothed auto- and cross-spectral estimates at that frequency. Methods for computing the degree of polarisation of the field as the ratio of the polarised part of the field to the total fields (polarised + unpolarised parts), and the polarisation parameters of the polarised part of the field only, are also given.

A FORTRAN subroutine was written to estimate the polarisation characteristics of the horizontal magnetic and telluric field variations using the technique of Fowler et al. The parameters derived from data section DZR9 are illustrated in figure 4.14. It is obvious by comparing figures 4.13 and 4.14 that much more information is obtained from studying the polarisation parameters in the frequency domain than in the time domain.

Many workers have adopted this technique for studying micropulsation phenomena (Rankin and Reddy, 1968; Rankin and Kurtz, 1970; Paulson, 1968) and MT data (Rankin and Reddy, 1970; Kurtz, 1973; Rooney, 1976).

4.4 Linear System Parameter Evaluation

In this section, the theoretical algorithms for estimating the response function (or functions) relating the output of a linear system to its input (or inputs) will be given. New types of coherence functions, which give a direct estimate of the correlating signal to random noise ratios, will be defined. The formulae derived will be

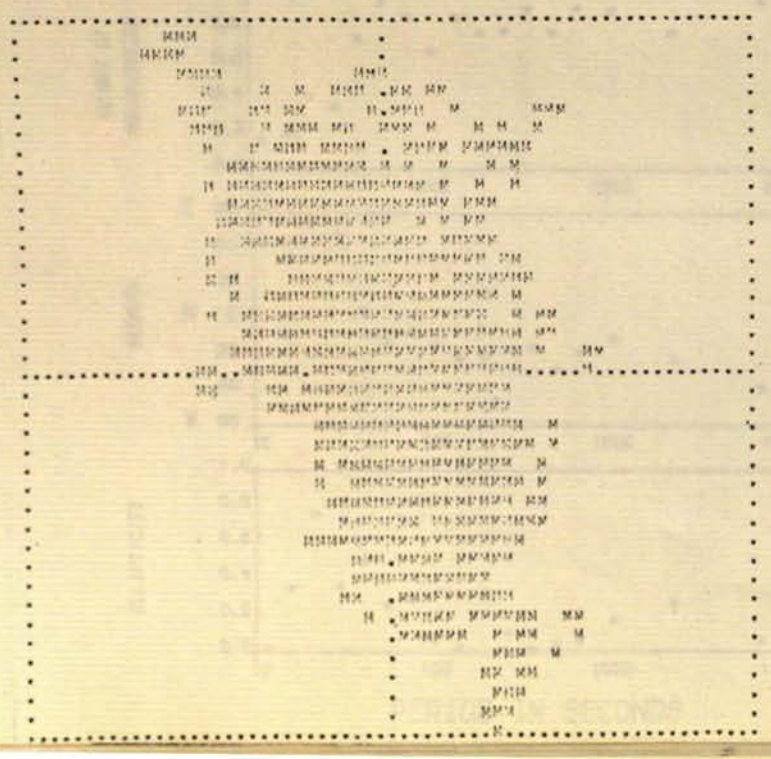

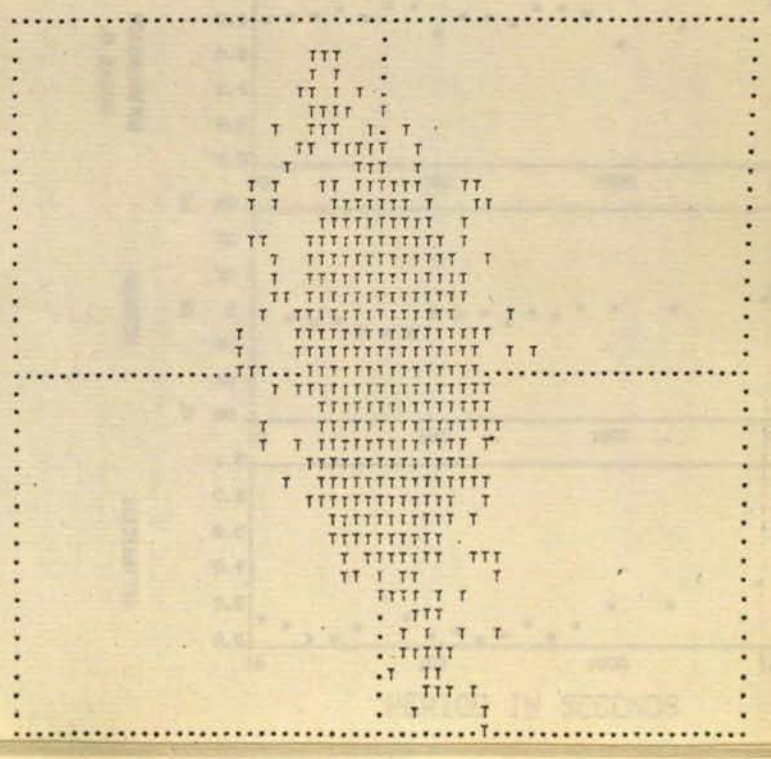

Figure 4.13 Hodograms of horizontal field polarisation for data section DZR9

Figure 4.14 Frequency domain horizontal field polarisation analysis for data section DZR9

shown in later sections to be useful for estimating the magneto-telluric impedance tensor elements (section 4.5) and the geomagnetic response functions (section 4.6).

4.4.1 Single input/single output system

Although the basic theory pertaining to the single input/single output linear system problem has been given in many standard texts (Jenkins and Watts, 1968; Bendat and Piersol, 1971; Otnes and Enochson, 1972), it is considered appropriate to restate it fully here because the mathematical procedures involved will be employed in later sections.

Consider the linear system model, figure 4.15a, with a single input time series, $x(t)$, and an output time series, $y(t)$. The output will be related to the input and the dynamic characteristics of the system, described by a weighting function $h(\tau)$, by the convolution integral, viz.

$$y(t) = \int_{-\infty}^{\infty} h(\tau)\, x(t-\tau)\, d\tau. \qquad (4.22)$$

(Bendat and Pierson, 1971, equation 2.2). However, for any system to be physically realisable, it can only respond to past inputs and not to any future ones. This implies $h(\tau) = 0$ for $\tau < 0$. Hence, the lower limit of equation 4.22 can be set to zero instead of minus infinity. Direct estimation of the impulse response function, $h(\tau)$, by auto-correlation methods is unwise because of the bad statistical properties of the estimates (Jenkins and Watts, 1968, pp 422-429). These difficulties may be removed by estimating the Fourier transform of the impulse response function, given by

$$H(f) = \int_{-\infty}^{\infty} h(\tau)\, e^{-2\pi i f \tau}\, d\tau. \qquad (4.23)$$

Figure 4.15 Single input/single output models

$x(t)$ - measured input

$y(t)$ - measured output

(a) - both inputs uncontaminated by noise conponents

(b) - output series contaminated by noise

$$y(t) = o(t) + n_y(t)$$

(c) - input series contaminated by noise

$$x(t) = i(t) + n_x(t)$$

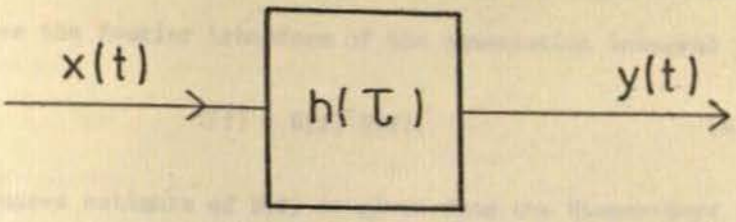

(a)

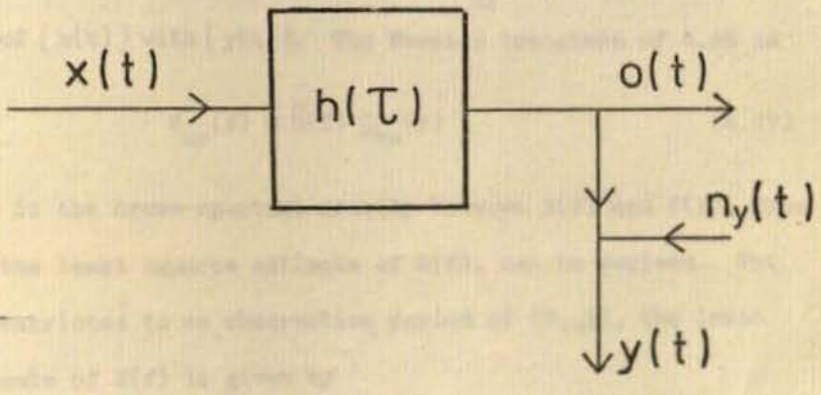

(b)

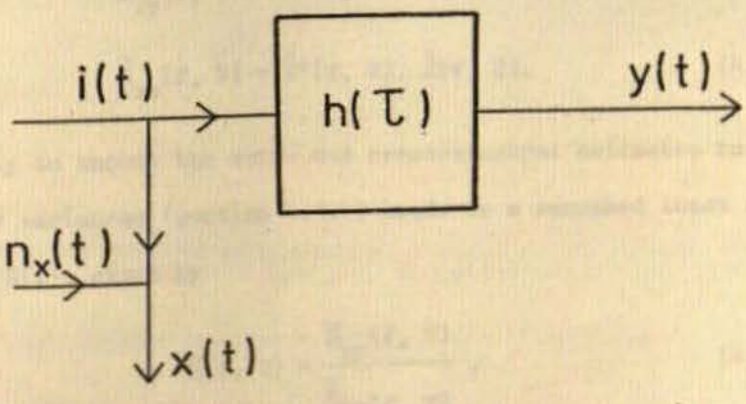

(c)

This function is derived by Fourier transforming the input and output series because the Fourier transform of the convolution integral yields

$$Y(f) = H(f)\, X(f). \tag{4.24}$$

The least squares estimate of H(f) is given from the Wiener-Hopf integral equation, which states

$$R_{xy}(U) = \int_{-\infty}^{\infty} \hat{h}(\tau)\, R_{xx}(U - \tau)\, d\tau \tag{4.26}$$

(Jenkins and Watts, 1968, pp 204-205), where $R_{xy}(U)$ is the cross-correlation of [x(t)] with [y(t)]. The Fourier transform of 4.26 is

$$S_{xy}(f) = \hat{H}(f)\, S_{xx}(f)\ , \tag{4.27}$$

where $S_{xy}(f)$ is the cross-spectral density between X(f) and Y(f), from which $\hat{H}(f)$, the least squares estimate of H(f), can be derived. For real data, restricted to an observation period of (0, T), the least squares estimate of H(f) is given by

$$\hat{H}(f, T) = \frac{\hat{S}_{xy}(f, T)}{\hat{S}_{xx}(f, T)} \tag{4.28}$$

where
$$\hat{S}_{xy}(f, T) = \hat{X}^*(f, T).\ \hat{Y}(f, T) \tag{4.29a}$$

and
$$\hat{S}_{xx}(f, T) = \hat{X}^*(f, T).\ \hat{X}(f, T). \tag{4.29b}$$

The necessity to smooth the auto- and cross-spectral estimates to reduce their variances (section 4.3.4) leads to a smoothed least squares estimate of H(f), given by

$$\overline{H}(f, T) = \frac{\overline{S}_{xy}(f, T)}{\overline{S}_{xx}(f, T)}\ , \tag{4.30}$$

where
$$\overline{S}_{xy}(f, T) = < \hat{S}_{xy}(f, T) > \tag{4.31a}$$

and $$\bar{S}_{xx}(f, T) = \langle \hat{S}_{xx}(f, T) \rangle. \qquad (4.31b)$$

Strictly, equation 4.30 is only valid if $\bar{S}_{xy}(f, T)$ and $\bar{S}_{xx}(f, T)$ represent the smoothed spectral estimates at a discrete frequency, i.e. if the smoothing has been done by averaging over an ensemble of events (section 4.3.4). However, if H(f) is a slowly varying function of frequency, smoothing of the raw estimates may be done by averaging over neighbouring frequencies.

Consider the effect of white noise, $n_y(t)$, on the output series $o(t)$, figure 4.15b. The mathematical model is expressed as

$$y(t) = \int_{-\infty}^{\infty} h(\tau)\, x(t - \tau)\, d\tau + n_y(t), \qquad (4.32)$$

where $y(t) = o(t) + n_y(t)$. The Fourier transform of 4.32 is

$$Y(f) = H(f)\, X(f) + N_y(f) \qquad (4.33)$$

If the noise series is orthogonal, i.e. not correlated, to the input series, then

$$\langle n_y(\tau)\, x(t + \tau) \rangle = 0 \qquad (4.34)$$

(Bendat and Piersol, 1973, p 161), and the cross spectral density between them will also be zero, i.e.

$$S_{XN}(f) = X^*(f)\, N_y(f) = 0 \qquad (4.35)$$

Thus, the equation

$$S_{xy}(f) = H(f)\, S_{xx}(f) + S_{xn}(f), \qquad (4.36)$$

obtained by multiplying equation 4.33 by $X^*(f)$, reduces to

$$S_{xy}(f) = H(f)\, S_{xx}(f),$$

which is exactly the same as equation 4.27. Hence, the estimate

of the response function, given by 4.30, is not biased by noise on the output which is uncorrelated to the input series.

If there is noise, $n_x(t)$, on the input series, $i(t)$, however (figure 4.15c), the mathematical model is

$$y(t) = \int_{-\infty}^{\infty} h(\tau).(x(t-\tau) - n_x(t-\tau))\, d\tau, \qquad (4.37)$$

where $x(t) = i(t) + n_x(t)$. Fourier transformation of 4.37 gives

$$Y(f) = H(f)(X(f) - N_x(f)). \qquad (4.38)$$

Multiplying equation 4.38 by the complex conjugate of the Fourier transform of the measured input series, i.e. $X^*(f)$, gives

$$S_{xy}(f) = H(f)(S_{xx}(f) - S_{xn}(f)). \qquad (4.39)$$

If the noise is uncorrelated to either the true input, $i(t)$, or the output, $y(t)$, then 4.39 reduces to

$$S_{xy}(f) = H(f)(S_{xx}(f) - S_{nn}(f)). \qquad (4.40)$$

Therefore, an estimate of $H(f)$ from equation 4.27, i.e.

$$\hat{H}'(f) = \frac{S_{xy}(f)}{S_{xx}(f)},$$

will be underestimated by an amount

$$\frac{\hat{H}'(f)}{\hat{H}(f)} = \frac{S_{xx}(f) - S_{nn}(f)}{S_{xx}(f)} = \frac{S_{ii}(f)}{S_{ii}(f) + S_{nn}(f)} \qquad (4.41)$$

Hence, estimate of the response function $H(f)$ by equation 4.27 will be unaffected by random noise on the measured output but will be downgraded by measured noise on the input. An alternative estimate of $H(f)$ can be derived by multiplying equation 4.24 by $Y^*(f)$ to give

$$S_{yy}(f) = \hat{H}(f)\, S_{yx}(f), \qquad (4.42)$$

from which $\hat{H}(f)$ can be calculated. It can be shown by an analysis similar to that above, that this estimate will be unaffected by noise on the measured input but will be overestimated, by a factor of $S_{yy}|(S_{yy} - S_{nn}) = (S_{oo} + S_{nn})|S_{oo}$, by noise present on the output. If it is known beforehand which series, either the input or the output, contains random noise, then one of the two equations, 4.27 and 4.42, can be selected to give the true response function. If noise is present on both the input and output, then neither 4.27 nor 4.42 will yield the correct result. Methods exist for deriving the true response function in this case by employing bispectral analysis techniques (Akaike, 1967; Parzen, 1967). These techniques however have not been generally adopted.

Information about the noise present in the measurements can be gained from the coherence between the input and output series. The coherence is defined as

$$\gamma^2_{xy}(f) = \frac{|S_{xy}(f)|^2}{S_{xx}(f)\, S_{yy}(f)} \qquad (4.43)$$

and is a totally real quantity. Some authors use the complex valued coherency, defined as

$$\gamma_{xy}(f) = \frac{S_{xy}(f)}{\left(S_{xx}(f)\, S_{yy}(f)\right)^{\frac{1}{2}}}.$$

This function has a modulus (the square root of the coherence) and a phase (the phase of $S_{xy}(f)$). As the majority of literature on spectral analysis quotes the former definition, the author has employed coherence rather than coherency throughout.

The coherence function given by 4.43 satisfies $0 < \gamma^2_{xy}(f) < 1$ for all frequencies (Bendat and Piersol, 1973, pp 79-80). As will be shown in section 4.4.4, the coherence function will always yield the value

of unity, even for totally uncorrelated series, unless the spectral estimates are smoothed. The smoothing operation increases the number of degrees of freedom from 2 to 2n - where n is the number of raw estimates averaged together - which is necessary to reduce the bias of the function (Bendat and Piersol, 1973, pp 194-196).

If $[x(t)]$ and $[y(t)]$ are totally uncorrelated, the coherence function will be theoretically zero. If they are totally correlated, the function will be one. If the function is between these limits, one or more of three possible situations exist:

(i) extraneous noise is present in the measurements,

(ii) the system relating $[y(t)]$ to $[x(t)]$ is not linear, or

(iii) $[y(t)]$ is an output due to input $[x(t)]$ and other (unknown) inputs.

To illustrate situation (i), if $x(t) = i(t) + n_x(t)$ and/or $y(t) = o(t) + n_y(t)$, then 4.43 yields

$$\gamma^2_{xy}(f) = \frac{|S_{io}(f)|^2}{(S_{ii}(f) + S_{nn}(f))(S_{oo}(f) + S_{nn}(f))}$$

which will be less than unity.

4.4.2 Two input/single output system

A two input/single output system is the simplest case of the class of multiple input/single output systems. The formulae derived can be generalised easily if there are more than two inputs.

The most general model possible, figure 4.17, of both measured inputs and measured outputs contaminated by noise is given by

$$y(t) - n_y(t) = \int_{-\infty}^{\infty} h_1(\tau)(x_1(t-\tau) - n_1(t-\tau))\, d\tau + \int_{-\infty}^{\infty} h_2(\tau)(x_2(t-\tau) - n_2(t-\tau))\, d\tau, \qquad (4.44)$$

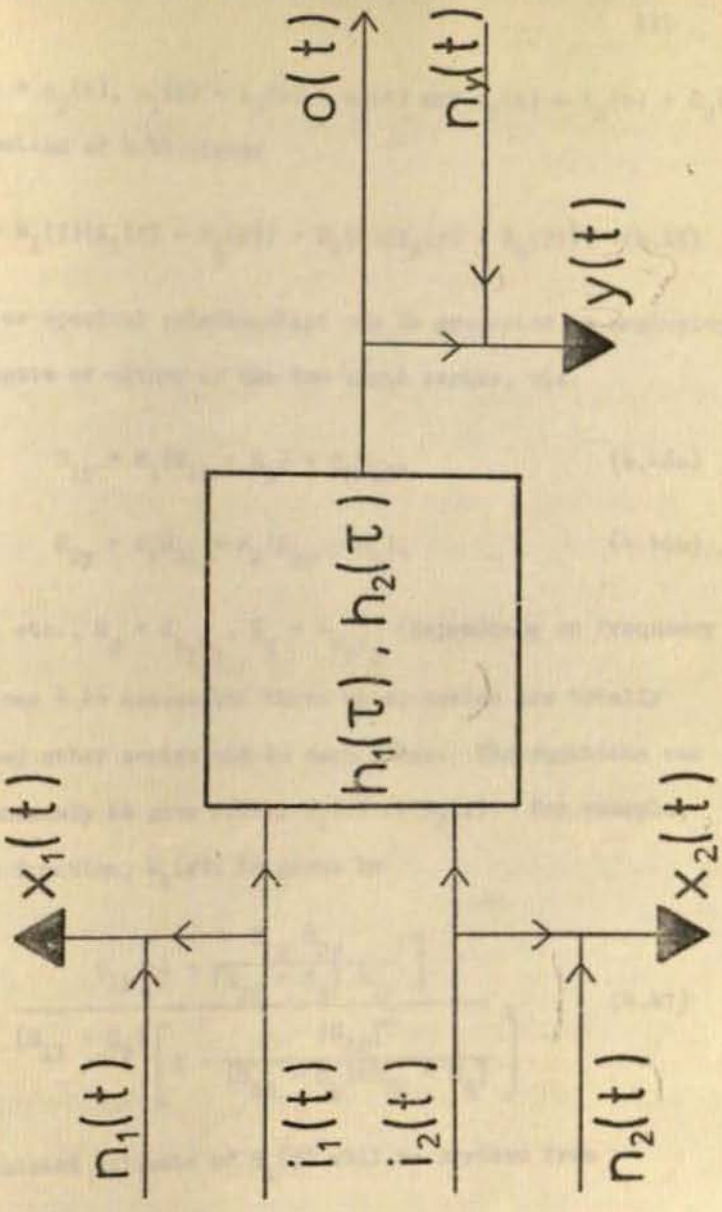

Figure 4.16 General two input/single output linear system model

where $y(t) = o(t) + n_y(t)$, $x_1(t) = i_1(t) + n_1(t)$ and $x_2(t) = i_2(t) + n_2(t)$. Fourier transformation of 4.44 yields

$$Y(f) - N_y(f) = H_1(f)(X_1(f) - N_1(f)) + H_2(f)(X_2(f) - N_2(f)). \quad (4.45)$$

The auto and cross-spectral relationships can be generated by employing the complex conjugate of either of the two input series, viz.

(i) $$S_{1y} = H_1(S_{11} - S_p) + H_2 S_{12}, \quad (4.46a)$$

and (ii) $$S_{2y} = H_1 S_{21} + H_2(S_{22} - S_q), \quad (4.46b)$$

where $S_{1y} \equiv S_{x_1 y}$, etc., $S_p = S_{n_1 n_1}$, $S_q = S_{n_2 n_2}$ (dependence on frequency assumed). Equations 4.46 assume the three noise series are totally uncorrelated to any other series and to each other. The equations can be solved simultaneously to give either $H_1(f)$ or $H_2(f)$. For example, the true response function, $H_1(f)$, is given by

$$H_1 = \frac{S_{1y}\left[1 - \dfrac{S_{12}\, S_{2y}}{(S_{22} - S_q)\, S_{1y}}\right]}{(S_{11} - S_p)\left[1 - \dfrac{|S_{12}|^2}{(S_{11} - S_p)(S_{22} - S_q)}\right]}. \quad (4.47)$$

However, the calculated estimate of $H_1(f)$ will be derived from

$$H_1' = \frac{S_{1y}\left[1 - \dfrac{S_{12}\, S_{2y}}{S_{22}\, S_{1y}}\right]}{S_{11}\left[1 - \dfrac{|S_{12}|^2}{S_{11}\, S_{22}}\right]}. \quad (4.48)$$

As with the simpler single input/single output case, $H_1'(f)$ will be an underestimate of $H_1(f)$ by a factor of:

$$\frac{H_1'}{H_1} = \frac{(S_{22}\, S_{1y} - S_{12}\, S_{2y})\,(1 - \gamma_{12}^2)\, S_{11}'\, S_{22}'}{(S_{22}'\, S_{1y} - S_{12}\, S_{2y})\,(1 - \gamma_{12}^{2\prime})\, S_{11}\, S_{22}}, \quad (4.49)$$

where $\gamma_{12}^{2'} = \dfrac{|S_{12}|^2}{(S_{11} - S_p)(S_{22} - S_q)}$, $S'_{11} = S_{11} - S_p$ and $S'_{22} = S_{22} - S_q$.

An indication of the magnitude of the various noise terms can be gained from the coherence between the output and the two inputs. This function is termed the 'multiple' coherence (or alternatively, the 'predicted coherence' as it describes the coherence between the measured output and the output predicted from the inputs convolved with the estimated response functions, Jenkins and Watts, 1968, p 487) and is given by

$$\gamma_{y12}^2 = \frac{S_{11}|S_{2y}|^2 + S_{22}|S_{1y}|^2 - 2\,\mathrm{Re}(S_{12}S_{2y}S_{y1})}{S_{yy}(S_{11}S_{22} - |S_{12}|^2)} \qquad (4.50)$$

(dependence on frequency assumed) (Jenkins and Watts, 1968, p 488). This function is also constrained to the limits $0 < \gamma_{y12}^2 < 1$ and its value can be interpreted in the same manner as the 'ordinary' coherence function defined in section 4.4.1.

If the ordinary coherence functions between either of the two inputs and the output, γ_{1y}^2 and γ_{2y}^2, are calculated by 4.43, their values may be erroneously high or erroneously low. The series $x_2(t)$, when computing γ_{1y}^2, appears as a noise component at the output $y(t)$. Thus, although there may be a true linear relationship between $x_1(t)$ and $y(t)$, it will be masked by the effect of $x_2(t)$. In order to derive the true coherence between the output and one of the inputs, the effect of the other input must be removed. This is done in a least-squares sence by computing the partial coherence functions (Bendat and Piersol, 1972, pp 153-160). These functions are given by

$$\gamma_{y1.2}^2 = \frac{\gamma_{y12}^2 - \gamma_{y2}^2}{1 - \gamma_{y2}^2} \qquad (4.51a)$$

and

$$\gamma^2_{y2.1} = \frac{\gamma^2_{y12} - \gamma^2_{y1}}{1 - \gamma^2_{y1}} \qquad (4.51b)$$

(Jenkins and Watts, 1968, p 489), where $\gamma^2_{y1.2}$ is the partial coherence between the input $x_1(t)$ and the output $y(t)$ with the effect of $x_2(t)$ removed.

4.4.3 Bias associated with coherence function estimation

Although the expectation value of the ordinary coherence between two random series, $r_1(t)$ and $r_2(t)$, is zero, the expectation value of the estimate of the ordinary coherence is not. This is due to the estimate being a biased estimate of the function. That is

$$E[\gamma^2_{r_1r_2}] = 0 \text{ but } E[\hat{\gamma}^2_{r_1r_2}] \neq 0.$$

The bias is given by

$$B(\hat{\gamma}^2_{r_1r_2}) = E[\hat{\gamma}^2_{r_1r_2} - \gamma^2_{r_1r_2}]$$

$$= E[\hat{\gamma}^2_{r_1r_2}] - E[\gamma^2_{r_1r_2}] \quad \text{(Kendall and Stuart, 1958, p 51)}$$

$$= E[\hat{\gamma}^2_{r_1r_2}] . \qquad (4.52)$$

Hence, the bias of the estimate is given by the expectation value of that estimate. Jenkins and Watts (1968, pp 396-399) show that the bias between two normal ergodic random series is

$$B(\hat{\gamma}^2_{r_1r_2}) = \frac{I}{T} ,$$

where $I = \int_{-\infty}^{\infty} W^2(f)df$ - the integrated squared smoothing window function

and T = data set time length.

The ratio I/T is called the variance ratio and, if the spectrum is smooth with respect to the spectral window (a valid assumption for white noise series), is given by

$$\frac{I}{T} = \frac{2}{n}$$

(Jenkins and Watts, 1968, pp 252-254), where n is the number of degrees of freedom associated with the estimate. Hence

$$E[\hat{\gamma}^2_{r_1 r_2}] = \frac{2}{n} . \qquad (4.53)$$

The bias of an estimate of multiple coherence between two random inputs and a random output is also given by the expectation value of that coherence. This is because $E[\gamma^2_{r_3 r_1 r_2}] = 0$ for random series. The expectation value of the estimate of the multiple coherence is given by the expectation value of 4.50. Assuming

$$E[\text{Re}(\hat{S}_{12}\hat{S}_{2y}\hat{S}_{y1})] = 0,$$

then $E[\hat{\gamma}^2_{y12}]$ reduces to

$$E[\hat{\gamma}^2_{y12}] = E\left[\frac{\hat{\gamma}^2_{y1} + \hat{\gamma}^2_{y2}}{1 - \hat{\gamma}^2_{12}}\right],$$

$$= \frac{E[\hat{\gamma}^2_{y1}] + E[\hat{\gamma}^2_{y2}]}{1 - E[\hat{\gamma}^2_{12}]}, \qquad \text{(Kendall and Stuart, 1958, pp 51-52),}$$

$$= \frac{\frac{2}{n} + \frac{2}{n}}{1 - \frac{2}{n}}, \qquad (4.54)$$

for three uncorrelated random series (equation 4.53). Thus

$$E[\hat{\gamma}^2_{y12}] = \frac{4}{n-2} \qquad (4.55)$$

if $y(t)$, $x_1(t)$ and $x_2(t)$ are random.

In a similar manner to that above, the expectation value, and therefore the bias, of an estimate of the partial coherence function for the case of random series is derived from

$$E[\hat{\gamma}^2_{y1.2}] = E\left[\frac{\hat{\gamma}^2_{y12} - \hat{\gamma}^2_{y2}}{1 - \hat{\gamma}^2_{y2}}\right] \quad \text{(equation 4.51a)}$$

$$= \frac{\frac{4}{n-2} - \frac{2}{n}}{1 - \frac{2}{n}} . \qquad (4.56)$$

Hence

$$E[\hat{\gamma}^2_{y1.2}] = E[\hat{\gamma}^2_{y2.1}] = \frac{2n + 4}{(n-2)^2} \qquad (4.57)$$

for three random series. Equation 4.57 will reduce to the form of 4.53 for n large.

A data set, comprising of 5 series of 1600 points each (figure 4.18) was generated using the NAG (Nottingham Algorithms Group) random number routine G05ADF. Each series was tested and found to be stationary, by a run test (Bendat and Piersol, 1972, pp 234-237), and normally distributed, by a chi-square goodness-of-fit test (Bendat and Piersol, 1972, pp 119-122). The three types of coherence functions, ordinary, multiple and partial, were estimated from various combinations of the five Fourier spectra. Those functions estimated were found after averaging to be in very close agreement (to within 5%) with the expected values given by equations 4.53, 4.55 and 4.57.

4.4.4 Normalised transformed coherence functions

As discussed in the previous section, there is an inherent bias of the estimate of any coherence function. This bias leads to a non-zero expectation value for random series. The ratio of the coherence value to its expected random value, which is dependent on n, can be

In a similar manner to that above, the expectation value, and therefore the bias, of an estimate of the partial coherence function for the case of random series is derived from

$$E[\hat{\gamma}^2_{y1.2}] = E\left[\frac{\hat{\gamma}^2_{y12} - \hat{\gamma}^2_{y2}}{1 - \hat{\gamma}^2_{y2}}\right] \quad \text{(equation 4.51a)}$$

$$= \frac{\frac{4}{n-2} - \frac{2}{n}}{1 - \frac{2}{n}} . \qquad (4.56)$$

Hence

$$E[\hat{\gamma}^2_{y1.2}] = E[\hat{\gamma}^2_{y2.1}] = \frac{2n + 4}{(n-2)^2} \qquad (4.57)$$

for three randon series. Equation 4.57 will reduce to the form of 4.53 for n large.

A data set, comprising of 5 series of 1600 points each (figure 4.18) was generated using the NAG (Nottingham Algorithms Group) random number routine G05ADF. Each series was tested and found to be stationary, by a run test (Bendat and Piersol, 1972, pp 234-237), and normally distributed, by a chi-square goodness-of-fit test (Bendat and Piersol, 1972, pp 119-122). The three types of coherence functions, ordinary, multiple and partial, were estimated from various combinations of the five Fourier spectra. Those functions estimated were found after averaging to be in very close agreement (to within 5%) with the expected values given by equations 4.53, 4.55 and 4.57.

4.4.4 Normalised transformed coherence functions

As discussed in the previous section, there is an inherent bias of the estimate of any coherence function. This bias leads to a non-zero expectation value for random series. The ratio of the coherence value to its expected random value, which is dependent on n, can be

considered as a coherent signal to random noise ratio. Using this procedure, it is possible to define normalised coherence functions in the following manner:

$$\text{normalised ordinary coherence function} = \hat{\gamma}^2_{yx}\left(\frac{n}{2}\right) \qquad (4.58a)$$

$$\text{normalised multiple coherence function} = \hat{\gamma}^2_{y12}\left(\frac{n-2}{4}\right) \qquad (4.58b)$$

$$\text{normalised partial coherence function} = \hat{\gamma}^2_{y1.2}\left(\frac{(n-2)^2}{2n+4}\right) \qquad (4.58c)$$

These functions have the expectation value of unity for random data and also are independent of the width of the smoothing window, i.e. the number of estimators averaged over. Accordingly, these functions can be directly and quantitatively compared to estimates derived at another frequency band.

However, the original coherence functions, and hence the normalised coherence functions defined by equations 4.58 also, do not have a normal distribution. Therefore, confidence limits and other statistical parameters cannot be calculated easily. Also, the variances of the estimates are functions of the estimate values (Jenkins and Watts, 1968, p 378). This causes a non-constant interval for confidence limits on the coherence scale. Jenkins and Watts (1968, p 379) note that the variance of the modulus of the ordinary coherency, i.e. the positive square root of the ordinary coherence, is identical to the variance of an ordinary correlation coefficient. They suggest therefore applying R. A. Fisher's Z-transformation (Hold, 1952, pp 608-609) to the ordinary coherency to obtain an estimator with a normal distribution. This transformed ordinary coherency is given by

$$\hat{T}_{xy}(f) = \operatorname{arctanh}\left(|\hat{\gamma}_{xy}|\right), \qquad (4.59)$$

and has a variance

$$\text{Var}\ (\hat{T}_{xy}(f)) = \frac{1}{n}, \tag{4.60}$$

which is independent of frequency and which suggests that $\hat{T}_{xy}(f)$ should be plotted rather than $\hat{\gamma}^2_{xy}$. This is because the confidence interval can be represented by a constant interval on the T scale. Empirical studies by Enochson and Goodman (1965) confirm that the transformation is valid for $0.3 < \gamma^2_{xy} < 0.98$ and $n > 20$. If the estimate of $\hat{\gamma}^2_{xy}$ is first corrected for the bias, then the transformation becomes valid for the whole range of $\hat{\gamma}^2_{xy}$ and for $n > 8$ (Benignus, 1969). This latter technique was not used however because most estimated coherences were within the empirical range.

The variance of the multiple coherence function is of the same form as that of the ordinary coherence function (Jenkins and Watts, 1968, p 492). This suggests the same transformation will also be valid for multiple coherence. Enochson and Goodman (1965) corroborated this and showed the transformed multiple coherency defined by

$$\hat{T}_{y12} = \text{arctanh}\ (|\hat{\gamma}_{y12}|) \tag{4.61}$$

has a normal distribution with a variance given by

$$\text{Var}\ (\hat{T}_{y12}) = \frac{2}{n-2}\ . \tag{4.62}$$

In a similar manner, the transformed partial coherency function

$$\hat{T}_{y1.2} = \text{arctanh}\ (|\hat{\gamma}_{y1.2}|) \tag{4.63}$$

will have an approximately normal distribution with variance

$$\text{Var}\ (\hat{T}_{y1.2}) = \frac{n+2}{(n-2)^2}\ . \tag{4.64}$$

The variances of each of these functions are half of their previously derived expectation values for random data.

It is desirable to normalise these three functions, 4.59, 4.61 and 4.63, to alleviate the dependence of each of them on n - the number of degrees of freedom of the smoothed spectral estimates. The usual statistical procedure of standardising the normally distributed variable to give a distribution with zero mean and unit variance, i.e.

$$Z = \frac{x - \mu'_x}{\sigma_x} \qquad (4.65)$$

where Z = standardised variable

x = original variable

μ'_x = first moment (mean) of [x] about zero

and σ_x^2 = second moment (variance) of [x] about μ'_x (Kendall and Stuart, 1952, p 48),

will not be employed. Equation 4.65 would not give a function that exhibited the required qualities. The normalisation procedure is required to generate a function which expresses the coherent signal to random noise ratio and also which is independent of the number of degrees of freedom, n. The latter requirement ensures that quantitative comparison between estimates made at different frequencies becomes possible even if a frequency dependent smoothing window is employed.

The method suggested by the author to result in a function with these properties is to normalise the transformed coherency functions by their expected value for random data. The three expected values are given by the transform of equations 4.53, 4.55 and 4.57. The normalised transformed coherency functions and their variances are thus given by

Function		Definition	Variance	
normalised transformed ordinary coherency	$\hat{N}_{yx}$	$\dfrac{\text{arctanh}\,(\lvert\hat{\gamma}_{yx}\rvert)}{\text{arctanh}\,((2/n)^{\frac{1}{2}})}$	$\dfrac{1}{n.\text{arctanh}^2\,((2/n)^{\frac{1}{2}})}$	(4.66a)
normalised transformed multiple coherency	$\hat{N}_{y12}$	$\dfrac{\text{arctanh}(\lvert\hat{\gamma}_{y12}\rvert)}{\text{arctanh}\,((4/(n-2))^{\frac{1}{2}})}$	$\dfrac{2}{(n-2)\,\text{arctanh}^2\,((4/(n-2))^{\frac{1}{2}})}$	(4.66b)
normalised transformed partial coherency	$\hat{N}_{y1.2}$	$\dfrac{\text{arctanh}\,(\lvert\hat{\gamma}_{y1.2}\rvert)}{\text{arctanh}\,((2n+4)^{\frac{1}{2}}/(n-2))}$	$\dfrac{n+2}{(n-2)^2\,\text{arctanh}^2\,((2n+4)^{\frac{1}{2}}/(n-2))}$.	(4.66c)

The following properties of these functions make them preferable to the usual coherence functions:

(i) they are normally distributed,

(ii) they are normalised to unity for random signals, so indicating directly the coherent signal to random noise ratio,

(iii) they are independent of n, thus enabling direct comparison between estimates made at different periods when a constant Q smoothing window (or an equivalent) is employed,

(iv) statistical parameters (e.g. confidence intervals) can easily be calculated, and

(v) the variance is less dependent on n.

For consistency with the use of coherence rather than coherency functions, the author chose to employ normalised transformed coherence functions, $\hat{N}^2_{yx}$, $\hat{N}^2_{y12}$ and $\hat{N}^2_{y1.2}$. The variances of these functions can be derived in the following manner, let

T = transform of the coherency function

V = $\text{Var}[\,T\,]$

T_r = expected value of T for random data

then N is defined by

$$N = \frac{T}{T_r} \tag{4.67}$$

with variance

$$\text{Var}(N) = \frac{T}{T_r^2}. \tag{4.68}$$

The definition of the normalised transformed coherences is

$$N^2 = \left(\frac{T}{T_r}\right)^2 \tag{4.69}$$

with variance by

$$\text{Var}(N^2) = E[N^4] - (E[N^2])^2. \tag{4.70}$$

From Kendall and Stuart (1958, p 55) $E[N^4] = \int_{-\infty}^{\infty} N^4 \, df = \mu_4'$ (the fourth moment of the function N about zero) and $E[N^2] = \int_{-\infty}^{\infty} N^2 \, df = \mu_2'$ (the second moment of N about zero). Therefore

$$\begin{aligned}\text{Var}(N^2) &= \mu_4' - (\mu_2')^2 \\ &= (\mu_4 - 4\mu_1'\mu_3 + 6\mu_1'^2\mu_2 + \mu_1'^4) \\ &\quad - (\mu_2 + \mu_1'^2)^2 \end{aligned} \tag{4.71}$$

(Kendall and Stuart, 1958, p 56) where μ_r' is the r'th moment of the function about zero and μ_r is the r'th moment about the mean (i.e. μ_1'). For a normally distributed variable (which N is), the moments about the mean are

$$\mu_1 = 0 \quad \mu_2 = \sigma^2 \text{ (i.e. Var (N))} \quad \mu_3 = 0 \quad \mu_4 = 3\sigma^4$$

(Kendall and Stuart, 1958, p 56). Letting $N = \mu_1'$, the sample mean (or in this case, the sample value) of the function N, then

$$\begin{aligned}\text{Var}(N^2) &= (3\sigma^4 + 6N^2\sigma^2 + N^4) - (N^2 + \sigma^2)^2 \\ &= 2\sigma^2(\sigma^2 + 2N^2) \\ &= 2\frac{V}{T_r^2}\left(\frac{V}{T_r^2} + 2N^2\right). \end{aligned} \tag{4.72}$$

This variance, as with the variance of coherence, is a function of the sample value (N^2) itself. Hence, constant confidence limits are not possible on an N^2 scale. However, equation 4.72 can be used to derive the minimum necessary normalised transformed coherence above the random noise level, i.e. $N_r^2 = 1$.

For example; to evaluate the minimum necessary normalised transformed coherence (N_m^2) which is non-random to 95% confidence level:

$$1 + 1.96\left(\frac{2V}{T_r^2}\left(\frac{V}{T_r^2} + 2N_m^2\right)\right) \leq N_m^2$$

Therefore

$$(N_m^2 - 1)^2 = 3.84\left(\frac{2V}{T_r^2}\left(\frac{V}{T_r^2} + 2N_m^2\right)\right),$$

which leads to a quadratic equation in N_m^2, viz.

$$N_m^4 - \left(\frac{15.36V}{T_r^2} + 2\right)N_m^2 + \left(1 - \frac{7.68V^2}{T_r^4}\right) = 0.$$

Solutions to this quadratic equation for varying degrees of freedom and for the three types of function, NTOC (normalised transformed ordinary coherence), NTMC (..multiple..) and NTPC (..partial..), are given in table 4.2 and are illustrated in figure 4.17.

To illustrate the use of these functions, the random data set (section 4.4.3, figure 4.18) was input to PROGRAM ONE and the estimated spectra gave the multiple and partial coherences illustrated in figure 4.19a. The incorrect conclusion that the traces are significantly coherent in the range 500 - 3000 s results. The true random characteristics are shown by the NTMC's and NTPC's (figure 4.19b), which are scattered about the expectation level for random signals of one. No value illustrated in 4.19b is above the 95% confidence minimum.

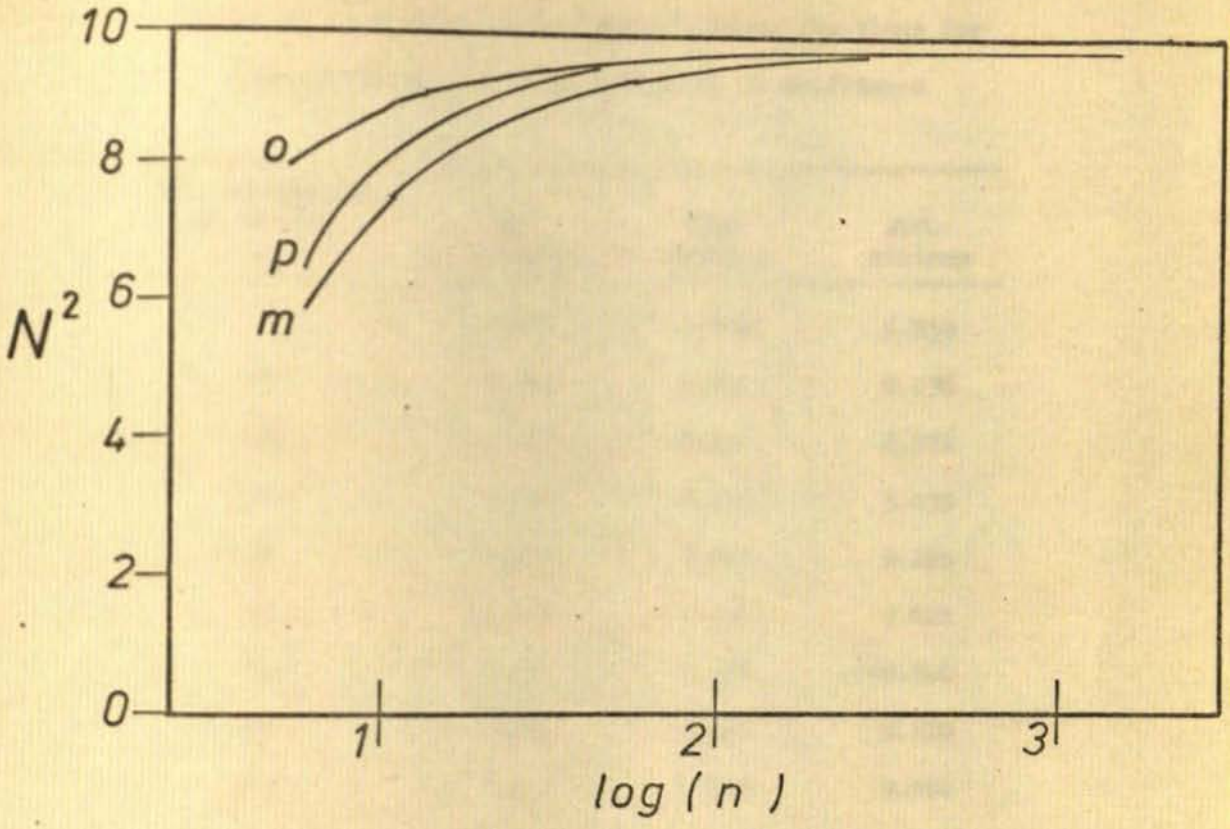

Figure 4.17 Normalised transformed coherence functions above random noise to 95% confidence

o - normalised transformed ordinary coherence

m - " " multiple "

p - " " partial "

TABLE 4.2

Minima of normalised transformed coherence functions for non-random series at the 95% level of confidence

No. of degrees of freedom n	NTOC minimum	NTMC minimum	NTPC minimum
8	8.401	5.810	6.559
12	8.869	7.527	8.230
16	9.098	8.197	8.774
20	9.235	8.558	9.039
28	9.390	8.940	9.296
36	9.476	9.139	9.421
48	9.551	9.306	9.521
64	9.607	9.428	9.590
100	9.667	9.556	9.661
200	9.721	9.666	9.719
400	9.747	9.721	9.747
800	9.761	9.747	9.761
1500	9.767	9.760	9.767

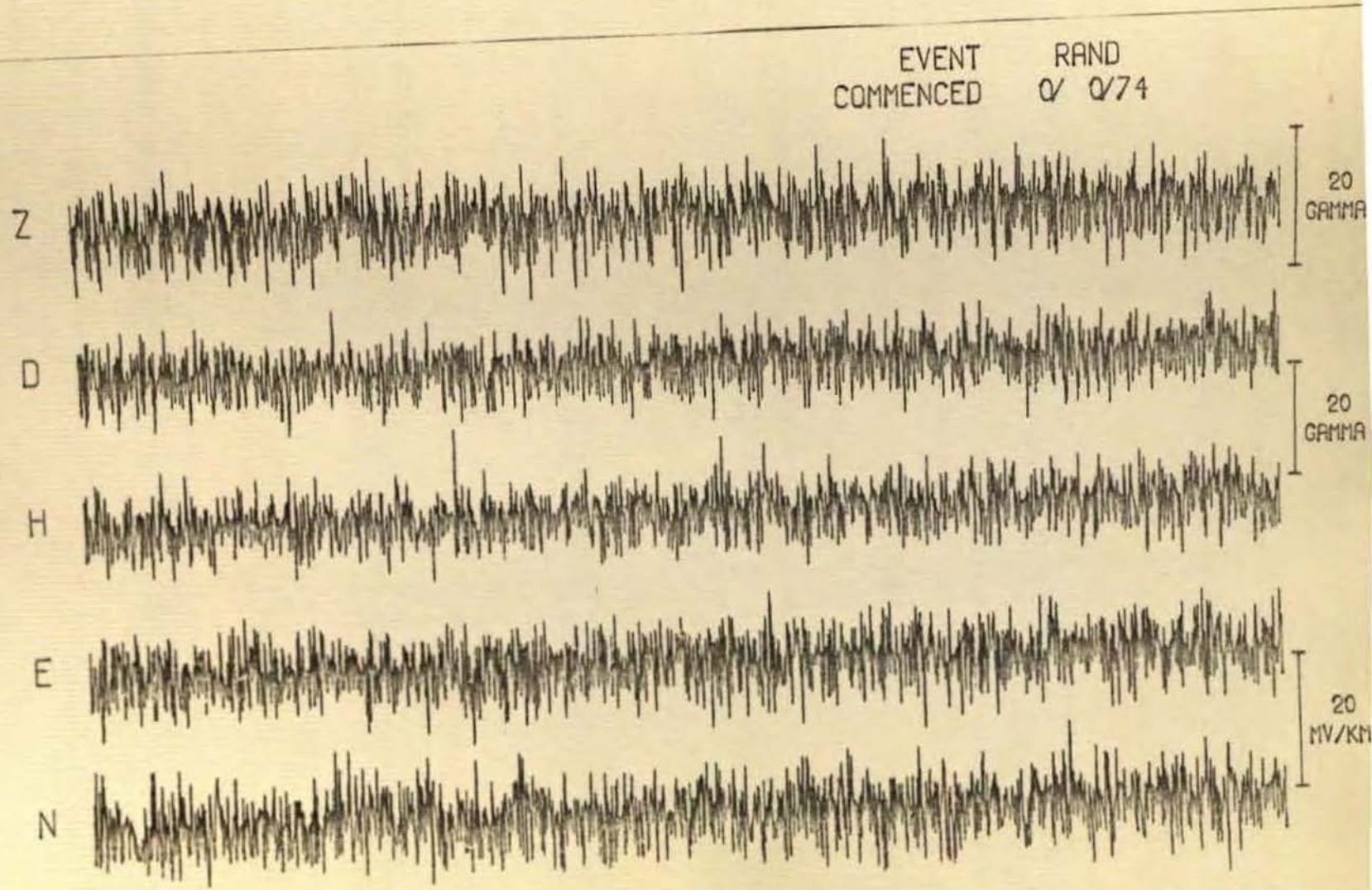

Figure 4.18 Data section RAND

Figure 4.19 Analysis of the coherence between random data series

(a) Multiple and Partial Coherences

(b) Normalised Transformed Multiple and Partial Coherences

STATION RAND

UNROTATED MULTIPLE AND PARTIAL COHERENCES

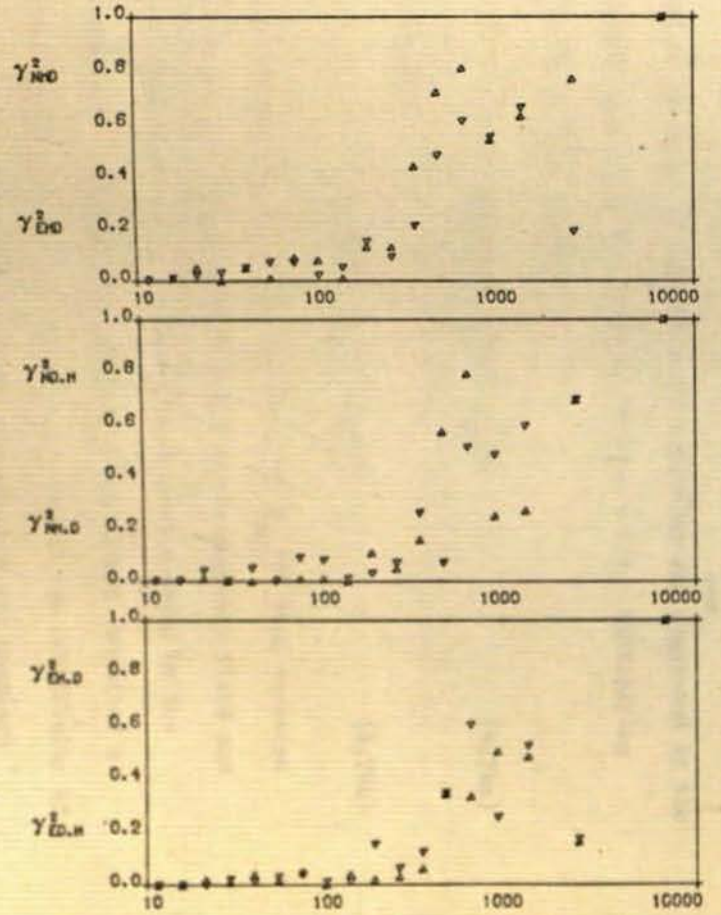

UNROTATED NORMALISED TRANSFORMED COHERENCIES

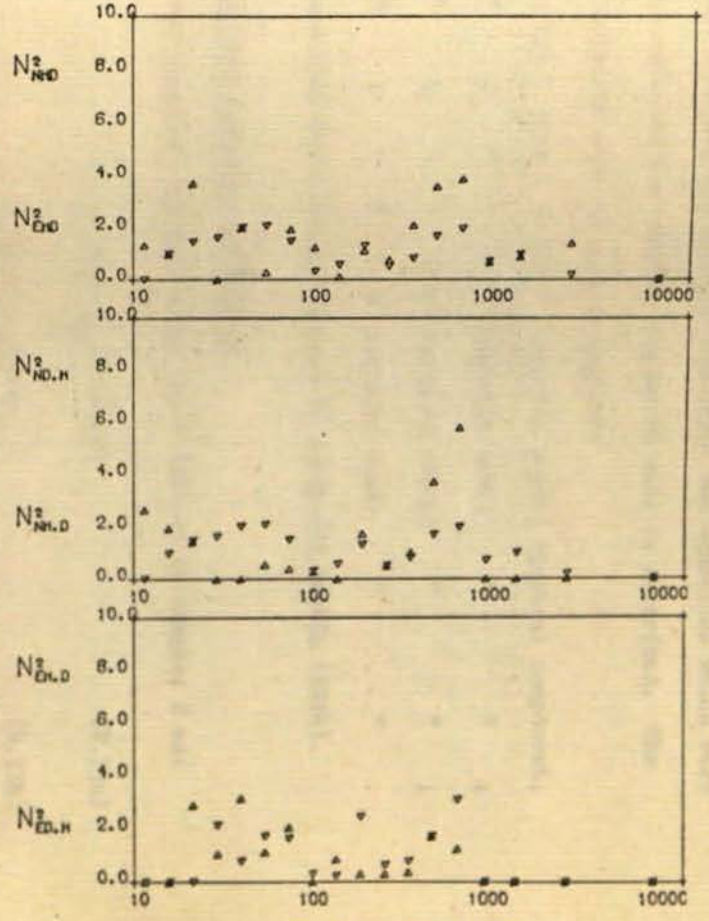

4.5 Magneto-Telluric Impedance Estimation

In this section, the various techniques and equations which were employed to estimate the complex impedances will be described. The following notation will be used throughout:

subscript 1 refers to the H (magnetic north) spectral component;
" 2 " " " D (magnetic east) " " ;
" 3 " " " N (telluric north) " " ;
" 4 " " " E (telluric east) " " .

This concurs with the notation adopted by Reddy and Rankin (1974).

4.5.1 Cagniard impedance estimation

The two Cagniard impedances are those defined in chapter 2 as:

$$E_x(f) = Z_{xy}(f)\, H_y(f) \tag{4.73a}$$

$$E_y(f) = Z_{yx}(f)\, H_x(f) \tag{4.73b}$$

Two methods of solution of each of these equations are suggested by the cross-spectral techniques discussed in section 4.4.1. Multiplying equation 4.73a by $H_y^*(f)$ yields

$$S_{23}(f) = Z_{xy}(f)\, S_{22}(f) \tag{4.74a}$$

or by $E_x^*(f)$ gives

$$S_{33}(f) = Z_{xy}(f)\, S_{32}(f) \tag{4.74b}$$

As concluded in section 4.4.1, the estimate of $Z_{xy}(f)$ from equation 4.74a will be biased down by random noise on the magnetic field and the estimate from 4.74b will be biased up by random noise on the telluric component. Because the telluric field always exhibited a greater noise level than the magnetic field, due to the sensitivity of the field to cultural disturbances, the estimates of the Cagniard impedances were calculated from

$$\hat{Z}_{xy}(f) = \frac{\bar{S}_{23}(f)}{\bar{S}_{22}(f)} \quad \text{and} \quad \hat{Z}_{yx} = \frac{\bar{S}_{14}(f)}{\bar{S}_{11}(f)} . \qquad (4.75a \text{ and } b)$$

An inherent assumption made in equations 4.75 is that $Z_{xy}(f)$ and $Z_{yx}(f)$ are smoothly varying functions of frequency (section 4.4.1). This facilitates estimation of the impedances with single data sets. Even in the limiting cases of either a perfectly conductive or a perfectly resistive substratum, $Z_{xy}(f)$ will be reasonably slowly varying over the bandwidths employed in the averaging procedure.

4.5.2 Tensor impedance estimation

Solution of the magneto-telluric impedance tensor given by

$$\begin{bmatrix} E_x \\ E_y \end{bmatrix} = \begin{bmatrix} Z_{xx} & Z_{xy} \\ Z_{yx} & Z_{yy} \end{bmatrix} \begin{bmatrix} H_x \\ H_y \end{bmatrix} \qquad (4.76)$$

is possible by the cross-spectral techniques discussed in section 4.4.2. As shown by Sims and Bostick (1969) and Sims et al. (1971), there are six possible equations for each of the tensor elements. This is because four cross-spectral equations can be written, by employing the complex conjugate of each of the field components (E_x^*, E_y^*, H_x^* and H_y^*), for each of the two matrix equations given in 4.76. Any pair of the four can then be solved simultaneously (there are six pairs) for the desired tensor element.

However, two of each of the four sets, one set for each element, of six equations become indeterminable if the earth is one-dimensional or if the fields are polarised. This is because the cross-spectra between E_x and H_x (S_{31} and S_{13}) and E_y and H_y (S_{42} and S_{24}) for a one-dimensional case, and between H_x and H_y (S_{12} and S_{21}) and E_x and E_y (S_{34} and S_{43}) for totally unpolarised fields, are zero.

Using arguments similar to those presented in section 4.4.2, it

is possible to show that two of the remaining four equations for each element are biased up by random noise on the telluric field (i.e. the output to the linear system represented by equation 4.67), and the other two are biased down by noise on the magnetic field (i.e. on the input). Sims et al. (1971) suggest that the arithmetic mean of these four equations for each impedance element represents the most reliable estimate possible or the element. However, one of these four equations for each set (one of the two biased up by random noise on the E-field) becomes unstable if the telluric field is strongly polarised, i.e. if $\hat{\gamma}^2_{34} = 1$. Because this was usually the case, and because the magnetic component records appeared much less contaminated by noise than the telluric field, it was decided to employ only one equation of the four for each impedance tensor element. The four expressions so chosen are least biased by noise on the telluric field. They are given by

$$\hat{Z}_{xx} = \frac{\bar{S}_{13}\,(1 - \bar{S}_{12}\,\bar{S}_{23}/\bar{S}_{22}\,\bar{S}_{13})}{\bar{S}_{11}\,(1 - \hat{\gamma}^2_{12})}, \qquad (4.77a)$$

$$\hat{Z}_{xy} = \frac{\bar{S}_{23}\,(1 - \bar{S}_{21}\,\bar{S}_{13}/\bar{S}_{11}\,\bar{S}_{23})}{\bar{S}_{22}\,(1 - \hat{\gamma}^2_{12})}, \qquad (4.77b)$$

$$\hat{Z}_{yx} = \frac{\bar{S}_{14}\,(1 - \bar{S}_{12}\,\bar{S}_{24}/\bar{S}_{22}\,\bar{S}_{14})}{\bar{S}_{11}\,(1 - \hat{\gamma}^2_{12})}, \qquad (4.77c)$$

$$\hat{Z}_{yy} = \frac{\bar{S}_{24}\,(1 - \bar{S}_{21}\,\bar{S}_{14}/\bar{S}_{11}\,\bar{S}_{24})}{\bar{S}_{22}\,(1 - \hat{\gamma}^2_{12})}, \qquad (4.77d)$$

and are equivalent to equation 4.47. Equations 4.77, or closely-related forms, have been used by many workers for estimating the tensor impedances, e.g. Swift (1967), Vozoff (1972), Kurtz (1973), Reddy and Rankin (1975) and Rooney (1976). Kurtz (1973) initially adopted the suggestion of Sims et al. (1971) of averaging four of the six possible equations for each element. However, the estimates so derived exhibited a large degree

of scatter. When the impedances were estimated by equations 4.77, a definite improvement in the quality of the results was reported. Kurtz therefore concluded that equations 4.77 gave more reliable estimates of the impedances than did the averaged estimates of Sims et al.

4.5.3 Rotation of the tensor impedances

As described in section 2.4, once the impedance tensor elements have been computed in the original coordinate system, it is necessary to rotate the elements to the direction of the gross structural strike of the anomaly. The rotated elements are derived by the matrix equation

$$\underline{\underline{Z}}' = \underline{\underline{R}}\,\underline{\underline{Z}}\,\underline{\underline{R}}^{T} \qquad (4.78)$$

where $\underline{R}$ is the Cartesian rotation matrix given by

$$\underline{\underline{R}} = \begin{bmatrix} \cos\theta & \sin\theta \\ -\sin\theta & \cos\theta \end{bmatrix}. \qquad (4.79)$$

In the case of a one-dimensional conductivity distribution, elements Z_{xx} and Z_{yy} are zero hence the rotation does not alter the off-diagonal elements, Z_{xy} and Z_{yx}.

For a two-dimensional structure, an angle, θ_o, may be found at which both the rotated diagonal elements, $Z'_{zz}(\theta_o)$ and $Z'_{yy}(\theta_o)$, become zero. Angle θ_o is then one of the principal axes, either major or minor, and one of the off-diagonal elements (either $Z'_{xy}(\theta_o)$ or $Z'_{yx}(\theta_o)$) represents the H-polarisation mode and the other the E-polarisation mode.

For quasi-two-dimensional structures, i.e. those with low skew factors at all frequencies, many methods have been proposed for estimating the gross structural strike of the anomaly (see for example Swift, 1967; Sims and Bostick, 1969; Reddy and Rankin, 1975). Some of these analytical and numerical methods were described in section 2.4. For real data, it is obviously desirable to maximise the signal content of Z_{xy} and Z_{yx},

or minimise that of Z_{xx} or Z_{yy}, or both. The partial coherence functions $\gamma^2_{32.1}$ and $\gamma^2_{41.2}$ give an indication of the signal content of the off-diagonal impedance tensor elements which are of the Cagniard form, i.e. the amount of coherent signal between one of the telluric field components and its orthogonal magnetic field component, with the influence of its parallel magnetic field component removed. Accordingly, the angle that maximises $\hat{\gamma}^{2'}_{32.1}(\theta)$ not only gives the gross structural strike but also the direction that gives the most coherent signal of the Cagniard-like form. This type of rotation was suggested by Reddy and Rankin (1975).

For three-dimensional structures, i.e. those structures with an associated large skew factor, none of the rotation criteria given in section 2.4 are sufficient to give interpretable results. Rankin et al. (1976) consider that once the 'principal' directions have been determined, a one-dimensional layering interpretation will yield a valid conductivity distribution with depth. The 'principal' directions are obviously those which give the most Cagniard-like impedances and the direction of the major axis will be given by that angle which maximises $\hat{\gamma}^{2'}_{32.1}(\theta)$.

Tests were conducted to compare the angle which maximised $|Z'_{xy}(\theta)|$ with that which maximised $\hat{\gamma}^{2'}_{32.1}(\theta)$. The author chose to maximise $\hat{\gamma}^{2'}_{32.1}(\theta)$ rather than minimise $\hat{\gamma}^{2'}_{31.2}(\theta)$, as suggested by Reddy and Rankin (1975), because sample rotated partial coherence plots (figure 4.20) indicated that minimising $\hat{\gamma}^{2'}_{32.1}(\theta)$ could give a low value for $\hat{\gamma}^{2'}_{31.2}(\theta_o)$. For data from a site with low skew, the two rotations produced the same angle. For data with skew greater than about 0.2, the angle that maximised $\hat{\gamma}^{2'}_{32.1}(\theta)$ gave a more smoothly varying value of $\theta_o(f)$ with frequency (figure 4.21a). Also the major apparent resistivity curves were smoother (figure 4.21b) and more estimates passed the acceptance criteria (section 4.7.1). The latter result is to be expected as $\hat{\gamma}^{2'}_{32.1}(\theta_o)$ is the highest coherent signal therefore $\hat{Z}_{xy}(\theta_o)$ will contain the highest possible signal level.

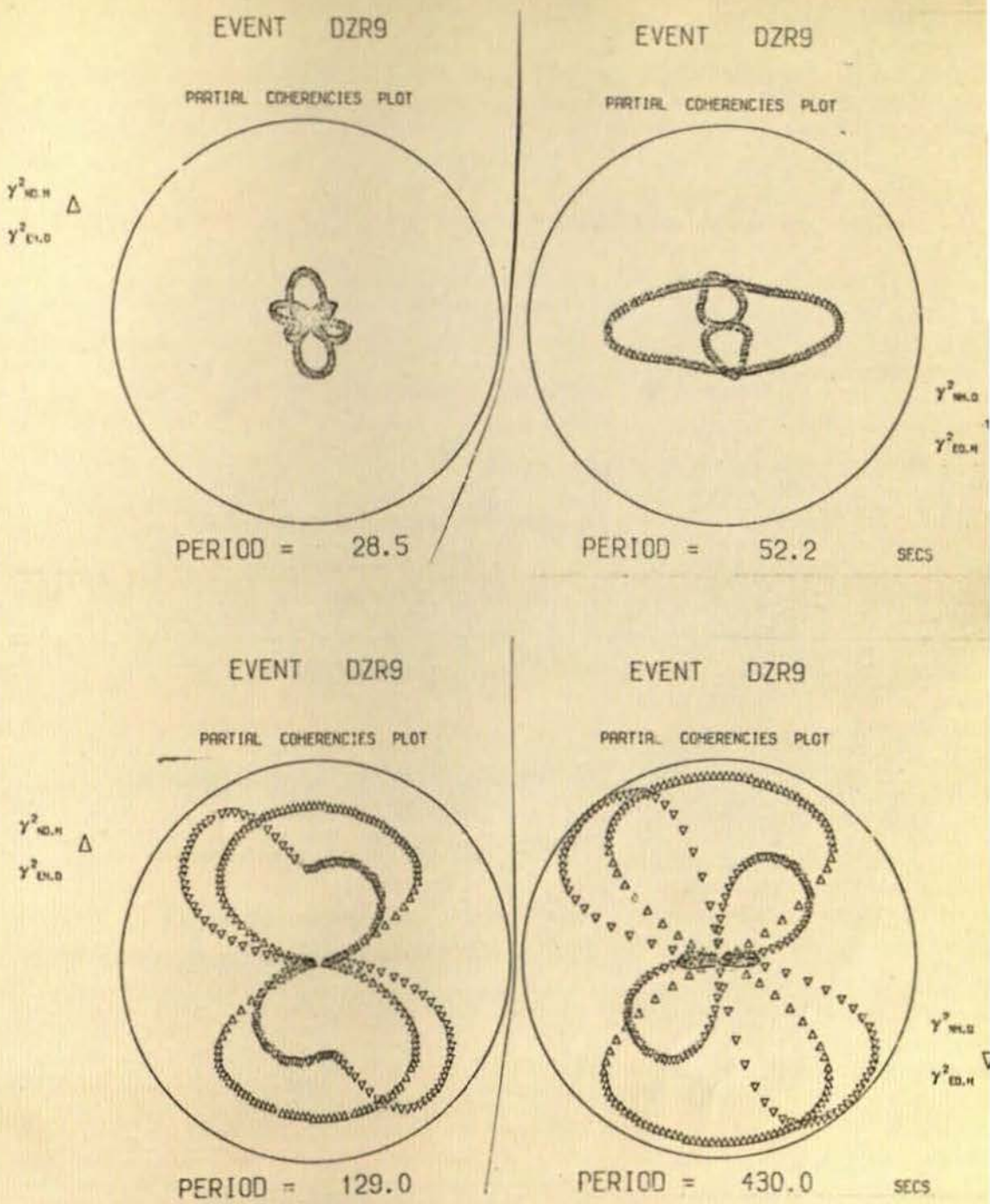

Figure 4.20 Examples of variation of the partial coherence functions with rotation angle

Δ - $\gamma^2_{32.1}$ (off-diagonal partial coherence)

∇ - $\gamma^2_{31.2}$ (diagonal partial coherence)

Figure 4.21 Comparison between maximising $|Z_{xy}|$ and maximising $\gamma^2_{32.1}$

(a) azimuthal angles for data sections CAP5, SALC & TOW1

(i) $|Z_{xy}|$ maximised

(ii) $\gamma^2_{32.1}$ maximised

(b) impedance estimates for data sections CAP5, SALC & TOW1

(i) $|Z_{xy}|$ maximised - open squares

(ii) $\gamma^2_{32.1}$ maximised - asterisks

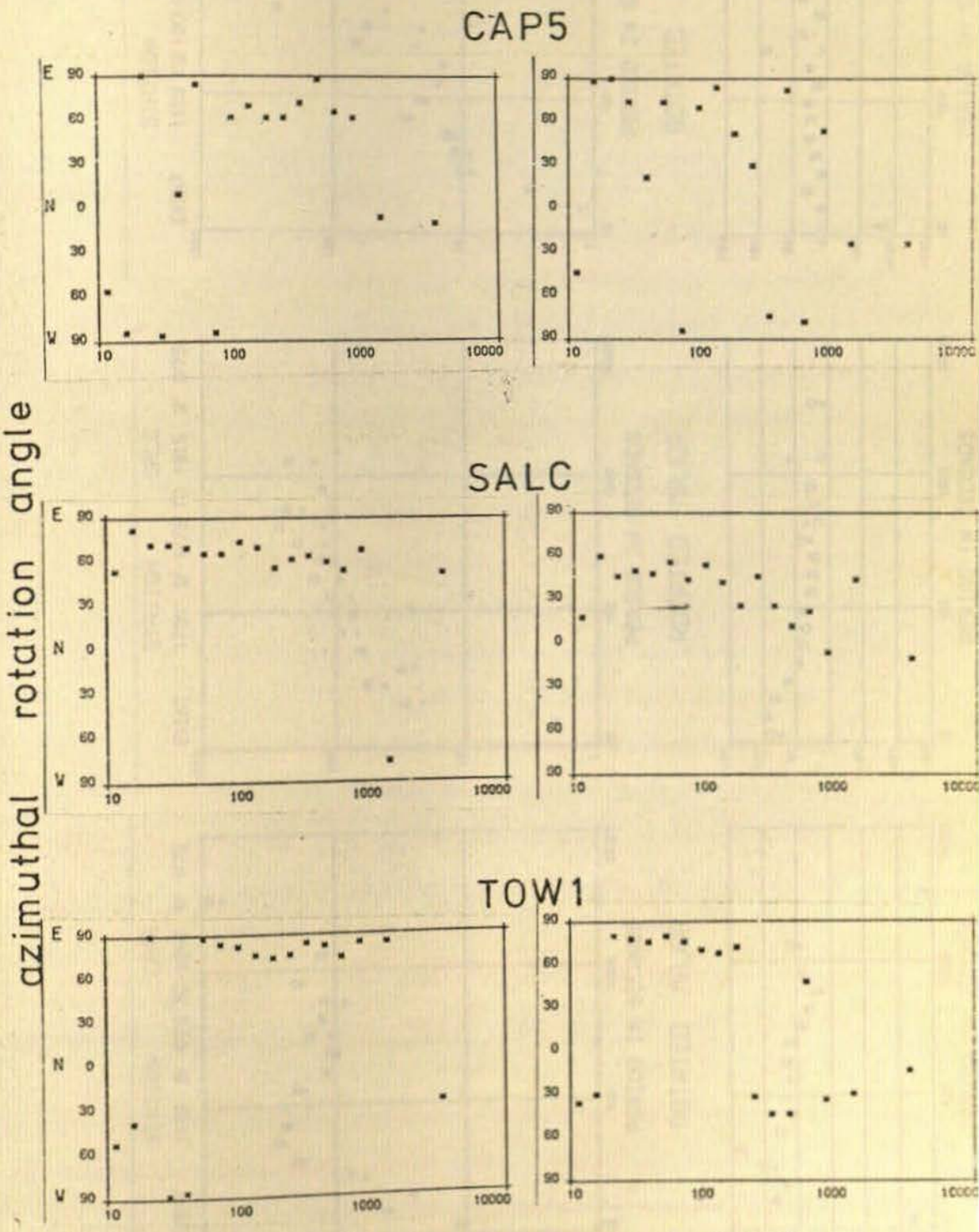
CAP5
SALC
TOW1
azimuthal rotation angle
E 90
60
30
N 0
30
60
W 90
10
100
1000
10000
(ii)
(i)

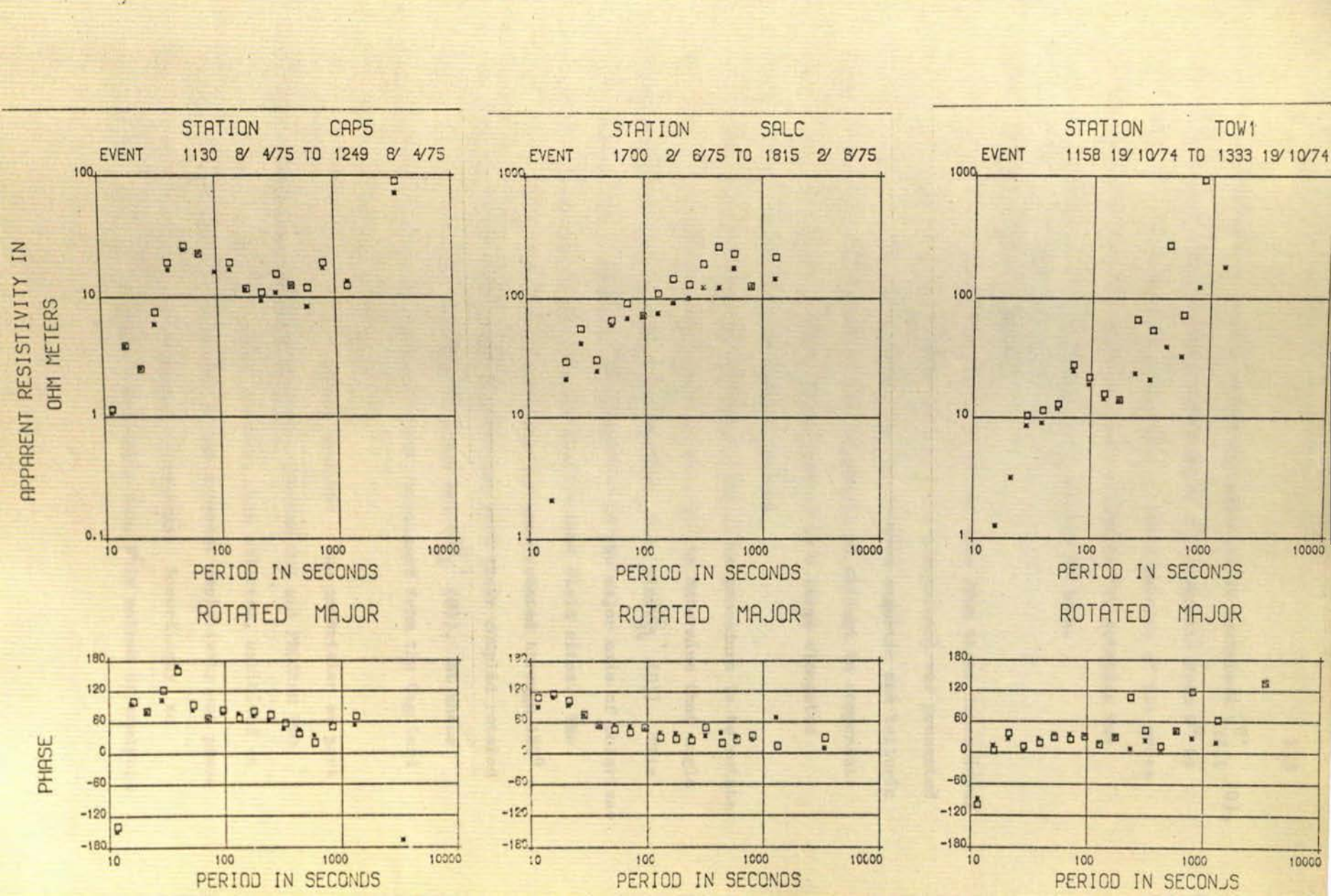
STATION CAP5
EVENT 1130 8/ 4/75 TO 1249 8/ 4/75
APPARENT RESISTIVITY IN OHM METERS
100
10
1
0.1
10
100
1000
10000
PERIOD IN SECONDS
ROTATED MAJOR
PHASE
180
120
60
0
-60
-120
-180
10
100
1000
10000
PERIOD IN SECONDS
STATION SALC
EVENT 1700 2/ 6/75 TO 1815 2/ 6/75
1000
100
10
1
10
100
1000
10000
PERIOD IN SECONDS
ROTATED MAJOR
120
60
0
-60
-120
-180
10
100
1000
10000
PERIOD IN SECONDS
STATION TOW1
EVENT 1158 19/10/74 TO 1333 19/10/74
1000
100
10
1
10
100
1000
10000
PERIOD IN SECONDS
ROTATED MAJOR
180
120
60
0
-60
-120
-180
10
100
1000
10000
PERIOD IN SECONDS

It was therefore concluded that the angle which maximised $\hat{\gamma}^{2'}_{32.1}(\theta)$, ascertained by rotation of equation 4.51 by 2° increments from 0° to 180°, gave the best possible indication of the direction of the gross structural strike of the anomaly. This criterion for rotation was accordingly adopted for the analysis of all the MT data.

4.5.4 Minimum-maximum analysis

An alternative approach for analysis of data from three-dimensional structures which may be regarded as quasi-two-dimensional was presented by Haak (1972). The requirement that the coupled magnetic and telluric field components be orthogonal was relaxed in an attempt to compensate for deflection of the electric field induced in a large elongated conducting structure by some local structure.

The method consists of two steps. The first procedure is to rotate the orthogonal telluric field vectors over 90° to determine that angle which minimises the coherence between them, i.e. $\min(\hat{\gamma}^{2}_{34}{}'(\theta))$. This angle usually corresponds to the direction of the major axis of polarisation due to the low ellipticity observed at most field sites. The horizontal magnetic field observations are then rotated through 180° to ascertain their most coherent direction with their coupled rotated telluric vectors, i.e. $\max(\hat{\gamma}^{2}_{23}{}'(\theta))$ and $\max(\hat{\gamma}^{2}_{14}{}'(\theta))$. At these maximising azimuths, two impedances are calculated from the Cagniard impedance equations 4.74a and 4.74b.

This procedure - called MINMAX analysis - was undertaken as part of the routine data analysis programs, PROGRAM ONE and PROGRAM TWO. The results for any one station however, when collated, exhibited an extremely high degree of scatter in the apparent resistivity and phase estimates and also in the azimuthal directions. Accordingly, no attempt was made to interpret the results from this method of analysis.

4.6 GDS Transfer Function Estimation

The single station transfer functions, A(f) and B(f), are given by

$$Z(f) = A(f)\, H(f) + B(f)\, D(f). \qquad (4.80)$$

Using cross-spectral methods, three equations can be derived from the complex conjugate of the measured fields, viz.

$$S_{15} = AS_{11} + BS_{12}, \qquad (4.81a)$$

$$S_{25} = AS_{21} + BS_{22}, \qquad (4.81b)$$

$$S_{55} = AS_{51} + BS_{52}, \qquad (4.81c)$$

where subscript 5 refers to the Z magnetic field component and the dependence on frequency is assumed. In a similar manner to the suggestion of Sims et al. (1971) for analysing MT data, any two of these three equations can be solved simultaneously for A(f) or B(f). However, the Z-component, due to its higher sensitivity, was more contaminated by cultural noise. Hence, estimates of A(f) and B(f) derived by employing 4.81c will be overestimated (section 4.4.2). Accordingly, 4.81a and 4.81b were solved simultaneously to yield equations for A(f) and B(f) similar to 4.48. The in-phase and quadrature induction vectors' magnitudes and directions were calculated from equations 2.4.

4.7 Station Data Averaging

In this section, the various acceptance criteria and averaging algorithms employed will be presented and discussed. The data from all analysed data sections from a station were first tested for acceptability, and those data which were accepted were assigned to period bands, then all data in each band were averaged by the relevant algorithm.

4.7.1 Acceptance criteria and averaging algorithms for GDS data

(a) Acceptance criteria - there were two for GDS data.

(i) Acceptance criterion one: the multiple coherence between the vertical magnetic field and the horizontal magnetic field components (i.e. γ^2_{512}) had to be greater than that possible for random data.

This criterion ensured that the signals were coherent. Because of the statistical nature of the signal, the test was undertaken at a required confidence level. The level chosen was 95%. Accordingly, employing the transformed multiple coherence which has a normal distribution and a known variance, the test for acceptance was

$$\text{arctanh}\,(|\hat{\gamma}_{512}|) > \text{arctanh}\left(\left(\frac{4}{n-2}\right)^{\frac{1}{2}}\right) + 1.96\left(\frac{2}{n-2}\right)^{\frac{1}{2}}$$

which can be written

$$\hat{T}_{512} > T_{rrr} + 1.96\left(\frac{2}{n-2}\right)^{\frac{1}{2}}. \qquad (4.82)$$

(ii) Acceptance criterion two: the power of each of the magnetic field components had to be greater than the digitiser error power.

This criterion ensured that the signals were real and not a manifestation of the digitising procedure. An estimate of the digitiser error power was obtained by digitising the same trace four times. Six error series were then computed by subtracting one series from another for each of the six possible pairs. These six digitising error series were then spectrally analysed, by PROGRAM ONE, and their autopowers plotted. The autopowers were equivalent to a digitising unrepeatability of up to 2 mm (i.e. ±1 mm). The full chart width was 250 mm thus the digitising error power for the i'th trace was given by

$$DEP_i = \left[\frac{2}{250} \times FSD_i\right]^2,$$

where FSD_i is the full scale deflection of the i'th component. The

acceptance criterion adopted therefore was

$$S_{ii}(f) > DEP_i. \qquad (4.83)$$

(b) Averaging algorithms - these algorithms gave the averaged number of degrees of freedom, averaged spectral autopowers, averaged transfer functions and averaged multiple coherence for a bandwidth.

(i) Estimate of the total number of degrees of freedom: As discussed in section 4.34, each raw spectral estimate has two degrees of freedom, one for the cosine part and one for the sine part of the estimate (assuming each estimate is independent of any other). Accordingly, the smoothed spectral estimate has n = 2 x NE degrees of freedom - where NE is the number of raw estimates averaged over in the windowing operation.

When deriving the number of degrees of freedom associated with the ensemble averaged estimate, the most optimistic choice available is to assume that each data set is strictly independent of any of the others analysed from the particular location. The total number of degrees of freedom is then given by

$$n_T(f) = \sum_{i=1}^{N} n_i(f)$$

for N data sets.

However, for totally independent data sets, each geomagnetic section analysed has to represent either (i) a different source mechanism, or (ii) a different polarisation of inducing field from the same source mechanism, compared to any other geomagnetic section. This places severe restrictions on data available for processing. The author chose the more conservative view that all information was contained in the data set with the greatest number of degrees of freedom. Any other data sets were considered not to contain additional information.

This assumption is certainly conservative but is less biased than any other estimators considered. The algorithm was accordingly given by

$$n_T(f) = \max(n_i(f)),\ i = 1,\ N. \qquad (4.84)$$

(ii) Estimate of the averaged power level: When deriving an algorithm that averages the auto-spectra, at frequency f, for all accepted data, consideration must be given to the form of the natural spectrum. As shown by figure 1.1, the fields exhibit an approximately logarithmic rise in amplitude with decreasing frequency in the frequency band of interest (0.1 - 0.0001 Hz). A logarithmic average will therefore be less biased than a normal average. Also, in section 4.4.4 an estimate of the coherent signal to random noise ratio, in the form of the normalised transformed multiple coherence, N^2_{512}, was developed. It seemed natural therefore to perform a weighted average, employing the estimates of $\hat{N}^2_{512}$ as the weights. A weighted average has previously been used for MT studies by Dowling (1970).

The weighted logarithmic averaging algorithm was accordingly given by

$$\overline{S}_k(f) = \text{antilog}\ \frac{\sum_{i=1}^{m} \hat{N}^2_{512}(f)_i \log(S_k(f)_i)}{\sum_{i=1}^{m} \hat{N}^2_{512}(f)_i} \qquad (4.85)$$

where k = 1, 2 or 5 and m is the total number of data sets.

Note: the weighted arithmetic mean of the logarithm of a function is equal to the weighted geometric mean of that function (Colquohoun, 1971, pp 24 - 26).

(iii) Estimate of the averaged transfer functions: When averaging complex numbers, the correct procedure is to average separately the real and imaginary parts, then compute the averaged complex number. It is incorrect to average modulii and phases.

For the same arguments as given in the previous section, it was desirable to perform a weighted average. The weights again chosen were the NTMCs. The averaging algorithms were given by

$$\overline{\text{Real }(A(f))} = \frac{\sum_{i=1}^{m} \hat{N}^2_{512}(f)_i \text{ Real } (A)_i}{\sum_{i=1}^{m} \hat{N}^2_{512}(f)_i}, \qquad (4.86)$$

similarly for $\overline{\text{Im }(A(f))}$, $\overline{\text{Re }(B(f))}$ and $\overline{\text{Im }(B(f))}$.

(iv) Estimate of averaged coherence: Because the transformed coherences have a normal distribution, it appears natural to average them rather than the coherences themselves. The averaged coherences, either ordinary, multiple or partial, were accordingly estimated by

$$\bar{\gamma}^2 = \tanh^2\left[\frac{1}{m}\sum_{i=1}^{m} \text{arctanh } (|\gamma_i|)\right]. \qquad (4.87)$$

4.7.2 Acceptance criteria and averaging algorithms for MT data

(a) Acceptance criteria - there were four for MT data.

(i) Acceptance criterion one: the maximised partial coherence function $\hat{\gamma}^{2\,'}_{32.1}(\theta_o)$ had to be greater than that possible for random data.

This criterion is analagous to that for GDS data except the signal to noise ratio of the $Z_{xy}(f)$ tensor element was indicated by the partial, rather than multiple, coherence. This criterion therefore ensured that the estimate was derived from coherent signals. Utilising the transformed coherency, the 95% confidence level acceptance test was hence

$$\text{arctanh } (|\hat{\gamma}_{32.1}|) > \text{arctanh}\left(\frac{(2n+4)^{\frac{1}{2}}}{n-2}\right) + \frac{1.96\,(n+2)^{\frac{1}{2}}}{n-2}$$

or

$$\hat{T}_{32.1} > \hat{T}_{rr.r} + \frac{1.96\,(n+2)^{\frac{1}{2}}}{n-2} \qquad (4.88)$$

(ii) Acceptance criterion two: the partial coherence function $\hat{\gamma}^2_{32.1}$ had to be greater than the partial coherence function $\hat{\gamma}^2_{31.2}$.

This criterion ensured there was more coherent signal in the off-diagonal elements than the diagonal elements. To account for statistical scatter, the following 95% confidence level acceptance test was employed.

$$\hat{T}_{32.1} > \hat{T}_{31.2} + \frac{1.96\,(n+2)^{\frac{1}{2}}}{n-2} \qquad (4.89)$$

(iii) Acceptance criterion three: the power of each of the four MT components (N, E, H and D) had to be greater than the digitiser error power.

This criterion is equivalent to criterion two for GDS data (4.7.1 (b) (ii)). It was applied in the same manner as 4.83 with i = 1, 2, 3 and 4.

(iv) Acceptance criterion four: the phase of the major impedance tensor element, $\hat{Z}'_{xy}(\theta_o)$, had to be between 0^o and 90^o.

This assured that the result is physically realisable. Phase was constrained to the limits of 0^o, over an infinite structure with zero conductivity, to 90^o, over an infinite structure of infinite conductivity. The acceptance test was accordingly

$$0^o < \phi_{major}(f) < 90^o \qquad (4.90)$$

This criterion was not applied to the rotated minor estimates because of their low signal to noise ratio which will degrade the estimates of phase.

(b) Averaging algorithms - these were as for the GDS data (section 4.7.1 (b)) with the inclusion of algorithms to average impedance elements, azimuthal angle, and skew factor.

(i) Estimate of total number of degrees of freedom: In the same manner as section 4.7.1 (b) (i), equation 4.84 was employed.

(ii) Acceptance criterion two: the partial coherence function $\hat{\gamma}^2_{32.1}$ had to be greater than the partial coherence function $\hat{\gamma}^2_{31.2}$.

This criterion ensured there was more coherent signal in the off-diagonal elements than the diagonal elements. To account for statistical scatter, the following 95% confidence level acceptance test was employed.

$$\hat{T}_{32.1} > \hat{T}_{31.2} + \frac{1.96\,(n+2)^{\frac{1}{2}}}{n-2} \qquad (4.89)$$

(iii) Acceptance criterion three: the power of each of the four MT components (N, E, H and D) had to be greater than the digitiser error power.

This criterion is equivalent to criterion two for GDS data (4.7.1 (b) (ii)). It was applied in the same manner as 4.83 with i = 1, 2, 3 and 4.

(iv) Acceptance criterion four: the phase of the major impedance tensor element, $\hat{Z}'_{xy}(\theta_o)$, had to be between 0^o and 90^o.

This assured that the result is physically realisable. Phase was constrained to the limits of 0^o, over an infinite structure with zero conductivity, to 90^o, over an infinite structure of infinite conductivity. The acceptance test was accordingly

$$0^o < \phi_{major}(f) < 90^o \qquad (4.90)$$

This criterion was not applied to the rotated minor estimates because of their low signal to noise ratio which will degrade the estimates of phase.

(b) Averaging algorithms - these were as for the GDS data (section 4.7.1 (b)) with the inclusion of algorithms to average impedance elements, azimuthal angle, and skew factor.

(i) Estimate of total number of degrees of freedom: In the same manner as section 4.7.1 (b) (i), equation 4.84 was employed.

(ii) Estimate of the averaged auto-spectra: This was undertaken in the same form as section 4.7.1 (a) (ii). In this case however, the signal to noise ratio is indicated by the NTPC $\hat{N}^2_{32.1}$ rather than the NTMC $\hat{N}^2_{312}$. Accordingly, the averaging algorithm was

$$\overline{S}_k(f) = \text{antilog}\left[\frac{\sum_{i=1}^{m} \hat{N}^2_{32.1}(f)_i \log(S_k(f)_i)}{\sum_{i=1}^{m} \hat{N}^2_{32.1}(f)_i}\right]. \qquad (4.91)$$

(iii) Estimate of averaged impedances: For reasons given in 4.7.1 (b) (iii), the correct method of averaging is to average the complex impedance estimates rather than their corresponding apparent resistivities and phases. Bentley (1973) considers that a lognormal rather than normal distribution is more appropriate for the impedance estimates. Accordingly, a logarithmic averaging procedure was employed. Also, a signal to noise ratio weighting, in the form of $\hat{N}^2_{32.1}$, was used.

$$\overline{Z}_{xy}(f) = \text{antilog}\left[\frac{\sum_{i=1}^{m} \hat{N}^2_{32.1}(f)_i \log(Z_{xy}(f)_i)}{\sum_{i=1}^{m} \hat{N}^2_{32.1}(f)_i}\right] \qquad (4.92)$$

similarly for $\overline{Z}_{xx}(f)$, $\overline{Z}_{yx}(f)$ and $\overline{Z}_{yy}(f)$.

(iv) Estimate of averaged azimuthal angle: The azimuthal angle, θ_o, was that angle in which $\hat{\gamma}^{2\,\prime}_{32.1}(\theta)$ was a maximum. This was averaged, in a weighted fashion, by the mean direction approach given by Mardia (1972, p 20). The algorithm was

$$\overline{\theta}_o(f) = \arctan\left[\frac{\sum_{i=1}^{m} \hat{N}^2_{32.1}(f)_i \sin(\theta_o(f)_i)}{\sum_{i=1}^{m} \hat{N}^2_{32.1}(f)_i \cos(\theta_o(f)_i)}\right]. \qquad (4.93)$$

(v) Estimate of averaged skew factor: This was done in a weighted manner by

$$\overline{\text{Skew}\ (f)} = \frac{\sum_{i=1}^{m} \hat{N}^2_{32.1}\ (f)_i\ \text{Skew}\ (f)_i}{\sum_{i=1}^{m} \hat{N}^2_{32.1}\ (f)_i} \quad . \tag{4.94}$$

(vi) Estimate of averaged coherences: This was undertaken by the same algorithm as equation 4.87.

4.8 Confidence Limit Estimation

When estimating a frequency response function, the effect of residual random noise on the estimate must be borne in mind. Consideration of the possible effect leads to a circle of confidence, centred on the estimate $\hat{H}(f)$, within which the true response function can be stated to lie, with a specific degree of confidence.

Bendat and Piersol (1971, pp 199 - 202) show that if the noise is random, the circle of confidence with a radius defined as

$$\hat{r} \geq |\hat{H}(f) - H(f)| \tag{4.95}$$

is given by

$$\hat{r}^2(f) = \frac{2}{n-2} F_{2:n-2:\alpha}\ (1 - \hat{\gamma}^2_{xy}(f)) \frac{\hat{S}_{yy}(f)}{\hat{S}_{xx}(f)} \tag{4.96}$$

where $F_{2:n-2:\alpha} = 100\alpha$ percentage point of an F distribution, for the single input [x(t)]/single output [y(t)] case. A circle of confidence in the complex H-plane is illustrated in figure 4.22a. This confidence region can be mapped onto the $(|H|,\phi)$ plane as shown in 4.22b. The rectangular region, an approximation of the confidence region, gives the confidence intervals for the gain $|H(f)|$ and phase $\phi(f)$ as

$$|\hat{H}(f)| - \hat{r}(f) < |H(f)| < |\hat{H}(f)| + \hat{r}(f) \tag{4.97a}$$

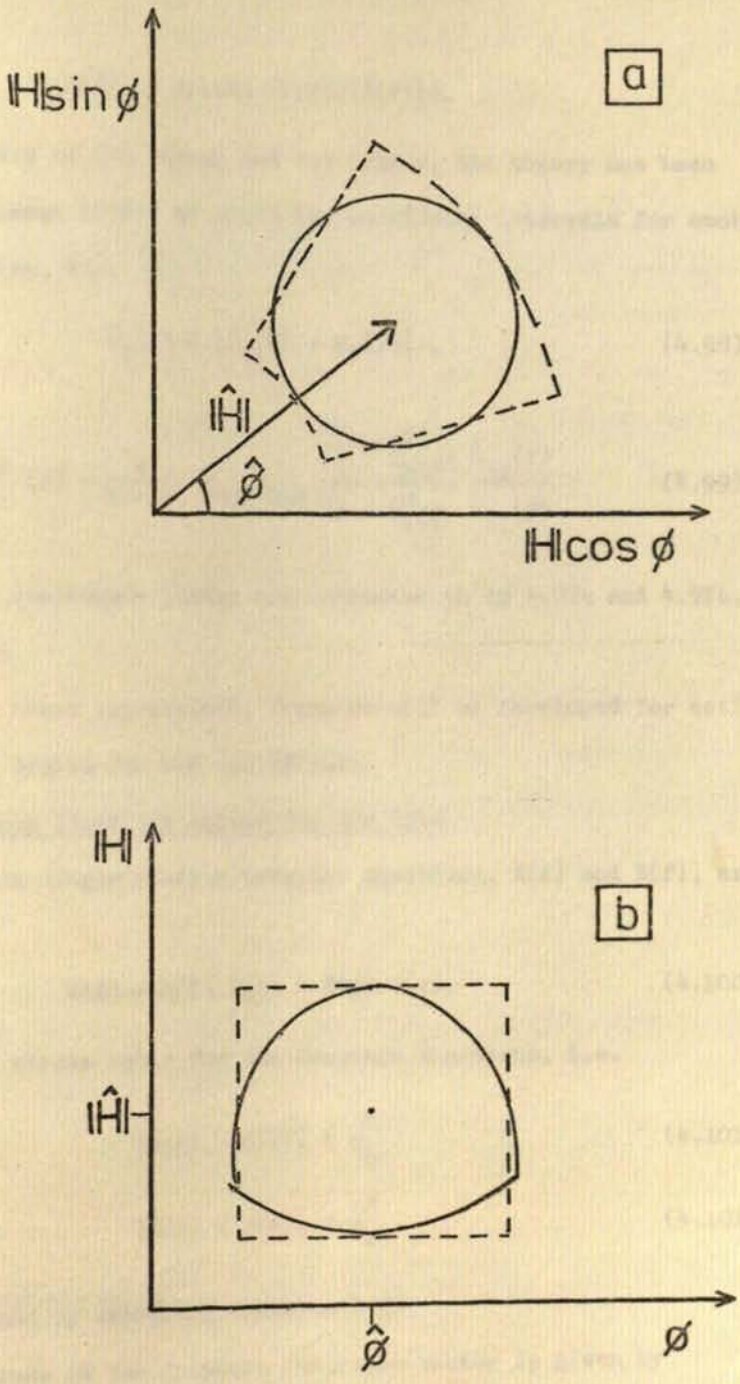

Figure 4.22 Confidence regions for gain and phase

———— exact

- - - - - - - - - approximate

$$\hat{\phi}(f) - \Delta\hat{\phi}(f) < \phi(f) < \hat{\phi}(f) + \Delta\hat{\phi}(f) \qquad (4.97b)$$

where

$$\Delta\hat{\phi}(f) = \arcsin\left(\hat{r}(f)/|\hat{H}(f)|\right).$$

For the case of two inputs and one output, the theory has been extended by Goodman (1965) to yield the confidence intervals for each response function, i.e.

$$\hat{r}_i(f) > |\hat{H}_i(f) - H_i(f)| \ , \qquad (4.98)$$

as given by

$$\hat{r}_i^2(f) = \frac{4}{n-4} F_{4:n-4:\alpha} \frac{(1 - \hat{\gamma}_{y12}^2)}{(1 - \hat{\gamma}_{12}^2)} \frac{\hat{S}_{yy}(f)}{\hat{S}_{ii}(f)} \qquad (4.99)$$

Gain and phase confidence limits are estimated as by 4.97a and 4.97b, with the subscript i.

Employing these expressions, formulae will be developed for estimating the confidence limits for GDS and MT data.

4.8.1 Confidence limit estimation for GDS data

The complex single station transfer functions, A(f) and B(f), are derived from

$$Z(f) = A(f)\,H(f) + B(f)\,D(f). \qquad (4.100)$$

The confidence circle radii for the response functions, i.e.

$$|\hat{A}(f) - A(f)| \leq \hat{r}_A^2 \qquad (4.101a)$$

and

$$|\hat{B}(f) - B(f)| \leq \hat{r}_B^2, \qquad (4.101b)$$

can be determined by employing equation 4.99.

The magnitude of the in-phase induction vector is given by

$$R^2(f) = Re^2(A(f)) + Re^2(B(f)). \qquad (4.102)$$

Hence, to derive the confidence limits for R, it is necessary to consider

the random error on the real parts of A(f) and B(f). Because $|\hat{A} - A|^2 > |\mathrm{Re}(\hat{A}) - \mathrm{Re}(A)|^2$, then $r_A > |\mathrm{Re}(\hat{A}) - \mathrm{Re}(A)|$, and similarly for r_B. Hence, the true response function, R(f), will be given by

$$(\mathrm{Re}(\hat{A}) - \hat{r}_A)^2 + (\mathrm{Re}(\hat{B}) - \hat{r}_B)^2 \leq R^2 \leq (\mathrm{Re}(\hat{A}) + \hat{r}_A)^2 + (\mathrm{Re}(\hat{B}) + \hat{r}_B)^2. \quad (4.103)$$

On expanding 4.103 and disregarding terms of $\hat{r}_A^2$ and $\hat{r}_B^2$, the inequality

$$R \leq \hat{R} \left(1 + \frac{2(\hat{r}_A \, \mathrm{Re}(\hat{A}) + \hat{r}_B \, \mathrm{Re}(\hat{B}))}{\hat{R}^2} \right)^{\frac{1}{2}} \quad (4.104)$$

(similarly for the lower bound with - instead of +) results. Equation 4.104 leads to

$$R < \hat{R} + \frac{\hat{r}_A \, \mathrm{Re}(\hat{A}) + \hat{r}_B \, \mathrm{Re}(\hat{B})}{\hat{R}} \quad (4.105)$$

after Binomial Expansion and neglecting terms involving powers of two and above. Hence, the confidence interval for the estimate of the magnitude of the in-phase induction vector, $\hat{R}$, is given by

$$\frac{\hat{r}_A \, \mathrm{Re}\,(\hat{A}) + \hat{r}_B \, \mathrm{Re}(\hat{B})}{\hat{R}} \quad (4.106a)$$

A similar treatment gives the confidence interval for the estimate of the magnitude of the quadrature vector, $\hat{I}$, as

$$\frac{\hat{r}_A \, \mathrm{Im}\,(\hat{A}) + \hat{r}_B \, \mathrm{Im}\,(\hat{B})}{\hat{I}} \quad (4.106b)$$

The estimate of the azimuth of the real induction arrow is given by

$$\hat{\theta}_R(f) = \arctan\left(- \frac{\mathrm{Re}\,(\hat{B}(f))}{\mathrm{Re}\,(\hat{A}(f))} \right), \quad (4.107)$$

similarly for $\hat{\theta}_I(f)$. The true azimuths will lie in the confidence

intervals given by

$$\frac{-\mathrm{Re}\,(\hat{B}) + \hat{r}_B}{\mathrm{Re}\,(\hat{A}) + \hat{r}_A} \leqslant \tan(\theta_R) \leqslant \frac{-\mathrm{Re}\,(\hat{B}) - \hat{r}_B}{\mathrm{Re}\,(\hat{A}) - \hat{r}_A}, \qquad (4.108)$$

similarly for θ_I. In expression 4.108 it has been assumed that $\mathrm{Re}(\hat{A})$ and $\mathrm{Re}(\hat{B})$ are both positive. If either, or both, are negative then various signs must be altered.

To illustrate the use of equations 4.106 and 4.108, figure 4.23a shows all the accepted GDS data for station FTH. The data were averaged, as described in section 4.7.1, and 95% confidence intervals were estimated. These are shown in figure 4.23b. It is apparent from comparing figure 4.23b with figure 4.23a that the confidence limits are well estimated. Equations 4.106 and 4.108 can be applied to estimates from only one data set and are therefore superior to statistical confidence limit estimating techniques which require more than one observation.

Equations 4.106 and 4.108 were employed to derive the confidence limits for the GDS data from all of the stations.

4.8.2 Confidence limit estimation for MT data

Reddy et al. (1976) employ the equations of Goodman (1965) - equations 4.98, 4.99 and 4.96 - to determine the confidence limits of their apparent resistivity and phase results. However, an inherent assumption in the technique is that the residual random noise has a normal distribution. This is because the estimates of the response functions are assumed to be distributed normally about the true response functions. If the estimates of the response functions are not distributed normally about the true response functions, then Goodman's equations give incorrect estimates of the confidence intervals. Bentley (1973) shows that MT apparent resistivity data is better approximated

Figure 4.23 Example of confidence limit estimation for GDS induction vectors

(a) All accepted GDS estimates from data recorded at station FTH

(b) Averaged GDS estimates with 95% confidence limits

STATION FTHB

INDUCTION VECTORS

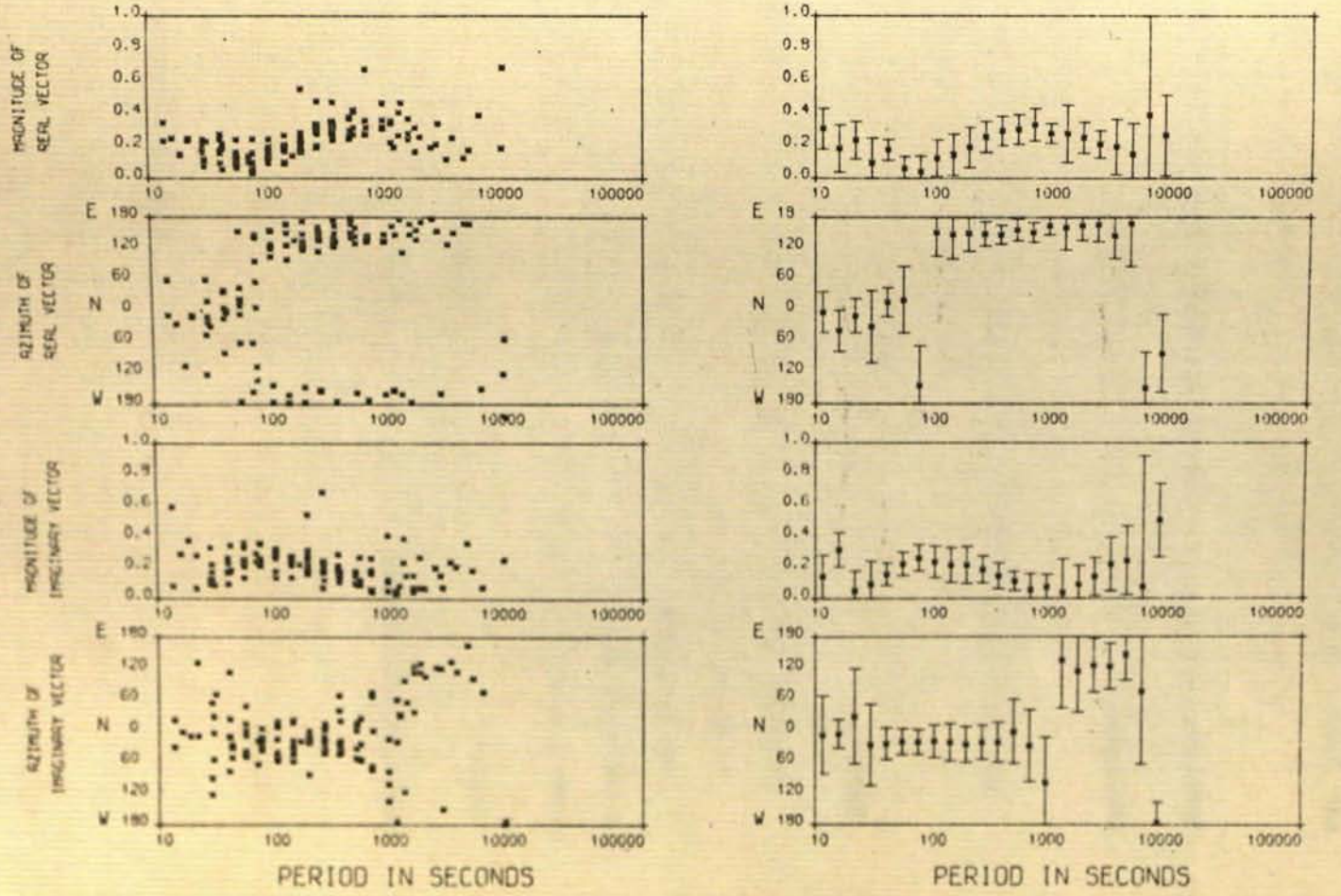

by a log normal, rather than a normal, distribution. Hence, Goodman's equations need revising before they are employed for MT data.

For a single input/single output linear system (figure 4.15a), the input and output are related by the response function given by

$$Y(f) = H(f)\, X(f). \tag{4.109a}$$

Hence

$$\log |Y| = \log |HX|, \tag{4.109b}$$

with the dependence on f omitted for clarity.

Following the same approach as given in Bendat and Piersol (1971, pp 199 - 202), the noise can be defined as

$$Z = \log |Y| - \log |HX|. \tag{4.110}$$

If the estimates, $|\hat{H}|$, of the modulus of the true response function, $|H|$, are distributed log normally about $|H|$, then the estimation of $\log |\hat{H}|$ will be distributed normally about $\log |H|$. Therefore, the random error, Z, defined by equation 4.110 will be normally distributed. Also Z is totally real. The best estimate of the noise term is given by

$$\hat{Z} = \log |Y| - \log |\hat{H}X|, \tag{4.111}$$

which will also be totally real and normally distributed. Substituting 4.111 into 4.102 for $\log |Y| - \log |X|$ gives

$$Z = \hat{Z} + (\log |H| - \log |\hat{H}|). \tag{4.112}$$

It follows, from squaring 4.112, that

$$\begin{aligned} Z^2 &= \hat{Z}^2 + 2\hat{Z}\,(\log |H| - \log |\hat{H}|) + (\log |H| - \log |\hat{H}|)^2 \\ &= \hat{Z}^2 + 2\hat{Z}\,(Z - \hat{Z}) + (\log |H| - \log |\hat{H}|)^2. \end{aligned} \tag{4.113}$$

Writing equation 4.113 in terms of spectral estimates

$$\hat{S}_{ZZ} = \hat{S}_{\hat{Z}\hat{Z}} + 2\hat{S}_{\hat{Z}Z} - 2\hat{S}_{\hat{Z}\hat{Z}} + \frac{2}{T}(\log|H| - \log|\hat{H}|)^2$$

$$= 2\,\hat{S}_{\hat{Z}Z} - \hat{S}_{\hat{Z}\hat{Z}} + \frac{2}{T}(\log|H| - \log|\hat{H}|)^2 \qquad (4.114)$$

term 1 term 2

from $\hat{S}_{ZZ} = \frac{2}{T}|Z|^2 = \frac{2}{T}Z^2$ (Z real), and $\hat{S}_{\hat{Z}Z} = \frac{2}{T}\hat{Z}^*Z = \frac{2}{T}\hat{Z}Z$.

Similarly to the analysis developed by Bendat and Piersol, both $\hat{S}_{\hat{Z}Z}$ and $\hat{S}_{\hat{Z}\hat{Z}}$ must have the same number of degrees of freedom as $\hat{S}_{ZZ}$ minus the number of additional constraints imposed on them. As $\hat{Z}(f)$ is defined in terms of $\log|\hat{H}(f)|$ rather than $\log|H(f)|$, this constitutes one constraint on $\hat{Z}(f)$. Hence, term 1 has $(n-1)$ degrees of freedom and term 2 has 1 degree of freedom. Because the two terms are statistically independent, their number of degrees of freedom will be additive, that is

$$\frac{\chi^2_n}{n} = \frac{\chi^2_{n-1}}{n} + \frac{\chi^2_1}{n} .$$

As shown by Bendat and Piersol (1971, p 111), the function

$$\frac{n\frac{2}{T}(\log|H| - \log|\hat{H}|)^2}{S_{ZZ}} = \chi^2_1 \qquad (4.115)$$

will be chi-square distributed with one degree of freedom.

To evaluate term 1 in terms of measured quantities and the true function $\log|H|$, the auto-spectral estimate $\hat{S}_{\hat{Z}\hat{Z}}$ can be written as

$$\hat{S}_{\hat{Z}\hat{Z}} = \frac{2}{T}(\log|Y| - \log|\hat{H}X|)^2 \text{ from 4.111}$$

$$= \frac{2}{T}C_o^2 , \qquad (4.116)$$

where $C_o = \log|\hat{H}X| - \log|Y|$, which is known.

The auto-spectral estimate $\hat{S}_{\hat{Z}Z}$ can be expanded by

$$\hat{S}_{Z\hat{Z}} = \frac{2}{T} (\log |Y| - \log |\hat{H}X|) (\log |Y| - \log |HX|)$$

$$\doteq \frac{2}{T} (C_o \log |H| + C_1), \qquad (4.117)$$

where C_o is as previously defined and

$$C_1 = \log^2 |Y| + \log^2 |X| + \log |X| \log |\hat{H}| -$$

$$\log |Y| (\log |\hat{H}| + 2 \log |X|),$$

which is known.

Substituting equations 4.116 and 4.117 in term 1 yields

$$2\hat{S}_{\hat{Z}Z} - \hat{S}_{\hat{Z}\hat{Z}} = \frac{2}{T} (2C_o \log |H| + 2C_1 - C_o^2).$$

Because term 1 has one degree of freedom less than $\hat{S}_{ZZ}$, the expression

$$\frac{n \frac{2}{T} (2C_o \log |H| - 2C_1 - C_o^2)}{S_{ZZ}} = \chi^2_{n-1} \qquad (4.118)$$

will be chi-square distributed with n-1 degrees of freedom.

From equations 4.115 and 4.118, it follows that

$$F_{1:n-1} = \frac{(n-1) (\log |H| - \log |\hat{H}|)^2}{2C_o \log |H| + 2C_1 - C_o^2} . \qquad (4.119)$$

Defining the circle of confidence for the logarithm of the modulus of the estimate of the response function, i.e. $\log |\hat{H}|$, as

$$\hat{r}^2 \geqslant (\log |H| - \log |\hat{H}|)^2 \qquad (4.120)$$

then it is given by

$$\hat{r}^2 = \frac{(2C_o \log |H| + 2C_1 - C_o^2) F_{1:n-1}}{n-1} . \qquad (4.121)$$

Therefore

$$2FC_o \log |H| + F(2C_1 - C_o^2) \geqslant (n-1) (\log^2 |H| - 2 \log |H| \log |\hat{H}| + \log^2 |\hat{H}|). \qquad (4.122)$$

Rearranging 4.122 gives the quadratic inequality in log $|H|$ of

$$(n-1)\log^2|H| - (2(n-1)\log|\hat{H}| + 2FC_o)\log|H| + ((n-1)\log^2|\hat{H}| - F(2C_1 - C_o^2)) < 0 . \qquad (4.123)$$

Inequality 4.123 is of the form $ax^2 + bx + c < 0$ which, because $a > 0$, will resemble figure 4.24. The shaded region in figure 4.24 indicates the permitted range of x that satisfies the inequality. The minimum and maximum permitted values of x are given by the two solutions to the quadratic equation $ax^2 + bx + c = 0$, which are

$$x = \frac{-b \pm \sqrt{b^2 - 4ac}}{2a} . \qquad (4.124)$$

Substituting the corresponding terms for a, b and c in equation 4.124 from inequality 4.122 gives

$$\log|H| = \log|\hat{H}| + \frac{FC_o}{n-1} \pm \left(\frac{2FC_o \log|\hat{H}|}{n-1} + \left(\frac{FC_o}{n-1}\right)^2 + \frac{F(2C_1 - C_o)}{n-1}\right)^{\frac{1}{2}} . \qquad (4.125)$$

The term $FC_o/(n-1)$ will be small compared to the others, hence the confidence interval for log $|H|$ is given by

$$\left(\frac{2FC_o \log|\hat{H}|}{n-1} + \left(\frac{FC_o}{n-1}\right)^2 + \frac{F(2C_1 - C_o)}{n-1}\right)^{\frac{1}{2}} . \qquad (4.126)$$

The phase of the estimate is shown by Bentley (1973) to be approximately normally distributed. Hence, because the argument of a complex number can be manipulated in the same way as logarithms, i.e. arg (HX) = arg (H) + arg (X), a similar analysis to that given will yield an expression equivalent to 4.125 for the confidence interval of arg (X), viz.

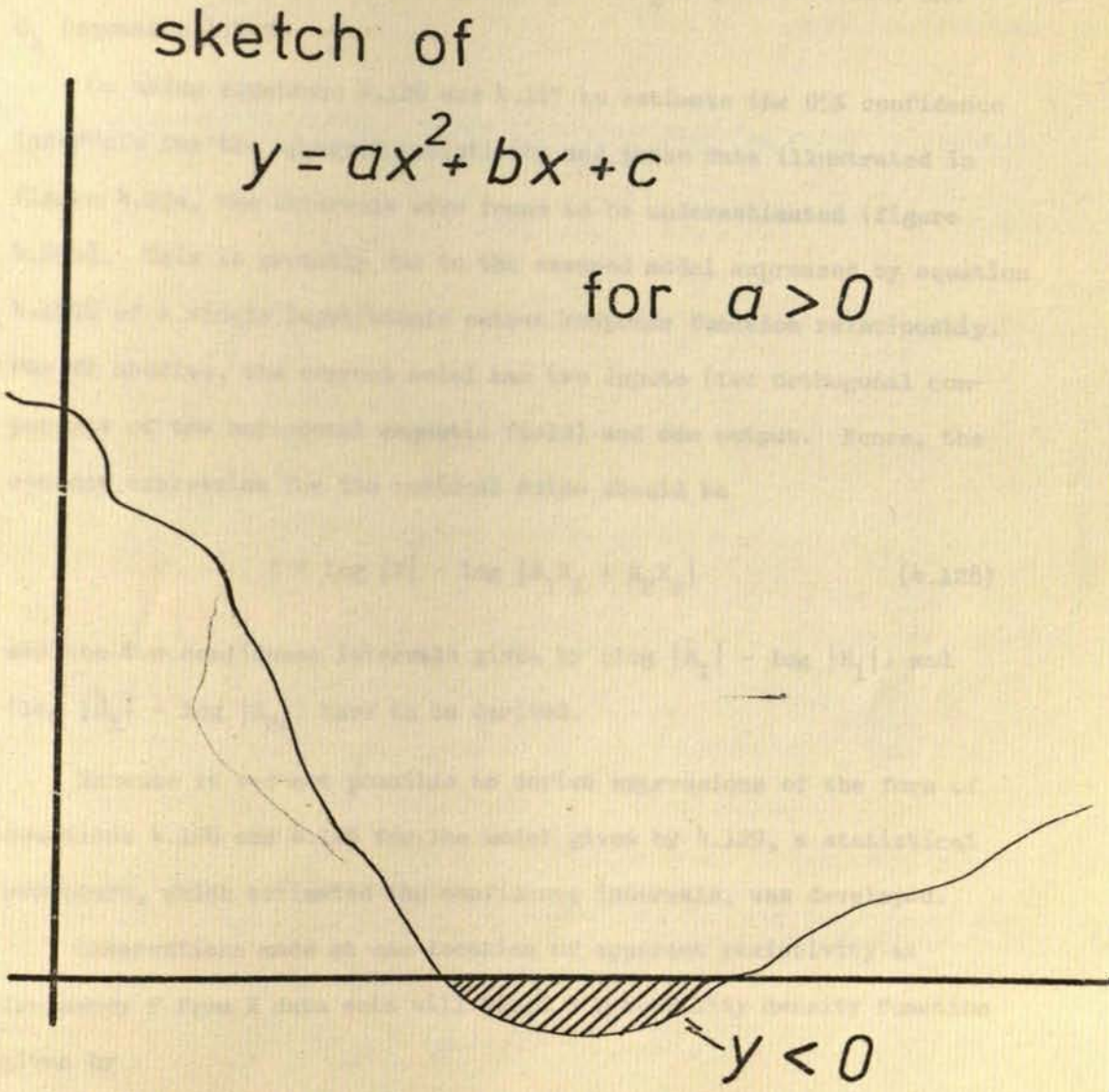

Figure 4.24 Sketch of function $y = ax^2 + bx + c$ showing region for $y < 0$

$$\left(\frac{2FC_o' \arg (H)}{n-1} + \left(\frac{FC_o'}{n-1} \right)^2 + \frac{F(2C_1' - C_o')}{n-1} \right)^{\frac{1}{2}} \qquad (4.127)$$

where C_o' and C_1' are argument equivalents of C_o (equation 4.116) and C_1 (equation 4.117).

On using equations 4.126 and 4.127 to estimate the 95% confidence intervals for the apparent resistivity and phase data illustrated in figure 4.25a, the intervals were found to be underestimated (figure 4.25b). This is probably due to the assumed model expressed by equation 4.109b of a single input/single output response function relationship. For MT studies, the correct model has two inputs (two orthogonal components of the horizontal magnetic field) and one output. Hence, the correct expression for the residual noise should be

$$Z = \log |Y| - \log |H_1X_1 + H_2X_2| \qquad (4.128)$$

and the two confidence intervals given by $(\log |\hat{H}_1| - \log |H_1|)$ and $(\log |\hat{H}_1| - \log |H_2|)$ have to be derived.

Because it was not possible to derive expressions of the form of equations 4.126 and 4.126 for the model given by 4.129, a statistical procedure, which estimated the confidence intervals, was developed.

Observations made at one location of apparent resistivity at frequency f from N data sets will yield a probability density function given by

$$p\,(\rho(f)) = \rho_1(f), \rho_2(f), \rho_3(f), \ldots, \rho_i(f), \ldots, \rho_N(f).$$

This density function, $p(\rho(f))$, will tend to a log normal distribution as indicated by Bentley (1973). Another related probability density function can be generated by

$$p_L(\log (\rho(f))) = \log (\rho_1(f)), \ldots, \log (\rho_i(f)), \ldots, \log (\rho_N(f))$$

and, by assuming the Central Limit Theorem, the function will obey

$$\lim_{N\to\infty} p_L(\log(\rho)) = p(\mathcal{N})$$

i.e. the probability density function will tend to a normal distribution as the number of observations becomes large.

The unbiased sample variance of the variable $\log \rho_i(f)$ is given by

$$S^2 = \frac{1}{m-1} \sum_{i=1}^{m} (\log \rho_i(f) - \overline{\log \rho(f)})^2$$

(Bendat and Piersol, 1971, pp 99 - 102) where $\log \rho(f)$ is the sample mean of the function.

However, a weighted sample variance is more appropriate for weighted mean data (as given by equation 4.91).

Consider the sample weighted variance given by

$$S_\omega^{2'}(x) = \frac{\sum \omega_i (x_i - \bar{x})^2}{\sum \omega_i} \qquad (4.129)$$

An analysis of the expectation value of this estimate of σ_ω^2 (the true weighted variance), in the same manner as that of Bendat and Piersol (1971, pp 99 - 102), will reveal that this estimate is biased by an amount $(N - 1)/N$. An efficient and consistent unbiased estimate of the true weighted variance is therefore given by

$$S_\omega^2(x) = \frac{N}{N-1} \frac{\sum \omega_i (x_i - \bar{x})^2}{\sum \omega_i}. \qquad (4.130)$$

Accordingly, this sample weighted variance for MT data is given by

$$S_\omega^2(\log(\rho)) = \frac{m}{m-1} \frac{\sum_{m}^{m} N_{32.1,i}^2 (\log(\rho_i) - \overline{\log(\rho)})^2}{\sum_{m}^{m} \hat{N}_{32.1,i}^2}. \qquad (4.131)$$

Because the true weighted variance, σ_ω^2, is unknown and is estimated by

S_ω^2, probability statements regarding future possible values of the sample weighted mean, $\overline{\log(\rho)}$, must be made with the Student t, rather than the normal, distribution. The probability that any mean will exceed the true mean plus an associated confidence interval is given by

$$\text{Prob}\left[\bar{x} > \left(\mu_x + \frac{S_\omega t_{n:\alpha}}{N^{\frac{1}{2}}}\right)\right] = \alpha \qquad (4.132)$$

(Bendat and Piersol, 1971, p 112)

where μ_x - true value

$\bar{x}$ - sample weighted mean

S_ω - sample weighted standard deviation

$t_{n:\alpha}$ - Student t distribution with n = N-1 degrees of freedom

α - probability level

N - total number of estimates averaged over.

Accordingly, the 100 (1 - 2α) confidence limits for $\bar{x}$ are given by

$$\left(\bar{x} - \frac{S_\omega t_{n:\alpha}}{N^{\frac{1}{2}}}\right) \leq \mu_x \leq \left(\bar{x} + \frac{S_\omega t_{n:\alpha}}{N^{\frac{1}{2}}}\right). \qquad (4.133)$$

This estimation technique was applied to the data illustrated in figure 4.25a. The 95% confidence limits for averages of 4 or more estimates, generated by equation 4.133, are illustrated in 4.25c. For averages of 3 or less estimates, equation 4.126 was used - these are indicated by black circles. The confidence limits for phase for averages of 4 or more values were derived from

$$\hat{\phi}(f) - \Delta\hat{\phi}(f) < \phi(f) < \hat{\phi}(f) + \Delta\hat{\phi}(f) \qquad (4.134a)$$

where

$$\Delta\hat{\phi}(f) = \arcsin\left(\frac{S_\omega t_{n:\alpha}}{N^{\frac{1}{2}}\,\bar{x}}\right) \qquad (4.134b)$$

and are also illustrated in figure 4.25c. The estimates with black circles again refer to confidence limits derived from using equation 4.127.

Figure 4.25 Example of confidence limit estimation for M-T responses

(a) All accepted M-T estimates from data recorded at station BOR

(b) Means of results in (a) with 95% confidence limits estimated by equation 4.125

(c) Means of results in (a) with 95% confidence limits estimated, for asterisked data, by statistical procedures (equations 4.133 & 4.134b)

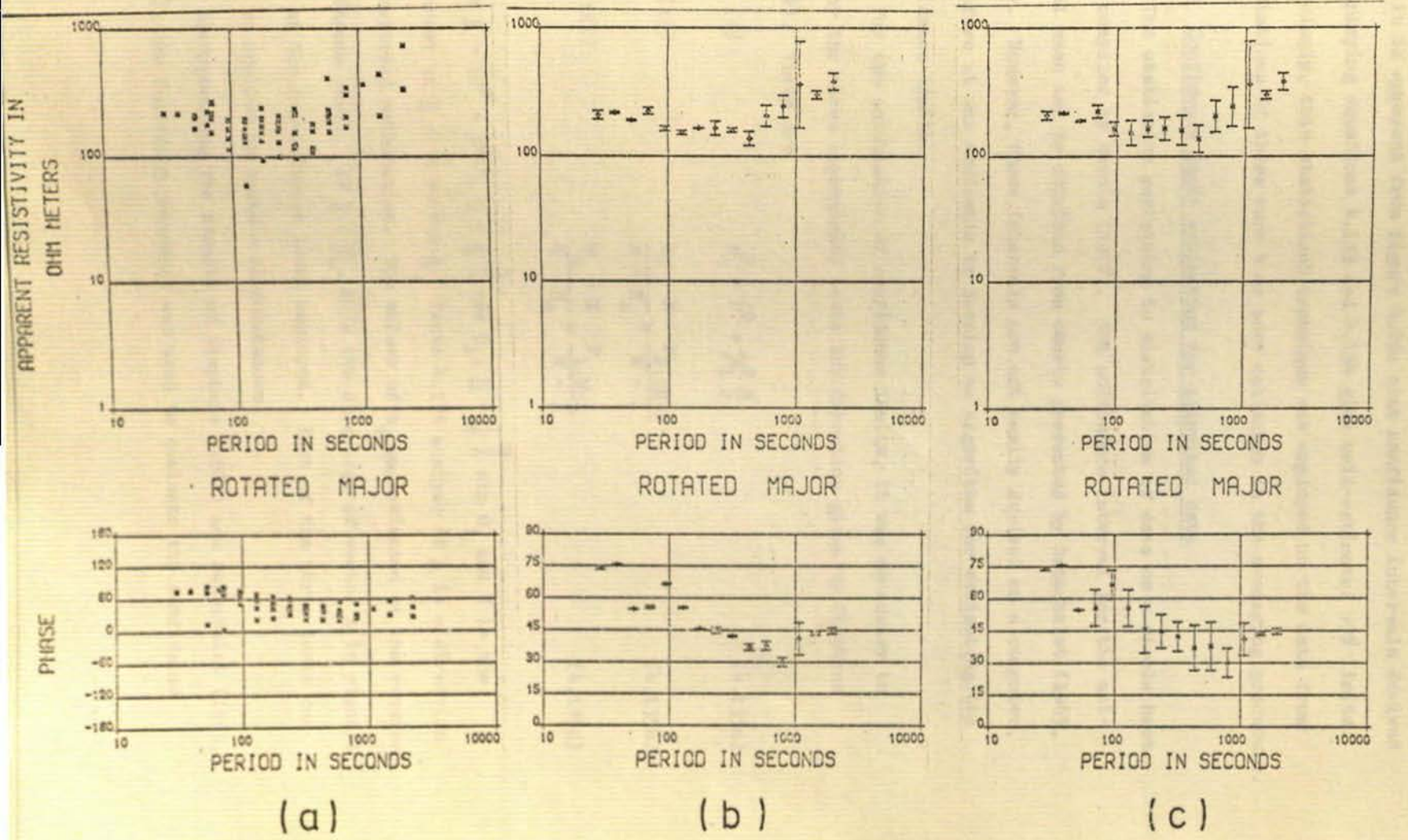
APPARENT RESISTIVITY IN OHM METERS
1000
100
10
1
10
100
1000
10000
PERIOD IN SECONDS
ROTATED MAJOR
PHASE
180
120
60
0
-60
-120
-180
90
75
60
45
30
15
0
PERIOD IN SECONDS
STATION BOR
(a)
(b)
(c)

It is apparent from figure 4.25c that confidence intervals derived by employing equations 4.133 and 4.134 give well-estimated 95% limits. Accordingly, this statistical technique was employed on the data from all stations if there were 4 or more estimates in the averaging procedure.

4.8.3 Confidence limit estimation for azimuthal data

The statistics pertaining to distribution of data on a circle have been compiled by Mardia (1972). The confidence interval for the azimuthal mean can be obtained from charts presented by Batschelet (1965, 1971). However, these intervals are not easily derived on a computer, therefore it was desirable to develop an algorithm for estimating the confidence limits.

For the calculation of confidence limits, it was necessary to employ the three approximate tests for direction given by Stephens (1962). These are

(i) $$R_o^2 = X^2 + \chi_1^2 \frac{N}{2} \qquad (4.135a)$$

(ii) $$\frac{R_c - X}{N - R_o} = \frac{F_{2:2N-2}}{N - 1} \qquad (4.135b)$$

and (iii) $$\frac{R_o - X}{N - R_o} = \frac{F_{1:N-1}}{N - 1} \qquad (4.135c)$$

where $\underline{R} = (\underline{C}^2 + \underline{S}^2)^{\frac{1}{2}}$, $\underline{C} = \frac{1}{N}\sum^{N} \cos\theta_i$, $\underline{S} = \frac{1}{N}\sum^{N} \sin\theta_i$ and X is the component of $\underline{R}$ on a vector $\underline{A}$. Tests 4.135 analyse if $\underline{A}$ is a direction of preferred orientation. The values of R_o are estimated at the required confidence level. If $\underline{R} < R_o$, then the direction of vector $\underline{A}$ is significant at the significance level employed. Each of the three tests can only be applied in certain circumstances.

Incorporating the results of Stephens (1962) and Batschelet (1965, 1971), the following procedure was used to evaluate the confidence

limits for the azimuthal data. Because the azimuthal data was in the range (0, π), and was therefore doubled to give a range of (0, 2π), the estimated confidence limits were halved.

If N was the number of estimates averaged, then for $N < 4$, statistical analysis was not possible.

For $N > 4$, a test for a uniform distribution was applied. The uniform distribution hypothesis was tested with the Rayleigh test (Batschelet, 1965).

If the data were uniformly distributed, then CL (confidence limits) = $\pm 90^{o}$.

If the azimuths were not uniformly distributed, $\underline{R}$ was calculated from $\underline{R}^2 = (\underline{C}^2 + \underline{S}^2)$, where $\underline{C}$ and $\underline{S}$ were computed from a weighted mean,

$$\underline{C} = \frac{\sum^{m} \hat{N}^2_{32.1,i} \cos(2\theta_i)}{\sum^{m} \hat{N}^2_{32.1,i}} \quad \text{and} \quad \underline{S} = \frac{\sum \hat{N}_{32.1,i} \sin(2\theta_i)}{\sum \hat{N}^2_{32.1,i}}$$

Then, if $N < 8$, X2 was derived from 4.135b with $R_o = \underline{R}$ and if $X2 < 3N/4$ then CL = 0.5 arccos (X2/R). Otherwise if $X2 > 3N/4$, X3 was calculated from 4.135c with $R_o = \underline{R}$ and if $X3 > 5N/6$ then CL = 0.5 arccos (X3/R). Alternatively, for $X3 < 5N/6$ then CL = 0.5 arccos ((X2 + X3)/R). For $N > 8$, X2 was calculated from 4.135b with $R_o = \underline{R}$ and for $X2 > 3N/4$, tests as for $N < 8$ were applied. Alternatively, for $N/2 < X2 < 3N/4$, then CL = 0.5 arccos (X2/R). Finally, if $X2 < N/2$, X1 was estimated from 4.126a and CL = 0.5 arccos ((X1 + X2)/2R).

Table 4.3 gives a comparison test, on 8 sets of sample azimuths, between the exact 95% confidence limits derived from the charts given by Batschelet (1971) and the approximate 95% confidence limits estimated by the above procedure. In only one case are the approximate limits an underestimate (by 6%) of the exact estimated limits. In all others, the intervals are either correctly estimated (to within 4%) or over-

TABLE 4.3

Comparison of exact, from Batschelet's charts (1965, 1971), and calculated, from section 4.8.3, confidence limits for azimuthal data

No. of estimates	Circular variance	Exact	Approximate	Error
4	0.03	12°	13.2°	+9%
4	0.08	19°	19.4°	+2%
6	0.01	5°	4.7°	-6%
4	0.01	7°	7.5°	+7%
5	0.04	10.5°	11.6°	+9%
7	0.08	11.5°	12.0°	+4%
5	0.21	23°	22.4°	-2%
4	0.25	Uniformly distributed	180°	-

estimated (up to 9%).

The sample azimuthal data illustrated in figure 4.26a were averaged by equation 4.93 and 95% confidence limits were estimated by the above procedure. The result is illustrated in figure 4.26b which shows that the limits have been well estimated. This procedure was therefore employed for all azimuthal data.

4.8.4 Confidence limit estimation for skew data

This was accomplished in the same manner as for apparent resistivity data. The sample weighted variance was estimated from 4.130 and then the limits derived by employing 4.133.

The skew data illustrated in figure 4.27a were averaged in each spectral band by 4.94 and the 95% confidence limits were estimated as described above. The result is shown in figure 4.27b.

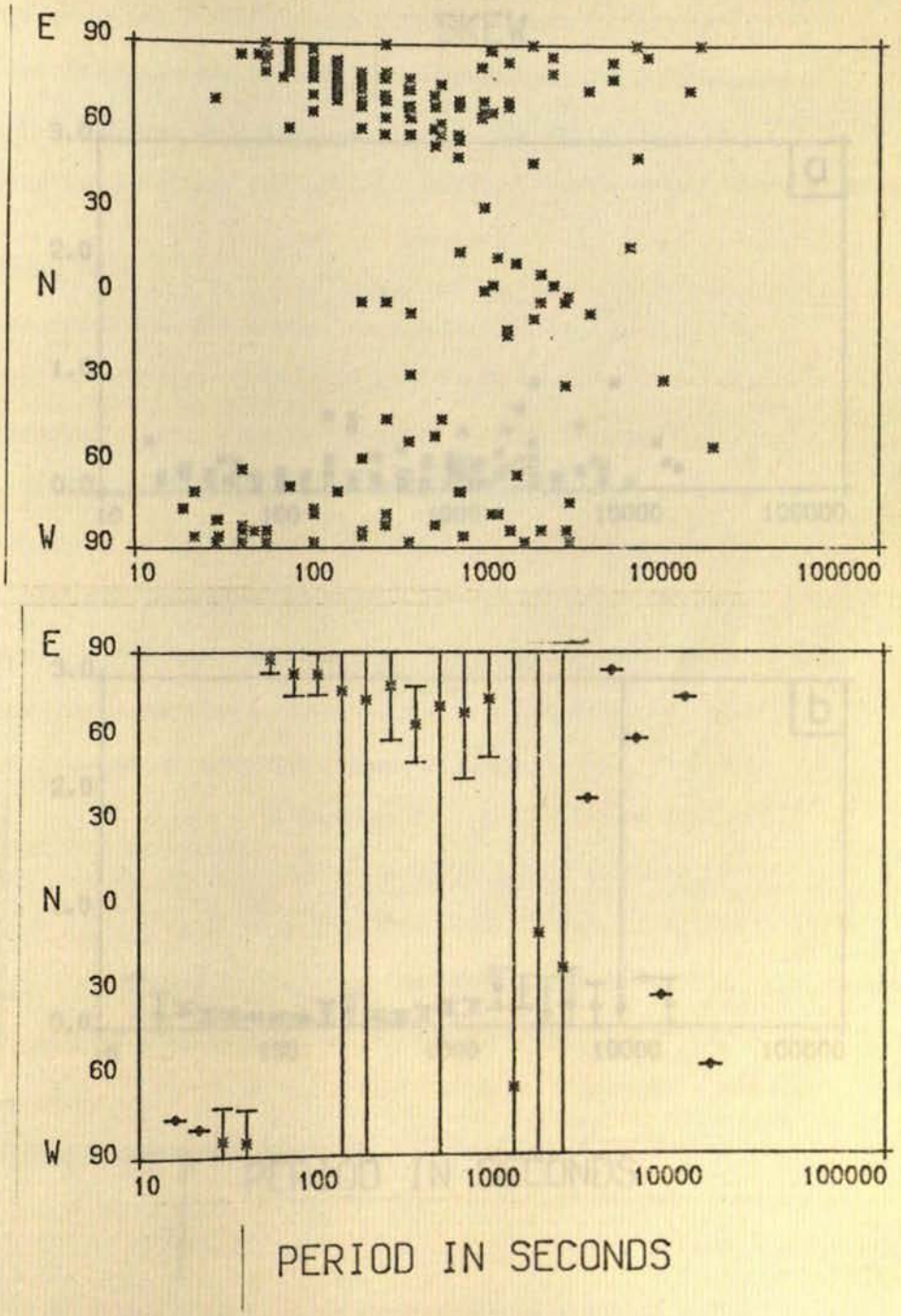

Figure 4.26 Example of confidence limit estimation for azimuthal data
a) azimuthal angles of accepted estimates
b) averaged values and 95% confidence

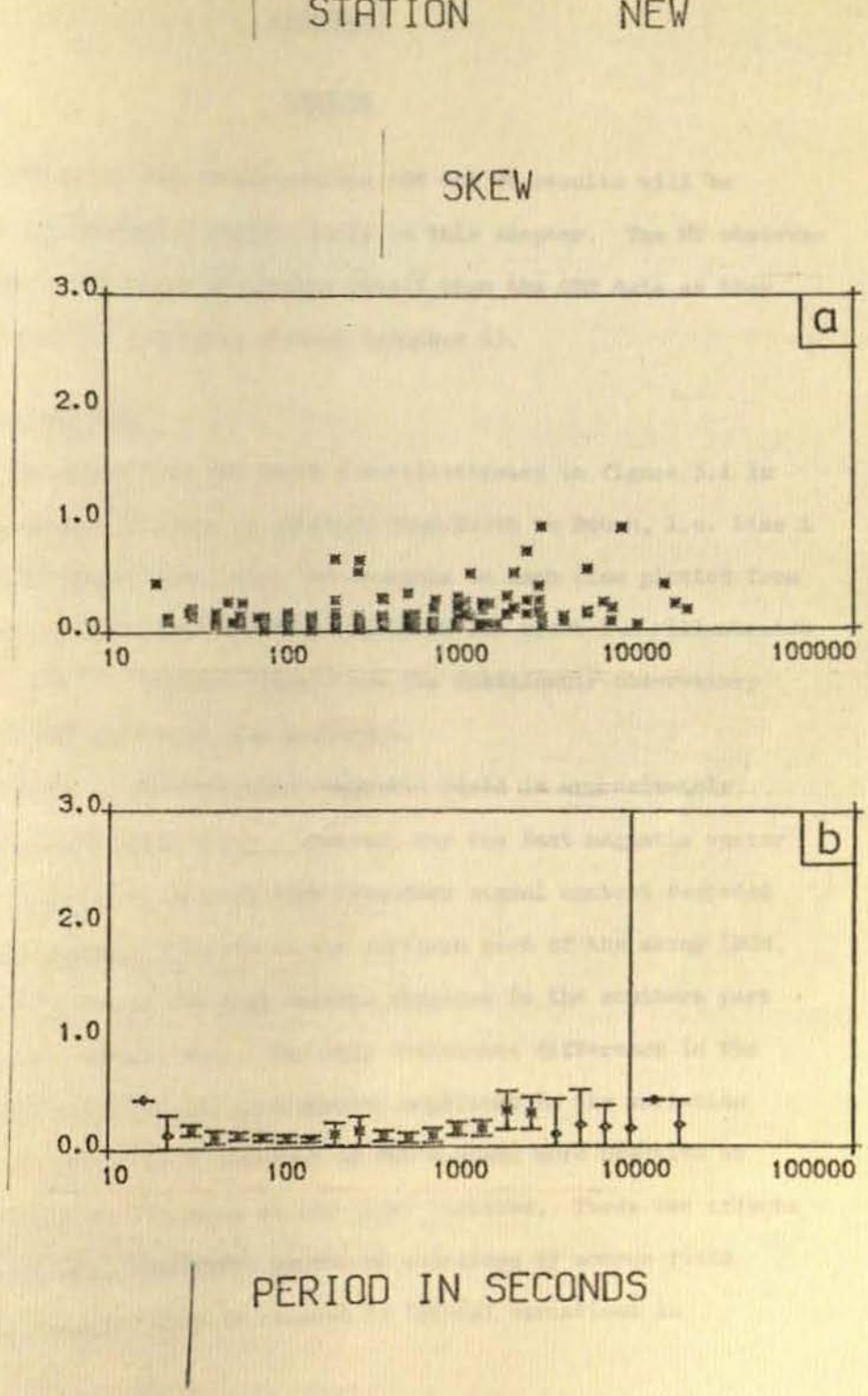

Figure 4.27 Example of confidence limit estimation for skew
a) skew values of accepted estimates
b) averaged values and 95% confidence limits

CHAPTER 5

RESULTS

The GDS array and single-station GDS and MT results will be presented and discussed qualitatively in this chapter. The MT observations will be discussed in greater detail than the GDS data as they were employed for modelling studies (chapter 6).

5.1 GDS Array Data

All the array data for event 3 are illustrated in figure 5.1 in the usual manner of lines of latitude from North to South, i.e. Line 1 is the northernmost line, with the stations on each line plotted from West to East. Those data which were analysed for event 2 are illustrated in figure 5.2. In neither figures are the Eskdalemuir observatory data shown although they were available.

For event 3, the horizontal magnetic field is approximately uniform over the whole array. However, for the East magnetic vector (D) there appears to be more high frequency signal content recorded at the most western stations in the northern part of the array (BON, HEL and GST), and at the most eastern stations in the southern part of the array (SGH and HAG). The only noticeable difference in the north magnetic vector (H) is a greater amplitude in the variation recorded at HAG. The H component at HAG becomes more negative by 25 nT compared to its value at the other stations. These two effects in the horizontal components cannot be explained by source field structure and hence must be related to lateral variations in conductivity.

For the vertical magnetic field component (Z), which is more sensitive to lateral conductivity variations than the horizontal

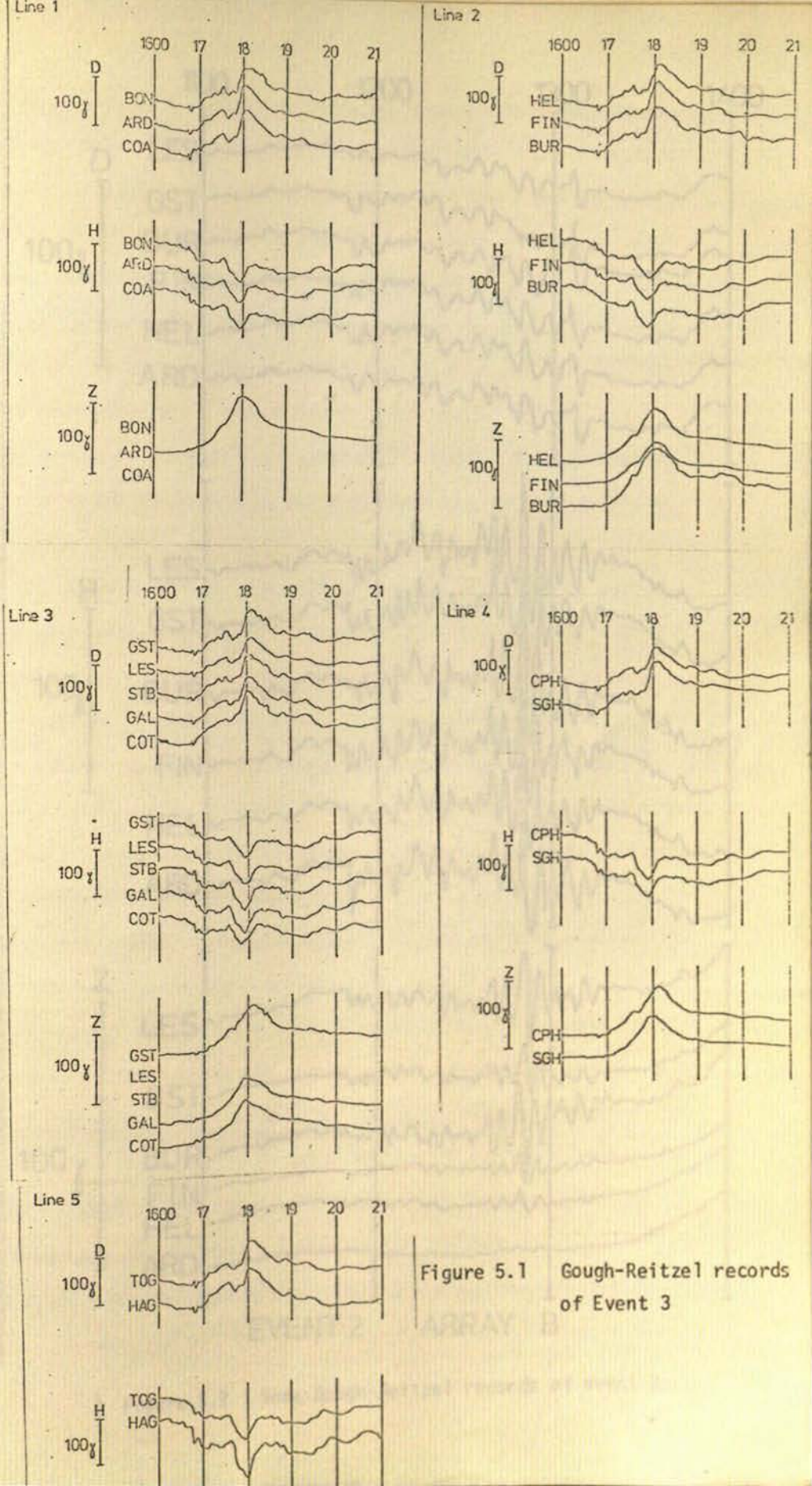

Figure 5.1 Gough-Reitzel records of Event 3

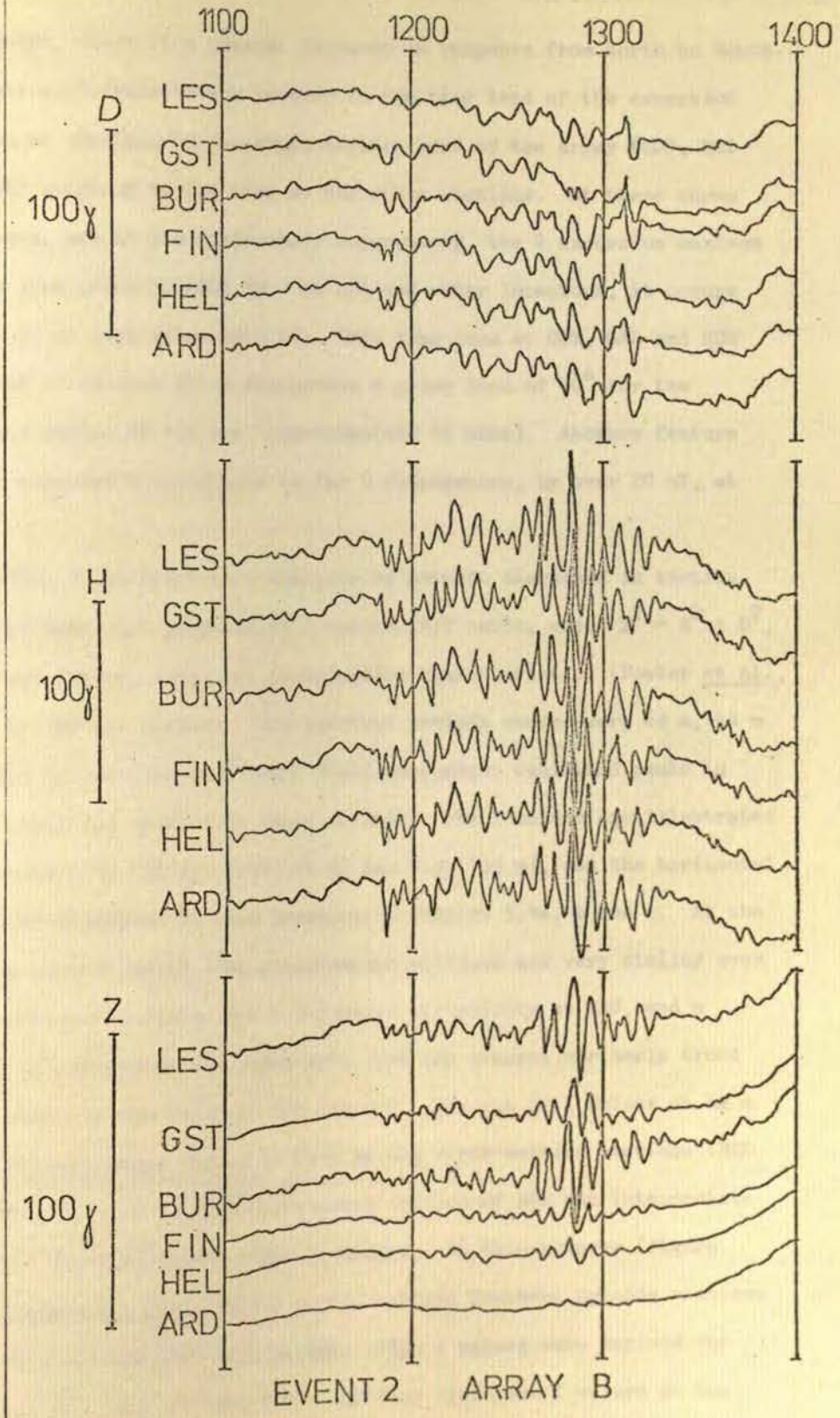

Figure 5.2 Some Gough-Reitzel records of event 2

components, there is a general decrease in response from North to South. The most noticeable effect however is the time lead of the excursion maximum at stations in the south-eastern part of the array (COT, GAL and SGH) compared to its time at the other stations. At these three locations, and at the Eskdalemuir observatory, the Z excursion maximum occurs just prior to 1800 UT. At all the other locations, it occurs either at or just after 1800 UT. This time lead at COT, GAL and SGH is about 13 minutes which represents a phase lead of 70° for the dominant period of the bay (approximately 66 mins). Another feature of the recorded Z variations is the Z attenuation, by over 20 nT, at FIN.

Event 3 was spectrally analysed by methods discussed in section 4.2, and maps were prepared of I values (Z/T ratio, where $T^2 = H^2 + D^2$, Caner and Cannon, 1965) and polarisation characteristics (Fowler et al., 1967) at various periods. The spectral periods chosen were 66 m, 44 m and 33 m because the horizontal field components exhibited peaks in their amplitude spectra at these periods. The I values are illustrated in figures 5.3a (66 m), 5.3b (44 m) and 5.3c (33 m), and the horizontal field polarisations at each location in figures 5.4a, b and c. At the longest period (66 m), the polarisation ellipses are very similar over the whole array, except for a decreased ellipticity at HAG, and a change in azimuth of the major axis from the general northerly trend to an easterly direction at SGH and COT. The map of I values at 66 m (figure 5.3a) shows high I (> 0.3) at the north-western stations (HEL and ARD), low I (< 0.2) at the coastal station of BUR and intermediate I ($0.2 < I < 0.3$) at the other locations. At 44 m however (figure 5.3b), there are low I values at the central Southern Uplands stations (GAL, ESK and SGH) and also at ARD. High I values were derived for stations HEl, BUR, COT and TOG. The very different I values at the

Figure 5.3 Maps of 'I' values calculated from Event 3 for periods of-

a) 66 minutes

b) 44.5 minutes

c) 33 minutes

Figure 5.4 Polarisation parameters calculated for Event 3 at periods of

a) 66 minutes

b) 44.5 minutes

c) 33 minutes

Note: all ellipses anti-clockwise polarised except at HAG for a period of 44.5 mins.

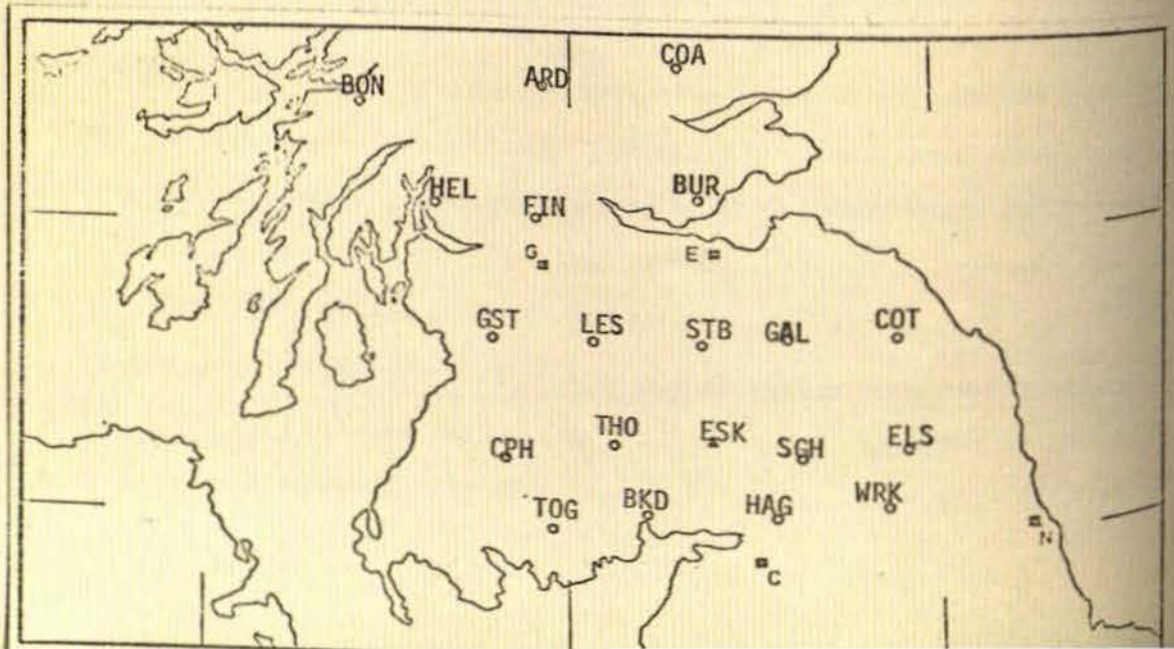

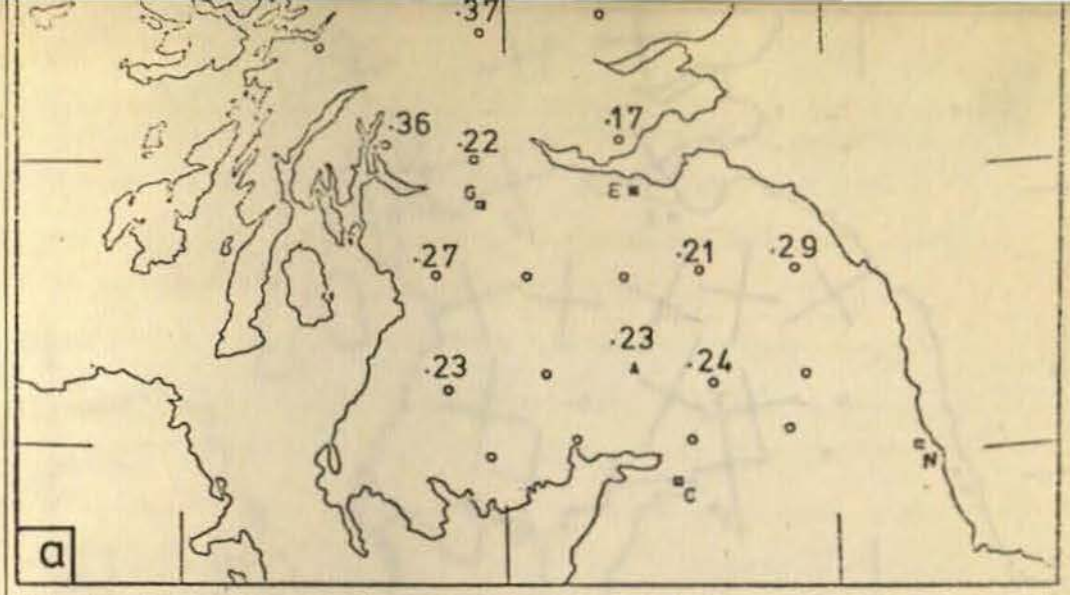
·37
·36
·22
·17
·27
·21
·29
·23
·24
·23
a

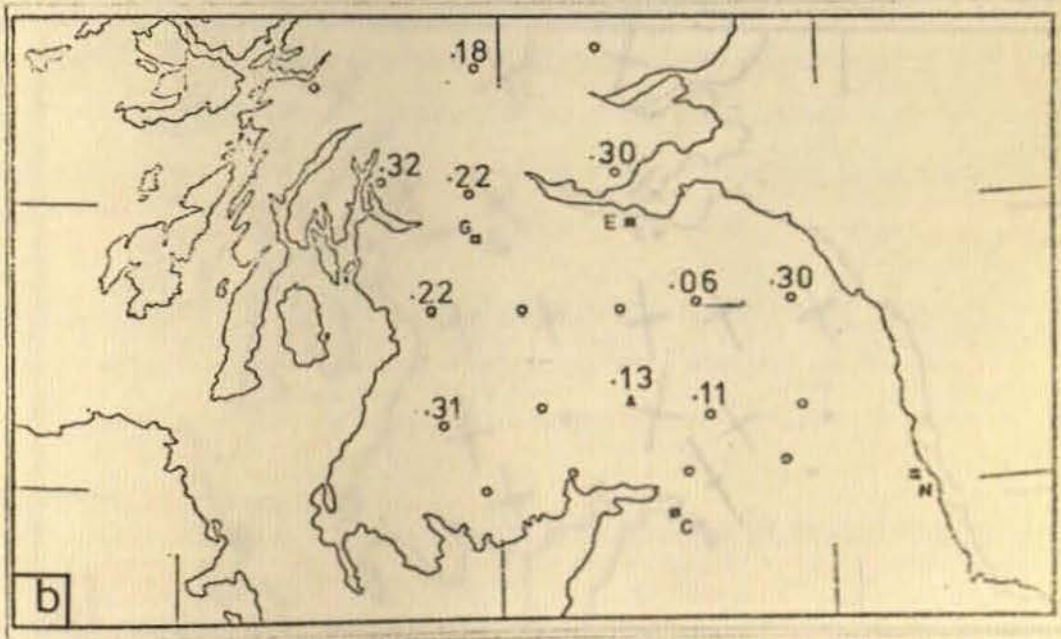
·18
·32
·22
·30
·22
·06
·30
·13
·11
·31
b

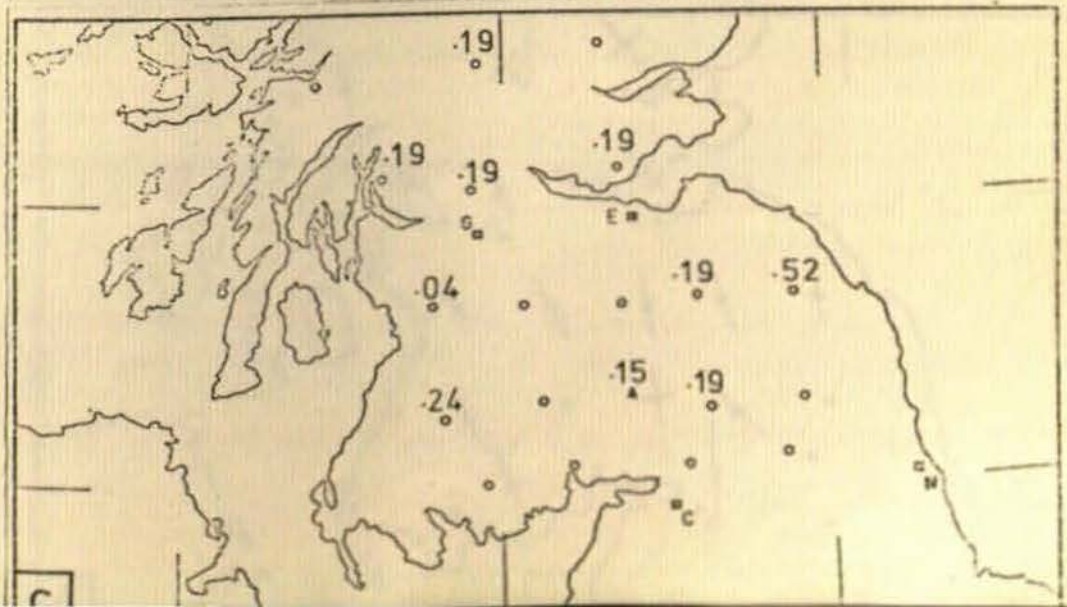
·19
·19
·19
·19
·19
·04
·52
·15
·19
·24
c

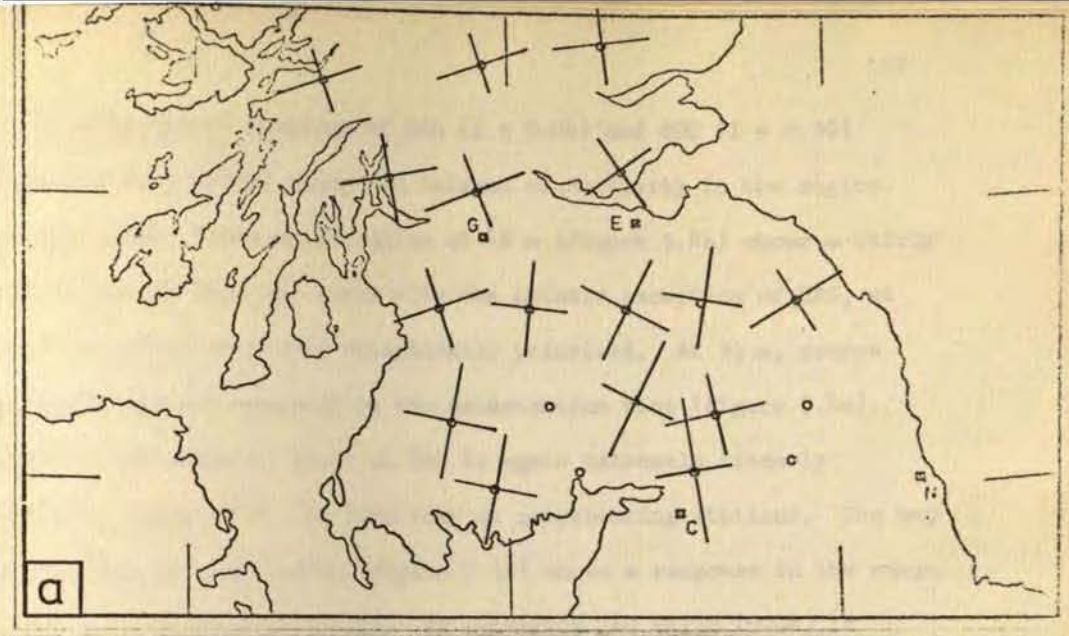
G
E
C
a

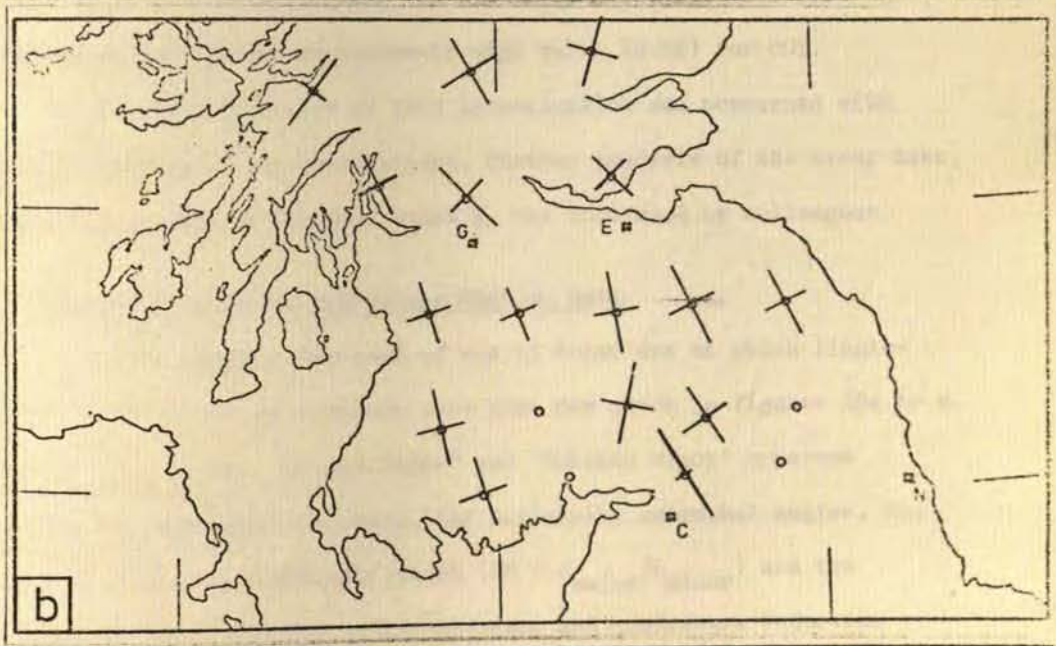
G
E
C
b

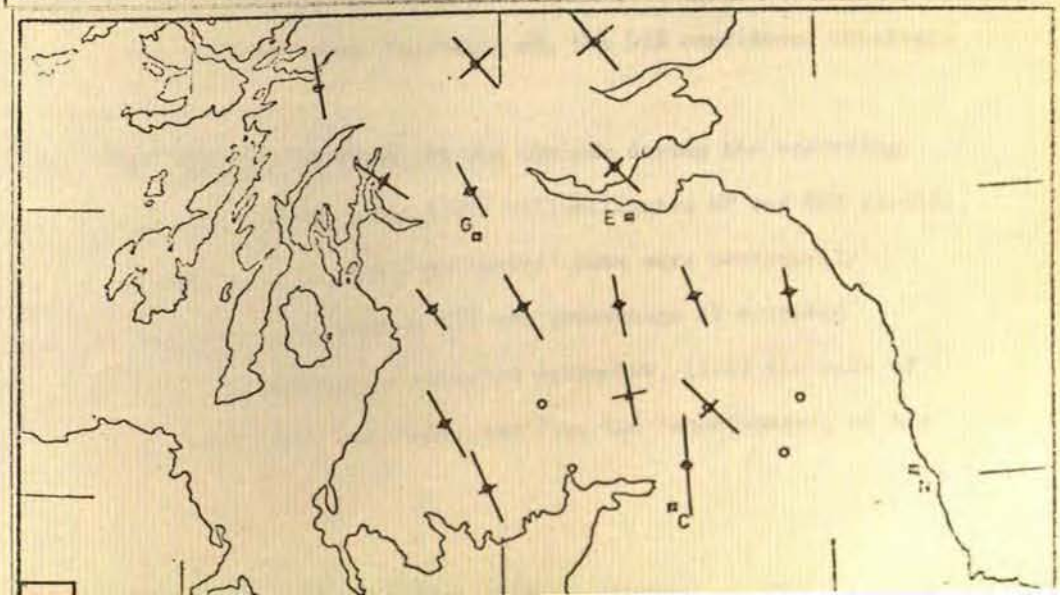
G
E
C

two closely-spaced stations of GAL (I = 0.06) and COT (I = 0.30) suggest a very marked change in lateral conductivity in the region. The horizontal field polarisation at 44 m (figure 5.4b) shows a fairly uniform nature over the array with the notable exception of HAG, at which the field is highly elliptically polarised. At 33 m, source field effects are apparent on the polarisation plot (figure 5.4c). However, the magnetic field at HAG is again extremely linearly polarised compared to its behaviour at neighbouring stations. The map of I values at this period (figure 5.3c) shows a response in the range 0.15 - 0.25 at most locations. An extremely low value (0.04) is calculated for GST and an extremely high value (0.52) for COT.

As the main objective of this investigation was concerned with the application of the MT technique, further analysis of the array data, including a detailed study of event 2, was continued by colleagues.

5.2 Synopsis of MT and GDS Single-Station Data

The full results from each of the 13 locations at which single-station MT and GDS observations were made are given in figures 5.5a to m. Illustrated are the 'Rotated Major' and 'Rotated Minor' apparent resistivity and phase estimates, the maximising azimuthal angles, the skew factors, the anisotropy ratios ($AR = \rho_{major}/\rho_{minor}$) and the magnitudes and directions of the in-phase and quadrature induction vectors. For all estimates, excluding AR, the 95% confidence intervals are also shown.

For the majority of sites, it was obvious during the recording stage whether the station would yield well-estimated MT and GDS results or not. The criteria for 'well-estimated' data were necessarily subjective but were dependent on (i) the percentage of accepted estimates, (ii) the scatter of accepted estimates, (iii) the size of the estimated confidence intervals, and (iv) the 'smoothness', of the

Figures 5.5 Total results from all 13 locations at which measurement of the M-T and GDS single-station variations were made.

top left - 'Rotated Major' apparent resitivities and phase

top right - 'Rotated Minor' apparent resistivities and phase

bottom left - azimuthal rotation angles, skew factors & anisotropy ratios

bottom right - real and imaginary induction vectors amplitudes & directions
(both vectors reversed)

STATION BOR

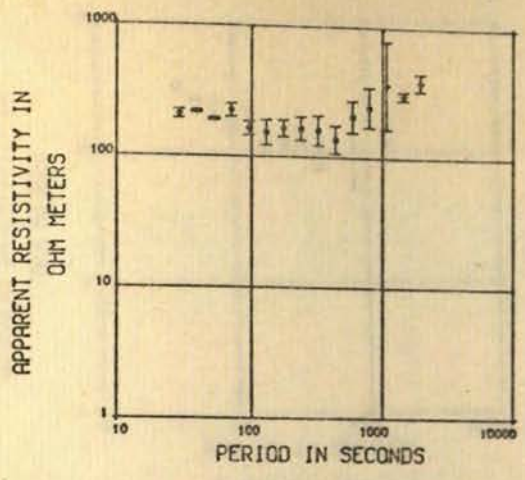

ROTATED MAJOR

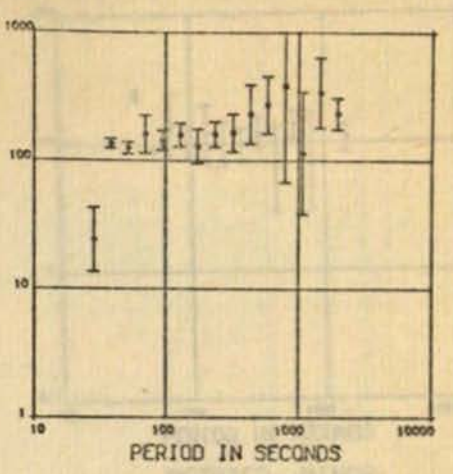

ROTATED MINOR

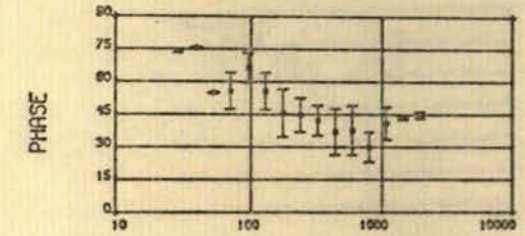

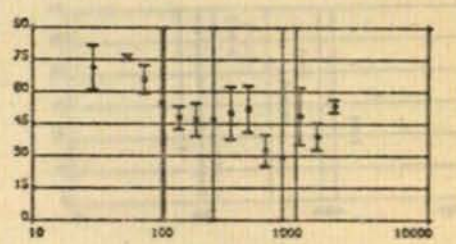

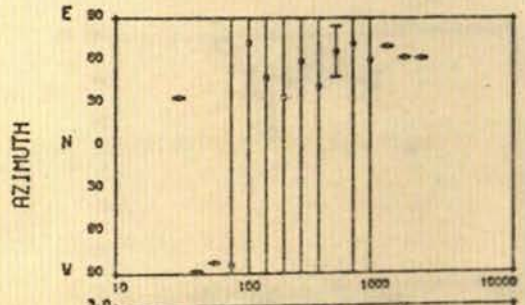

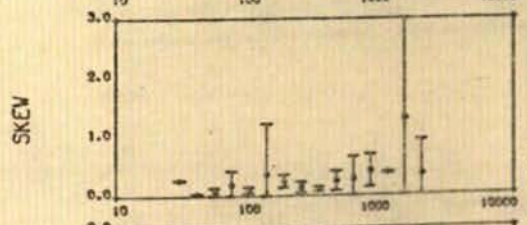

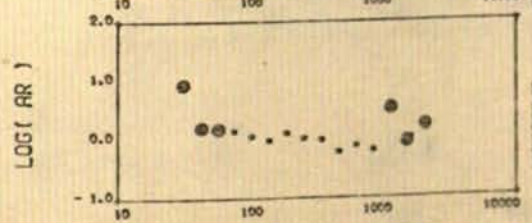

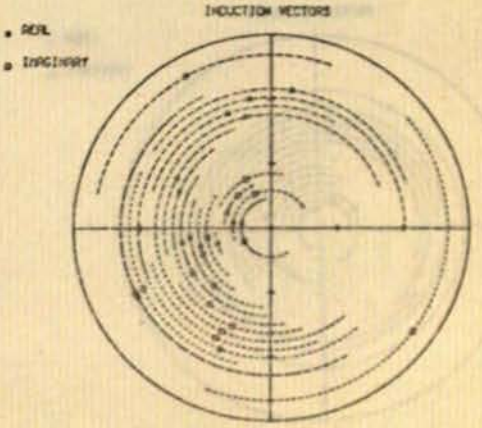

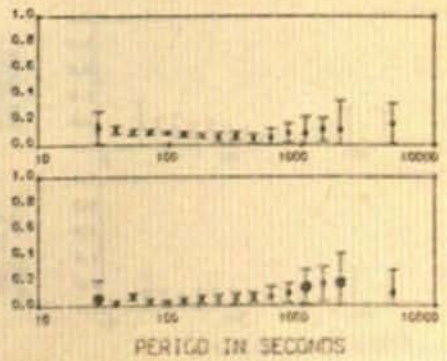

Figures 5.5 Total results from all 13 locations at which measurement of the M-T and GDS single-station variations were made.

top left - 'Rotated Major' apparent resitivities and phase

top right - 'Rotated Minor' apparent resistivities and phase

bottom left - azimuthal rotation angles, skew factors & anisotropy ratios

bottom right - real and imaginary induction vectors amplitudes & directions
(both vectors reversed)

STATION BOR

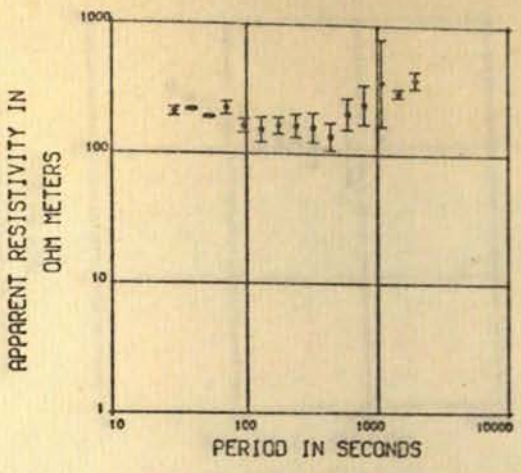
APPARENT RESISTIVITY IN OHM METERS
PERIOD IN SECONDS
ROTATED MAJOR

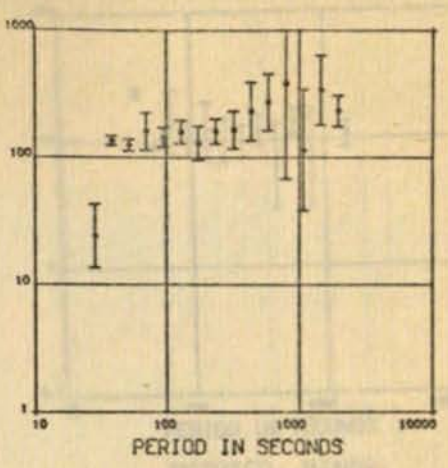
PERIOD IN SECONDS
ROTATED MINOR

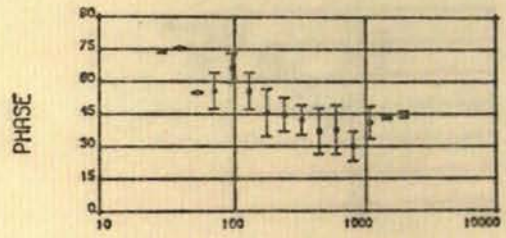
PHASE

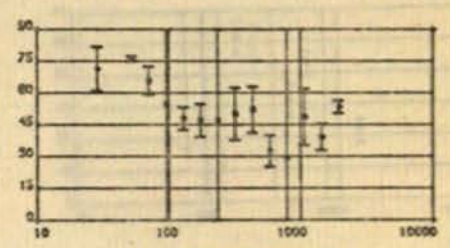

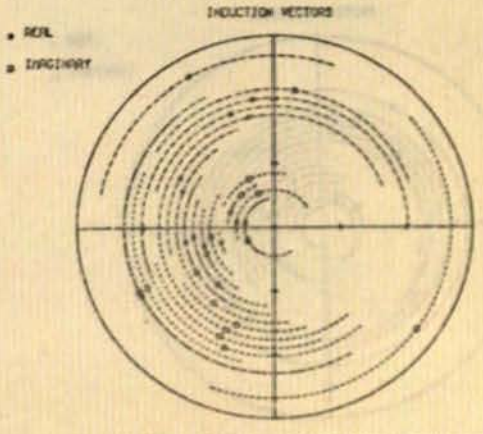
INDUCTION VECTORS
REAL
IMAGINARY
INNER PERIOD = 10 SECS
OUTER PERIOD = 10000 SECS

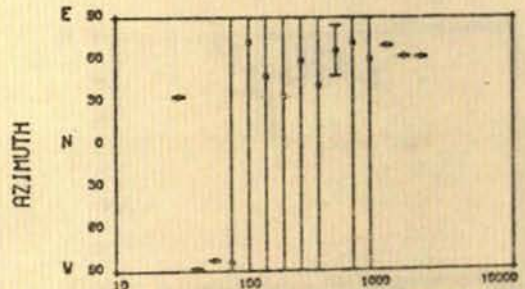
AZIMUTH
E
N
W
SKEW

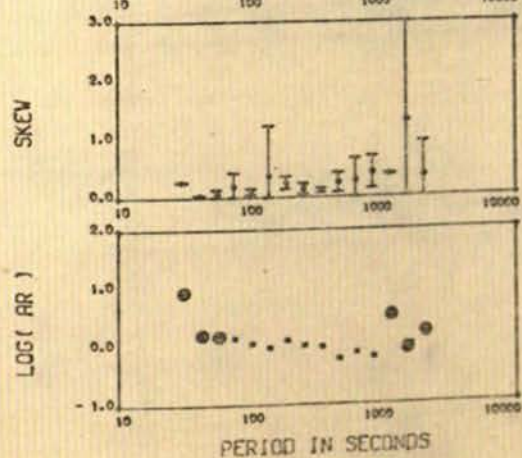
LOG(AR)
PERIOD IN SECONDS

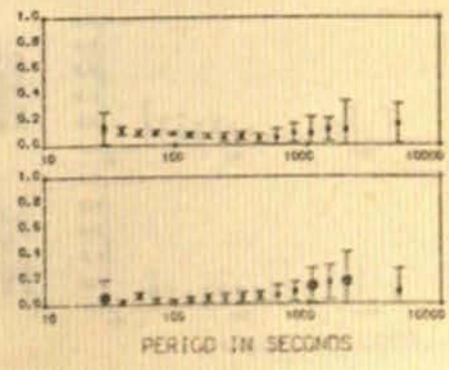
PERIOD IN SECONDS

STATION CAP

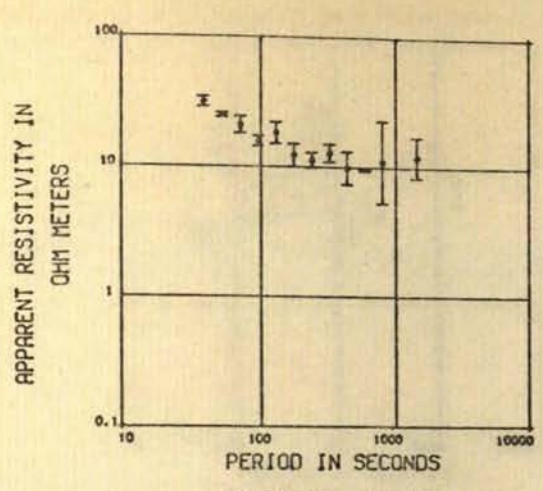

ROTATED MAJOR

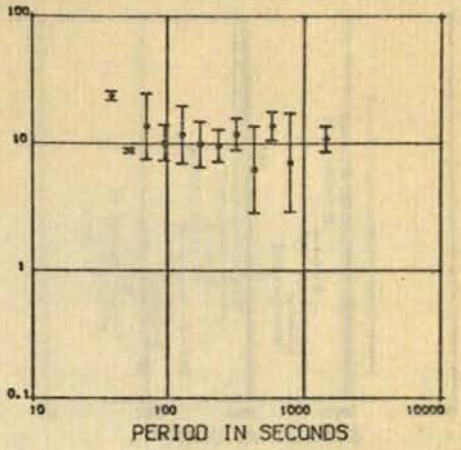

ROTATED MINOR

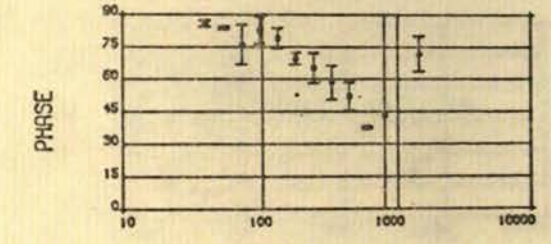

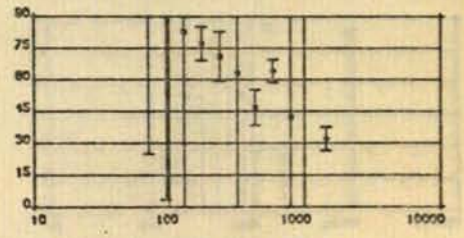

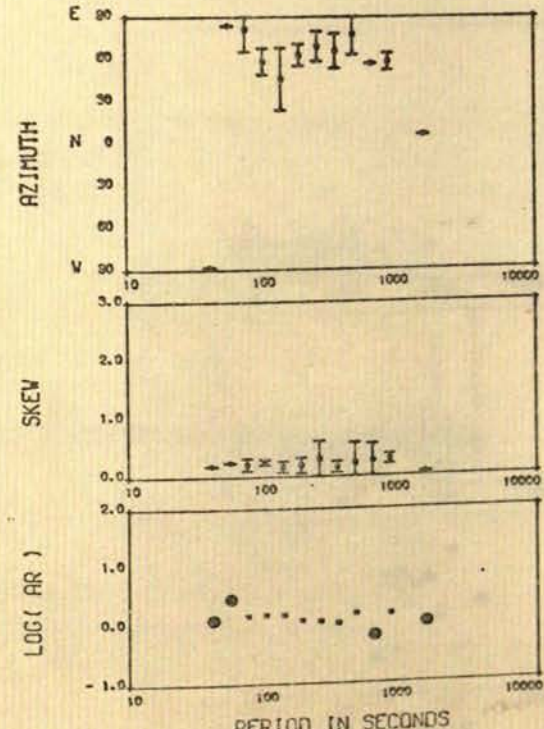

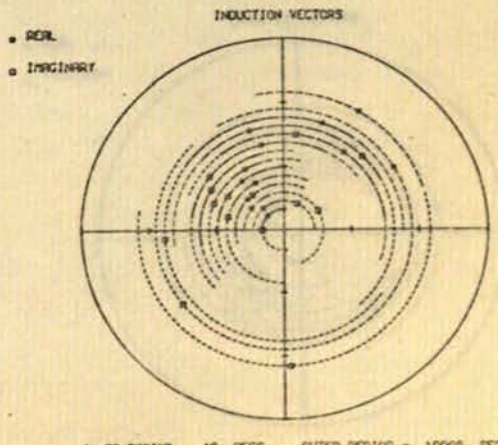

STATION CRK

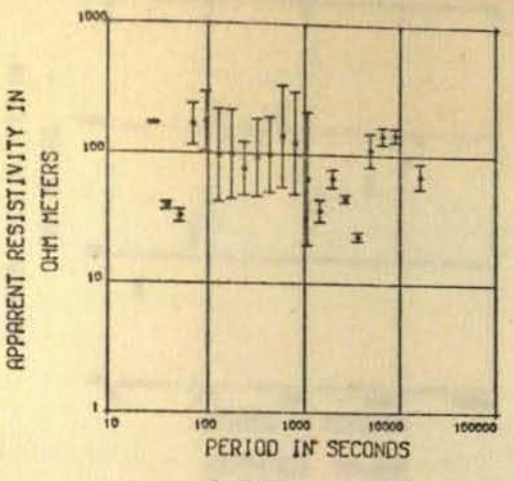

ROTATED MAJOR

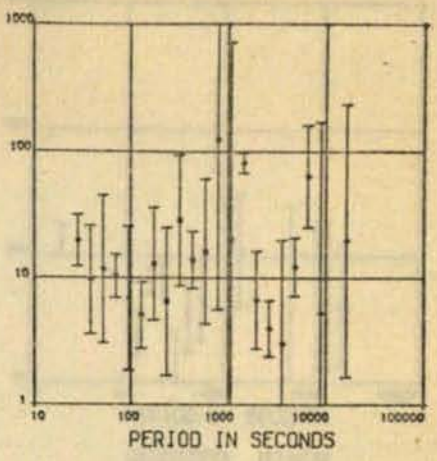

ROTATED MINOR

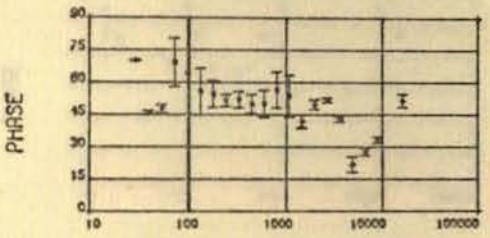

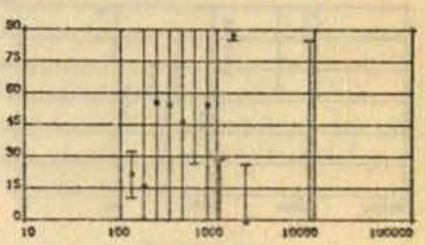

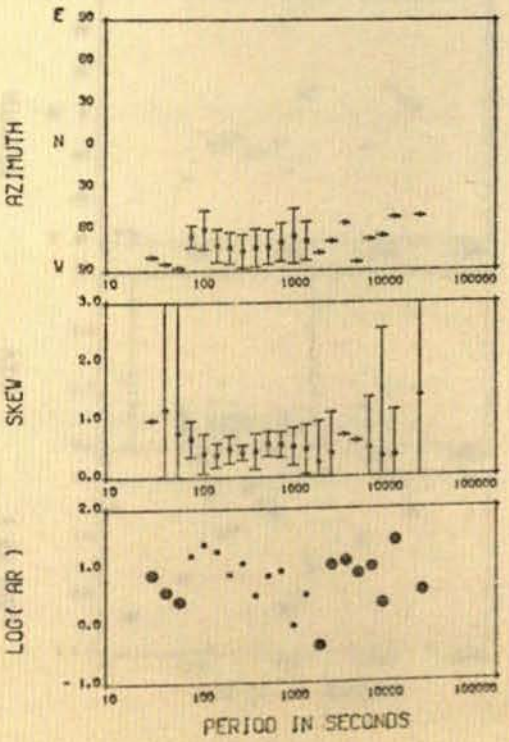

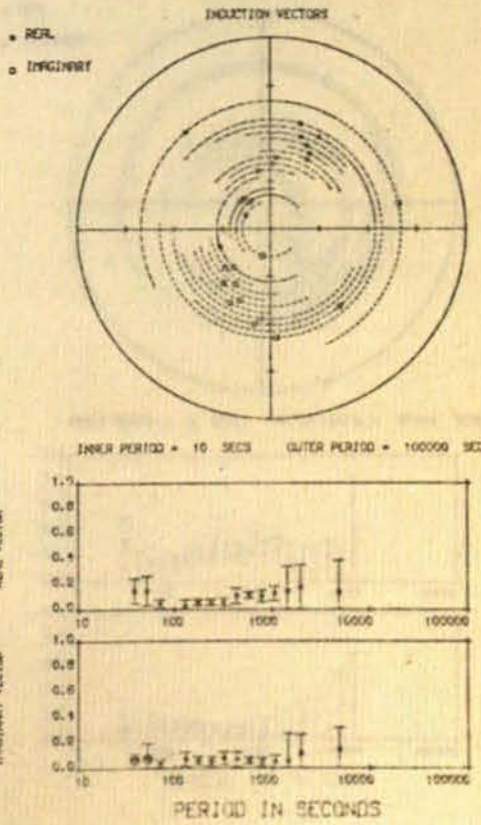

STATION DZR

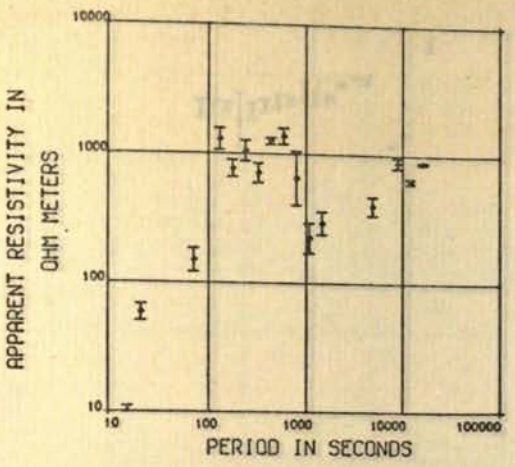

ROTATED MAJOR

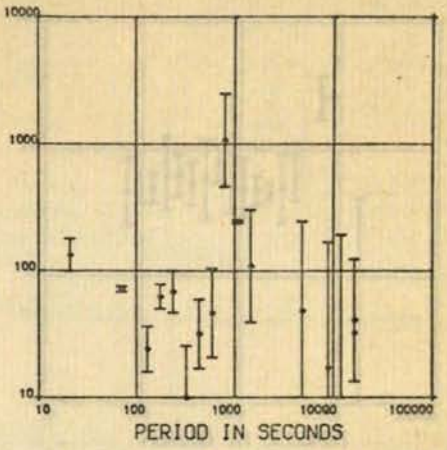

ROTATED MINOR

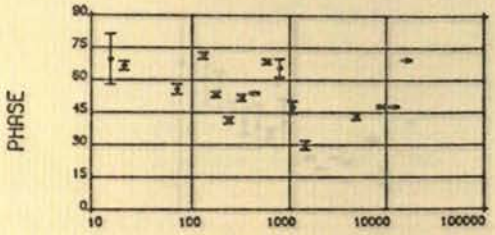

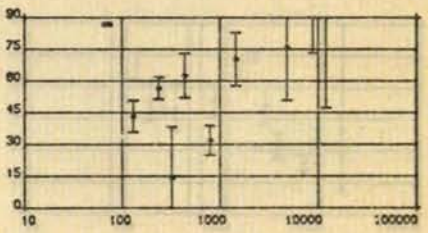

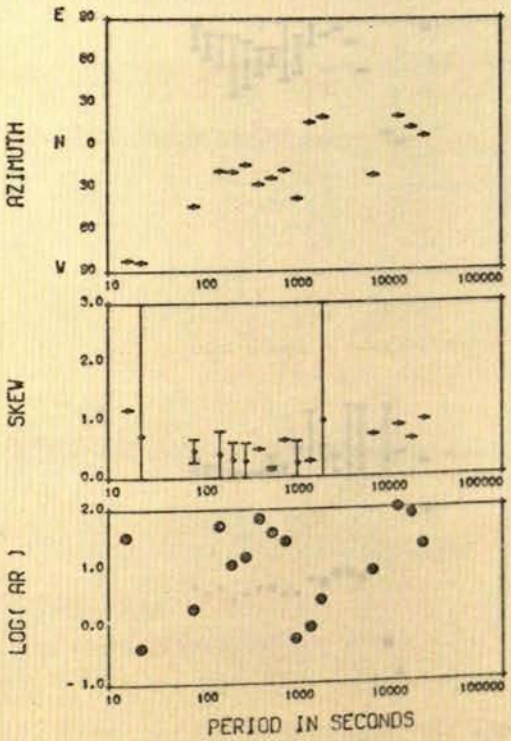

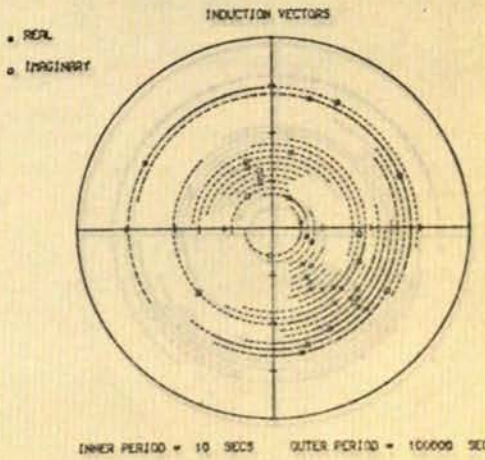

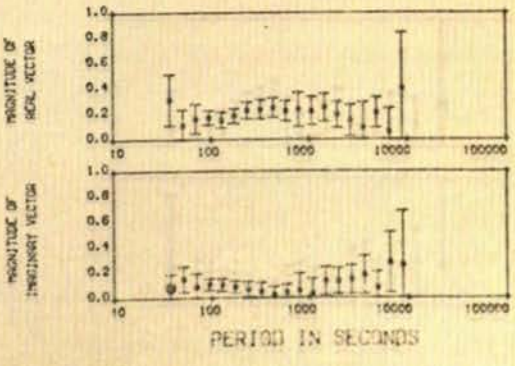

STATION ELC

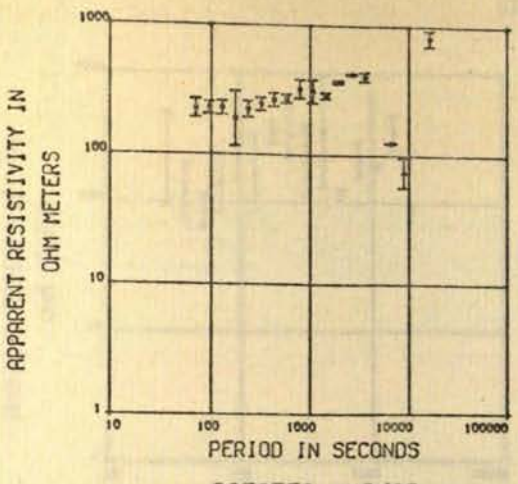

ROTATED MAJOR

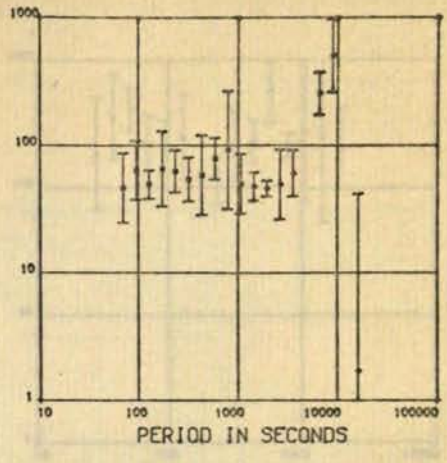

ROTATED MINOR

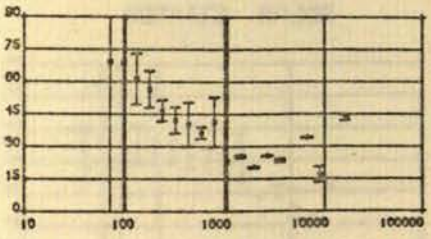

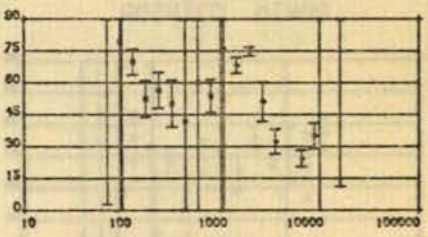

INDUCTION VECTORS

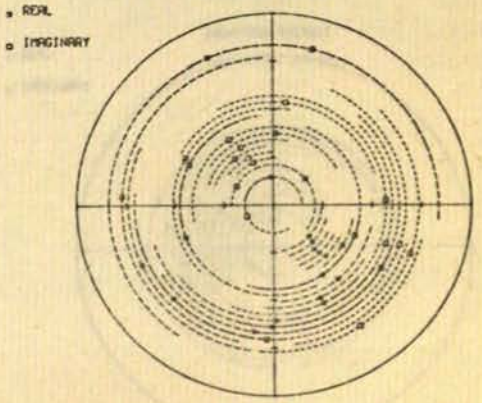

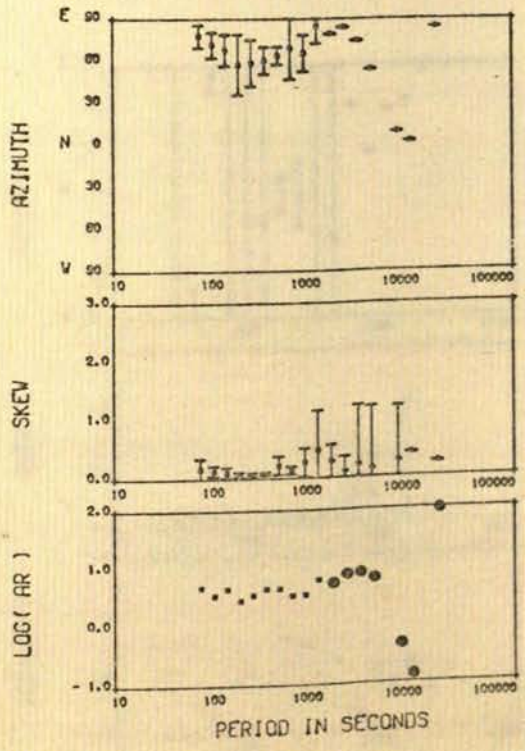

INNER PERIOD = 10 SECS OUTER PERIOD = 100000 SECS

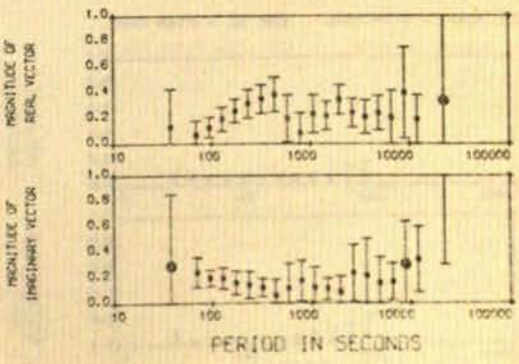

STATION ESK

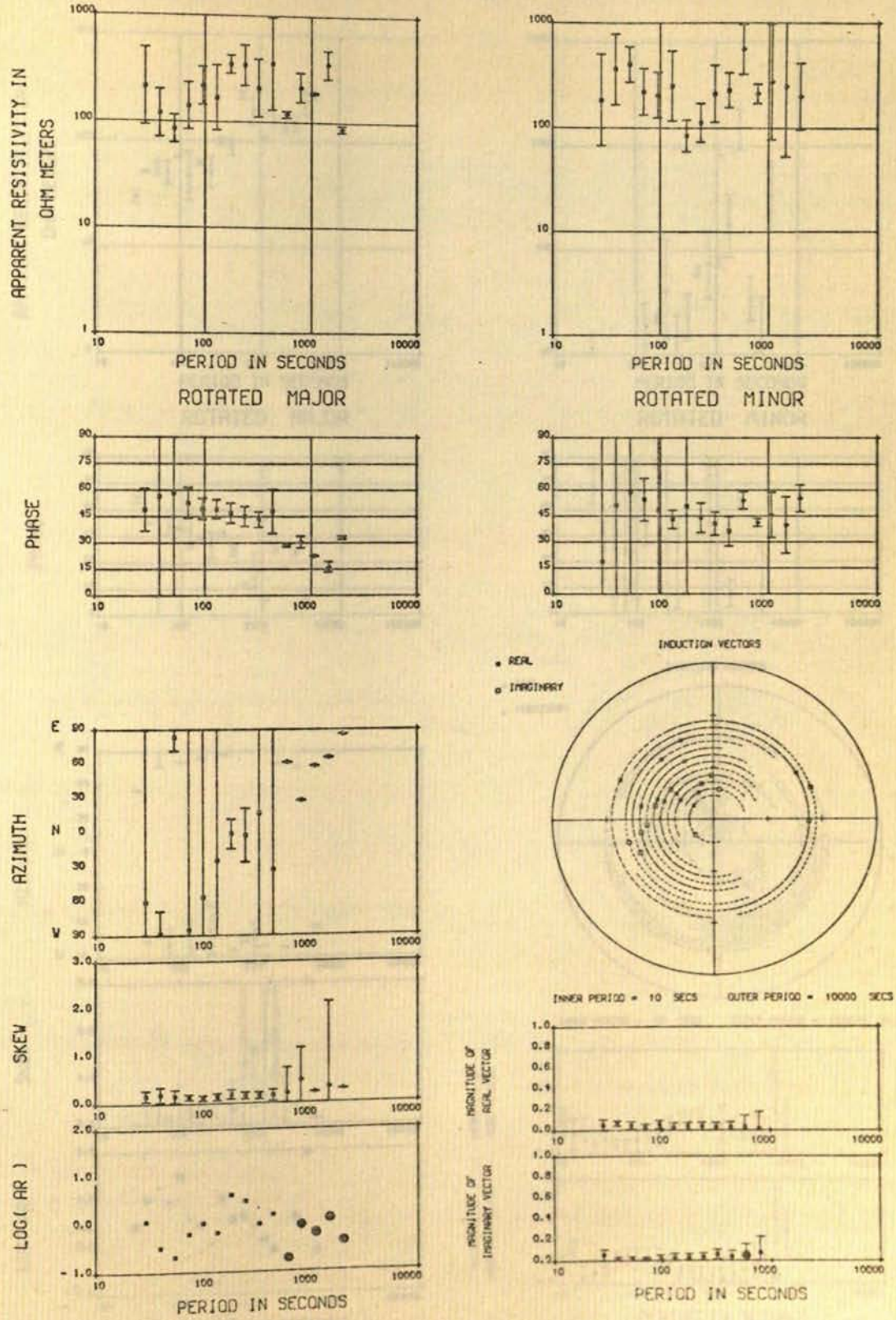
APPARENT RESISTIVITY IN OHM METERS
1000
100
10
1
10
100
1000
10000
PERIOD IN SECONDS
ROTATED MAJOR
ROTATED MINOR
PHASE
90
75
60
45
30
15
0
AZIMUTH
E
N
W
SKEW
3.0
2.0
1.0
0.0
LOG(AR)
-1.0
INDUCTION VECTORS
REAL
IMAGINARY
INNER PERIOD = 10 SECS
OUTER PERIOD = 10000 SECS
MAGNITUDE OF REAL VECTOR
MAGNITUDE OF IMAGINARY VECTOR
0.8
0.6
0.4
0.2

STATION FTH

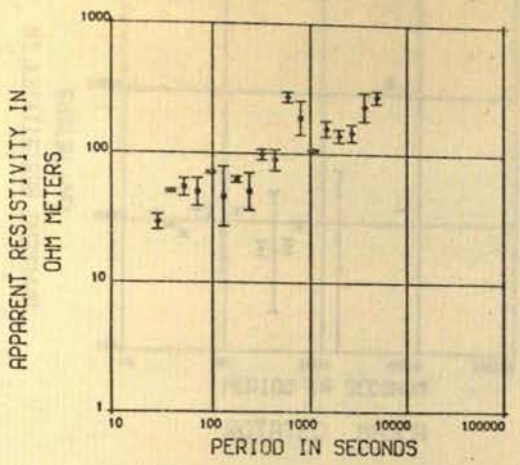

ROTATED MAJOR

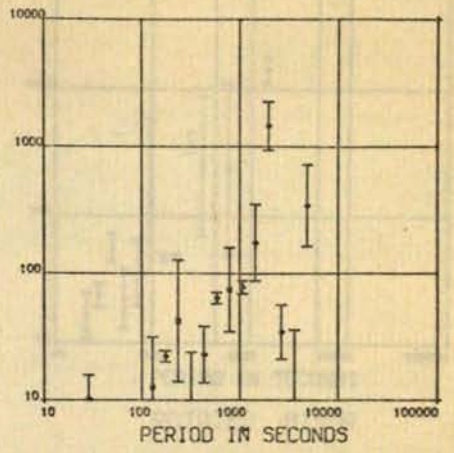

ROTATED MINOR

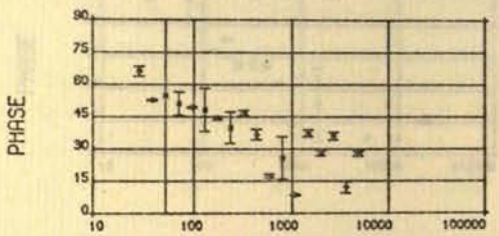

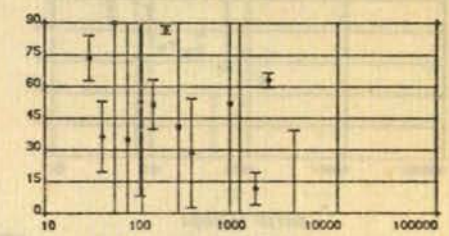

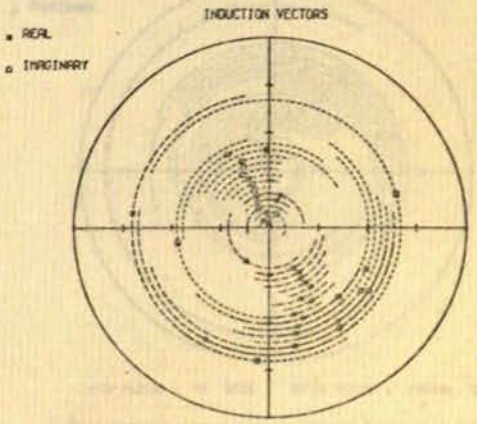

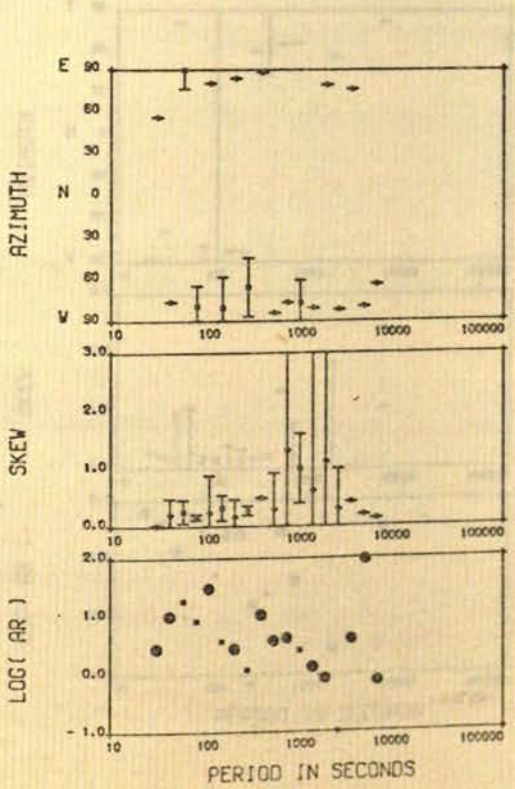

INNER PERIOD = 10 SECS OUTER PERIOD = 100000 SECS

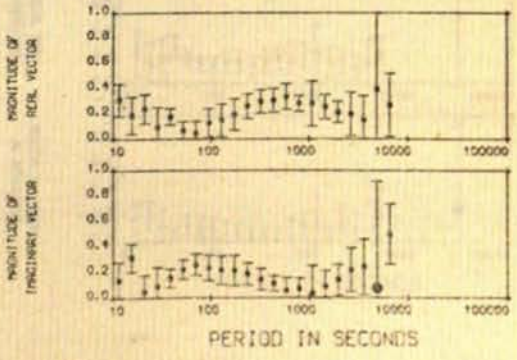

STATION GOR

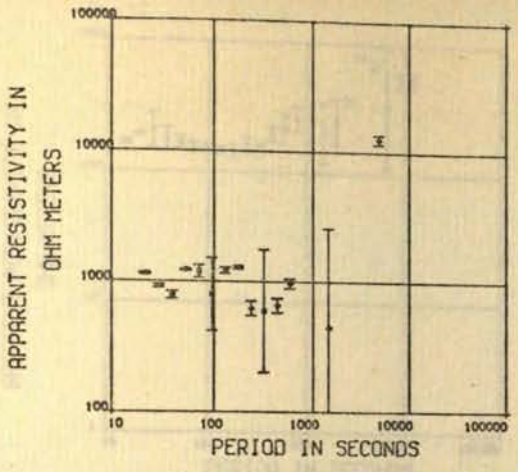

ROTATED MAJOR

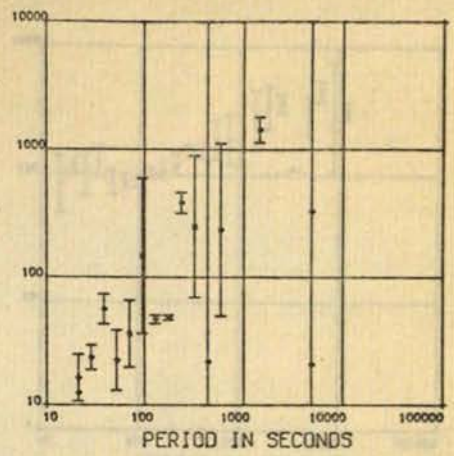

ROTATED MINOR

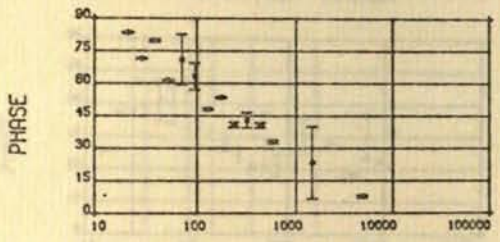

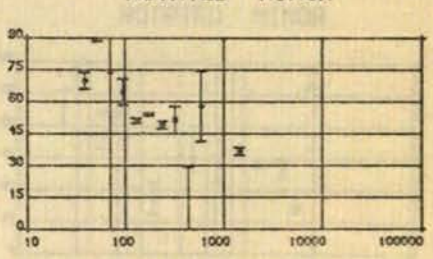

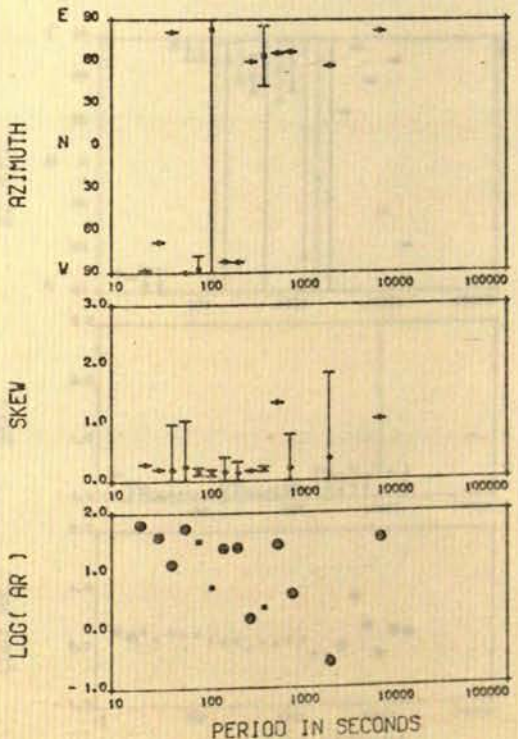

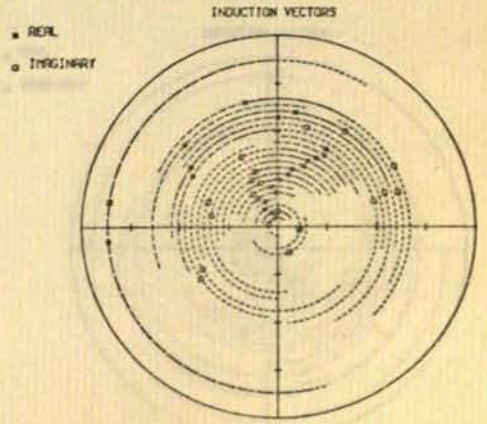

STATION NEW

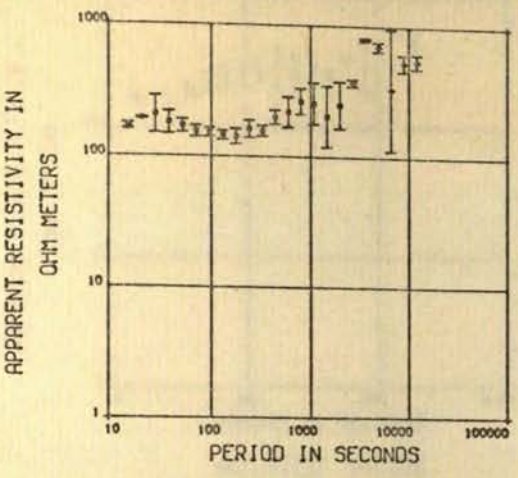

ROTATED MAJOR

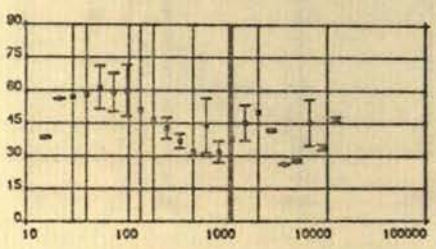

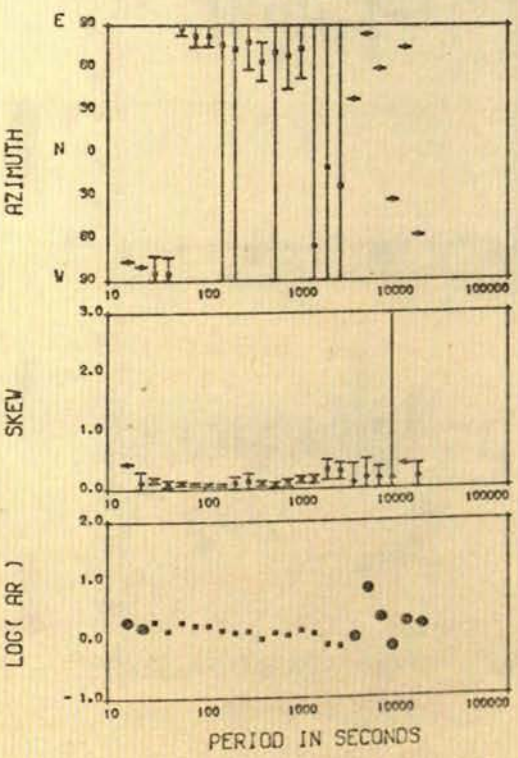

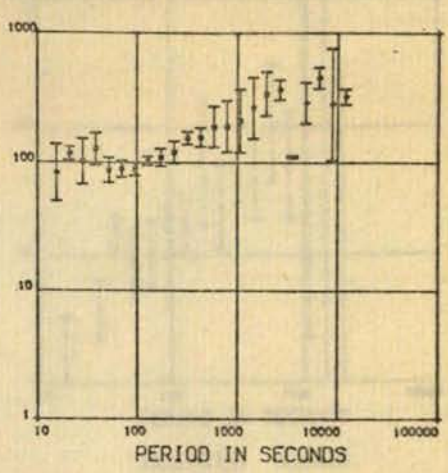

ROTATED MINOR

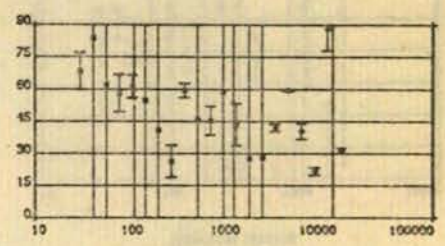

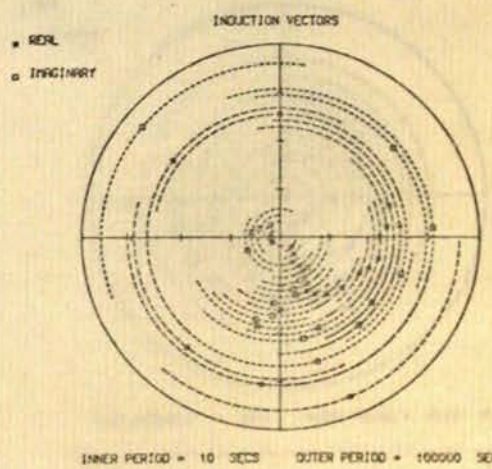

INNER PERIOD = 10 SECS OUTER PERIOD = 100000 SECS

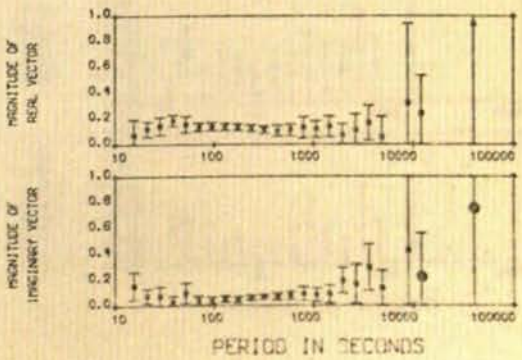

STATION PRE

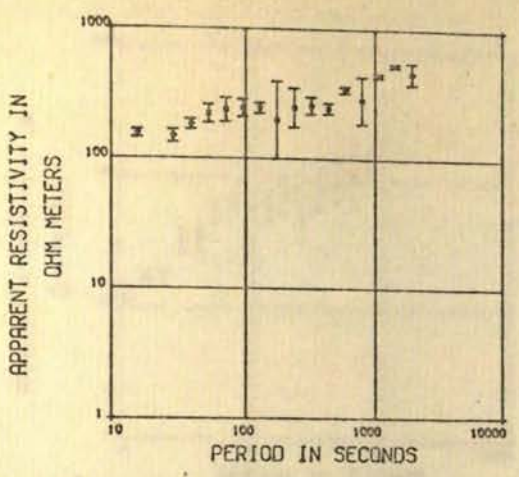

ROTATED MAJOR

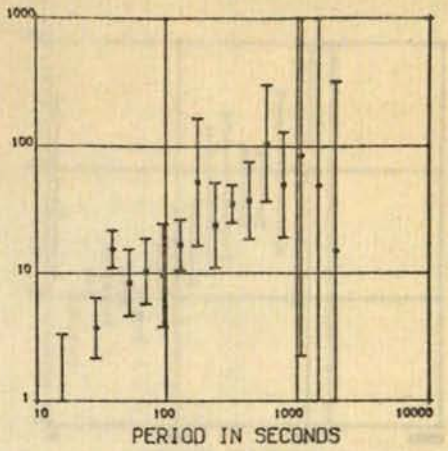

ROTATED MINOR

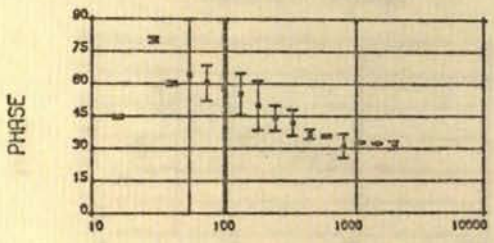

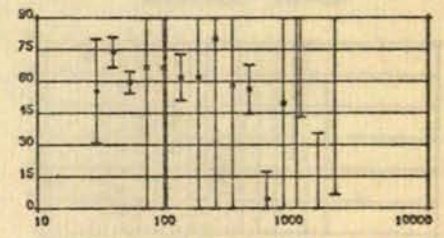

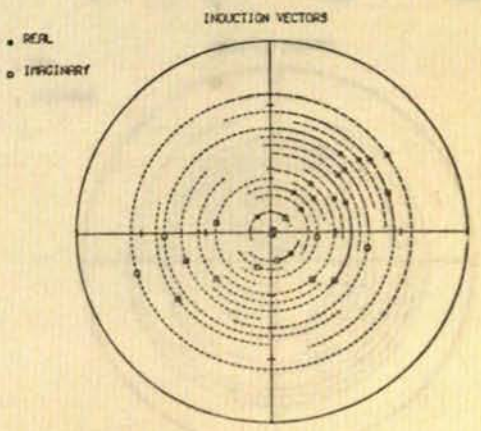

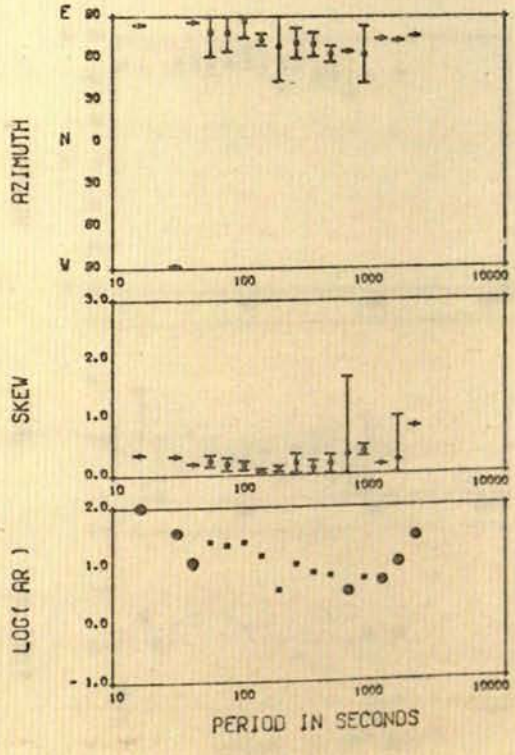

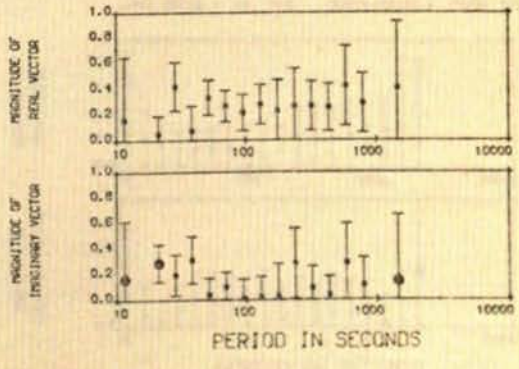

STATION SAL

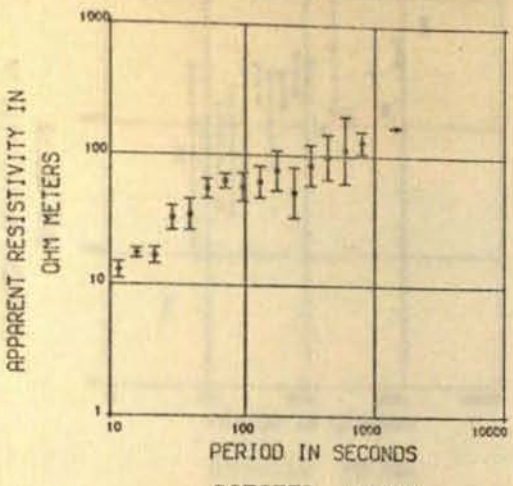

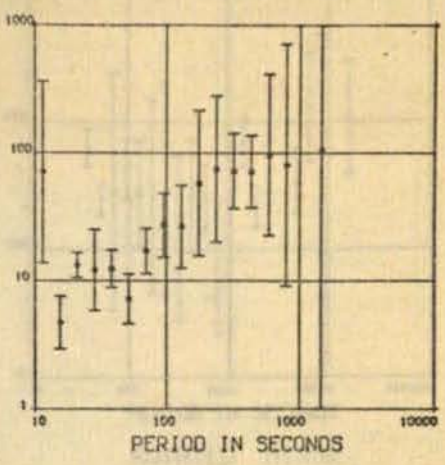

ROTATED MAJOR

ROTATED MINOR

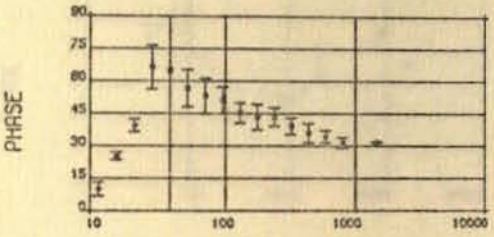

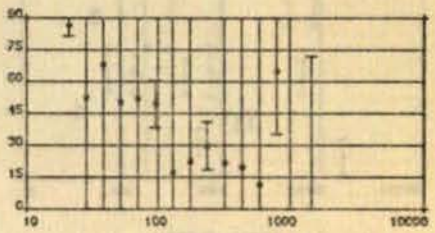

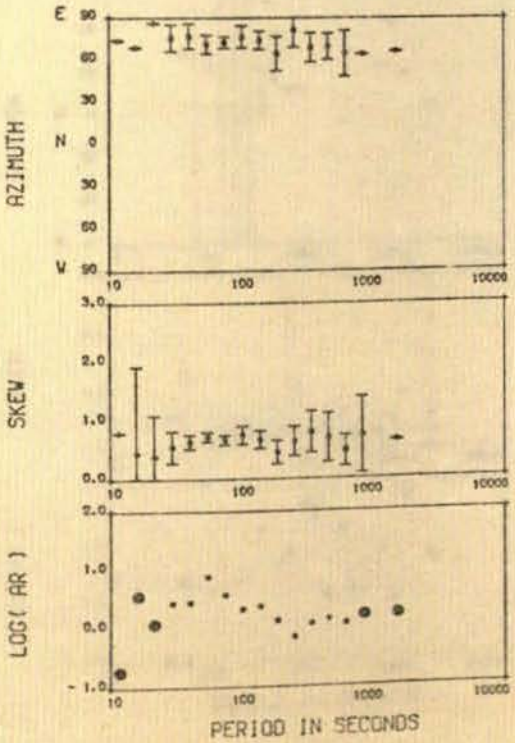

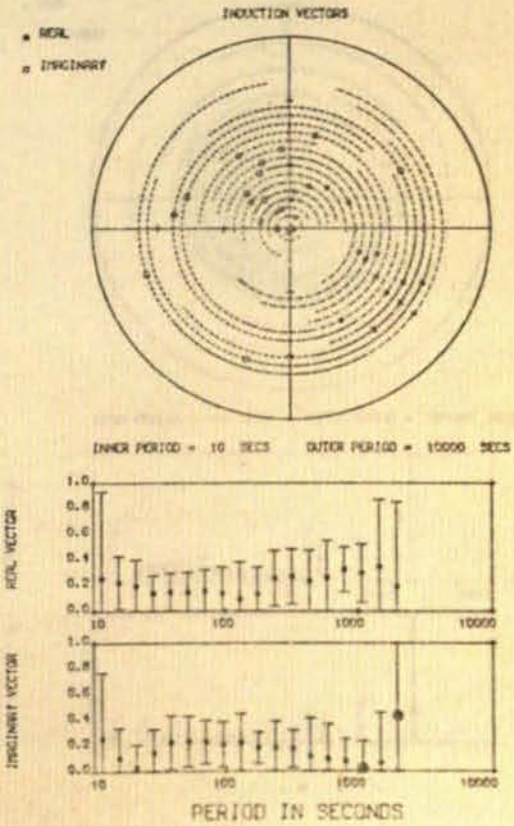

STATION TIN

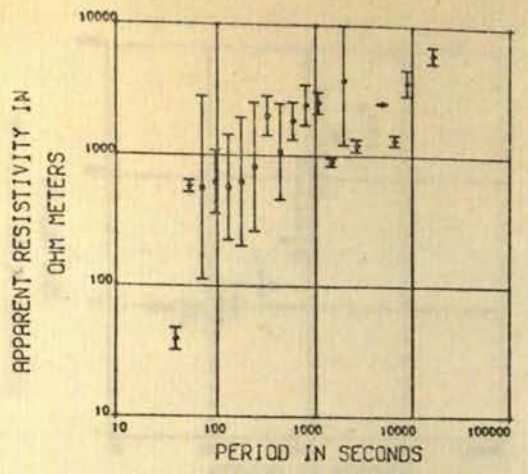

ROTATED MAJOR

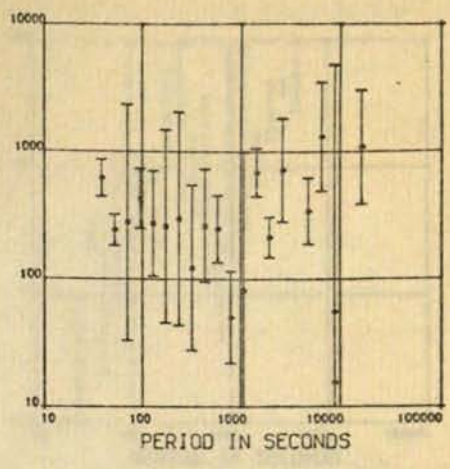

ROTATED MINOR

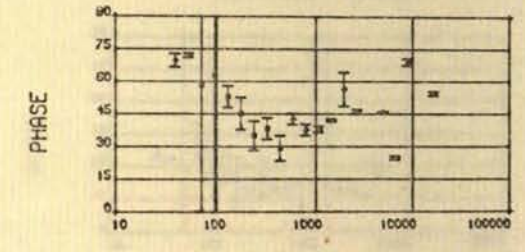

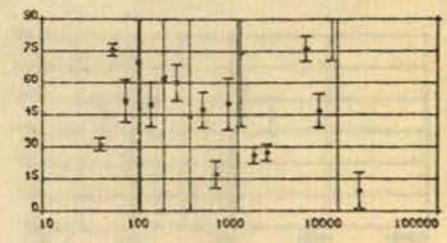

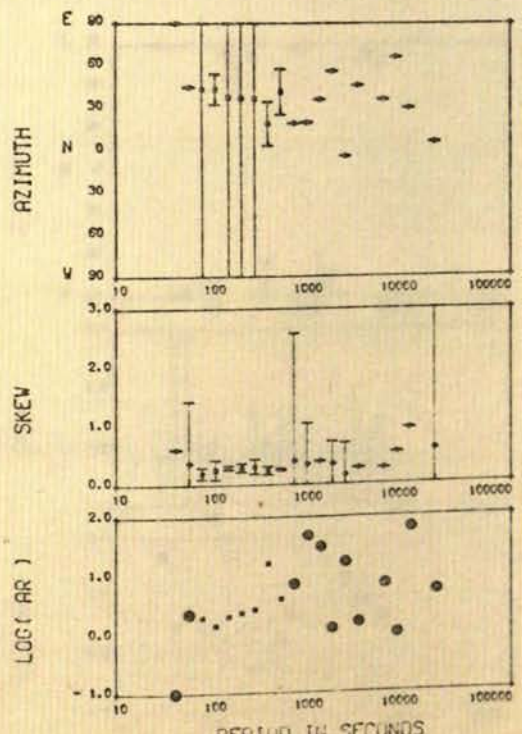

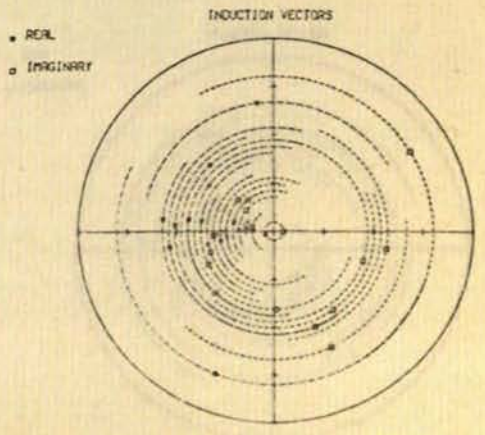

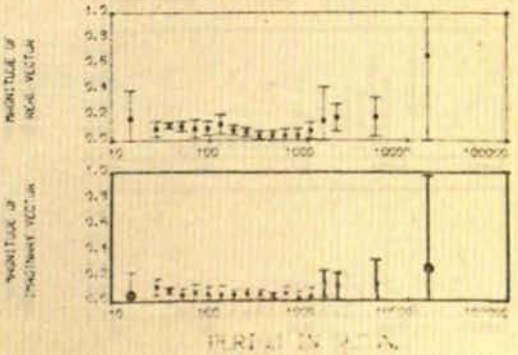

STATION TOW

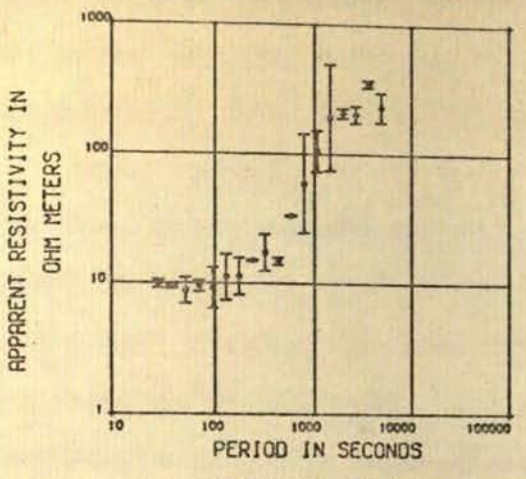

ROTATED MAJOR

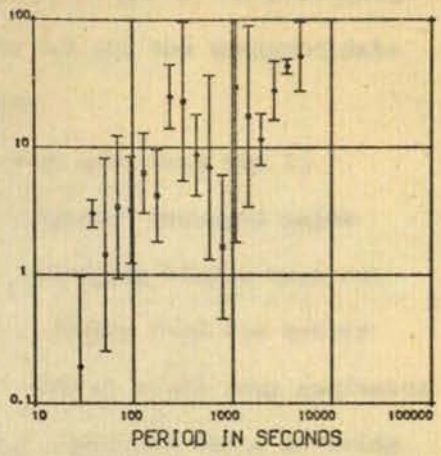

ROTATED MINOR

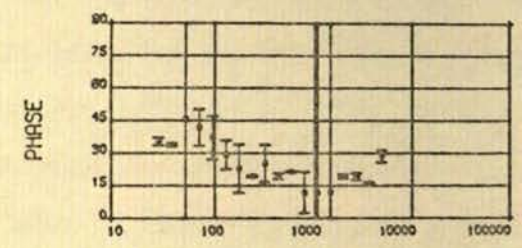

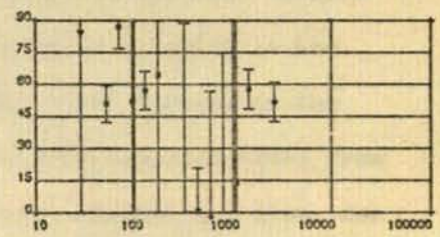

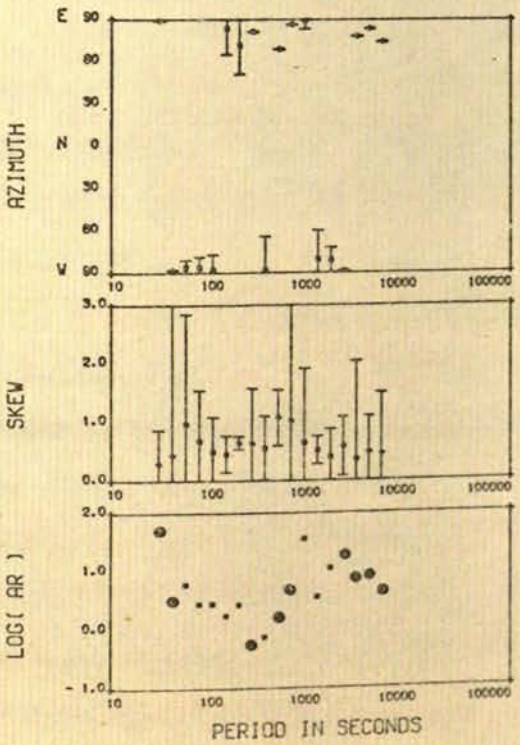

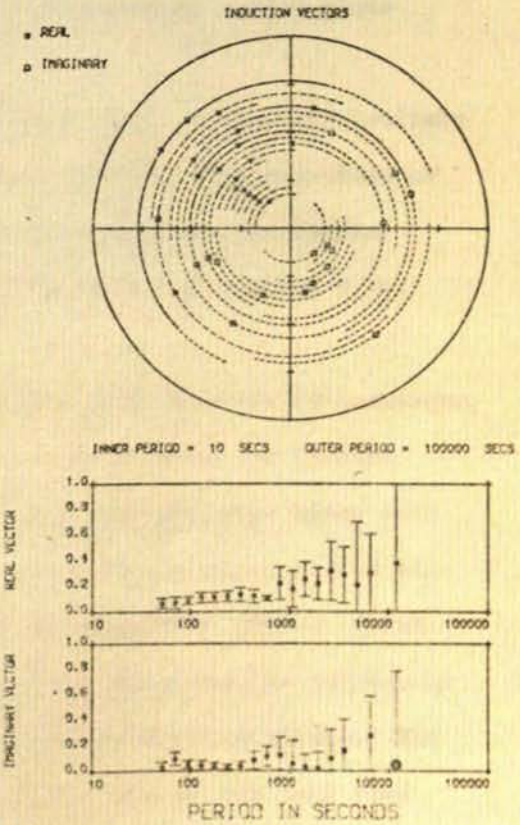

means of the accepted data, with period. Table 5.1 gives the percentage and actual fraction of the accepted estimates for all the analysed data from each site after PROGRAM ONE had been used.

After inspecting all the available accepted data from the 13 stations, it was apparent that for a 'well-estimated' averaged major impedance value, one or two estimates in the averaging window were not sufficient. Obviously the more estimates in a window then the better estimated is the mean value. It was decided that at least four estimates were required in order to acknowledge the mean impedance value as being 'well-estimated'. Those averaged values compounded from four or more estimates in the frequency window are denoted by an asterisk in the ensuing data plots. Their confidence intervals were derived by the statistical procedures given in 4.8.2. Those mean values derived from three or less estimates are indicated by an open diamond and also, for clarity, by a large black circle in the AR (anisotropy ratio) plots in figures 5.5.

For the GDS data, only 'averaged' vectors derived from one estimate appeared inconsistent with vectors at other periods. The magnitude of the quadrature arrow of these estimates, which were not considered well-estimated, are indicated by a black circle in the figures 5.5a, ..., 5.5m.

All the 'well-estimated' major impedance data from the 13 locations (excluding DZR for which no MT data was well-estimated) are plotted together in figure 5.6. The apparent resistivity estimates range over two orders of magnitude at all periods. However, the phase curves all exhibit a decreasing asymptote in the period range 80 - 800 s. Great effort was expended, during both the recording stage and the subsequent data processing, to ensure that the phase data would be reliable. The facts that (a) the phase data from all stations are of the same form

TABLE 5.1

Percentage of estimates accepted after analysis by PROGRAM ONE

Station	MT	GDS
BOR	50% (73/147)	50% (66/131)
CAP	52% (45/87)	63% (36/57)
CRK	33% (72/221)	35% (60/170)
DZR	14% (25/180)	53% (95/180)
ELC	39% (59/150)	55% (75/136)
ESK	58% (81/139)	46% (34/74)
FTH	30% (49/161)	67% (108/161)
GOR	17% (32/184)	54% (100/184)
NEW	61% (171/280)	60% (169/280)
PRE	41% (61/147)	51% (39/76)
SAL	52% (100/194)	65% (126/194)
TIN	34% (56/166)	46% (77/166)
TOW	39% (62/157)	50% (69/138)

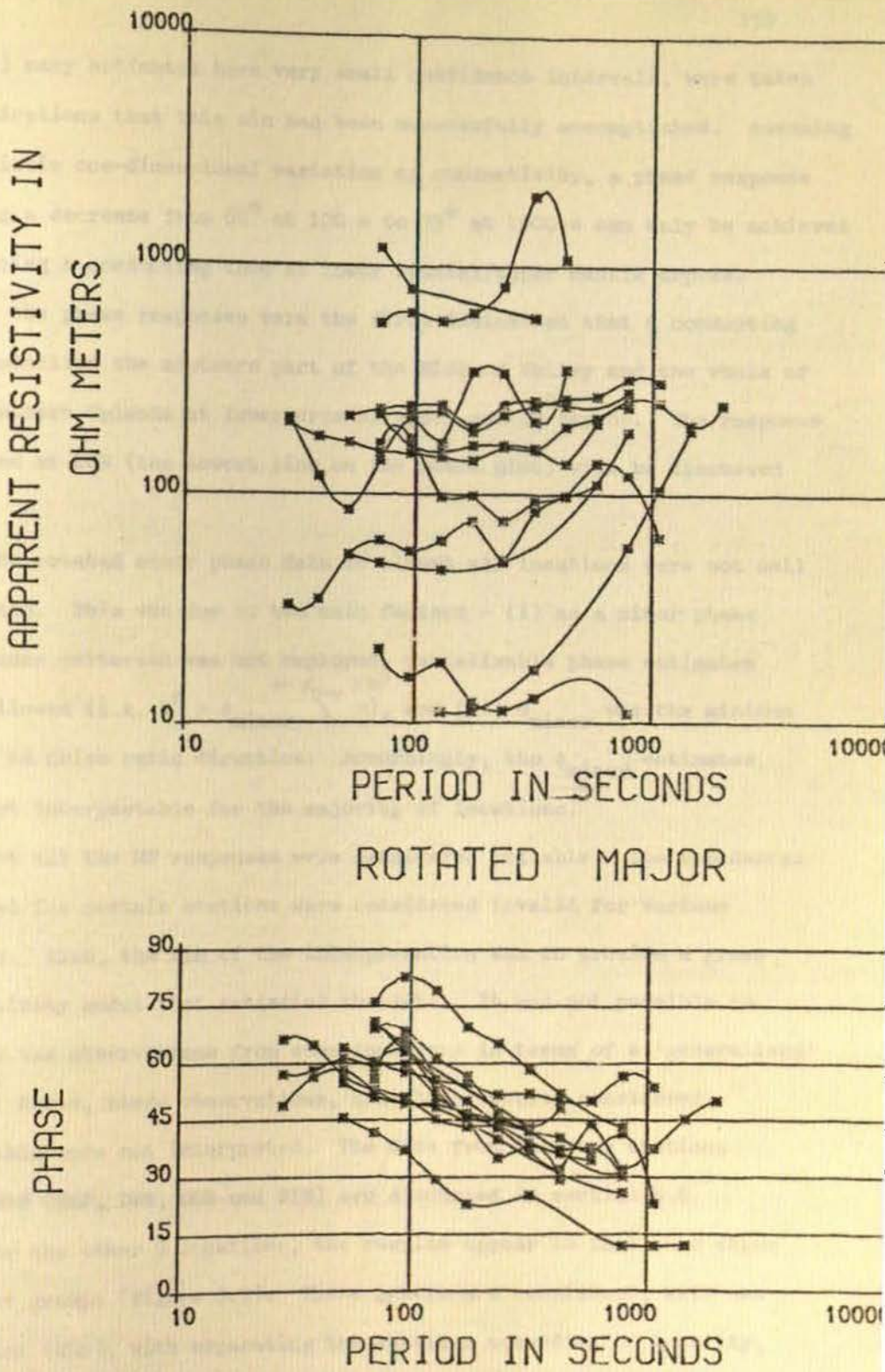

Figure 5.6 'Rotated Major' Curves for all stations

and (b) many estimates have very small confidence intervals, were taken as indications that this aim had been successfully accomplished. Assuming a realistic one-dimensional variation of conductivity, a phase response showing a decrease from 60° at 100 s to 35° at 1000 s can only be achieved by placing a conducting zone at lower crustal/upper mantle depths. Hence, the phase responses were the first indication that a conducting zone underlies the southern part of the Midland Valley and the whole of the Southern Uplands at lower crustal/upper mantle depths. The response observed at TOW (the lowest line on the phase plot) will be discussed later.

The rotated minor phase data at almost all locations were not well estimated. This was due to two main factors - (i) as a minor phase acceptance criterion was not employed, unrealisable phase estimates were allowed (i.e. $0° > \phi_{minor}$ or $\phi_{minor} > 90°$), and (ii) θ_{minor} was the minimum signal to noise ratio direction. Accordingly, the ϕ_{minor} estimates were not interpretable for the majority of locations.

Not all the MT responses were considered reliable. The impedances computed for certain stations were considered invalid for various reasons. Also, the aim of the interpretation was to provide a gross conductivity model that satisfied the data. It was not possible to explain the observations from some locations in terms of a 'generalised' model. Hence, these observations, and those results considered unreliable were not interpreted. The data from the four stations concerned (CAP, DZR, GOR and TIN) are discussed in section 5.6.

For the other 9 locations, the results appear to fall into three distinct groups (figure 5.7). These groups are consistent, with one exception (ELC), with separating the stations according to locality, i.e. Midland Valley, Southern Uplands and Northern England.

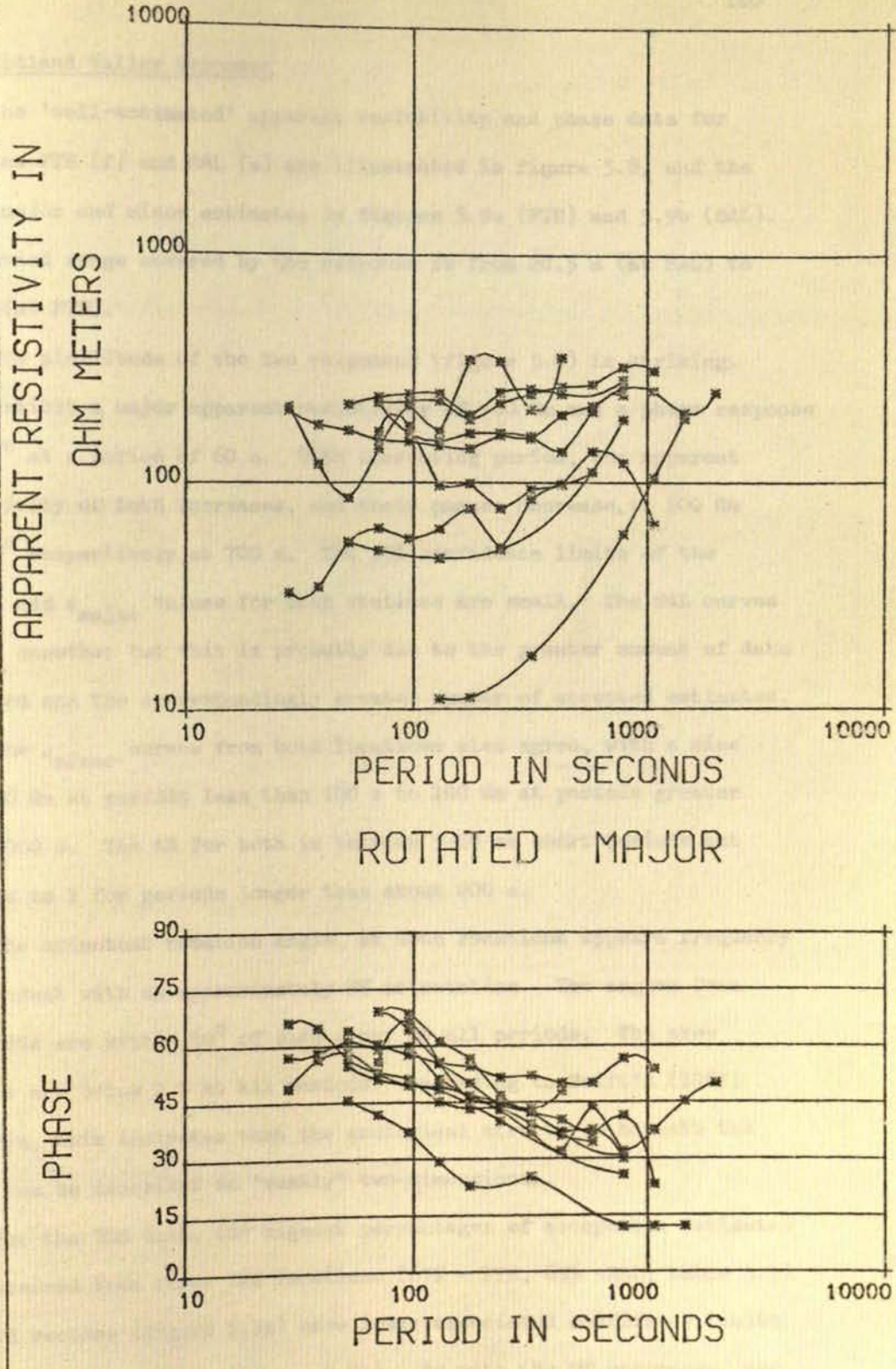

Figure 5.7 'Rotated Major' Curves for 9 stations

5.3 Midland Valley Response

The 'well-estimated' apparent resistivity and phase data for stations FTH (f) and SAL (s) are illustrated in figure 5.8, and the total major and minor estimates in figures 5.9a (FTH) and 5.9b (SAL). The period range covered by the response is from 28.5 s (at SAL) to 800 s (at FTH).

The similitude of the two responses (figure 5.8) is striking. Both exhibit a major apparent resistivity of ~60 Ωm and a phase response of ~50° at a period of 60 s. With increasing period, the apparent resistivity of both increases, and their phases decrease, to 100 Ωm and 30° respectively at 700 s. The 95% confidence limits of the ρ_{major} and ϕ_{major} values for both stations are small. The SAL curves appear smoother but this is probably due to the greater amount of data analysed and the correspondingly greater number of accepted estimates.

The ρ_{minor} curves from both locations also agree, with a rise from 10 Ωm at periods less than 100 s to 100 Ωm at periods greater than 1000 s. The AR for both is between 5-10 at short periods but reduces to 1 for periods longer than about 200 s.

The azimuthal rotation angle at both locations appears frequency independent with an approximately EW orientation. The angles from each site are within 60° of each other at all periods. The skew factors are below 0.5 at all periods. According to Swift's (1967) criteria, this indicates that the geological structures beneath the sites can be described as 'weakly' two-dimensional.

For the GDS data, the highest percentages of acceptable estimates are obtained from these two locations (67% - FTH, 65% -SAL, table 5.1) The FTH vectors (figure 5.5g) have lower associated confidence limits than do the SAL vectors (figure 5.5k). As with the MT responses, the induction vectors observed at both locations appear remarkably similar.

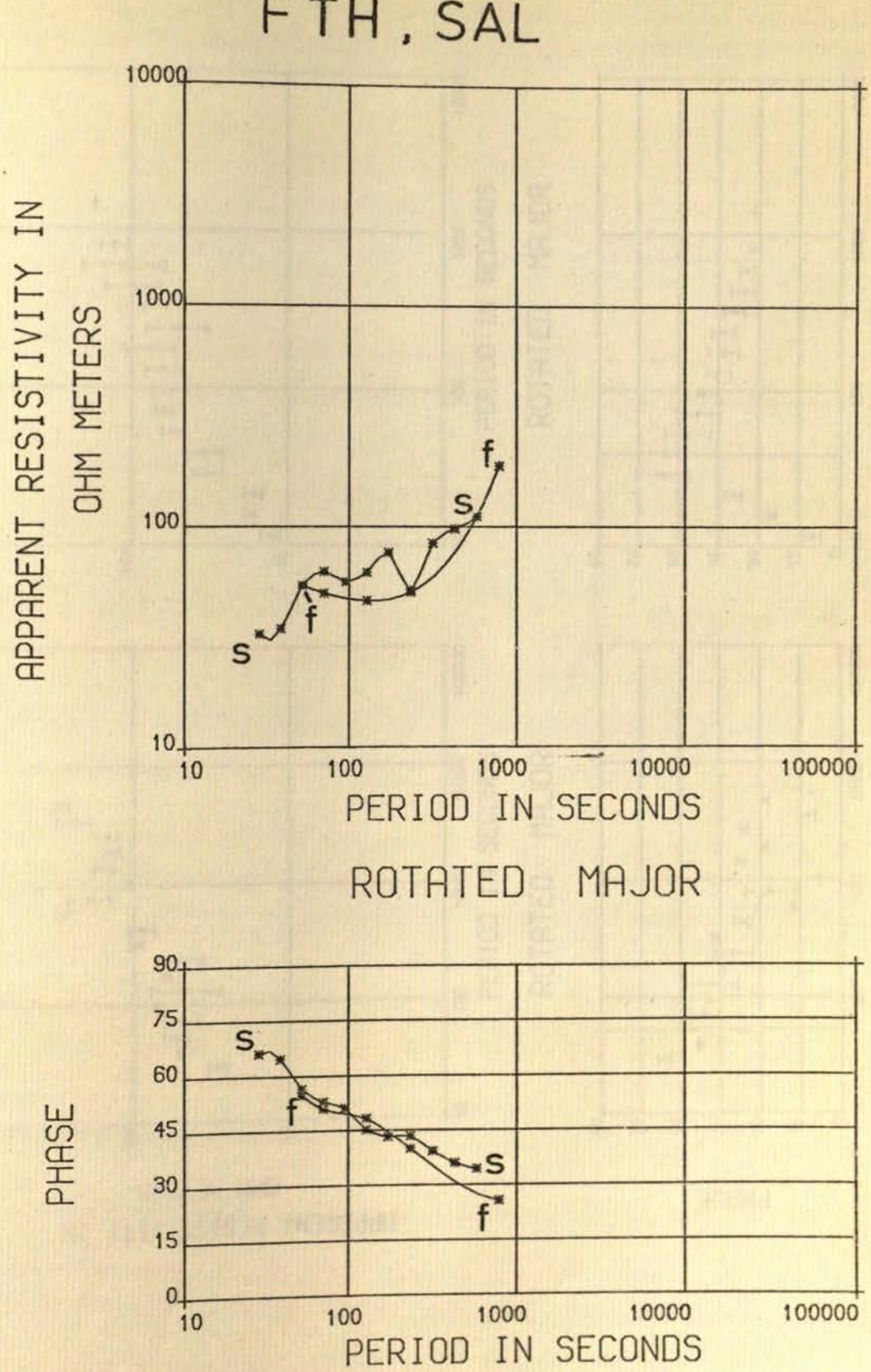

Figure 5.8 'Rotated Major' curves for stations FTH & SAL

Figure 5.9 'Rotated Major' data for stations (a) FTH & (b) SAL

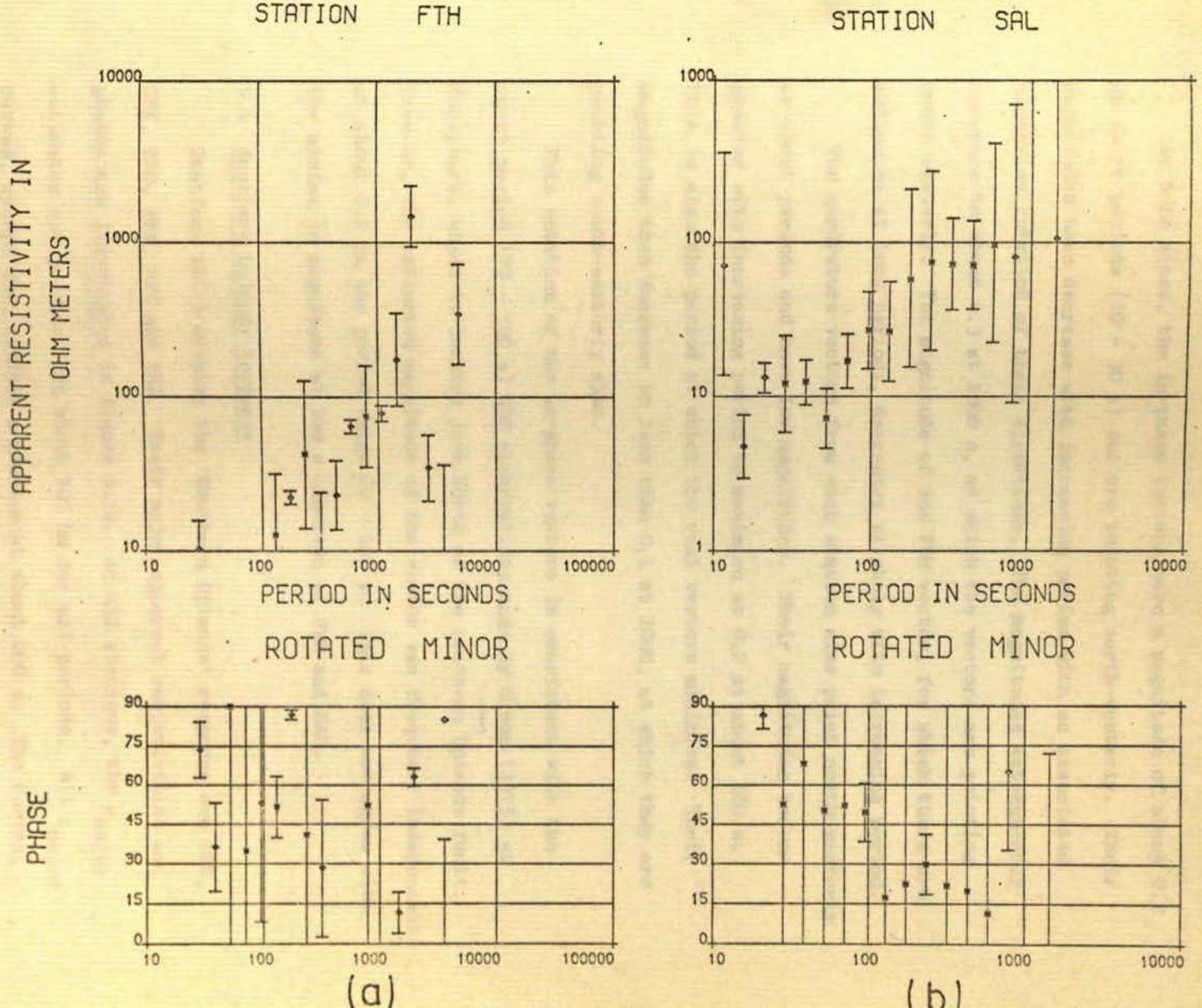

Figure 5.9 'Rotated Minor' data for stations (a) FTH & (b) SAL (cont)

At both sites, the in-phase vectors have a magnitude of about 0.2 at short periods (10 - 30 s) and are pointing north-westerly. Their magnitudes then decrease with increasing period with an associated clockwise rotation of their directions. The magnitudes subsequently increase to about 0.3 at 1000 s, at which the vectors are pointing south-easterly. The magnitude of the FTH vector, for which there are estimates at long periods, decreases slightly with increasing period.

The quadrature vectors from each station also point north-westerly at short periods and have low magnitudes. Their magnitudes become greater with increasing period to maximise at 0.2 at about 100 s. This is also the period at which the real vectors minimise. Their magnitudes then decrease to less than 0.1 at 1000, at which they are pointing south-easterly also.

This rotation of the in-phase vectors is consistent with the short period (20 - 500 s) GDS observations made by Green (1975) at Earlyburn, which is located just North of the Southern Uplands fault. However, the estimated magnitude of the vector was frequency independent at about 0.2 in the period range 20 - 125 s. This does not agree with the minima in magnitude at 100 s observed at FTH and SAL.

5.4 Southern Uplands Response

Stations which display the 'Southern Uplands' response are BOR, CRK, ELC, ESK, NEW and PRE. Their major apparent resistivities and phases are illustrated in figure 5.10. At all stations, the ρ_{major} estimates are greater than about 100 Ωm for all periods. All ρ_{major} curves, except ESK, exhibit a minimum at about 200 s. The curves, excluding CRK, are asymptotic to a value of about 750 Ωm at long periods. The rotated major phase estimates from these stations are greater than 60° for a period of 100 s. Except CRK, the phase responses all decrease with increasing period to 30° at 1000 s.

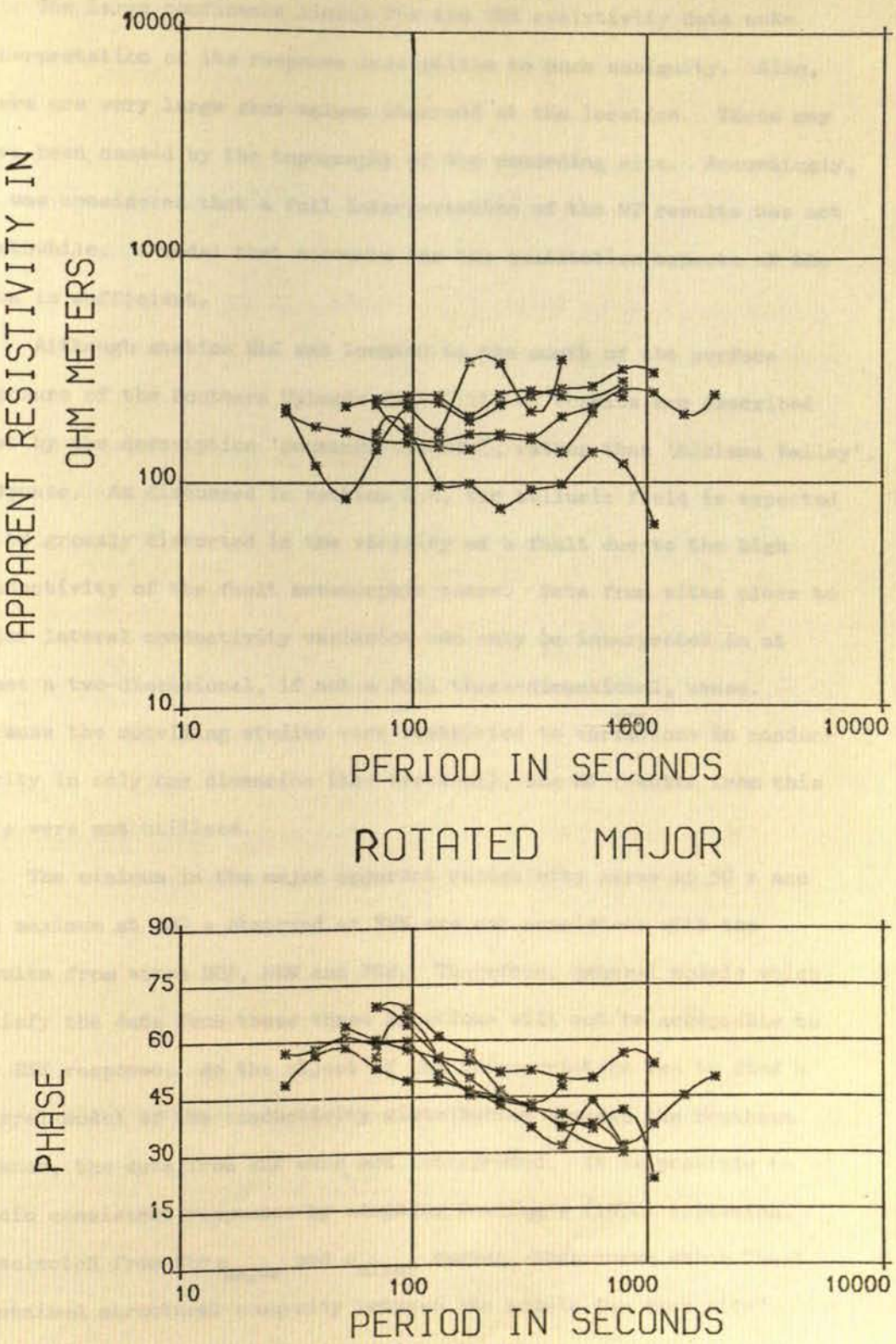

Figure 5.10 'Rotated Major' curves for stations with the 'Southern Uplands' type response

The large confidence limits for the CRK resistivity data make interpretation of its response susceptible to much ambiguity. Also, there are very large skew values observed at the location. These may have been caused by the topography of the recording site. Accordingly, it was considered that a full interpretation of the MT results was not worthwhile. A model that accounts for the qualitative aspects of the data is sufficient.

Although station ELC was located to the north of the surface exposure of the Southern Uplands fault, its MT results are described best by the description 'Southern Uplands", rather than 'Midland Valley', response. As discussed in section 2.4, the telluric field is expected to be grossly distorted in the vicinity of a fault due to the high conductivity of the fault metamorphic zones. Data from sites close to major lateral conductivity variation can only be interpreted in at least a two-dimensional, if not a full three-dimensional, sense. Because the modelling studies were restricted to variations in conductivity in only one dimension (the vertical), the MT results from this site were not utilised.

The minimum in the major apparent resistivity curve at 50 s and the maximum at 200 s observed at ESK are not consistent with the results from sites BOR, NEW and PRE. Therefore, general models which satisfy the data from these three locations will not be acceptable to the ESK response. As the object of the interpretation was to find a general model of the conductivity distribution beneath the Southern Uplands, the data from ESK were not interpreted. It is possible to obtain consistent responses by adopting Dowling's (1970) criterion. He selected from the ρ_{major} and ρ_{minor} curves, that curve which "best maintained structural congruity between the models for each site". The ρ_{minor} curve for ESK does exhibit, like the ρ_{major} curves of the

other three stations, a minimum at 200 s. Hence, the ρ_{minor}, rather than the ρ_{major}, curve would have been selected and interpreted if Dowling's criterion had been adopted. As previously mentioned, the θ_{min} direction gives the worst possible signal to noise ratio and, because of this, Rankin (1975, personal communication) has warned against interpreting the ρ_{minor} curve. However, the problems are not so critical for the ESK data because θ_{max} passes the Rayleigh uniform distribution test, at the 95% level of confidence, in the period range 30 - 450 s (figure 5.5f). Hence, it is possible to make a strong case for interpreting the ρ_{minor} results from ESK. However, the more prudent approach was taken of only interpreting fully consistent results. Accordingly, the data from ESK, although appearing interpretable on its own, was not employed because of lack of consistency with the majority of responses observed in the Southern Uplands.

The ρ_{major} and ϕ_{major} averaged estimates from BOR (b), NEW (n) and PRE (p) are illustrated in figure 5.11, and the full major and minor data in figures 5.11a (BOR), 5.11b (NEW) and 5.11c (PRE). The major impedances from these three stations are extremely similar in both amplitude and phase responses. All the 'well-estimated' resistivity estimates, and the majority of the phase estimates, have very small associated confidence limits. For all three locations, the skew factor (figures 5.5a, i and j) is less than 0.2 at all periods, and less than 0.1 for the majority of periods. Hence, it can be concluded that the conductivity distribution beneath these sites is one- or two-dimensional.

Stations BOR and NEW have many other features in common. Their rotated minor resistivity estimates, except at short periods, are within the confidence limits of the major estimates at the same period (figures 5.12a and 5.12b). Also, their anisotropy ratios are very

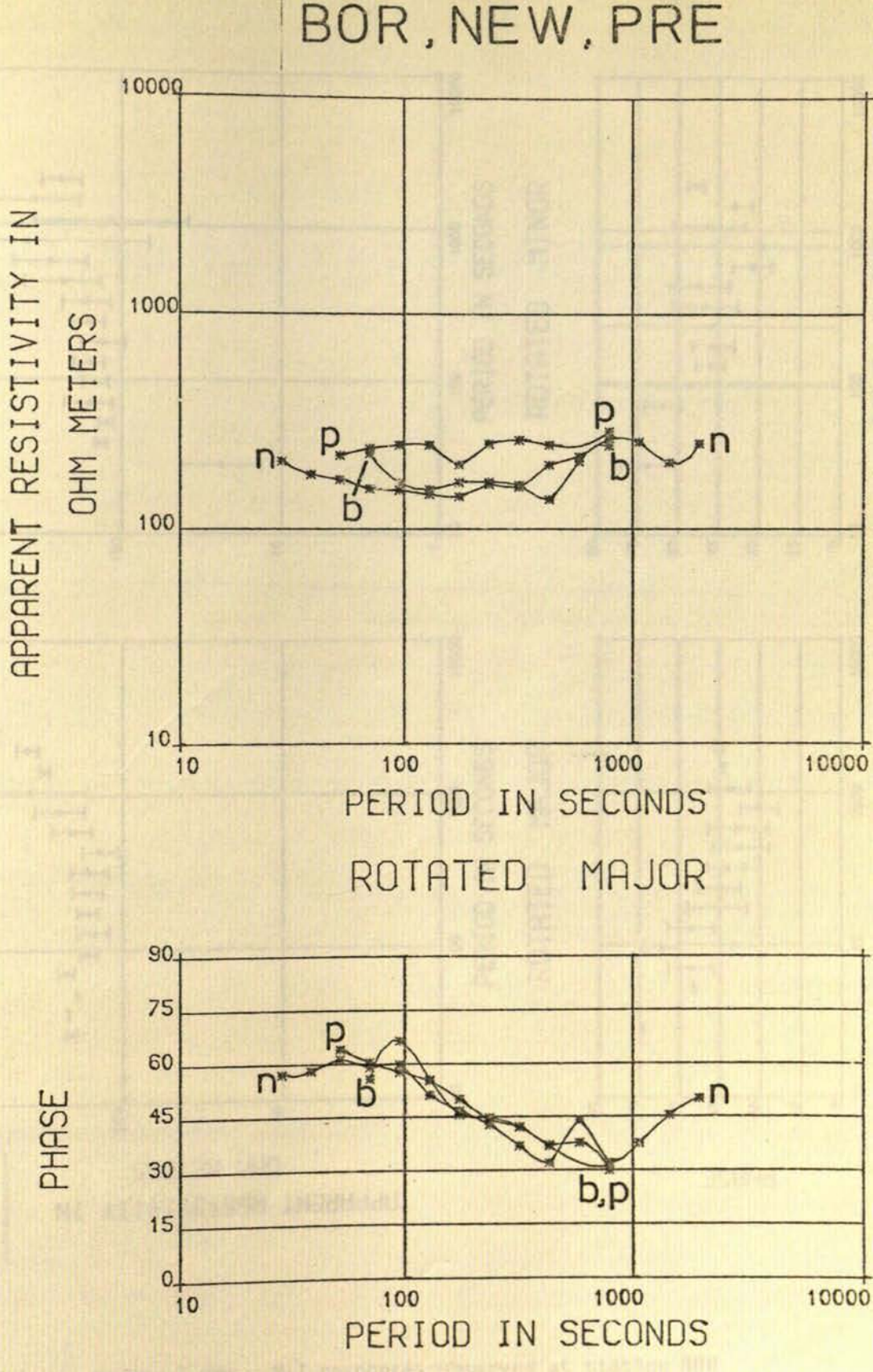

Figure 5.11 'Rotated Major' curves for stations BOR (b), NEW (n) & PRE (p)

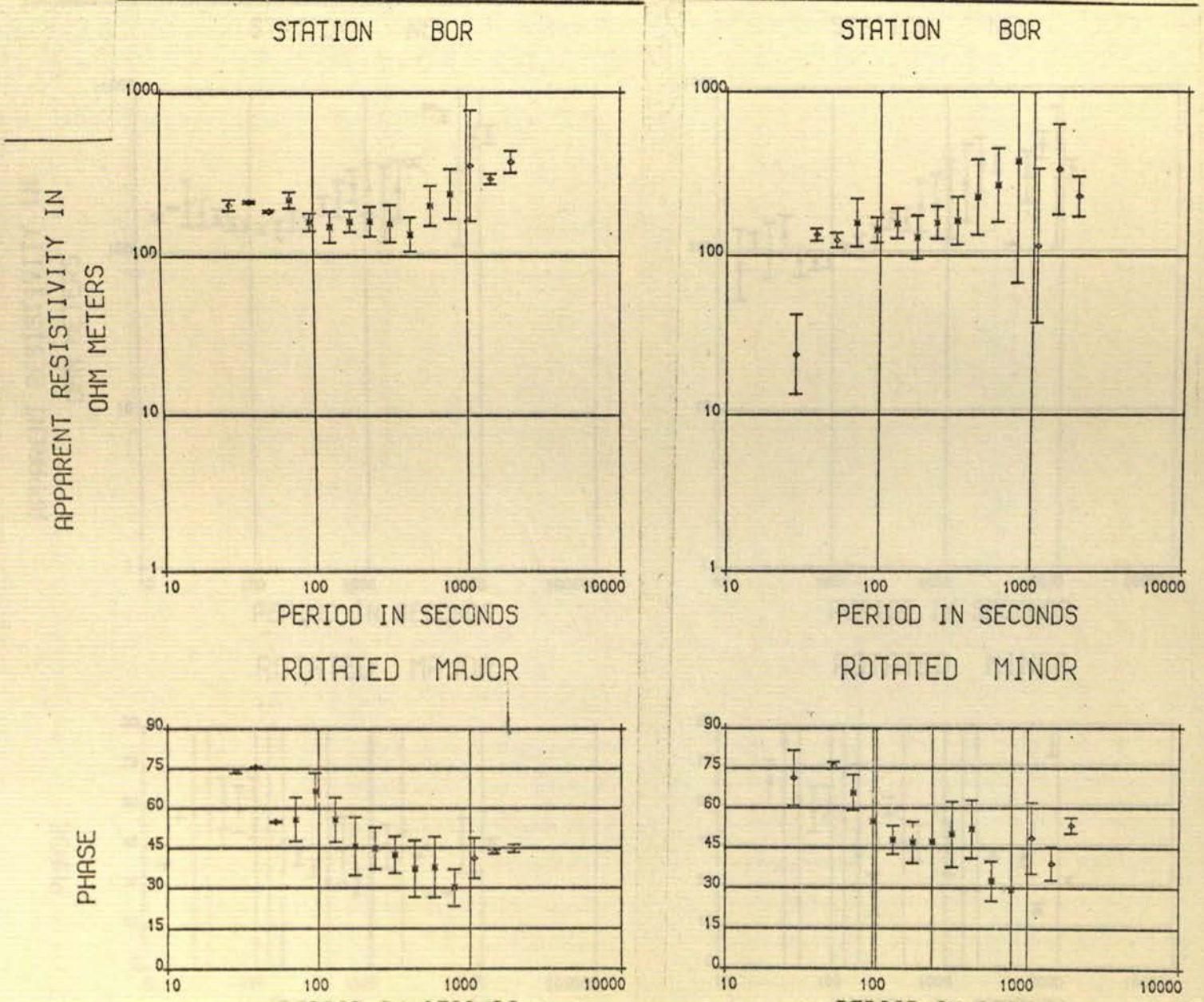

Figure 5.12a M-T responses observed at station BOR

Figure 5.12b M-T responses observed at station NEW

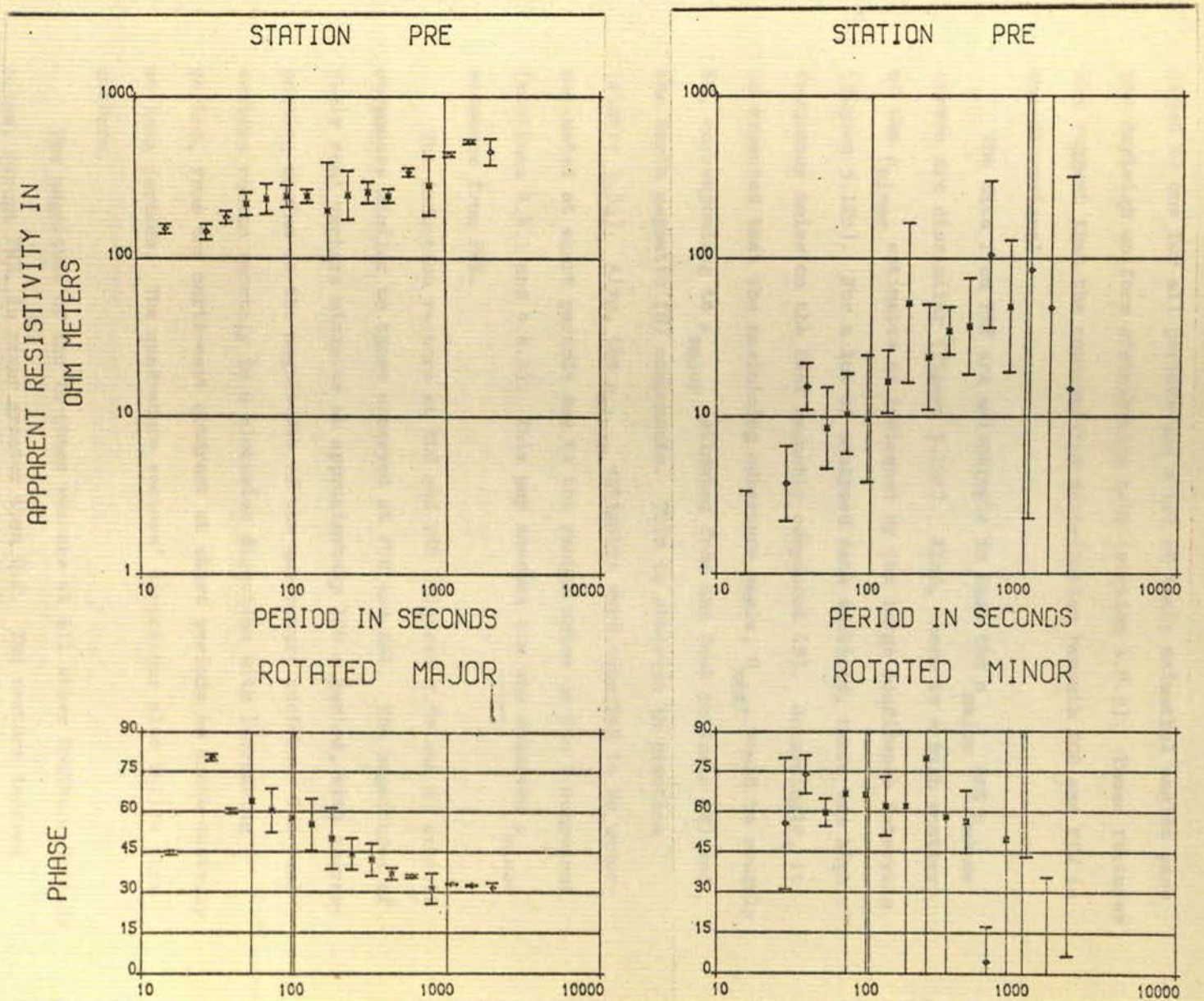

Figure 5.12c M-T responses observed at station PRE

close to one for all periods and a lot of their azimuthal angles pass the Rayleigh uniform distribution test (section 4.8.3). These features all suggest that the conductivity distribution beneath BOR and NEW is one-dimensional.

The data from PRE are anisotropic in that the ρ_{major} and ρ_{minor} curves are dissimilar (figure 5.12c). Also, there is a high scatter of the ρ_{minor} estimates as indicated by the large confidence intervals (figure 5.12c). For a lot of analysed data sections, there was high frequency noise on the East magnetic component (D). Accordingly, it is expected that the maximising coherence angle, θ_{max}, would be roughly EW, corresponding to ρ_{major} estimated from the East telluric (E) and the North magnetic (H) components. This is observed in practice (figure 5.5j). Also, the ρ_{minor} estimates were expected to be underestimated at short periods due to the random noise on the D component (sections 4.4.1 and 4.4.2). This may account for the observed ρ_{minor} response from PRE.

The induction vectors at ELC and DZR (figures 5.5e and d) exhibit responses similar to those observed at FTH and SAL. The magnitudes of their real vectors minimise at approximately 100 s period, with corresponding maxima in the magnitudes of the quadrature vectors. The real vectors rotate smoothly in a clockwise direction with increasing period, from the north-east quadrant at short periods to south-easterly at long periods. The quadrature vectors' directions also follow this pattern.

The magnitude of the in-phase vectors at all other Southern Uplands sites, except PRE, is never greater than 0.2. The vectors derived from the data recorded at PRE are suspect because of the previously mentioned random noise on the D component. The large confidence limits for the vectors may be a manifestation of this effect. However, the

directions of the vectors at PRE should be fairly reliable because of the ellipse of confidence effect (section 4.7.1).

Stations BOR, CAP, CRK, ESK, NEW and TIN all have values of R (the real vector magnitude) less than 0.1, but significantly different from zero in the period range 20 - 1000 s. At periods greater than 1000 s, there is some evidence for an increase in R at these locations. The quadrature vector magnitude (I) is also less than 0.1, and frequently less than 0.05, in this short period range. This suggests there is little near surface lateral inhomogeneity to distort the induced vertical component.

The real vectors at BOR and TIN point westwards at short periods ($T < 300$ s) then rotate clockwise to a northerly direction at long periods ($T > 1000$ s). Their imaginary vectors also point westwards at short periods but they rotate anti-clockwise to a south-easterly direction at the longer periods.

At short periods, the real vectors at CAP, CRK, ESK and GOR point north-westerly. At all 4 stations, the vector rotates clockwise with increasing period to point north-easterly at long periods. The quadrature vectors from these locations do not exhibit the same response. This may be due to their low magnitudes giving rise to statistical random orientation of their azimuths.

The induction vector response at NEW is very different in character to that at all the other Southern Uplands stations. The magnitudes of the in-phase and quadrature vectors have very small 95% confidence intervals for periods less than 3000 s, suggesting they are extremely well estimated. The real vector points south-east at short periods ($T < 100$ s) then, with increasing period, rotates anti-clockwise in a very smooth manner to point north-easterly at long periods ($T > 1000$ s). The quadrature vector also follows this pattern except that it initially

points north-westerly at the shortest period (15 s), then rotates anti-clockwise to a south-easterly direction by 70 s period.

5.5 Northern England Response

The response observed at the one station in Northern England, TOW, was unusual in many respects. Although a dominant orientation of the telluric field, with a high ellipticity of polarisation, is commonly observed on MT records, it is not typical to find the polarisation of the horizontal magnetic field as linear as that found at TOW. The power in the magnetic field was almost all oriented in a NS direction for any source structure. The telluric field was also linearly polarised but with an EW azimuth. Accordingly, the θ_{max} direction is EW (figure 5.5m), corresponding to ρ_{major} estimated from H magnetic and E telluric components.

The rotated major and rotated minor responses observed at TOW are illustrated in figure 5.13. The ρ_{major} and ϕ_{major} estimates are very different from those observed at any other location. At short periods ($T < 200$ s), the major apparent resistivity is of the order of 10 Ωm. It increases, with increasing period, to 200 Ωm at 1500 s. The major phase is smaller at all periods than that observed at any other location. Because there was little power in either the D magnetic or N telluric components, the ρ_{minor} values are not well estimated. This is exhibited by their large confidence intervals and their high degree of scatter with period (figure 5.13). The large skew factors and their large associated confidence intervals, are also due to the power being contained solely in one component of each field.

The induction vector response observed at TOW shows a frequency independent azimuth of the real vector in a north-west direction. The magnitude of the vector rises from 0.1 at short periods ($T < 100$ s) to

Figure 5.13 M-T responses observed at station TOW

0.3 at longer periods (T > 2500 s). The quadrature vector has small magnitude (less than 0.1) for periods shorter than 2500 s. Its azimuth scatters at the long periods but is south-easterly at the shortest periods, then turning clockwise to south-westerly.

5.6 Unreliable and Anomalous Responses

It is obvious from table 5.1 that DZR and GOR were not good MT recording sites. When recording at both of these locations, a high telluric noise level was present. This resulted in the rejection of over 80% of their estimates of rotated major impedances. Also, those estimates which were accepted exhibit a high degree of scatter (figures 5.5d and h). Therefore, it was concluded that the MT data were grossly corrupted by cultural electric disturbances and were not meaningful. Accordingly, no attempt was made to explain the derived impedance responses for these locations. However, over 50% of the GDS data from both stations were accepted and the estimates appear smoothly varying with frequency (figures 5.5d and h). Hence, the GDS data were considered indicative of conductivity variations.

The resistivity estimates for CAP are not congruent with those of nearby stations (CRK, ESK and NEW). Both the major and minor apparent resistivity estimates are of the order of 10 Ωm for all periods (figure 5.5b). At all other locations however, the major resistivity curves exhibit ascending asymptotes to a value of about 750 Ωm in the period range 10^3 - 10^4 s. The NS telluric line had to be relocated once because of obvious interference from a mains transformer (section 3.4 (c)). It was concluded that the data did not reflect the true conductivity distribution but were a manifestation of distortion of the natural telluric field. The water of St. Mary's Loch, which was close to the recording site, may also have attenuated the electric

field. As with DZR and GOR however, the induction vectors appear reasonable.

The MT results derived for TIN are also not consistent with those for other Southern Uplands stations. The low frequency asymptote is of the order of 5000 Ωm (figure 5.51) whilst for most other locations is 750 Ωm. Hence, the MT results from CAP and TIN were not interpreted because they were not consistent with the other data.

CHAPTER 6

INTERPRETATION AND CONCLUSIONS

In this chapter, various techniques for inverting magnetotelluric data, to derive a conductivity distribution with depth, will be reviewed and discussed. Also, the validity of a one-dimensional interpretation of two-dimensional data will be investigated. The results of inverting apparent resistivity and phase data, obtained during this project, by a Monte-Carlo technique will be presented. The geophysical and geological conclusions drawn from the derived conductivity profiles will be discussed. Suggestions for further work will be given.

6.1 Introduction

The purpose of interpreting any geophysical parameter(s) is to derive a unique model whose theoretical response satisfies the observed data. Many methods for inverting geophysical data to obtain such a model are available. Some of these methods are totally automatic , some totally empirical and the rest are semi-automatic. With the advent of high speed computers, there has been, in most branches of geophysics, a general trend away from subjective 'trial-and-error' inversion techniques towards the more objective computer-oriented automatic inversion procedures. However, even these methods may suffer from the effects of personal, or other, bias due to oversimplification of the problem. This vulnerability inherent in modelling studies has been emphasised by many workers, and perhaps most aptly by Professor A. T. Price (1973), who states:

"One of the dangers we have to guard against is that of including some feature in our Earth model, for mathematical convenience or simplicity,

and then drawing inferences from the results of our mathematical solution about some feature in the real Earth, whereas this stems only from the particular model we have chosen."

When considering the problem of uniqueness, i.e. that the derived model may not be the only model whose response satisfies the data, it must be remembered that no geophysical parameter can be measured with absolute precision. Accordingly, each geophysical response function, derived from the observations, has an associated confidence interval. This will permit more than one acceptable model. Hence, the rational objective of inverting real data should be to determine the bounds of the family of acceptable models, and not one single model, even the 'optimum' model, of that family.

For electromagnetic induction studies on a regional scale, there is a twofold aim to interpreting the data. The first objective is to derive a conductivity distribution which satisfies the observed response functions. This distribution may then be interpreted in terms of geological structure and/or tectonic history.

Initially, the modelling studies of geomagnetic data should be undertaken without regard to any other information other than that determined by the investigation. Preconceived ideas of the likely form of the conductivity distribution will greatly bias the model studies by excluding whole sets of models which are not compatible with these ideas. If, and only if, initial modelling gives conductivity distributions which are concordant with any other geophysical data for the region, e.g. results of previous induction studies, seismic velocity profiles, heat flow data, gravity and magnetic anomalies, etc., then, and only then, should these other data be taken into consideration. To give an illustration, conductivity interfaces are often constrained to a specified depth because of seismic information - see for example

Jain and Wilson (1967), Hermance and Grillot (1973), Cochrane and Hyndman (1974), Kurtz and Garland (1976). However, an acoustic interface may not represent a change in conductivity. Admittedly, the probability of this is high, but it is certainly not one. Unfortunately, two-dimensional modelling studies are computationally expensive. Hence, to reduce the cost, as few models as possible are investigated. To aid this aim, other geophysical data, particularly seismic, are employed to reduce the number of models tried to a minimum.

In contrast to the interpretation of induction data, a geological interpretation of the derived conductivity distributions, in terms of bulk composition of the rocks, should take all known data into account. The dangers of speculating about probable geological structure from conductivity models alone have been stressed in section 1.4. A geological interpretation, if attempted, should be tentative, and not definitive, because many geologists are too ready to accept the interpretation implicitly, without realising the limitations of the geophysical method(s) employed. An excellent example of this problem is the suggestion by Gunn (1973) and Jeans (1973) that the Midland Valley, and not the Southern Uplands, was the location of the Iapetus ocean during early Palaeozoic times. This postulate was to explain Powell's (1971) conclusion, from geophysical evidence, that the Southern Uplands is underlain by a Precambrian basement of Lewisian type rocks. The models of Gunn and Jeans are not considered tenable, by the majority of geologists, because of faunal evidence (Williams, 1972; Moseley, 1975).

6.2 One-Dimensional Interpretation Techniques

6.2.1 Validity

The validity of a one-dimensional interpretation of MT data has been the subject of much discussion since Cagniard first proposed the

method. If the conductivity beneath the recording site varies as a function of depth alone, then a 1D interpretation is certainly valid. If however, the conductivity varies significantly in one, or both, horizontal directions, then a 1D interpretation of the data is open to criticism.

As shown in section 2.3, for one-dimensional conductivity structures the two apparent resistivities (ρ_{xy} and ρ_{yx}), and their phases (ϕ_{xy} and ϕ_{yx}) are equal for all frequencies. Hence, the anisotropy ratio (AR) is one at all frequencies. Also, the diagonal elements of the impedance tensor (Z_{xx} and Z_{yy}) are zero and therefore the skew factor is also zero. Because $Z'_{xy}(\theta) = Z'^{*}_{yx}(\theta)$, for any θ, the azimuthal angle, θ_{max}, does not exhibit any preferred orientation.

If the apparent resistivity data are isotropic therefore, i.e. $\rho_{xy}(f) = \rho_{yx}(f)$ for all f, it may be safely concluded that the conductivity beneath the recording site only varies significantly with depth. If the other two effects are also observed, i.e. zero skew and no preferred maximising orientation, then the assumption can be made even more confidently. The data from sites BOR and NEW display all three of these indicators and hence one-dimensional interpretations of their responses are certainly valid. Also, BOR, NEW and PRE exhibit similar responses (figure 5.10), which is fairly conclusive evidence for assuming that a 1D model is valid for the central NE/SW zone of the Southern Uplands.

For locations in the centre of a conducting graben, Reddy and Rankin(1972) show that the conductivity variation with depth can be derived by interpreting the E-polarisation apparent resistivity curve (i.e. $\rho_{//}$) in a one-dimensional sense. The E-polarisation data for such a site is given by the ρ_{major} and ϕ_{major} curves. The H-polarisation curve ($\rho_{\perp}$) is shown to be frequency independent at the

value of the graben resistivity. The 'minor' data from TOW exhibits a frequency independence and also it is known that the site was located above the Northumberland sedimentary basin. Reddy and Rankin (1972) also show that the magnetic field component normal to the strike is altered by the secondary field generated by induction. This results in a change in the polarisation characteristics of the total field compared to the source field. The total magnetic field has a tendency to orient itself normal to the strike direction. This effect could account for the highly linearly polarised magnetic field, for periods up to 2500 s, oriented NS observed at both TOW (an MT/GDS station) and HAG (a GDS array station). Hence, it was concluded that a one-dimensional interpretation of the rotated major data from TOW would give a valid conductivity distribution with depth.

Wright (1970) also studied the problem of the perturbation of electromagnetic fields by a two-dimensional structure, namely one possible Rhine-graben model. His interest was in the anisotropy of the tensor elements Z_{xy} and Z_{yx} caused by the structure. He showed that at a sufficiently large distance from a lateral inhomogeneity, in his case 15 km, the H- and E-polarisation apparent resistivity and phase curves are very similar, both in shape and in magnitude. Also, he showed that a one-dimensional interpretation of either would yield the correct resistivity-depth profile beneath the location. At locations close to a lateral inhomogeneity however, the two polarisations give widely different responses, both in magnitude and in phase. However, the Cagniard one-dimensional apparent resistivity curve for locations on the resistive side of the inhomogeneity has exactly the same shape as the H-polarisation curve but it is of different magnitude, i.e. there is a frequency independent scaling factor between them. Also, the Cagniard phase curve, at periods greater than 5 s, is within 5° of

the H-polarisation phase curve. Hence, on the resistive side of a lateral inhomogeneity, and close to that inhomogeneity, a one-dimensional interpretation of the H-polarisation curve ($\rho_{\perp}$) yields a structure whose interface depths are correct but whose layer resistivities are overestimated. The overestimation factor, the logarithm of which is the same for all layers, can be obtained from the long period E-polarisation resistivites ($\rho_{//}$) because, at long periods the Cagniard and E-polarisation curves coalesce. H-polarisation results when the magnetic field is parallel to, and the telluric field perpendicular to, the strike of the anomaly. For locations on the resistive side of the inhomogeneity, this is the ρ_{major} and ϕ_{major} data.

Hence, for two-dimensional structures on the conductive side of the inhomogeneity, a one-dimensional interpretation of the E-polarisation - or $\rho_{//}$ and $\phi_{//}$ - data yields the correct conductivity distribution with depth whilst the H-polarisation - or $\rho_{\perp}$ and $\phi_{\perp}$ - curves should be interpreted on the resistive side. Both the $\rho_{//}$ on the conductive side, and the $\rho_{\perp}$ on the resistive side, are given by their respective ρ_{major} curves. This is also true for the phase response

Hence, for MT data that appears two-dimensional, an interpretation of the major impedance data appears to give correct interface depths. It is only necessary to know whether the location is on the conductive side, or the resistive side, of the lateral inhomogeneity in order to correct, or not, as the case may be, the layer resistivities. To illustrate the validity of this approach, comparisons between the one- and two-dimensional modelling studies for two investigations are given below.

The MT results obtained at nine locations in Southern Australia were presented by Tammemagi and Lilley (1973). In order to explain, in terms of geoelectric structure, the observed responses at six of

these, Lilley and Tammemagi (1972) undertook 'trial-and-error' two-dimensional modelling employing the Jones-Pascoe programs (section 2.4.2 (c)). Apart from the station Partacoona (PAR), the E- and H-polarisation apparent resistivity curves derived from each location for one of the 'best compromised models' (the compromise is between the MT and GDS data) are equal (to within experimental accuracy). The Cagniard theoretical curves derived for the conductivity profiles below the observation sites are equal to their respective E- and H-polarisation curves presented. Hence, for the MT data, the same information as was obtained by the computationally expensive 2D modelling study could have been obtained by 1D modelling.

As reviewed in chapter 1, Kurtz (1973) and Kurtz and Garland (1976) have undertaken an MT study in eastern Canada. Initial interpretation was by 1D inversion - by empirical methods - of both the rotated major and rotated minor resistivity curves. Because of the anisotropy in the data, i.e. $\rho_{major} \neq \rho_{minor}$, they then undertook 2D modelling studies, again with the Jones-Pascoe program. They concluded that the generalised model structure illustrated in figure 1.5b was the optimum model examined. However, the 1D model fit to station 10 data gave a conducting crust underlain by a resistive upper mantle. The 1D model for station 14 data was of a resistive crust with a conducting upper mantle. Thus, the same general conclusions as those illustrated by the model in figure 1.5b could have been drawn without resorting to 2D modelling.

These two examples discussed above illustrate that 2D modelling is not always necessary to explain the observed MT data. The gross features can be derived by a 1D interpretation of the rotated major apparent resistivity and phase curves from sites sufficiently distant from large lateral variations in electrical conductivity. Two-

dimensional modelling studies of all but the simplest structures must at present be accomplished by numerical techniques on high-speed computers. These methods involve a high use of computing time and only result in establishing finer details to the conductivity model. Also, many questions have been raised about the fundamental theories of the most widely employed 2D modelling program, namely the Jones-Pascoe program (section 2.4.2 (c)). Until these problems are resolved and the programs are made much more computationally efficient - with regard to the required core time - it is the opinion of the author that extensive trial-and-error 2D modelling studies by these numerical methods, are not essential for the interpretation of the observed MT responses.

Rankin and his colleagues (Rankin, Reddy and Kao, 1976; Rankin, Reddy and Schneider, 1976) believe that a one-dimensional interpretation of the rotated major data is valid even for three-dimensional structures. Although this may be regarded as somewhat speculative, it is probably true if the structure is on a large enough scale and if the data were obtained from locations sufficiently distant from major lateral variations in conductivity.

6.2.2 First approximation inversion schemes

A method for directly inverting MT and GDS data was presented by Schmucker (1970, pp 68-69) and, in a slightly different form by Kuckes (1973a, 1973b). The method involves approximating the real Earth to a two-layer model. The 'depth to a perfect substitute conductor' - h^* - is then derived with an associated apparent resistivity at that depth.

The method is as follows: Consider a conducting substratum of conductivity σ_2, overlain by a resistive top layer, of thickness h. The surface impedance, at frequency ω, above the model is given by

$$Z_o(\omega) = \frac{+i\mu\omega}{k_1} \coth\left[k_1 h + \coth^{-1}\left(\frac{k_1}{k_2}\right)\right], \qquad (6.1)$$

from equation 2.23. The attenuation of the incident field within the base layer is determined solely by its skin depth value, hence k_2 may be replaced by $(1 + i)/\delta_2$, where δ_2 is the skin depth of the base layer as defined by equation 2.14. Also, from equation 2.25, k_1 may be approximated by the wavenumber k_T, in the top layer. If $k_1 h << 1$, i.e. the upper layer is small compared to the dimensions of the source, then equation 6.1 can be reduced to

$$Z_o(\omega) = \frac{+i\omega\mu}{k_1}\left(\frac{1 + k_2 h}{k_1 h + k_2/k_1} \right) \qquad (6.2)$$

(Keller and Frischknecht, 1966, p 221). If the basement is much more conducting than the top layer, then $k_1 << k_2$, therefore $k_2/k_1 >> k_1 h$. Accordingly, equation 6.2 can be approximated by

$$Z_o(\omega) = i\omega\mu\left(h + \tfrac{1}{2}\delta_2 - i\,\tfrac{1}{2}\delta_2 \right), \qquad (6.3)$$

by neglecting $k_1 h$ and substituting $k_2 = (1 + i)/\delta_2$. Hence, from equation 2.12, the inductive scale length, $C(\omega)$, given by $i\,\mu\omega\, C(\omega) = Z_o(\omega)$, is equal to

$$C(\omega) = h + \tfrac{1}{2}\delta_2 - i\,\tfrac{1}{2}\delta_2. \qquad (6.4)$$

Hence, the value of h and ρ_2 are given by

$$h = \mathrm{Re}(C) - \mathrm{Im}(C) = \frac{1}{\omega\mu}\,(\mathrm{Im}(Z_o) - \mathrm{Re}(Z_o)) \qquad (6.5a)$$

and

$$\rho_2 = 2\omega\mu\,(\mathrm{Im}(C))^2 = \frac{2}{\omega\mu}\,(\mathrm{Re}(Z_o))^2. \qquad (6.5b)$$

Keller and Frischknecht (1966, pp 222-223) show that for $\delta_2 << h$ i.e. that $\sigma_2 >> \sigma_1$, then $h' \sim h$ is given by

$$Z_o(\omega) = i\omega\mu h'.$$

substituting $\rho_a(\omega)$ for $Z_o(\omega)$ (equation 2.13) gives

$$\rho_a(\omega) = \omega\mu h'^2(\omega)$$

and hence

$$h'(\omega) = \left(\frac{\rho_a}{\omega\mu}\right)^{\frac{1}{2}} = 800\left(\frac{\rho_a}{\omega}\right)^{\frac{1}{2}}.$$

However, the depth to the perfect substitute conductor, h^*, defined by

$$h^* = h + \tfrac{1}{2}\delta_2 = \mathrm{Re}(C) = \frac{1}{\omega\mu}\,\mathrm{Im}(Z_o), \qquad (6.6)$$

has been shown by Weidelt (1972) to be the mean depth of eddy current flow in a multi-layered conductor. For σ_2 very large, then $h^* \simeq h \simeq h'$.

Schmucker (1970, p 69) proposed a method for deriving a first approximation to the 1D conductivity distribution. He suggested evaluating $h^*(\omega)$ and $\rho^*(h^*)$, from either the inductive scale length, $C(\omega)$, for GDS data or the impedance function, $Z_o(\omega)$, for MT data, by utilising equations 6.5b and 6.6. This ρ^*-h^* approximation was shown by Schmucker (1970, p70) to give the Lahiri and Price (1939) model 'd' when applied to global data.

However, the substitution is only meaningful when the approximation of a resistive layer overlying a conducting sub-stratum is valid, i.e. that the conductivity is a monotonically increasing function with depth. If, as was the case with the MT results for this work, the ρ_a curve does not exhibit a decreasing asymptote with increasing period, then the approximation is invalid. Hence, the Schmucker approximation scheme was not applied to the results presented in this work.

Another first approximation algorithm, which employs the integrated skin depth, was presented by Laird and Bostick (1970). A depth versus frequency curve is generated from

$$D(f) = \frac{0.13}{(\pi\mu)^{1/3}} \int_f^\infty \frac{\rho_a(f_o)^{\frac{1}{2}}}{f_o^{\,3}}\, df_o$$

and resistivity $\rho_a(f)$ is assigned to depth D(f). However, this technique has not been widely employed.

6.2.3 Curve fitting procedures

The simplest form of curve matching is to generate the theoretical response of a model and compare that response with the observed response. For the MT problem, the theoretical response of a multi-layered substratum is given by equation 2.23. The parameters of the model can then be adjusted and further theoretical curves generated until an 'optimum' model is found whose response best agrees with the data.

Such 'trial-and-error' procedures are employed in many branches of geophysics. This is because the forward problem is inherently easier to solve than the inverse problem. One major advantage of the technique is that an intuitive feeling is obtained of which are the most critical model parameters.

A procedure which interprets MT apparent resistivity data by the sequential addition of base layers was suggested by Nabetani and Rankin (1969). The initial procedure is to interpret the highest frequency response in terms of a two-layer structure. A three-layer model is then employed, the upper two layers as previously interpreted, to match the theoretical and observed data at the point where the observed response departs from the theoretical two-layer response. This process is continued by adding further layers to the base of the resistivity profile until the whole field curve has been modelled. An interactive graphics program to choose the best possible 'new' layer parameters for the Nabetani-Rankin inversion scheme was written by Mozeson (1971). Patella (1976) has given a similar procedure for a partial curve-matching technique. However, Patella's method also inverts the phase data, simultaneously with the apparent resistivity data.

Various automatic techniques for deriving the model whose response best matches the observed response has been given. Most are by non-linear least squares procedures which minimise the residual between some function of the model response and that of the observed response. Laird and Bostick (1970) have examined many methods of minimising

$$\psi_1 = \sum_i |Z_{oi}(f) - Z_{mi}(f)|^2,$$

whilst Wu (1968) has given a procedure for minimising

$$\psi_2 = \sum_i (\rho_{oi}(f) - \rho_{mi}(f))^2,$$

where subscripts 'o' and 'm' refer to the observed and modelled responses respectively. Muller (1976) has generalised Wu's application of Marquardt's least squares method (Marquardt, 1963) to allow a complex valued parameter, ψ_3, given by

$$\psi_3 = \sum_i (Z_{oi}(f) - Z_{mi}(f))^2$$

to be minimised by his iteration scheme.

A novel least squares procedure, in the time-domain, was suggested by Kunetz (1972). It involves evaluating the operator u(t), given from the convolution

$$e(t) = u(t) * \frac{d}{dt} h(t)$$

where e(t) is the electric field

and h(t) is the orthogonal magnetic field. The function ψ_4, given by

$$\psi_4 = \int (u'(t) - U_m(t, \rho_i, h_i))^2 \, dt$$

where u'(t) is the best least squares estimate of u(t)

and $u_n(t)$ is the model operator given by ρ_i and h_i, the model layer resistivities and thickness.

Kunetz shows that $U(\omega)$, the Fourier transform of $u(t)$, is related to the impedance function $Z_o(\omega)$ by

$$U(\omega) = \frac{Z}{i\mu\omega}$$

and hence it is directly related to Schmucker's inductive scale length by $U(\omega) = -C(\omega)$. However, Kunetz considers that rather than undertake the two-step procedure of (i) deriving $u'(t)$ by a least-squares procedure, from $e(t)$ and $h(t)$, and then (ii) evaluating the 'optimum' model by minimising ψ_4, also by a least squares procedure, a superior algorithm is to derive $u_m(t, \rho_i, h_i)$ directly by minimising

$$\psi_r = \int (e(t) - U_m(t, \rho_i, h_i)^* \frac{d}{dt} h(t))^2 \, dt.$$

However, as Kunetz points out, this time-domain inversion involves infintely long functions of time, $e(t)$ and $h(t)$. Hence, it is very approximate for short data sets and it is computationally expensive for long data sets.

All the procedures presented in this section - 'trial-and-error' curve matching, partial curve matching and automatic least squares procedure - only derive one conductivity distribution that satisfies the data. The automatic techniques do not even allow an intuitive insight into the relative importance of each layer or its parameters. Because real data are subject to scatter, there is no reason to assume that the means of the apparent resistivity or phase data are the true responses. Accordingly, it is desirable to ascertain the bounds of the family of models that satisfy the confidence limits of the data.

6.2.4 Monte-Carlo inversion schemes

As stated by Jackson (1973), the complete solution to an inverse problem consists of two tasks: (i) finding a solution, and (ii) representing in a meaningful way the degree of non-uniqueness of that solution.

For most geomagnetic data, an acceptable model may be found using methods discussed in section 6.2.3. On some occasions, the least-squares procedures are not convergent to a solution (Wu, 1968). However, they do not satisfy (ii) above. As previously stated, an inherent feeling of which are the most critical model parameters is obtained by curve-matching methods. However, this 'feeling' cannot be quantified.

A technique used much in geophysics for investigating the non-uniqueness of a solution is the random search, or Monte-Carlo, procedure. A model is picked at random from the N-dimensional parameter space, corresponding to the N permitted variables of the model, and the theoretical response of the model is compared with the measured response. If certain criteria are satisfied, then the model is accepted. The criteria are usually of the form of a maximum level of the sum of the squares of departure of the theoretical response from the measured response or that the departure does not exceed a present limit at any response value. If the criteria are not satisfied, then the model is rejected. Another model, not statistically related to the first, is then selected from the parameter space and the procedure repeated. This random selection of models is continued until either the whole parameter space - which is infinite if the variables are continuous - has been examined or the computing time limit is exceeded.

For large N or continuous variables, the latter of the two situations given above limits the number of models which can be examined. If there is only one closed set of acceptable models in the N-dimensional parameter space, then a more efficient search is undertaken by the Hedgehog procedure (Keilis-Borok and Yanovskaja, 1967). Initially, the search is implemented by a Monte-Carlo procedure but, once an acceptable solution has been found, the search is then conducted in an organised manner about the solution. Hence, if there are two, or more, enclosed

sets of solutions which are unconnected with each other in the parameter space, only one of these will be found and subsequently locally explored.

In seismology, Monte-Carlo and/or Hedgehog inversion procedures have been applied to Rayleigh wave attenuation data (Mills and Fitch, 1977 - Monte-Carlo; Burton, 1977 - Hedgehog), surface wave dispersion data (Biswas and Knopoff, 1974 - Hodgehog) and global seismic velocity profile data (Press, 1968, 1970 - Monte Carlo; Anderssen et al., 1972 - Monte-Carlo) and many other problems.

In geomagnetic induction studies, the Hedgehog inversion procedure does not appear to have been employed. Monte-Carlo inversion was applied by Anderssen (1970), to global electromagnetic induction data, and by Hermance and Grillot (1974), to regional MT data. In his review on inversion of global electromagnetic data, Anderssen (1975) considers that Monte-Carlo inversion has an advantage over linearised heuristic methods, of the type employed by Parker (1971), because the averaging inherent in the latter is avoided.

A simple Monte-Carlo inversion scheme was developed by the author for deriving the range of acceptable models permitted by the observed MT responses.

Initially, a model of 'n' layers was found, by empirical curve-matching, the response of which satisfied the observed apparent resistivity and phase data to within the 95% confidence limits. If such a model was not found easily, a model whose theoretical response was within as many of the confidence intervals as possible was chosen. The departure of the response of this model from the observed response was obtained from the expression

$$\psi = \sum (\log (\hat{\rho}(f)) - \log (\rho_m(f))^2 + \sum (\hat{\phi}(f) - \phi_m(f))^2 \qquad (6.7)$$

where $\rho(f)$ and $\hat{\phi}(f)$ are the estimated apparent resistivity and phase at frequency f and $\rho_m(f)$ and $\phi_m(f)$ are those of the model at f.
The logarithm of the apparent resistivity was used because $\hat{\rho}(f)$ is distributed lognormally, rather than normally, about $\rho(f)$ (Bentley, 1973). A new model, whose response was to be examined, was generated by perturbing the initial model in a random manner. The resistivities and the thicknesses of the i'th layer of the new model was derived from

$$h_i' = h_i \, 2^{r_i} \tag{6.8a}$$

$$\rho_i' = \rho_i \, 10^{r_{i+n}} \tag{6.8b}$$

where ρ_i and h_i is the resistivity and thickness of the i'th layer of the initial model. The 'dashed' parameters refer to the new model layers, and r represents random numbers.
The random numbers (r_i and r_{i+n}) which generated the new model were derived from the NAG subroutine G05ADF. A sequence of numbers from this subroutine is normally distributed with zero mean and unit variance. Hence, 68% of the h_i' thicknesses generated were between $h_i/2$ and $2h_i$ and 68% of the ρ_i' resistivities generated were in the range $\rho_i/10$ - $10\,\rho_i$.

The theoretical response for the new model was calculated and compared with the measured response. If the theoretical response was within more than a set number of the 95% confidence intervals, then the model was accepted. Otherwise it was rejected. If the model was accepted, the value of ψ' was calculated from 6.7 by replacing $\rho_m(f)$ with $\rho_m'(f)$ (the apparent resistivity of the response of the new model at frequence f) and $\phi_m(f)$ with $\phi_m'(f)$ (similarly for phase). If $\psi' < \psi$, then the initial model parameters were replaced by those of the new model. For $\psi' > \psi$, no action was taken. Hence, the parameters which

were perturbed, by equations 6.8, to give the new model, related to the best fitting model at that moment.

The procedure was repeated by generating other 'new' models from equation 6.8 (note: each call on G05ADF gives a number statistically independent of any other number given by previous calls, until 10^{77} calls have been made). Tests were incorporated to ensure the thicknesses and resistivities, h_i' and ρ_i', of the new model were between preset limits. These constraints not only ensured that the parameters were physically realisable but also were used to restrict the search to that region of the parameter space where acceptable models were likely to be found. This region was approximately delineated by initial tests with only physically realisable constraints applied.

It was decided to generate the new model from values chosen out of the continuous distributions of each of the parameters. An alternative would be to choose at random from discrete values of each of the parameters, as was undertaken by Hermance and Grillot (1973). This decision was taken to ensure that the models would be as randomly selected as possible and therefore not subject to Haddon and Bullen's (1969) objection to Press' (1968) Monte-Carlo method. They claimed that a misleading predominance of complex models resulted because the probability of generating a parametrically simple random walk was small. However, they made the implicit assumption that the points of the random model were generated sequentially (Anderssen et al., 1972). This cannot be true for the method outlined above.

Incorporated in the procedure was a facility for keeping any one, or more, of the layer parameters to its initial value. Hence, the thicknesses could be kept constant and the layer resistivities altered or vice versa.

To illustrate the proposed inversion scheme, the three-layer model, model 1 illustrated in figure 6.1, was used as the initial model to invert station BOR's rotated major data. The theoretical (crosses) and observed (asterisks and open-diamonds) responses are also shown in figure 6.1. For the MT data from station BOR, there were nine periods at which the impedances were considered 'well-estimated'. Hence, there were 18 confidence intervals, 9 for apparent resistivity and 9 for phase. These can be employed to constrain the responses of the acceptable models.

In the first trial, the resistivities were held constant at 700 Ωm/50 Ωm/750 Ωm, and the depths to the interfaces were permitted to vary in the range 15-40 km, for the top interface d_1, and 25-80 km, for the lower interface d_2. Because there are only two variables, the parameter space was two-dimensional and it is illustrated in figure 6.2. This is termed the d-space of the model. The triangle in the top left-hand corner of the d-space is a region from which models were not selected because they would require a negative thickness for the second layer, h_2. The position of the initial model in the parameter space is indicated by the full circle in figure 6.2. Each of the other symbols represents a model that was randomly selected from the parameter space and its theoretical response compared with the measured response. The asterisks denote models whose responses are within the confidence limits of greater than 75% (0.75 x 18 = 13.5, i.e. 14 limits) of the data. The vertical crosses indicate those models whose responses are within all the apparent resistivity confidence intervals (i.e. 9) but an insufficient number of phase intervals (i.e. less than 5). The open diamonds are models rejected because their responses do not satisfy either of these two sets of acceptance criteria.

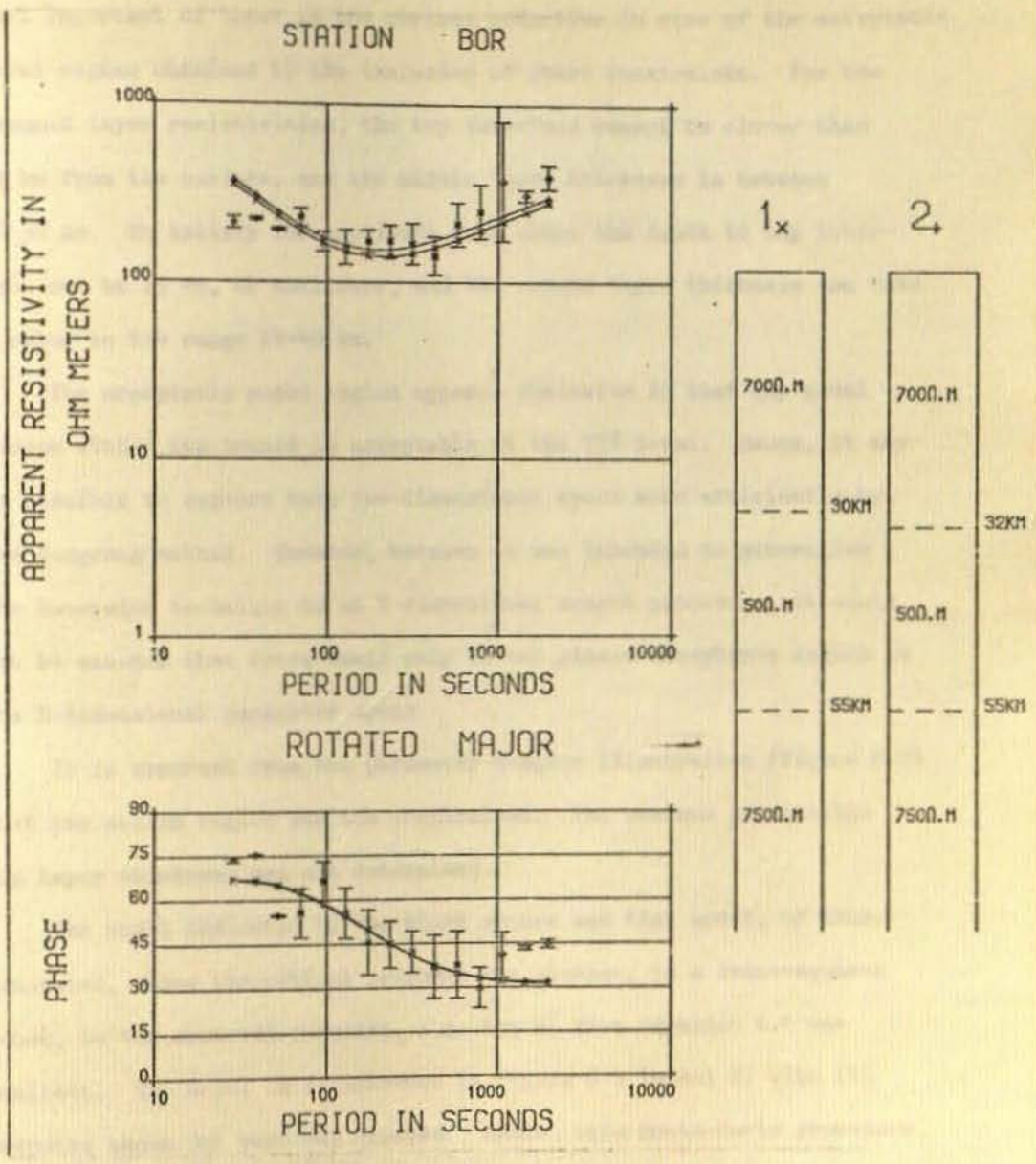

Figure 6.1 Initial (1) and final (2) models of Monte-Carlo inversion, with fixed layer resistivities, of BOR major data

Several features of the parameter d-space are worthy of note. The most important of these is the obvious reduction in size of the acceptable model region obtained by the inclusion of phase constraints. For the assumed layer resistivities, the top interface cannot be closer than 23 km from the surface, and the middle layer thickness is between 16-30 km. To satisfy the amplitude data alone the depth to top interface can be 15 km, or shallower, and the second layer thickness can take a value in the range 14-42 km.

The acceptable model region appears exclusive in that any model chosen within its bounds is acceptable at the 75% level. Hence, it may be possible to explore this two-dimensional space more efficiently by the Hedgehog method. However, because it was intended to generalise the inversion technique to an N-dimensional search procedure, it could not be assumed that there would only be one closed acceptance region in the N-dimensional parameter space.

It is apparent from the parameter d-space illustration (figure 6.2) that the search region was too constrained. The maximum permissible top layer thickness was not determined.

The model indicated by the black square was that model, of those generated, whose theoretical response was closest, in a least-squares sense, to the observed response, i.e. its ψ' from equation 6.7 was smallest. The model is illustrated in figure 6.1 (model 2) with its response shown by vertical crosses. Hence, this Monte-Carlo procedure not only finds the bounds of the acceptable model parameters but also finds an 'optimum' model.

When the acceptance level is increased from 75% to 89% (i.e. 16 of the 18 intervals), only those models whose layer depths were within region A of figure 6.1 had acceptable theoretical responses. When the acceptance level was further increased to 94% (17 intervals minimum),

Figure 6.2 Parameter 'd-space' for Monte-Carlo inversion of the 'rotated major' data from station BOR -layer resistivities held constant.

triangle - negative h_2 zone, unacceptable models

asterisks- models accepted at the 75% level of acceptance

crosses - models acceptable to the amplitude response but not the phase response

diamonds - unacceptable model parameters

circle - starting model for the inversion procedure

square - 'optimum model' found by random choice

zone A - acceptable model region at the 89% acceptance level

zone B - acceptable model region at the 94% acceptance level

PARAMETER SPACE FOR STATION BOR -MAJ

RESISTIVITIES HELD CONSTANT , DEPTHS ALTERED

d-space

ρ_1 = 700.0

ρ_2 = 50.0 0.75 ACCEPTANCE

ρ_3 = 750.0

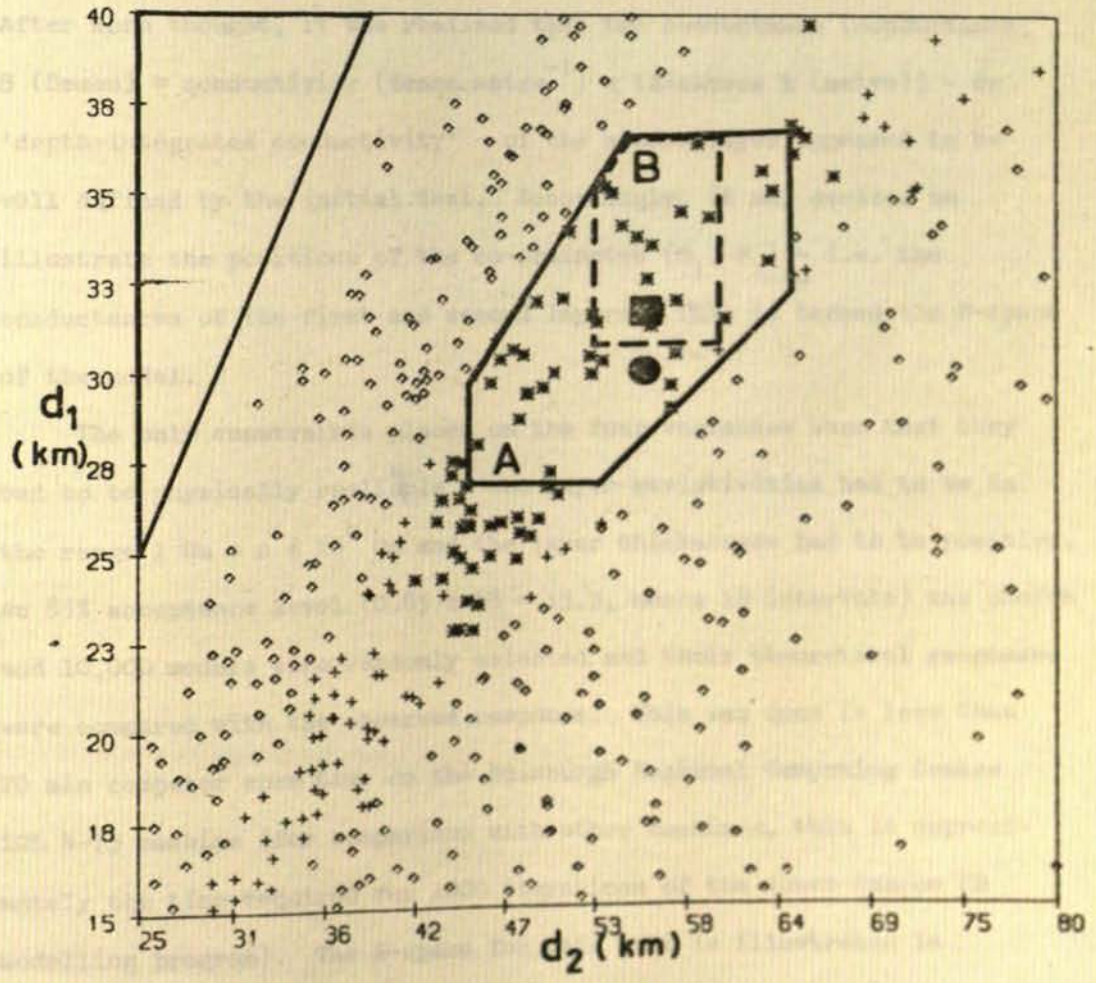

the region of acceptable models was further reduced in size to zone B. Note that the initial model was not acceptable at the 94% level.

This initial test illustrated that the method was viable and could produce worthwhile results. Hence, the best-fitting model (the black square in figure 6.1) was employed as the initial model to a random search procedure with four parameters of a three-layer model allowed to vary. These four were the top layer resistivity and thickness and the second layer resistivity and thickness. The base layer resistivity was again kept constant at 750 Ωm. One major problem with multi-variate inversion studies is the difficulty of displaying the parameter space. After much thought, it was realised that the conductance (conductance, S (Semen) = conductivity (Semen.metre^{-1}) x thickness h (metre)) - or 'depth-integrated conductivity' - of the middle layer appeared to be well defined by the initial test. Accordingly, it was decided to illustrate the positions of the co-ordinates (S_1, S_2) - i.e. the conductances of the first and second layers. This is termed the S-space of the model.

The only constraints placed on the four variables were that they had to be physically realisable - the layer resistivities had to be in the range 1 Ωm < ρ < 10^4 Ωm and the layer thicknesses had to be positive. An 85% acceptance level (0.85 x 18 = 15.3, hence 16 intervals) was chosen and 10,000 models were randomly selected and their theoretical responses were compared with the observed response. This was done in less than 20 min computer core time on the Edinburgh Regional Computing Centre ICL 4-75 machine (for comparison with other machines, this is approximately the time required for 1000 iterations of the Jones-Pascoe 2D modelling program). The S-space for this test is illustrated in figure 6.3 and the resistivity-depth profiles (ρ-d profiles) of the accepted models are illustrated in figure 6.4. For clarity, the S

Figure 6.3 Parameter 'S-space' for Monte-Carlo inversion of the 'rotated major' data from station BOR. S_1 & S_2 are the conductances of the first and second layer respectively.
- three layer models with the base layer resistivity held constant at 750 ohm.m . All other four parameters allowed to vary randomly

circles - acceptable model parameters

diamonds- unacceptable model parameters

PARAMETER SPACE FOR STATION BOR -MAJ

BASEMENT RESISTIVITY HELD CONSTANT

S - space

ρ_3 = 750.0

0.85 ACCEPTANCE

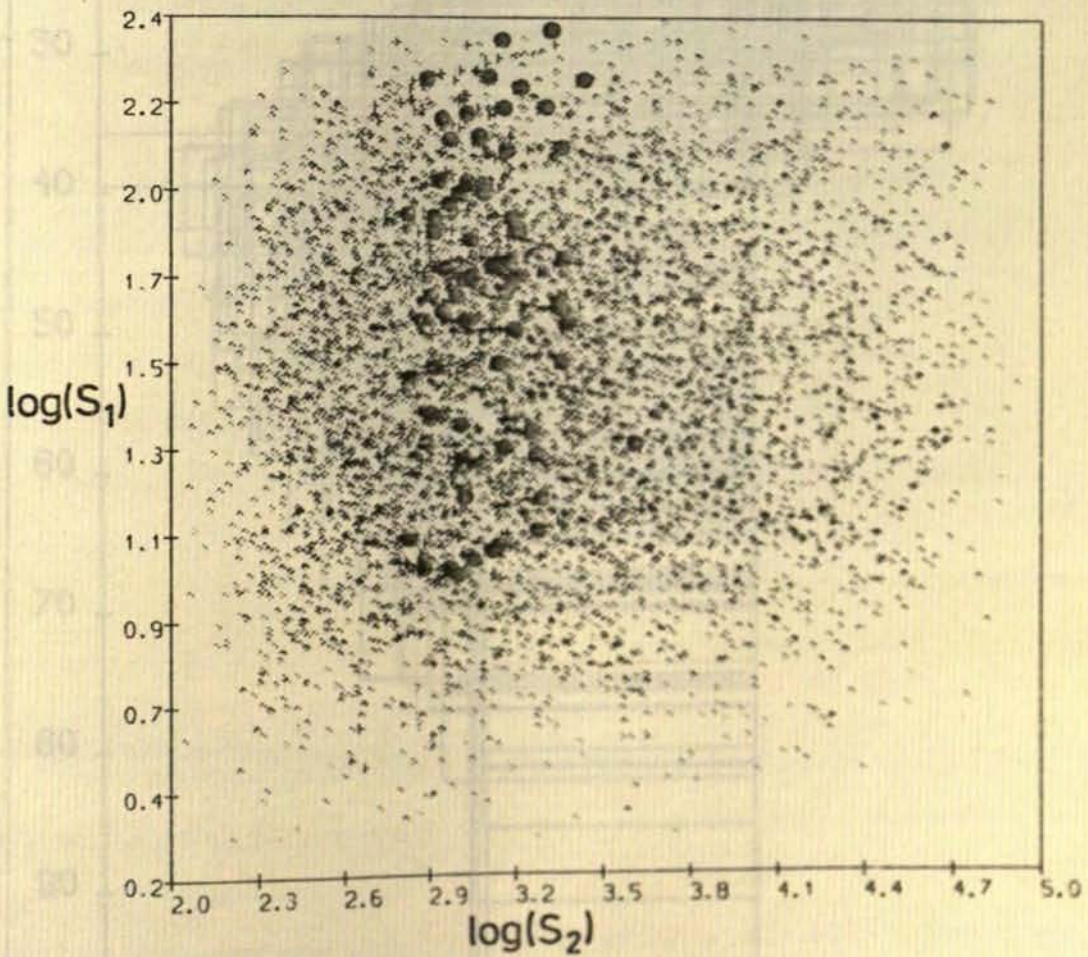

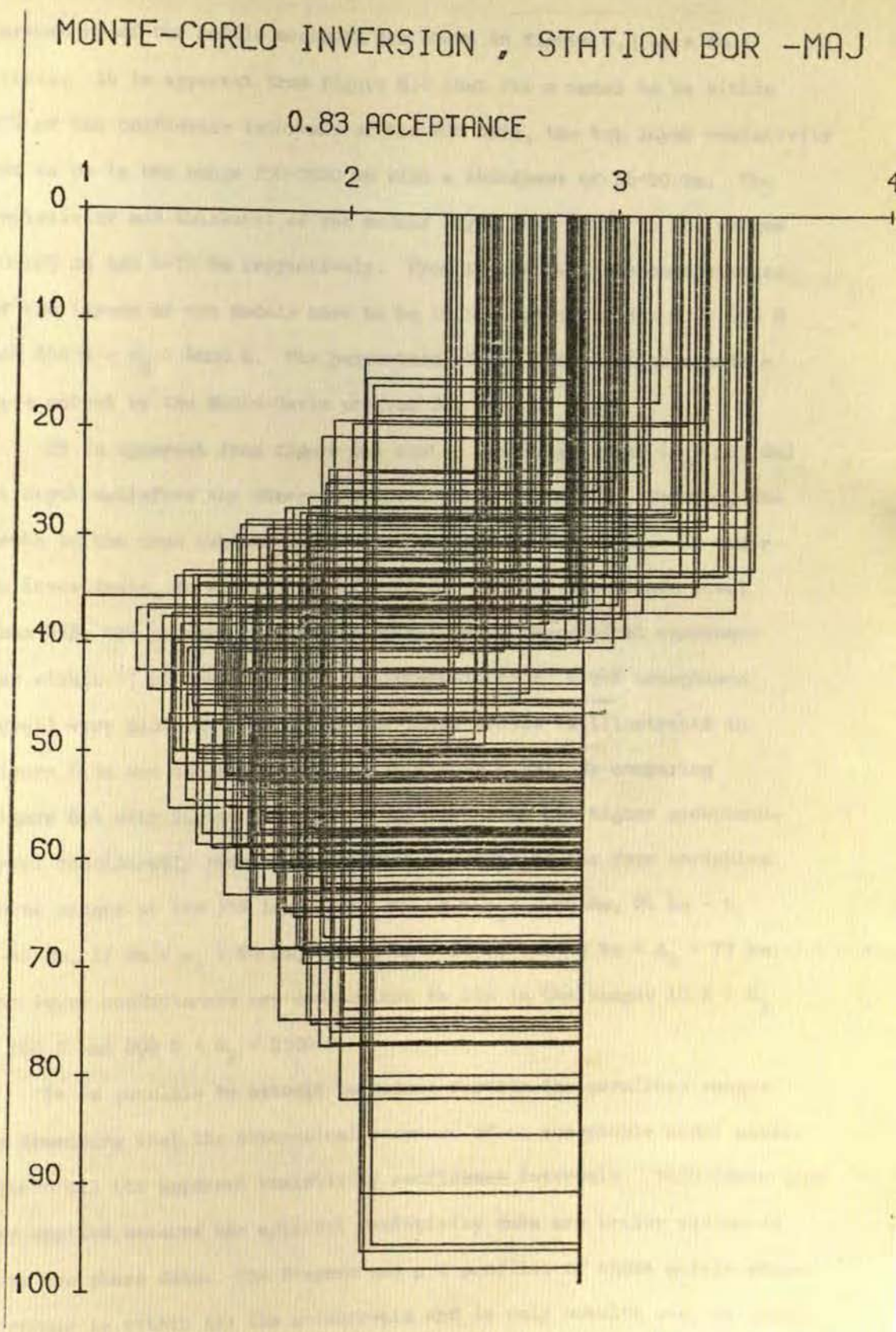

Figure 6.4 Monte-Carlo inversion - BOR major data
ρ-d profiles for acceptance level of 83%

parameters of the models accepted are shown in figure 6.3 by a full circle. It is apparent from figure 6.4 that for a model to be within 85% of the confidence intervals of the BOR data, the top layer resistivity has to be in the range 250-3000 Ωm with a thickness of 16-50 km. The resistivity and thickness of the middle layer have to be in the ranges 10-125 Ωm and 4-70 km respectively. From figure 6.3, the conductances of the layers of the models have to be in the ranges $10 \text{ S} < S_1 < 250 \text{ S}$ and $650 \text{ S} < S_2 < 4000 \text{ S}$. The parameters of all the acceptable models were output by the Monte-Carlo program for further use.

It is apparent from figure 6.4 that a conducting zone ($\rho < 125$ Ωm) at depth satisfies the observed response at station BOR. However, the depth to the zone can take any value in the range 16-50 km. In order to investigate, as before, the effects of a higher acceptance level than 85%, the parameters of those models whose theoretical responses lay within 17 of the 18 confidence intervals (i.e. a 94% acceptance level) were plotted. The S-space of these models is illustrated in figure 6.5a and their ρ-d profiles in figure 6.5b. By comparing figure 6.4 with figure 6.5b, it is apparent that the higher acceptance level considerably reduced the permitted ranges of the four variables. These ranges at the 94% level are: $300 \text{ Ωm} < \rho_i < 3000 \text{ Ωm}$, $24 \text{ km} < h_1 < 45 \text{ km}$, $17 \text{ Ωm} < \rho_2 < 90 \text{ Ωm}$, $8 \text{ km} < h_2 < 54 \text{ km}$ and $44 \text{ km} < d_2 < 77 \text{ km}$. The layer conductances are constrained to lie in the ranges $10 \text{ S} < S_1 < 160 \text{ S}$ and $800 \text{ S} < S_2 < 2500 \text{ S}$.

It is possible to attempt to reduce further the permitted ranges by demanding that the theoretical response of an acceptable model passes within all the apparent resistivity confidence intervals. This constraint was applied because the apparent resistivity data are better estimated than the phase data. The S-space and ρ-d profiles of those models whose response is within all the ρ-intervals and is only outwith one, or less,

parameters of the models accepted are shown in figure 6.3 by a full circle. It is apparent from figure 6.4 that for a model to be within 85% of the confidence intervals of the BOR data, the top layer resistivity has to be in the range 250-3000 Ωm with a thickness of 16-50 km. The resistivity and thickness of the middle layer have to be in the ranges 10-125 Ωm and 4-70 km respectively. From figure 6.3, the conductances of the layers of the models have to be in the ranges 10 S < S_1 < 250 S and 650 S < S_2 < 4000 S. The parameters of all the acceptable models were output by the Monte-Carlo program for further use.

It is apparent from figure 6.4 that a conducting zone (ρ < 125 Ωm) at depth satisfies the observed response at station BOR. However, the depth to the zone can take any value in the range 16-50 km. In order to investigate, as before, the effects of a higher acceptance level than 85%, the parameters of those models whose theoretical responses lay within 17 of the 18 confidence intervals (i.e. a 94% acceptance level) were plotted. The S-space of these models is illustrated in figure 6.5a and their ρ-d profiles in figure 6.5b. By comparing figure 6.4 with figure 6.5b, it is apparent that the higher acceptance level considerably reduced the permitted ranges of the four variables. These ranges at the 94% level are: 300 Ωm < ρ_i < 3000 Ωm, 24 km < h_1 < 45 km, 17 Ωm < ρ_2 < 90 Ωm, 8 km < h_2 < 54 km and 44 km < d_2 < 77 km. The layer conductances are constrained to lie in the ranges 10 S < S_1 < 160 S and 800 S < S_2 < 2500 S.

It is possible to attempt to reduce further the permitted ranges by demanding that the theoretical response of an acceptable model passes within all the apparent resistivity confidence intervals. This constraint was applied because the apparent resistivity data are better estimated than the phase data. The S-space and ρ-d profiles of those models whose response is within all the ρ-intervals and is only outwith one, or less,

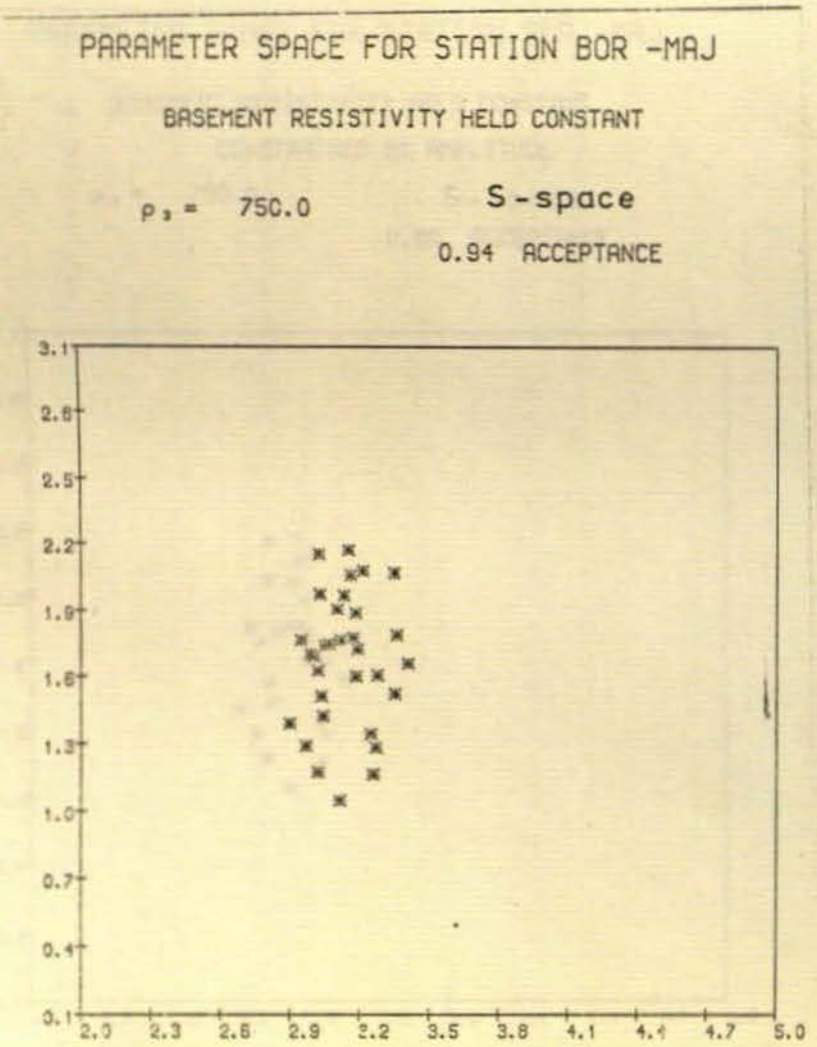

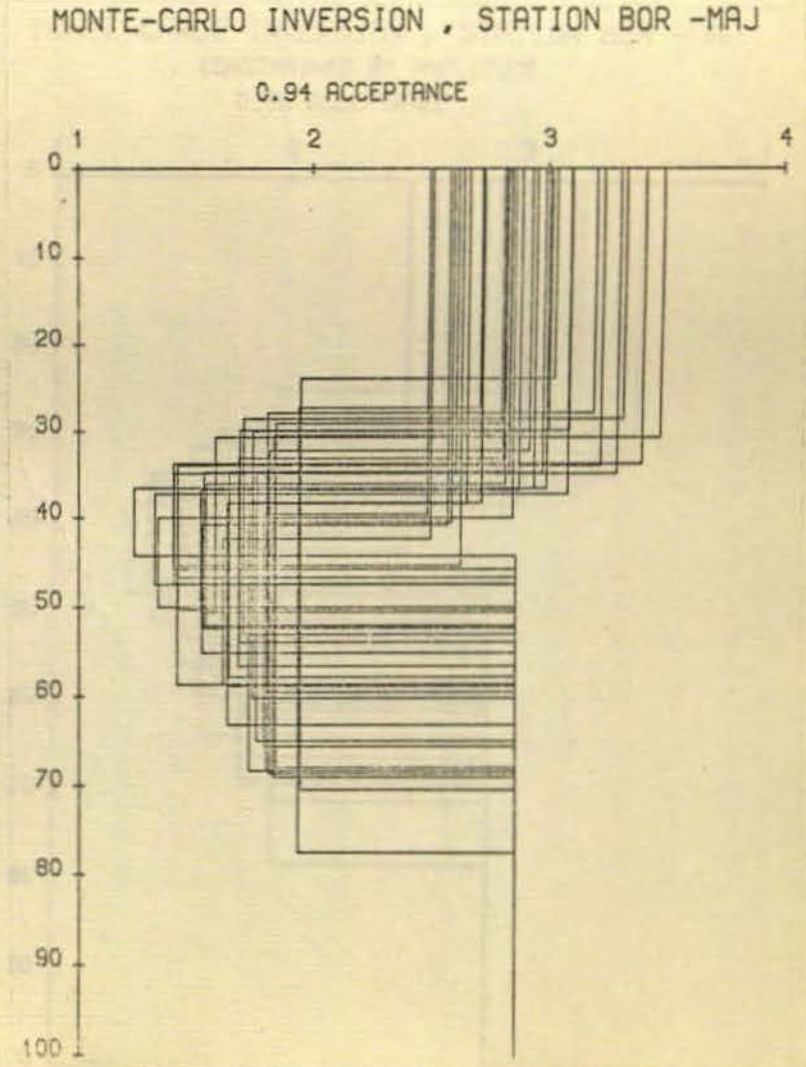

Figure 6.5 Monte-Carlo inversion - BOR major data
acceptance level of 94%
a) S-space b) ρ-d profiles

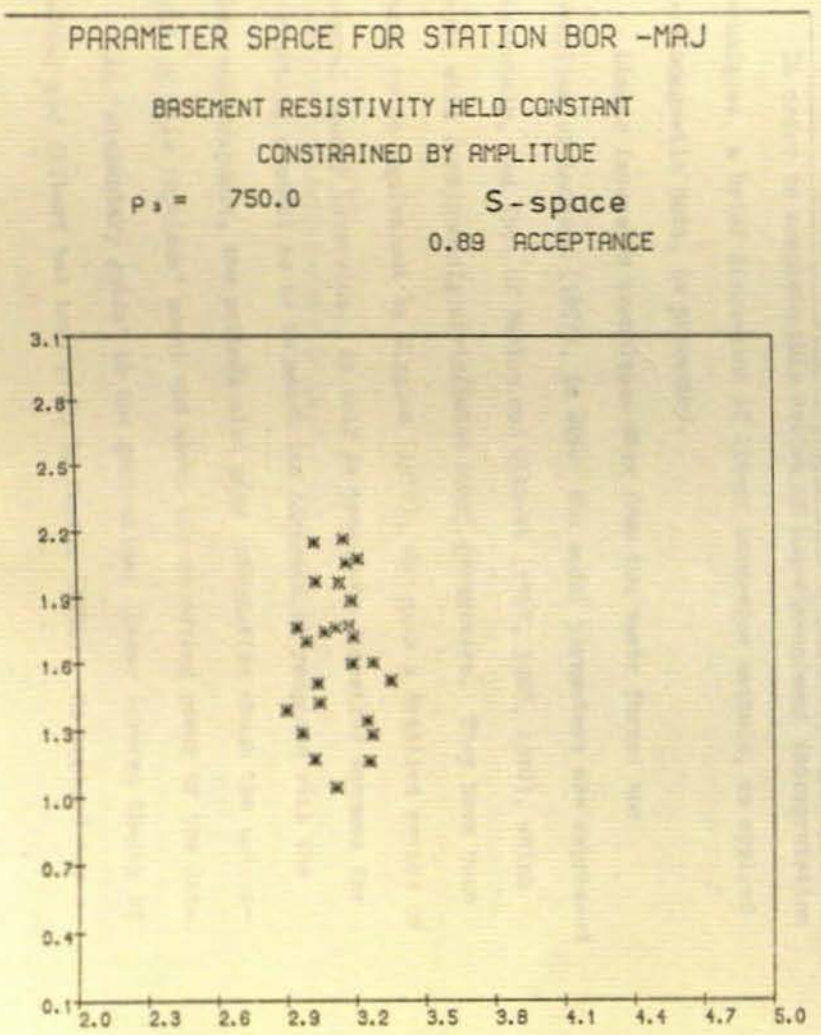

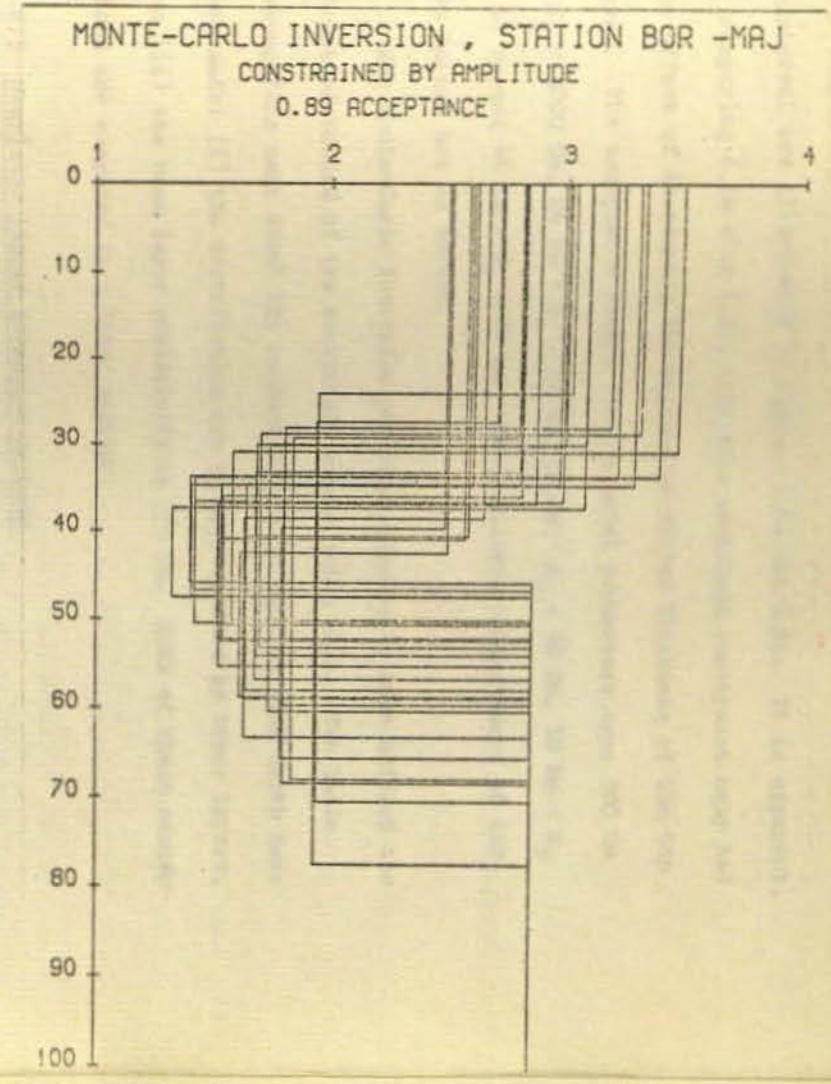

Figure 6.6 Monte-Carlo inversion - BOR major data
acceptance level of 89% & amplitude constraint
a) S-space
b) ρ-d profiles

ϕ-interval are illustrated in figures 6.6a and 6.6b. It is apparent, by comparing 6.5b with 6.6b, that this amplitude constraint only had the effect of decreasing the maximum permitted thickness of the top layer. The acceptable ranges for the model parameters are: 300 Ωm $< \rho_1 <$ 3000 Ωm, 24 km $< h_1 <$ 42 km, 20 Ωm $< \rho_2 <$ 90 Ωm, 10 km $< h_2 <$ 54 km and 46 km $< d_2 <$ 77 km. The permitted conductances of the two layers are as before.

The Monte-Carlo inversion procedure appears to have defined the permitted bounds of the acceptable models quite well. Two basic assumptions made about the conductivity distribution with depth have been made: (i) the distribution can be approximated by three layers, and (ii) the base layer resistivity is 750 Ωm. Both of these assumptions are examined in a later section.

6.2.5 Heuristic linear inversion methods

In order to complete this review of one-dimensional interpretation techniques, a brief discussion of linear inversion methods, as applied to geomagnetic data, is presented.

Linear inversion techniques stem from two basic forms: the formalism of Lanczos (1967), in which the model parameters are expressed discretely, and that of Backus and Gilbert (1967, 1968, 1970), which deals with continuously distributed model parameters. They have been shown to be equivalent by Wiggins (1972), who gave a detailed review of general linear inversion. As well as providing iterative schemes for perturbing a model so as to match its theoretical response with the observed response, the methods also give information about the uniqueness of this 'optimum' model and about the resolving power of the data.

An 'elementary guide' to the generalised linear inverse theory of Backus and Gilbert has been given by Parker (1970). He applied the

theory to the global induction problem using the observed response derived by Banks (1969). Parker was not able to find a starting model which gave converging iterates. He concluded this was due to the fact that either (i) the starting models were too far from the true structure, or (ii) no earth model existed which was compatible with the data. Considering the errors involved in measurement, alternative (ii) seemed the most likely. However, satisfactory models could be found, whose theoretical responses were within one standard deviation of the observed response, but none of these gave the low near-surface conductivity derived by Banks. Parker also showed that the inclusion of phase information gave better surface resolution. This feature has also been concluded from the Monte-Carlo exercise discussed in section 6.2.4 and illustrated in figure 6.2. However, Parker considered that the inclusion of phase data does not introduce off-diagonal components in the covariance matrix. This has been shown to be in error by Summers (1976, p 177) because the diagonal elements of the off-diagonal sub-matrices are non-zero. Hence, an element of approximation was introduced by Parker, and is introduced whenever such a procedure of matrix extension is adopted (e.g. Muller, 1976).

The Backus-Gilbert formalism has also been applied by Hobbs (1973) to a response derived from data obtained from one magnetometer on the surface of the moon and one in lunar orbit. Hobbs concluded that there was not any evidence in the observed response for the 'spiked' conductivity profile of Sonnet et al. (1971). He considered that the limit of knowledge attainable by linear inversion theory is that the outer 170 km of the moon is less conducting than the interior, which is of uniform conductivity in the range 170 km < d < 700 km. In later papers, Hobbs (1977) and Hobbs and Parker (1977) illustrate one of the strengths of linear inversion methods by estimating the conductivity distribution

permitted by just two points at the high frequency end of Sonnet et al.'s (1972) response curve. They concluded that the majority of models examined by Sonnet et al. (1972) could not satisfy these two data points alone. Hence, these models were also unacceptable to the total response function.

Word et al. (1974) have applied inversion theory to galvanic resistivity data and to electromagnetic sounding data whilst Vozoff and Jupp (1975) have inverted, in a joint scheme, both galvanic resistivity data and MT sounding data. Larsen (1975) has inverted low frequency electromagnetic data to derive the conductivity structure beneath Hawaii.

Anderssen (1975), in a review of inversion of global electromagnetic induction data, argued that because the Lahiri and Price (1939) equations are already linear, once a conductivity model is specified, the linearisations of the problem by Parker (1971) and Bailey (1973) are unnecessary. It may be true that the relationship between the internal and external fields is linear for any specified conductivity model, but it is not obvious that the inversion problem, i.e. choosing the next 'optimum' model, is also linear. Parker (1977) has shown his linearisation is valid for a restricted class of conductivity models and has given the bounding constants.

Summers (1976) examined linear inversion theory with special reference to inverting magnetotelluric data. He applied his procedure to the preliminary response derived by the author for station NEW. Summers initially inverted the rotated major apparent resistivity data alone. Various starting models were chosen and the iterations all converged to different 'optimum' models. This dependence on starting model is not surprising as the Backus-Gilbert scheme seeks that model, closest to the starting model, which satisfies the data (Parker, 1970). However, all six 'optimum' models illustrated by Summers have several similar characteristics. They all exhibit a conducting upper crust

($\rho \sim 100$ m) and a conducting zone ($\rho \sim 10$ m) at upper mantle depths. None of these models however, satisfied the short period phase data. When the phase information was included and the inversion procedure was repeated, the derived 'optimum' models all displayed a resistive upper crust ($\rho \sim 10^3 - 10^4$ Ωm). The conducting zone at upper mantle depths however, was still present. Hence, Summers concurred with Parker, and with the conclusions of section 6.2.4, that the inclusion of phase information gives better surface resolution.

In conclusion, generalised linear inversion theory is obviously a formidable tool for not only deriving an 'optimum' model, whose theoretical response 'best' satisfies the data, but also for examining the uniqueness of the model and the resolving power of the data. However, it was not within the scope of this work to devise algorithms for inverting the observed MT responses by these methods.

6.3 Monte-Carlo Inversion of the MT Results

This section will discuss the inversion of the MT results by the proposed Monte-Carlo method (section 6.2.4). It is subdivided in the same manner as sections 5.3, 5.4 and 5.5 to discuss separately the inversion of the data from the three regions, i.e. the Midland Valley, the Southern Uplands and Northern England.

6.3.1 Midland Valley results - FTH and SAL

The FTH and SAL results, which were inverted, are illustrated in figures 5.8a and 5.8b. Their qualitative aspects were discussed in section 5.3.

For station FTH, there are 'well-estimated' data at five periods from 50 s to 800 s. Although there are 10 confidence intervals, 5 for apparent resistivity and 5 for phase, the interval for the phase at 50 s is from 0° to 90°. This range permits any conductivity model to be

PARAMETER SPACE FOR STATION FTH -MAJ

BASEMENT RESISTIVITY HELD CONSTANT

ρ_3 = 750.0

S-space

0.80 ACCEPTANCE

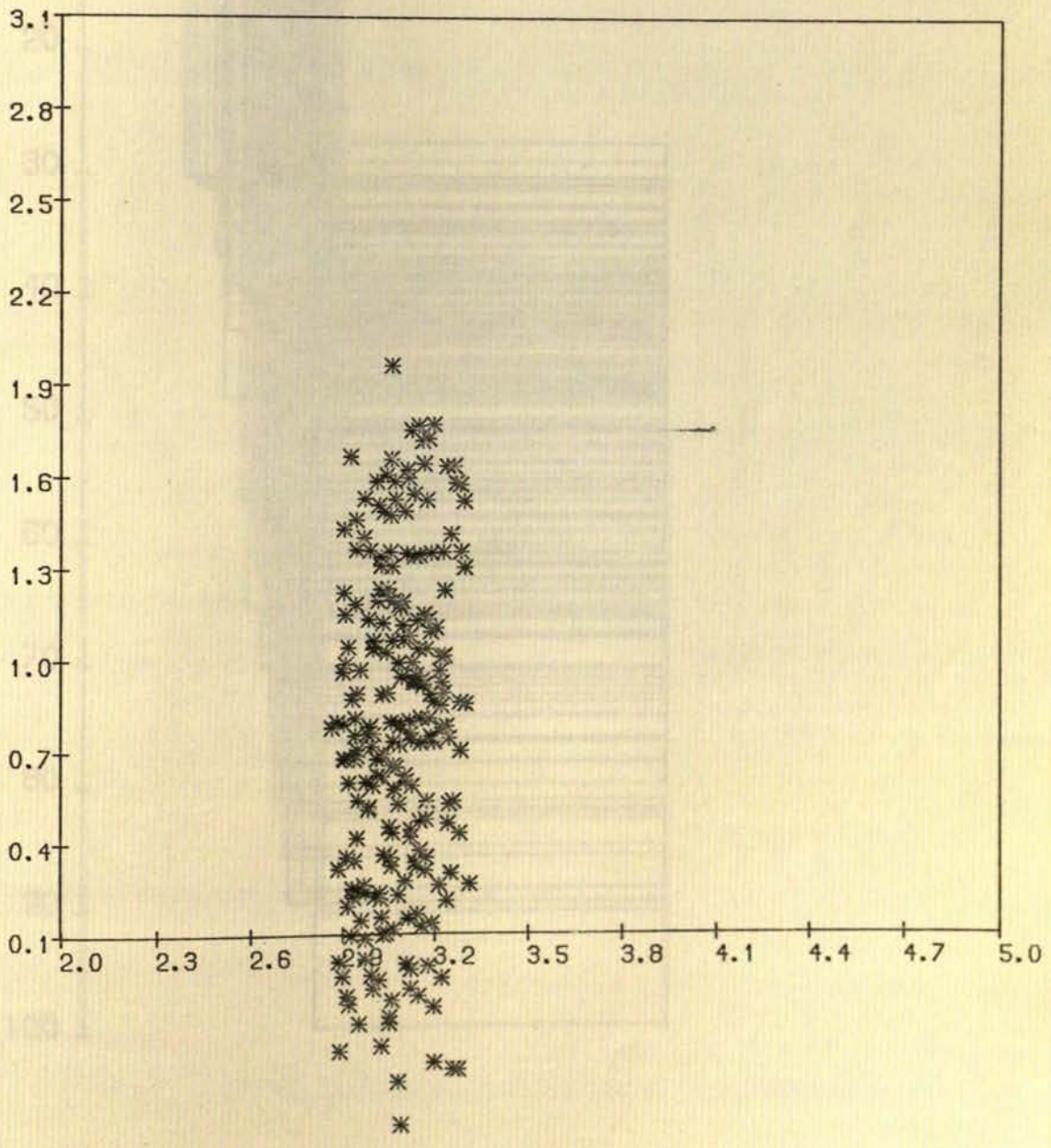

Figure 6.7a Monte-Carlo inversion - FTH major data
S-space for acceptance level of 80%

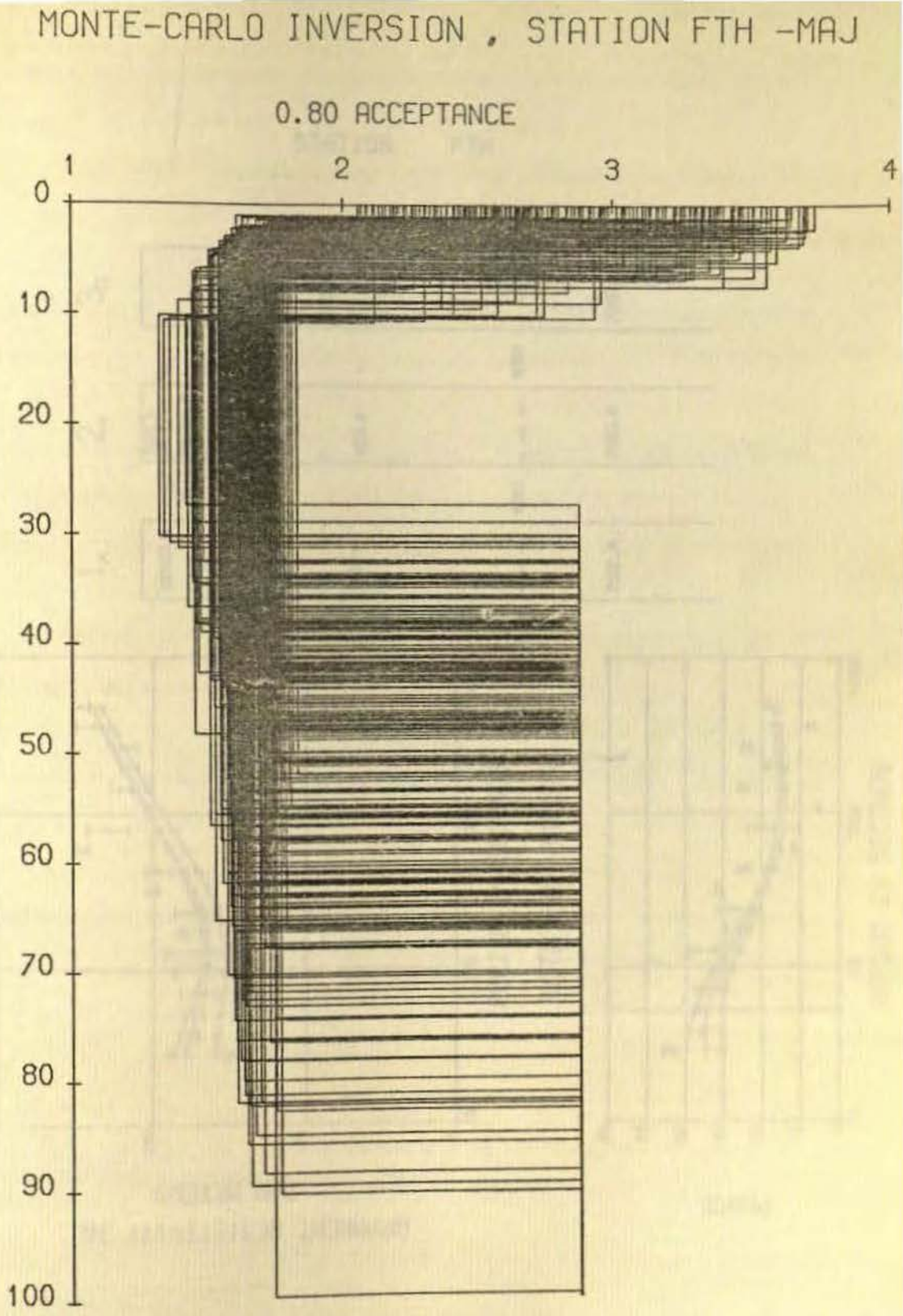

Figure 6.7b Monte-Carlo inversion - FTH major data
ρ-d profiles for acceptance level of 80%

Figure 6.8 Theoretical model responses to FTH major data

Midland Valley. However, the data do require a resistive zone in the upper crust as illustrated by curve 3 of figure 6.8.

There are 11 impedances considered well-estimated for station SAL (figure 5.8b). The period range of these data is from 28.5 s to 600 s. One of the confidence intervals for phase spans the total possible range (i,e. 0° - 90°), hence there are 21 intervals which can determine the acceptable models. However, the apparent resistivities of the two estimates at the shortest periods (i.e. 28.5 s and 38.5 s) are inconsistent with the observed phase response. These two estimates require a conducting upper crust to model their responses but the first five phase intervals require a resistive upper crust. A similar situation occurred when Summers (1976) inverted some MT data.

The magnetic field at location SAL was measured by the 3-component Fluxgate magnetometer as the Jolivet sensors were not operating satisfactorily at that time (section 3.3 (b)). The Fluxgate records appeared to be more contaminated by noise than did Jolivet records. From the comparison test undertaken, it was concluded that the noise was due to the instrumentation. As shown in sections 4.4.1 and 4.4.2, the magnitude of a response function is underestimated if there is any random noise on the input(s) to the linear system. However, because both the real and imaginary parts of the response function are underestimated by the same fraction, the phase of the response function should be unaffected. This argument could explain the apparent contradiction in the data because the phase estimates may be unbiased but the apparent resistivity estimates may be biased downwards by random noise.

Because of this inconsistency in the data, the maximum number of intervals within which the responses of a model of any conductivity distribution can lie is thus 19 of the total 21.

The SAL data were inverted, in exactly the same manner as the FTH data, and the S-space co-ordinates and ρ-d profiles of the models accepted at the 75% level (i.e. a minimum of 16 of the 19 intervals) are illustrated in figures 6.9a and 6.9b. The resemblance between figures 6.7b for FTH and 6.8b for SAL is striking, but perhaps not surprising considering that the two data sets are congruent. The maximum depth to the conducting zone is 13 km and the conducting zone resistivity is in the range 35 Ωm < ρ_2 < 80 Ωm. The base of the zone is at a depth of 33-80 km.

When the acceptance level is increased to 77% (i.e. 17 of the 19 intervals), the permitted models have a depth to the second interface, i.e. the base of the conducting zone, of 44 < d_2 < 67 km. The resistivity of the conducting zone is in the range 35 Ωm < ρ_2 < 70 Ωm and its top interface is at a depth less than 12 km.

The similarity of the permitted resistivity-depth profiles whose responses match the FTH and SAL data lends considerable weight to the argument that the rotated major results may, in certain circumstances, be interpreted in a one-dimensional sense.

6.3.2 Southern Uplands results - BOR, NEW and PRE

The data are illustrated in figures 5.11a (BOR), 5.11b (NEW) and 5.11c (PRE). For reasons discussed in section 6.1, it is considered that a one-dimensional treatment of these data is valid.

The inversion of the BOR data was discussed in section 6.2.4. To recapitulate, for completeness, the conclusions of that section: the parameters of a three-layer model, which has a base-layer resistivity of 750 Ωm and which is acceptable to the data, are contrained to the following bounds; 300 Ωm < ρ_1 < 3000 Ωm, 24 km < h_1 < 42 km, 20 Ωm < ρ_2 < 90 Ωm, 10 km < h_2 < 54 km, 46 km < d_2 < 77 km, 10 S < S_1 < 160 and 800 S < S_2 < 2500 S.

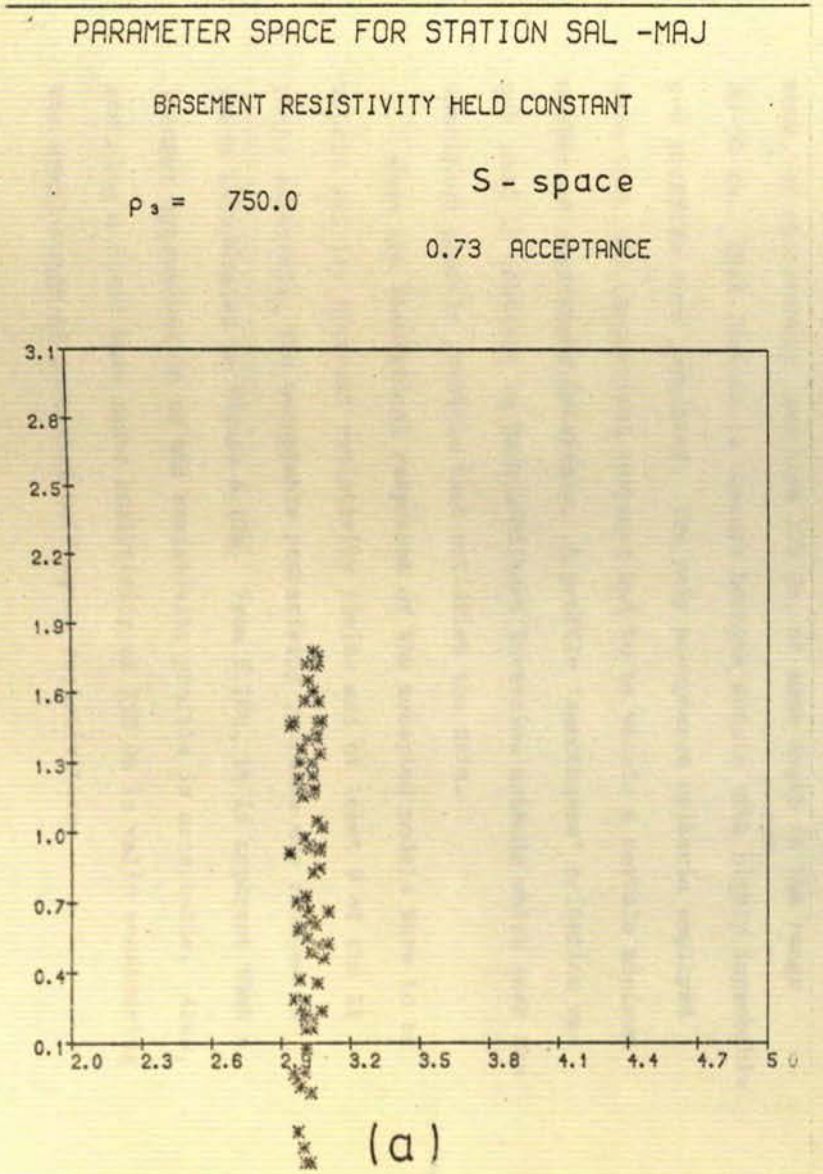

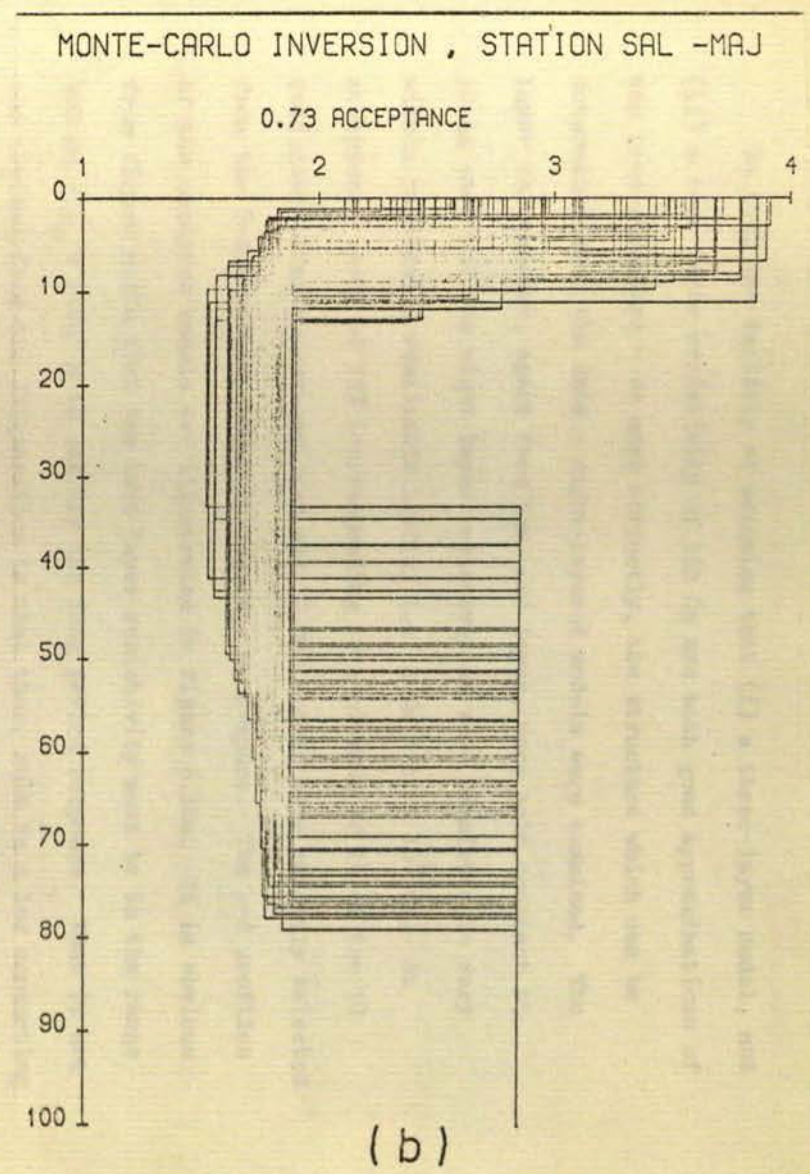

Figure 6.9 Monte-Carlo inversion - SAL major data acceptance level of 73%
(a) S-space (b) ρ-d profiles

To test the validity of assuming that (i) a three-layer model, and (ii) a base layer resistivity of 750 Ωm are both good approximations of the true structure - or more correctly, the structure which can be determined from the data - eight-layered models were examined. The layer thicknesses, apart from the base layer, were held constant at 10 km each and the eight layer resistivities were permitted to vary within physically realisable limits, i.e. $1\ \Omega m < \rho_i < 10^4\ \Omega m$. An acceptance level of 75% (corresponding to a minimum of 14 of the 18 confidence limits) was employed and 10,000 models were randomly selected from the 8-dimensional parameter space - or ρ-space. The ρ-d profiles of the accepted models are illustrated in figure 6.10a. It is obvious from figure 6.10a that the base layer resistivity must be in the range $400\ \Omega m < \rho_b < 2000$ m to satisfy the long period response. What is not too obvious from the illustration is that there must be a low conducting zone, of resistivity less than 100 Ωm, at some depth in the range 20-50 km. This feature is obscure because models with highly improbable ρ-d profiles were permitted. The only acceptance criteria employed were that the theoretical response had to be within a certain minimum number of confidence intervals. A profile 'smoothness' criterion was not used in contrast to Backus-Gilbert inversion methods which seek the smoothest profile possible that satisfies the data.

When the theoretical responses of the accepted models have to be within all the apparent resistivity limits and at least 9 of the 11 phase intervals, the acceptable resistivity profiles are reduced to those illustrated in figure 6.10b. From 6.10b, it is apparent that a 3-layer approximation to the resistivity profile is acceptable. Also, assuming a fixed base layer resistivity of 750 Ωm is valid considering the small range of permitted half-space resistivities.

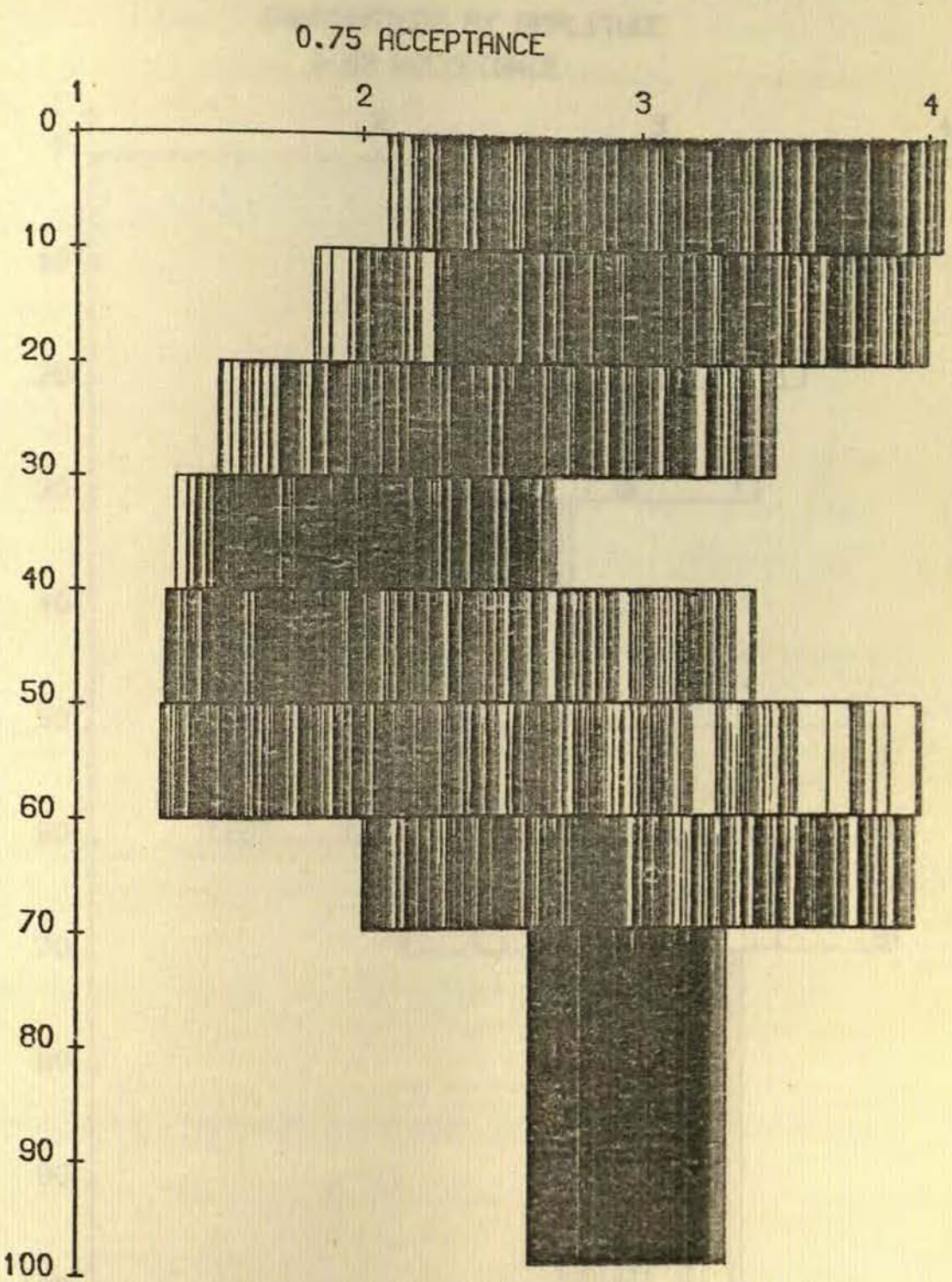

Figure 6.10a Monte-Carlo inversion - BOR major data
ρ-d profiles of 8-layer models
acceptance level of 75%

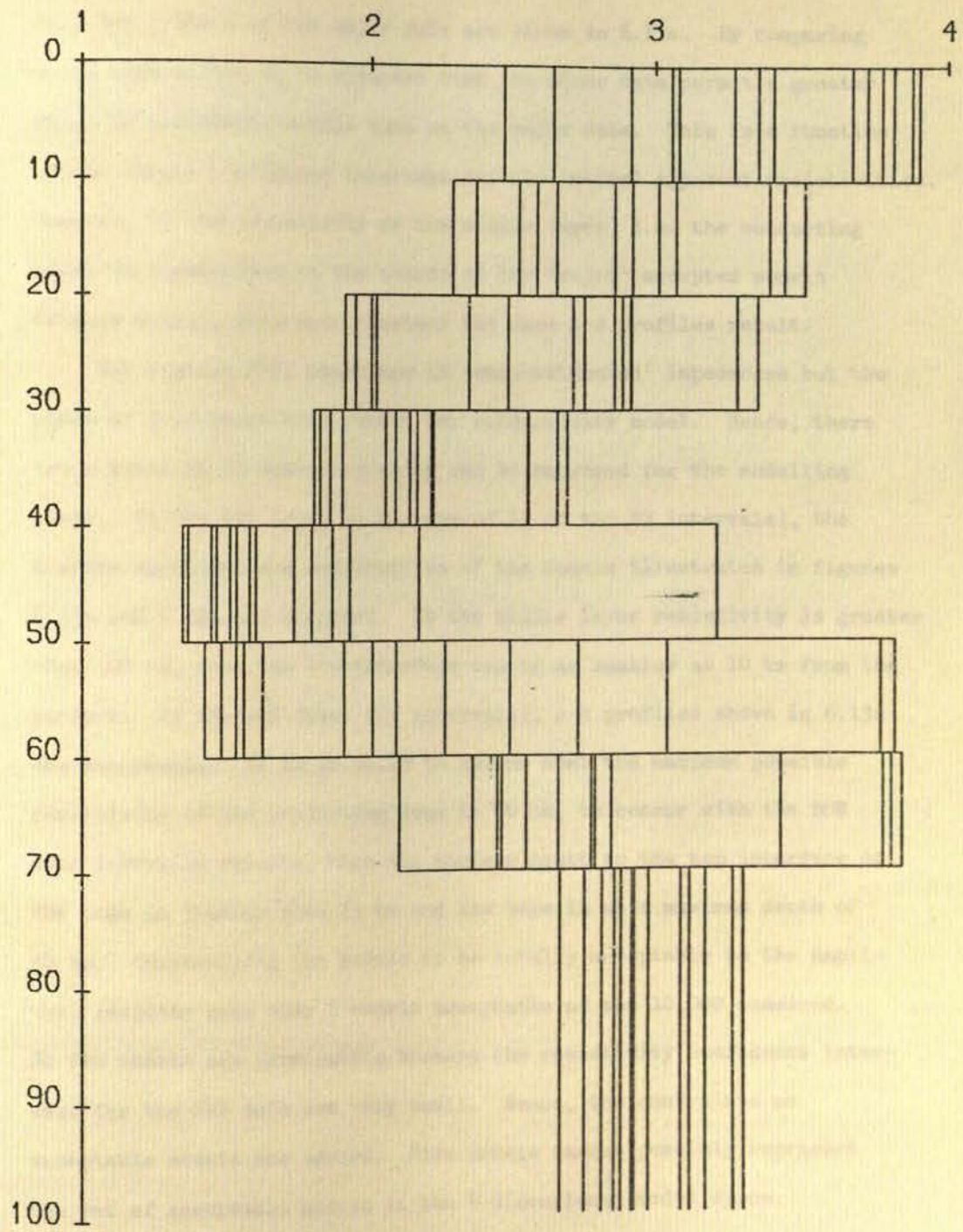

Figure 6.10b Monte-Carlo inversion - BOR major data
ρ-d profiles of 8-layer models
acceptance level of 89%

Because the 'rotated minor' resistivities appear well estimated, it was thought worthwhile to invert these data also. Acceptable models, constrained to be within all the amplitude intervals, are illustrated in 6.11b. Those of the major data are shown in 6.11a. By comparing 6.11a with 6.11b, it is apparent that the minor data permit a greater range of acceptable models than do the major data. This is a function of the larger confidence intervals for the 'minor' apparent resistivities. However, if the resistivity of the middle layer, i.e. the conducting zone, is constrained to the bounds of the 'major' accepted models (figure 6.11a), then approximately the same ρ-d profiles result.

For station NEW, there are 15 'well-estimated' impedances but the phase of 7 of these will permit any conductivity model. Hence, there are a total of 23 intervals which can be employed for the modelling study. At the 80% level (a minimum of 17 of the 23 intervals), the S-space locations and ρ-d profiles of the models illustrated in figures 6.12a and 6.12b are accepted. If the middle layer resistivity is greater than 100 Ωm, then its top interface can be as shallow as 10 km from the surface. At the 90% level (20 intervals), ρ-d profiles shown in 6.13a are acceptable. If it is valid to assume that the maximum possible resistivity of the conducting zone is 90 Ωm, to concur with the BOR data inversion results, then the minimum depth to the top interface of the zone is greater than 15 km and its base is at a maximum depth of 60 km. Constraining the models to be totally acceptable to the amplitude response gave only 5 models acceptable of the 10,000 examined. So few models are permissible because the resistivity confidence intervals for the NEW data are very small. Hence, the contraints on acceptable models are severe. Five models cannot possibly represent the set of acceptable models in the 4-dimensional model space.

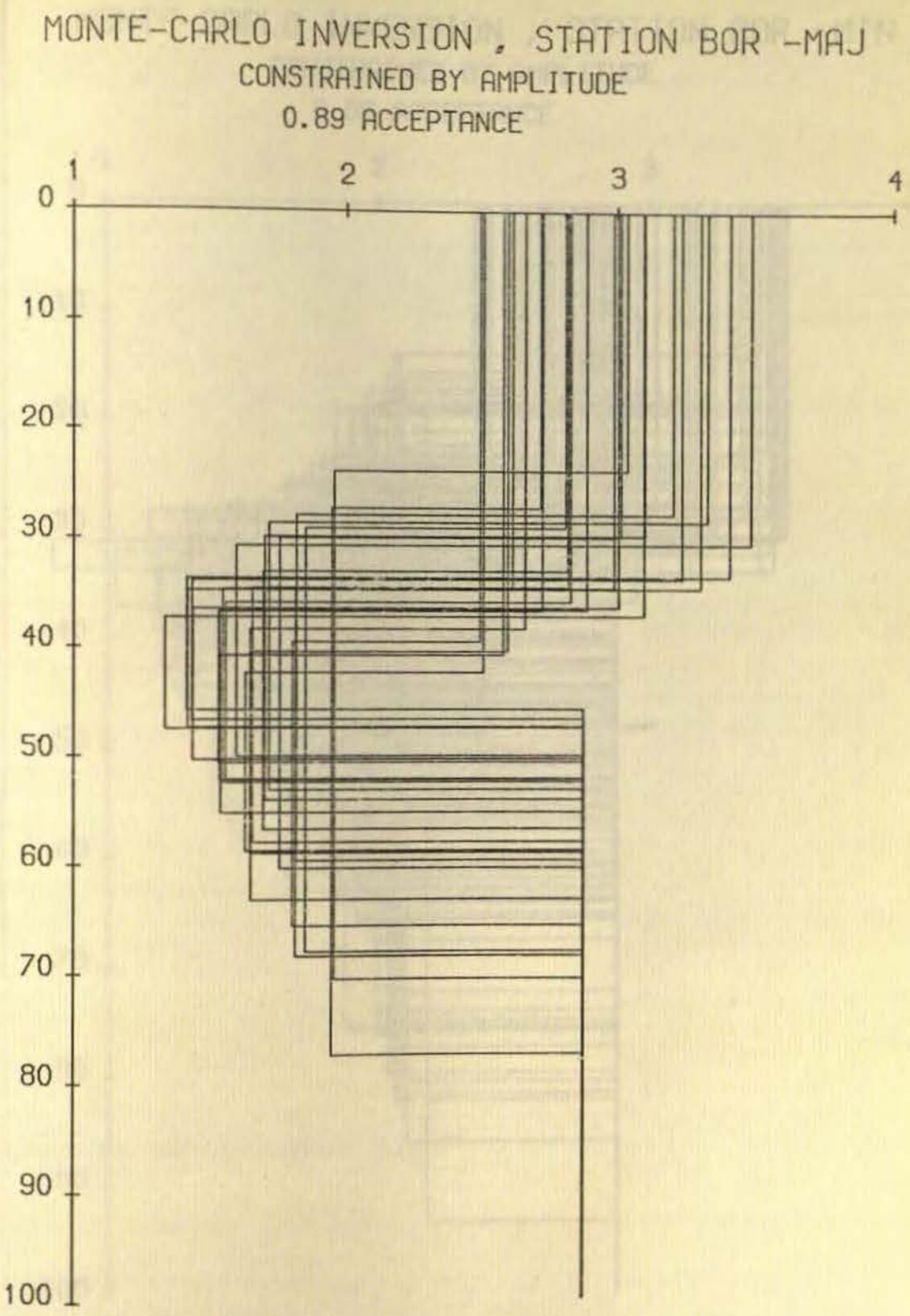

Figure 6.11a Monte-Carlo inversion - BOR major data ρ-d profiles for acceptance level of 89% with amplitude constraint

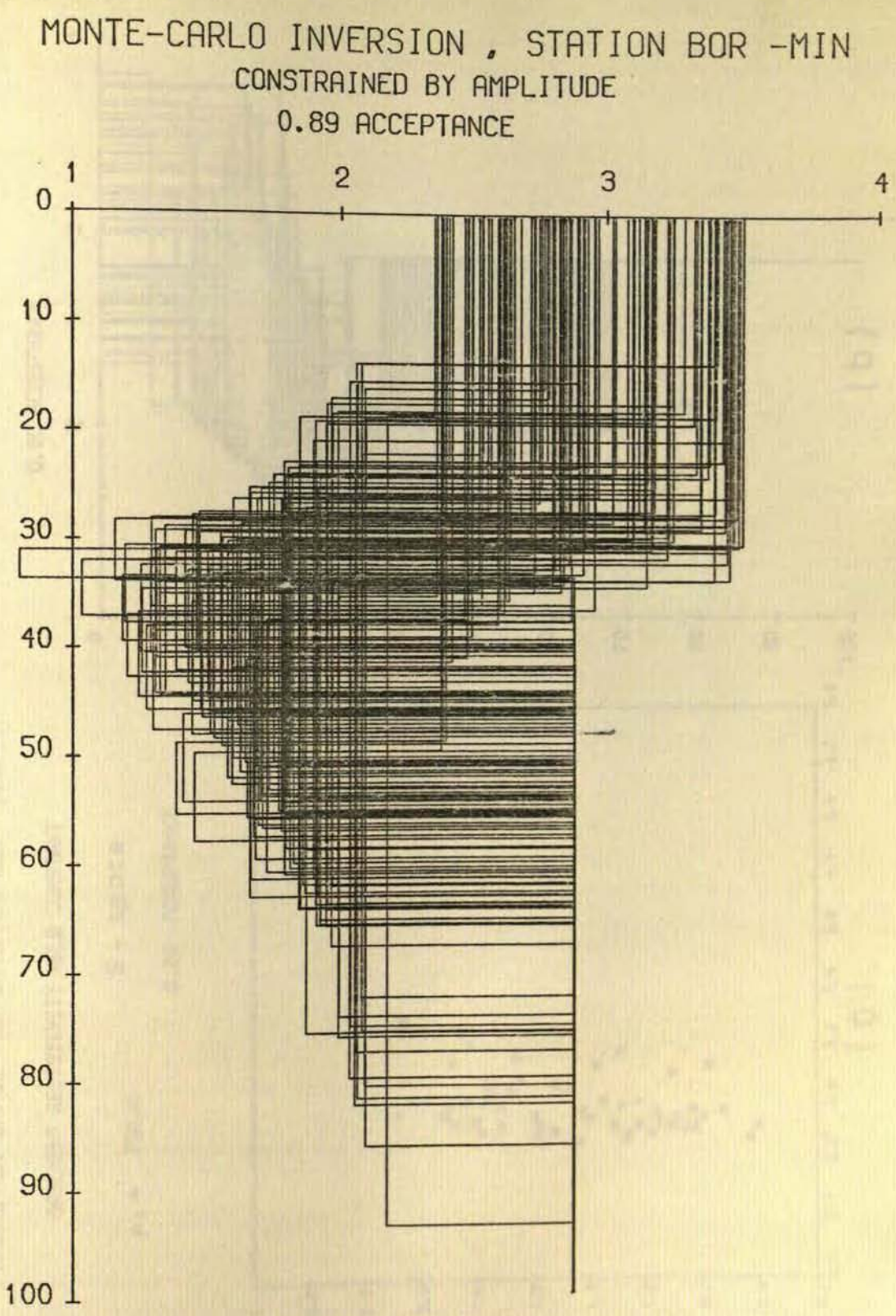

Figure 6.11b Monte-Carlo inversion - BOR minor data ρ-d profiles for acceptance level of 89% with amplitude constraint

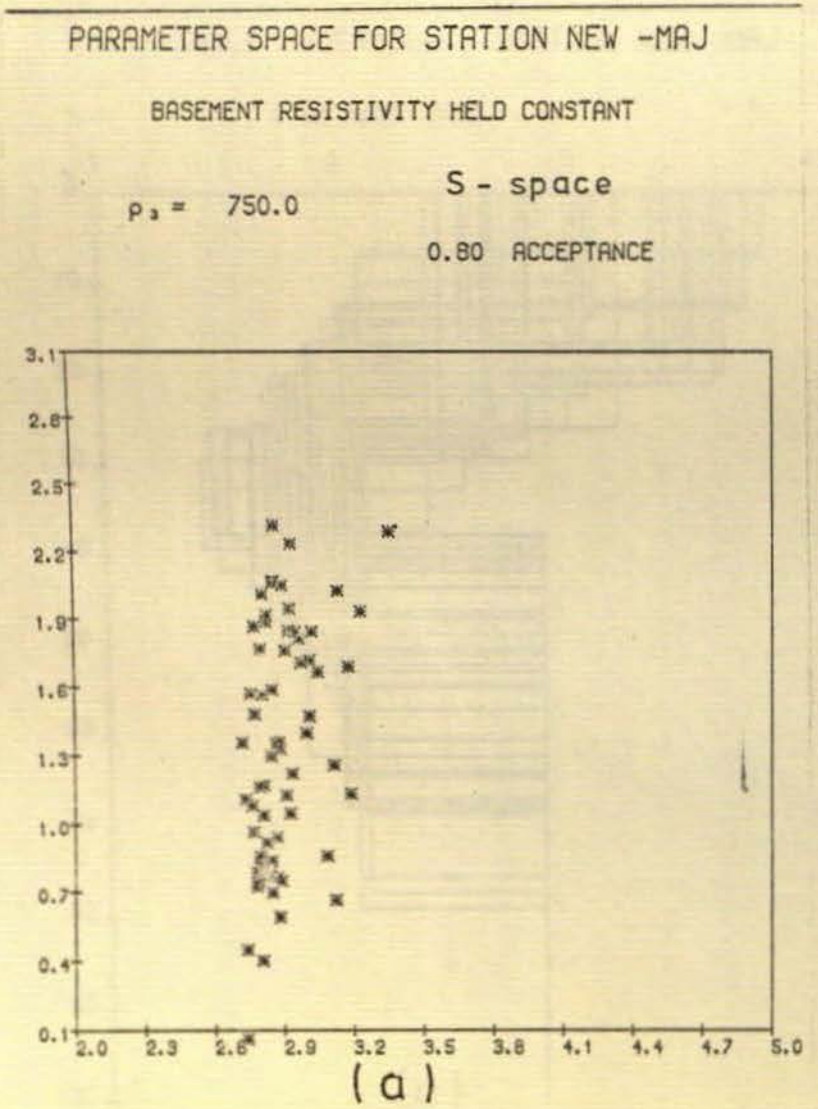

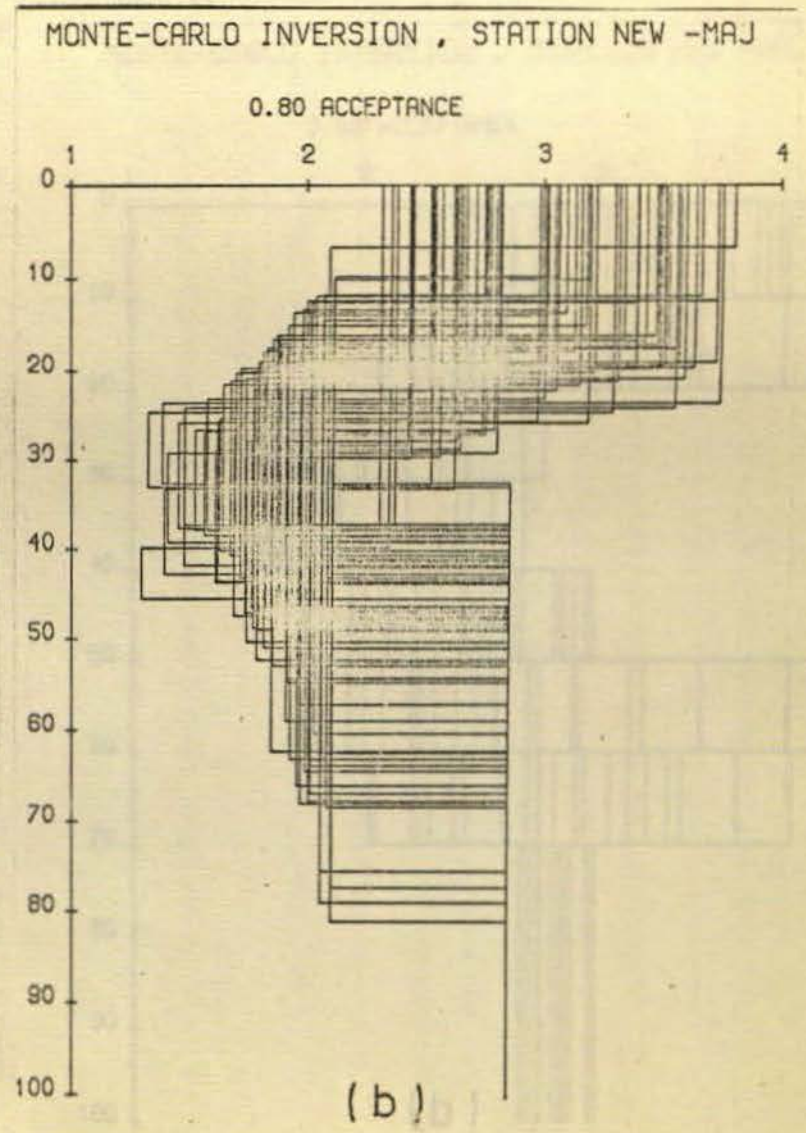

Figure 6.12 Monte-Carlo inversion - NEW major data
acceptance level of 80%
(a) S-space (b) ρ-d profiles

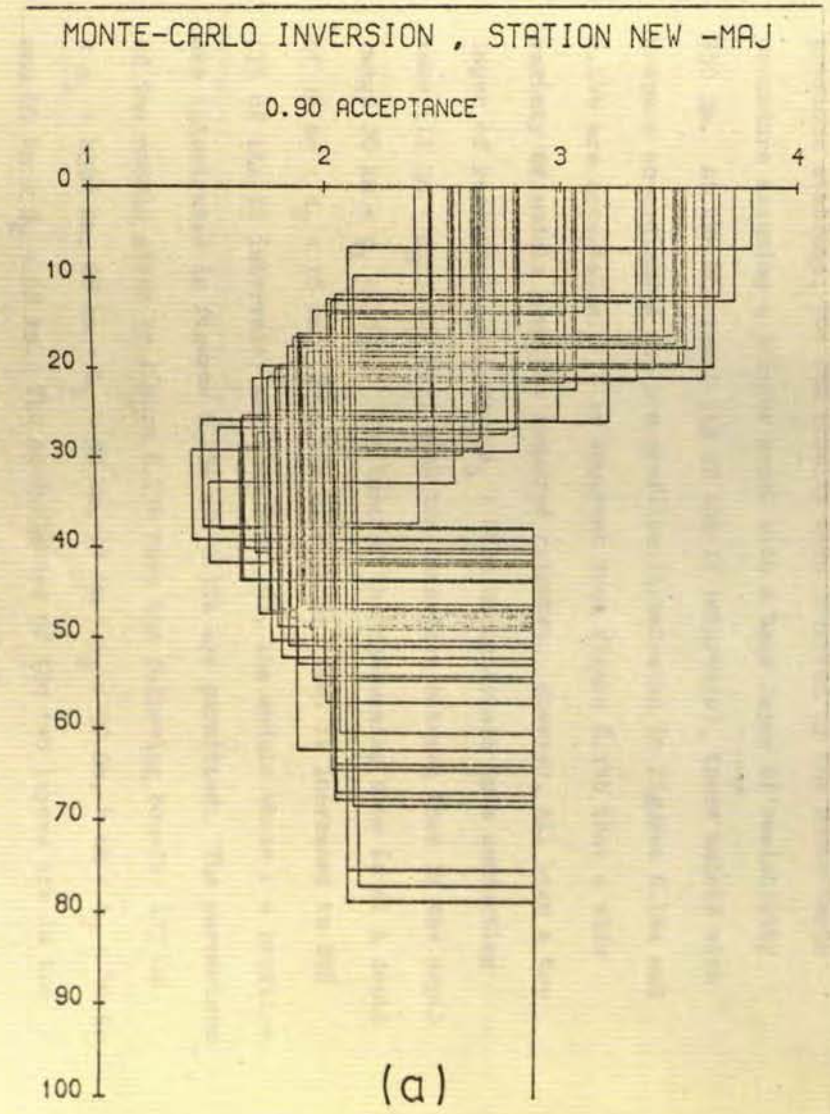

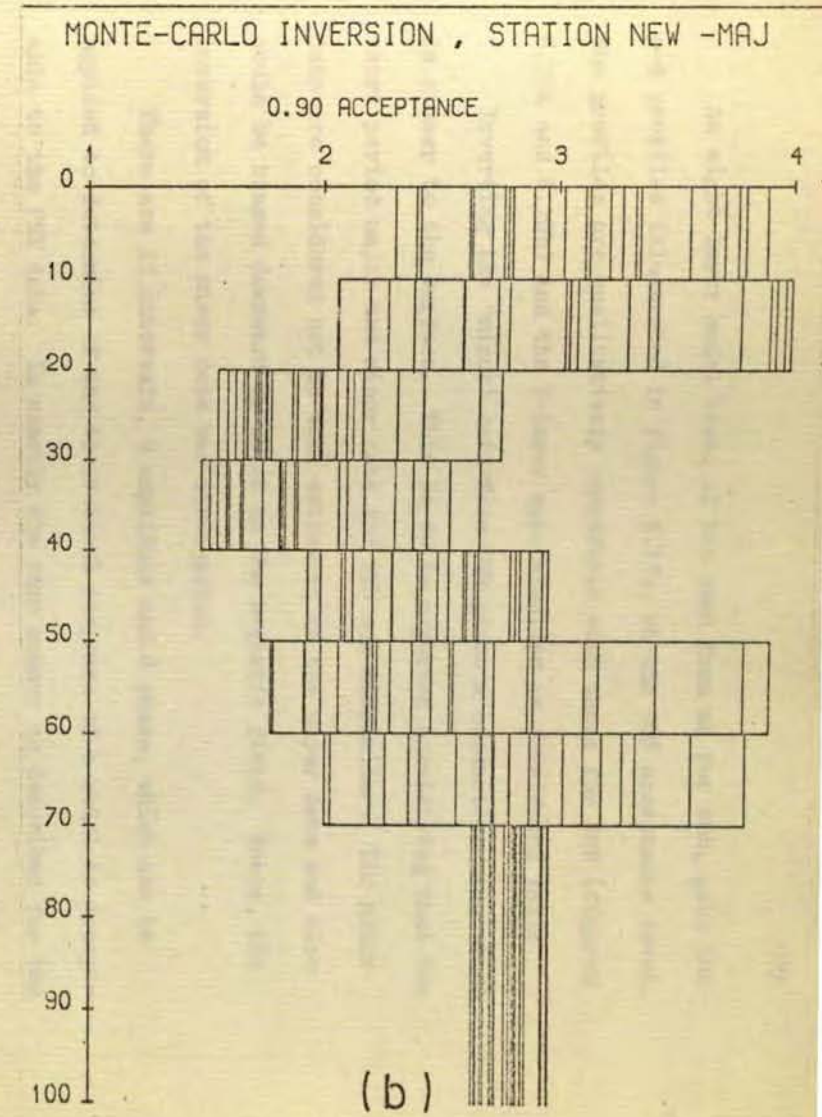

Figure 6.13 Monte-Carlo inversion - NEW major data
ρ-d profiles of
(a) 3-layer models, acceptance level 90%
(b) 8-layer models, acceptance level 90%

An eight-layer model test, of the same form as for BOR, gave the ρ-d profiles illustrated in figure 6.13b, at the 90% acceptance level. The profiles are qualitatively comparable with those for BOR (figures 6.10a and 6.10b) and the 3-layer approximation is considered valid.

Inverting the 'minor' data from NEW gives a conducting zone which is closer to the surface. This is to be expected considering that the short period major and minor data for NEW are dissimilar. The minor data are considered not as well estimated as the major data and also could be biased downward by noise on the magnetic field. Hence, the inversion of the minor data was disregarded.

There are 17 intervals, 9 amplitude and 8 phase, which can be applied to determine if the theoretical responce of a model is acceptable to the PRE data. In exactly the same manner as described for the previous stations, the PRE results were inverted by the Monte-Carlo procedure assuming a 3-layer model with a base layer of resistivity 750 Ωm. At the 80% level (14 of the 17 intervals), those models with S-space co-ordinates and ρ-d profiles illustrated in figures 6.14a and 6.14b are acceptable. It is apparent from figure 6.14b that a wide variety of models give the required response. However, all have a top layer of resistivity 250 Ωm $< \rho_1 <$ 8700 Ωm underlain by a conducting zone (11 Ωm $< \rho_2 <$ 100 Ωm), with the interface between them in the depth range 20 km $< d_1 <$ 55 km. The base of the conducting zone is at a depth of 38 km $< d_2 <$ 78 km. When the acceptance level is increased to 89% (15 of the 17 intervals) and then 94% (16), the models whose ρ-d profiles are illustrated in figures 6.15a and 6.15b are permitted. The parameters of the models given by figure 6.15b have the following bounds: 425 Ωm $< \rho_1 <$ 4000 Ωm, 28 km $< h_1 <$ 50 km, 17 Ωm $< \rho_2 <$ 90 Ωm, 4 km $< h_2 <$ 40 km and 40 km $< d_2 <$ 68 km. The conductances of the two layers are in the range 10 S $< S_1 <$ 125 S and 630 S $< S_2 <$ 2000 S.

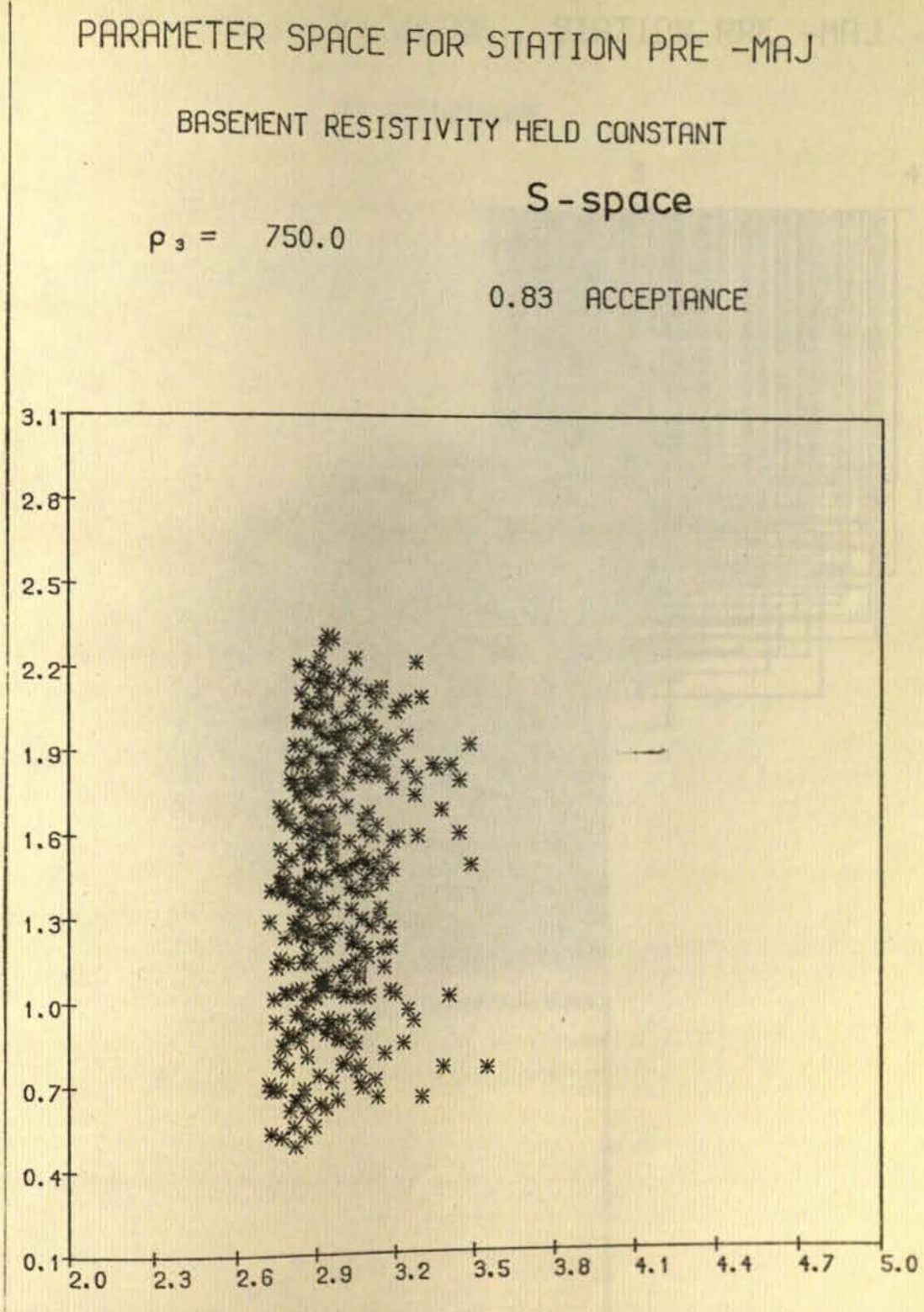

Figure 6.14a Monte-Carlo inversion - PRE major data
S-space for acceptance level of 83%

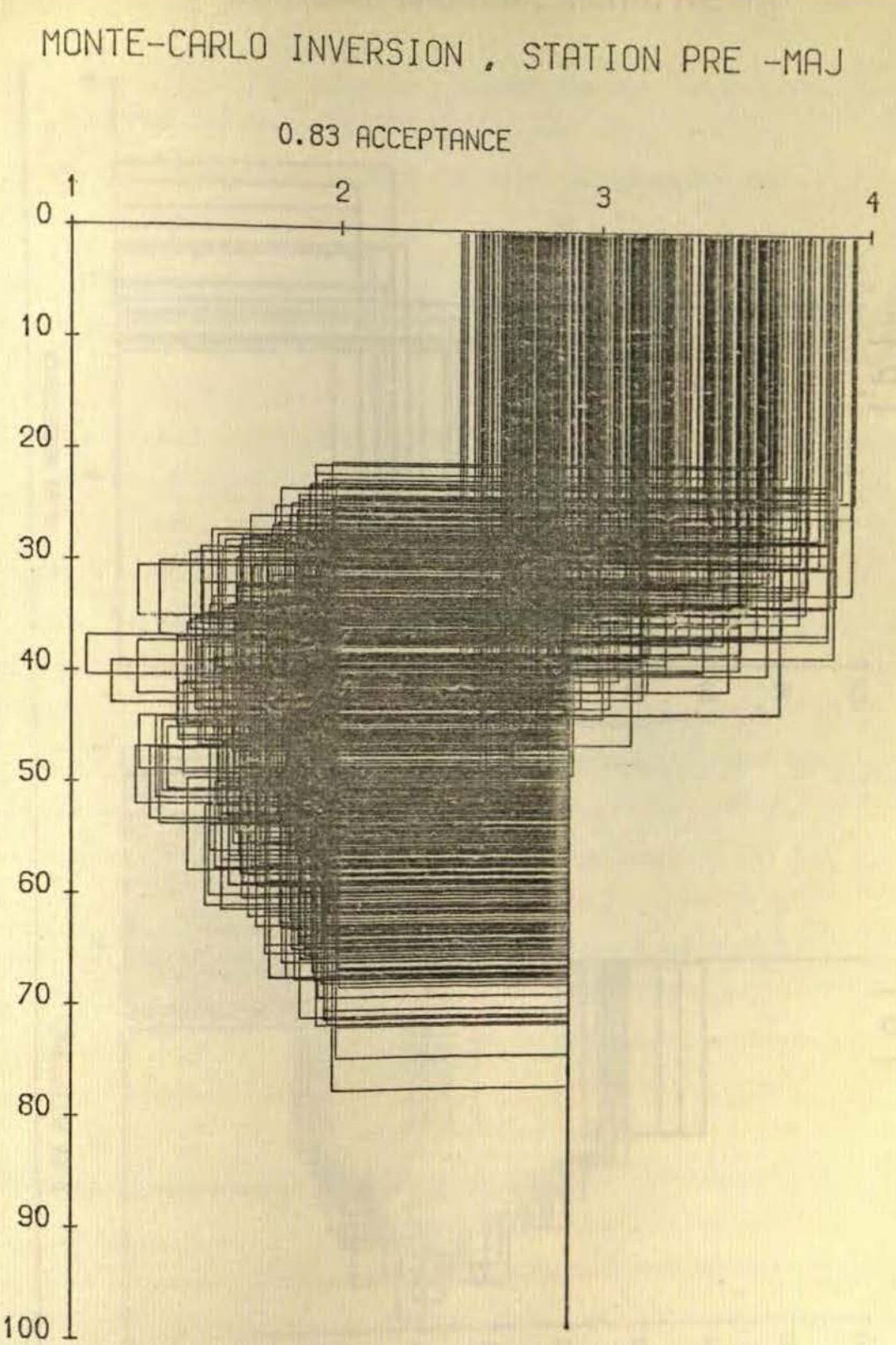

Figure 6.14b Monte-Carlo inversion - PRE major data
ρ-d profiles for acceptance level of 83%

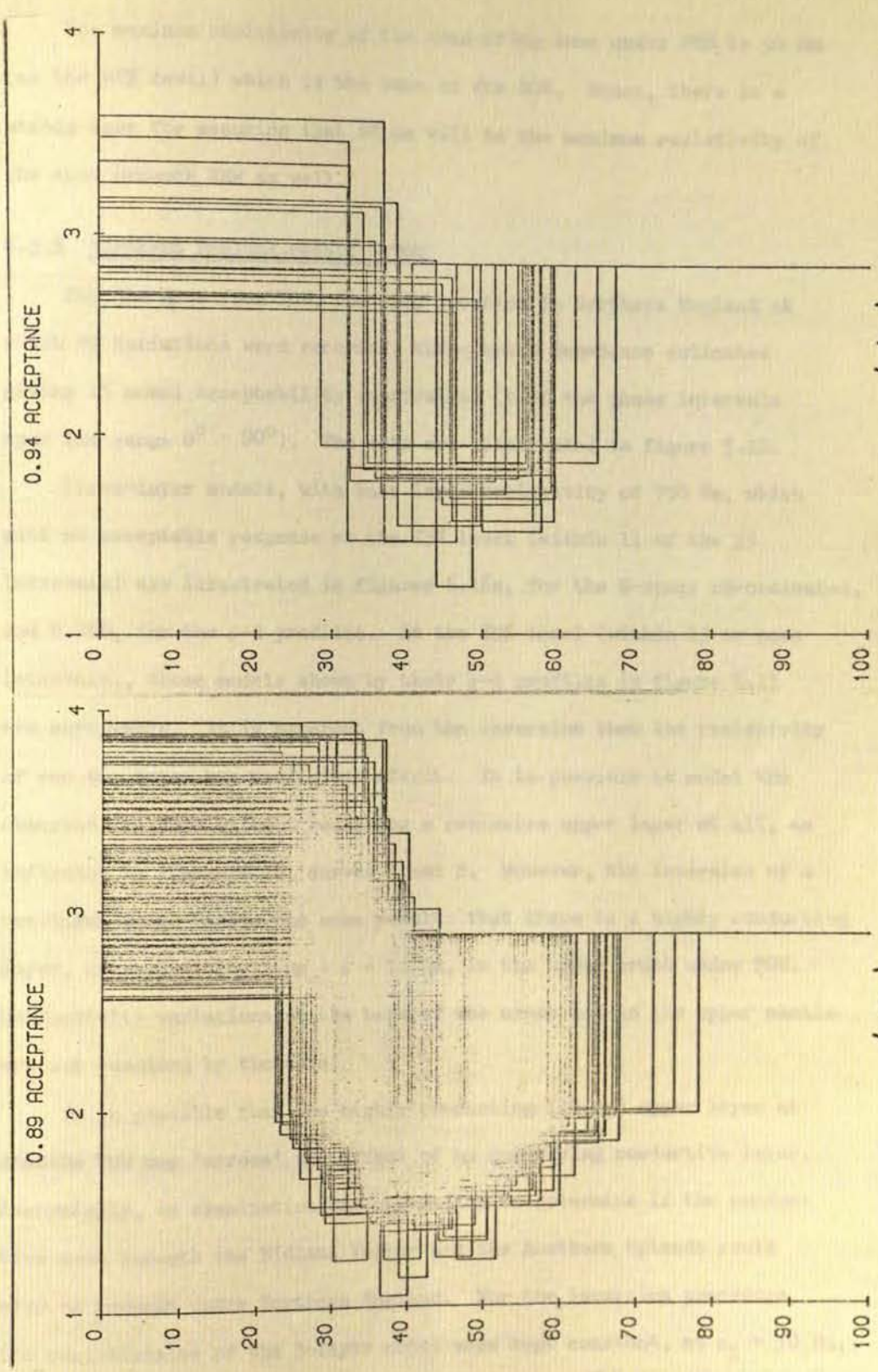

Figure 6.15 Monte-Carlo inversion - PRE major data
ρ-d profiles for an acceptance level
(a) 89% & (b) 94%

The maximum resistivity of the conducting zone under PRE is 90 Ωm (at the 94% level) which is the same as for BOR. Hence, there is a strong case for assuming that 90 Ωm will be the maximum resistivity of the zone beneath NEW as well.

6.3.3 Northern England result - TOW

For the data from TOW, the only location in Northern England at which MT variations were recorded, there are 9 impedance estimates giving 15 model acceptability constraints (3 of the phase intervals span the range 0^{o} - 90^{o}). The data are illustrated in figure 5.12.

Three-layer models, with base layer resistivity of 750 Ωm, which give an acceptable response at the 75% level (within 11 of the 15 intervals) are illustrated in figures 6.16a, for the S-space co-ordinates, and 6.16b, for the ρ-d profiles. At the 89% level (within 13 or more intervals), those models shown by their ρ-d profiles in figure 6.17 are acceptable. It is apparent from the inversion that the resistivity of the top layer has negligible effect. It is possible to model the observed response without requiring a resistive upper layer at all, as indicated by figure 6.18, curves 1 and 2. However, the inversion of a two-layer model yields the same result: that there is a highly conducting layer, of resistivity 3 Ωm < ρ < 11 Ωm, in the upper crust under TOW. Conductivity variations at the base of the crust and in the upper mantle are not resolved by the data.

It is possible that the highly conducting (10 Ωm) upper layer at station TOW may 'screen' the effect of an underlying conductive layer. Accordingly, an examination was undertaken to determine if the conductive zone beneath the Midland Valley and the Southern Uplands could also be present under Northern England. For the inversion procedure, the resistivities of the 3-layer model were kept constant, at ρ_1 = 10 Ωm,

PARAMETER SPACE FOR STATION TOW -MAJ

BASEMENT RESISTIVITY HELD CONSTANT

ρ_3 = 750.0

0.78 ACCEPTANCE

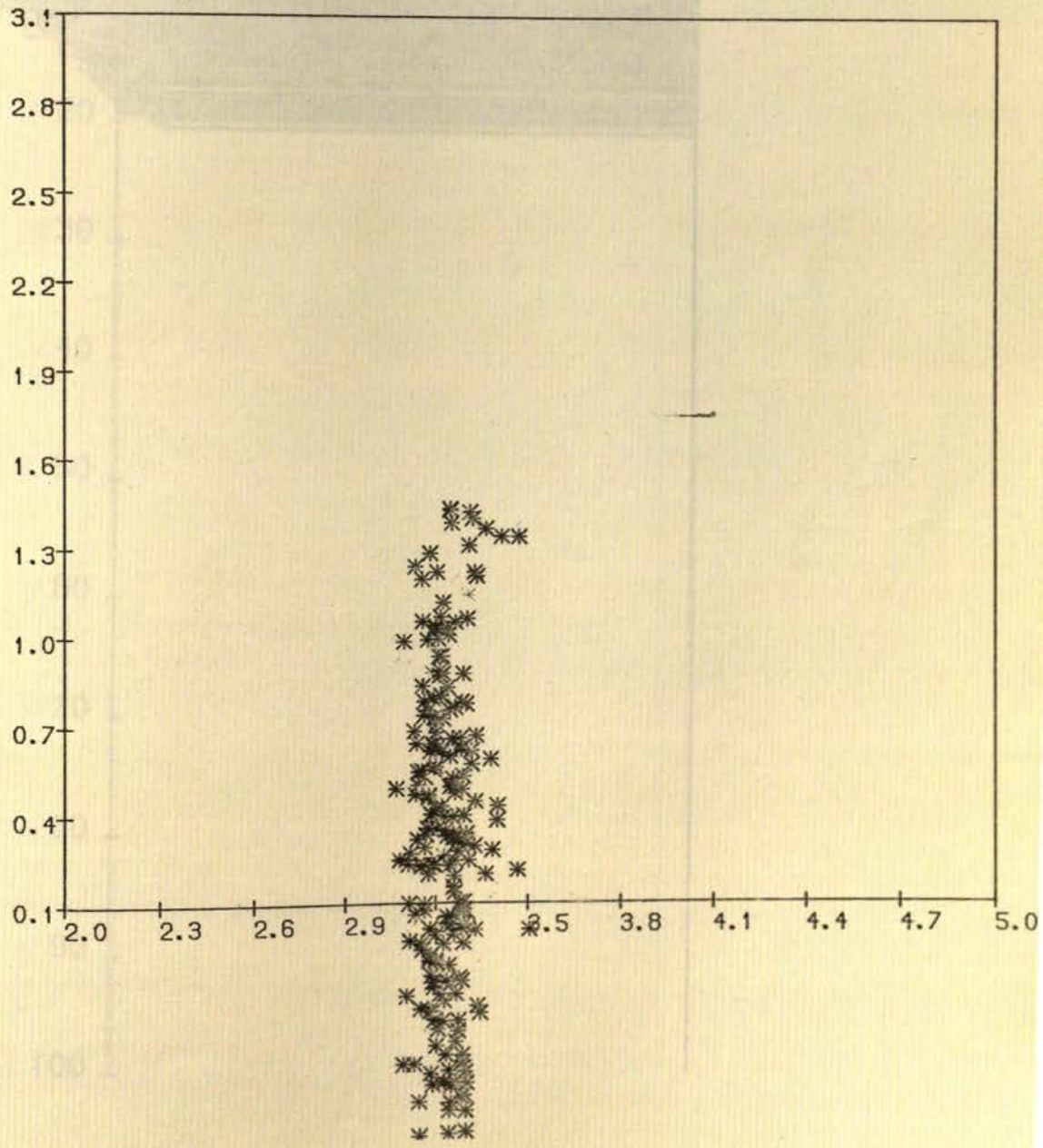

Figure 6.16a Monte-Carlo inversion - TOW major data S-space for acceptance level of 78%

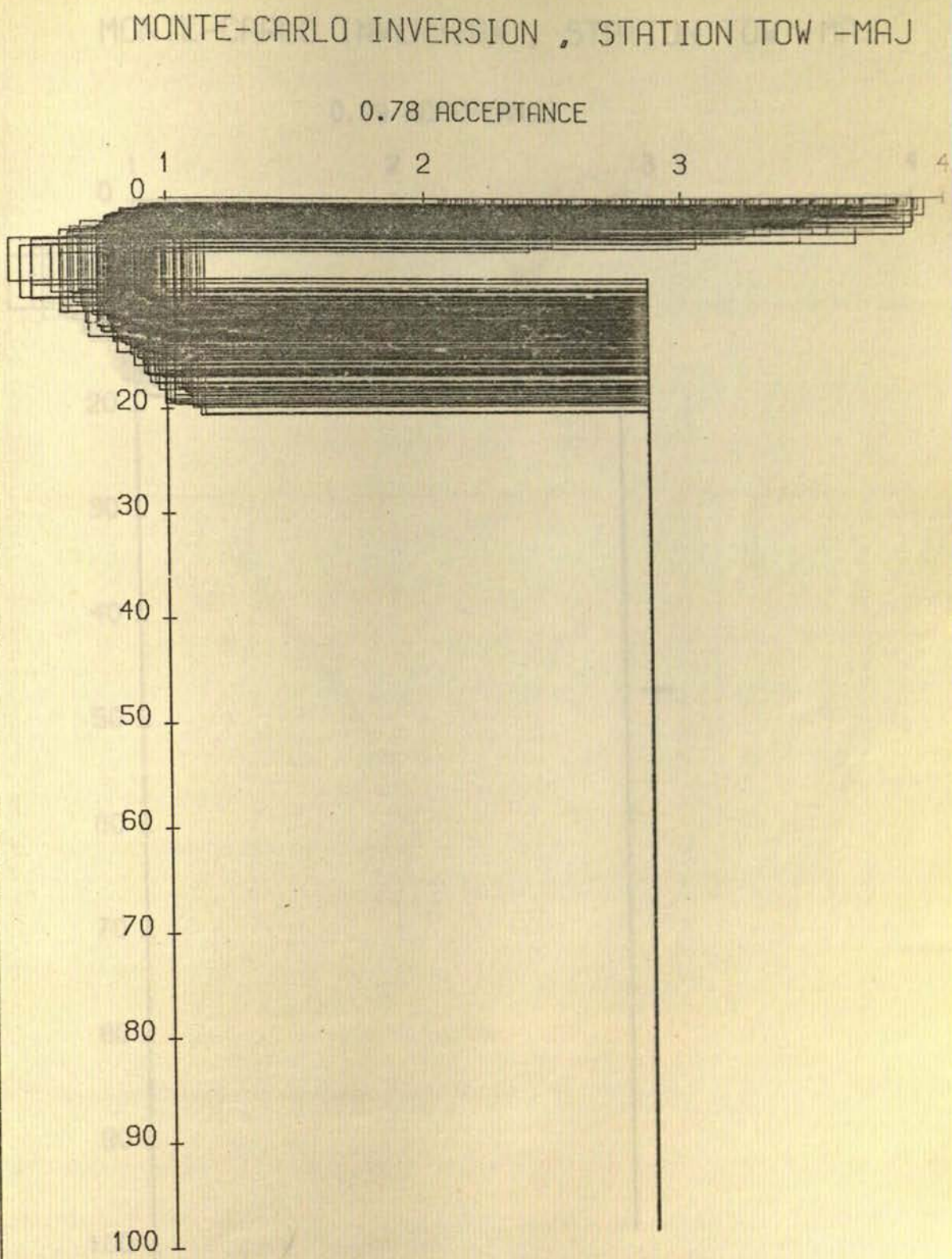

Figure 6.16b Monte-Carlo inversion - TOW major data
ρ-d profiles for acceptance level of 78%

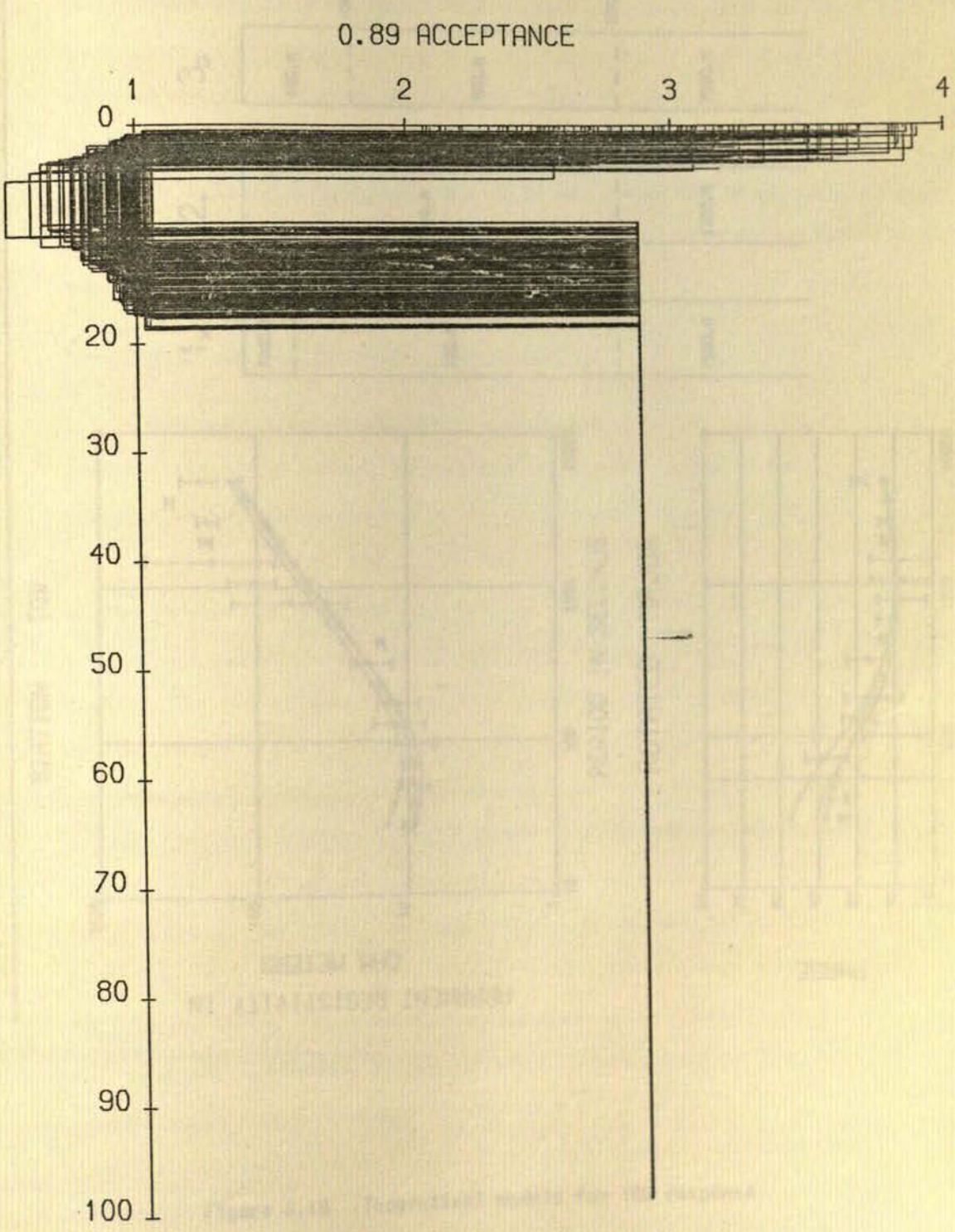

Figure 6.17 Monte-Carlo inversion - TOW major data
ρ-d profiles for acceptance level of 89%

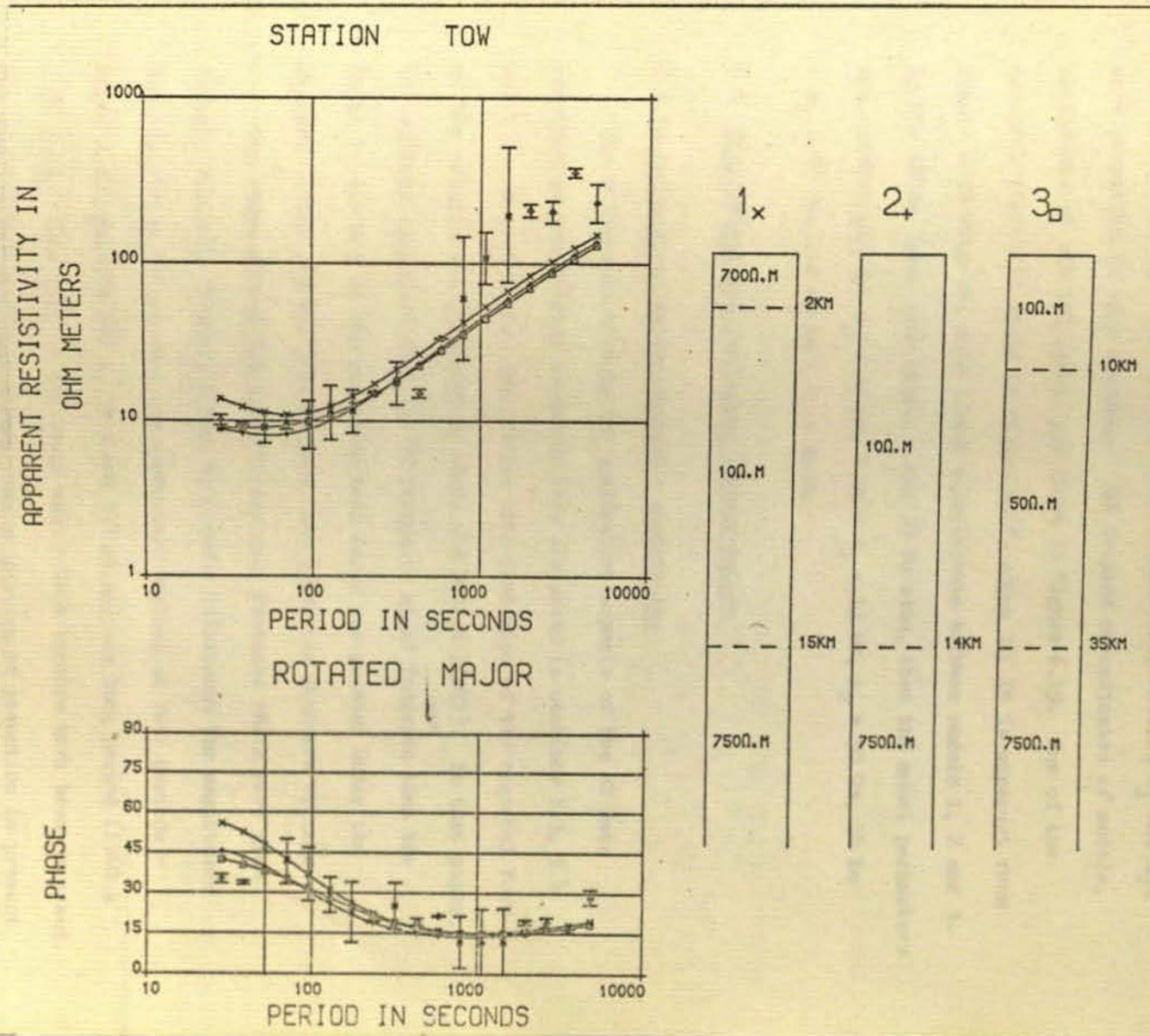

Figure 6.18 Theoretical models for TOW response

ρ_2 = 50 Ωm and ρ_3 = 750 Ωm, and the two-layer thicknesses, h_1 and h_2, were permitted to vary randomly. The d-space co-ordinates of models, acceptable at the 90% level, are shown in figure 6.19. One of the accepted models is shown in figure 6.18, curve 3. It is apparent from figure 6.18 that the data cannot discriminate between models 1, 2 and 3. If the 50 Ωm layer does underlie the 10 Ωm zone, then the model parameters are constrained by: ρ_1 = 10 Ωm, 8 km < d_1 < 13 km, ρ_2 = 50 Ωm, 28 km < h_2 < 40 km and 28 km < d_2 < 40 km.

6.4 Geophysical and Geological Interpretation

6.4.1a Geophysical interpretation - qualitative

The difference between the qualitative aspects of the MT data recorded at the various locations were discussed in sections 5.3, 5.4 and 5.5. A preliminary qualitative interpretation of the regional form of the results was presented by Jones and Hutton (1977). In that paper, the authors suggested that the MT responses might indicate that the depth to the top of the resistive base layer was greater under the Midland Valley and Northern England than under the Southern Uplands.

The short period GDS data display many features which were previously unknown. Figures 6.20a, b, c and d illustrate the magnitudes and directions of the real and quadrature vectors at four periods - three short periods (40 s, 70 s and 129 s) and one long period (1960 s ≡ 32.7 m). Note that in the usual manner both vectors have been reversed. The vectors indicate that a very complex pattern of induction is present in the region. Inclusion of the GDS array results, derived from non-synoptic single event analyses of the GDS data by Dr. D. Rooney, supports the results of the long period single station responses (see Appendix). At a period of 2000 s (figure A1a), the results are fairly consistent with those of Edwards et al. (1970). However, at the shorter

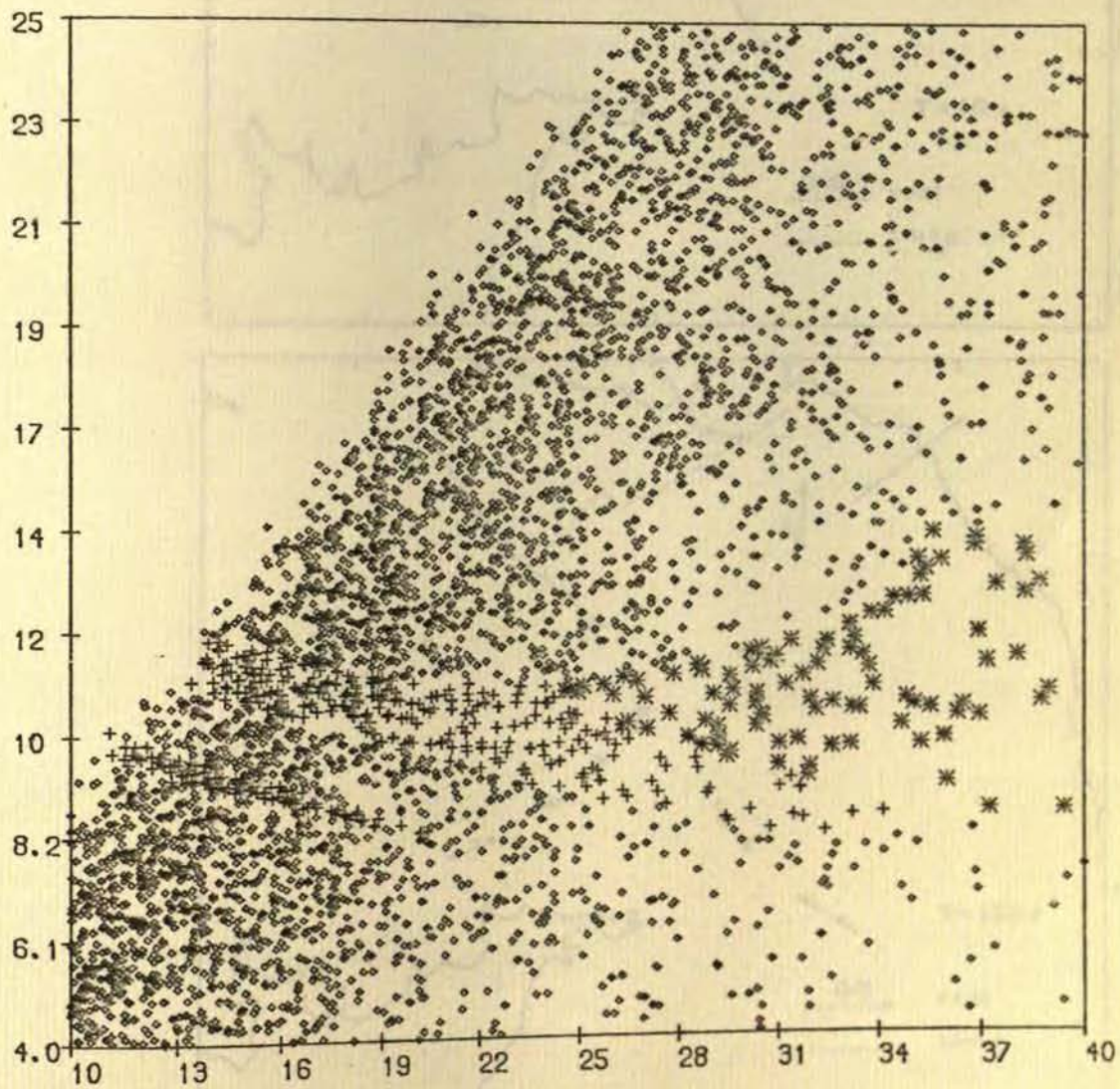

Figure 6.19 Monte-Carlo inversion - TOW major data
d-space for acceptance level of 90%

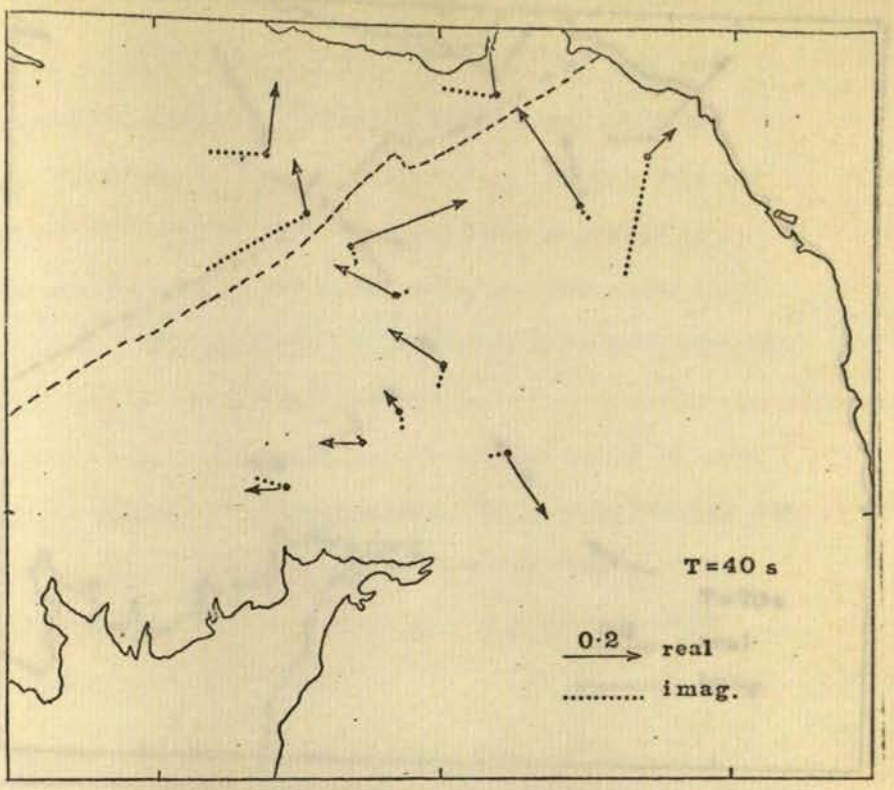

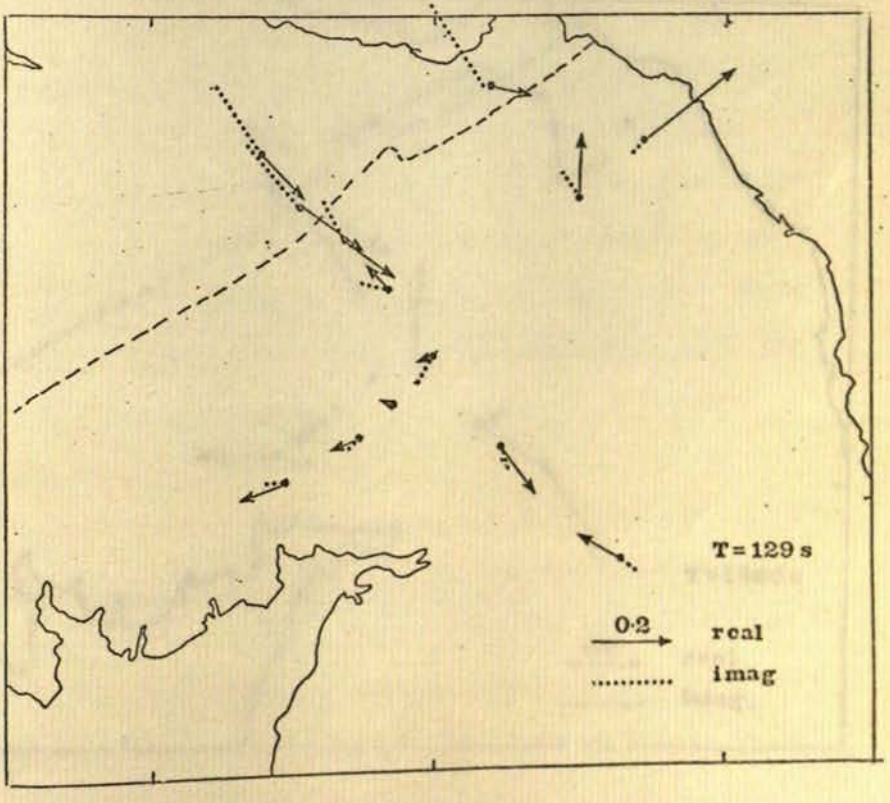

Figure 6.20 Induction vectors for single-station data -both vectors reversed

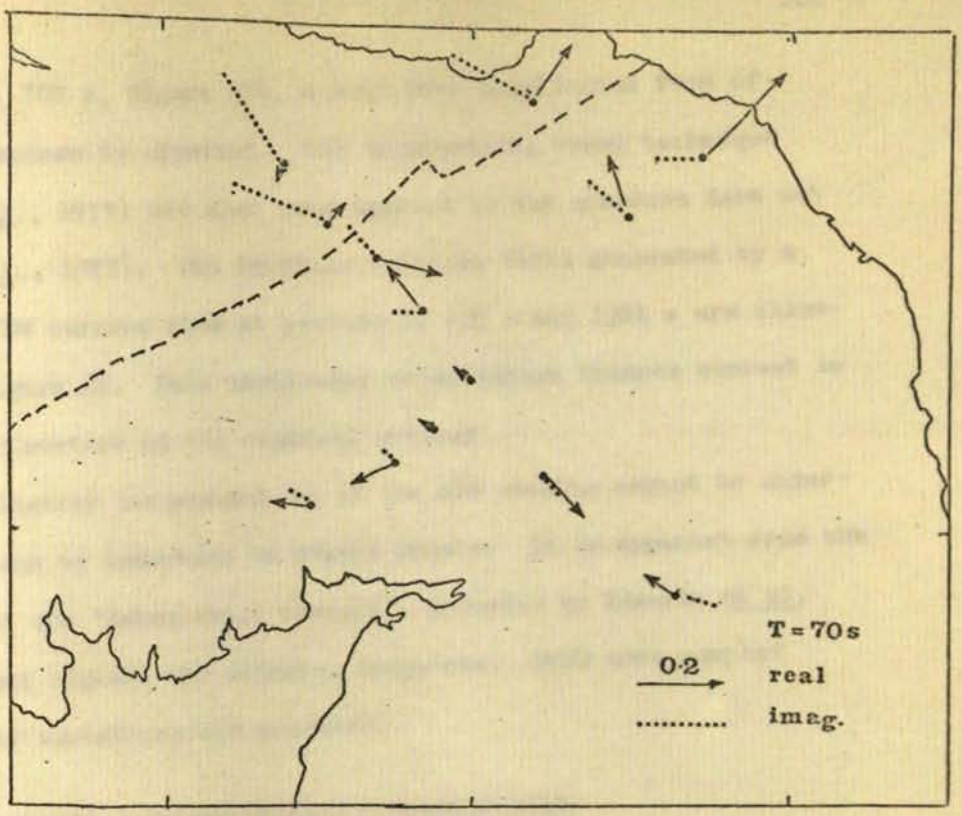

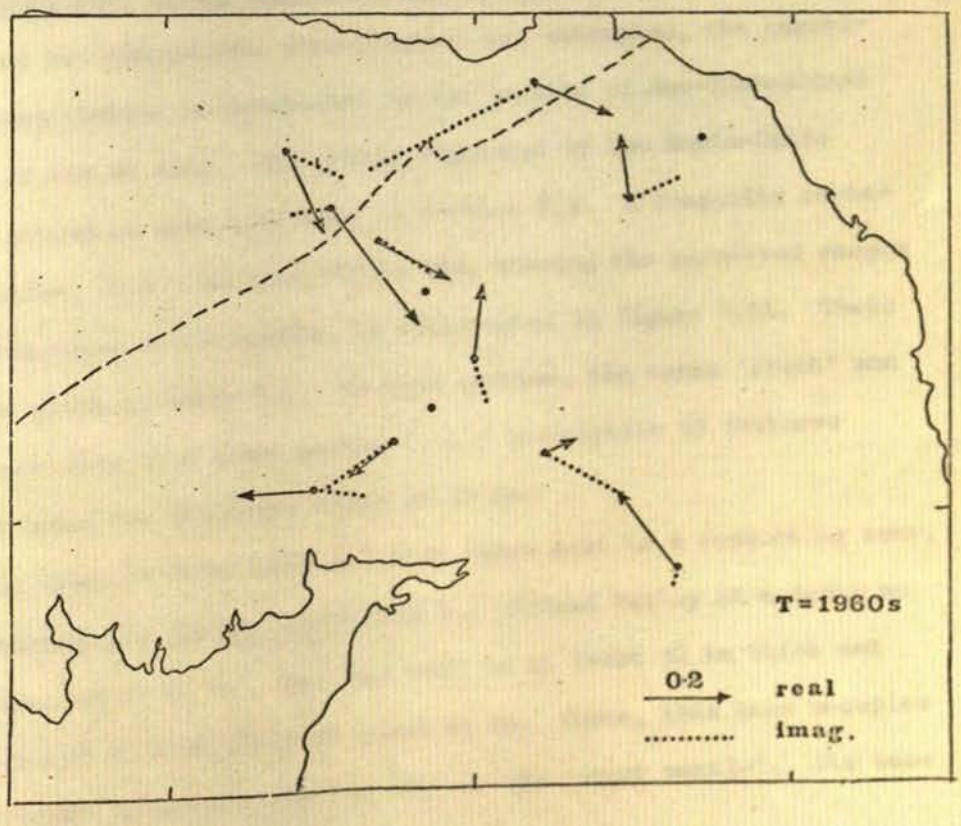

Figure 6.20 (cont) Induction vectors for single-station data -both vectors reversed

periods, e.g. 700 s, figure A1b, a much more complicated form of induction response is apparent. The hypothetical event technique (Bailey et al., 1974) has also been applied to the combined data set (Hutton et al., 1977). The in-phase vertical field generated by a regional NE/SW current flow at periods of 236 s and 1961 s are illustrated in figure A2. This particular polarisation induces current in the strike direction of the regional geology.

A qualitative interpretation of the GDS results cannot be undertaken in terms of induction in simple models. It is apparent from the figures that the 'Eskdalemuir anomaly', proposed by Edwards et al. (1971) cannot explain the observed responses. Much more complex conductivity variations are required.

6.4.1b Geophysical interpretation - quantitative

Because two-dimensional modelling was not attempted, the quantitative interpretation is restricted to the results of one-dimensional inversion of the MT data. The models suggested by the Monte-Carlo inversion procedure were discussed in section 6.3. A composite resistivity section, on a line from FTH to TOW, showing the permitted ranges of the parameters of the models, is illustrated in figure 6.21. These ranges are given in table 6.1. In this section, the terms 'crust' and 'mantle' are used in a loose manner to aid description of features above and below the arbitrary depth of 30 km.

It is apparent from table 6.1 that there must be a conducting zone, of resistivity 35 - 60 Ωm, underlying the Midland Valley at a depth no greater than about 12 km. The zone must be at least 32 km thick and it must extend to a depth of at least 44 km. Hence, this zone occupies all the 'lower crust' and the top part of the 'upper mantle'. Its base is not well resolved by the data.

Figure 6.21 Resistivity cross-section from station FTH to station TOW.

The permitted ranges of the model parameters for a three-layer model fit to the 'rotated major' data from the locations FTH,SAL,BOR, PRE,NEW & TOW are shown

The conductive zones are indicated by circles.

The zone under TOW cannot be resolved and hence is questionable.

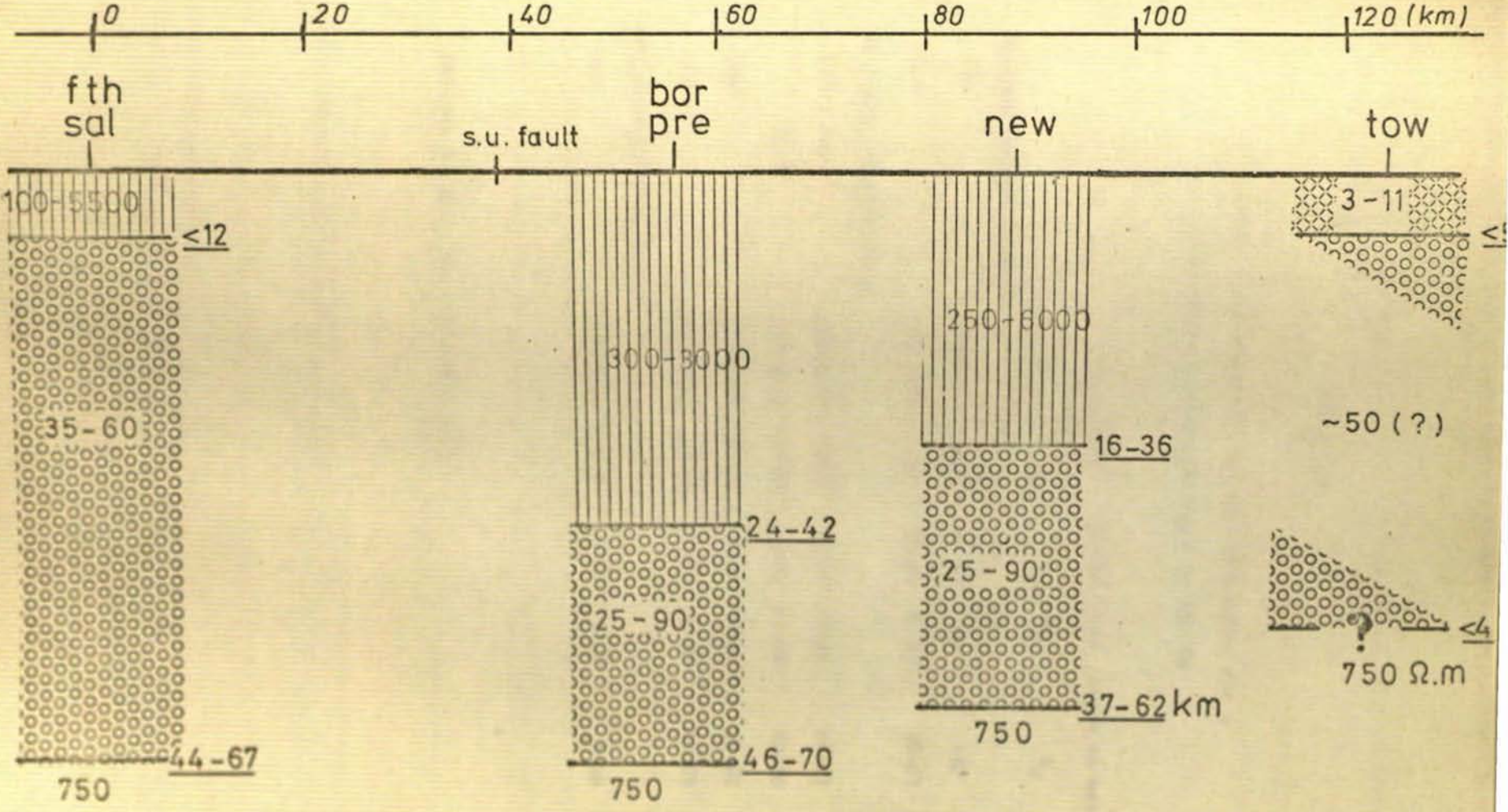
0
20
40
60
80
100
120 (km)
fth
sal
s.u. fault
bor
pre
new
tow
100-5500
<12
35-60
44-67
750
300-3000
24-42
25-90
46-70
750
250-6000
16-36
25-90
37-62 km
750
3-11
~50 (?)
<4
?
750 Ω.m

TABLE 6.1

Permitted layer resistivities and thicknesses for a 3-layer model with a base layer of 750 Ωm

	First Layer		Second Layer		Depth to basement
	ρ_1	h_1	ρ_2	h_2	d_2
Midland Valley Sites					
FTH	100-5500	<11	25-60	>21	>32
SAL	125-7500	<13	35-70	32-63	44-67
Southern Uplands Sites					
BOR - maj	300-3000	24-42	20-90	10-54	46-77
min*	250-3250	18-50	20-90	11-58	42-76
NEW*	250-6300	16-37	25-90	9.46	37-62
PRE	400-4000	28-50	17-90	4-40	40-68
Northern England Sites					
TOW	120-8000	0.5-5	3-11	9-19	5-19

* Reduced ranges, see text for details.

There is also a conducting zone underlying the Southern Uplands, with a resistivity of 25 Ωm < ρ < 90 Ωm. Under BOR and PRE, which lie on a line of geological strike, this zone is at a depth greater than 28 km. Therefore, the crust under these sites is resistive and the upper mantle conductive. There is some evidence that the zone may become shallower to the south-east because its top interface is permitted to be as close as 16 km to the surface under NEW. The maximum permitted depth of the base of the zone under all three of these stations is of the order of 65 - 75 km.

Whether the conducting zone under the Midland Valley is due to the same conditions that cause the low resistivities under the Southern Uplands cannot be confirmed, or otherwise, from this analysis. However, there is a high probability that the two are related because of their similar resistivities.

There are many possible causes for low resistivity zones at lower crustal/upper mantle depths. As stated in the introduction (section 1.3), the suggestion most usually given for such a zone in the crust is hydration processes, with or without associated partial melting. A temperature of greater than 950 K is required to partially melt rocks under water-saturated conditions in the crust. Hence, partial melting at the crust-mantle interface generates a geothermal gradient in the crust in excess of 20 K km^{-1}. This would normally result in an above average heat flow. Only one heat flow measurement has been taken in the area but which is suspect because it was taken down a mineshaft. It is a value of 1.85 HFU (Osemeikhan and Everett, 1968), taken near Glasgow, which is higher than the average continental value of 1.2 HFU. However, the conducting zone is considered to be within 12 km of the surface. If partial melting were responsible for the low resistivities at these shallow depths, a geothermal gradient of greater than 60 K km^{-1}

would normally exist. Such a high gradient would usually generate hot springs, as in Iceland. These however, are not observed. Hence, hydration processes are probably responsible for the conducting zone at shallow depths under the Midland Valley.

It is possible that partial melting of the hydrated rocks could be responsible for the observed low resistivities at upper mantle depths under both the Midland Valley and the Southern Uplands. A partial melt might also explain why Bamford and Prodehl (1977) did not observe clear arrivals from the Moho when they analysed the LISPB seismic data for the region (Bamford et al., 1976). However, as stated by Duba (1976), many conducting phases, about which little is known, may be possible in the upper mantle.

The conducting zone under Northern England, as detected by the data from TOW, is very different in character from that under the other stations. It is apparently in the upper crust and has a conductivity which is an order of magnitude greater than the other conducting zone(s). It is possible that this zone could 'screen' an underlying layer of resistivity the same as that for the zones under the Midland Valley and the Southern Uplands, i.e. 20 - 90 Ωm. This would provide continuity of the same zone under these regions to the south to underlie Northern England. However, this feature cannot be resolved by the data so its assumption is unjustifiable. The most likely explanation for a highly conducting zone ($\sigma \sim 0.1$ S m^{-1}) in the upper crust is electrolytic conduction in the water-saturated sediments which infill the Northumberland Basin. This basin is known to extend to a greater depth than 3 km. The 'graben-like' feature of the conducting basin could also account for the predominant magnetic field polarisation in a NS orientation, as shown by Reddy and Rankin (1972).

It is obvious from table 6.1 that the preliminary qualitative interpretation of the MT data (Jones and Hutton, 1977), based on the apparent resistivity data only, cannot be proven or otherwise. The different responses, observed for amplitude and phase data recorded in each of the three regions, are due to the top of the conducting zone being closer to the surface, rather than its base being deeper, under the Midland Valley than the Southern Uplands.

It is difficult to reconcile the GDS data with the quantitative interpretation of the MT data.

Many effects are exhibited by the GDS induction vectors which cannot be explained by the generalised cross-section shown in figure 6.2.1. Work is in progress at this time (Hutton et al., 1977) to combine the results from the two methods - MT and GDS.

An examination was made to discover if the data resolved any of the olivine phase transformations discussed in section 1.3. The longest period at which estimates of the impedance were made were from data recorded at NEW. Well-estimated resistivities and phases for periods up to 2000 s were obtained from the NEW records. A three-layer model, whose theoretical response is very close to the observed response, is illustrated, together with its response and the data from NEW, in figure 6.22 (model 1). The responses of three models, with their upper layers as for model 1 but with a base layer of 1 Ωm at 400 km, 600 km and 800 km, were calculated and were compared with the observational data. It is apparent from their responses, shown in figure 6.22 as curves 1, 2 and 3, that the well-estimated data (those plotted with asterisks) cannot resolve the deep structure. However, if all the estimates are considered, it appears that the transition to a high conducting zone must be at some depth greater than 800 km. A conducting zone at such depths satisfies both the amplitude and the phase long

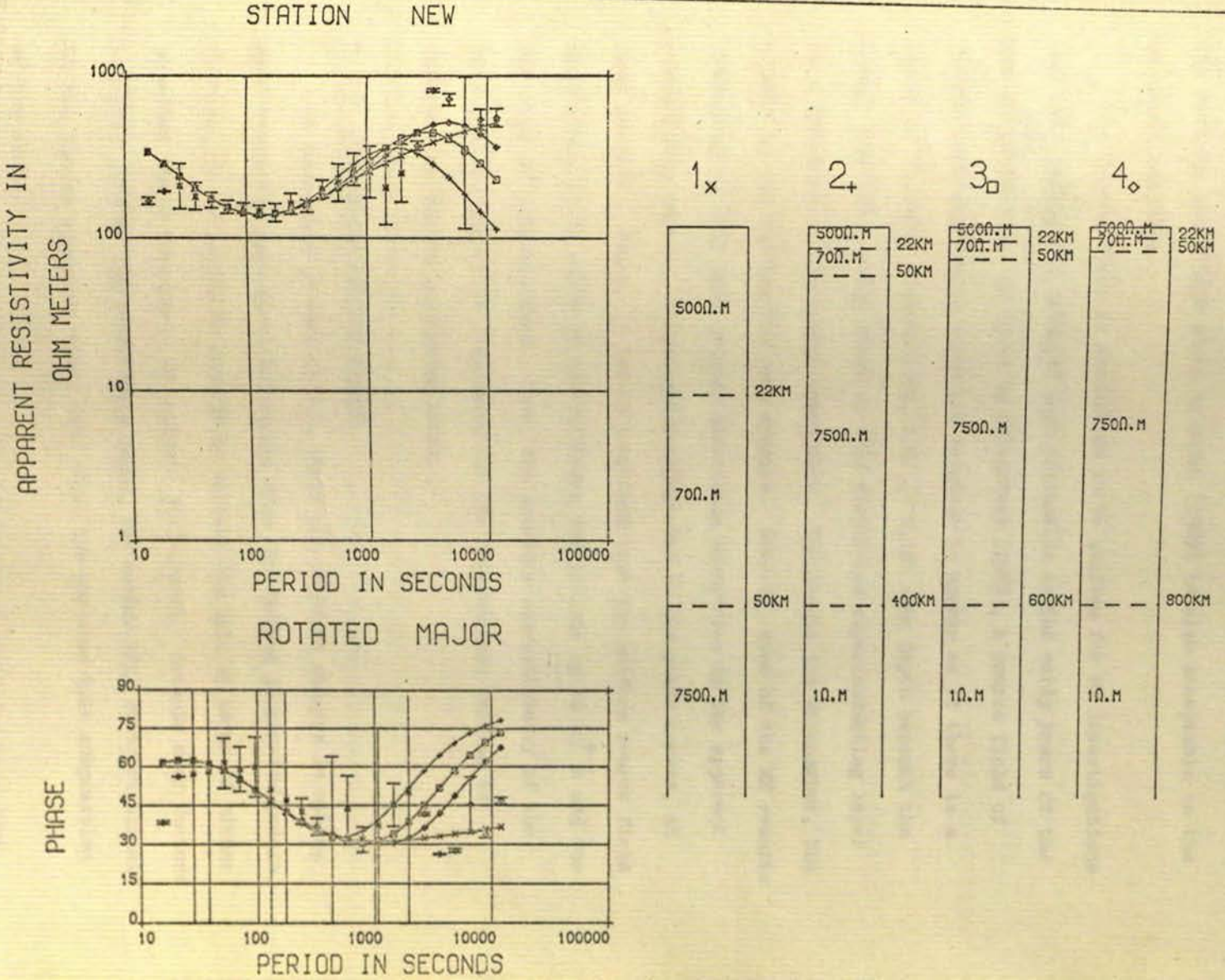

Figure 6.22 Theoretical models for NEW response

period responses. A gradational transition over 200 km, suggested as the maximum transition width by Banks (1969) is also acceptable to the observed response.

The source field is considered to be uniform for MT investigations and this assumption prompted much discussion in the early years of the use of the technique. As shown by Srivastava (1965), a source field of finite wavelength will cause the response to appear as if there is a layer of infinite conductivity, i.e. $\rho = 0$, at some depth beneath the site. The interpreted depth of this fictitious superconducting layer is a function of the source wavenumber. The larger the wavenumber, the closer to the surface the zone appears. However, none of the MT results presented in this work display decreasing asymptotes in the apparent resistivity curves, or increasing asymptotes in the phase curves, at long periods. Hence, it can be concluded that the uniform source field approximation is valid in mid-latitudes for periods up to 10^4 s and for the type of data analysed. Thus, the possible non-uniformity of the source field cannot be considered for the observations failing to resolve the mantle conducting zones.

6.4.2 Geological interpretation

As discussed in section 6.1, there are inherent dangers in making even tentative geological inferences from the derived geophysical models. However, it is useful to attempt to explain the data in terms of either possible Earth structures or tectonic environment. Because many factors can give rise to low resistivity zones, the author will restrict himself to the latter approach rather than state the possible bulk composition of the rocks.

The association of the tectonic histories of Eastern Canada with the Southern Uplands has been described by many geologists, and most

recently by Phillips et al (1976). Accordingly, it is useful to compare the results of this study with those of Kurtz and Garland (1976). As discussed in section 1.3 (figure 1.5b), the response observed at station 10 was interpreted by Kurtz and Garland as indicating a conducting crust (45 Ωm) underlain by a resistive upper mantle (5000 Ωm). This interpretation is directly comparable to the accepted models for the structure beneath stations FTH and SAL (figure 6.21), which also indicate a conducting crust underlain at upper mantle depths by a resistive layer. The interpretation of station 14 (figure 1.5b) however, gave a resistive crust (1000 Ωm) underlain by a conducting upper mantle (100 Ωm). This is also the interpretation of the structure beneath the Southern Uplands, i.e. stations BOR, NEW and PRE.

Hence, the conductivity variations beneath eastern Canada can be strongly correlated with those beneath the Midland Valley and the Southern Uplands. If, on this basis, a parallel tectonic development of the two regions can be concluded, then there is strong foundation for proposing that the Iapetus suture zone in Britain is now represented by the Southern Uplands region. This conclusion is drawn because station 14 of Kurtz and Garland lies directly on the line of continuation of the Reach Bay fault in Newfoundland. This fault has recently been shown to be the manifestation of the Iapetus suture in Newfoundland (McKerrow and Cocks, 1977). The natural parallel conclusion that the Iapetus suture zone is represented by the Southern Uplands is contrary to the postulate of Phillips et al. that it is in the region of the Northumberland Basin.

6.5 Conclusions

A number of conclusions can be drawn from this work. The result of paramount importance is that the 'Eskdalemuir anomaly' is not the

simple conductivity structure proposed by Edwards et al. (1971). The existence of much more complex conductivity variations is shown by both the GDS and the MT results.

2. Under the Midland Valley, there is a conducting zone at a depth of no greater than 12 km. The whole of the lower crust, and possibly part of the upper mantle, under stations FTH and SAL is of low resistivity ($35\ \Omega m < \rho < 60\ \Omega m$).

3. In contradiction to the conclusions of Jain and Wilson (1967), the conducting zone underlying the Southern Uplands is at a depth greater than 24 km. Hence, this zone is in the 'upper mantle' and not in the 'lower crust' as was previously conjectured. There is some evidence that the top interface of the zone might become closer to the surface to the south-east, i.e. under NEW. The permitted resistivity of the zone is in the range 25 - 90 Ωm, which is comparable to the permitted resistivity of the zone under FTH and SAL. Whether the two are due to the same dominant conducting mechanisms cannot be evaluated from this study, but their similar resistivities give some weight to such a supposition.

The most likely explanation for the zones are hydration processes in the crust and upper mantle, with possibly associated partial melting at upper mantle depths. These effects must not be exclusively assumed however, because many other conducting phases could give low resistivity in the upper mantle (Duba, 1977) and metamorphic rocks, such as graphitic schists, could give low resistivity zones in the crust. The latter was postulated by Alabi et al. (1975) to explain the North American Central Plains (NACP) anomaly. Partial melting of the rocks at the crust-mantle boundary could explain the 'blurred' Moho observed in the region (figure 1.9) from seismic evidence (Bamford and Prodehl, 1977).

4. Under Northern England, there is a very highly conducting zone ($0.1 < \sigma < 0.35$ S m^{-1}) very close to the surface. This zone is probably due to the conducting sediments which fill the Northumberland Basin. The conducting processes will be dominated by electrolytic conduction in the pore fluid, as given by Archie's Law (equation 1.1). For rocks of conductivity 0.1 S m^{-1}, and probable pore water conductivity of 1 S m^{-1} (Keller, 1966), the required porosity is from 0.1, for $m = 1$, to 0.3, for $m = 2$. This porosity range is acceptable for most limestone and sandstone formations (Keller, 1966). The rocks of the Silurian, Ordovician and Carboniferous systems, which fill the Northumberland Basin, contain vast thicknesses of sandstone (or greywacke) and limestone sediments (Eastwood, 1953). This conducting zone may 'screen' an underlying layer which is the southward continuation of the zone beneath the Midland Valley and the Southern Uplands. However, this feature cannot be resolved by the data.

5. A comparison can be made between the conductivity structure beneath eastern Canada, postulated from MT observations by Kurtz and Garland (1976), and the structure derived in this work (figure 6.21). This comparison supports the view that there was parallel tectonic development of the two regions. This suggests that the Iapetus suture zone in Britain is represented by the Southern Uplands.

6. In this work, the complementary nature of the GDS and MT techniques has been shown. However, the GDS technique mapped the region of 'anomalous' current flow caused by the conductivity structure. The strength of the MT method, in deriving quantitative conductivity profiles, has been proven. Without the MT observations, very different models and conclusions would have been reached.

7. The importance of estimating the phase response has been shown in the modelling studies. It is possible to satisfy the amplitude data

alone without a conducting layer (figure 6.23) but the phase response for such a model is totally unacceptable. The phase response gives better resolution of the surface structure, as shown by Summers (1976) and by section 6.2.4.

8. At the highest frequencies of this study (10^{-2} - 10^{-1} Hz), it is not possible to resolve the surface structure if there are resistive strata close to the surface. The conducting sediments in the Midland Valley are indicated by the short period induction vectors but the thickness of the sediments could not be determined by the MT data. If the upper layers are very conducting, as at TOW, the underlying successions are difficult to resolve.

9. The long period MT data (10^{3} - 10^{4} s) do not indicate the depth to the conducting transition in the upper mantle. There is a suggestion (section 6.4.1b) that the 1 S m^{-1} layer must be at a depth greater than 800 km. However, this is in contradiction to the results of the majority of global geomagnetic studies (see Price, 1970; Banks, 1972; Rikitake, 1973) and hence must be treated with some caution.

10. The response of the MT data at long periods indicates that the source field approximation is valid in mid-latitudes and for the type of activity examined.

11. It has been shown possible to extract information without resorting to 2-dimensional modelling of the data. The rotated major data from sites located sufficiently distant from lateral inhomogeneities can be interpreted in a one-dimensional sense and valid conductivity-depth distributions will result. However, it is extremely important to choose such data with care. It is not meaningful to interpret the data from all locations but only those data which are consistent with their neighbouring stations - or stations in the same region - and which appear reliable.

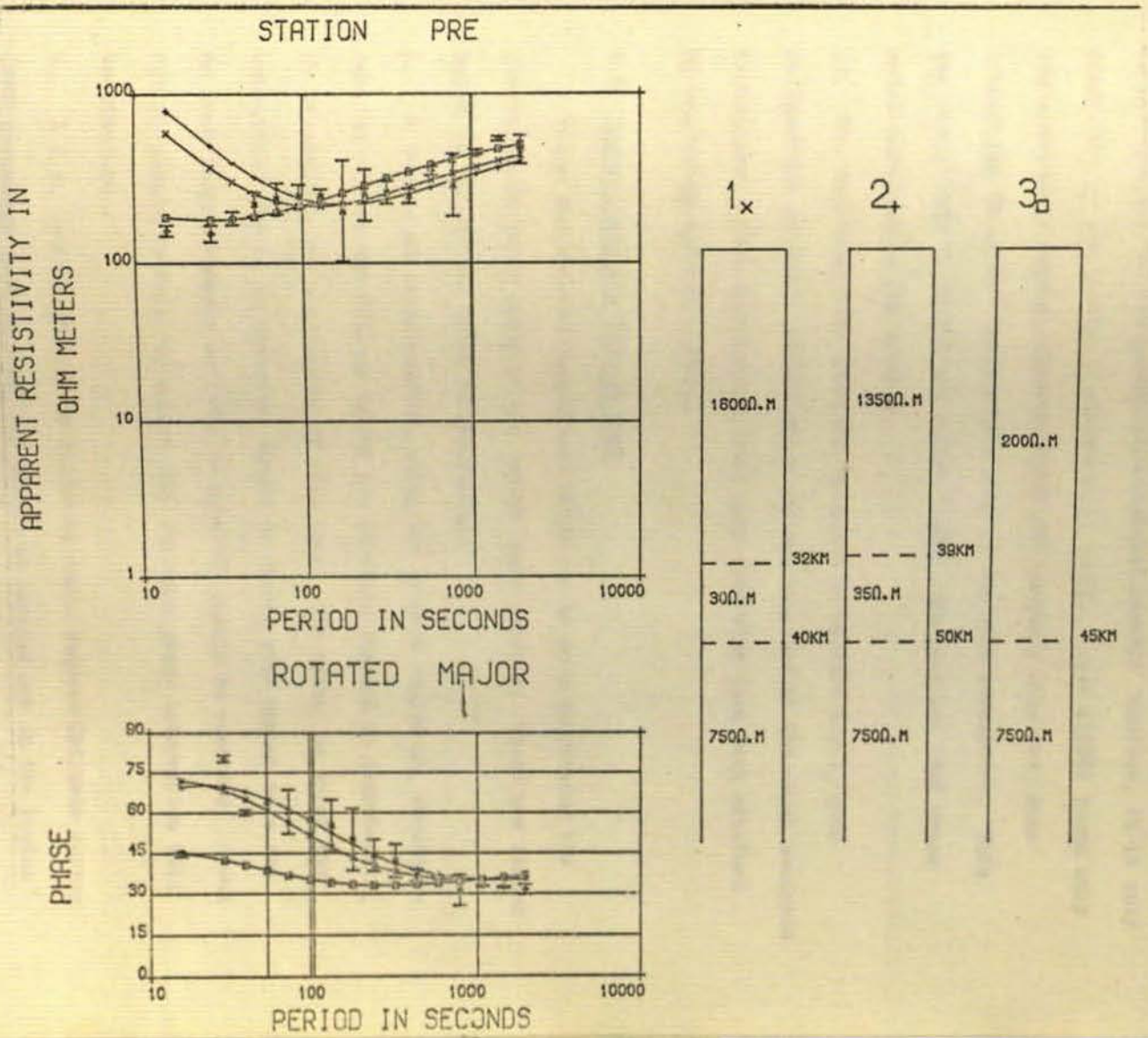

Figure 6.23 Theoretical models for PRE data

12. The Monte-Carlo inversion procedure has been shown to give information regarding the uniqueness of acceptable models. However, it is only feasi ble if the number of variables is small. Press (1968) found only six acceptable models, from the 5,000,000 randomly selected, when attempting to invert seismic data with 23 variable parameters. This was criticised by Haddon and Bullen (1969), who consider that Press under-constrained the problem.

13. The frequency-time analysis, proposed in section 4.3.7, gave information at short periods which was not realised by the usual analysis techniques. Such information could only otherwise have been attained by employing digital filters.

6.6 Suggestions for Further Work

There are various suggestions which can be made concerning the direction in which study of the region could proceed. These are listed below in an advised order of importance.

1. A fuller MT investigation, using the present equipment, should be carried out in the Midland Valley and Northern England to corroborate, or otherwise, the conclusions of this work. The sites, at which the variations are to be measured, should be chosen with utmost care and as much hign frequency activity as possible should be recorded. Great effort should be taken to ensure that reliable phase information will be obtained.

2. A d.c. resistivity survey and/or an Audio Magneto-Telluric survey (AMT frequency band 10 - 10^4 Hz) should be carried out in the region to delineate the upper crustal layers. The resistivity of these layers could then be employed to constrain further the models acceptable to the observed MT responses.

3. The MT results presented in this work should be analysed by the Backus-Gilbert, or closely-related, inversion technique. This is not

to derive the 'optimum' models that satisfy the data, but to investigate the resolution of the data and the possibility that more than three layers should be modelled. As pointed out by Parker (1970), with the Monte-Carlo procedure "it is difficult to be sure that an adequate search has been carried out and, more importantly, very little understanding is gained of the fundamental problems".

4. More sections of the data obtained for this study should be analysed. This would lead to smaller confidence intervals and hence more well-defined conductivity profiles.

5. Two-dimensional modelling of the data should be undertaken to examine the GDS responses for various models. Only the gross features of the data should be modelled as the finer details do not warrant the prohibitively high computing costs of running the programs.

6. Heat-flow measurements should be undertaken to determine if there is a high heat flow in the region, as suggested by the one measurement taken (Osemeikhan and Everett, 1967). High heat flow might be expected in the Midland Valley if the conducting zone is partly due to partial melting of the rocks.

It is the opinion of the author that the data analysis procedures given in chapter 4 are sufficiently advanced not to warrant further sophistication. It may be possible that some of the acceptance criteria, particularly the minimum power level requirement, are too severe. However, the author considered it better to err on the side of caution.

APPENDIX

The preliminary analysis of the GDS array data is described in section 4.2 and the results are presented in section 5.1. A full analysis was not undertaken by the author because the main objective of the research was the application of the MT technique.

The data processing of further events from the array records has been continued by Dr. Rosemary Hutton and Dr. Dennis Rooney. The advantages of analysing variations recorded simultaneously at an array of magnetometers are apparent from many papers published on the subject. However, intermittent recording by a few instruments made this objective difficult. It was decided that more information could be gained by treating the data in a non-synoptic manner. Accordingly, record sections were chosen and analysed in the same way as for single-station data.

The in-phase induction vectors determined at periods of 750 s and 2000 s by this analysis are illustrated in figures A1.1a and A1.1b. The real vectors from the MT stations are also included in the figure. The results from the two studies appear to be in agreement. A very complex pattern of induction which was previously unknown is shown by the vectors.

The derived GDS response functions have also been analysed employing the Hypothetical Event Technique of Bailey *et al.* (1974). The in-phase vertical fields generated by a regional NE/SW current flow at periods of 236 s and 1960 s are illustrated in figures A1.2a and A1.2b.

A tentative interpretation of these results has been presented recently by Hutton *et al.* (1977).

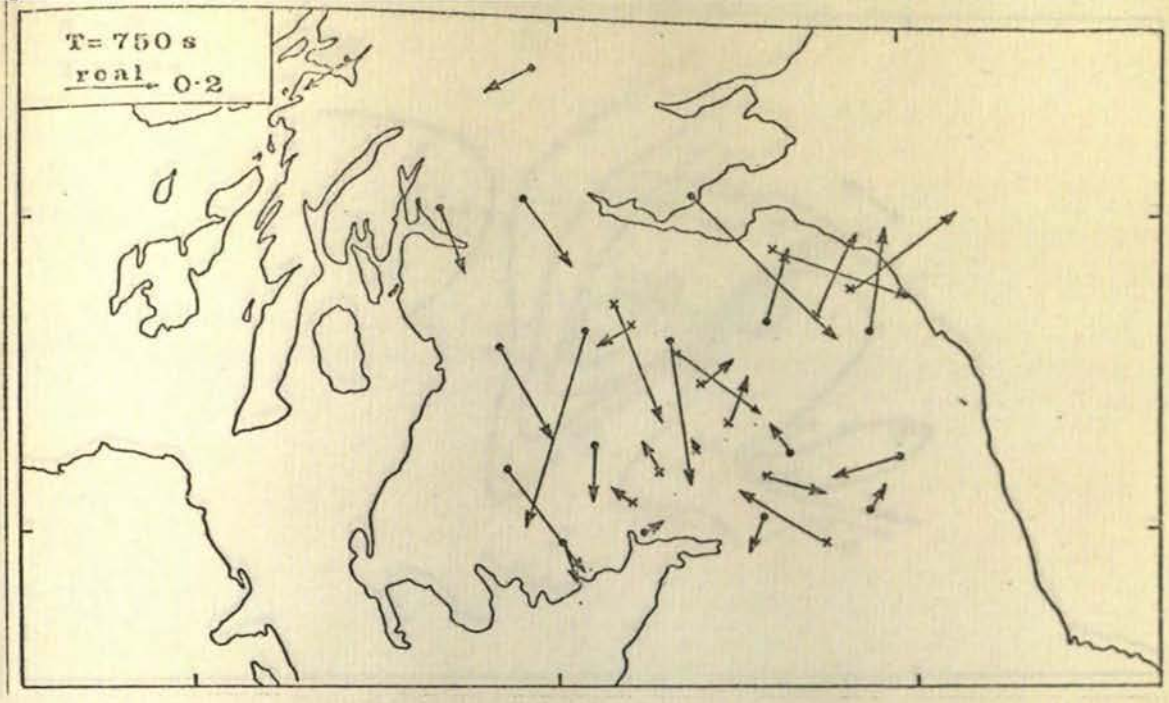

(a)

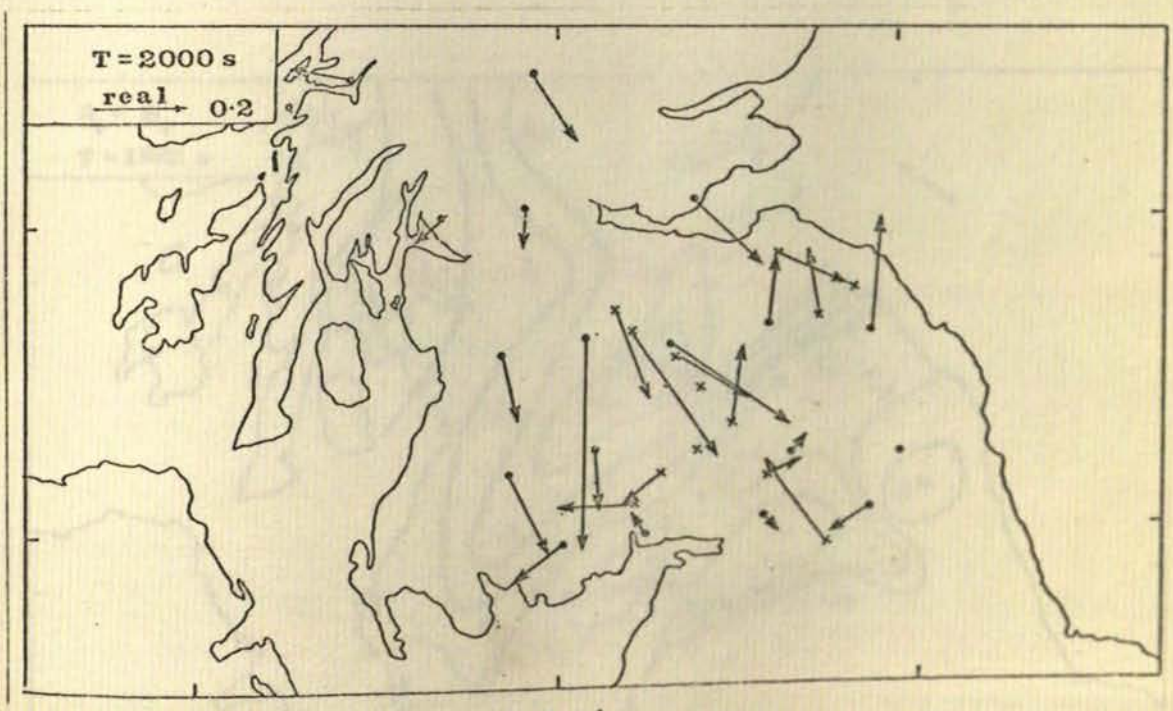

(b)

Figure A1.1 In-phase induction vectors for array and single-station data at (a) 750s & (b) 2000s

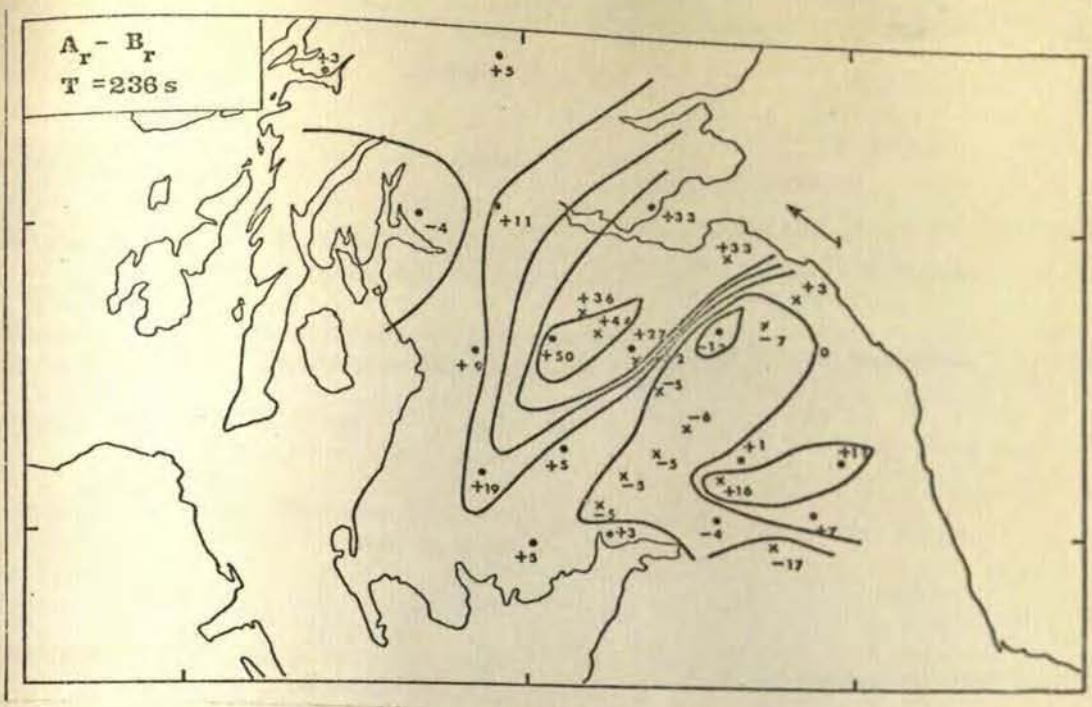

(a)

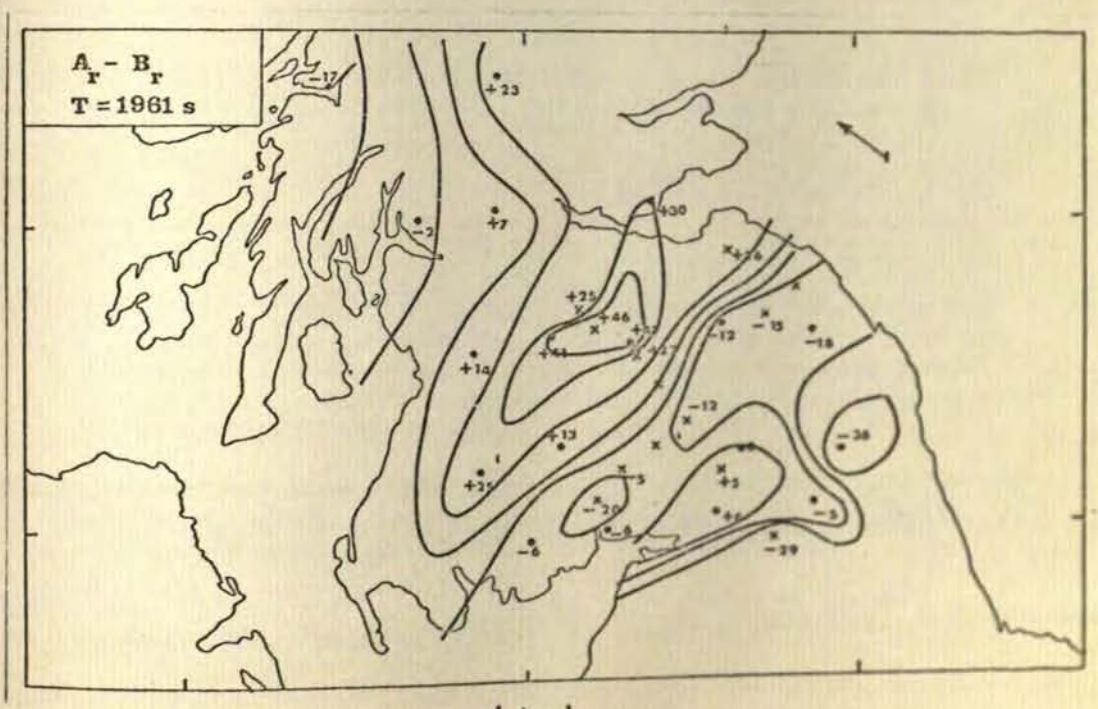

(b)

Figure A1.2 Hypothetical Event Analysis: in-phase vertical field generated by a regional NE/SW current flow at (a) 236s & (b) 1961s

REFERENCES

Papers given at various conferences are indicated as follows:-

Edinburgh: First Workshop on Electromagnetic Induction in the Earth, held in Edinburgh, Scotland, 20-27 September 1972.

Ottawa: Second Workshop on Electromagnetic Induction in theEarth, held in Ottawa, Canada, 22-28 August 1974.

Grenoble: 16th General Assembly of the IUGG, held in Grenoble, France, 25 August - 6 September 1975.

Sopron: Third Workshop on Electromagnetic Induction in the Earth, held in Sopron, Hungary, 4-10 July 1976.

Abramovici, F., 1974. The forward MT problem for an inhomogeneous and anisotropic structure, Geophysics, 56-68.

Adam, A., 1974. Geotektonische Interpretation der elektromagnetischen Tiefsondierungen im Karpaten-Becken, Acta. Geol. Acad. Sci. Hung., 18, 267-277.

Adam, A., 1976. Geoelectric and Geothermal Studies, KAPG Geophysical Monograph. Akadémiai Kiadó, Budapest.

Adam, A. and Vero, J., 1970. Das Elektrische Modell des Oberan Erdmantels Im Karpatenbecken. Acta. Geod. Geoph. et Mont., 5, 5-20.

Agger, H.E. and Carpenter, E.W., 1964. A crustal study in the vicinity of Eskdalemuir seismological array station. Geophys. J. R. astr. Soc., 9, 69.

Airy, G.B., 1868. Comparison of magnetic disturbances recorded by the self-registering magnetometers at the Royal Observatory, Greenwich with magnetic disturbances deduced from the corresponding terrestrial galvanic currents recorded by the self-registering galvanometer of the Royal Observatory. Phil. Trans. Roy. Soc., 158, 465.

Akaike, H., 1967. Some problems in the application of the cross-spectral method, in Advanced Seminar on Spectral Analysis of Time Series, ed. Bernard Harris, John Wiley & Sons Ltd., pp 81-107.

Alabi, A.O., 1974. A study of the North American Central Plains conductivity anomaly, Ph.D. Thesis, University of Alberta.

Alabi, A.O., Camfield, P.A. and Gough, D.I., 1975. The North American Central Plains conductivity anomaly, Geophys. J. R. astr. Soc., 43, 815-834.

Albouy, Y., Godivier, R. and Perichon, P., 1971. Le Sondage Magnetotellurique, O.R.S.T.O.M., Paris.

Aldrich, T., Casaverde, M., Bannister, J.R. and Beach, L., 1975. Electrical Conductivity Studies in South America-Argentina-Central Chile, Carnegie Inst. Washington Yearbook, pp 291-292.

Anderson, D.L., 1967. Phase changes in the upper mantle, Science, 157, 1165-1173.

Anderssen, R.S., 1970. Pure Appl. Geophys., 80, 238-259.

Anderssen, R.S., 1975. On the inversion of global electromagnetic induction data, Phys. Earth Planet. Int., 10, 292-298.

Anderssen, R.S., Worthington, M.H. and Cleary, J.S., 1972. Density modelling by Monte-Carlo inversion - I. Methodology, Geophys. J. R. astr. Soc., 29, 433-444.

Archie, 1942. The electrical resistivity log as an aid in determining some reservoir characteristics, A.I.M.E. Trans., 146, 54-61.

Backus, G. and Gilbert, F., 1967. Numerical application of a formalism for geophysical inverse problems, Geophys. J. R. astr. Soc., 13, 247-276.

Backus, G. and Gilbert, F., 1968. The resolving power of gross Earth data, Geophys. J. R. astr. Soc., 16, 169-205.

Backus, G. and Gilbert, F., 1970. Uniqueness in the inversion of inaccurate gross Earth data, Phil. Trans. R. Soc., A266, 123-192.

Bailey, R.C., 1970. Inversion of the geomagnetic induction problem, Proc. R. Soc., 315, 185-194.

Bailey, R.C., 1973. Global geomagnetic sounding - methods and results, Phys. Earth Planet. Int., 7, 234-244.

Bailey, R.C. and Edwards, R.N., 1976. The effect of source field polarisation on geomagnetic anomalies in the British Isles, Geophys. J. R. astr. Soc., 45, 97-104.

Bailey, R.C., Edwards, R.N., Garland, G.D., Kurtz, R. and Pitcher, D.H., 1974. Electrical conductivity studies over a tectonically active area in Eastern Canada. J. Geomag. Geoelectr., 26, 125-146.

Bamford, D., 1977. Deep structure of the Southern Uplands and adjacent areas from the 1000 km seismic refraction line experiment (LISPB), contributed paper: S.U. Workshop, Edinburgh.

Bamford, D., Faber, S., Jacob, B., Kaminski, W., Nunn, K., Prodehl, C., Fuchs, K., King, R. and Willmore, P., 1976. A lithosphere seismic profile in Britain. I - Preliminary results, Geophys. J. R. astr. Soc., 44, 145-160.

Bamford, D. and Prodehl, C., 1977. Explosion seismology and the continental crust-mantle boundary, Jl. geol. Soc., Lond., in press.

Banks, R.J., 1969. Geomagnetic variations and the electrical conductivity of the upper mantle, Geophys. J. R. astr. Soc., 17, 457-487.

Banks, R.J., 1972. The overall conductivity distribution of the Earth, J. Geomag. Geoelectr., 24, 337-351.

Banks, R.J., 1973. Data processing and interpretation in geomagnetic deep sounding, Phys. Earth Planet. Int., 7, 339-348.

Banks, R.J., 1975. Complex demodulation of geomagnetic data and the estimation of transfer functions, Internal Report, Dept. of Environmental Sciences, University of Lancaster, U.K.

Banks, R.J. and Ottey, P., 1974. Geomagnetic deep sounding in and around the Kenya Rift Valley, Geophys. J. R astr. Soc., 36, 321-335.

Barsczus, H.G., 1970. Sondages Geomagnetiques Bibliographies, Paris: Ostrom.

Bartlett, M.S., 1948. Smoothing periodograms from time series with continuous spectra, Nature, 161, 666-668.

Bartlett, M.S., 1950. Periodogram analyses and continuous spectra, Biometrika, 37, 1-16.

Batschelet, E., 1965. Statistical methods for the analysis of problems in animal orientation and certain biological rhythms, Amer. Inst. Biol. Sci., Washington, D.C.

Batschelet, E., 1971. Recent statistical methods for orientation data in Animal Orientation, Symposium 1970 on Wallops Island. Amer. Inst. Biol. Sciences, Washington.

Beblo, M., 1976. Electrical conductivity in the geothermal anomaly of the Urach Volcanic Area, S.W. Germany. Sopron.

Behannon, K.W. and Ness, N.F., 1966. The design of numerical filters for geomagnetic data analysis, N.A.S.A. Technical Note D 3341, July.

Bendat, J.S. and Piersol, A.G., 1971. Random Data: Analysis and Measurement Procedures: Wiley-Interscience, New York.

Benignus, V.A., 1969. Estimation of the coherence spectrum and its confidence interval using the Fast Fourier Transform, I.E.E.E. Trans. Audio Electroacoustics, AU-17, 145-150.

Bentley, C.R., 1973. Error estimation in two-dimensional magnetotelluric analysis. Phys. Earth Planet. Int., 7, 423.

Bentley, C.R., 1974. Magnetotelluric evidence for lateral variations of crustal structure along the margin of the Canadian shield, contributed paper: Ottawa.

Berdichevsky, M.N., 1960. Principles of magneto-telluric profiling theory, Applied Geophys., (Prikl. Geofiz.), 28.

Berdichevsky, M.N., 1963. Linear relationships in the magnetotelluric field, Applied Geophys., (Prikl. Geofiz.), 38.

Berdichevsky, M.N., Bezruk, I.A. and Chinareva, O.M., 1973. Magneto-telluric sounding using mathematical filters, IZV, Earth Physics, 76.

Berdichevsky, M.N., Borisova, V.P., Bubnov, V.P., Vanyan, L.L. Feldman, I.S. and Yakovlev, I.A., 1969. Anomaly of the Earth's crust electroconductivity in Yakutiya, Fizika. Zemli., 10, 43-49.

Berdichevsky, M.N., Safonov, A.S., Bubnov, V.M., Sysoev, T.K., Chernyavsky, G.A. and Chinareva, O.M., 1975. Results of abyssal magnetotelluric soundings in Siberia on the data of amplitude and phase curves interpretation, Voprosy Geofiziki.

Berdichevsky, M.N., Vanyan, L.L., Feldman, I.S. and Porstendorfer, G., 1972. Conducting layers in the Earth's crust and upper mantle, Gerlands Beitr. Geophysik, Leipzig, 81, 187-196.

Berktold, A, Bennet, D.J., Angenheister, G., Dziewonski, A., Gouin, P., Haak, V. and Porath, H., 1974. The distribution of the electrical conductivity in eastern Ethiopia (A far depression and main rift), contributed paper: Ottawa.

Bingham, C., Godfrey, M.D. and Tukey, J.W., 1967. Modern techniques for power spectrum estimation, I.E.E.E. Trans. Audio Electroacoust., AU-15, 56-66.

Birch, F., 1952. Elasticity and constitution of the Earth's interior, J. Geophys. Res., 57, 227-286.

Birch, F., 1970. Density and composition of the upper mantle: first approximation as an olivine layer, in The Earth's Crust and Upper Mantle, AGU Monograph 13.

Biswas, N.N. and Knopoff, L., 1974. The structure of the upper mantle under the United States from the dispersion of Rayleigh waves, Geophys. J. R. astr. Soc., 36, 515-539.

Blackman, R.B. and Tukey, J.W., 1958. The measurement of power spectra. Dover Publications Inc., New York.

B.M.D., 1970. Biomedical Computer Programs, ed. W.J. Dixon. University of California Publications in Automatic Computation No. 2.

Born, J. and Wolf, E., 1964. Principles of Optics. The Macmillan Company, New York.

Bostick, F.X. and Smith, H.W., 1962. Investigation of large scale inhomogeneities in the Earth by the magnetotelluric method, Proc. Inst. Radio Engineers, 50, 2339-2346.

Bowden, K.F. and Hughes, P., 1961. The flow of water through the Irish Sea and its relation to wind, Geophys. J. R. astr. Soc., 5, 265-291.

Brace, W.F., Orange, A.S. and Madden, T.R., 1965. The effect of pressure on the electrical resistivity of water-saturated crystalline rocks, J. Geophys. Res., 70, 5669-5678.

Bradley, R.S., Jamil, A.K. and Munro, D.C., 1964. The electrical conductivity of olivine at high temperature and pressure, Geochim. Cosmochim. Acta., 28, 1669-1678.

Brewitt-Taylor, C.R. and Weaver, J.T., 1976. On the finite difference solution of two-dimensional induction problems, Geophys. J. R. astr. Soc., 47, 375-396.

Briden, J.C., Morris, W.A. and Piper, J.D.A., 1973. Palaeomagnetic studies in the British Caledonides - IV. Regional and global implications, Geophys. J. R. astr. Soc., 34, 107-134.

Burdick, L. and Anderson, D.L., 1975. Interpretation of velocity profiles in the mantle, J. Geophys. Res., 80, 1070-1074.

Burg, J.P., 1967. Maximum entropy spectral analysis: paper presented at 37th Annual Int. S.E.G. Meeting Oklahoma, Oct. 31, 1967.

Burg, J.P., 1968. A new analysis technique for time series data: paper presented at N.A.T.O. Advanced Study Institute on Signal Processing.

Burg, J.P., 1970. New concepts in power spectra estimation: paper presented at 40th Annual International S.E.G. Meeting, New Orleans, Louisiana, November 11, 1970.

Burg, J.P., 1972. The relationship between maximum entropy spectra and maximum likelihood spectra. Geophysics, 37, 375-

Burg, J.P., 1973. Recommendations concerning maximum entropy spectral estimation: private circulation.

Burton, P.W., 1977. Inversions of high frequency $Q_\gamma^{-1}(f)$, Geophys. J. R. astr. Soc., 48, 29-51.

Cagniard, L., 1953. Basic theory of the magnetotelluric method of geophysical prospecting, Geophys., 18, 605-635.

Camfield, P.A., 1976. Magnetometer array in a tectonically-active region of Quebec, Canada: Preliminary results: paper presented Sopron.

Camfield, P.A., Gough, D.I. and Porath, H., 1971. Magnetometer array studies in the northwestern United States and Southwestern Canada, Geophys. J. R. astr. Soc., 22, 201-222.

Caner, B., Camfield, P.A., Andersen, F. and Niblett, E.R., 1969. A large-scale magnetotelluric survey in Western Canada, Can. J. Earth. Sci., 6, 5.

Caner, B. and Cannon, W.H., 1965. Geomagnetic depth-sounding and correlation with other geophysical data in western North America, Nature, 27, 927-928.

Caner, B., Cannon, W.H. and Livingstone, C.E., 1967. Geomagnetic depth-sounding and upper mantle structure in the Cordillera region of western North America, J. Geophys. Res., 72, 6335-6351.

Cantwell, T., 1960. Detection and analysis of low frequency magnetotelluric signals, Ph.D. Thesis, Dept. Geology & Geophysics, M.I.T. Cambridge, Massachusetts.

Capon, J., 1969. High-resolution frequency-wave-number spectral analysis, Proc. I.E.E.E., 57, 1408-1418.

Chan, T., Nyland, E. and Gough, D.I., 1973. Partial melting conductivity anomalies in the upper mantle, Nature Physical Sci., 244, 89-90.

Channon, M.J. and Orr, D., 1970. Planet. Space Sci., 18, 229.

Chapman, S., 1919. The solar and lunar diurnal variation of the Earth's magnetism, Phil. Trans. Roy. Soc. Lond., Ser. A, 218, 1-118.

Chapman, S. and Bartels, J., 1940. Geomagnetism, Oxford University Press, London.

Chapman, S. and Price, A.T., 1930. The electric and magnetic state of the interior of the earth as inferred from terrestrial magnetic variations, Phil. Trans. Roy. Soc. Lond. Ser. A, 229, 427-460.

Chen, W.Y. and Stegen, G.R., 1974. Experiments with maximum entropy power spectra of sinusoids, J. Geophys. Res., 79, 20, 3019-3022.

Church, W.R. and Gayer, R.A., 1973. The Ballantrae ophiolite, Geol. Mag., 110, 497-510.

Cochrane, N.A. and Hyndman, R.D., 1970. A new analysis of geomagnetic depth-sounding data from western Canada, Can. J. Earth. Sci., 7, 1208-1218.

Cochrane, N.A. and Hyndman, R.D., 1974. Magnetotelluric and magneto-variational studies in Atlantic Canada, Geophys. J. R. astr. Soc., 39, 385-406.

Coggon, J.H., 1971. Electromagnetic and electrical modeling by the finite element method, Geophysics, 36, 132-155.

Collette, B.J., Lagaay, R.A., Ritsema, A.R. and Schouten, J.A., 1970. Seismic investigations in the North Sea, 3 to 7, Geophys. J. R. astr. Soc., 19, 183-200.

Cooley, J.W. and Tukey, J.W., 1965. An algorithm for the machine calculation of complex fourier series, Math. Comput., 19, 297-301.

Colquhoun, D., 1971. Lectures on Biostatistics. Clarendon Press, Oxford.

Courtillot, V. and LeMouel, J.L., 1975. On the long period variations of the earth's magnetic field (from 2 months to 20 years): paper presented at 16th General Assembly of IUGG, Grenoble, 25 August - 6 September 1975.

Cox, C.S., Filloux, J.H. and Larsen, J.C., 1971. Electromagnetic studies of ocean currents and electrical conductivity below the ocean floor, in The Sea, ed. A.E. Maxwell, v.4, part 1.

Currie, R.G., 1966. The geomagnetic spectrum 40 days - 5.5 years, J. Geophys. Res., 71, 4579-4598.

Dadunashvily, H.S., Gegunava, G.E., Logvinov, I.M., Rokityanskaya, D.A., Rokityansky, I.I., Shuman, V.N., Smolnikov, B.M. and Vanyan, L.L., 1976. Induction studies in the Caucus: paper presented Sopron.

Daniel, P.J., 1946. Discussion on symposium on auto-correlation in time series, Supplement to J. Royal Statist. Soc., 8, 88-90.

D'Erceville, I. and Kunetz, E., 1962. The effect of a fault on the earth's natural electromagnetic field, Geophysics, 27, 651-665.

Dewey, J.F., 1974. The geology of the southern termination of the Caledonides, in The Ocean Basins and Margins, Vol. 2 The North Atlantic. Plenum Press, New York and London.

Dixon, W.J., 1971. B.M.D. - Biomedical Computer Programs, University of California Publications in Automatic Computation No. 2. University of California Press, Berkeley, California.

Dowling, F.L., 1970. Magnetotelluric measurements across the Wisconsin arch, J. Geophys. Res., 75, No. 14, 2683-2698.

Dragert, H., 1974. A field evaluation of Caner's broad band geomagnetic induction instrument, J. Geophys. Res., 40, 121-129.

Duba, A., 1976. Are laboratory electrical conductivity data relevant to the earth? Review paper presented Sopron.

Duba, A., Heard, H.C. and Schock, R.N., 1974. Electrical conductivity of olivine at high pressure and under controlled oxygen fugacity, J. Geophys. Res., 79, 1667-1673.

Duba, A. and Lilley, F.E.M., 1972. Effect of an ocean ridge model on geomagnetic variations, J. Geophys. Res., 77, 7100-7105.

Duba, A. and Nicholls, I.A., 1973. The influence of oxidation state on the electrical conductivity of olivine, Earth. Planet. Sci. Lett., 18, 59-64.

Dubrovskiy, V.G., Nikolayeva, L.S. and Firsova, V.E., 1970. Attempt to use Sq varuations for deep magnetotelluric sounding work in Turkmenia, Izv. Earth Phys., 11, 82-85.

Dulaney, E.N. and Madden, T.R., 1962. Analogue relaxation net calculations of two-dimensional magneto-telluric response curves, S.E.G. Yearbook, p 265 (Abstract)

Dyck, A.V. and Garland, G.D., 1969. A conductivity model of certain features of the Alert anomaly in geomagnetic variations, Can. J. Earth. Sci., 6, 513-516.

Eastwood, T., 1953. Northern England. British Regional Geology handbook, 3rd ed. Her Majesty's Stationery Office.

Edwards, R.N. and Greenhouse, J.P., 1975. Geomagnetic variations in the eastern U.S.: evidence for a highly conducting lower crust? Science, 188, 726-728.

Edwards, R.N., Law, L.K. and White, A., 1971. Geomagnetic variations in the British Isles and their relation to electrical currents in the ocean and shallow seas, Phil. Trans. Roy. Soc. Lond., No. 1204,, 270, 289-323.

Enochson, L.D. and Goodman, N.R., 1965. Gaussian approximation to the distribution of sample coherence, A.F.F.D.L. T.R. 65-57 Air Force Flight Dynamics Lab., Wright-Patterson A.F.B., Ohio, February.

Everett, J.E. and Hyndman, R.D., 1967a. Geomagnetic variations and electrical conductivity structure in S.W. Australia, Phys. Earth. Planet. Int., 1, 24-34.

Everett, J.E. and Hyndman, R.D., 1967b. Magneto-telluric investigations in South-Western Australia, Phys. Earth. Planet. Int., 1, 49-54.

Febrer, J., Demicheli, J., Garcia, E. and Fournier, H., 1976. Magneto-telluric sounding in Pilar - Cordoba, Argentina: paper presented Sopron.

Fitton, J.G. and Hughes, D.J., 1970. Volcanism and plate tectonics in the British Ordovician, Earth. Plan. Sci. Lett., 8, 223-228.

Floyd, J., 1976. Recent work in the Southern Uplands. Seminar presented at Grant Institute of Geology, King's Buildings, University of Edinburgh on 7 December 1976.

Fougere, P.F., Zawalick, E.J. and Radoski, M.R., 1975. Spontaneous line splitting in maximum entropy power spectrum analysis: paper presented Grenoble.

Fournier, H.G., 1966. Essai d'un historique des counaissances magneto-telluriquer, Note 17, Institut de Physique du Globe, Universite de Paris.

Fournier, H.G., Adam, A., DeMiguel, L. and Sanclement, G., 1971. Acta. Geodaet. Geophys. Montanist. Acad. Sci. Hung., 6, 459-477.

Fournier, H., Babour, K., Dupis, A. and Clerc, G., 1974. Identite possible entre les lignes geostructurales et les directions tensorielles magnetotelluriques d'interpretation dans le Bassin de Paris: paper presented Ottawa.

Fournier, H. and Rossignol, J.C., 1974. A magnetotelluric experiment in Nozay-en-Dunois (Eure-et-Loir, France): Results, interpretation and critical study, Phys. Earth. Planet. Int., 8, 13-18.

Fowler, R.A., Kotick, B.J. and Elliot, R.D., 1967. Polarisation analysis of natural and artificially induced geomagnetic micropulsations, J. Geophys. Res., 72, 2871.

Fujisawa, H., 1968. Temperature and discontinuities in the transition layer within the earth's mantle: geophysical application of the olivine-spinel transition in the Mg_2SiO_4-$FeSiO_4$ system, J. Geophys. Res., 73, 3281-3294.

Garland, G.D., 1960. Earth-currents, in Methods and Techniques in Geophysics, ed. S.K. Runcorn. John Wiley & Sons Inc., London.

Garland, G.D. and Ward, J., 1965. Magnetic variation measurements in Iceland, Nature, 205, 269-270.

Garson, M.S. and Plant, J., 1973. Alpine type ultramafic rocks and episodic mountain building in the Scottish Highlands, Nature Phys. Sci., 242, 34-38.

Gentleman, W.M. and Sande, G., 1966. Fast Fourier transforms for fun and profit, Proceedings of the Fall Joint Computer Conference, San Francisco, 563-578.

Gough, D.I., 1973. The geophysical significance of geomagnetic variation anomalies, Phys. Earth. Planet. Int., 7, 379-388.

Gough, D.I., McElhinny, M.W. and Lilley, F.E.M., 1974. A magnetometer array study in southern Australia, Geophys. J. R. astr. Soc., 36, 345-362.

Gough, D.I. and Reitzel, 1967. A portable 3-component magnetic variometer, J. Geomag. & Geoelectr., 19, 203.

Grant, A.L., 1972. The continental margin off Labrador and Eastern Newfoundland - morphology and geology, Can. J. Earth. Sci., 9, 1394-1440.

Grant, F.S. and West, G.F., 1965. Interpretation theory in applied geophysics. McGraw-Hill New York.

Green, C.A., 1975. An induction study at micropulsation periods in the British Isles, Geophys. J. R. astr. Soc., 40, 225.

Green, D.H., 1973. Experimental melting studies on a model of upper mantle composition at high pressure under water saturated and water under-saturated conditions, Earth. Planet. Sci. Lett., 19, 37-53.

Greenberg, R.J. and Brace, W.F., 1969. Archie's law for rocks modelled by simple networks, J. Geophys. Res., 74, 2099-2102.

Greenfield, R.J. and Turnbull, L.S., 1970. Monte-Carlo inversion of magneto-telluric data, E.O.S. Trans. A.G.U., 51, 426.

Greig, D.C., 1971. The South of Scotland. British Regional Geology Handbook - 3rd edition. Her Majesty's Stationery Office.

Grillot, L.R., 1975. Calculation of the magnetotelluric tensor impedance: Analysis of band limited MT signal pairs, Geophys., 40, 790-797.

Goodman, N.R., 1965. Measurement of Matrix Frequency Response Functions and Multiple Coherence Functions, AFFDL TR 65-56, Air Force Flight Dynamics Lab., Wright-Patterson AFB, Ohio, February 1965.

Gunn, P.J., 1973. Location of the proto-Atlantic suture in the British Isles, Nature, 242, 111-112.

Haak, V., 1972. Magnetotelluric method: the determination of transfer functions in areas with lateral variation of electrical conductivity, Zeitschrift fur Geophysik, 38, 85-102.

Haak, V., 1976. Interpretation of magnetotelluric data from the Afar-depression in Ethiopia, in particular of variations at long periods: paper presented Sopron.

Haak, V. and Reitmayr, G., 1974. The distribution of electrical resistivity in the Rheingraben area as determined by telluric and magnetotelluric methods, in Approaches to Taphrogenesis, pp 366-369, ed. J.H. Illies and K. Fuchs. Schweizerbart, Stuttgart.

Haddon, R.A.W. and Bullen, K.E., 1969. An Earth model incorporating free earth oscillation data, Phys. Earth. Planet. Int., 2, 35-49.

Hald, A., 1952. Statistical theory with engineering applications. John Wiley, New York.

Hall, J., 1970. The correlation of seismic velocities with formations in the south-west of Scotland, Geophys. Prosp., 18, 134-148.

Hall, J., 1971. A preliminary seismic survey adjacent to the Rashiehill borehole near Slamannan, Stirlingshire, Scott. J. Geol., 7, 170-174.

Hall, J., 1974. A seismic reflection survey of the Clyde Plateau Lavas in North Ayrshire and Renfrewshire, Scott. J. Geol., 9, 253-279.

Hasegawa, M., 1936. Representation of the field of diurnal variations of terrestrial magnetism on quiet days by the method of graphical integration, Proc. Imp. Acad. Tokyo, 12, 225-228.

Hatakeyama, H., 1938. On the bay disturbance and the pulsation of the earth current, Geophys. Mag., 12, 189-210.

Heirtzler, J.R., LePichon, X. and Baron, J.G., 1966. Magnetic anomalies over the Reykjanes Ridge, Deep-Sea Res., 13, 427-443.

Hermance, J.F., 1973a. Processing of magnetotelluric data, Phys. Earth. Planet. Int., 7.

Hermance, J.F., 1973b. An electrical model for the sub-Icelandic crust, Geophys., 38, 3-13.

Hermance, J.F. and Garland, G.D., 1968. Magnetotelluric deep sounding experiments in Iceland, Earth. Planet. Sci. Lett., 4, 469-474.

Hermance, J.F. and Grillot, L.R., 1970. Correlation of magnetotelluric, seismic and temperature data for southwest Iceland, J. Geophys. Res., 75, 6582-6591.

Hermance, J.F. and Grillot, L.R., 1974. Constraints on temperatures beneath Iceland from magnetotelluric data, Phys. Earth. Planet. Int., 8, 1-12.

Hewson-Browne, R.C. and Kendall, P.C., 1976. Magneto-telluric modelling and inversion in three-dimensions: review paper presented Sopron.

Hirayama, M., 1934. On the relations between the variations of earth potential gradient and terrestrial magnetism, J. Met. Soc. Japan, 12, 16-22.

Hobbs, B.A., 1973. The inverse problem of the Moon's electrical conductivity, Earth. Planet. Sci. Letts., 17, 380-384.

Hobbs, B.A., 1977. The electrical conductivity of the Moon: An application of inverse theory: paper presented at U.K.G.A., Edinburgh, 12-15 April 1977: abstract Geophys. J. R. astr. Soc., 49, 275.

Hobbs, B.A. and Parker, R.L., 1977. The parameter space for the lunar electromagnetic induction inverse problem, in preparation.

Honkura, Y., Kurtz, R.D. and Niblett, E.R., 1977. Geomagnetic Depth Sounding and Magnetotelluric results from a seismically active region northeast of Quebec City, Can. J. Earth. Sci., 14, 256-267.

Hutton, J., 1795. Theory of the Earth. Cadell and Davies, Edinburgh.

Hutton, V.R.S., 1976a. Induction studies in rifts and other active regions: review paper presented Sopron.

Hutton, V.R.S., 1976b. The electrical conductivity of the Earth and planets, Rep. Prog. Phys., 39, 487-572.

Hutton, V.R.S., Sik, J., Jones, A.G. and Rooney, D., 1977. The interpretation of geomagnetic variation observations in Scotland using the hypothetical event technique: paper presented at U.K.G.A., Edinburgh, 12-15 April 1977: abstract Geophys. J. R. astr. Soc., 49, 275.

Hyndman, R.D. and Cochrane, N.A., 1971. Electrical conductivity structure by geomagnetic induction at the continental margin of Atlantic Canada, Geophys. J. R. astr. Soc., 25, 425-446.

Hyndman, R.D. and Hyndman, D.W., 1968. Water saturation and high electrical conductivity in the lower continental crust, Earth. Planet. Sci. Letts., 4, 427-432.

Iliceto, V., 1974. Some remarks on Magnetotelluric digital equipment; Magnetotelluric field examples: contributed paper: Ottawa.

Jackson, D.D., 1973. Marginal solutions to quasi-linear inverse problems in geophysics: The Edgehod Method. Geophys. J. R. astr. Soc., 35, 121-136.

Jacob, A.W.B., 1969. Crustal phase velocities observed at the Eskdalemuir seismic array, Geophys. J. R. astr. Soc., 18, 189.

Jacobs, J.A., 1970. Geomagnetic micropulsations. Springer-Verlag, New York.

Jain, S., 1964. Electrical conductivity of the crust and upper mantle at Eskdalemuir, S. Scotland, Nature, 203, 631-632.

Jain, S. and Wilson, C.D.V., 1967. Magnetotelluric investigations in the Irish Sea and Southern Scotland, Geophys. J. R. astr. Soc., 12, 165-180.

Jankowski, J. Szymanski, A., Pec, K., Pekova, J., Petr, V. and Praus, O., 1976. Electromagnetic studies of the Carpathian conduction anomaly: contributed paper Sopron.

Jeffrey, A., 1971. Mathematics for Engineers and Scientists. Nelson, London.

Jenkins, G.M. and Watts, D.G., 1968. Spectral Analysis and its Application. Holden-Day.

Jessop, A.M., 1968. Three measurements of heat flow in eastern Canada, Can. J. Earth. Sci., 8, 711-716.

Jolivet, J., 1966. Ph.D. Thesis, University of Paris, France.

Jones, A.G. and Hutton, V.R.S., 1977. Magnetotelluric investigation of the Eskdalemuir anomaly - Preliminary results, Acta. Geodaet. Geophys. Montanist. Acad. Sci. Hung., in press.

Jones, F.W., 1973a. Induction in laterally non-uniform conductors: theory and numerical models, Phys. Earth. Planet. Int., 7, 282-293.

Jones, F.W., 1973b. The perturbation of alternating geomagnetic fields by an island near a coastline: Reply, Can. J. Earth. Sci., 10, 1703-1704.

Jones, F.W. and Pascoe, L.J., 1971. A general computer programme to determine the perturbation of alternating electric currents in a two-dimensional model of a region of uniform conductivity with an embedded inhomogeneity, Geophys. J. R. astr. Soc., 24, 3-30.

Jones, F.W. and Price, A.T., 1970. The perturbations of alternating geomagnetic fields by conductivity anomalies, Geophys. J. R. astr. Soc., 20, 317-334.

Jones, F.W. and Thomson, D.J., 1974. A discussion of the finite difference method in computer modelling of electrical conductivity structures. A reply to the discussion by Williamson, Hewlett and Tammemagi. Geophys. J. R. astr. Soc., 37, 537-544.

Jupp, D.L.B. and Vozoff, K., 1976. Discussion on "The magnetotelluric method in the exploration of sedimentary basins" by Vozoff, 1972, Geophys., 41, 325-328.

Kaila, K.L. and Krishna, V.G., 1976. Nature of the 400 km discontinuity in the Earth's mantle, Geophys. J. R. astr. Soc., 46, 185-188.

Kanasewich, 1973. Time Sequence Analysis in Geophysics. University of Alberta Press.

Kasameyer, P.W., 1974. A low frequency magnetotelluric survey in New England: contributed paper Ottawa.

Keilis-Borok and Yanovskaya, T.B., 1967. Inverse problems of seismology (structural review), Geophys. J. R. astr. Soc., 13, 223-234.

Keller, G.V., 1966. Electrical properties of rocks and minerals. Handbook of Physical Constants, Geol. Soc. Amer. Mem., 97, 553-577.

Keller, G.V., 1971. Electrical studies of the crust and upper mantle, in The Structure and Properties of the Earth's Crust, A.G.U. Monograph 14.

Keller, G.V. and Frischknecht, F.C., 1966. Electrical methods in geophysical prospecting, International series of Monographs in Electromagnetic Waves, Vol. 10. Pergamon Press.

Kemmerle, K., 1976. The influence of small near-surface anomalies in magnetotellurics: contributed paper Sopron.

Kendall, M.G. and Stuart, A., 1958. The Advanced Theory of Statistics Vol. I. Distribution Theory. Charles Griffin & Company Ltd., London.

Kharin, E.P., Csipova, I.L. and Spivak, 1976. Interpretation of sea-floor spreading near California: contributed paper Sopron.

Kisak, E., 1976. A recursive method in the E-polarisation of magneto-telluric modelling by high order finite elements: contributed paper Sopron.

Kisak, E. and Silvester, P., 1975. A finite-element program package for magneto-telluric modelling, Compt. Phys. Comm., 10, 421-433.

Kittel, C., 1953. An introduction to solid state physics. John Wiley and Sons Inc., New York.

Kovtun, A.A., 1976. Induction studies in stable shield and platform areas: review paper Sopron.

Kovtun, A.A. and Chicherina, N.D., 1973. Investigations in the north-eastern part of the Russian platform, in Investigations of Thermal and Electromagnetic Fields in the U.S.S.R., pp 61-68. Publ. House 'Nauka'.

Kovtun, A.A., Porokhova, L.N. and Chicherina, N.D., 1975. The evaluation of the effective reverse problem solution based on the magnetotelluric sounding data in the north-west of the Russian plate: contributed paper Grenoble.

Krasnobaeva, A.G., 1976. About the nature of the geomagnetic field and Earth's current and their relation with the geological and geotectonic structure of the Urals geargneline: contributed paper Sopron.

Kuckes, A.F., 1973a. Relations between electrical conductivity of a mantle and fluctuating magnetic fields, Geophys. J. R. astr. Soc., 32, 119-131.

Kuckes, A.F., 1973b. Correspondence between the magnetotelluric and field penetration depth analysis for measuring electrical conductivity, Geophys. J. R. astr. Soc., 32, 381-385.

Kunetz, G., 1972. Processing and interpretation of magnetotelluric soundings, Geophys., 37, 1005-1021.

Kuppers, F., 1976. Versatility of Gough and Reitzel type magnetometers: presented paper Sopron.

Kurtz, R., 1973. A magneto-telluric investigation of Eastern Canada, Ph.D. Thesis, University of Toronto.

Kurtz, R.D. and Garland, G.D., 1976. Magneto-telluric measurements in Eastern Canada, Geophys. J. R. astr. Soc., 45, 321-348.

Lacoss, R.T., 1971. Data adaptive spectral analysis methods, Geophys., 36, 661-675.

Lahiri, B.N. and Price, A.T., 1939. Electromagnetic induction in non-uniform conductors, and the determination of the conductivity of the earth from terrestrial magnetic variations, Phil. Trans. Roy. Soc. London, Ser. A, 237, 509-540.

Laird, C.E. and Bostick, Jr., F.X., 1970. One-dimensional magneto-telluric inversion techniques, Tech. Rep. No. 10, Electrical Geophysics Research Laboratory, University of Texas at Austin, Austin, Texas.

Lancczos, C., 1961. Linear Differential Operators. D. Van Nostrand, London.

Lapworth, C., 1889. On the Ballantrae rocks of South Scotland and their place in the Upland sequence, Geol. Mag., 26, 20-24, 59-69.

Larsen, J.C., 1975. Low frequency (0.1-6.0 cpd) electromagnetic study of deep mantle electrical conductivity beneath the Hawaiian Island, Geophys. J. R. astr. Soc., 43, 17-46.

Larsen, J.C., 1976. Conductivity structure beneath Tucson, Arizona and Bermuda: presented paper Sopron.

Law, L.K. and Riddihough, R.P., 1971. A geographical relation between geomagnetic variation anomalies and tectonics, Can. J. Earth. Sci., 8, 1094-1106.

Leary, P. and Phinney, R.A., 1974. A magnetotelluric traverse across the Yellowstone region, Geophys. Res. Letts., 1, 265-268.

Leeder, M.R., 1974. The origin of the Northumberland basin, Scott. J. Geol., 10, 283,296.

Levadny, V.T., Bazarzhapov, L.D., Shpinev, G.B., Pavlova, I.V. and Fedorov, A.N., 1976. Magnetovariational investigation in Baikal area: presented paper Sopron.

Liebermann, R.C., 1973. Elasticity of the olivine-spinel and olivine-beta phase transformations and the 400 km discontinuity of the mantle, J. Geophys. Res., 78, 7015-7017.

Lilley, F.E.M., 1974. Analysis of the geomagnetic induction tensor, Phys. Earth. Planet. Int., 8, 301-316.

Lilley, F.E.M., 1975. Magnetometer array studies: A review of the interpretation of observed fields, Phys. Earth. Planet. Int., 10, 231-240.

Lilley, F.E.M. and Sloane, M.N., 1976. On estimating electrical conductivity using gradient data from magnetometer arrays, J. Geomag. Geoelectr., 28, 321-328.

Lilley, F.E.M. and Tammemagi, H.Y., 1972. Magnetotelluric and geomagnetic depth sounding methods compared, Nature Phys. Sci., 240, 184-187.

Lines, L.R. and Jones, F.W., 1973a. The perturbation of alternating geomagnetic fields by an island near a coastline. Can. J. Earth. Sci., 10, 510-518.

Lines, L.R. and Jones, F.W., 1973b. The perturbation of alternating geomagnetic fields by three-dimensional island structures, Geophys. J. R. astr. Soc., 32, 133-154.

Lipskaya, N.V., Deniskin, N.A. and Rudneva, T.L., 1973. Abyssal magnetotelluric soundings of the Byelorussian massif, Izvestia A.N. S.S.S.R., Fizika. Zemli., 10, 63-71.

Lipskaya, N.V. and Troitskaya, V.A., 1955. The actual alternating electromagnetic field, Report on the Work of Inst. Phys. Earth. Funds of the Acad. Sci. U.S.S.R.

Losecke, W., 1970. Ergebnisse magnetotellurisher Messungen bei speyer, in Graben Problems, pp 242-244, ed. J.H. Illier and St. Mueller. Schweizerbart, Stuttgart.

Losecke, W. and Muller, W., 1975. Two-dimensional magnetotelluric model calculations for overhanging, high-resistivity structures, Zeitschrift fur Geophysik, 41, 311-319.

McDonald, K.L., 1957. Penetration of the geomagnetic secular variation through a mantle with variable conductivity, J. Geophys. Res., 62, 117-141.

MacGregor, I.D. and Basu, A.R., 1974. Thermal structure of the lithosphere: a petrological model, Science, 187, 1007-1011.

MacGregor, M. and MacGregor, A.G., 1948. The Midland Valley of Scotland. British Regional Geology Handbook - 2nd edition. Her Majesty's Stationery Office.

McKenzie, D.P., 1970. The Mohorovicic Discontinuity, in The Earth's Crust and Upper Mantle, A.G.U. Monograph 13.

McKerrow, W.S. and Cocks, L.R.M., 1977. The location of the Iapetus Ocean suture in Newfoundland, Can. J. Earth. Sci., 488-495.

McLean, A.C. and Qureshi, I., 1966. Regional gravity anomalies in the western Midland Valley of Scotland, Trans. Roy. Soc. Edin., 66, 267-283.

Madden, T. and Nelson, P., 1964. A defence of Cagniard's magneto-telluric method, Geophys. Lab. O.N.R. proj. NR-371-401, M.I.T., Cambridge, Massachusetts.

Madden, T. and Swift, C.M., 1969. Magnetotelluric studies of the electrical conductivity structure of the crust and upper mantle, in A.G.U. Monograph 13, The Earth's Crust and Upper Mantle, pp 469-479.

Marquardt, D.W., 1963. An algorithm for least squares estimation of non-linear parameters, J. Geophys. Res., 67, 1907-1918.

Masse, R.P., 1974. Compressional velocity distribution beneath central and eastern North America in the depth range 450-800 km, Geophys. J. R. astr. Soc., 36, 705-716.

Matsushita, S., 1967. Solar quiet and lunar daily variation fields, in Physics of Geomagnetic Phenomena, ed. S. Matsushita and W.H. Campbell. Academic Press, New York.

Mercier, J.C. and Carter, N.L., 1975. Pyroxene geotherms, J. Geophys. Res., 80, 334913362.

Meyer, O., 1951. Uber eine besondere Art von Bayskurungen, Devt. Hydrograph Z., 4, 61-65.

Migaux, L., Astier, J.L. and Reval, P.H., 1960. Un essai de determination experimentale de la resistivite electrique des couches profondes de l'ecorce terreste, Ann. geophys., 16, 555-560.

Mills, J.M. and Fitch, T.J., 1977. Thrust faulting and crust-upper mantle structure in East Australia, Geophys. J. R. astr. Soc., 48, 351-384.

Mishin, V.M., Bazarzapov, A.D., Matveev, M.I. and Nemtsova, E.I., 1975. On nature of Sq variations. Siberian Instit. of Terr. Mag., Ionosp. and Radio Wave Prop., Siberian Dept. of Academy of Sciences, U.S.S.R.

Mitchell, B.J. and Landisman, M., 1971. Electrical and seismic properties of the earth's crust in the southwestern great plains of the U.S.A., Geophys., 36, 363-381.

Mitchell, A.H.G. and McKerrow, W.S., 1975. Analogous evolution of the Burma orogen and the Scottish caledonites, Bull. geol. Soc. Am., 86, 305-315.

Monteith, J.L., 1973. Principles of Environmental Physics. Edward Arnold.

Morrison, H.F., Wombwell, E., and Ward, S.H., 1968. Analysis of Earth impedances using magnetotelluric fields, J. Geophys. Res., 73, 2769-2778.

Moseley, F., 1975. Caledonian plate tectonics and the place of the English Lake District, paper presented at the Colloquium on "Early stages of evolution of the Caledonian Orogen in Britain", at University of Birmingham, 3 December.

Mostow, G.D., Sampson, J.H. and Meyer, J.-P., 1963. Fundamental Structures of Algebra. McGraw-Hill, New York.

Mozeson, C.E., 1971. Inverse magnetotelluric analysis by the method of sequential layering, M.Sc. Thesis, University of Alberta, Edmonton, Canada.

Muller, W., 1976. Inversion by simultaneous fitting of apparent resistivity and phase angle, contributed paper Sopron.

Nabetani, S. and Noritomi, K., 1974. Investigation of crustal structure of northern Japan with electromagnetic induction studies, contributed paper Ottawa.

Nabetani, S. and Rankin, 1969. An inverse method of magnetotelluric analysis of a multilayered earth, Geophys., 34, 75-86.

Nagata, T., and Fukushima, N., 1971. Morphology of magnetic disturbance, in Encyclopedia of Physics, Vol. 49-3, Geophysics III, Part III, ed. K. Rawer.

Nakamura, Y. and Howell, Jr., B.F., 1964. Maine seismic experiment: Frequency spectra of refracted arrivals and the nature of the Mohorovicic discontinuity, Bull. Seismol. Soc. Am., 54, 9-18.

Neves, A.S., 1957. The magnetotelluric method in two-dimensional structures, Ph.D. Thesis, Massachusetts Institute of Technology, Cambridge, Massachusetts.

Niblett, E.R. and Sayn-Wittgenstein, C., 1960. Variations in electrical conductivity with depth by the magneto-telluric method, Geophys., 25, 998-1008.

Nienaber, W., Auld, D.R. and Dosso, H.W., 1973. Analysis of anisotropic magnetotelluric measurements at Victoria, B.C., Can. J. Earth. Sci., 10, 557-570.

Nunn, K., and LISPB Working Group, 1977. The crustal structure beneath Northern Britain, contributed paper U.K.G.A., Edinburgh, 12-15 April 1977.

O'Neill, E.L., 1963. Introduction to statistical optics. Addison-Wesley.

Osemeikhian, J.E.A. and Everett, 1968. Anomalous magnetic variations in S.W. Scotland, Geophys. J. R. astr. Soc., 15, 361-366.

Otnes, R.K. and Enochson, L., 1972. Digital Time Series Analysis, John Wiley & Sons, New York.

Parker, R.L., 1970. The inverse problem of electrical conductivity in the mantle, Geophys. J. R. astr. Soc., 22, 121-138.

Parker, R.L., 1977. The Frechet derivative for the one-dimensional electromagnetic induction problem, Geophys. J. R. astr. Soc., 49, 543-547.

Parkinson, W.D., 1959. Directions of geomagnetic fluctuations, Geophys. J. R. astr. Soc., 2, 1-14.

Parkinson, W.D., 1962. The influence of continents and oceans on geomagnetic variations, Geophys. J. R. astr. Soc., 6, 441-449.

Parkinson, W.D., 1964. Conductivity anomalies in Australia and the coast effect, J. Geomag. Geoelect., 15, 222-226.

Parslow, G.R., 1968. The physical and structural features of the Cairnsmore of Fleet granite and its aurole, Scott. J. Geol., 4, 91-108.

Parslow, G.R. and Randall, B.A.O., 1973. A gravity survey of the Cairnsmore of Fleet granite and its environs, Scott. J. Geol., 9, 219-231.

Parzen, E., 1969. Multiple time series modeling, in Multivariate Analysis - II, ed. P.R. Krishnaiah. Academic Press, New York.

Pascoe, L.J. and Jones, F.W., 1972. Boundary conditions and calculation of surface values for the general two-dimensional electromagnetic induction problem, Geophys. J. R. astr. Soc., 27, 179-194.

Patella, D., 1976. Interpretation of magneto-telluric resistivity and phase soundings over horizontal layers, Geophys., 41, 96-105.

Paulson, K.V., 1968. The polarisation and spectral characteristics of some high-latitude irregular geomagnetic micropulsations, Annales de Geophysique, 24, 1-6.

Pecova, J., Petr, V. and Praus, O., 1970. Depth distribution of the electrical conductivity in the Czechoslovak territory, J. Geomag. Geoelectr., 22, 235-240.

Peeples, W.J. and Rankin, D., 1973. A magnetotelluric study in the Western Canadian sedimentary basin, Pure & Applied Geophys., 102, 134-147.

Phillips, W.E.A., Stillman, C.J. and Murphy, T., 1976. A Caledonian plate tectonic model, Jl. Geol. Soc. Lond., 132, 576-609.

Pitcher, D.H., 1972. A study of geomagnetic variation in eastern Canada, M.Sc. Thesis, Department of Physics, University of Toronto.

Piwinsky, A.J. and Duba, A., 1975. Geothermal exploration: An additional ambiguity in the interpretation of resistivity anomalies, paper III.76 presented at Second United Nations Symposium on the Development and Use of Geothermal Resources, San Francisco, 20-29 May 1975.

Porath, H., 1971. A review of the evidence on low-resistivity layers in the Earth's crust, in Structure and Physical Properties of the Earth's Crust, A.G.U. Monograph 14.

Porath, H. and Dziewonski, A., 1970. Crustal electrical conductivity anomalies in the Great Plains Province of the United States, Geophys., 36, 382-395.

Porath, H. and Dziewonski, A., 1971. Crustal resistivity anomalies from geomagnetic deep sounding studies, Rev. Geophys. Space Phys., 9, 891-915.

Porath, H. and Gough, D.I., 1971. Mantle conductive structures in the western United States from magnetometer array studies, Geophys. J. R. astr. Soc., 22, 261-276.

Porath, H., Oldenburg, D.W. and Gough, D.I., 1970. Separation of magnetic variation fields and conductive structures in the western United States, Geophys. J. R. astr. Soc., 19, 237-260.

Porstendorfer, G., 1975. Principles of Magneto-Telluric Prospecting. Bontraeger, Berlin.

Portnyagin, M.A., 1968. On anomalous electrical conductivity at crust-mantle boundary in the Irkutsk amphitheatre, Geologika i Geofizika, 12, 93-100.

Pospeev, V.J., Mikhalevsky, V.J. and Gornostaev, V.P., 1969. Results of measurements with the magnetotelluric method in east Siberia and the Far East, in Magnetotelluric Method for Studying the Structure of the Crust and Upper Mantle, pp 139-149. Nauka Press.

Powell, D.W., 1970. Magnetised rocks within the Lewisian of Western Scotland and under the Southern Uplands, Scott. J. Geol., 6, 353-371.

Powell, D.W., 1971. Comment on "A model for the Lower Palaeozoic evolution of the southern margin of the early Caledonides of Scotland and Ireland" by Dewey (1971), Scott. J. Geol., 7. 369-372.

Powell, D.W., 1977a. Gravity and magnetic interpretations of Ballantrae ophiolites, contributed paper: Southern Uplands Workshop held in Edinburgh, 11 March 1977.

Powell, D.W., 1977b. Gravity and magnetic interpretations of Southern Upland granites, contributed paper: Southern Uplands Workshop held in Edinburgh, 11 March 1977.

Praus, O., Pecova, J., Petr, V., Pec, K., Jankowski, J. and Szymanski, A., 1975. Anomalous induction in the Carpathians, contributed paper Grenoble.

Press, F., 1968. Earth models obtained by Monte-Carlo inversion, J. Geophys. Res., 73, 5223-5234.

Press, F., 1970. Earth models consistent with geophysical data, Phys. Earth. Planet. Int., 3, 3-22.

Price, A.T., 1950. Electromagnetic induction in a semi-infinite conductor with a plane boundary, Quart. J. Mech. Appl. Maths., 3, 385-410.

Price, A.T., 1962. The theory of magnetotelluric fields when the source field is considered, J. Geophys. Res., 67, 1907.

Price, A.T., 1970. The electrical conductivity of the Earth, Q. Jl. R. astr. Soc., 11, 23-42.

Price, A.T., 1973. The theory of geomagnetic induction, Phys. Earth. Planet. Int., 7, 227.

Rader, C.M., 1970. An improved algorithm for high speed auto-correlation with applications to spectral estimation, I.E.E.E. Trans. Audio. Electroacoust., AU-18, 439-441.

Rankin, D., 1973. The perturbation of alternating geomagnetic fields by an island near a coastline: discussion. Can. J. Earth. Sci., 10, 1702.

Rankin, D. and Kurtz, R., 1970. Statistical study of micropulsation polarisations, J. Geophys. Res., 75, 5444-5458.

Rankin, D. and Reddy, I.K., 1968. Polarisation of micropulsation sources, Earth. Planet. Sci. Lett., 3, 347-350.

Rankin, D. and Reddy, I.K., 1970. Polarisation of the magnetotelluric fields over an anisotropic earth, Pure Appl. Geophys., 78, 58-65.

Rankin, D. and Reddy, I.K., 1973. Crustal conductivity anomaly under Black Hills, a magnetotelluric study, Earth. Planet. Sci. Lett., 20, 275-279.

Rankin, D., Reddy, I.K. and Kao, D., 1976. The Black Hills anomaly, a magnetotelluric study, paper presented Sopron.

Rankin, D., Reddy, I.K. and Schneider, K., 1976. On the interpretation of continuous resistivity distributions in the magnetotelluric method, Geophys. J. R. astr. Soc., 45, 89-95.

Reddy, I.K. and Rankin, D., 1971. Magnetotelluric measurements in central Alberta, Geophys., 36, 739-753.

Reddy, I.K. and Rankin, D., 1972. On the interpretation of magnetotelluric data in the Plains of Alberta, Can. J. Earth. Sci., 9, 514-527.

Reddy, I.K. and Rankin, D., 1973. Magnetotelluric response of a two-dimensional sloping contact by finite element method, Pure Appl. Geophys., 105, 847.

Reddy, I.K. and Rankin, D., 1974. Coherence functions for magnetotelluric analysis, Geophys., 312.

Reddy, I.K., Phillips, R.J., Whitcomb, J.H., Cole, D.M. and Taylor, R.A., 1976. Monitoring of time-dependent electrical resistivity by magnetotellurics, J. Geomag. Geoelectr., 28, 165-178.

Rikitake, T., 1966. Electromagnetism and the Earth's Interior. Elsevier Publishing Co.

Rikitake, T., 1973. Global electrical conductivity of the Earth, Phys. Earth. Planet. Int., 7, 245-250.

Ringwood, A.E., 1966. Mineralogy of the mantle, in Advances in Earth Sciences, ed. P.M. Hurley. M.I.T. Press, Cambridge, Massachusetts.

Ringwood, A.E. and Green, D.H., 1970. Phase transitions, in The Earth's Crust and Upper Mantle, A.G.U. Monograph 13.

Ringwood, A.E. and Major, A., 1970. The system Mg_2SiO_4-Fe_2SiO_4 at high pressures and temperatures, Phys. Earth. Planet. Int., 3, 89-108.

Robinson, B., 1976. Electromagnetic induction in the seas around the Orkney Islands, paper presented at Sopron.

Robinson, E.A., 1967. Statistical communication and detection. Hafner Publication Co., New York.

Rokityansky, I.I., 1974. Non-synoptic array studies: a review, paper presented at Ottawa.

Rokityansky, I.I., 1975. Investigation of anomalies of electro-conductivity by the method of magneto-variational profiling, p 279. 'Naukou Dumka', Kiev.

Rokityansky, I.I., Amirov, V.K., Kulick, S.N., Logvinov, I.M. and Shuman, V.N., 1974. Electrical conductivity anomaly in Carpathians, contributed paper Ottawa.

Rokityansky, I.I. and Logvinon, I.N., 1972. Anomaly of electro-conductivity on Kirovograd block of the Ukranian shield, Izv. An. S.S.S.R., Fizika. Zemli, 6.

Rokityansky, I.I., Logvinov, I.M. and Maksimov, V.M., 1976. Magneto-meter array study in the central part of the Russian platform, contributed paper Sopron.

Ronov, A.B. and Yarcshevsky, 1969. Chemical composition of the Earth's crust, in The Earth's Crust and Upper Mantle, A.G.U. Monograph 13.

Rooney, D., 1976. Magnetotelluric measurements across the Kenyan Rift Valley, Ph.D. Thesis, University of Edinburgh.

Rooney, W.J., 1939. Earth-currents, in Terrestrial Magnetism and Electricity, ed. J.A. Fleming. McGraw-Hill, New York.

Saito, T., 1964. J. Geomag. Geoelectr., 16, 115.

Saito, T. and Matsushita, S., 1968. Solar cycle effects on geomagnetic Pi2 pulsations, J. Geophys. Res., 73, 267-286.

Scheelke, I., 1972. Magnetotellurische Messungen im Rheingarben and ihre Deutung mit Zweidimensionaler Modelles. Gamma 20, Inst. geophys. meterol. Tech. Univ. Braunschweig.

Schelkunoff, S.A., 1938. The impedance concept and its application to problems of reflection, refraction, shielding and power absorption, Bell System Tech. Journ., 17, 17.

Schloessen, H.H., 1976. Electrical and dielectric properties of mantle materials from high pressure experiments, paper presented at a discussion meeting of the R.A.S. on 'Solid State Physics and Geophysics', London, 12 November 1976.

Schmidt, A., 1909. Die magnetische Storung am 25 September 1909 zu Potsdam and Seddin, Meteorol. Z., 36, 509-511.

Schmucker, U., 1970. Anomalies of geomagnetic variations in the south-western United States, Bull. Scripps Inst. Ocean., Univ. of Calif., San Diego, Calif., Vol. 13.

Schmucker, U., 1971. Interpretation of induction anomalies above non-uniform surface layers, Geophys., 36, 156-165.

Schmucker, U., 1973. Regional induction studies: a review of methods and results., Phys. Earth. Planet. Int., 7, 365-378.

Schuster, A., 1889. The diurnal variation of terrestrial magnetism, Phil. Trans. Roy. Soc. London, Ser. A, 180, 467-518.

Scrutton, R.A., 1974. The Gibbs Fracture Zone, Nature, 251, 165-166.

Serson, P.H., 1973. Instrumentation for induction studies on land, Phys. Earth. Planet. Int., 7, 313.

Shankland, T.J., 1969. Transport properties of olivine, in The Application of Modern Physics to the Earth and Planetary Interiors, ed. S.K. Runcorn. Interscience, New York.

Shankland, W.J., 1975. Electrical conduction in rocks and minerals, parameters for interpretation, Phys. Earth. Planet. Int., 10, 209-219.

Shankland, T.J. and Waff, H.S., 1974. Conductivity of fluid bearing rocks, J. Geophys. Res., 79, 4863-4868.

Shanks, J.L., 1967. Recursion filters for digital processing, Geophys. 32, 33-51.

Simon, G. and Rossignol, J.C., 1974. A recording system for the earth's telluric field with either analogue or numerical output, Phys. Earth. Planet. Int., 8, 19-22.

Sims, W.E. and Bostick, Jr. F.X., 1969. Methods of magnetotelluric analysis, Elec. Geophys. Res. Lab. Tech. Rep. 58, University of Texas.

Sims, W.E., Bostick, F.N. and Smith, H.W., 1971. The estimation of magnetotelluric impedance tensor elements from measured data, Geophys. 36, 938-942.

Sochelnikov, V.V., 1976. The theory and methods of marine magneto-telluric sounding, contributed paper Sopron.

Sonett, C.P., Colburn, D.S., Dyal, P., Parkin, C.W., Smith, B.F., Schubert, G. and Schwartz, K., 1971. Lunar electrical conductivity profile, Nature, 230, 359-362.

Sonett, C.P., Smith, B.F., Colburn, D.S., Schubert, G. and Schwartz, K., 1972. The induced magnetic field of the Moon: conductivity profiles and inferred temperatures, Proc. Third Lunar Sci. Conf., 2309-2336.

Slutsky, E., 1937. The summation of random causes as the source of cyclic processes, Econometrica, 5, 105.

Smith, G.D., 1965. Numerical solution to partial differential equations, Oxford University Press, London.

Srivastava, S.P., 1965. Method of interpretation of magneto-telluric data when source field is considered, J. Geophys. Res., 70, 945-954.

Srivastava, S.P., 1967. Magnetotelluric two- and three-layer master curves, Dom. Obs. Publ., 35, no. 7, Canada Dept. of Energy, Ottawa.

Srivastava, S.P., Douglass, J.L. and Ward, S.H., 1963. The application of magnetotelluric and telluric methods in central Alberta, Geophys., 28, 426-446.

Srivastava, S.P. and Jacobs, J.A., 1964. Determination of the electrical resistivity at Meanook, Alberta, Canada by the magneto-telluric method, J. Geomag. Geoelectr., 15, 280-288.

Srivastava, S.P. and White, A., 1971. Inland, coastal and offshore magnetotelluric measurements in eastern Canada, Can. J. Earth. Sci., 8, 204-216.

Steinhart, J.S. and Meyer, R.P., 1961. Explosion studies of continental structure, Carnegie Inst. Wash. Publ. 622, Washington, D.C.

Stephens, M.A., 1962. Exact and approximate tests for directions I, Biometrika, 49, 463-477.

Stuart, W.F., Sherwood, V. and MacIntosh, S.M., 1971. The power spectral density technique applied to micropulsation analysis, PAGEOPH, 92, 150-164.

Summers, D. McN., 1976. The inversion of geomagnetic data, Ph.D. Thesis, University of Edinburgh.

Swift, C.M., 1967. A magneto-telluric investigation of an electrical conductivity anomaly in the south-western United States, Ph.D. Thesis, Department of Geology & Geophysics, M.I.T., Cambridge, Massachusetts.

Swift, C.M., 1971. Theoretical magnetotelluric and Turan response from two-dimensional inhomogeneities, Geophys., 36, 38-52.

Tammemagi, H.Y. and Lilley, F.E.M., 1973. A magneto-telluric traverse in Southern Australia, Geophys. J. R. astr. Soc., 31, 433-445.

Terada, T., 1917. On rapid periodic variations of terrestrial magnetism, J. Col. Sci., Tokyo Imp. Univ., 37, 56-84.

Tikhonov, A.V., 1950. Determination of the electrical characteristics of the deep strata of the earth's crust, Dokl. Akad. Nauk., 73, 295.

Tikhonov, A.N. and Berdichevskii, M.N., 1966. Experience in the use of magneto-telluric methods to study the geological structures of sedimentary basins, Izv. Earth. Phys., 2, 34-41.

Tkachev, G.N., 1973. Experiment of abyssal magnetotelluric soundings at the Ukrainian shield, Geofiz. Sbornik. A.N. Uk.S.S.R., 52, 62-65.

Tolland, H.G. and Strens, R.G.J., 1972. Electrical conduction in physical and chemical mixtures. Application to planetary mantles, Phys. Earth. Planet. Int., 5, 380-386.

Trigg, D.F., 1972. An amplifier and filter system for telluric signals, Publ. Earth. Phys. Branch, 41, 66.

Trigg, D.F., Serson, P.H. and Camfield, P.A., 1971. Publ. Earth. Phys. Branch, 41 (5), 66.

Ulrych, T., 1975. A review of the maximum entropy method of spectral analysis and some applications, paper presented at Grenoble.

Untiedt, J., 1970. Conductivity anomalies in central and southern Europe, J. Geomag. Geoelectr., 22, 131-150.

Van Ngoc, P. and Boyer, D., 1974. Magnetotelluric mapping of deep structure in the Parisian basin, contributed paper Ottawa.

Vanyan, L.L. and Kharin, E.P., 1967. Deep magnetic variation sounding in the Baikal region, in Regional Geophysical Investigations in Siberia, Isdat, Nanka, Novosibirska.

Vozoff, K., 1972. The magnetotelluric method in the exploration of sedimentary basins, Geophys., 37, 98-141.

Vozoff, K. and Ellis, R.M., 1966. Magneto-telluric measurements in southern Alberta, Geophys., 31, 1153-1157.

Vozoff, K. and Jupp, D.L.B., 1975. Joint inversion of geophysical data, Geophys. J. R. astr. Soc., 42, 977-999.

Vozoff, V. and Swift, C.M., 1968. Magneto-telluric measurements in the North German Basin, Geophys. Prosp., 16, 454-473.

Wagenitz, V., 1974. A systematic magnetotelluric mapping of the North German sedimentary basin, contributed paper Ottawa.

Wait, J. R., 1954. On the relationship between telluric currents and the earth's magnetic field, Geophys., 19, 281-289.

Wait, J.R., 1962. Electromagnetic Waves in Stratified Media. Pergamon Press, Oxford.

Walton, E.K., 1960. Some aspects of the succession and structure in the Lower Palaeozoic rocks of the Southern Uplands of Scotland, Geol. Rdsch., 50, 63-77.

Ward, S.H., Peebles, W.J. and Ryu, J., 1973. Analysis of geomagnetic data, in Methods in Computational Physics, Vol. 13, Geophysics. Academic Press, New York.

Weaver, J.T., 1963. The electromagnetic field with a discontinuous conductor with reference to geomagnetic micropulsations near a coastline, Can. J. Phys., 41, 484-495.

Weidelt, P., 1971. The electromagnetic induction in two thin half-sheets, Zeitschrift fur Geophysik, 37, 649-665.

Weidelt, P., 1972. The inversion problem of geomagnetic induction, Zeitschrift fur Geophysik, 38, 257-289.

Weidelt, P., 1975a. Inversion of two-dimensional conductivity structures, Phys. Earth. Planet. Int., 10, 282-291.

Welch, P.D., 1967. The use of fast Fourier transform for the estimation of power spectra: A method based on time averaging over short, modified periodograms, I.E.E.E. Trans. Audio. Electroacoust., AU-15, 70-73.

Wiese, H., 1963. Geomagnetische Tiefentellurik, Dt. Akad. Wiss. Berlin, Geomagn. Institut. Potsdam, 36.

Wiggins, R.A., 1972. The general linear inverse problem: implications of surface waves and free oscillations for Earth structure, Rev. Geophys. Space Phys., 10, 251-285.

Wiggins, R.A. and Miller, S.P., 1972. New noise-reduction technique applied to long-period oscillations from the Alaska earthquake, Bull. Seis. Soc. Am., 62, 471-479.

Williams, A., 1972. Distribution of brachiopod assemblages in relation to ordovician palaeo-geography, in Organisms and Continents through Time, ed. N.F. Hughes, Spec. Pap. Palaeont., 12, 241-269.

Williamson, K., Hewlett, C. and Tammemagi, H.Y., 1974. Computer modeling of electrical conductivity structures. Geophys. J. R. astr. Soc., 37, 533-536.

Wilson, J.T., 1966. Did the Atlantic close and then re-open? Nature, 211, 676-681.

Winter, R., 1973. Der Oberrheingraben als Anomalie der elektrischen Leitfahigkeit untersucht mit Methoden der Erdmagnetischen Tiefensonderung, Diss. Math. - Naturwiss, Fak. Univ. Gottingen.

Winter, R., 1976. Analysis and first interpretation of magnetotelluric soundings on the deep sea floor in the North Atlantic, paper presented Sopron.

Word, D.R., Smith, H.W. and Bostick, F.W., 1970. An investigation of the magnetotelluric tensor impedance method, Tech. Rep. No. 82, Elec. Geophys. Res. Lab., Univ. of Texas at Austin, Austin, Texas.

Wright, J.A., 1969. The electromagnetic response of two-dimensional structures, Gamma 7, Inst. f. Geoph. Meteorol., Tech. Univ. Braunschweig, 102.

Wright, J.A., 1970. Anisotropic apparent resistivities arising from non-homogeneous two-dimensional structures, Can. J. Earth. Sci., 7, 527-531.

Wu, F.T., 1968. The inverse problem of magnetotelluric sounding, Geophys. 33, 972-979.

Yungul, S.H., 1961. Magnetotelluric sounding three-layer interpretation curves, Geophys. 26, 465.

Zhemaletdinov, A.A., Semenov, A.S. and Veselow, I.I., 1970. Influence of horizontal inhomogeneity on the results of abyssal electric soundings in the Pechenega region, Vestnik. I.G.U., 18.